

Soft Ferrites

Properties and Applications

E. C. Snelling

Soft Ferrites

Soft Ferrites

Properties and Applications

E. C. Snelling, B.Sc.(Eng.), C.Eng., F.I.E.E.

Mullards Research Laboratories

LONDON ILIFFE BOOKS LTD

Iliffe Books Ltd
42 Russell Square
London, W.C.1

First published in 1969

© E. C. Snelling, 1969

Digitized and polished by PE1ABR

Filmset by Photoprint Plates Ltd

Wickford, Essex

Printed in England by J. W. Arrowsmith Ltd
Bristol

592 02790 2

Contents

Preface

Acknowledgements

1	Ferrites; their Nature, Preparation and Processing	1
2	The Expression of Electrical and Magnetic Properties	18
3	Properties of some Manganese Zinc and Nickel Zinc Ferrites	38
4	Magnetic Circuit Theory	171
5	Inductors	193
6	High Frequency Transductors	225
7	Wide Band Transformers	237
8	Pulse Transformers	269
9	Power Transformers	297
10	Ferrite Antennas	327
11	Properties of Windings	337
	Appendix A Wire Tables	359
	Appendix B Calculation of the Core Factors of a Pot Core	377
	Appendix C Symbols	379
	<i>Index</i>	385

Preface

Ferrites have become firmly established as one of the most important classes of present day magnetic materials and are widely used in linear, digital and microwave branches of electrical engineering. Of these applications, those in the digital and microwave fields are rather well served by the literature, whereas it appears that hitherto there has been no textbook specifically devoted to the properties and applications of the largest and most established group of ferrites, i.e. those having high permeability and low losses. It is to remedy this deficiency that this book has been written. It is concerned with the technically important properties of magnetically soft ferrites at frequencies up to about 100 MHz, and the applications of these ferrites to inductors, transformers and related devices. It is primarily intended for electrical engineers and physicists whose work involves design or development using these ferrites. Thus the treatment of each aspect of the subject is direct and functional. But it is not superficial; adequate detail and analysis is given where it is relevant to the main purpose. Data, theoretical relations, and design or selection procedures have been given in the most accessible and useful forms. Wherever possible the labour of design or selection has been minimized by the computation of the functions involved and the presentation of the results in tabular or graphical form.

The four opening chapters deal with the properties of ferrites and magnetic circuits in general. The first gives a broad introduction to ferrite materials and a qualitative description of the origin of the magnetic properties. It also describes those aspects of manufacture and processing that may be of interest to the user. The next chapter considers in detail the expression of the electrical and magnetic properties of ferrites ranging from the Rayleigh relations to recent recommendations of the International Electrotechnical Commission.

Chapter 3 is devoted to a wide-ranging survey of the properties of currently available manganese zinc and nickel zinc ferrites. It starts with a tabulation of all the ferrite manufacturers known to the author; entered against each manufacturer are the current material grade numbers classified according to application. There follows an extensive presentation of material properties containing over 180 separate graphs. In the case of Mullard Ferroxcube the data were largely generated by the author and his colleagues whereas the other data were exclusively supplied by the manufacturers concerned. Every effort has been made to ensure that the selection is as comprehensive and representative as possible. The author expresses his gratitude to the many manufacturers who have contributed data to this section and he apologises for any omissions or unbalance that may become apparent. The fourth chapter considers the relations between the properties and the geometry of the practical magnetic circuit, e.g. the effect of non-uniform cross section, air gaps, etc.

The next six chapters each deal with a basic type of ferrite-cored device. In order to prevent repetition and excessive proliferation the aim has been to treat the fundamental principles in some detail and to avoid consideration of the more specific versions of the device. Thus important applications such as telephone loading coils, I.F. transformers, T.V. line output transformers, etc., have not been separately described, but inasmuch as their design is concerned with ferrite cores the essential information will be found in these chapters. They consider in turn inductors, transducers, wide band transformers, pulse transformers, power transformers and magnetic antennas. Each is a study of the basic theory and design

concepts with special reference to core properties and geometry. These chapters contain much specially computed data and original work.

Finally all the design aspects that relate particularly to the winding and are common to a number of the applications, e.g. resistance, eddy currents in conductors, self capacitance and leakage inductance, are grouped together in Chapter 11.

The quantities and units used in this book are primarily in accordance with the International System (S.I.) and the symbols are as far as possible consistent with IEC Publication 27. This representation is rapidly superseding the C.G.S. practical system. However, as many readers will be more familiar with this latter system it has been included as an alternative in the following way. In the main text the equations are in S.I. units except in rare cases where an equation is applicable only in some other (stated) system. If the C.G.S. version of a numbered equation differs from the S.I. version, the C.G.S. version is given in a footnote. Unless multiples or sub-multiples are specifically indicated, the symbols refer to the basic units of the appropriate system. If a numbered equation does not have a footnote version it means that the S.I. and C.G.S. versions are identical provided the appropriate units are used. In the graphs, scales have been given in both systems of units where necessary.

E.C.S.

Acknowledgements

In gathering the material for this book and preparing it for publication the author has been fortunate in having the assistance and co-operation of a number of people and organizations, and he wishes to express his gratitude to all of them. Although it is not possible to mention them all by name he would like to make the following specific acknowledgements.

Mr. H. Jackson provided useful data on ferrite manufacture, and Dr. F. W. Harrison, Mr. J. E. Knowles and Mr. C. V. Newcomb contributed helpful suggestions concerning the first and third chapters. The acquisition and marshalling of the data for Chapter 3 was a major task and valuable assistance was provided by his colleagues Mr. A. G. Dabney, Mr. F. G. Pronger, Mr. A. Waters and in particular Mr. N. C. O. Jackson. In Chapter 4 the discussion of core factors benefited from correspondence with Mr. E. Olsen and the measurements on ferrite rods were made by Mr. P. Johnson. Mr. B. Astle assisted by checking the pot core optimization results on the computer and he provided helpful comments on a number of subjects. Chapter 7 contains much that has its origins in the author's early training in transformer design and he acknowledges the tuition in this subject that he received from the late Dr. J. Mole and from an unpublished report by Mr. C. Hooijkamp. Grateful acknowledgement is due to Mrs. V. B. Ingram who typed most of the final manuscript, to Mrs. L. Strudwick and Miss P. A. Webb who typed much of the preparatory material, to Mrs. A. I. Pronger who prepared all the diagrams and illustrations, and to those colleagues who assisted with the checking of the proofs. Finally, on a more personal note, the author wishes to recognize the help and enormous patience of his wife who expected that the work would occupy months but found that it consumed years.

Special acknowledgement is due to the Directors of Mullard Ltd for permission to publish in this book the results of work done on their behalf. Referring particularly to Chapter 3 the author wishes to express his appreciation to all the manufacturers who kindly made available data on their ferrite materials, and who subsequently checked and approved the detailed presentation of their contributions. The manufacturers who co-operated in this are as follows: Aladdin Components Ltd., Greenford, Middlesex, England. Allen Bradley Company, Milwaukee, Wisconsin, U.S.A. Ceramic Magnetics Inc., Fairfield, New Jersey, U.S.A. Compagnie des Ferrite Electroniques, Paris, France. COPRIM, Evreux, Eure, France. Fair-Rite Products Corp., Wallkill, New York, U.S.A. Ferroxcube Corporation, Saugerties, New York, U.S.A. Fried. Krupp Widia-Fabrik, Essen, Germany. Indiana General Corp., Keasbey, New Jersey, U.S.A. Lignes Telegraphiques et Telephoniques, Paris, France. Magnetics Inc., Bulter, Pennsylvania, U.S.A. Mullard Ltd., London, England. National Moldite Company Inc., Newark, New Jersey, U.S.A. Neosid Ltd., Welwyn Garden City, Hertfordshire, England. Neosid Pemetzrieder G.m.B.H., Halver in Westfalen, Germany. Nippon Electric Co. Ltd., Minato-ku, Tokyo, Japan. Nippon Ferrite Industrial Co. Ltd., Shinjuku-ku, Tokyo, Japan. N. V. Philips Gloeilampenfabrieken, Eindhoven, Holland. The Plessey Company Ltd., Towcester, Northamptonshire, England. Salford Electrical Instruments Ltd., Heywood, Lancashire, England. Siemens A.G., Munich, Germany. Sony Corporation, Shinagawa-ku, Tokyo, Japan. Stackpole Carbon Company, St. Mary's, Pennsylvania, U.S.A. Standard Telephones and Cables Ltd., Harlow, Essex, England. Steatite Magnesia, Porz, Rhein bei Köln, Germany. D.M. Steward Manufacturing Company, Chattanooga, Tennessee, U.S.A. Toholcu Metal Industries Ltd., Chuo-ku, Tokyo, Japan. Valvo G.m.b.H., Hamburg, Germany.

Ferrites; Their Nature, Preparation and Processing

1.1. INTRODUCTION

Ferrimagnetic oxides, or ferrites as they are usually known, have become available as practical magnetic materials over the course of the last twenty years. During this time their use has become established in many branches of communication and electronic engineering and they now embrace a very wide diversity of compositions, properties and applications. The scope of this book is restricted to the properties of those ferrites which are magnetically soft and which are of technical importance, and to the applications of such ferrites in devices which, in the broadest sense, may be described as inductors or transformers. In the pages that follow, unqualified reference to ferrites will usually imply this restricted scope. It is appropriate, therefore, that this introduction should put these particular ferrites and their applications into a proper perspective by surveying briefly the wider field.

Magnetite, or ferrous ferrite, is an example of a naturally occurring ferrite. It has been known since ancient times and its weak permanent magnetism found application in the lodestone of the early navigators. Hilpert¹ in 1909 attempted to improve the magnetic properties of magnetite and in 1928 Forestier² prepared ferrites by precipitation and heat treatment. Magnetic oxides were also studied by Japanese workers^{3, 4} between 1932 and 1935. In 1936 Snoek⁵ was studying magnetic

oxides in Holland; by 1945 he had laid the foundations of the physics and technology of ferrites and a new industry came into being.⁶

Ferrites are ceramic materials, dark grey or black in appearance and very hard and brittle.

The magnetic properties arise from interactions between metallic ions occupying particular positions relative to the oxygen ions in the crystal structure of the oxide. In magnetite, in the first synthetic ferrites and indeed in the majority of present-day magnetically soft ferrites the crystal structure is cubic; it has the form of the mineral spinel. The general formula of the spinel ferrite is MeFe_2O_4 where Me usually represents one or, in mixed ferrites, more than one of the divalent transition metals Mn, Fe, Co, Ni, Cu and Zn, or Mg and Cd. Other combinations, of equivalent valency, are possible and it is possible to replace some or all of the trivalent iron ions with other trivalent metal ions.

In the early practical ferrites Me represented Cu+Zn, Mn+Zn, or Ni+Zn. The first of these compounds was soon abandoned and the other two, referred to as manganese zinc ferrite and nickel zinc ferrite (often abbreviated to MnZn ferrite and NiZn ferrite) were developed for a wide range of applications where high permeability and low loss were the main requirements.⁷ These two compounds are still by far the most important ferrites for high-permeability, low-loss applications and

constitute the vast majority of present-day ferrite production. By varying the ratio of Zn to Mn or Ni, or by other means, both types of ferrite may be made in a variety of grades, each grade having properties that suit it to a particular class of application. The range of permeabilities available extends from about 15 for nickel ferrite to several thousand for some manganese zinc ferrite grades.

The applications started in the field of carrier telephony where the combination of good magnetic properties and high resistivity made these materials very suitable as cores for inductors and transformers. Since the resistivities were at least a million times greater than the values for metallic magnetic materials, laminated or powdered cores could be replaced with solid ferrite cores and these could often be made in a more convenient shape than their laminated counterparts.

The application was extended to domestic television receivers where they became, and still remain, the undisputed core material for the line time-base transformer and the magnetic yoke used in the deflection system. In domestic radio receivers, rods or plates of ferrite are used as cores for magnetic antennas. Many other high-permeability, low-loss applications have been found.^{8, 9}

Meanwhile ferrites having hard magnetic properties were discovered.¹⁰ They have a hexagonal crystal structure and a typical chemical formula is $\text{BaFe}_{12}\text{O}_{19}$. They are characterized by having very large coercivities, e.g. greater than 160 A.mm^{-1} (2000 Oe). Because these ferrites were introduced at a time when the more important constituents of metal permanent magnets, e.g. Co and Ni, were scarce they found ready application. The crystallite axes may be orientated during manufacture so that anisotropic properties are induced and greater magnetic energies may be stored.¹¹ In both isotropic and anisotropic form these ferrites are used for a wide range of permanent magnet applications, e.g. loud speaker magnets, magnetic chucks, small electric motors and focussing magnets. Other hexagonal ferrites were developed^{12, 13} having useful soft magnetic properties that are maintained up to frequencies approaching 1000 MHz.

Another class of application arose when it was found possible to prepare spinel ferrites, such as Mn Mg, Mn Cu and Li Ni ferrite, having substantially rectangular hysteresis loops. The main use of these materials is for memory cores.^{14, 15} These are very small toroids which are used in large numbers as elements in rapid access data stores. The storage function depends on the two distinct states of remanence that these materials have and the ease by which they may be selected and switched from one state to the other. Rectangular loop ferrites are also applied in devices such as switching cores, used to send pulses of energy into selected memory core circuits, and multi-aperture cores, used for performing a variety of logic functions.

Applications at microwave frequencies resulted from the discovery that the aligned moments of the electron spins within the crystal lattice may be made to precess at a frequency that depends on the strength of the steady internal magnetic field. An incident circularly polarized electromagnetic wave will only produce precessional resonance (and the accompanying absorption) if the rotation is in the right sense with respect to the direction of the steady field. This gives rise to non-reciprocal devices in which the transmission properties in one direction are quite different to those in the other.¹⁶ A variety of microwave devices have been developed which depend basically on this principle. They include wave guide isolators, switches, circulators, modulators, etc. The performance of these devices depends among other things on the saturation magnetization of the ferrite and the width of the resonance absorption peak. Many different ferrites have been used to meet the diversity of requirements that occur in the field of microwave engineering. Among the most important are spinel ferrites, such as Ni ferrite, Mg Mn ferrite and Ni Cu Co Mn Al ferrite, hexagonal ferrites such as $\text{BaFe}_{12}\text{O}_{19}$ and garnet ferrites, such as yttrium iron garnet with various substitutions.

Permanent magnet ferrites, rectangular loop ferrites and microwave ferrites are extensive subjects, each meriting its own specialised literature. As previously stated, this book excludes them from further consideration and concentrates on the properties and applications of magnetically soft MnZn and NiZn ferrites. Further, it is not intended to consider in this book the physics of magnetism in general or of ferrites in particular. This subject is extensively covered in the literature. However a short qualitative description of the spinel lattice, the magnetic domain and the magnetization process will be useful as a basis for the discussion of the properties of ferrites. The reader is referred to standard text books for a more complete treatment.^{17, 18, 19, 20}

1.2. MAGNETISM IN FERRITES

1.2.1. The spinel lattice

Fig. 1.1 shows a unit cell of the spinel lattice and the sites of the various ions. The small cubic diagram shows how the unit cell is composed of octants of alternate kind: in the large diagram only the four nearest octants are shown complete, the remainder having the symmetry shown in the smaller diagram. All the octants contain the same tetrahedral arrangement of oxygen ions, the sites being defined by four corners of a smaller cube, which in practice is usually slightly distorted. In the octants corresponding to the unshaded parts of the small diagram, the remaining corners of the smaller cube are occupied by

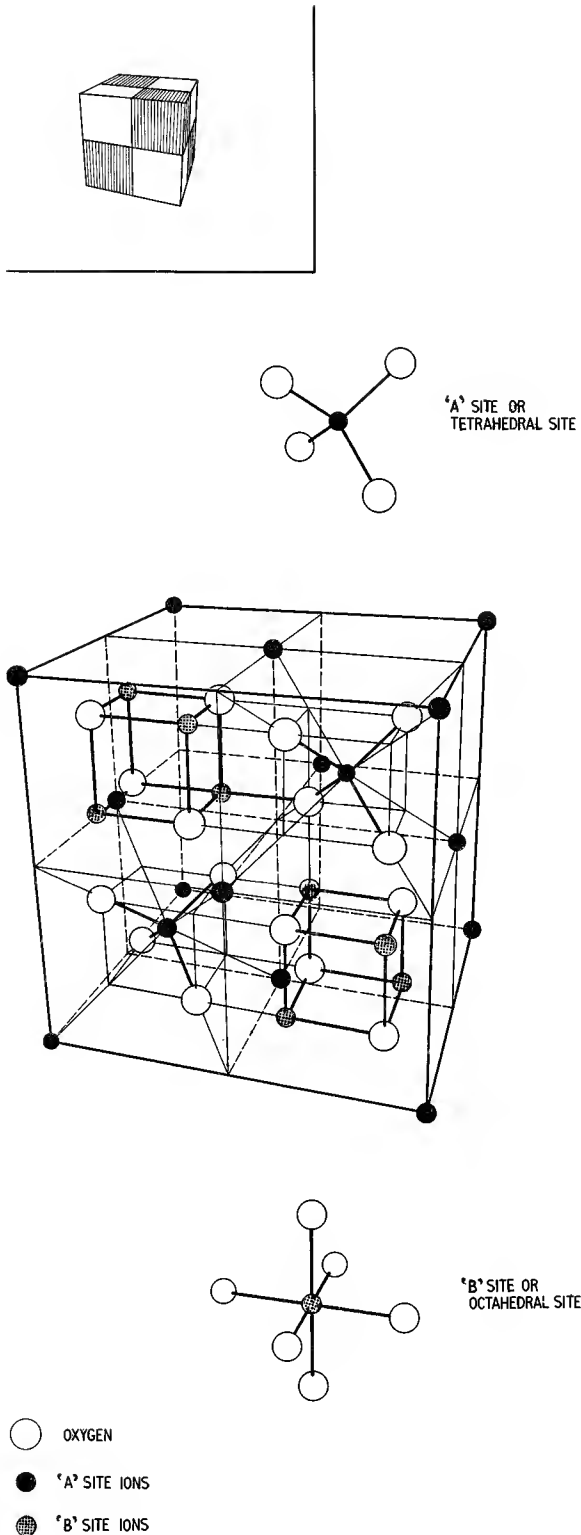


Fig. 1.1. Unit cell of the spinel lattice

metal ions. In the alternate octants these corners are not occupied; instead there is a site in the centre of the octant. This site, being surrounded by a tetrahedral arrangement of oxygen ions, is called a tetrahedral site or *A* site. A tetrahedral site is shown separately at the top of the diagram. All the black spheres are in tetrahedral sites although this is not obvious when considering only one isolated unit cell. The remaining metal ion sites are surrounded by six oxygen ions in the form of an octahedron. These are referred to as octahedral sites or *B* sites; an isolated octahedral site is shown at the bottom of the diagram.

In the unit cell there are 64 possible tetrahedral sites and 32 possible octahedral sites. Of these only 8 tetrahedral and 16 octahedral sites are occupied in a full unit cell. If, in the preparation, the ratio of metal ions to oxygen ions is too small, i.e. there is excess oxygen then some of the metal ion sites may be unoccupied. These sites are then referred to as vacancies. If the ratio is correct, then the unit cell contains 24 metal ions and 32 oxygen ions, i.e. there are 3 metal ions for every 4 oxygen ions. Thus the spinel unit cell may be considered from the chemical point of view to consist of 8 molecules having the formula MeFe_2O_4 . Of the three metal ions, one is on a tetrahedral site and two are on octahedral sites. If the spinel were 'normal' the divalent *Me* ion would occupy a tetrahedral (*A*) site while the trivalent *Fe* ions would occupy the octahedral (*B*) sites. In an 'inverse' spinel the divalent *Me* ion occupies one of the *B* sites while the trivalent *Fe* ions occupy the other *B* site and the *A* site. In terms of a unit cell:

	Me	Fe ₂	O ₄
Number of { <i>A</i> site ions { <i>B</i> site	— 8	8 8	32

In practice spinel ferrites have an ion distribution somewhere between 'normal' and 'inverse'.

The spinel structure consists of a number of interlaced face-centred cubic lattices. The most obvious one in Fig. 1.1 is that formed by the *A* sites on the cell corners and face centres. The remaining *A* sites (octant centres) form another face-centred cubic lattice displaced from the first along the cube diagonal.

The positions of the oxygen ions are also defined by a set of interlaced face-centred cubic lattices. Any oxygen ion may be taken as occupying a corner of a face-centred cube having the same dimensions as the unit cell; all other sites in this face-centred cube are also occupied by oxygen ions. Again, the octahedral (*B*) ions occupy sites on four face-centred cubic lattices. Each of these lattices has the same dimensions as the unit cell and they are displaced from one another along the edges of the smaller cube in the unshaded octants.

These interlaced lattices are called sub-lattices and they play an important part in the magnetism of ferrites.

1.2.2. Magnetization

Electrons spin about an axis and, by virtue of this spin and their electrostatic charge, exhibit a magnetic moment. Normally, in an ion with an even number of electrons, the spins or moments cancel, and when the number of electrons is odd there will be one uncompensated spin. For the transition metals the number of uncompensated spins is larger, e.g. the trivalent Fe ion has a moment equivalent to five uncompensated spins.

When the atoms of these transition metals are combined in metallic crystals, as they are, for example, in iron, the atomic moments are spontaneously held in parallel alignment over regions within each crystallite. The net number of uncompensated spins will be less than for the isolated ion due to the band character of the electron energies in a metal. The regions in which alignment occurs are called domains and may extend over many thousands of unit cells. The spin orientation is along a direction of minimum energy, i.e. external energy is required to deflect the magnetization from this direction and if the external constraint is removed the magnetization will return to a preferred direction. This directional or anisotropic behaviour may arise from a number of factors. Crystal anisotropy is inherent in the lattice structure; the magnetization always preferring the cube diagonal or cube edge. Mechanical strain can cause anisotropy and the shape of the grain boundary will nearly always produce anisotropy. The result is that the magnetization is held to a certain direction, or to one of a number of directions, as if by a spring. The greater the anisotropy, the stiffer the spring and the more difficult it is to deflect the magnetization by an external magnetic field, i.e. the lower the permeability (see Chapter 2 for definitions of permeability, etc.)

The parallel spin alignment implies that the material within the domain is magnetically saturated. The magnetization is defined as the magnetic moment per unit volume and is therefore proportional to the density of magnetic ions and to their magnetic moments. This magnetism arising from parallel alignment is called ferromagnetism.

In a ferrite the metal ions are separated by oxygen ions. As a result of this the ions in the *A* sub-lattice (tetrahedral sites) are orientated antiparallel to those in the *B* sub-lattice (octahedral sites). If these sub-lattices were identical the net magnetization would be zero in spite of the alignment and the ferrite would be classified as anti-ferromagnetic. In the majority of practical ferrites the two sub-lattices are different in number and in the type of ions so that there is a resultant magnetization. Such materials are classified as ferrimagnetic. For example, in the foregoing section it was stated that in the general spinel molecule MFe_2O_4 one metal ion occupies an *A* site while two occupy *B* sites; thus in the case of MnFe_2O_4

where both metal ions have 5 uncompensated spins the net magnetization is 5 spins per molecule. This compares with a net moment of 2.2 spins per *atom* in the case of metallic iron. For this reason a ferrite has a much lower saturation magnetization ($\mu_0 M_{\text{sat}} \approx 0.5 \text{ Wb.m}^{-2}$) than metallic iron (about 20 Wb.m^{-2}). However, in spite of the partial cancellation of the spin moments, ferrites possess sufficient saturation magnetization to make them useful in a wide range of applications.

The crystallite is normally divided into a number of domains of various spin orientations, e.g. opposite (180°) and orthogonal (90°), so that the crystallite has very little external field arising from the internal magnetization, i.e.

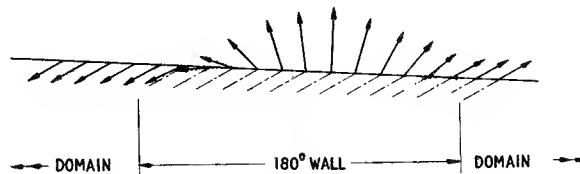


Fig. 1.2. Transition of spin direction at a 180° Bloch wall (domain boundary)

the demagnetizing fields are small. The domain boundaries (Bloch walls) consist of regions many unit cells in thickness in which there is a gradual transition of spin orientation, see Fig. 1.2. This transition must act against the anisotropic forces and the forces which tend to hold the spins in alignment and therefore involves storage of energy. The number and arrangement of domains in a crystallite is such that the sum of the energies, mainly the wall energy and the demagnetizing field energy, is a minimum. Fig. 1.3 shows an idealized arrangement of domains. If an external field is applied, the domain walls

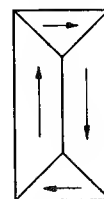


Fig. 1.3. Idealized domain pattern

experience a pressure which tends to make those domains having a component of magnetization in the direction of the field grow at the expense of the unfavourably orientated domains.

In practice it is energetically favourable for domain walls to pass through certain imperfections such as voids, stressed regions, non-magnetic inclusions, etc. Fig. 1.4 is a simplified representation of the situation. In the absence of an applied field the walls are straight and might occupy the positions shown in (a). The dots represent imperfections. If a small field is applied in the direction shown (b) the walls remain pinned by the imperfections but bulge

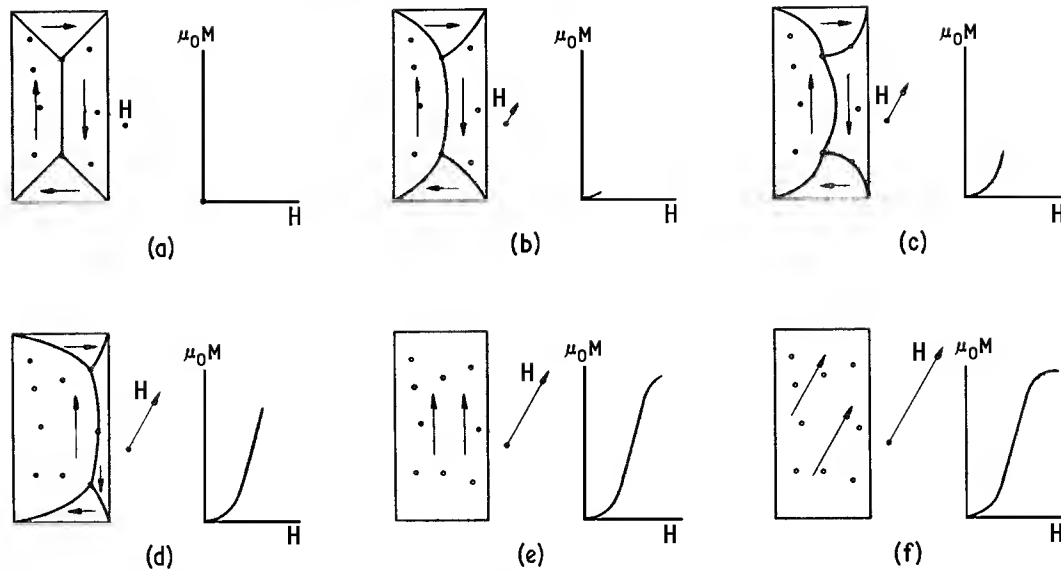


Fig. 1.4. A simplified representation of the part played by domain boundaries in the process of magnetization

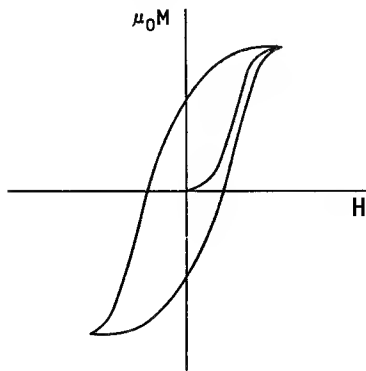


Fig. 1.5. Hysteresis loop

as would a membrane under pressure. These movements are reversible. The change in magnetization is restricted by the stiffness of the walls. Under these circumstances the lower part of the magnetization curve is traced. As the field increases, the pressure on the walls overcomes the pinning effect and the walls move by a series of jumps (c, d, e). These movements are irreversible, i.e. if a certain field change is required to produce a jump, the reversal of that change, i.e. the restoration of the field, will not in general cause the wall to jump back. During this part of the process the magnetization curve rises steeply. Finally, when all the domains have been swept away, further increases in field strength cause the magnetization vector to rotate reversibly towards the external field direction until complete alignment is approached (f). No further increase in magnetization is then possible and the material is said to be saturated. Normally in a polycrystalline material there is a wide distribution of

grain sizes, domain sizes, orientations, etc., and irreversible and reversible processes merge together. However the above illustration represents the main stages in the magnetization process.

If the magnetic field, having reached the maximum value corresponding to Fig. 1.4(f), is made to alternate cyclically about zero at the same maximum amplitude, the initial magnetization curve will not be retraced. Due to the irreversible domain wall movements the magnetization will always lag behind the field and an open loop will be traced. This phenomenon is known as magnetic hysteresis and the loop is called a hysteresis loop, see Fig. 1.5.

The ease with which the magnetization may be changed by a given magnetic field depends on the anisotropy, i.e. magnetic stiffness, whether the change is due to reversible or irreversible wall movements or rotations. A low anisotropy leads to a large induced magnetization for a given magnetic field and therefore to a large value of susceptibility and permeability (see Chapter 2).

1.3. MANUFACTURE

1.3.1. Manufacturing processes

The processes used in ferrite manufacture on an industrial scale are similar to those used in the manufacture of other ceramics. The description of these processes given in this chapter is intended mainly for the information of the user, so that the possibilities and limitations of manufacture may be taken into account when a particular ferrite core design or application is being considered.

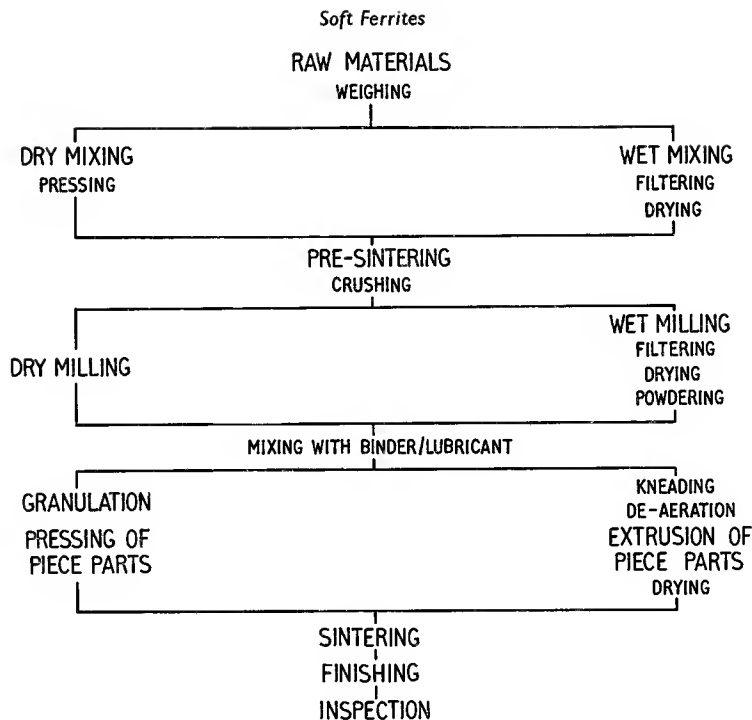


Fig. 1.6. Typical flow diagram for the manufacture of polycrystalline ferrites

There are, of course, other methods of preparation which are far less common and which have been used in special cases, usually on a small scale. A brief mention of these will be made before giving a more extended description of the normal processes.

One such method of powder preparation is chemical co-precipitation in which the constituents may be precipitated from salt solutions in the form of hydrated oxides or oxalates. This technique has the disadvantage that the product is susceptible to changes in the conditions of the solution during the preparation of a batch. Also, unwanted products are formed and these are difficult to remove. Electrolytic co-precipitation²¹ overcomes these disadvantages while retaining the intimate mixing inherent in co-precipitation. In this method the composition is formed by electrolysis from anodes consisting of metals corresponding to the required oxides. The oxides are formed continuously in an alkali salt electrolyte. Good control and a high degree of purity are claimed.

The mixture of oxides, however prepared, is usually sintered into a dense mass of the required shape. The alternative, fusion, is another method that has been used on a laboratory scale for the preparation of both single crystals and for polycrystalline ferrite preparation.

Returning to conventional manufacture of polycrystalline ferrites, a typical flow diagram is shown in Fig. 1.6. This diagram shows alternative processes, e.g. wet and dry milling, and forming of final shapes by pressing or extrusion. It is not intended to imply that in practice the

manufacture follows only the left hand or only the right hand paths; in fact wet milling is often used in the production of both pressed and extruded parts. Other process variations are possible; some will be mentioned in the more detailed description that follows.

The effect of the process variables on the magnetic properties of the ferrite is a subject of great significance to the manufacturer but it is beyond the scope of the present treatment. However, a brief mention of the more important relations will be included as appropriate in the process descriptions. Inasmuch as this procedure introduces the magnetic properties it will anticipate some of the more elementary parts of Chapter 2.

1.3.2. Raw materials

The raw materials are normally oxides or carbonates of the constituent metals. Chemical analysis, particle size and price are important characteristics of these starting materials. Because minor constituents or impurities may have a great influence on the properties of the finished ferrite it is normal to analyse incoming materials in an attempt to ensure that the composition does not deviate significantly from batch to batch. Particle size of the starting material has a profound effect on the behaviour of the product during manufacture.²² The ease of mixing, the compressibility, the shrinkage and the reactivity all depend on the particle size so it is normal to keep a check

on this parameter to ensure uniformity between batches. Materials of adequate purity and uniformity are usually prohibitively expensive, and successful large-scale manufacture depends on the skill with which reasonably-priced materials may be used to produce consistently ferrites having the required magnetic properties.

The constituent raw materials are weighed into batches to give the proportions required for the composition. Ignoring the influence of the minor constituents, the relative proportions of the principal metal ions and the oxygen ions have a basic effect on the magnetic properties. In mixed ferrites there are three or more different metal ions and this gives a wide range of possible relations.

Figs. 3.3.1 and 3.3.2 give an indication of the effect on the saturation flux density of changes in the ratio of zinc to other non-ferrous metal. Figs. 3.8.1 and 3.8.2 give the corresponding effects on the permeability-temperature relation. Zinc ferrite is paramagnetic at room temperatures; it is seen that an increasing proportion of zinc has the effect of reducing the Curie temperature and, except at the higher temperatures, it gives rise to a maximum saturation flux density. If more iron is used than the amount required for the exact composition, MeFe_2O_4 , then the excess iron appears in the form of divalent ions. Then Me, representing the divalent ions, includes some ferrous ions, e.g. manganese-zinc-ferrous ferrite. The effects of excess iron are complicated.^{23, 24} A small excess can minimise losses and cause a secondary peak in the permeability-temperature curve (see Fig. 3.8.4). It also provides conduction electrons and reduces the resistivity; for this reason the amount of iron is not normally allowed to exceed about 10% of the amount needed to supply the trivalent ions.

Trace elements such as cobalt or calcium are often added to modify the properties of the ferrite.²⁵ Since these elements, and others, are usually present in small quantities as impurities in the main raw materials the amount to be added depends on the amount present when the materials are received.

1.3.3. Mixing

The main purpose of this process is to combine the starting materials into a thoroughly homogeneous mixture. If crystallites of uniform composition and properties are subsequently to be formed then the constituents must be present in the correct proportions in any microscopic volume of the bulk material. It is difficult to avoid unmixing, i.e. one or more constituents becoming slightly more concentrated in certain regions of the mass, by virtue of the particle size or density. This may be due to agitation, either during mixing or transport, or in the wet process, due to sedimentation or selective filtration.

The mixing may be carried out dry, or the constituents may have water added to form a slurry which may be stirred with a turbine blade. Another method is wet ball-milling. The constituents are placed in a rotating steel-lined drum with steel balls and a medium such as water. Steel is used because any iron picked up by the mixture due to wear of the lining and balls may be allowed for in the initial composition of the powder. The fluid is mainly for cooling and mixing purposes. Wet milling usually continues for periods up to about twelve hours. Particle size reduction is not a primary aim of this process and is not usually very great.

After wet mixing the product is poured off as a slurry into a filter press where the water is squeezed out. The resulting blocks are then dried in an oven. In the dry process the powder has to be loosely pressed into blocks ready for pre-sintering. The pressing into blocks makes the product easier to manage in the kilns and improves the thermal conductivity.

1.3.4. Pre-sintering

Pre-sintering or pre-firing is a calcining process in which the temperature of the powder is raised to the region of 1000°C. Strictly this is not essential to the preparation of ferrites but it is a very important means of obtaining the necessary degree of control over the properties of the finished product.

Swallow and Jordan²⁶ state that pre-sintering is carried out for the following reasons:

1. It decomposes the carbonates or higher oxides, thereby reducing the evolution of gases in the final sintering.
2. It assists in homogenizing the material.
3. It reduces the effects of variations in the raw materials.
4. It reduces or controls the shrinkage occurring during the final sintering.

A typical pre-sintering cycle for manganese zinc and nickel zinc ferrites consists of passing the powder down a tunnel kiln in air so that its temperature is raised to a peak of 940–1060°C in about 8 h and then allowed to fall until it emerges from the kiln at about 200°C, about 20 h after entry. During this process the constituents partially react to form ferrite, i.e. spinel crystals begin to form and are normally allowed to grow to about 1 μ in size. The extent to which spinel is formed depends on the reactivity of the material, the temperature of the kiln and the time for which the material is heated. Middel²⁷ gives a linear relation between spinel content and sintering temperature starting at about 25% spinel formed at 800°C and going to 100% at about 1350°C.

After pre-sintering, the porous lumps of partly formed ferrite are easily crushed ready for milling.

1.3.5. Processing of the pre-sintered powder

The pre-sintered powder is milled to reduce it to small, uniformly sized crystallites. This process is carried out in a wet ball mill or a vibrating mill. In either case steel balls are normally used and as previously stated the inevitable wear of the balls may be allowed for in the composition; balls of other materials might cause contamination.

Milling times of up to 12 h are commonly used. After an initial period of rapid breakdown the particle size decreases in proportion to the milling time and then approaches a limiting value. The extent of the milling affects the forming characteristics of the powder, the sintered density and the magnetic properties such as permeability and losses. Since the extent of the milling depends on milling efficiency as well as the milling time it is preferable to mill to a certain particle size rather than a certain time. Particle size may be controlled by measuring the aggregate surface area of the particles in a sample of the powder.

After wet milling, the slurry is drawn off and the bulk of the liquid is removed by a pressure filter. The filtered material is then oven-dried and powdered. The dry-milled powder does not, of course, require this treatment.

At this stage it is usual to add the binder and lubricants. The choice of these additives depends on the subsequent granulation process, the method of forming (pressing or extrusion), the required strength of the formed piece-part before firing, and the avoidance of undesirable residues after burning-out during sintering. Commonly used binders are gum arabic, ammonium alginate, acrylates, polyvinyl alcohol, while waxes and wax emulsions, zinc or ammonium stearate may be used as lubricants to ease powder flow during forming. The quantities involved are quite small; using water as a vehicle these additives are blended with the powder to give the right consistency. Sometimes the lubricant is added later, when the powder has been granulated.

For the extrusion process the consistency must be that of a stiff dough. This is obtained by kneading. The batch is then divided into separate charges of the right size and shape for the cylinders of the extrusion machines. They are de-aerated to remove voids which would be detrimental to the extrusion process and to prevent excessive porosity of the sintered extrusion.

For dry pressing the powder must be in a form in which it will flow readily and uniformly into the die. This may be achieved by granulation. Methods of granulation in common use are:

- (a) Forming the powder (with binder) into tablets and then partially breaking these down by a method such as sieving.
- (b) Pan granulation. The powder is loaded into a rotating pan which has its axis inclined at about 45° to the horizontal. The tumbling action causes

the particles to agglomerate into small granules.

- (c) Spray drying. The powder, with binder and lubricant, is formed into a high solid content slurry. Alternatively the binder and lubricant may be added during milling and the milled slurry used direct. The slurry is sprayed into a chamber where it is atomized as high velocity particles in the presence of currents of hot air. The arrangement is such that the droplets scribe long trajectories before dropping into the collecting zone as dry granules.

The optimum size of granule is dictated mainly by the die in which the part is to be pressed. If the granules are too small or contain too many fines, the powder will work its way in between the sliding faces of the tool and cause excessive wear and friction. If they are too large they may not adequately fill the extremities of the die. Uniformity of size is important for a good flow of the granules and, to ensure a dense compact, the granules must readily break down under the pressure in the die.

1.3.6 Forming

For the ferrites that are the subject of this book, the usual forming method is dry-pressing or extrusion. Normally the main purpose of this operation is, of course, to form the powder into a shape which is as near as possible to the final shape required. The dimensions of the forming tools must be larger than the final part dimensions by a factor which allows for shrinkage during sintering. The product when sintered is very hard, and shape modification at that stage is usually expensive. Another, equally important, purpose of forming is to force the crystallites into close proximity so that, during sintering, they may grow to form a dense material, i.e. one having a low porosity. There are occasions when the compacting is more important than the shaping, e.g. in the iso-static technique described among the miscellaneous methods at the end of this section, the powder is pressed into a simple shape of high density from which the required final shape is cut after sintering, the quality of the product justifying the cost of the technique.

Dry pressing

In its simplest form this process consists of pouring the correct quantity of granulated powder into the die and then closing the die with a prescribed pressure which is usually in the range 1.6 to 16 kg.mm^{-2} (1 to 10 ton.in^{-2}). In practice the flow properties of the powder must be taken into account and therein lies the art of dry pressing. As the powder is compressed it builds up a friction between its outer surface and the adjacent die walls. Due to this friction and the viscosity of the powder, the

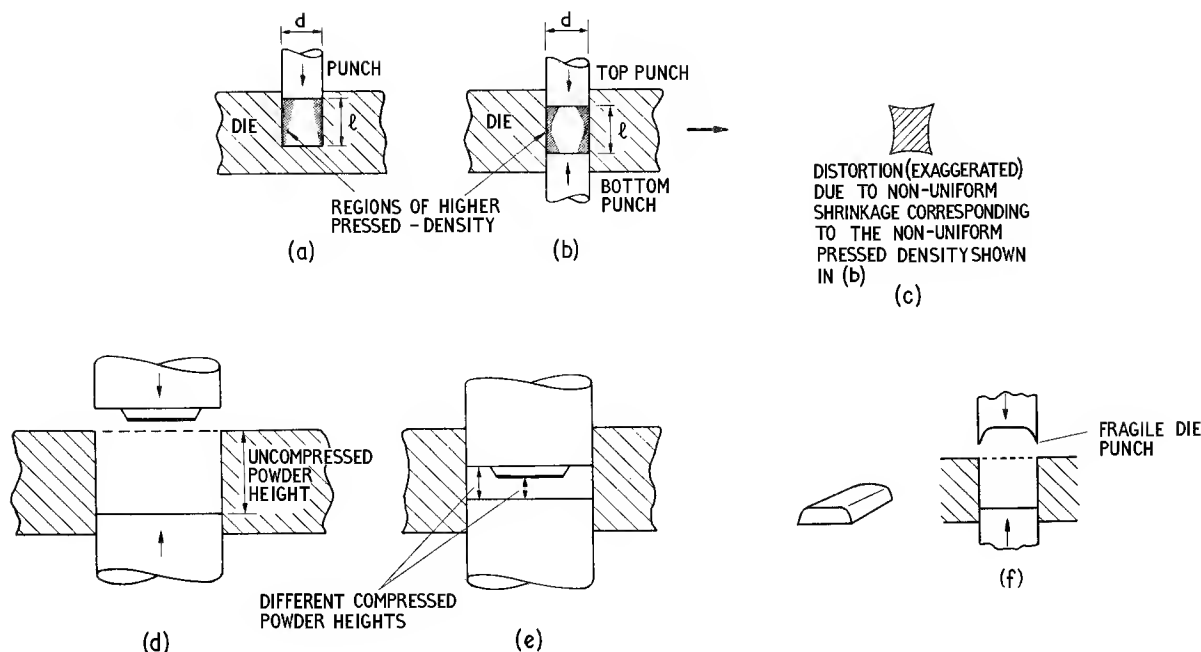


Fig. 1.7. Some aspects of pressing technique

pressure (and therefore the density) in the pressed powder is not uniform. Fig. 1.7(a) shows the simple pressing of a cylinder and indicates by shading the higher pressure zones caused by friction. If the length l were long enough, the friction alone would be enough to balance the applied force and the powder at the bottom of the die would not be compressed at all. This difficulty may be somewhat alleviated by compressing the powder from both ends as in Fig. 1.7(b). In practice it is usual for the die to move in a vertical line during pressing, the movements of die and punches being so related that the most uniform pressed density is obtained. Even so, shapes having l/d ratios of greater than about 5 are difficult to press successfully.

Inhomogeneous pressed density leads to inhomogeneous magnetic properties and so degrades the product. It also leads to non-uniform shrinkage during the sintering and this causes shape distortion as shown in exaggerated form in Fig. 1.7(c). In more complicated shapes, non-uniform pressed density may result from some zones being compressed more than others, see Figs. 1.7(d) and (e). The simpler the shape the more successful is the pressing and the better is the control of the electrical and mechanical parameters. On the other hand, as the understanding of the flow properties of the powder improves and pressing technology advances, more complicated shapes may be successfully pressed. However, some shapes will always be

inherently difficult to press and control. Such shapes are those that include:

- (a) zones of widely unequal powder compression
- (b) zones having large aspect ratios (l/d) in the direction of pressing
- (c) abrupt change of cross-section
- (d) features that lead to fragile die punches (see Fig. 1.7(f))

Shapes having cavities extending perpendicular to the line of pressing cannot normally be pressed as they would require split dies. Such dies are rare in ferrite pressing technology.

The pressed parts have the consistency of drawing chalk. They are said to be in the green state. As the parts leave the press a proportion of them are weighed to check the density and they are then stacked on trays to await sintering.

Extrusion

The extrusion process is used mainly for rods and tubes. Such shapes cannot easily be dry-pressed, because if the pressing were axial the length/diameter ratio would be too great whereas if they were pressed transversely the die punches would have feather edges.

The extrusion process is very simple. The de-aerated

charge of plasticized powder is placed in the cylinder of an extrusion machine. A ram then forces the charge through a suitable orifice to form a length of rod or tube. When a convenient length, e.g. about 0.7 m, has emerged, the extrusion is stopped and the length is detached from the machine to be laid on a tray. The tray has a number of parallel grooves in which the still-plastic extrusions may rest and be held straight while they dry. When the extrusions are dry and hard the ends, which have been deformed by handling, are removed and the remainder may be sawn into pieces of the required length (allowing for shrinkage during sintering). Where a large production is required it is possible for the extrusion, cutting and drying to be done automatically and this leads to a more consistent product. Sometimes, particularly for shorter lengths or where greater length accuracy is necessary, the final cutting is done after sintering.

Miscellaneous forming methods

Iso-static pressing. The inhomogeneity arising from the friction and flow of granulated or plasticized powders may be avoided by iso-static pressing. In this method the finely milled powder (particle size $0.1-0.3\mu$) is placed, either loose or after being compacted approximately to the required shape, into a latex envelope itself approximating to the required shape, e.g. a cylindrical compact may be formed and placed into a cylindrical sleeve. The air is evacuated and the sleeve is sealed. It is placed in a hydraulic pressure vessel and the pressure is raised to about 1000 atmospheres. This pressure, acting on all sides of the envelope, compresses the powder evenly and with the minimum interference from friction.

This process may contribute to the preparation of high density ferrites, e.g. having porosities of 0.1% or less but the shapes obtainable from iso-static pressing are relatively simple and this normally leads to cutting and shaping. The cutting and shaping may either be carried out before sintering or, if greater final accuracy is required, after sintering. For items such as ferrite recording heads for industrial or professional equipment, high density is a prerequisite to good wear characteristics, and production cost is less important than good performance. Accordingly the ferrite parts for these heads are often cut from blocks that have been iso-statically pressed and sintered to a high density.

Slurry pressing. This technique is used when it is necessary to induce orientation of the particles during forming. The powder is made into a slurry and when the required amount has been admitted to the die a strong magnetic field is applied so that the orientation is obtained. With the field maintained, the die closes and the fluid is expelled by the pressure through filters at the bottom of the die. This process is mainly used to make

anisotropic barium ferrite permanent magnets and anisotropic high frequency hexa-ferrites such as Ferroxlana.

Hot pressing. This is a relatively new process in which the pressing and sintering occur simultaneously. The die is made of a refractory material heated to the sintering temperature by a surrounding electric furnace and pressure is applied by die punches which do not enter the sintering zone. This process, which is virtually confined to cylindrical shapes, enables dense ferrites to be obtained at relatively low sintering temperatures.

1.3.7. Sintering

In the compacted form the partially reacted particles press against each other over part of their surface, the remaining surface forming the boundaries of the interstitial voids or pores. At temperatures in the region of 1000°C and above, the free surface containing the voids decreases, the particles grow together to form crystallites and the density rises. During this process the linear dimensions of the piece part shrink between 10% and 25% depending on the powder and the pressing technology and this must be allowed for in the design of the forming tool. The grain growth and the elimination or the persistence of pores both have profound effects on the properties of the sintered ferrites.^{28, 29} Typical crystallite sizes range from about 5 to 40μ .

The properties are, of course, also affected by changes occurring within the crystallite structure. These changes are influenced not only by the temperature but also by the atmosphere in which the sintering takes place,³⁰ in particular the partial pressure of the oxygen in the atmosphere.

A mixed ferrite in a quaternary system such as Mn-Zn-Fe-O can exist in a wide variety of compositions within the limitations of the spinel structure. Even when the proportion of the three metals is fixed during powder preparation the valency states and the phase depend on the amount of oxygen in the structure and this will depend on the oxygen equilibrium between the structure and the surrounding atmosphere. If, for instance, the partial pressure of oxygen in the atmosphere is very small, any excess iron in the composition would be present as ferrous ions and would take its place with the other divalent ions, e.g. Mn and Zn. A small proportion of ferrous ions together with manganese ions tends to increase the permeability and reduce the losses, but the co-existence of trivalent and divalent ions of the same element lowers the electrical resistivity. On the other hand excessive oxygen in the atmosphere would prevent the formation of ferrous iron. As well as leading to higher magnetic losses and higher resistivity this would cause the formation of cation vacancies since the ratio of oxygen ions (anions) to metal ions (cations) would be excessive. The presence

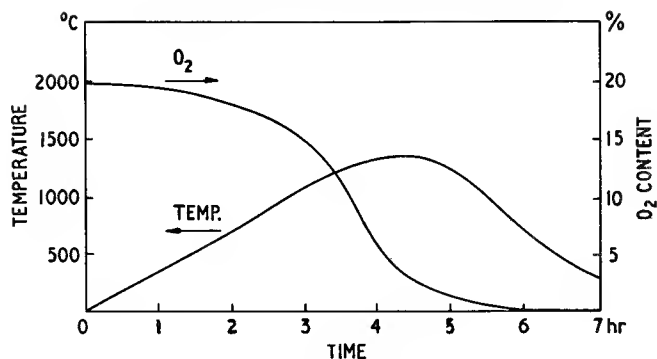


Fig. 1.8. Typical sintering cycle

of vacancies gives rise to after-effects such as change of permeability with time, known as disaccommodation (see Fig. 3.10).

The chemistry and physics of mixed ferrites comprise a large and complex subject and many aspects remain unexplored. The above brief excursion into this field is intended to illustrate that the atmosphere control has a direct bearing on the composition of the sintered ferrite and therefore on its properties. The control is complicated because equilibrium oxygen partial pressure varies with temperature and at any one temperature the optimum with respect to iron may not be the optimum with respect to the other metals, e.g. manganese. In practice a compromise has to be found empirically. Another difficulty is that uniform equilibrium may not be attainable because, as the sintering proceeds and the porosity decreases, the inner regions of the material become less susceptible to the kiln atmosphere and inhomogeneity results.

Fig. 1.8 shows a typical sintering cycle for a production ferrite. During the heating period the oxygen pressure is often made relatively high; this may be done to assist the burn-out of the binder. As the maximum temperature is approached the oxygen pressure is normally reduced as quickly as possible to a low value. However for some ferrites, where the properties are not critical, this reduction of oxygen is not necessary and it is possible to carry out the whole sintering process in air.

There are many types of kiln used in the manufacture of ferrite.³¹ They may be classified according to the method of heating—oil, town gas or electricity, and according to whether the charge remains stationary (static kiln) or is passed through the kiln (continuous kiln).

Oil firing, although the cheapest, presents some disadvantages in process control and is not often used. Kilns fired with town gas are extensively used where a large throughput is required and where sintering in air is permissible, e.g. for pre-sintering of powder and for the final sintering of parts which are not required to have a high magnetic stability. Gas-fired kilns are usually of the continuous type. Such a kiln might be 43 m (140 ft) long and produce nearly 500 kg ($\frac{1}{2}$ ton) of pre-sintered powder

per hour or 250 kg ($\frac{1}{4}$ ton) of sintered parts per hour. The charge is passed slowly through the tunnel of the kiln. It is stacked on silicon carbide plates carried on trucks and is protected from burning gas. The temperature increases with distance along the kiln until the central sintering zone is reached, thereafter the temperature falls until it reaches about 200°C at the exit. The horizontal scale of the firing-cycle, see Fig. 1.8, may be expressed as distance along the kiln instead of time. Control is obtained by a series of thermo-couples connected to potentiometric recorders and to electronic equipment operating gas valves.

Static electric kilns are used mainly for development work, for short production runs and for the sintering of parts requiring special firing cycles. They have two main disadvantages. It is difficult to maintain uniform conditions, particularly temperature, throughout the zone occupied by the charge, and it is difficult to control the process because there is no output to monitor until the process is complete.

The majority of high-quality ferrite is sintered in electrically-heated continuous kilns. Fig. 1.9 shows the side elevation and alternative sections of a pusher-type kiln. The charge is stacked on silicon carbide pusher plates which slide along either a track formed of tiles (a) or along grooves formed in the lower parts of the tunnel walls (b). The plates, which press against each other, are slowly moved through the kiln by a ram which pushes against the plate nearest the entrance. After the ram has completed a stroke equal to the length of the pusher plate it returns and another loaded plate is introduced. Care must be taken to avoid the plates being obstructed and causing a catastrophic hold-up or pile-up inside the kiln.

The kiln is heated by elements consisting of either silicon-carbide rods or wire such as Kanthal. The elements may be placed either in the side walls of the tunnel as in section (a) of Fig. 1.9 or along the roof and floor as in section (b). The temperature may be kept more uniform if the aperture of the kiln is shallow; for this reason the roof and floor offer better accommodation

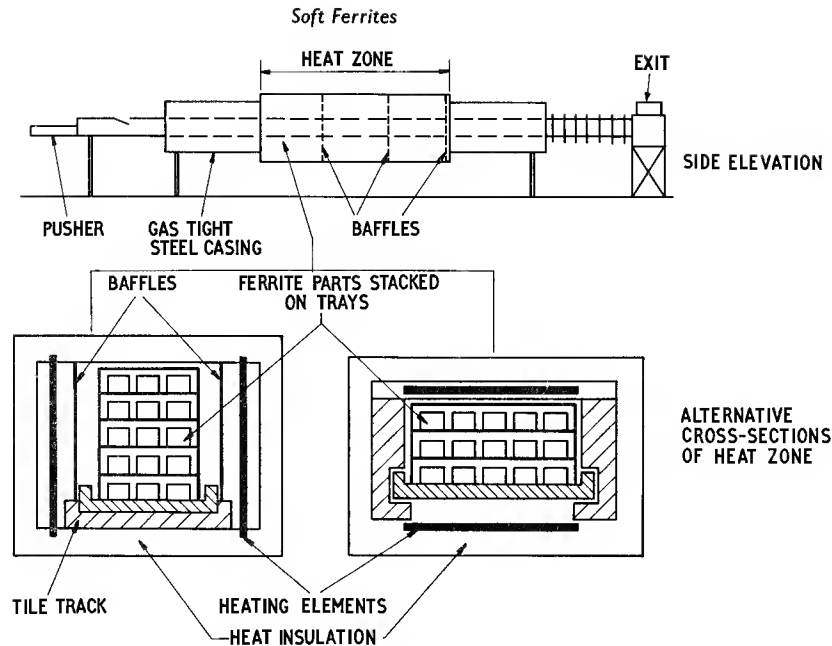


Fig. 1.9. Diagram of a pusher type kiln

for the elements and this system is preferred.

An alternative arrangement is to use trucks instead of plates. The trucks butt together so that they virtually form a floor to the kiln, their sides dipping into sand troughs to provide a seal. Trucks allow larger loads and greater immunity from obstruction but since the loads tend to be tall and narrow and the elements must be located in the tunnel walls there is an appreciable temperature gradient between the bottom and the top of the charge.

The temperature control in the various zones of an electrically-heated continuous kiln is obtained by means of thermo-couples placed in the walls and almost touching the charge. The thermo-couples, which must be screened against leakage currents from the elements, operate potentiometric recorders and means of controlling the element currents.

Atmosphere control is normally required to produce a pre-determined transition from air or oxygen in the rising temperature zones to a low oxygen partial pressure at or about the zone of maximum temperature. This may be obtained by feeding air in at the entrance of the kiln and nitrogen in at the exit. Inlets for air or nitrogen are also provided at intermediate points. The flow of gas past the charge is impeded by baffles. The nitrogen and air pass along the kiln towards the centre until they reach a point determined by relative air/nitrogen pressures where they rise and pass above the charge to be exhausted at a point above the entrance. An air-lock is necessary at the exit end to prevent air leaking into the cooling zone.

Instruments are used to measure and record the oxygen content at a number of points in the kiln and by means of these instruments the oxygen content is automatically controlled.

1.3.8. Finishing

When the sintered part leaves the kiln it is 10–25% smaller in linear dimensions than its pressed size. If the pressed density and the firing cycle have been correctly controlled it is normally possible to hold the dimensions of the sintered part to better than $\pm 2\%$ for pressed parts and $\pm 3\%$ for extruded parts. As explained in the section on pressing, non-uniform pressed density can lead to distortion during sintering, and where the geometric form of the part (e.g. straightness, roundness) is important it may be necessary to specify geometric tolerances or form gauges.

If the specified tolerances of dimensions or form are smaller than those which may easily be achieved by sintering alone then some form of finishing process will be required. Such a process usually consists of grinding or cutting. As the sintered product is hard and abrasive, the grinding and cutting will significantly increase the production cost. For this reason it is usual to avoid, where possible, tolerances smaller than those obtained by sintering.

The most usual, and often unavoidable, finishing process is the grinding of surfaces which are required to

give low-reluctance butt-joints in the assembled magnetic circuit. Fig. 1.10 shows typical mating parts. The surfaces $A-A$ must be made flat and smooth so that the residual gap obtained on assembly is as small and as stable as possible. Surface grinding may also be required to control a dimension, such as h , to close tolerances.

As far as mating surfaces are concerned the degree of flatness and smoothness obtainable depends to a large extent on the acceptable cost of the operation. In principle a reasonable surface may be obtained by the use of a normal surface grinder and this is often used when only a few parts are involved. In mass production it is usual to use a plough grinder. In this the work, perhaps a hundred pieces or more, is attached magnetically to a large circular surface plate. This rotates slowly in a horizontal plane.

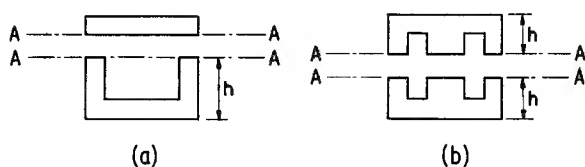


Fig. 1.10. Typical mating parts

Above this plate and laterally removed from it is another circular plate carrying an abrasive annulus. This plate is rotated rapidly and the vertical clearance between the lower plate and the abrasive segments is adjusted to equal the required height of the ground piece part. The work is flooded with coolant, usually water, and the lower plate is moved laterally under the upper plate until all the parts have been ground to size by the abrasive wheel. It is usually necessary to grind the back face of the work first so that a stable base is formed. Such a process will give a total residual air gap (two butt-joints) equivalent to about 5μ . If a substantially smaller gap is required then lapping techniques must be used. As these are not easily adapted to mass production the cost of this improvement can be high.

Another widely used finishing process is the cutting to length of extruded rods or tubes. This is done with a diamond-impregnated metal-bonded wheel. Where it is necessary to remove sharp edges, e.g. the edges of a ring on which a conductor is to be wound, this may be successfully done by tumbling (rumbling).

Finally there is the cracking process commonly used in the manufacture of television deflection yokes. These yokes are normally pressed in the shape of a bottomless flower pot. Before being fitted over the neck of a picture tube the deflection coils will have to be fitted and this necessitates dividing the yoke into mating halves. This is done during manufacture; the yoke is cracked along a diametral plane by the heat of two fish tail gas burners applied along the required dividing lines. Sometimes the

required dividing lines are defined by notches or grooves formed during pressing. Due to the somewhat random nature of the cracks, the cracked parts must remain paired so that when incorporated in the deflection assembly they may be restored to an almost perfect magnetic circuit.

1.3.9. Inspection

The mechanical dimensions are checked by conventional techniques. The magnetic properties pose greater problems. For a typical ferrite core it is necessary to control about seven magnetic parameters and some of these present appreciable measuring difficulty, e.g. the measurement of very low magnetic losses, temperature coefficients of permeability, etc. Some measurements cannot easily be done on the production line and usually require the specialized resources of a quality control laboratory. Although such facilities, used on a sampling basis, give adequate inspection of the manufactured product, the inevitable time delay makes the effective feed-back of process control information rather difficult. This latter aspect of inspection is probably the more important because it can ensure that the process will be maintained in a high-yield condition. In practice adequate inspection and control is attained by a combination of on-line and laboratory testing backed up by the accumulated inspection records from which control relations may be derived.

1.4. FINISHING PROCESSES AVAILABLE TO THE USER

Usually a ferrite part leaves the factory in its final form and the user has only to combine it with the required winding and hardware to complete the wound assembly. There are, however, instances where the user must carry out some finishing process on the ferrite itself: (a) in the development of a prototype design it may be necessary to carry out machining operations, (b) in the production of inductors or transformers the design often requires core halves to be cemented together and (c) the encapsulation of the complete wound assembly is sometimes necessary to provide adequate environmental protection of the winding. In many cases users have developed their own techniques; in this section some brief notes on these topics will be given for the guidance of those encountering these problems for the first time.

1.4.1. Machining

Normal ceramics machining techniques and standard machine shop equipment may be used for most shaping

operations on ferrites; see Section 3.3 for data on hardness, etc.

For surface (and cylindrical) grinding, 'green' silicon carbide wheels may be used. Roughing operations require a fairly hard grade of wheel with a coarse texture while for finishing a softer wheel with finer grains may be used. A peripheral speed of 1500 to 1800 m.min⁻¹ (5000 to 6000 ft.min⁻¹) is suitable. The cut should be limited to about 0.025 mm (0.001 in) and the traverse should be rapid so that local heating is restricted. The work should be flooded with coolant; water or a dilute soluble oil solution is suitable. The wheel must be dressed true so that 'hammering' of the work due to eccentricity is avoided. The dressing must be repeated at frequent intervals because ferrite rapidly dulls the wheel.

Diamond machining is a much better technique. Diamond-impregnated metal-bonded cutters may be used for surface grinding, drilling, reaming and sawing. Because the cutting is much more efficient, less heat is generated and larger cuts and slower traverse may be used. For surface grinding, wheels having diamond particles of 150 to 180 μ (100 to 80 mesh approx.) are normally used and the peripheral speeds should be similar to those quoted for silicon carbide wheels. Cuts of 0.6 mm (0.025 in) may be taken. For sawing, the size of the diamond particles may vary from 150 to 90 μ (100 to 170 mesh approx.) depending on the thickness of the wheel. As before, peripheral speeds of 1500 to 1800 m.min⁻¹ (5000 to 6000 ft.min⁻¹) are recommended. The cut may be as large as the available radius of the wheel; a 25 mm (1 in) cut is quite common. Again an ample quantity of coolant is essential; water or dilute soluble oil solution may be used.

A valuable technique, which cannot be classed as normal machine shop routine, is ultrasonic drilling. A tool, having a cross-section identical to that of a required hole, is attached vertically to the end of an electro-mechanical transducer which is resonated longitudinally at ultrasonic frequency, e.g. 20 kHz. The end of the tool is brought into contact with the ferrite and it delivers a rapid succession of minute blows. An abrasive slurry, such as 45 μ (325 mesh approx.) boron carbide in water, submerges the end of the tool and the result is that a downward pressure on the tool causes it to cut its way through the ferrite. In this way holes or patterns of holes of any cross-section may be drilled. Large holes may be trepanned by using hollow tools thus reducing the amount of ferrite cutting to a minimum. The tool is usually made of mild steel or brass and an ultrasonic power of 300 W is suitable for most purposes.

1.4.2. Cementing

Ferrite-ferrite bonds may be made with thermo-setting

resin adhesives, in particular the epoxy resins, but if the bond is to be strong and permanent a number of precautions must be observed. The main cause of the deterioration of bond strength between ferrite parts appears to be the ingress of water vapour between the ferrite and the resin. Some resins are more resistant to this deterioration than others and the porosity of the ferrite is probably also a factor. The test of a good bond is its strength after it has been subjected to a number of damp heat cycles. Often a wound component, e.g. an inductor, must be protected from dampness in order to prevent corrosion or degradation of the winding during its service life. If such protection includes the ferrite core, the deterioration of joint strength due to dampness ceases to be a problem. Before subjection to dampness, a good bond has a tensile strength that is greater than that of the ferrite. Not all the factors contributing to a good bond are understood, but experience has shown that the following points are significant.

Choice of adhesive

The available range is very large. The most important factors influencing the choice are the required curing temperature and the viscosity. The economic curing temperature must not be above the maximum temperature to which the assembly may be safely raised. If the assembly consists only of ferrite and other inorganic parts it will not usually impose a limit to the curing temperature. To bond the parts of such an assembly a hot setting resin may be used. Such resins cure quickly at about 180°C to give very strong bonds. They are available in solid, powder or liquid form. As solids or powders they present some difficulties in application on a production scale. The liquid form usually consists of two components, the resin and the hardener, and these are mixed together by the user. Usually one or both components contain a solvent and in that case the manufacturer generally recommends that as much of the solvent as possible be driven off by warming the mixture in free air conditions. This may be done after the adhesive has been applied but before the mating surfaces have been brought together, or alternatively the process may be carried out on the adhesive in bulk before application. While this appears to be essential for a good ferrite-metal bond experience has shown that solvent removal is not necessary for ferrite-ferrite bonds.

If the assembly includes temperature limiting materials such as thermoplastic or other organic insulating parts then resins with lower curing temperatures, e.g. 100 to 120°C, will have to be used. Cold or warm setting resins are also available but they are usually inferior to the hot setting resins in bond durability and stability. Flexible adhesives have advantages under some circumstances,

but they tend to creep under load and may have poor stability even when unstressed. If the bond is required to withstand adverse environmental conditions, particularly damp heat, the strength of sample joints should be determined experimentally after exposure to such conditions.

The other important factor is the viscosity. If it is too high application is difficult; if it is too low the resin may run out of a poorly-fitting joint or, in a well-fitting joint, it may be absorbed by the porosity of the ferrite. It is sometimes an advantage to incorporate a filler such as finely powdered chalk or silica. This will reduce the temperature coefficient of linear expansion, reduce the shrinkage occurring during curing and increase the viscosity. On the other hand it makes the exclusion of air or water vapour from the mixture more difficult and it is usually advisable to remove the water vapour from the filler before mixing.

The selected adhesive should be easy to prepare, it should have an adequate pot life and a simple and reasonably short curing cycle. Needless to say, the manufacturer's instructions for a particular resin must be meticulously followed. The constituents must not have exceeded the permitted shelf life and must not have been exposed to excessive atmospheric moisture before or after mixing. Quite often bond weakness may be traced to insufficient care in the preparation of the resin mixture.

Preparation of surfaces

The surfaces to be bonded must be perfectly dry and free from contamination. It is advisable to clean the surfaces before bonding. Degreasing in solvents is widely employed but it has been found that ultrasonic washing in hot water containing a small amount of detergent is the most effective process. After cleaning, the surfaces should not be touched by hand.

Application

For maximum bond strength, the resin manufacturers usually specify the thickness of the adhesive in the joint; figures between 0.025 and 0.25 mm (0.001 and 0.01 in) are often given. However, in a ferrite-ferrite bond it is usually necessary to make the joint as thin as possible in order to minimize the reluctance of the residual gap in the magnetic circuit. In practice adequate joint strengths are possible between flat ferrite surfaces from which all the surplus resin has been expelled by the application of pressure or by rubbing the surfaces together. It is obviously preferable to use resins that have an optimum joint thickness that is near the lower end of the above-quoted range. Joints prepared in this way have effective

gaps in the magnetic circuit that are not significantly larger than those obtained when the joints are dry.

Curing

After application of the adhesive, the mating surfaces should be clamped lightly together to provide contact pressure, e.g. a pressure of 0.02 kg.mm^{-2} (27 lb.in^{-2}) has been found satisfactory. The manufacturer's curing instructions should then be followed. If a warm or cold setting resin has been used it is usually preferable to cure at a suitable elevated temperature (e.g. $60\text{--}80^\circ\text{C}$) as this will result in improved strength. However if the viscosity becomes very low at the curing temperature so that there is a risk of excessive absorption by the ferrite, it is recommended that partial curing be allowed at room temperature and that this is followed by a suitable heat cycle to complete the cure.

Bonds between ferrite and other materials are more difficult insofar as there is a difference in the temperature coefficients of linear expansion. This coefficient, α , for ferrites is about $10 \times 10^{-6} \text{ }^\circ\text{C}^{-1}$. Thus steel ($\alpha = 12 \times 10^{-6} \text{ }^\circ\text{C}^{-1}$) may be successfully bonded (although steel, having large magnetic losses, is not recommended for intimate connection to a ferrite core), while brass ($\alpha = 19 \times 10^{-6} \text{ }^\circ\text{C}^{-1}$) presents the difficulty of accommodating the differential expansion or contraction. In practice the interfaces are locked together as the resin cures at a temperature which is usually well above room temperature. On subsequent cooling a stress is created. The attachment is then prone to failure due to the resin or the ferrite fracturing under the stress. The best remedy is to alleviate the stress by reducing the shear strain in the adhesive. This may be done either by using a flexible resin or by making the adhesive layer as thick as possible, e.g. by including an open glass cloth scrim wetted with adhesive. As stated earlier, if the resin mixture contains solvent it is usually advisable to remove as much of it as possible by warming the mixture in free air conditions. This may be done after application but before the mating surfaces have been brought together or it may be done before the adhesive has been applied.

Apart from the additional aspects, the procedures described for the ferrite-to-ferrite bonds apply equally well to these dissimilar bonds.

1.4.3. Encapsulation

Encapsulation is a technique of protection whereby an electrical component or assembly is embedded in a casting of insulating material, e.g. synthetic resin. The component or assembly is suitably mounted in a mould and the encapsulant is poured in until it is covered.

Usually all air and water vapour is removed by evacuation, thus ensuring that the finished casting is without voids. The encapsulant is then allowed to set or cure into a solid or elastic mass. The main protection is against mechanical shock and vibration, and against hostile atmospheric constituents such as water vapour, sulphur dioxide and salt. Ferrites, being inert to atmospheric conditions, do not normally require such protection, but in most wound assemblies it is difficult to provide the essential protection of the winding without including the core.

There are many encapsulants available, the main ones being epoxy resins and silicone compounds. To perform its task successfully an encapsulant should be tough, impervious to the atmosphere (particularly to water vapour) and capable of adhering to any parts of the assembly, e.g. terminal connections, which break the surface of the casting. The latter point is of importance because lack of adhesion could provide capillary paths by which water vapour may reach the inside of the assembly.

The encapsulation of a wound ferrite assembly presents special difficulties. It has been observed that except for mechanical protection the ferrite core does not need to be encapsulated. In practice the core must usually be included and it is the resultant stresses that give rise to the difficulties. The main factors are:

- (a) Most resins shrink during the curing process and exert a compressive stress on the core. If the curing has been done at an elevated temperature the differential temperature coefficient will increase the compressive stress. It is shown in Chapter 3 that mechanical stress can appreciably change the initial permeability of a ferrite, so the process of encapsulation may cause a change of inductance. This difficulty may be overcome by using a non-rigid resin, e.g. a silicone elastomer or an epoxy resin which has been made flexible by the addition of liquid polyamide resin or polysulphide rubber. Such non-rigid resins must be selected with great care because they may lack toughness, or the ability to adhere to the terminal connections or they may not be a sufficient barrier to water vapour.

Another possibility is to load the resin with a filler in an attempt to equate the temperature coefficients of the encapsulant and the ferrite. However, because filled resin sets hard and exact temperature coefficient compensation is unlikely, appreciable residual stress must be expected.

- (b) If the resin completely fills the winding space, and has been cured at room temperature, a rise of temperature will cause a bursting stress on the core as the differential temperature coefficient reverses any stress due to curing shrinkage. This effect can

easily break any ferrite core which, like a pot core, encloses the winding, even if the encapsulant is quite flexible. For this reason it is undesirable to allow the encapsulant to fill spaces enclosed by ferrite.

A particular case in this category is the effect of a hard resin in the air gap of a pot core. Differential expansion will cause the gap to increase with temperature and this will tend to make the temperature coefficient of inductance negative. Even if fracture does not occur the resultant temperature coefficient of inductance will be unpredictable. The stresses due to volumetric expansion of the encapsulant in ferrite cavities may be made negligible by the use of foam encapsulants since the gas in the foam is easily compressible. The foam encapsulant must of course be satisfactory in all other respects.

- (c) If the resin sets hard and adheres to the surface of the ferrite, the differential temperature coefficient will cause shear stresses in the surface of the ferrite, an action similar to that of a bimetal strip. Such stresses could cause fracture, so it is good practice to prevent adhesion to the ferrite.
- (d) Most resins have fairly high permittivity and dielectric loss angle. Such resins, if allowed to enter the winding or the winding space, could increase the losses of most medium or high frequency inductors. This may be another reason for preventing the resin from entering the winding space.

Summing up:

The encapsulant should be:

- sufficiently tough,
- a sufficient barrier to adverse environmental conditions,
- sufficiently flexible to prevent compressive stresses in the ferrite,
- capable of good adhesion to parts of the assembly which break the surface, e.g. terminal connections.

The encapsulation technique should:

- avoid solid filling ferrite-enclosed spaces, e.g. winding spaces and air gaps,
- avoid adhesion to the ferrite if a hard encapsulant is used.

It is not easy to select an encapsulant and develop a technique which fulfils these requirements. For this reason encapsulation is not widely employed in the production of high performance inductors and transformers using ferrite cores.

REFERENCES AND BIBLIOGRAPHY

Section 1.1.

1. HILPERT, S., 'Genetische und konstitutive Zusammenhänge in den magnetischen Eigenschaften bei Ferriten und Eisenoxiden', *Ber. dtsh. chem. Ges.*, **42**, 2248, (1909).
2. FORESTIER, H., 'Transformations magnétiques du sesquioxide de fer, de ses solutions solides, et des ses combinaisons ferromagnétiques', *Ann. Chim., Xe Serie*, **IX**, 316, (1928).
3. KATO, V. and TAKEI, T., 'Permanent oxide magnet and its characteristics', *J. Instn elect. Engrs Japan*, **53**, 408, (1933).
4. KAWAI, N., 'Formation of a solid solution between some ferrites', *J. Soc. chem. Ind. Japan*, **37**, 392, (1934).
5. SNOEK, J. L., 'Magnetic and electrical properties of the binary systems $\text{MO.Fe}_2\text{O}_3$ ', *Physica, Amsterdam*, **3**, 463, (1936).
6. SNOEK, J. L., *New developments in ferromagnetic materials*, Elsevier Publishing Company, Inc., New York-Amsterdam, (1947).
7. POLDER, D., 'Ferrite materials', *Proc. Instn elect. Engrs*, **97**, Part II, 246, (1950).
8. OWENS, C. D., 'A survey of the properties and applications of ferrites below microwave frequencies', *Proc. Inst. Radio Engrs*, **44**, 1234, (1956).
9. SNELLING, E. C., 'Properties of ferrites in relation to their applications', *Proc. Br. Ceram. Soc.*, **2**, 151, (1964).
10. WENT, J. J., RATHENAU, G. W., GORTER, E. W. and VAN OOSTERHOUT, G. W., 'Ferroxdure, a new class of permanent magnet materials', *Philips tech. Rev.*, **13**, 194, (1951-52).
11. STUITS, A. L., RATHENAU, G. W. and WEBER, G. H., 'Ferroxdure II and III, anisotropic permanent magnet materials', *Philips tech. Rev.*, **16**, 141, (1954-55).
12. JONKER, G. H., WUN, H. P. J. and BRAUN, P. B., 'Ferroxplana, hexagonal ferromagnetic iron-oxide compounds for very high frequencies', *Philips tech. Rev.*, **18**, 145, (1956-57).
13. NECKENBÜRGER, E., SEVERIN, H., VOGEL, J. K. and WINKLER, G., 'Ferrite hexagonaler Kristallstruktur mit hoher Grenzfrequenz', *Z. angew. Phys.*, **18**, 65, (1964).
14. ALBERS-SCHONBERG, E., 'Ferrites for microwave circuits and digital computers', *J. appl. Phys.*, **25**, 152, (1954).
15. PELOSCHKE, H. P., 'Square loop ferrites and their applications', *Progress in Dielectrics*, **5**, Editors—J. B. Birks and J. Hart, Heywood & Co. Ltd., London, (1963).
16. LAX, B. and BUTTON, K. J., *Microwave ferrites and ferrimagnetics*, McGraw-Hill Book Co., (1962).
17. BOZORTH, R. M., *Ferromagnetism*, Van Nostrand Company, Inc., (1951).
18. SMIT, J. and WUN, H. P. J., *Ferrites*, Philips Technical Library, Eindhoven, (1959).
19. CHIKAZUMI, S., *Physics of magnetism*, John Wiley & Son, Inc. New York, (1964).
20. BATES, L. F., *Modern magnetism*, Cambridge University Press, 4th Edition, (1963).

Section 1.3.1.

21. BEER, H. B. and PLANER, G. V., 'Preparing ferrites by continuous electrolytic co-precipitation', *Br. Commun. Electron.*, **5**, 939, (1958).
- FRESH, D. L., 'Methods of preparation and crystal chemistry

of ferrites', *Proc. Inst. Radio Engrs*, **44**, 1303, (1956).

- GUILLAUD, C., 'The properties of manganese-zinc ferrites and the physical processes governing them', *Proc. Instn elect. Engrs*, **104**, Part 8, 165, (1957).
- BROWN, C. S., 'The effect of ceramic technology on the properties of ferrites', *Proc. Br. Ceram. Soc.*, **2**, 55, (1964).
- CLEVENGER, T. R., 'Advances in ferrite technology', *Bull. Am. Ceram. Soc.*, **44**, 216, (1965).
- KLAMER, K., 'Technologie van elektrokeramiek', *Klei en Keramiek*, **15**, 30, (1965).

Section 1.3.2.

22. ERZBERGER, P., 'Correlation of partial size with other physical properties of iron oxides for ferrite synthesis', *Proc. Brit. Ceram. Soc.*, **2**, 19, (1964).
23. GORTER, E. W., 'Some properties of ferrites in connection with their chemistry', *Proc. Inst. Radio Engrs*, **43**, 1945, (1955).
24. STUITS, A. L., 'Sintering of ceramic permanent magnetic material', *Trans. Br. Ceram. Soc.*, **55**, 57, (1956).
25. VAN DER BURGT, C. M., 'Controlled crystal anisotropy and controlled temperature dependence of the permeability and elasticity of various cobalt-substituted ferrites', *Philips Res. Rep.*, **12**, 97, (1957).

Section 1.3.4.

26. SWALLOW, D. and JORDAN, A. K., 'The fabrication of ferrites', *Proc. Br. Ceram. Soc.*, **2**, 1, (1964).
27. MIDDEL, V. J. and MACDONALD, G. L., private communication. See also ref. 26 above.

Section 1.3.7.

28. GUILLAUD, C. and PAULUS, M., 'Permeabilité initiale et grosser des grains dans les ferrites de manganèse-zinc', *C.R. Acad. Sci. Paris*, **242**, 2525, (1956).
29. STUITS, A. L., 'Microstructural considerations in ferromagnetic ceramics', *Proc. 3rd Int. Mater. Symp. on Ceramic Microstructures*, Univ. Calif., Berkeley, (June, 1966).
30. HECK, C. and WEBER, J., 'How firing atmospheres influence ferrite properties', *Ceramic Ind.*, **77**, Part 1, no. 5, 75, Part 2, no. 6, 66, (1961).
31. JACKSON, H., 'Kilns for the manufacture of ferrites', *Proc. Br. Ceram. Soc.*, **2**, 43, (1964).

Section 1.4.2.

- SKEIST, I., *Handbook of adhesives*, Reingold Publishing Corp., New York, (Chapman and Hall, Ltd., London), (1962).
- HOUWINK, R. and SALOMON, G., *Adhesion and adhesives*, Elsevier Publishing Co., Vol. 1, 2nd edition, (1965), Vol. 2, 2nd edition, (1967).

Section 1.4.3.

- LUNDBERG, C. V., 'A guide to potting and encapsulation materials', *Mater. Des. Engng*, **51**, no. 5, 123, (1960).
- DAVIS, J. H., REES, D. W. and RILEY, I. H., 'Silicone encapsulating and potting materials', *Proc. Instn elect. Engrs*, **109**, Part B, 266, (1962).
- VOLK, M. C., LEFFORGE, J. W. and STETSON, R., *Electrical encapsulation*, Reingold Publishing Corp., (1962).
- LICARI, J. J. and BROWNING, G. V., 'Plastics for packaging: handle with care', *Electronics*, **40**, no. 8, 101, (1967).

The Expression of Electrical and Magnetic Properties

2.1. MAGNETIZATION

The magnetic field strength, H , inside a very long uniform solenoid having N_1 turns per axial length l and carrying I amperes is given by

$$H = \frac{N_1 I}{l} \quad \text{A.m}^{-1} \quad (2.1)^*$$

Its direction is parallel to the axis of the solenoid and it is uniform across the internal cross section.

The associated flux density, B , is given by

$$B = \mu_0 H \quad \text{tesla}^\dagger (\text{T}), \text{ i.e. } \text{Wb.m}^{-2} \quad (2.2)$$

where μ_0 is the magnetic constant or the permeability of free space. It has the numerical value $4\pi \times 10^{-7}$ and has the dimensions henries/metre or $[\text{LMT}^{-2}\text{I}^{-2}]$. Thus in

*Many of the quantities used in this section are vector quantities and therefore the equations involving them are vector equations. However, in the present limited treatment, the relative directions of the vectors are implied in the text so no special symbols will be used to denote vector quantities or vector operations. For a more general treatment the reader is referred to textbooks on electromagnetic theory.

†The unit of flux density in the SI units has been named the 'tesla' and has the symbol T, (see IEC Publication No. 27). It has the units Wb.m^{-2} so there is no change in its value:

$$\begin{aligned} 1 \text{ T} &= 1 \text{ Wb.m}^{-2} = 10^4 \text{ Gs} \\ 1 \text{ mT} &= 10 \text{ Gs} \end{aligned}$$

the SI units, flux density is dimensionally different from field strength.

If the solenoid is now filled with a magnetic material, the applied magnetic field will act upon the magnetic moments of the ions composing the material. This process has been described qualitatively in Section 1.2.2. The ions, by virtue of the spinning electrons, behave as microscopic current loops each having a magnetic moment. These moments may, in general, be considered to be aligned parallel to each other over small regions, or domains, within the material. In the demagnetized state the domains are distributed so that the vector sum of the magnetization of the domains is zero. Under the influence of an applied field the ion moments are re-orientated, either by the growth and contraction of the various domains or by the rotation of the magnetization within them, so that the ionic moments effectively augment the

$$(2.1) \quad H = \frac{4\pi N_1 I}{10l} \quad \text{Oe} \\ (1 \text{ Oe} \approx 80 \text{ A.m}^{-1})$$

$$(2.2) \quad B = H \quad \text{Gs}$$

In the CGS system of units H and B have the same dimensions and therefore the oersted and the gauss are strictly the same units.

applied field. This increase in magnetic field is called the magnetization, M , and it is expressed in A.m^{-1} . It is the vector sum of the magnetic area moments* of all the microscopic currents in a given volume of material, divided by that volume. The internal magnetic field, H_i , becomes

$$H_i = \frac{N_1 I}{l} + M \quad \text{A.m}^{-1} \quad (2.3)$$

and the flux density becomes:

$$B = \mu_0 H_i = \mu_0 (H + M) \quad \text{T, (Wb.m}^{-2}) \quad (2.4)$$

$$\text{or } B = \mu_0 H + J \quad \text{T, (Wb.m}^{-2}) \quad (2.5)$$

where J is the magnetic polarization in teslas; it is sometimes referred to as intrinsic flux density

$$J = \mu_0 M \quad \text{T} \quad (2.6)$$

Thus M is the increase in the field strength due to the magnetic material and J is the corresponding increase in flux density. The ratio of the magnetization and the applied field strength is called the susceptibility, κ ; it is dimensionless.

From Eqn 2.4

$$\frac{B}{H} = \mu_0 \left(1 + \frac{M}{H} \right) = \mu_0 (1 + \kappa) \quad (2.7)$$

This quotient of flux density and applied field strength is called the absolute permeability and is sometimes denoted by μ . However it is more usual to show it as the product of the magnetic constant and a dimensionless constant called the relative permeability, μ_r . In the chapters that follow, the relative permeability is such a widely used parameter and is given such a variety of qualifying subscripts that it is convenient to drop the adjective 'relative'. Thus permeability will refer to the dimensionless ratio and in equations it will normally be associated with the magnetic constant, μ_0 . The absolute permeability, as such, will not be used.

*Magnetic area moment, m , is the product of a current and the area of the loop in which it flows, the direction is normal to the plane of the loop and when viewed in this direction the current has clockwise rotation.

$$\frac{B}{H} = \mu_0 \mu \quad (2.8)$$

from which it follows that

$$\kappa = \mu - 1 \quad (2.9)$$

The applied field strength may be determined by measuring the current and using Eqn 2.1. The measurement of flux density depends on the law of induction, i.e.

$$e = -d\phi/dt \quad \text{V} \quad (2.10)$$

where ϕ is the magnetic flux i.e. the area integral of the flux density; it is expressed in Wb.

In the ideal solenoid $\phi = BA$ where A is the cross-sectional area of the magnetic material. If N_2 turns are wound tightly round the magnetic material the e.m.f. induced will be

$$e = -N_2 A dB/dt \quad \text{V} \quad (2.11)$$

By integration, the average e.m.f. during a change of flux density, ΔB , is:

$$\bar{E} = -N_2 A \Delta B \quad \text{V} \quad (2.12)$$

The negative sign indicates that the e.m.f. is in such a direction that it would produce current opposing the change of flux. If the flux density is sinusoidal, e.g. if $B = \hat{B} \sin \omega t$, then from Eqn 2.11, dropping the sign:

$$e = N_2 A \hat{B} \omega \cos \omega t = \hat{E} \cos \omega t \\ \therefore \bar{E} = \omega \hat{B} A N_2 \quad \text{V}$$

$$\text{or } E = \frac{\omega \hat{B} A N_2}{\sqrt{2}} \quad \text{V} \quad (2.13)$$

If the current in the ideal solenoid is increased from zero, the field strength increases and the magnetization will increase non-linearly by the processes illustrated in Fig. 1.4. It is more usual to consider the dependence of the flux density on field strength. Such a B - H curve is shown in Fig. 2.1. Starting with the magnetic material in an unmagnetized or neutralized state the B - H curve will follow the path *oba*. If, on reaching the point *a*, the field strength is decreased, the B - H curve will follow the

$$(2.3) \quad H_i = \frac{4\pi N_1 I}{10l} + 4\pi M \quad \text{Oe}$$

$$(2.4) \quad \left. \begin{aligned} B &= H_i = H + 4\pi M \quad \text{Gs} \end{aligned} \right\}$$

$$(2.7) \quad \frac{B}{H} = 1 + 4\pi \frac{M}{H} = 1 + 4\pi \kappa$$

$$(2.8) \quad \frac{B}{H} = \mu$$

$$(2.9) \quad 4\pi \kappa = \mu - 1$$

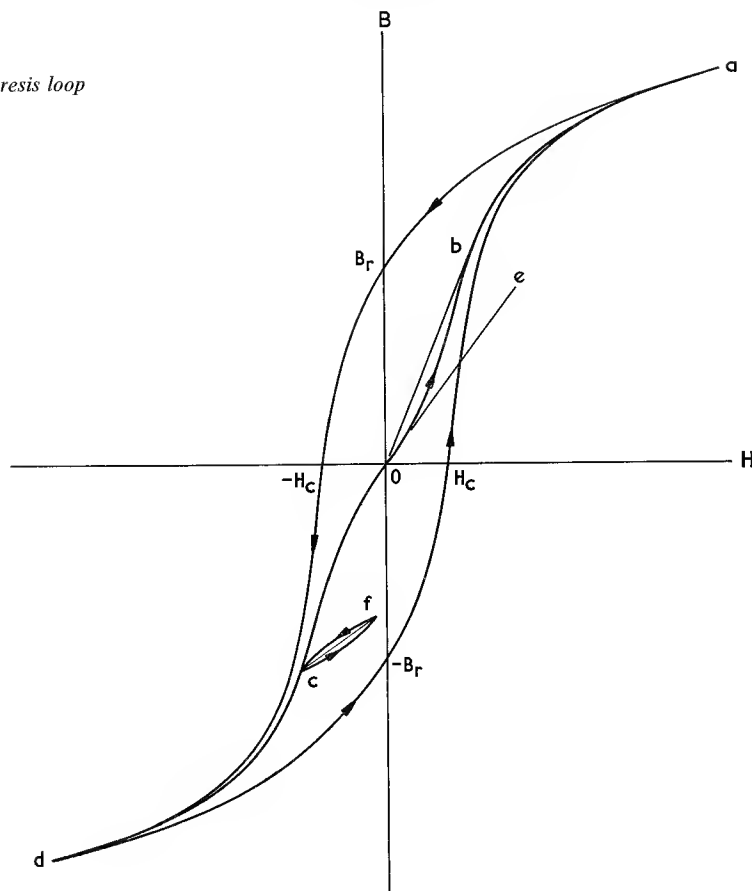
$$(2.10) \quad e = -\frac{d\phi}{dt} \times 10^{-8} \quad \text{V}$$

$$(2.11) \quad e = -N_2 A \frac{dB}{dt} \times 10^{-8} \quad \text{V}$$

$$(2.12) \quad \bar{E} = -N_2 A \Delta B \times 10^{-8} \quad \text{V}$$

$$(2.13) \quad E = \frac{\omega \hat{B} A N_2}{\sqrt{2}} \times 10^{-8} \quad \text{V}$$

Fig. 2.1. Hysteresis loop



upper limb of the open loop. As explained in Chapter 1, a reason for this lag in the change of flux density is the irreversible movement of the domain walls. If, on reaching point *d*, symmetrical with *a*, the field strength is increased again towards its former positive maximum value, the lower limb of the loop will be traced. The loop is called a hysteresis or *B-H* loop. Although, on the first cycle, the loop may not close exactly, a number of cycles will result in a closed loop. If the excursions of *H* are symmetrical about the origin the material is then said to be in a symmetrical cyclic magnetic state.

If the field strength is large enough to take the material substantially into saturation, i.e. to a point where the magnetization *M* cannot be significantly increased, then the intercept of the hysteresis loop with the *B*-axis, *B_r* (or $-B_r$), is referred to as the remanence of the material and the intercept with the *H*-axis, *H_c* (or $-H_c$), is referred to as the coercivity. The tips of loops for smaller excursions of *H* lie very close to the initial magnetization curve *oba*.

Since *B* is a two-valued function of *H*, the instantaneous ratio *B/H* depends on the magnetic history. However in alternating magnetization it is usually relevant only to

consider the peak amplitudes of *B* and *H*, i.e. the tips of the loops. If the material is in a symmetrical cyclic state and *H* is vanishingly small, the permeability is designated μ_i , the initial permeability. It is $1/\mu_0$ times the slope of the line *oe*. If *H* is not vanishingly small, then the permeability is referred to as the amplitude permeability designated μ_a . It is $1/\mu_0$ times the slope of the line connecting the origin to the tip of the loop produced by that particular value of *H*. As *H* increases, μ_a increases, until the tip of the loop reaches *b* and the slope of the line *ob* is the maximum value of $\mu_0\mu_a$.

A non-symmetrical or minor loop is traced if, on reaching a point such as *e*, the field variation is reversed and the material is cycled between *c* and *f*. The slope of *cf* divided by μ_0 is called the incremental permeability, μ_A , and if the amplitude of the excursion is made vanishingly small it becomes the reversible permeability, μ_r . Finally, the slope at any point on a hysteresis loop or curve is referred to as the differential permeability.

In principle *B*, *H* and μ have meaning and may be observed without the need for windings, e.g. in a waveguide or a cavity. However, in the present context, it is by means of windings on magnetic cores that magnetic

properties may be observed and put to useful purposes. The ideal solenoid is not a practical arrangement but it may be simulated by a uniformly wound toroidal core. An ideal toroidal core is radially thin so that it approaches an elementary ring and consequently has a uniform distribution of field strength and flux density across its cross-section. Such an ideal toroid is assumed in the remainder of this chapter. It is further assumed that the windings fit closely to the core, the flux is contained entirely in the core and that the effects of stray inductance, capacitance or resistance due to the winding are negligible so that the impedance measured across a winding is due entirely to the properties of the core material.

The methods of expressing core properties will be related to such a core. In a practical device the core departs from the ideal, having, in general, a relatively large non-uniform cross-section and perhaps an air gap in the magnetic circuit. The modifications to the theoretical relations required to cover such a core are considered in Chapter 4.

2.2 THE EXPRESSION OF THE LOW-AMPLITUDE PROPERTIES

In the majority of applications of magnetic materials in inductors and transformers, the field strength or flux density is varying in a more-or-less complex way. For the purpose of expressing material properties and design relations it is convenient to consider only sinusoidal wave forms. Ferrite cores are often used at quite low amplitudes. At these low amplitudes the non-linearity between B and H is small so that, to a first order, the waveform distortion may usually be neglected. Under these conditions, if the field strength is sinusoidal then the flux density and the e.m.f. (proportional to dB/dt) may be taken as sinusoidal. Thus simple a.c. theory may be used to describe the influence of a magnetic material on an electric circuit. When distortion must be taken into account this may be done by specifically introducing non-linearity into the relations.

For the present purpose, low-amplitude may be taken as corresponding to flux densities of the order of, or less than, 1% of the saturation flux density.

2.2.1. Complex permeability

The inductance of a circuit may be defined as the flux linkage per unit current, i.e. for an alternating current of peak amplitude \hat{I} ,

$$L = \frac{N\hat{\phi}}{\hat{I}} \quad \text{H}$$

For a winding of N turns on an ideal toroid of magnetic

length l and cross-sectional area A

$$\left. \begin{aligned} L &= \frac{N\hat{B}A}{\hat{I}} = \frac{NA}{\hat{I}} \mu_0 \mu \frac{N\hat{I}}{l} \\ \therefore L &= \frac{\mu_0 \mu N^2 A}{l} \\ &= L_0 \mu \end{aligned} \right\} \quad \text{H} \quad (2.14)$$

where

$$L_0 = \frac{\mu_0 N^2 A}{l}$$

= the inductance that would be measured if the core had unity permeability, the flux distribution remaining unaltered.

In general the impedance of the winding will not be a pure reactance; there will be a resistive component due to the loss of energy incurred as the magnetization alternates. The impedance may be expressed in terms of a complex permeability.

Whereas a loss-free core will present a reactance $X = j\omega L$, a core having magnetic loss may be represented by an impedance:

$$\begin{aligned} Z &= j\omega L_s + R_s \\ &= j\omega L_0 (\mu'_s - j\mu''_s) \end{aligned} \quad (2.15)$$

where R_s is the series loss resistance

L_s is the series inductance

μ'_s is the real component of the series complex permeability

and μ''_s is the imaginary component of the series complex permeability.

Then

$$\left. \begin{aligned} \omega L_s &= \omega L_0 \mu'_s \\ R_s &= \omega L_0 \mu''_s \end{aligned} \right\} \quad \text{and the magnetic loss tangent:} \quad (2.16)$$

$$\begin{aligned} \tan \delta_m &= \frac{R_s}{\omega L_s} \\ &= \frac{\mu''_s}{\mu'_s} \end{aligned}$$

where δ_m is the loss angle, i.e. the phase angle between B and H .

Fig. 2.2(a) shows the vector diagram corresponding to the series circuit.

An alternative approach is to represent the same impedance in terms of parallel components. Fig. 2.2(b) shows the equivalent vector diagram, the applied voltage U and current I in each case corresponding exactly in magnitude and phase. Then the admittance,

$$(2.14) \quad L = 4\pi\mu \frac{N^2 A}{l} \times 10^{-9} \quad \text{H}$$

$$= L_0 \mu \quad \text{where } L_0 = 4\pi \frac{N^2 A}{l} \times 10^{-9}$$

$$Y = \frac{1}{j\omega L_p} + \frac{1}{R_p} = \frac{1}{j\omega L_o} \left(\frac{1}{\mu'_p} - \frac{1}{j\mu''_p} \right) \quad \Omega^{-1} \quad (2.17)$$

where R_p is the parallel loss resistance
 L_p is the parallel inductance
 μ'_p is the real component of the parallel complex permeability
and μ''_p is the imaginary component of the parallel complex permeability

Then

$$\left. \begin{aligned} \omega L_p &= \omega L_o \mu'_p \\ R_p &= \omega L_o \mu''_p \\ \text{and the magnetic loss tangent:} \\ \tan \delta_m &= \frac{\omega L_p}{R_p} = \frac{\mu'_p}{\mu''_p} \end{aligned} \right\} \quad (2.18)$$

By analogy with the conversion of series to parallel impedances quoted in Fig. 2.2 the following relations

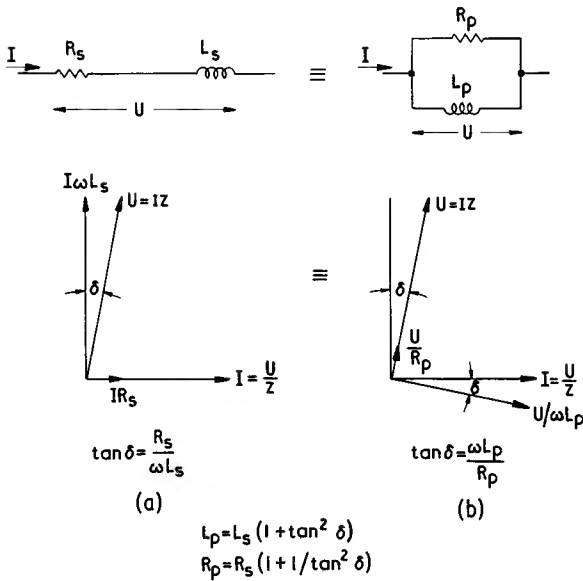


Fig. 2.2. Equivalence of series and parallel inductive circuits

exist between the series and parallel components of the permeability.

$$\left. \begin{aligned} \mu'_p &= \mu'_s (1 + \tan^2 \delta_m) \\ \mu''_p &= \mu''_s (1 + 1/\tan^2 \delta_m) \end{aligned} \right\} \quad (2.19)$$

Graphical representation of the components of the complex permeability and of the values of $\tan \delta_m$ as functions of frequency are common methods of indicating the performance of ferrites at low field strengths. Where the term 'permeability' or the symbol μ is used without any identification of the complex components, the real component is assumed.

2.2.2. Variability

The permeability of a magnetic material may change for a variety of reasons. When such changes occur as the result of unavoidable variations in the operating conditions, they are usually detrimental to the performance of the magnetic material and must be minimized or their magnitude controlled. These changes are referred to as variability and the quantitative expression of the types of variability will now be considered briefly. Experimental observations and some discussion of the phenomena are given in Chapter 3.

The most obvious cause of variation is the change of temperature. Over a limited temperature range the reversible variation of permeability with temperature may be described by a temperature coefficient defined by:

$$\text{Temp. Coeff.} = \frac{\Delta \mu_i}{\mu_i \Delta \theta} \quad (2.20)$$

It is usually expressed in parts per million per degree centigrade. In principle this and the following expressions may be applied to any of the previously described forms of permeability, including the loss components; in practice they usually refer only to the initial permeability.

If the range of temperature is small the above expression is satisfactory but, if $\Delta \mu_i / \mu_i$ becomes appreciable, it is necessary to define the value of μ_i used in the denominator. Further, if the relation is non-linear or has a turning point within the temperature range considered, further ambiguity may arise. In present practice the above expression is interpreted as:

$$\text{Temp. Coeff.} = \frac{(\mu_2 - \mu_1)}{\mu_1 (\theta_2 - \theta_1)} \quad (2.21)$$

where μ_1 is the initial permeability observed at θ_1 and μ_2 at θ_2 . If the permeability change is large, the value in the denominator should be a mean value. It has been suggested¹ that the geometric mean gives a more satisfactory result.

Then

$$\text{Temp. Coeff.} = \frac{(\mu_2 - \mu_1)}{\sqrt{\mu_1 \mu_2} (\theta_2 - \theta_1)} \quad (2.22)$$

If the relation is very non-linear or has a turning point between θ_2 and θ_1 then it is better to abandon the concept of temperature coefficient and to specify that the curve shall lie within a prescribed area, bounded on either side by θ_1 and θ_2 and at the top and bottom by lines giving the permissible change of fractional permeability. Such an area might be rectangular or, if some compensation of another temperature coefficient, e.g. that of a capacitor, is to be attempted, the shape may be that of a parallelogram.

In Chapter 4 it is shown that when an air gap is inserted into a magnetic circuit so that its permeability is reduced

to an effective value, μ_e , the effect of permeability variations are reduced in the ratio μ_e/μ_i . It is therefore convenient to divide the temperature coefficient by μ_i . This gives the temperature factor of permeability. Corresponding to Eqn 2.20.

$$\text{Temp. Factor} = \frac{\Delta \mu_i}{\mu_i^2 \Delta \theta} \quad (2.23)$$

while corresponding to Eqn 2.22

$$\text{Temp. Factor} = \frac{(\mu_2 - \mu_1)}{\mu_1 \mu_2 (\theta_2 - \theta_1)} \quad (2.24)$$

To obtain the temperature coefficient of the effective permeability it is only necessary to multiply the temperature factor, by μ_e . Temperature factor as defined by Eqn 2.23 is at present the usual method of expressing the temperature dependence of the initial permeability of a ferrite material.

Normally the initial permeability rises monotonically with temperature until it reaches a peak just below the Curie temperature. Then, as the forces that hold the spins in alignment are overcome by thermal agitation the permeability falls abruptly to values approaching unity and the material becomes paramagnetic. It is possible to introduce secondary peaks and even minima in the μ/θ characteristic in order to produce a low temperature factor within a limited operating temperature range.

A second form of variability is the variation of permeability with time, or disaccommodation as it is sometimes called. This phenomenon is described in some detail in the introduction to Fig. 3.10. It is sufficient here to state that if a magnetic material is given some form of disturbance, the initial permeability is, in general, instantaneously raised to an unstable value from which it returns as a function of time. Let t_1 and t_2 represent two time intervals measured from the time of the disturbance, and let μ_1 and μ_2 be the corresponding values of the permeability observed at these times, then in general the instability is defined as

$$\frac{\mu_1 - \mu_2}{\mu_1} \text{ and is usually expressed in percent.} \quad (2.25)$$

The times must also be defined. Usually the fractional change in permeability is small so there is no need to use a mean value of permeability in the denominator. By a similar reasoning to that used for temperature factor, the instability factor is

$$\frac{\mu_1 - \mu_2}{\mu_1^2} \quad (2.26)$$

In the discussion of Fig. 3.10, specific types of disturbance are referred to and specific measuring techniques are described. These lead to particular forms of the above

expressions. The one most commonly used in the past, and still often quoted, expresses the time change of permeability, at constant temperature, between 1 min and 24 h after the material has been disturbed by an alternating field which decreases to zero from a value corresponding to saturation, i.e. disaccommodation

$$D = \frac{\mu_1 - \mu_2}{\mu_1} \text{ (usually expressed in percent)} \quad (2.27)$$

where μ_1 is measured at $t = 1$ min and μ_2 is measured at $t = 24$ h after the disturbance.

The corresponding value of disaccommodation factor is

$$\frac{\mu_1 - \mu_2}{\mu_1^2} \quad (2.28)$$

More recently time intervals of 10 min and 100 min have come into use.

Because it is observed that the change of permeability is approximately proportional to the logarithm of time, the IEC has proposed that the disaccommodation factor be expressed as

$$\frac{\mu_1 - \mu_2}{\mu_1^2 \log_{10} \frac{t_2}{t_1}} \quad (2.29)$$

Within the validity of the assumed relations this expression will yield a value which is independent of the times of the measurement.

2.2.3. Hysteresis

There are a variety of coefficients that have been used to express hysteresis loss.² In this section only the Rayleigh and Peterson coefficients will be introduced because they are derived from consideration of ideal hysteresis loop shapes and have formed the basis for the more recent methods of expression. In a later section these current expressions will be considered and compared.

The Rayleigh relations

Rayleigh,³ 1887, observed experimentally that at low and decreasing values of magnetization the amplitude permeability linearly approached the initial permeability,

$$\text{i.e. } \mu_a = \mu_i + v\hat{H} \quad (2.30)$$

$$(2.30) \mu_a = \mu_i + v\hat{H}$$

v is a hysteresis coefficient having the units Oe^{-1}

$$v_{\text{CGS}} = \frac{10^3}{4\pi} v_{\text{SI}}$$

where v is a hysteresis coefficient having the units m.A^{-1}

Multiplying by $\mu_0 \hat{H}$ this relation becomes:

$$\hat{B} = \mu_0 (\mu_i \hat{H} + v \hat{H}^2) \quad \text{T} \quad (2.31)$$

He further observed that, for the specimen examined, the sides of the hysteresis loop would be represented by parabolic curves such that

$$B = \mu_0 \{ (\mu_i + v \hat{H}) H \pm \frac{v}{2} (\hat{H}^2 - H^2) \} \quad \text{T} \quad (2.32)$$

where B and H are instantaneous values and \hat{H} is the maximum value of H .

It should be noted that Rayleigh used only one constant to express the change of permeability with field strength and to express the width of the hysteresis loop, two properties of a magnetic material which are not obviously related.

The hysteresis loop is essentially a d.c. loop. With alternating magnetization the non-hysteresis losses will result in a phase angle between B and H . This will give rise to an elliptical B - H relation which will be superimposed on the hysteresis loop. If hysteresis predominates

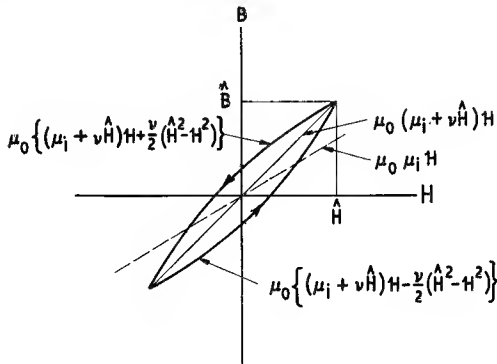


Fig. 2.3. The Rayleigh loop

in the range of amplitudes for which the Rayleigh loop applies then the overall loop will tend to be parabolic. If the other losses predominate the loop will tend to be elliptical, but the parabolic component and the associated hysteresis phenomena will still be present.

The Rayleigh loop is shown in Fig. 2.3. The vertical width of the loop at any given field strength is, from Eqn 2.32, $\mu_0 v (\hat{H}^2 - H^2)$ and, by integration of this width from $-\hat{H}$ to $+\hat{H}$, the area of the loop is $4\mu_0 v \hat{H}^3/3$.

The energy lost during each cycle in a unit volume of the material due to hysteresis is equal to the loop area. It is called the hysteresis energy loss (volume) density and is denoted by w_h

$$w_h = \oint B dH = \frac{4\mu_0 v \hat{H}^3}{3} = \frac{4v \hat{B}^3}{3\mu_0^2 \mu_a^3} \quad \text{J.m}^{-3} \cdot \text{cycle}^{-1} \quad (2.33)$$

The hysteresis power dissipated in a core of volume Al which is subjected to an alternating field of amplitude \hat{H} and frequency f is

$$P_h = w_h A l f \quad \text{W} \\ = I^2 R_h \quad \text{W}$$

where R_h is the series hysteresis loss resistance and I is the r.m.s. current $= \hat{H}l/\sqrt{2N}$.

Combining these equations with Eqn 2.33

$$R_h = \frac{4v \hat{B}}{3\pi \mu_0 \mu_a^2} \cdot 2\pi f \cdot \frac{N^2 A \mu_0 \mu_a}{l} \quad \Omega \\ = \frac{4v \hat{B}}{3\pi \mu_0 \mu_a^2} \cdot \omega L \quad \Omega \quad (2.34)$$

\therefore The hysteresis loss tangent:

$$\tan \delta_h = \frac{R_h}{\omega L} = \frac{4v \hat{B}}{3\pi \mu_0 \mu_a^2} \left. \begin{array}{l} \\ \\ \frac{4v \hat{H}}{3\pi \mu_a} \end{array} \right\} \quad (2.35)$$

As far as a.c. bridge measurements are concerned, the Rayleigh relations are embodied in Eqns 2.30 and 2.35. For a magnetic material to obey the Rayleigh relations the measured properties should follow each of these equations with the same value of constant, or, combining the equations to eliminate the constant, it should obey the following equation:

$$\mu_a = \mu_i + \frac{3\pi \mu_a \tan \delta_h}{4} \\ \text{or } \mu_a = \frac{\mu_i}{1 - \frac{3\pi}{4} \tan \delta_h} \quad (2.36)$$

There is no obvious reason why this relation should be obeyed however low the field strength is. The Rayleigh

$$(2.31) \quad \hat{B} = \mu_i \hat{H} + v \hat{H}^2 \quad \text{Gs}$$

$$(2.32) \quad B = \{ (\mu_i + v \hat{H}) H \pm \frac{v}{2} (\hat{H}^2 - H^2) \} \quad \text{Gs}$$

$$(2.33) \quad w_h = \frac{1}{4\pi} \times \text{loop area} = \frac{1}{3\pi} v \hat{H}^3 = \frac{v \hat{B}^3}{3\pi \mu_a^3}$$

$\text{ergs.cm}^{-3} \cdot \text{cycle}^{-1}$

$$(2.34) \quad R_h = \frac{4v \hat{B}}{3\pi \mu_a^2} \cdot \omega L \quad \Omega$$

$$(2.35) \quad \frac{R_h}{\omega L} = \tan \delta_h = \frac{4v \hat{B}}{3\pi \mu_a^2} = \frac{4v \hat{H}}{3\pi \mu_a}$$

region is a term loosely applied to the low amplitude region in which $\tan \delta_h$ is approximately proportional to \hat{B} or \hat{H} , the value of μ_a in Eqn 2.35 being assumed equal to μ_i ; this is equivalent to saying that the hysteresis energy loss is proportional to \hat{B}^3 (see Eqn 2.33).

Fig. 3.5 shows relations between μ_a and low amplitude flux density measured on typical ferrites. Values of ν have been determined from the tangents of the curves at zero flux density. Fig. 3.15 gives the corresponding $\tan \delta_h$ relations measured on the same specimens and from these the values of ν have also been derived. Comparison shows that, for the materials considered, the two independently derived values of ν approximately agree. However, in both figures, the relations are not linear but tend to fall away from the tangent at $\hat{B} = 0$ as the flux density increases.

The Peterson relations

Peterson,⁴ in 1928, expressed the flux density as a double power series of the instantaneous and maximum field strengths (H , \hat{H}). Making certain assumptions about the loop symmetry and ignoring terms higher than those of the third degree, he obtained for the magnetization curve (not loop)

$$\left. \begin{aligned} B &= \mu_0 [a_{10}H + a_{11}H^2 + (a_{12} + a_{30})H^3 + \dots] \text{ T} \\ \text{or } \mu_a &= a_{10} + a_{11}H + (a_{12} + a_{30})H^2 + \dots \end{aligned} \right\} \quad (2.37)$$

where a_{10} , etc., are coefficients in the power series.

In particular a_{10} = the initial permeability μ_i
and $a_{11} = d\mu/dH$ and has the units m.A^{-1}

From the power series he also deduced that the hysteresis energy (volume) density is

$$w_h = \mu_0 \frac{8}{3} (a_{02}\hat{H}^3 + a_{03}\hat{H}^4 + \dots) \quad \text{J.m}^{-3}.\text{cycle}^{-1} \quad (2.38)$$

where a_{02} has the units m.A^{-1} .

Therefore at low field strength, using the same reasoning as that used to obtain Eqn 2.35 and taking only the first term of Eqn 2.38,

$$(2.37) \left\{ \begin{aligned} B &= a_{10}H + a_{11}H^2 + (a_{12} + a_{30})H^3 + \dots \quad \text{Gs} \\ \mu_a &= a_{10} + a_{11}H + (a_{12} + a_{30})H^2 \end{aligned} \right.$$

where a_{10} = the initial permeability = μ_i

$a_{11} = d\mu/dH$ and has the units Oe^{-1}

$$(a_{11})_{\text{CGS}} = \frac{10^3}{4\pi} (a_{11})_{\text{SI}}$$

$$\frac{R_h}{\omega L} = \tan \delta_h = \frac{8a_{02}\hat{B}}{3\pi\mu_0\mu_a^2} \quad (2.39)$$

Whereas Rayleigh started with limited experimental observations and found relations to express them, Peterson assumed only that the loop is symmetrical about the origin, that the locus of its tips is the initial magnetization curve and that it disappeared when $H = 0$. Thus Peterson's approach was more general; provided the hysteresis loop is regarded as a continuous function and enough terms are taken, the hysteresis loop can always be expressed.

Comparing Eqns 2.30 and 2.37 and ignoring Peterson's third degree term

$$a_{10} = \mu_i \quad \text{and} \quad a_{11} = \nu \quad (2.40)^*$$

Similarly comparing Eqns. 2.35 and 2.39

$$a_{02} = \frac{\nu}{2} \quad (2.41)^*$$

Thus for a material which satisfies the Rayleigh relations the following correspondence must exist in the Peterson coefficients:

$$a_{11} = 2a_{02}. \quad (2.42)$$

Both Rayleigh and Peterson considered only the loss of energy that is proportional to the area of the low frequency or static B - H loop. This is hysteresis loss by definition.

2.2.4. Eddy current phenomena

Resistivity and permittivity

Ferrites are semiconductors and commercial grades have resistivities ranging from $0.1\Omega\text{m}$ to greater than $10^6\Omega\text{m}$ ($10\Omega\text{cm}$ to $> 10^8\Omega\text{cm}$) at room temperatures. Associated with the resistivity there is an effective permittivity which in the case of the low resistivity ferrites can be as

*The discrepancy between these equations and those of Peterson's original paper is due to his use of 2ν in place of ν used here.

$$(2.38) \quad w_h = \frac{2}{3\pi} (a_{02}\hat{H}^3 + a_{03}\hat{H}^4 + \dots) 10^{-7} \quad \text{J.cm}^{-3}.\text{cycle}^{-1}$$

where a_{02} is a Peterson hysteresis coefficient having the units Oe^{-1} .

$$(a_{02})_{\text{CGS}} = \frac{10^3}{4\pi} (a_{02})_{\text{SI}}$$

$$(2.39) \quad \frac{R_h}{\omega L} = \tan \delta_h = \frac{8a_{02}\hat{B}}{3\pi\mu_a^2}$$

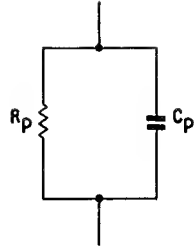


Fig. 2.4. Equivalent circuit of a dielectric

high as 100,000. A ferrite rarely forms a part of a physical electrical circuit, but nevertheless the dielectric properties are important. Significant eddy currents may flow in the bulk of a ferrite core and give rise to energy losses or dispersion of permeability. It is also possible that a ferrite core may contribute to the stray capacitance of a winding. In this section the theory of ferrite dielectric properties will be considered.⁵

The bulk resistivity may be measured on a block of ferrite by the four-probe method, i.e. a known direct current is passed through the block by means of probes at each end of the block and the voltage drop across two intermediate probes of known separation is measured with a high resistance voltmeter. The ratio of the voltage to the current gives the resistance of the section between the voltage probes. The result is independent of the contact resistance of the probes. Alternatively metallic contacts may be deposited on each end of the block. If the contact resistance can be made negligible the resistivity, ρ , and the relative parallel permittivity, ϵ , of the block may be measured in terms of the equivalent two terminal impedance (or admittance). On an admittance bridge the equivalent admittance is expressed in the parallel components of Fig. 2.4.

If A is the cross-sectional area of the block and l is the length separating the contacts then

$$\left. \begin{aligned} C_p &= \epsilon_0 \epsilon \frac{A}{l} & \text{F} \\ R_p &= \frac{\rho l}{A} & \Omega \end{aligned} \right\} \quad (2.43)$$

where ϵ_0 is the electric constant or permittivity of free space = 8.854×10^{-12} F.m.⁻¹ It has the dimensions [L⁻³M⁻¹T⁴I²].

An alternative presentation is the parallel complex permittivity which is analogous to parallel complex permeability (see Eqn 2.17).

$$\left. \begin{aligned} \text{Then} \quad \epsilon &= \epsilon'_p - j\epsilon''_p \\ \therefore Y &= j\omega C_p + \frac{1}{R_p} = j\omega \epsilon_0 \frac{A}{l} (\epsilon'_p - j\epsilon''_p) \quad \Omega^{-1} \\ \therefore \epsilon''_p &= \frac{l}{\omega \epsilon_0 A R_p} = \frac{1}{\omega \epsilon_0 \rho} \end{aligned} \right\} \quad (2.44)$$

The dielectric loss tangent is given by

$$\tan \delta_d = \frac{1}{\omega C_p R_p} = \frac{\epsilon''_p}{\epsilon'_p} = \frac{1}{\omega \epsilon_0 \epsilon'_p \rho} \quad (2.45)$$

Some writers remove the d.c. resistance contribution from ϵ''_p thus representing the impedance as a constant d.c. resistance in parallel with a capacitance having dielectric loss. This is not the procedure adopted here.

Consideration of the polycrystalline structure of ferrites and the variation of their resistivity and permittivity with

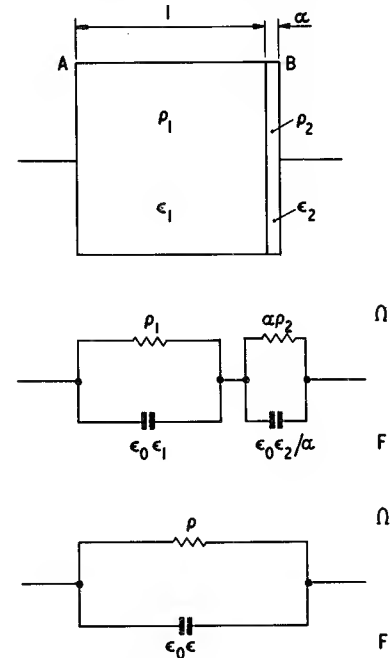


Fig. 2.5. Equivalent circuit of a crystallite and boundary

$$(2.43) \quad \left\{ \begin{aligned} C_p &= \frac{\epsilon A 10^{-12}}{3.6\pi l} & \text{F} \\ &= 0.0885 \epsilon A / l & \text{pF} \\ R_p &= \rho l / A & \Omega \end{aligned} \right.$$

$$(2.44) \quad Y = j\omega C_p + \frac{1}{R_p} = \frac{j\omega A 10^{-12}}{3.6\pi l} (\epsilon'_p - j\epsilon''_p) \quad \Omega^{-1}$$

$$\therefore \epsilon''_p = \frac{3.6\pi 10^{12}}{\omega A R_p} = \frac{3.6\pi 10^{12}}{\omega \rho}$$

$$(2.45) \quad \tan \delta_d = \frac{1}{\omega C_p R_p} = \frac{\epsilon''_p}{\epsilon'_p} = \frac{3.6\pi 10^{12}}{\epsilon'_p \omega \rho}$$

frequency (see Fig. 3.21) has led to the view that polycrystalline ferrite may be regarded as a compound dielectric consisting of semiconducting regions (crystallites) surrounded by thin boundaries having much higher resistivity. Fig. 2.5 shows a unit cube of material, of resistivity ρ_1 and real permittivity ϵ_1 , having a boundary layer, of thickness α , with corresponding dielectric properties ρ_2 and ϵ_2 . This represents a single crystallite. The admittance between the faces A and B will characterize the admittance of a material built up of a chain of such blocks, or more generally, a polycrystalline material.

Applying Eqn 2.43, the crystallite and boundary may be represented by the equivalent electrical circuit as shown. This circuit may at a given frequency be resolved into a capacitance, $\epsilon_0\epsilon$ in parallel with a resistance, ρ ; ϵ and ρ represent the apparent dielectric properties of the composite dielectric.

It has been found that in polycrystalline ferrites $\alpha \ll 1$, $\epsilon_2 \approx \epsilon_1$ and $\alpha\rho_2 \gg \rho_1$. Therefore at low frequencies the impedance of the crystallite is negligible compared to that of the boundary; so the resistivity approximates to $\alpha\rho_2$ while the permittivity approaches ϵ_2/α . This is analogous to calculating dielectric properties from measurements on a specimen between the plates of a capacitor, using a dielectric length $1/\alpha$ times the actual value.

At very high frequencies the boundary capacitance short circuits the boundary resistance and the bulk dielectric properties approach those of the crystallite.

Summarizing

$$\left. \begin{array}{ll} \text{when } f \rightarrow 0 & \rho \rightarrow \alpha\rho_2 \\ & \epsilon \rightarrow \epsilon_2/\alpha \\ \text{when } f \rightarrow \infty & \rho \rightarrow \rho_1 \\ & \epsilon \rightarrow \epsilon_1 \end{array} \right\} \quad (2.46)$$

It follows that if the boundary layer is relatively thin, i.e. $\alpha \ll 1$, then at low frequencies the bulk resistivity will be low and the permittivity will be high. The properties will transform from the low frequency values to the high frequency values in accordance with a relaxation curve.

The relaxation time for both ρ and ϵ is given by

$$\tau = \epsilon_0 \frac{\epsilon_1 + \epsilon_2/\alpha}{\frac{1}{\rho_1} + \frac{1}{\alpha\rho_2}} \quad \text{s} \quad (2.47)$$

$$\tau = 1/\omega_r$$

where ω_r is $2\pi \times$ the relaxation frequency.

This is the frequency at which the value of the property is midway between the values at the two extreme frequencies. Fig. 3.21 shows some experimental results.

Eddy current loss

An alternating magnetic flux in a conductive medium will induce eddy currents in that medium and these will result in an energy loss called eddy current loss.

The magnitude of this loss depends, among other things, on the size and shape of the conductive medium and, as is well known, may be reduced by subdivision of the medium into electrically insulated regions, e.g. laminations or grains. When a material is thus subdivided the magnitude of the eddy current loss per unit volume depends on the size and shape of the insulated regions and not on the shape of the bulk material. Ferrites, on the other hand, are usually regarded as homogeneous materials as far as eddy currents are concerned. Under certain circumstances significant micro-eddy currents may circulate within the crystallites and cause additional loss. Any loss due to this cause is usually included with the residual loss and not separately considered; this is the practice adopted in these chapters.

At any given frequency, the effective dielectric properties discussed in the previous section may be used to calculate the magnitudes of the eddy currents that may flow through the material as a whole. Fig. 3.21 shows some measured dielectric properties.

At low frequencies, where the inductive effect of the eddy currents may be neglected, the eddy current power loss (volume) density is given by

$$P_F = \frac{(\pi \hat{B} f d)^2}{\rho \beta} \quad \text{W.m}^{-3} \quad (2.48)$$

where \hat{B} is the peak value of the flux density assumed perpendicular to the plane containing dimension d ,

ρ is then the bulk resistivity,
and $\beta = 6$ for laminations of thickness d m,
= 16 for a cylinder of diameter d m,
= 20 for a sphere of diameter d m.

Using a similar reasoning to that which led to Eqn 2.35 the eddy current core loss tangent is:

$$\tan \delta_F = \frac{R_F}{\omega L} = \frac{\pi \mu_0 \mu d^2 f}{\rho \beta} \quad (2.49)$$

where R_F is the eddy current series loss resistance.

$$(2.47) \quad \tau = \frac{10^{-12}}{3.6\pi} \times \frac{\epsilon_1 + \epsilon_2/\alpha}{\frac{1}{\rho_1} + \frac{1}{\alpha\rho_2}} \quad \text{s}$$

$$(2.48) \quad P_F = \frac{(\pi \hat{B} f d)^2}{\rho \beta} 10^{-16} \quad \text{W.cm}^{-3}$$

$$(2.49) \quad \tan \delta_F = \frac{R_F}{\omega L} = \frac{4\pi^2 \mu d^2 f}{\rho \beta} \cdot 10^{-9}$$

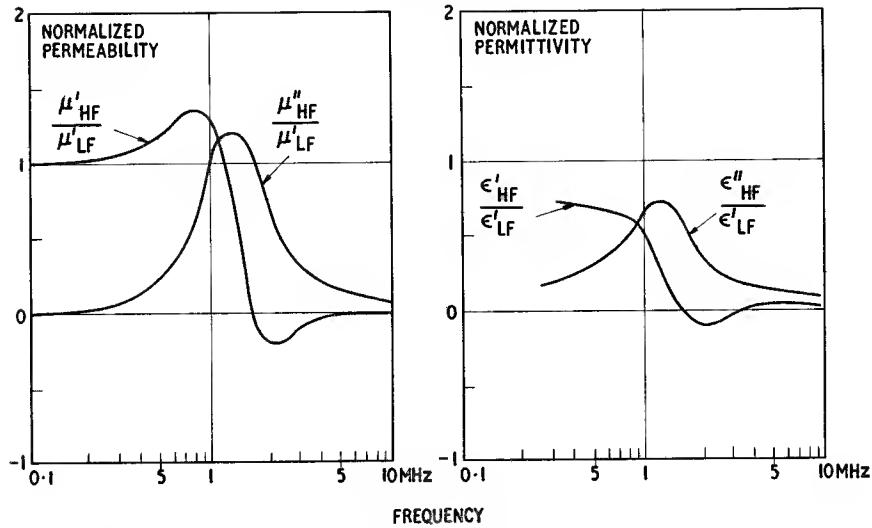


Fig. 2.6. Dimensional resonance in a manganese zinc ferrite calculated for a sample of thickness 12.5 mm, using typical complex permeability and permittivity data. The imaginary part of the permittivity has the contribution from the d.c. resistivity removed—see Eqn 2.44. The results are normalized with respect to the low frequency values. (Courtesy Brockman et al.⁷)

These expressions may be used to calculate the eddy current loss in simple core shapes; the result for a square cross-section bar may be taken as approximately equal to that for the cylinder of the same cross-sectional area. For more complicated shapes expressions must be derived from first principles. An elementary eddy current path is assumed and the flux linkage is expressed in terms of its dimensions. From the corresponding induced e.m.f. and the resistance of the path, an expression for the power loss may be obtained. This may then be integrated over the whole cross-section.

Dimensional resonance

The calculation of eddy current loss in the previous section assumed that the flux density is uniformly distributed across the section of the core. At higher frequencies this may not be true because in some ferrites the high values of permeability and permittivity give rise to standing electromagnetic waves within the ferrite. This is called dimensional resonance.

In a loss-free medium the velocity of propagation of electromagnetic waves is given by

$$v = (\mu_0 \mu \epsilon_0 \epsilon)^{-\frac{1}{2}} = f\lambda \quad \text{m.s}^{-1} \quad (2.50)$$

where λ = the wavelength in the medium.

In a typical manganese zinc ferrite, $\mu = 10^3$ and $\epsilon = 10^5$.

Therefore at a frequency of 1 MHz

$$v = (4\pi \times 10^{-7} \times 10^3 \times 8.854 \times 10^{-12} \times 10^5)^{-\frac{1}{2}} \\ \approx 3 \times 10^4 \quad \text{m.s}^{-1}$$

and $\lambda \approx 0.03 \text{ m}$

If the smallest cross-sectional dimension of the core (perpendicular to the magnetic field) is half a wavelength, i.e. 15 mm, then a fundamental mode standing wave will be set up across the section. Under these conditions the net reactive flux is zero; the surface flux which is in phase with the surface magnetic field is cancelled by antiphase flux at the centre of the core. Thus dimensional resonance is characterized by the observed permeability dropping to zero. Since the phenomenon is essentially electromagnetic there is a corresponding standing wave in the electric flux density. This gives rise to a similar dispersion in the observed permittivity. It occurs when the smallest dimension of the cross-section perpendicular to the electric field equals half a wave length. Since the electric and magnetic fields are perpendicular both standing waves appear across the same dimension.

If the medium has some loss then μ and ϵ in Eqn 2.50 must be replaced by $\mu'_s - j\mu''_s$ and $\epsilon'_p - j\epsilon''_p$. If $\tan \delta_m = \mu''_s/\mu'_s$ and $\tan \delta_d = \epsilon''_p/\epsilon'_p$, and $\tan \delta_m \tan \delta_d \ll 1$ then

$$(2.50) \quad v = \frac{c_0}{\sqrt{\mu\epsilon}} = f\lambda \quad \text{cm.s}^{-1}$$

where c_0 = velocity of electromagnetic waves in vacuo

$$c_0 \approx 3 \times 10^{10} \quad \text{cm.s}^{-1}$$

and λ = wavelength in cm

dimensional resonance will still be observed but the resonant dimension is now obtained by replacing $\mu\epsilon$ in Eqn 2.50 by the real part of the complex product. The resonant dimension is then given by⁶

$$\frac{\lambda}{2} = \frac{\sqrt{2\pi c_0}}{\omega \sqrt{[\mu] [\epsilon] + \mu'_s \epsilon'_p (1 - \tan \delta_m \tan \delta_d)}} \quad \text{m (2.51)}$$

where c_0 is the velocity of electromagnetic waves in vacuo $= (\mu_0 \epsilon_0)^{-\frac{1}{2}}$

In such a medium there is a quadrature standing wave which gives rise to a peak in the observed magnetic loss, μ'_s , and dielectric loss ϵ'_p at resonance.

If $\tan \delta_m \tan \delta_d \gg 1$ the material will not support standing waves and there is no dimensional resonance. Instead the flux will be attenuated as it is propagated through the cross-section and there will be a penetration depth, Δ , as in metal magnetic materials.⁶

$$\Delta = \frac{\sqrt{2c_0}}{\omega \sqrt{[\mu] [\epsilon] + \mu'_s \epsilon'_p (1 - \tan \delta_m \tan \delta_d)}} \quad \text{m (2.52)}$$

As with the resonant dimension, Δ is measured perpendicular to the magnetic field or the electric field. In calculating $\lambda/2$ and Δ , the variation of the permeability and permittivity components with frequency must be taken into account. Relevant data may be found in Figs. 3.11 and 3.21. Strictly the above expressions apply only to the thickness of an infinite plate but in practice they may be applied to practical core cross-sections for the purpose of estimation. $\lambda/2$ and Δ have been calculated from these expressions using the properties of a typical manganese zinc ferrite and the result is given in Fig. 4.5.

An analytical study of dimensional resonance was made by Brockman *et al.*⁷ They give expressions for the real and imaginary parts of the complex permeability and permittivity as functions of frequency and they calculate these functions for a typical manganese zinc ferrite. Their results are reproduced in Fig. 2.6.

2.2.5. Residual loss

Two forms of magnetic loss have so far been distinguished, namely, hysteresis loss which gives rise to a loss tangent which is proportional to \hat{B} (see Eqn 2.35) and eddy current loss which gives rise to a loss tangent which is proportional to f (see Eqn 2.49), i.e.

$$\tan \delta_h \propto \hat{B}$$

$$\tan \delta_F \propto f$$

If, for a metallic magnetic material, e.g. a laminated or powder core, the total loss tangent is measured as a function of \hat{B} and f at low frequencies where eddy current screening effects are negligible, a set of curves similar to that shown in Fig. 2.7 is obtained. It is seen that when

$\hat{B} \rightarrow 0$ and $f \rightarrow 0$, the total loss tangent is not zero. The remainder is called the residual loss.

The total loss tangent may be written

$$\tan \delta_m = \tan \delta_h + \tan \delta_F + \tan \delta_r \quad (2.53)$$

where $\tan \delta_r$ is the residual loss tangent.

This is the original definition of residual loss. In a ferrite, which has high resistivity, it is very easy to ensure that the bulk eddy current loss is negligible by making

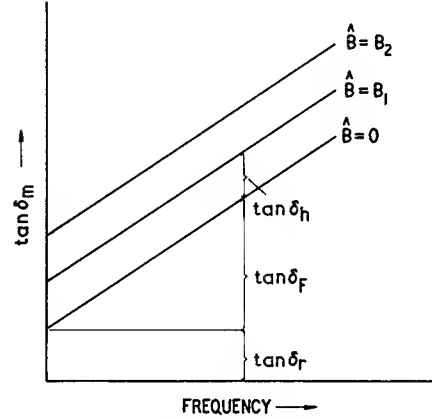


Fig. 2.7. Loss tangent as a function of frequency; illustration of Eqn 2.53

measurements on an adequately small sample. On such a sample it is also possible to measure the loss tangent at vanishingly small flux densities. By this procedure the bulk eddy current and hysteresis losses may be eliminated at any frequency and the remaining loss tangent is due to residual loss. This is the usual meaning of the term residual loss in ferrites, and the residual loss tangent expressed as a function of frequency is an important loss parameter relating to ferrites.

There are probably several loss processes that contribute to residual loss and different processes may apply at different parts of the spectrum. A brief discussion of this aspect of residual loss is given in the introduction to Fig. 3.11 and Fig. 3.12 where typical residual loss spectra are illustrated.

2.2.6. General loss expressions

Loss factor

If a loss-free winding having N turns is placed round a closed magnetic core and an alternating voltage U is applied, a power loss (volume) density, $P_m = U^2 G / Al$, will be observed, where G is the conductance appearing across the winding due to the magnetic loss in the core. The induced e.m.f., the frequency and flux density are related by Eqn. 2.13. If the loss tangent is small the applied voltage will approximately equal the induced e.m.f. so

$$U = \frac{\hat{B}AN\omega}{\sqrt{2}} \quad V \quad (2.54)$$

Thus for a given core cross-sectional area A and number of turns, the voltage and frequency determine the flux density.

The loss tangent due to the magnetic core,

$$\tan \delta_m = \frac{\omega L_p}{R_p} = \omega L_p G$$

It has already been postulated that $\tan \delta_m \ll 1$, therefore the distinction between series and parallel inductance may be dropped.

Substituting $L_p = \mu_0 \mu N^2 A / l$

$$\tan \delta_m = \omega \mu_0 \mu N^2 A G / l \quad (2.55)$$

Putting $G = P_m A l / U^2$ and substituting for U from Eqn 2.54

$$\frac{\tan \delta_m}{\mu} = \frac{\mu_0}{\pi f \hat{B}^2} \cdot P_m \quad (2.56)$$

The factor $(\tan \delta_m) / \mu$ depends on the power loss (volume) density and this depends on the frequency and flux density. If the eddy current core loss is negligible the loss density is independent of core shape and is a material property dependent only on f and B . Under these conditions $(\tan \delta_m) / \mu$ is also a material property and a function of only f and B .

The analysis of the effect of an air gap must now be anticipated. If an air gap is introduced into a magnetic circuit the inductance will be reduced so that the core appears to have an effective permeability μ_e . It is shown in Chapter 4 that the loss tangent of a gapped core is related to the material loss tangent by the following expression (see Eqn. 4.48):

$$\frac{(\tan \delta_m)_{\text{gapped}}}{\mu_e - 1} = \frac{\tan \delta}{\mu - 1} \quad (2.57)$$

These expressions are referred to as loss factors. Because μ_e and μ are usually much greater than unity the above equation is usually approximated to

$$\frac{(\tan \delta)_{\text{gapped}}}{\mu_e} = \frac{\tan \delta}{\mu} \quad (2.58)$$

The subscript m has been dropped because clearly the loss tangent need not be due to the total loss; it may refer to any specific form of loss. Within the conditions stated the loss factor is independent of the gap and therefore

for those ferrites which are normally gapped in use it is an important material property. Residual loss of a ferrite material is frequently expressed by the corresponding loss factor.

An important practical consequence of Eqn 2.58 is that the loss tangent due to the magnetic loss of a gapped core is given by

$$(\tan \delta)_{\text{gapped}} = \left(\frac{\tan \delta}{\mu} \right) \mu_e \quad (2.59)$$

i.e. loss factor \times effective permeability

Considering again the total loss factor, Eqn 2.53 may be written in terms of loss factors

$$\frac{\tan \delta_m}{\mu} = \frac{\tan \delta_h}{\mu} + \frac{\tan \delta_F}{\mu} + \frac{\tan \delta_r}{\mu} \quad (2.60)$$

Substituting for the loss tangent expressions from Eqns 2.35 and 2.49 and letting $\mu_a \rightarrow \mu$:

$$\left. \begin{aligned} \frac{\tan \delta_m}{\mu} &= \frac{4v\hat{B}}{3\pi\mu_0\mu^3} + \frac{\pi\mu_0 d^2 f}{\rho\beta} + \frac{\tan \delta_r}{\mu} \\ &= k_1 \hat{B} + k_2 f + k_3 \end{aligned} \right\} \quad (2.61)$$

where k_1 and k_3 are hysteresis and residual loss coefficients characterizing the material and k_2 is an eddy current loss coefficient that depends on the material and its shape. Eqn 2.61 is the basis of a number of well-known loss expressions, several of which will now be considered.

The Jordan expression

Jordan,⁸ in 1924, proposed that the series loss resistance due to a magnetic core could be expressed as follows:

$$R_s = h \cdot \frac{NI}{l} \cdot \frac{f}{800} \cdot L + F \cdot \frac{f^2}{800^2} \cdot L + t \cdot \frac{f}{800} \cdot L \quad (2.62)$$

where h is the hysteresis loss coefficient in Ω/H at a frequency of 800 Hz for a field strength corresponding to $NI/l = 1$ ampere turn/cm (rms)
 F is the eddy current loss coefficient and
 t is the residual loss coefficient, both in Ω/H at a frequency of 800 Hz.

This method of expression is the basis of the loss coefficients used in France and Germany. Dividing both sides of the equation by $\mu f L$:

$$(2.54) \quad U = \frac{\hat{B}AN\omega}{\sqrt{2}} \times 10^{-8} \quad V$$

$$(2.55) \quad \tan \delta_m = \omega 4\pi\mu N^2 A G \cdot 10^{-9} / l$$

$$(2.56) \quad \frac{\tan \delta_m}{\mu} = \frac{4P_m 10^7}{f \hat{B}^2}$$

$$(2.61) \quad \frac{\tan \delta_m}{\mu} = \frac{4v\hat{B}}{3\pi\mu^3} + \frac{4\pi^2 d^2 f \times 10^{-9}}{\rho\beta} + \frac{\tan \delta_r}{\mu}$$

$$\frac{R_s}{\mu f L} = \frac{h}{\mu} \cdot \frac{NI}{l} \cdot \frac{1}{800} + \frac{F}{\mu} \cdot \frac{f}{800^2} + \frac{t}{\mu} \cdot \frac{1}{800} \quad (2.63)$$

The hysteresis component is expressed in terms of field strength, instead of flux density as in Eqn 2.61. The alternative version is easily derived:

$$\frac{R_h}{\mu_a f L} = \frac{h}{\mu_a^2} \frac{10B}{4\pi 800} = \frac{h\hat{B}}{\mu_a^2 1422} \quad (2.64)$$

where h is in $\Omega \cdot H^{-1} \cdot f^{-1} \cdot cm^{-1} \cdot A$ as before, or more simply Gs^{-1} ,

B is in Gs

R_h is the series hysteresis loss resistance,

and the subscript a indicates that strictly it is the amplitude permeability in the denominator.

The Jordan hysteresis loss is usually quoted as a value of h/μ^2 .

Often a modified version of this expression is used for the hysteresis component. The hysteresis loss resistance is then given by

$$R_h = h L f H \quad \Omega \quad (2.65)$$

where h is in $cm \cdot A^{-1}$

L is in H

f is in Hz

and H is in ampere turns/cm

Comparing this with Eqn 2.63 it follows that

$$h = h/800$$

$$\therefore \frac{R_h}{\mu f L} = 0.563 \frac{h}{\mu^2} \hat{B}. \quad (2.66)$$

Sometimes the Jordan coefficients are expressed in SI units and the reference frequency of 800 Hz replaced by 1 Hz. These coefficients usually carry the suffix K .

The conversion is as follows:

$$F = 640\,000 F_K$$

$$h = 80\,000 h_K$$

$$t = 800 t_K$$

The Legg expression

Legg, in 1936, introduced the following relation to express the loss in a magnetic material operating at low flux densities.

$$\frac{R_s}{\mu f L} = a \hat{B} + e f + c \quad (2.67)$$

where a is the hysteresis loss coefficient in T^{-1} ,

e is the eddy current loss coefficient in seconds,

c is the residual loss coefficient and is a number.

[In CGS units a has the units Gs^{-1}

$$\therefore (a)_{CGS} = 10^{-4} (a)_{MKS}]$$

This expression has a direct similarity to Eqn 2.61. Since $R_s/\mu f L$ equals $(2\pi \tan \delta_m)/\mu$ it may be written in terms of loss factor:

$$\frac{\tan \delta_m}{\mu} = \frac{1}{2\pi} (a \hat{B} + e f + c). \quad (2.68)$$

Although this expression corresponds to that proposed by Legg it should be remembered that strictly the loss factor has $\mu-1$ in the denominator, see Eqn 2.57.

The Snoek expressions

All the expressions considered hitherto were proposed before the introduction of ferrites. In 1947 Snoek¹⁰ expressed the losses in ferrites by an equation which is identical in form with the Legg equation:

$$\frac{R_s}{\mu f L} = c_h \hat{B} + c_e f + c_r \quad (2.69)$$

where c_h is the hysteresis loss coefficient in T^{-1} or Gs^{-1} depending on units of B ,

c_e is the eddy current loss coefficient in seconds,

c_r is the residual loss coefficient.

It was also proposed to use a further hysteresis coefficient which was related to the performance of loading coils. The CCITT (formerly CCIF) laid down¹¹ that in loading coils the hysteresis resistance should not exceed a value quoted in the form

$$R_h = q_2 \sqrt{L} \quad \Omega / mA \cdot H \text{ at } 800 \text{ Hz} \quad (2.70)$$

where q_2 has a specific value, e.g. 12 for low grade circuits and 6 for high grade circuits.

For an arbitrary inductor

$$R_h = \frac{q_2 L^{3/2} I f 10^3}{800} \quad \Omega \quad (2.71)$$

where L is the inductance of the coil.

The coefficient q_2 thus characterizes the hysteresis loss of an inductor; it was suggested that if it were related to a particular inductor design, then it could be used as a convenient material constant. The particular design chosen has an effective volume,* V_e , of 24 cm^3 and effective permeability, μ_e , of 100; these values being typical of the loading coils used at that time. The derived coefficient was therefore designated $q_{2-24-100}$. The steps in the derivation are rather tedious and are unnecessary for the present discussion. It is sufficient to state that using this hysteresis loss coefficient the value of q_2 for a general inductor having an effective volume $V_e \text{ cm}^3$ and an effective permeability μ_e is given by

*See Section 4.2.1.

Table 2.1 SUMMARY OF EXPRESSIONS FOR MAGNETIC LOSSES AT LOW FIELD STRENGTH

<i>Method of Expression</i>	<i>Hysteresis Loss</i>		<i>Eddy Current Loss</i>		<i>Residual Loss</i>	
	$\frac{\tan \delta_h}{\mu_a} =$		$\frac{\tan \delta_F}{\mu} =$		$\frac{\tan \delta_r}{\mu} =$	
	Coeff.	Factor	Coeff.	Factor	Coeff.	Factor
Rayleigh	ν	$\frac{4}{3\pi} \frac{\hat{B}}{\mu_o \mu_a^3}$				
Peterson	a_{02}	$\frac{8}{3\pi} \frac{\hat{B}}{\mu_o \mu_a^3}$				
Jordan: based on A.cm ⁻¹ Gs and 800 Hz	$\left\{ \begin{array}{l} h \\ \frac{h}{\mu_a^2} \end{array} \right.$	$\frac{NI}{2\pi \mu_a l 800}$ $\frac{\hat{B}}{2\pi 1422}$	F	$\frac{f}{2\pi \mu 800^2}$	t	$\frac{1}{2\pi \mu 800}$
based on A.cm ⁻¹ Gs and 1 Hz	$\left\{ \begin{array}{l} h \\ \frac{h}{\mu_a^2} \end{array} \right.$	$\frac{NI}{2\pi \mu_a l}$ $\frac{0.563 \hat{B}}{2\pi}$				
based on MKS and 1 Hz	$\left\{ \begin{array}{l} h_K \\ \frac{h_K}{\mu_a^2} \end{array} \right.$	$\frac{NI}{2\pi \mu_a l}$ $\frac{0.707 \hat{B}}{2\pi \mu_o}$	F_K	$\frac{f}{2\pi \mu}$	t_k	$\frac{1}{2\pi \mu}$
Legg	a	$\frac{\hat{B}}{2\pi}$	e	$\frac{f}{2\pi}$	c	$\frac{1}{2\pi}$
Snoek	c_h	$\frac{\hat{B}}{2\pi}$	c_e	$\frac{f}{2\pi}$	c_r	$\frac{1}{2\pi}$
	$q_{2-24-100}$	$0.386 \times 10^{-6} \frac{\hat{B}}{2\pi}$				
IEC	η_B	\hat{B}				

Any coefficient multiplied by the adjacent factor equals the corresponding $(\tan \delta)/\mu$. Some of the conversion factors strictly apply only when the value of the permeability corresponds to the level of flux density considered; in most applications this level is low enough to allow the use of the initial permeability without significant error. However in the conversion factors for the hysteresis loss expressions the permeability has been designated

μ_a to draw attention to the fact that in general the amplitude permeability is meant. When the distinction is not essential the symbol μ is sufficient.

Apart from the Jordan coefficients the table applies to both MKS and CGS units provided the system used is consistent e.g. if a_{02} is the CGS value then B is in gauss and $\mu_o = 1$. The Jordan coefficients are based on a hybrid system and the versions in current use are quoted separately.

$$\left. \begin{aligned} q_2 &= q_{2-24-100} \sqrt{\left(\frac{\mu_e}{100}\right)^3 \times \frac{24}{V_e}} \\ \text{or } \frac{R_h}{L} &= q_{2-24-100} I \sqrt{L} \frac{f}{0.8} \sqrt{\left(\frac{\mu_e}{100}\right)^3 \times \frac{24}{V_e}} \end{aligned} \right\} \Omega \cdot \text{H}^{-1} \quad (2.72)$$

These equations are used only in CGS (practical) units.

The following relation to the Legg hysteresis loss coefficient applies

$$q_{2-24-100} = 2.59a \cdot 10^6 \quad \text{Gs}^{-1} \quad (2.73)$$

This coefficient is used mainly in the Netherlands.

The IEC expression

Technical Committee 51 of the International Electrotechnical Commission, considering their recommendations for standard forms of loss expression^{1,2}, agreed to the following proposal for hysteresis

$$\frac{\tan \delta_h}{\mu} = \eta_B \hat{B} \quad (2.74)$$

where η_B is a hysteresis loss coefficient in T^{-1}
 \hat{B} is in T.

Summary of loss expressions

Not all the loss expressions in current use have been included in the foregoing survey. There are a number of national variations, but most of them stem from the expressions described above. Table 2.1 gives a summary of the above expressions and lists the multiplying factors required to convert each term to the corresponding value of $(\tan \delta)/\mu$ (see also ref. 1). There is a growing tendency to accept $(\tan \delta)/\mu$ as the basic form of expression.

Discussion of loss expressions

The losses in magnetic materials are fundamentally energy losses and may be expressed as such, e.g. in terms of $\text{J} \cdot \text{m}^{-3} \cdot \text{cycle}^{-1}$, but at low amplitudes it is more convenient to express them in terms of loss angle or loss resistance. This is because at these low amplitudes the influence of the core on the associated electrical circuit is best studied by expressing the core properties in terms of resistances and inductances. These may then be readily combined with other circuit elements by the normal processes of circuit theory. In particular, time constants and Q -factors may easily be derived.

It has been previously observed that the power loss

per unit volume is a function of flux density and frequency. A double power series in f and B may easily be set up to express the loss per unit volume. Common observation will lead to the discarding of some of the lower order terms. If all the higher order terms are also discarded one obtains an expression identical in form with the Legg expression (Eqn 2.67). Such an exercise does not introduce such concepts as hysteresis or eddy current loss and yet for $(\tan \delta)\mu$ it yields one term proportional to B , one proportional to f and another that is independent of either. The point of this digression is that although it is appropriate to describe these terms as due to hysteresis, eddy current and residual loss respectively, in practice the adequate expression of the behaviour of a material requires higher terms and the distinction between the phenomena can become obscure.

It is not usual to invoke these higher power terms. It is more convenient to express the losses in general by three coefficients and to regard these coefficients as empirical functions of frequency and flux density. Thus the hysteresis coefficient is usually specified at a low frequency and at a low flux density, under which conditions it may be regarded as a material constant. If the frequency or flux density is raised appreciably the measured value of the hysteresis coefficient will change and it is convenient to express this change by means of a graph which is characteristic of the particular material.

The eddy current loss coefficient depends on the degree of sub-division in the case of laminated or powdered cores, or, in the case of homogeneous cores, on the dimensions of the core cross-section. Ferrite cores, although not entirely homogeneous, come into the latter category so the eddy current loss coefficient is not a material property but depends on the core size and shape (see Eqn 2.61). For this reason the eddy current loss coefficient is rarely used in a ferrite material specification; the value of the bulk resistivity is a more useful parameter.

So the loss coefficients most commonly used to express losses in ferrites are the hysteresis and the residual loss coefficients. In this context residual loss is taken as referring to the loss angle or loss resistance remaining when the eddy current loss is negligible and the flux density is vanishingly small. In practice it depends on frequency but by definition does not depend on flux density.

Some experimental data on these losses are given in Chapter 3.

2.2.7. Waveform distortion and intermodulation

At very low field strengths the low frequency hysteresis loop approximates to the parabolic form considered by Rayleigh and Peterson; it is illustrated in Fig. 2.3. If a

sinusoidal field of constant peak amplitude \hat{H} is applied to such a material the flux density will alternate at a peak amplitude \hat{B} but due to the non-linear relation between B and H the waveform will be distorted. Because the loop has symmetry about the origin this distortion may be expressed in terms of only the odd harmonics of the applied field.

Assuming the parabolic loop equation, an expression may easily be derived for the flux density as a function of time and by Fourier analysis the amplitude of the harmonics may be obtained. Peterson's⁴ expression for the flux density when the applied field is $\hat{H} \cos pt$ is

$$B = \mu_0 \left\{ \hat{H}(a_{10} + a_{11}\hat{H}) \cos pt + \frac{8a_{02}}{3\pi} \hat{H}^2 \sin pt + a_{30} \frac{\hat{H}^3}{4} \cos 3pt - \frac{8a_{02}}{15\pi} \hat{H}^2 \sin 3pt \dots \right\} \quad (2.75)$$

The first term is the fundamental frequency inductance term, the second is the fundamental frequency hysteresis loss term, the third term is the third harmonic resulting from the permeability change and is negligible, and the fourth is the main third harmonic term. The third harmonic term depends on the hysteresis loss coefficient a_{02} . It usually has much larger amplitude than any of the higher order harmonics and its amplitude is usually taken as a measure of the total distortion. Denoting the fundamental and the third harmonic by subscripts a and $3a$ respectively, the amplitude of the third harmonic flux density is

$$\hat{B}_{3a} = \frac{8}{15\pi} \mu_0 a_{02} \hat{H}_a^2 \quad T \quad (2.76)$$

$$\frac{\hat{B}_{3a}}{\hat{B}_a} = \frac{8a_{02}\hat{B}_a}{15\pi\mu_0\mu^2} \quad (2.77)$$

Since the induced e.m.f. is proportional to frequency

$$\begin{aligned} \frac{E_{3a}}{E_a} &= \frac{3\hat{B}_{3a}}{\hat{B}_a} = \frac{8a_{02}\hat{B}_a}{5\pi\mu_0\mu^2} \\ &= 0.6 \tan \delta_h \\ &\text{from Eqn 2.39} \end{aligned} \quad (2.78)$$

If the amplitude of the applied field is increased, the loop will increase in length and breadth and $\tan \delta_h$ will increase in proportion to \hat{H} , (see Eqn 2.35). At the same

time the slope of the major axis of the loop, i.e. the permeability, will increase in accordance with Eqn 2.37. The permeability rise has negligible effect in the production of third harmonic distortion. However, in the intermodulation of two simultaneously applied currents of different frequency, both hysteresis phenomena play a part.

If two alternating fields of equal amplitude \hat{H} and angular frequencies $2\pi f_a = (p + \omega)$ and $2\pi f_b = (p - \omega)$ respectively are simultaneously applied to a magnetic material the resultant field has the equation:

$$H = \hat{H} \cos 2\pi f_a t + \hat{H} \cos 2\pi f_b t = 2\hat{H} \cos \omega t \cdot \cos pt \quad (2.79)$$

The combined r.m.s. amplitude is numerically equal to \hat{H} , i.e. it is $\sqrt{2}$ times the r.m.s. amplitude of the single frequency field considered in the analysis of third harmonic. If the difference between f_a and f_b is small, i.e. $\omega \ll p$, then Eqn 2.79 represents a wave of angular frequency p , the peak amplitude of which varies relatively slowly from $2\hat{H}$ to $-2\hat{H}$. Thus the distortion arising in the flux wave will be partly due to the parabolic shape of the loop (characterized by the hysteresis loss coefficient) and partly due to the rise and fall of the slope of the loop axis (permeability) as the amplitude varies. The flux wave will contain components corresponding to the intermodulation of the two applied fields.

Latimer¹³ in 1935 and Kalb¹⁴ and Bennett in the same year derived analytically the amplitudes of the third order intermodulation products arising from the application of such simultaneous fields to a material having a B - H loop described by the parabolic loop equation.

In Eqn 2.75 the applied field strength $\hat{H} \cos pt$ is replaced by the R.H.S. of Eqn 2.79, i.e. the amplitude \hat{H} becomes $2\hat{H} \cos \omega t$. By resolving the resultant expression into terms containing only first order sines and cosines, the amplitudes of the intermodulation products were derived. A similar analysis was made for the case of two applied fields of very different amplitude; the amplitude corresponding to f_a being \hat{H} and that corresponding to f_b being $k\hat{H}$, where $k \ll 1$. The r.m.s. amplitude is $\hat{H}/\sqrt{2}$.

The results of these analyses are given in Table 2.2.

In the above discussion it has been assumed that the B - H loop is symmetrical. If there is a magnetic bias,

$$(2.75) \quad B = \hat{H}(a_{10} + a_{11}\hat{H}) \cos pt + \frac{8a_{02}}{3\pi} \hat{H}^2 \sin pt + a_{30} \frac{\hat{H}^3}{4} \cos 3pt - \frac{8a_{02}}{15\pi} \hat{H}^2 \sin 3pt \quad \text{Gs}$$

$$(2.76) \quad \hat{B}_{3a} = \frac{8}{15\pi} a_{02} \hat{H}_a^2 \quad \text{Gs}$$

$$(2.77) \quad \frac{\hat{B}_{3a}}{\hat{B}_a} = \frac{8a_{02}\hat{B}_a}{15\pi\mu^2}$$

$$(2.78) \quad \frac{E_{3a}}{E_a} = \frac{3\hat{B}_{3a}}{\hat{B}_a} = \frac{8a_{02}\hat{B}_a}{5\pi\mu^2} = 0.6 \tan \delta_h$$

Table 2.2 THIRD HARMONIC AND INTERMODULATION PRODUCT AMPLITUDES

Harmonic or intermodulation product	Peak amplitude of the harmonic or intermodulation products of the flux density \hat{B}_{3a} or $\hat{B}_{2a \pm b}$	$\frac{\hat{B}_{3a}}{\hat{B}_a}$ or $\frac{\hat{B}_{2a \pm b}}{\hat{B}_a}$	$\frac{E_{3a}}{E_a}$ or $\frac{E_{2a \pm b}}{E_a}$ assuming $f_a \approx f_b$
Applied field = $\hat{H}_a \cos 2\pi f t$			
$3f$	$\frac{8}{15\pi} \mu_o a_{02} \hat{H}_a^2$	$\frac{8}{15\pi} \cdot \frac{a_{02}}{\mu_o \mu^2} \hat{B}_a$	$0.6 \tan \delta_h$
Applied field = $\hat{H}_a(\cos 2\pi f_a t + \cos 2\pi f_b t)$, $f_a \rightarrow f_b$			
$2f_a - f_b$	$\frac{16}{15\pi} \mu_o a_{02} \hat{H}_a^2 \sqrt{\left[F^2 + \left(\frac{8}{3\pi}\right)^2\right]}$	$\frac{16}{15\pi} \frac{a_{02}}{\mu_o \mu^2} \hat{B}_a \sqrt{\left[F^2 + \left(\frac{8}{3\pi}\right)^2\right]}$	$0.4 \sqrt{\left[F^2 + \left(\frac{8}{3\pi}\right)^2\right]} \cdot \tan \delta_h$
$2f_b - f_a$		$= 0.740 \frac{a_{02}}{\mu_o \mu^2} \hat{B}_a$ if $F = 2$	$= 0.869 \tan \delta_h$ if $F = 2$
$2f_a + f_b$	$\frac{128}{45\pi^2} \mu_o a_{02} \hat{H}_a^2$	$\frac{128}{45\pi^2} \frac{a_{02}}{\mu_o \mu^2} \hat{B}_a$	$\frac{16}{5\pi} \tan \delta_h$
$2f_b + f_a$			$= 1.019 \tan \delta_h$
$3f_a$	$\frac{128}{225\pi^2} \mu_o a_{02} \hat{H}_a^2$	$\frac{128}{225\pi^2} \frac{a_{02}}{\mu_o \mu^2} \hat{B}_a$	$\frac{16}{25\pi} \tan \delta_h$
$3f_b$			$= 0.2037 \tan \delta_h$
Applied field = $\hat{H}_a(\cos 2\pi f_a t + k \cos 2\pi f_b t)$, $k \ll 1$, $f_a \rightarrow f_b$			
$2f_a - f_b$	$\frac{k}{2} \mu_o a_{02} \hat{H}_a^2 \sqrt{\left[F^2 + \left(\frac{8}{3\pi}\right)^2\right]}$	$\frac{k}{2} \frac{a_{02}}{\mu_o \mu^2} \hat{B}_a \sqrt{\left[F^2 + \left(\frac{8}{3\pi}\right)^2\right]}$	$\frac{3\pi k}{16} \sqrt{\left[F^2 + \left(\frac{8}{3\pi}\right)^2\right]} \cdot \tan \delta_h$
		$= 1.09k \frac{a_{02}}{\mu_o \mu^2} \hat{B}_a$ if $F = 2$	$= 1.28k \tan \delta_h$ if $F = 2$
$2f_b - f_a$	$\longrightarrow 0$	$\longrightarrow 0$	$\longrightarrow 0$
$2f_a + f_b$	$\frac{4k}{3\pi} \mu_o a_{02} \hat{H}_a^2$	$\frac{4k}{3\pi} \frac{a_{02}}{\mu_o \mu^2} \hat{B}_a$	$\frac{3k}{2} \tan \delta_h$
$2f_b + f_a$	$\longrightarrow 0$	$\longrightarrow 0$	$\longrightarrow 0$
$3f_a$	$\frac{8}{15\pi} \mu_o a_{02} \hat{H}_a^2$	$\frac{8}{15\pi} \frac{a_{02}}{\mu_o \mu^2} \hat{B}_a$	$0.6 \tan \delta_h$
$3f_b$	$\longrightarrow 0$	$\longrightarrow 0$	$\longrightarrow 0$

The results are based on the Rayleigh or Peterson parabolic hysteresis loop characterized by a permeability rise coefficient, a_{11} , and a hysteresis loss coefficient, a_{02} . The ratio a_{11}/a_{02} is designated F and equals 2 for a Rayleigh material.

The subscripts a and b refer to the applied fields of frequency f_a and f_b respectively; $3a$ refers to the third harmonic of f_a and $2a+b$ to one of the sum products, etc.

In the second case considered in the table, i.e. that for two equal amplitude fields, the ratios are relative to the amplitude of one of the two fundamentals. For ratios relative to the combined amplitude of the fundamentals, divide by 2.

The expressions are in SI units but they are readily converted to CGS units by putting $\mu_0 = 1$ and expressing B , H and a_{02} in gauss, oersteds and oersteds⁻¹ respectively.

e.g. due to a direct current in the winding, the analysis is invalidated. Both even and odd harmonics will be generated and their amplitudes cannot be predicted from any simple magnetic parameters. Data must be obtained experimentally for particular values of bias.

It is important to note that the third order summation products and the third harmonics of single or simultaneous fields depend only on the field strength and the hysteresis loss coefficient a_{02} . Thus a measure of the third harmonic amplitude is a good guide to the third order summation products. However the third order difference products depend on a_{02} and a_{11} . Unless the true value of $F (= a_{11}/a_{02})$ is known the amplitude of the third order difference products cannot be obtained from a knowledge of the third harmonic amplitude.

Although the values of a_{02} and F may easily be measured at low frequencies it cannot be assumed that these values will apply at high frequencies. That part of the magnetization process which gives rise to hysteresis is due to irreversible domain wall displacements. These walls have effective mass, compliance and friction which affects their motion when a field is applied. It has been observed in the high permeability manganese zinc ferrites that there is a relaxation of the domain wall motion at frequencies above 100 kHz. At these frequencies the amplitude permeability approaches the initial permeability and the third harmonic distortion decreases.

Latimer¹⁵ calculated the third order intermodulation products for the case of an elliptical loop in which the slope of the major axis, corresponding to the permeability, and the area, corresponding to the loss, obeys the Peterson relation, Eqn 2.37 and 2.38. The results show that the difference products are unchanged from the expressions shown in Table 2.2 except that the hysteresis coefficient and F are no longer the usual low frequency values. All the other terms are zero.

Thus the transition of the $B-H$ loop from parabolic to elliptical would be accompanied by a fading out of the third harmonic and the third order sum products but not the difference products. Such a transition is probably an over-simplification but the results given in Fig. 3.18 tend to support the general hypothesis.

The conclusion must be that while the results quoted in Table 2.2 are a useful guide to the amplitudes of the distortion products, their use at higher frequencies is limited because the values of the material constants are generally unknown at these frequencies and the parabolic loop equation is probably not applicable.

2.3. THE EXPRESSION OF HIGH-AMPLITUDE PROPERTIES

At the beginning of this chapter the $B-H$ loop was described and the amplitude permeability was defined as

$$\mu_a = \frac{\hat{B}}{\mu_0 \hat{H}} \quad (2.80)$$

As the field strength or flux density increases from zero the amplitude permeability rises until it reaches a maximum value at the knee of the magnetization curve and then it falls progressively as the amplitude is further increased.

At these high amplitudes the $B-H$ relation becomes increasingly non-linear so that there is appreciable waveform distortion. There are two limiting cases, (1) the field strength waveform may be made sinusoidal by driving the magnetizing winding from a high impedance source or (2) the flux waveform may be made sinusoidal by driving from a low impedance source. In the latter case the winding resistance must not be high enough to cause appreciable voltage drop. The waveforms associated with each case are shown in Plate 2.1.

Due to this appreciable non-linearity it becomes prohibitively difficult to express the magnetic performance with any accuracy in terms of coefficients and a.c. theory. It is usual therefore to express the high-amplitude loss of a magnetic material as power dissipated per unit volume. This may be measured by a wattmeter or a calorimeter and may be expressed as a function of frequency and flux density. For such data to be truly descriptive of the material, i.e. independent of size and shape of the core, the eddy current loss must be excluded either by using cores suitably dimensioned to make this loss negligible or by calculating its magnitude (e.g. from Eqn 2.48) and subtracting it from the measured loss. Thus the high-amplitude loss normally quoted is the loss due to the area of the $B-H$ loop. It is normally called hysteresis loss although at high frequencies other loss processes may contribute. To obtain the total loss for a given core, the eddy current loss must be calculated for that core and, if significant, it must be added to the hysteresis loss.

REFERENCES AND BIBLIOGRAPHY

Section 2.1.

HARRINGTON, R. F., *Introduction to electromagnetic engineering*, McGraw-Hill Book Co., Inc., (1958).

BLEANEY, B. I. and BLEANEY, B., *Electricity and magnetism*, Oxford at the Clarendon Press, 2nd edition, (1965).

Section 2.2.2.

1. OLSEN, E., private communication.

Section 2.2.3.

2. OLSEN, E., See 'General'.

3. RAYLEIGH, LORD, 'Notes on electricity and magnetism III. On the behaviour of iron and steel under the

$$(2.80) \mu_a = \Delta \hat{B} / \Delta \hat{H}$$

operation of feeble magnetic forces', *Phil. Mag.*, **23**, 225, (1887).

4. PETERSON, E., 'Harmonic production in ferromagnetic materials at low frequencies and low flux densities', *Bell, Syst. Tech. J.*, **7**, 762, (1928).

Section 2.2.4.

5. VAN UITERT, L. G., 'Dielectric properties of and conductivity in ferrites', *Proc. Inst. Radio Engrs*, **44**, 1294, (1956).
6. VAN DER BURGT, C. M. and GEVERS, M., unpublished report.
7. BROCKMAN, F. G., DOWLING, P. H. and STENECK, W. G., 'Dimensional effects resulting from a high dielectric constant found in a ferromagnetic ferrite', *Phys. Rev.*, **77**, 85, (1950).

Section 2.2.6.

8. JORDAN, H., 'Die ferromagnetischen Konstanten für schwache Wechselfelder', *Elekt. Nachr. Tech.*, **1**, 7, (1924).
9. LEGG, V. E., 'Magnetic measurements at low flux densities using the alternating current bridge', *Bell Syst. tech. J.*, **15**, 39, (1936).
10. SNOEK, J. L., *New developments in ferromagnetic materials*,

Elsevier Publishing Company, Inc., New York—Amsterdam, (1947).

11. Specification A-II and III, C.C.I.F., Firenze, **Tome III**, 227, (1951).
12. *I.E.C. Publication 125*—see General.

Section 2.2.7.

13. LATIMER, K. E., 'Intermodulation in loaded telephone cables', *Electr. Commun.*, **14**, 275, (1935–36).
14. KALB, R. M. and BENNET, W. R., 'Ferromagnetic distortion of a two-frequency wave', *Bell Syst. tech. J.*, **14**, 322, (1935).
15. LATIMER, K. E., 'Non-linearity in magnetic core materials at low field strengths', *Soft Magnetic Materials*, Editors, C. E. Richards and A. C. Lynch, Pergamon Press Ltd., London, (1953).
- KÖHLER, J. W. L., 'Non-linear distortion phenomena of magnetic origin', *Philips tech. Rev.*, **2**, 193, (1937).

General

- OLSEN, E., *Applied magnetism, a study in quantities*, Philips Technical Library, Eindhoven, (1966).
- 'General classification of ferromagnetic oxide materials and definitions of terms', *International Electrotechnical Commission, Publication 125*, Geneva, (1961), plus Amend. no. 1, (1965).

Properties of some Manganese Zinc and Nickel Zinc Ferrites

3.1. INTRODUCTION

This chapter presents a wide range of data relating to the technical properties of currently available manganese zinc and nickel zinc ferrites. In the majority of cases the information is intrinsic to the material, i.e. it is not, in the theoretical sense, dependent on the core geometry. The purpose is to provide the designer with the data necessary to predict the performance of a given core under a wide variety of conditions, e.g. frequency, flux density, temperature, etc. The relations between the material properties described here and the core performance are considered in the next chapter; they depend essentially on the core geometry.

In practice the intrinsic material properties may also depend somewhat on the size and shape of the core due to the limitations imposed by the manufacturing processes, e.g. a core with a large cross-section may have a material permeability that differs from that of a smaller cross-section core made from the same powder because the exposure to kiln conditions is different in the two cases (see Section 1.3.7). Thus, although in theory the data presented here may be used to predict the properties of a given core, in practice some margin must be allowed for geometry-dependent variations arising in manufacture.

All the data appearing in this chapter refer, as far as possible, to typical properties of the materials indicated.

Although the designer usually requires limit values it would not be appropriate to include them here as they are essentially a matter of contract between the supplier and purchaser. In any case, the range of data required by a designer is far larger than the scope of a normal magnetic material specification.

Any survey of material properties must in some respects be inadequate. It will be incomplete because (i) it must be kept to a reasonable size by selection, (ii) data from some manufacturers may be more easily accessible than from others and (iii) some manufacturers, or particular grades of material, may have been over-looked. The data were selected according to the following procedure. The first step was to compile a list describing the electrical and magnetic data that are useful in ferrite applications. These data are usually available as measured functions expressed graphically. An attempt was made to obtain such data from all the principal manufacturers known to the author; he apologises now for any omissions. All available data were correlated to the prepared list and the selection was made on the widest possible basis. The data for some of the figures were specially prepared by the author and his colleagues and consequently relate only to ferrites manufactured by the Company with which the author is associated. However the range of materials and manufacturers represented has been as wide as possible, and the emphasis has been on the variety of

types and grades currently available rather than on comparisons of competitive products. Indeed quantitative comparisons based on typical data would be quite unreliable.

In cases where particular information on a grade of ferrite is, for some reason, omitted it may often be inferred from the corresponding data of a similar grade of ferrite, the similarity being established by a comparison of those properties that are given for both types.

All types and grades are referred to by the manufacturer's codes. At first they are classified broadly according to applications and tabulated against the manufacturer's name. This table provides a general guide to types currently available at the time of going to press and enables any code number to be identified with a manufacturer.

The application classification is followed by data on the mechanical and thermal properties. The next section starts with a table of electrical and magnetic properties in which typical values are given for the parameters that are normally quoted in manufacturers' catalogues. Then follows the main part of the chapter, i.e. the graphical data. This starts with the $B-H$ loops and ranges through all the more important properties.

3.2. SURVEY AND CLASSIFICATION

A study has been made of the catalogues and trade literature of all manufacturers of manganese zinc and nickel zinc ferrites known to the author. Only magnetically soft ferrites suitable for inductors and transformers (in the broadest sense of these terms) were considered. It appeared that although there are very many grades and types of ferrite, nearly all of them could be placed into relatively few categories according to the principal application for which they are intended. The application classification is as follows:

Manganese zinc ferrites

- I Inductors for frequencies up to about 200 kHz.
- II Inductors for the approximate frequency range 100 kHz to 2 MHz. Antenna rods for medium and long wave broadcast bands
- III High permeability applications, in particular wide band transformers (lower cut-off frequency up to about 10 MHz) and low power pulse transformers.
- IV Applications requiring high saturation flux density and low loss at high flux densities, in particular television line scanning transformers, deflection yokes and power transformers for the approximate frequency range 700 Hz to 100 kHz.

Nickel zinc ferrites

- V $\mu > 1000$. Wide band transformers for the approximate frequency range 1 to 300 MHz, pulse transformers for short duration pulses, e.g. $t_d < 0.1 \mu s$.
- VI μ : 500 to 1000. Wide band transformers for the approximate frequency range 5 to 300 MHz. Antenna rods for medium and long wave broadcast bands. Power transformers for the approximate frequency range 100 kHz to 1 MHz.
- VII μ : 160 to 490. Antenna rods for medium and long wave broadcast bands. Power transformers for the approximate frequency range 500 kHz to 5 MHz.
- VIII μ : 70 to 150. Inductors in the approximate frequency range 2 to 20 MHz. Antenna rods for short wave broadcast bands. Power transformers for the approximate frequency range 2 to 30 MHz.
- IX μ : 35 to 65. Inductors for the approximate frequency range 10 to 40 MHz.
- X μ : 12 to 30. Inductors for the approximate frequency range 20 to 60 MHz.
- XI $\mu < 10$. Inductors for frequencies above about 30 MHz.

The classification of all the grades and types of material which were included in the survey is shown in Table 3.1. Although great care has been taken omissions are inevitable and it must be recognized that in due course such a table becomes out-of-date. Nevertheless it does give a broad picture of the commercial availability of manganese zinc and nickel zinc ferrites that have been developed for inductors and transformers.

Notes: Where a manufacturer has several grades of ferrite in one category this may be due to the introduction of improved grades or because there are several versions of a given grade, each having a special specification, e.g. a particular temperature factor. The relative merit of different manufacturers' ferrites should not be assumed from the relative positions of entries. Relative performance may only be established by reference to manufacturers' specifications; the vertical columns of the table simply indicate application classification.

Sometimes the application of a particular grade is obscure or the catalogue places a given grade in several categories; in such cases the grade may appear several times.

Finally there are a number of special grades of these ferrites which are intended for applications not covered by the scope of this book, e.g. magnetostrictive ferrites and specially dense ferrites used for recording heads; in general these have not been included.

Table 3.1. SURVEY OF SOME FERRITE GRADES

APPLICATION					
Class	I	II	III	IV	V
Initial permeability	800-2500	500-1000	1500-10 000	1000-3000	> 1000
Main applications	Inductors	Inductors Antenna rods	Wide band & pulse transformers	High B_{sat} applns., T.V. & power transformers	Wide band & pulse transformers
Approx. frequency range	< 200 kHz	100 kHz-2 MHz	LF-200 MHz	< 100 kHz	1-300 MHz
Manufacturer and trade name					
UNITED KINGDOM					
1 Aladdin Components Ltd. Feradin					
2 Mullard Ltd. Ferroxcube	A1 A5 A13	A10	A5T A8 A7 A15	A2 A3 A9 A16	
3 Neosid Ltd.	F7 F8 F8A	F11	F7 F8A		
4 The Plessey Company Ltd.	M2 T5 T11	T21 T31	T5 T5T	NW27 NW29 NW26	
5 S.E.I. Ltd. Feralex	P R	S	P	R	
6 S.T.C. Ltd. Stanferite	SA503 SA502 SA500L	SA401	SA500T SA601		
HOLLAND					
7 N.V. Philips Ferroxcube	3B 3B3 3B5 3H1 3B7	3D3	3E1 3E2 3E3	3C2 3C6 3C7 3C8	
FRANCE					
8 Cofelec Ferrinox	T4 T6 T10 T14 T22	B10* T31*	B50 T6	B30 B42 B50	
9 Coprim Ferroxcube	3B 3B3 3B5 3H1 3B7	3D3	3E1 3E2 3E3	3C6 3C7 3C8	
10 L.T.T. Fermalite Fernilite	2002 1004 1002 2005	1005	2002 2003	3002 3001	2101
GERMANY					
11 Krupp Widia-Fabric Hyperox	D1S4 D1S2 D1S3		C3 D1 D1S1	C2 C22 C21	E1
12 Neosid Pemetzrieder GmbH					
13 Siemens A.G. Siferrit	N22 N28 N29	M33	T26 N30 T35 T38	N20 N27	
14 Steatite Magnesia Keraperm	417	615	417	407 417	
15 Valvo GmbH Ferroxcube	3B 3B3 3B5 3H1 3B7	3D3	3E1 3E2 3E3	3C6 3C7 3C8	

<i>CLASSIFICATION</i>							
<i>Class</i>	<i>V</i>	<i>VI</i>	<i>VII</i>	<i>VIII</i>	<i>IX</i>	<i>X</i>	<i>XI</i>
<i>Initial permeability</i>	> 1000	500-1000	160-490	70-150	36-65	12-30	< 10
<i>Main applications</i>	Wide band & pulse transformers	H.F. Wide band & power transformers, Antenna rods	Antenna rods, H.F. power transformers	Inductors, Antenna rods, H.F. power transformers	Inductors	Inductors	Inductors
<i>Approx. frequency range</i>	1-300 MHz	100 kHz 300 MHz	500 kHz-5 MHz	2-30 MHz	10-40 MHz	20-60 MHz	> 30 MHz

Manufacturer and trade name

UNITED KINGDOM

1	Aladdin Components Ltd. Feradin			R1	R4 R5	R6 R8	R9 R10	
2	Mullard Ltd. Ferroxcube		B1	B2	B10	B4	B5	
3	Neosid Ltd.			F14A	F16 F17	F25		F29
4	The Plessey Company Ltd.			NW25	NW6 NW10 H32			
5	S.E.I. Ltd. Feralex		K2	K4	K6	K8		
6	S.T.C. Ltd. Stanferite		SB700	SB600	SB500	SB400	SB300	

HOLLAND

7	N.V. Philips Ferroxcube		4A1 4A4	4B1	4C1 4C6 4C7	4D1 4D2	4E1	1Z3
---	----------------------------	--	---------	-----	-------------	---------	-----	-----

FRANCE

8	Cofelec Ferrinox			H20	H30 H32	H50	H60 H52	
9	Coprim Ferroxcube		4A1 4A3	4B1	4C1 4C7	4D1	4E1	
10	L.T.T. Fermalite Fermalite	2101	1101	1102	1112 1103	1104	1105	

GERMANY

11	Krupp Widia-Fabric Hyperox	E1	E2 E3	E4	E5	E6	E7	
12	Neosid Pemetzrieder GmbH		F1	F2	F106	F20	F40	F100
13	Siemens A.G. Siferrit			M11	K1		K12	U17 U60
14	Steatite Magnesia Keraperm		503	606 612	602		704 814	
15	Valvo GmbH Ferroxcube		4A1 4A3 4A4	4B1	4C1 4C6 4C7	4D1	4E1	

APPLICATION					
Class	I	II	III	IV	V
Initial permeability	800–2500	500–1000	1500–10 000	1000–3000	> 1000
Main applications	Inductors	Inductors Antenna rods	Wide band & pulse transformers	High B_{sat} applns., T.V. & power transformers	Wide band & pulse transformers
Approx. frequency range	< 200 kHz	100 kHz–2 MHz	LF–200 MHz	< 100 kHz	1–300 MHz
Manufacturer and trade name					

U.S.A.

16	Allen-Bradley Co.	W-O3 W-5			W-O3 W-O4 W-5	
17	Ceramic Magnetics Inc.	MN-30 MN-60	MN-30 MN-31	MN-30	MN-31	CM-2002
18	Fair-rite Products Corp.	71 72 73	31 32 33			
19	Ferroxcube Corp. Ferroxcube	3B9 3B7	3D3	3E 3E2A 3E3	3E 3C5	4A6
20	Indiana General Corp. Ferramic	TC-6 TC-7	TC-3	O-5 O-6	O-5	
21	Magnetics Inc.	C D G	A	A C D G	C D	
22	National Moldite Co. Inc.	D*	71*			
23	Stackpole Carbon Co. Ceramag	C24 C26	C27A	C24	C24A	
24	D. M. Steward Manufacturing Co.	F-112				

JAPAN

25	Nippon Electric Co. Ltd. Neferrite	C*		D1* D2 D3		
26	Nippon Ferrite Industrial Co. Ltd.	VL-71 VL-74 FQ-2 GP-5 GP-3 GQ-2 SB-5 FB-5	AL-3 CL-81	VL-71 VL-74 FB-3 GP-5	VL-71 VL-74 SB-5 FB-5 FB-3	
27	Sony Corp.	407*FBM FB1 FB4 FB4A	503* 403 FB1	204 FBL FC1 FC2 FC4	304 307	4B1*
28	Tohoku Metal Industries Ltd.	1801F	801F	4000H 7000H 12000H	1300B 1500B 3000B	2000L

- (i) See text for the description of this table.
- (ii) The application classifications are summarized at the heads of the columns; they are defined more completely in the text.
- (iii) As far as is known classifications I to IV are basically manganese zinc ferrites and V to XI are basically nickel zinc ferrites. Exceptions are 1Z2 and 1Z3, which are hexagonal structures, and AL-3 and CL-81 which, although appearing in column II are nickel zinc ferrites.

CLASSIFICATION							
Class	V	VI	VII	VIII	IX	X	XI
Initial permeability	> 1000	500-1000	160-490	70-150	36-65	12-30	< 10
Main applications	Wide band & pulse transformers	H.F. Wide band & power transformers, Antenna rods	Antenna rods, H.F. power transformers	Inductors, Antenna rods, H.F. power transformers	Inductors	Inductors	Inductors
Approx. frequency range	1-300 MHz	100 kHz 300 MHz	500 kHz-5 MHz	2-30 MHz	10-40 MHz	20-60 MHz	> 30 MHz

Manufacturer and trade name

U.S.A.

16	Allen-Bradley Co.		W-O1	R-O2			
17	Ceramic Magnetics Inc.	CM-2002	CN-20 C-2025	C-2050 C-2075	C-2075 N-51	N-50	N-40
18	Fair-rite Products Corp.			64 62	61 65 51	63	
19	Ferroxcube Corp. Ferroxcube	4A6	4A	4B	4C 4C4	4D	4E 1Z2
20	Indiana General Corp. Ferramic		H		TC-4 Q-1	Q-2	Q-3
21	Magnetics Inc.				N		
22	National Moldite Co. Inc.				M	M2*	
23	Stackpole Carbon Co. Ceramag		C7A C5N	C9	C11 C11A	C12	C2285 C2285A
24	D. M. Steward Manufacturing Co.		F4S-1		F-220		F6-21

JAPAN

25	Nippon Electric Co. Ltd. Neferrite						
26	Nippon Ferrite Industrial Co. Ltd.		L-84 L-85 T-314 TH-100 CL-81	LK-100 QL-400 L-81 QM-051 KQ-1 L-82	QM-101 QM-201 LM-81	MH-81 VH-40 KM-45 1T-1 MH-90	VH-50 VH-100 VH-150 VH-200 VH-300
27	Sony Corp.	4B1*	5A5 KT23	KT21 KT41	6A6 KM21	6A7	KH51 KH72 KH75
28	Tohoku Metal Industries Ltd.	2000L		250L 400L	80L 100L	40L	20L 10L

*(iv) Often associated companies use the same code number for equivalent material grades. However, sometimes quite different ferrites manufactured by unrelated companies have by chance identical code numbers; to avoid ambiguity in the graphical data only those material grades printed in bold type are quoted in Figs. 3.1 to 3.24.

INDEX TO FERRITE CODE NUMBERS LISTED IN TABLE 3.1

<i>Ferrite code number</i>	<i>Manufacturer ref.</i>	<i>Ferrite code number</i>	<i>Manufacturer ref.</i>	<i>Ferrite code number</i>	<i>Manufacturer ref.</i>
A	21	D3	25	KM21	27
AL-3	26			KM-45	26
A1	2	E1	11	KQ-1	26
A2	2	E2	11	KT21	27
A3	2	E3	11	KT23	27
A5	2	E4	11	KT41	27
A5T	2	E5	11	K1	13
A7	2	E6	11	K2	5
A8	2	E7	11	K4	5
A9	2			K6	5
A10	2	FBL	27	K8	5
A13	2	FBM	27	K12	13
A15	2	FB1	27		
A16	2	FB-3	26	LK-100	26
		FB4	27	LM-81	26
B1	2	FB4A	27	L-81	26
B2	2	FB-5	26	L-82	26
B4	2	FC1	27	L-84	26
B5	2	FC2	27	L-85	26
B10	2	FC4	27		
B10*	8	FQ-2	26	M	22
B30	8	F1	12	MH-81	26
B42	8	F2	12	MH-90	26
B50	8	F4S-1	24	MN-30	17
		F6-21	24	MN-31	17
C	21	F7	3	MN-60	17
C*	25	F8	3	M2	4
CL-81	26	F8A	3	M2*	22
CM-2002	17	F11	3	M11	13
CN-20	17	F14A	3	M33	13
C2	11	F16	3		
C3	11	F17	3	N	21
C5N	23	F20	12	NW6	4
C7A	23	F25	3	NW10	4
C9	23	F29	3	NW25	4
C11	23	F40	12	NW26	4
C11A	23	F100	12	NW27	4
C12	23	F106	12	NW29	4
C21	11	F-112	24	N20	13
C22	11	F-220	24	N22	13
C24	23			N27	13
C24A	23	G	21	N28	13
C26	23	GP-3	26	N29	13
C27A	23	GP-5	26	N30	13
C-2025	17	GQ-2	26	N-40	17
C-2050	17			N-50	17
C-2075	17	H	20	N-51	17
C2285	23	H20	8		
C2285A	23	H30	8	O-5	20
		H32	4, 8	O-6	20
		H50	8		
D	21	H52	8	P	5
D*	22	H60	8		
D1	11			QL-400	26
D1*	25			QM-051	26
D1S1	11	IT-1	26	QM-101	26
D1S2	11			QM-201	26
D1S3	11	KH51	27	Q-1	20
D1S4	11	KH72	27	Q-2	20
D2	25	KH75	27		

continued

<i>Ferrite code number</i>	<i>Manufacturer ref.</i>	<i>Ferrite code number</i>	<i>Manufacturer ref.</i>	<i>Ferrite code number</i>	<i>Manufacturer ref.</i>
Q-3	20	W-03	16	64	18
R	5	W-04	16	65	18
R1	1	W-5	16		
R-O2	16			71	18
R4	1	1Z2	19	71*	22
R5	1	1Z3	7, 15	72	18
R6	1			73	18
R8	1	3B	7, 9, 15		
R9	1	3B3	7, 9, 15	80L	28
R10	1	3B5	7, 9, 15	100L	28
		3B7	7, 9, 15, 19	204	27
S	5	3B9	19	250L	28
SA401	6	3C2	7	304	27
SA500L	6	3C5	19	307	27
SA500T	6	3C6	7, 9, 15		
SA502	6	3C7	7, 9, 15	400L	28
SA503	6	3C8	7, 9, 15	403	27
SA601	6	3D3	7, 9, 15, 19	407	14
SB-5	26	3E	19	407*	27
SB-300	6	3E1	7, 9, 15	417	14
SB-400	6	3E2	7, 9, 15		
SB-500	6	3E2A	19	503	14
SB-600	6	3E3	7, 9, 15, 19	503*	27
SB-700	6	3H1	7, 9, 15		
		4A	19	602	14
TC-3	20	4A1	7, 9, 15	606	14
TC-4	20	4A3	9, 15	612	14
TC-6	20	4A4	7, 15	615	14
TC-7	20	4A6	19	704	14
TH-100	26	4B	19	801F	28
T4	8	4B1	7, 9, 15	814	14
T5	4	4B1*	27	1002	10
T5T	4	4C	19	1004	10
T6	8	4C1	7, 9, 15	1005	10
T10	8	4C4	19	1101	10
T11	4	4C6	7, 15	1102	10
T14	8	4C7	7, 9, 15	1103	10
T21	4	4D	19	1104	10
T22	8	4D1	7, 9, 15	1105	10
T26	13	4D2	7	1112	10
T31	4	4E	19		
T31*	8	4E1	7, 9, 15	1300B	28
T35	13			1500B	28
T38	13	5A5	27	1801F	28
T-314	26	6A6	27	2000L	28
		6A7	27		
U17	13			2002	10
U60	13	10L	28	2003	10
		20L	28	2005	10
				2101	10
VH-40	26				
VH-50	26	31	18	3000B	28
VH-100	26	32	18	3001	10
VH-150	26	33	18	3002	10
VH-200	26				
VH-300	26	40L	28	4000H	28
VL-71	26	51	18	7000H	28
VL-74	26	61	18	12000H	28
		62	18		
W-01	16	63	18		

Table 3.2 MECHANICAL PROPERTIES OF SOME FERRITES

Ferrite grade No.	Pressed or Extruded	ρ_s p	Ultimate tensile strength			Ultimate compressive strength			Young's modulus of elasticity			Impact strength (Charpy) ft lb		
			x	s	n	x	s	n	x	s	n	x	s	n
A1	P	4700-4800 8.4-6.4	6.4 9.1×10^3	0.19 0.27×10^3	6	53 75×10^3	0.7 1.0×10^3	4	15.0×10^3 2.13×10^7	0.28×10^3 0.04×10^7	6			
	E		3.6 5.1×10^3	0.77 1.1×10^3	8	74 105×10^3	9.4 13.4×10^3	5	15.9×10^3 2.36×10^7	4.2×10^3 0.60×10^7	8	0.0319	0.0012	5
A5	P	4700-4800 8.4-6.4	4.0 5.7×10^3	1.05 1.5×10^3	3	60 86×10^3	4.8 6.8×10^3	2	12.9×10^3 1.84×10^7	0.21×10^3 0.03×10^7	3			
	E		3.2 4.6×10^3	0.91 1.3×10^3	4	42 60×10^3	13.3 19×10^3	5	13.6×10^3 1.93×10^7	0.49×10^3 0.07×10^7	4	0.0320	0.0012	5
A9	P	4700-4770 7.5-6.1	4.6 6.5×10^3	0.70 1.0×10^3	6	22 31×10^3	2.5 3.6×10^3	2	12.5×10^3 1.78×10^7	0.56×10^3 0.08×10^7	6			
	E		4.8 6.8×10^3	0.14 0.2×10^3	5	60 85×10^3	5.9 8.4×10^3	5	12.5×10^3 2.08×10^7	0.35×10^3 0.05×10^7	5	0.0334	0.0009	5
A10	P	4500-4600 10.6-9.6	3.7 5.3×10^3	1.12 1.6×10^3	5			5	9.2×10^3 1.31×10^7	0.84×10^3 0.12×10^7	5			
	E		3.9 5.5×10^3	0.51 0.72×10^3	5	44 62×10^3	8.8 12.5×10^3	5	11.0×10^3 1.56×10^7	0.56×10^3 0.08×10^7	5	0.0310	0.0011	5
B1	P	4810-4970 9.1-6.1	5.1 7.3×10^3	0.32 0.46×10^3	6	69 98×10^3	13.3 19×10^3	5	14.6×10^3 2.07×10^7	0.49×10^3 0.07×10^7	6			
	E		3.9 5.6×10^3	0.37 0.53×10^3	5	42 60×10^3	3.6 5.1×10^3	5	12.7×10^3 1.80×10^7	1.4×10^3 0.20×10^7	5	0.0344	0.0005	5
B2	P	4660-4840 14.0-8.7	5.1 7.3×10^3	0.53 0.75×10^3	6	41 58×10^3	7.7 11×10^3	5	14.0×10^3 1.99×10^7	0.56×10^3 0.08×10^7	6			
	E		6.4 9.1×10^3	0.53 0.75×10^3	5	51 73×10^3	5.1 7.3×10^3	5	14.4×10^3 2.04×10^7	0.28×10^3 0.04×10^7	5	0.0311	0.0011	5
B3	P	4600-4880 13.4-8.1	5.1 7.2×10^3	0.63 0.89×10^3	6	44 63×10^3	13.3 19×10^3	3	11.5×10^3 1.64×10^7	0.35×10^3 0.06×10^7	6			
	E		5.3 7.6×10^3	1.34 1.9×10^3	6				11.4×10^3 1.62×10^7	0.28×10^3 0.04×10^7	6	0.0331	0.0020	5
B4	P	4360-4620 18.0-13.2	6.0 8.5×10^3	0.50 0.71×10^3	6				12.5×10^3 1.78×10^7	0.56×10^3 0.08×10^7	6			
	E		4.0 5.8×10^3	0.84 1.2×10^3	3	42 60×10^3	5.6 8×10^3	5	9.8×10^3 1.40×10^7	1.83×10^3 0.26×10^7	3	0.0328	0.0011	5
B5	P	4070-4290 24-20	3.2 4.6×10^3	0.34 0.48×10^3	6	18 26×10^3	0.84 1.2×10^3	4	8.2×10^3 1.16×10^7	0.63×10^3 0.09×10^7	6			
	E		6.1 8.7×10^3	1.55 2.2×10^3	5	27 39×10^3	6.9 9.8×10^3	5	8.7×10^3 1.23×10^7	0.35×10^3 0.05×10^7	5	0.0303	0.0011	5
Average values	P		4.9 7.0×10^3			44			11.3×10^3 1.61×10^7					
	E		4.6 6.5×10^3			48 68×10^3			12.2×10^3 1.74×10^7			0.0322		

 ρ_s = sintered density in kg.m^{-3} ($1000\text{kg.m}^{-3} = 1 \text{ g.cm}^{-3}$) p = porosity, per cent x = mean value in $\left\{ \begin{array}{l} \text{kgf.mm}^{-2} \\ \text{lb.in}^{-2} \end{array} \right\}$ s = standard deviation, in $\left\{ \begin{array}{l} \text{kgf.mm}^{-2} \\ \text{lb.in}^{-2} \end{array} \right\}$

in experimental determination

 n = number of specimensNote. kgf = weight of 1 kg \approx 9.81 newtons

Apart from being a broad survey of ferrite grades Table 3.1 provides a means of identifying the grade numbers in the graphical data which forms the major part of this chapter. In some instances different manufacturers use the same code numbers to designate quite different materials; to avoid ambiguity all grades quoted in the graphical data are printed in heavy type.

3.3 MECHANICAL AND THERMAL PROPERTIES

Ferrites, being ceramic materials formed by sintering, have mechanical properties similar to those of pottery. In particular the properties depend on the sintered density. As described in Chapter 1, the pressed core before firing consists of a relatively porous compact of oxides. During sintering the oxides react to form crystallites of the required composition, these crystallites nucleating at discrete centres and growing outwards until the boundaries meet those of neighbouring crystallites. During this process the density of the mass rises; if this process were to yield perfect crystals meeting at perfect boundaries the density would rise to the theoretical maximum, i.e. the X-ray density, ρ_x , which is the mass of material in a perfect unit crystal cell divided by the cell volume. In practice imperfections occur and the sintered mass has microscopic voids both within the crystallites and at the crystallite boundaries. The resulting density is referred to as the sintered density, ρ_s .

If the porosity is denoted by p then

$$p = 100(1 - \rho_s/\rho_x) \quad \text{per cent} \quad (3.1)$$

In normal production the porosity might range from 3% to 20% depending on the grade of ferrite.

In Table 3.2 typical values of the sintered density and porosity are given for a number of representative polycrystalline ferrites. The porosity has an effect on the mechanical and magnetic properties and low porosities are usually preferable. Since the majority of the pores do not open to the surface there is relatively little absorption from the environment and normally no protecting finish is required.

Recently ferrites have been developed having porosities less than 1%; indeed values of 0.1% have been reported.¹ These are particularly valuable in the manufacture of devices such as recording heads which require intricately formed, highly polished surfaces having the greatest possible wear resistance. High density ferrites having high permeability are used for transformer cores; for this application accurately lapped pole faces are essential.

Some of the principal mechanical properties of a representative selection of ferrite specimens have been determined by Sellwood.² The results, which have not been previously published, are given in Table 3.2. For each grade of ferrite there were two sets of measurements, one for pressed specimens and other for extrusions. The table gives the mean value, \bar{x} , the standard deviation, s , and the number of specimens used for each determination. It should be made clear that the specimens used for any set of measurements, e.g. A1 pressed specimens, were generally all obtained from one production batch because they had to be specially made to the required shape. Thus the standard deviations should not be applied to estimate normal spreads in production. Such production spreads may however be inferred from an inspection of the results for several closely related grades. Care should be exercised in using these figures, particularly the tensile strength values, since the presence of porosity, voids or hair-line cracks will in practice make the breaking load

Table 3.3. TYPICAL THERMAL PROPERTIES OF FERRITES

Property	Conditions	Value	Units
Coeff. of linear expansion			
MnZn ferrites	0–50°C	10×10^{-6}	$^{\circ}\text{C}^{-1}$
	0–200°C	11×10^{-6}	$^{\circ}\text{C}^{-1}$
NiZn ferrites	0–50°C	7×10^{-6}	$^{\circ}\text{C}^{-1}$
	0–200°C	8×10^{-6}	$^{\circ}\text{C}^{-1}$
Specific heat⁵			
MnZn ferrites	25°C	$\begin{cases} 1100 \\ 0.26 \end{cases}$	$\begin{cases} \text{J. kg}^{-1} \text{ } ^{\circ}\text{C}^{-1} \\ \text{cal. g}^{-1} \text{ } ^{\circ}\text{C}^{-1} \end{cases}$
NiZn ferrites	25°C	$\begin{cases} 750 \\ 0.18 \end{cases}$	$\begin{cases} \text{J. kg}^{-1} \text{ } ^{\circ}\text{C}^{-1} \\ \text{cal. g}^{-1} \text{ } ^{\circ}\text{C}^{-1} \end{cases}$
Thermal conductivity			
MnZn ferrites } NiZn ferrites }	25–85°C	$\begin{cases} 3500 \text{ to } 4300 \\ 35 \text{ to } 43 \\ 0.0083 \text{ to } 0.010 \end{cases}$	$\begin{cases} \mu\text{W. mm}^{-1} \text{ } ^{\circ}\text{C}^{-1} \\ \text{mW. cm}^{-1} \text{ } ^{\circ}\text{C}^{-1} \\ \text{cal. s}^{-1} \text{ cm}^{-1} \text{ } ^{\circ}\text{C}^{-1} \end{cases}$

Table 3.4 TYPICAL VALUES OF SPECIFICATION PARAMETERS FOR MANGANESE ZINC FERRITES

Property	Symbol or expression	Measuring conditions*				Principle application categories (see Table 3.1)				Units
		f kHz	B		Misc.	I L.F. inductors	II M.F. inductors, antenna rods	III W.B. and pulse transformers	IV High B _{sat} applns. T.V. and power transformers	
			mT	Gs						
Initial permeability	μ _i	< 10	< 0.1	< 1		800-2500	500-1000	1500-10,000	1000-3000	
Saturation flux density	B _{sat}				H = 1 A.mm ⁻¹ = 12.5Oe	0.35-0.5 3500-5000	~ 0.4 ~ 4000	0.3-0.5 3000-5000	0.35-0.52 3500-5200	T Gs
Remanence	B _r				from sat	0.08-0.14 800-1400	0.15-0.20 1500-2000	0.07-0.14 700-1400	0.1-0.25 1000-2500	T Gs
Coercivity	H _c				from sat	10-30 0.12-0.38	40-100 0.5-1.2	2.8-24 0.035-0.3	10-30 0.12-0.38	A.m ⁻¹ Oe
Residual loss factor	(tan δ _r)/μ	10 30 100 300 1000	< 0.1	< 1		0.8-1.8 1.3-3.0 2.0-10	5-15 10-40	1-10 2-20 4-60		10 ⁻⁶ 10 ⁻⁶ 10 ⁻⁶ 10 ⁻⁶ 10 ⁻⁶
Hysteresis coeff.	η _B	10	from 1 to 3	from 10 to 30		0.3-1.3	0.48-1.9	0.1-1.3		mT ⁻¹ × 10 ⁻⁶
	a	10	from 1 to 3	from 10 to 30		0.2-0.8	0.3-1.2	0.06-0.8		Gs ⁻¹ × 10 ⁻⁶
Power loss density	P _m	10 16	200 200	2000 2000	{ 25°C 85°C 25°C 85°C	45-130 60-130 70-210 95-210	250	50-150	50-120 50-120 80-190 80-190	{ μW.mm ⁻³ = mW.cm ⁻³
Curie point	θ _c	< 10	< 0.1	< 1		140-210	200-280	90-200	180-280	°C
Temperature factor	$\frac{(\mu_2 - \mu_1)}{\mu_1 \mu_2 (\theta_2 - \theta_1)}$	< 10	< 0.25	< 2.5	θ ₁ -40 + 5 + 25 + 25 θ ₂ + 25 + 55 + 70	1.0 to 2.5 -1.5 or 0.5 to 2.0 -0.6 to +0.6/or 0.5 to 1.5 0.5 to 1.8	5.0 1.0 to 3.0 1.0 to 3.0 1.0 to 3.0		}	°C ⁻¹ × 10 ⁻⁶
Disaccommodation factor	$\frac{(\mu_2 - \mu_1)}{\mu_1^2 \log_{10}(t_2/t_1)}$	< 10	< 0.25	< 2.5	e.g. t ₁ = 10 min t ₂ = 100 min	1-3	2-10	1-4		10 ⁻⁶
Resistivity	ρ	d.c.				0.5-7 50-700	1-20 100-2000	0.02-0.5 2-50	0.2-1.0 20-100	Ω.m Ω.cm

Table 3.5 TYPICAL VALUES OF SPECIFICATION PARAMETERS FOR NICKEL ZINC FERRITES

Property	Symbol or expression	Measuring conditions*				Principle application categories (see Table 3.1)							Units
		f	\hat{B}		Misc.	V W.B. and pulse trans- formers	VI H.F. W.B. and power transformers, antenna rods	VII Antenna rods, H.F. power transformers	$VIII$ Inductors, antenna, rods, H.F. power transformers	IX Inductors	X Inductors	XI Inductors	
			mT	Gs									
Initial permeability	μ_i	< 10 kHz	< 0.1	< 1		2000	500-1000	160-490	70-150	35-65	12-30	10	
Saturation flux density	B_{sat}					0.26 at $H = 1$ 2600 at $H = 12.5$	0.28-0.34 at $H = 1$ 2800-3400 at $H = 12.5$	0.3-0.36 at $H = 2$ 3000-3600 at $H = 2.5$	0.25-0.42 at $H = 4$ 2500-4200 at $H = 50$	0.24-0.28 at $H = 4$ 2400-2800 at $H = 50$	0.15-0.26 at $H = 8$ 1500-2600 at $H = 100$	0.1-0.2 at $H = 8$ 1000-2000 at $H = 100$	T A mm ⁻¹ Gs Oe
Remanence	B_r				from sat	0.85 850	0.15-0.19 1500-1900	0.12-0.16 1200-1600	0.24-0.34 2400-3400	0.15-0.20 1500-2000	0.08-0.15 800-1500	0.05-0.1 500-1000	T Gs
Coercivity	H_c				from sat	20 0.25	16-50 0.2-0.6	80-160 1.0-2.0	160-500 2.0-6.0	300-500 4.0-6.0	500-1600 6.0-20	800-1600 10-20	A m ⁻¹ Oe
Residual loss factor	(tan δ_r)/ μ	100 kHz 300 kHz 1 MHz 3 MHz 10 MHz 30 MHz 100 MHz	< 0.1	< 1		20	50 150-300	25-70 50-200	20-50 25-60 60-120	50-130 200-1000	150-200 200-500	130-1300 400-2000	10 ⁻⁶ 10 ⁻⁶ 10 ⁻⁶ 10 ⁻⁶ 10 ⁻⁶ 10 ⁻⁶ 10 ⁻⁶
Hysteresis coeff.	η_B a	10 kHz 10 kHz	from 1 to 3	from 10 to 30	{	6.4 4	4.8-14 3-9	11-16 7-10	1.6-48 1-30	64-95 40-60	64-130 40-80	8†, 400 5†, 250	mT ⁻¹ × 10 ⁻⁶ Gs ⁻¹ × 10 ⁻⁶
Curie point	θ_c	< 10 kHz	< 0.1	< 1		100	90-200	200-370	350-490	300-500	250-510	250-510	°C
Temperature factor	$\frac{(\mu_2 - \mu_1)}{\mu_1 \mu_2 (\theta_2 - \theta_1)}$	< 10 kHz	< 0.25	< 2.5	θ_1 θ_2 + 25 + 55	4	2 to 16	0 to 14	0 to 10	12 to 40	-10 to + 20		°C ⁻¹ × 10 ⁻⁶
Resistivity	ρ					10 10 ³	10-10 ⁷ 10 ³ -10 ⁹	> 10 ³ > 10 ⁵	> 10 ³ > 10 ⁵	> 10 ³ > 10 ⁵	> 10 ³ > 10 ⁵	> 10 ³ > 10 ⁵	Ω m Ω cm

These tables list the parameters that may be found in a ferrite material specification. In each of the application categories typical values of these parameters are given. They normally refer to toroidal specimens of the material; no limits are implied.

*The measuring temperature is 25°C unless otherwise stated.
†This low figure of hysteresis loss is obtained on specially heat treated nickel zinc ferrites (see Fig. 3.1. 24(b)).

uncertain. Some additional data are given in the literature.^{3, 4}

The average hardness of ferrite was measured on a limited number of samples. The results in terms of the Vickers Pyramid Number were 600 to 700 for manganese zinc ferrite and 800 to 900 for nickel zinc ferrite.

Table 3.3. gives typical values of the thermal properties of ferrites.

3.4. MAGNETIC AND ELECTRICAL PROPERTIES

Before presenting the graphical data it will be useful to give in tabular form, for each application category, typical values for those parameters which may be quoted in manufacturers' catalogues. These Tables, 3.4 and 3.5, enable comparisons between the categories of ferrite to be readily made. However it must be emphasized that the figures are merely representative of the category and should not be interpreted as being typical of any particular grade.

The rest of this chapter consists of graphical data presented as a series of figures, each dealing with a specific property as a function of an independent variable.

Each figure is accompanied by a brief commentary intended to draw attention to the salient features, to indicate in a qualitative way any underlying physical processes that may be relevant, and to provide cross-references and relevant formulae. Each commentary serves as an extended caption for all graphs in one figure. It indicates, after the heading, the values of those quantities, e.g. f , B , θ , etc., that were constant during the variation of the independent variable(s).

In general each figure consists of a number of graphs each displaying typical data for the grade or grades of ferrite indicated in the panel at the top right-hand corner. The order of the graphs appearing under one figure number is approximately in accordance with the application classifications listed in Section 3.1, e.g. any data relating to LF inductor grades would appear first while the data on higher frequency nickel zinc ferrites would appear in the later graphs. The grade references are those used by manufacturers and appear in the survey in Table 3.1.

It is emphasized once again that the data are typical and should not be used to compare the performance of similar grades manufactured by different Companies. Where comparison is required reference should be made to the manufacturer's specification.

INDEX TO GRAPHICAL DATA

		<i>Page.</i>		
Fig. 3.1.	<i>B-H</i> loops	47- 53	Fig. 3.14.	Residual loss tangent as a function of frequency with superimposed steady field as a parameter
Fig. 3.2.	Minor <i>B-H</i> loops	54- 60		135-137
Fig. 3.3.	Saturation flux density as a function of temperature	61- 64	Fig. 3.15.	Hysteresis loss factor as a function of flux density
Fig. 3.4.	Permeability as a function of high amplitude flux density	65- 71		138-140
Fig. 3.5.	Permeability as a function of low amplitude flux density	72- 73	Fig. 3.16.	Hysteresis loss factor as a function of frequency
Fig. 3.6.	Incremental permeability as a function of steady field strength	74- 83		141
Fig. 3.7.	Hanna curves	84- 90	Fig. 3.17.	Hysteresis loss factor as a function of temperature
Fig. 3.8.	Initial permeability as a function of temperature	91-100		142
Fig. 3.9.	Incremental permeability as a function of temperature with a steady field strength as a parameter	101-104	Fig. 3.18.	Magnetic distortion
Fig. 3.10.	Disaccommodation	105-107		143-147
Fig. 3.11.	Complex initial permeability	108-121	Fig. 3.19.	Power loss as a function of frequency at high flux densities
Fig. 3.12.	Residual loss factor spectrum	122-131		148-156
Fig. 3.13.	Residual loss factor as a function of temperature	132-134	Fig. 3.20.	Resistivity as a function of temperature
				157-159
			Fig. 3.21.	Resistivity and permittivity as functions of frequency
				160-163
			Fig. 3.22.	High frequency resistivity and permittivity as functions of temperature
				164-165
			Fig. 3.23.	Static magnetostriction
				166
			Fig. 3.24.	Initial permeability as a function of stress
				167-168

B-H Loops Fig. 3.1

$f \rightarrow 0$ (ballistic measurement)

A basic property of any magnetic material is the relation between flux density and field strength, the *B-H* loop. This figure shows the *B-H* loops for a wide and representative range of ferrites.

The *B-H* loops for the manganese zinc ferrites are given first and the later loops are for the nickel zinc ferrites. The saturation flux density depends on the composition and decreases as the temperature rises (see also Fig. 3.3); its effective value is also decreased by the porosity of the specimen.

At room temperature the saturation flux densities range from 0.30 to 0.45 T (3000 to 4500 Gs) for the manganese zinc ferrites quoted and from 0.12 to 0.41 T (1200 to 4100 Gs) for the nickel zinc ferrites.

The coercivities range from 16 to 80 A.m^{-1} (0.2 to 1.0 Oe) for the manganese zinc ferrites and from 16 A.m^{-1} (0.2 Oe) for the nickel zinc ferrite having the highest zinc content to about 1400 A.m^{-1} (18 Oe) for nickel ferrite having no zinc.

The area of the *B-H* loop is a measure of the energy loss due to hysteresis in a unit volume during one cycle

of magnetization. At high frequencies residual loss and eddy current loss will generally modify the loop shape. Thus the loop area is only an indication of the high amplitude low frequency loss; the losses at small amplitudes, e.g. the loss represented by the hysteresis coefficient, cannot be inferred.

Fig. 3.1.24 illustrates *B-H* loops obtained by special heat treatment of nickel zinc ferrites having small cobalt additions.

(See also Section 2.1)

Field strength $H = NI/l$ A.m^{-1} (See Eqn 2.1)

Flux density $B = \mu_0 \mu H$ T (See Eqn 2.8)

Magnetic polarization $J = B - \mu_0 H$ T (See Eqn 2.5)

Hysteresis energy loss density $w_h = \oint B dH$ $\text{J.m}^{-3} \text{ cycle}^{-1}$ (See Eqn 2.33)

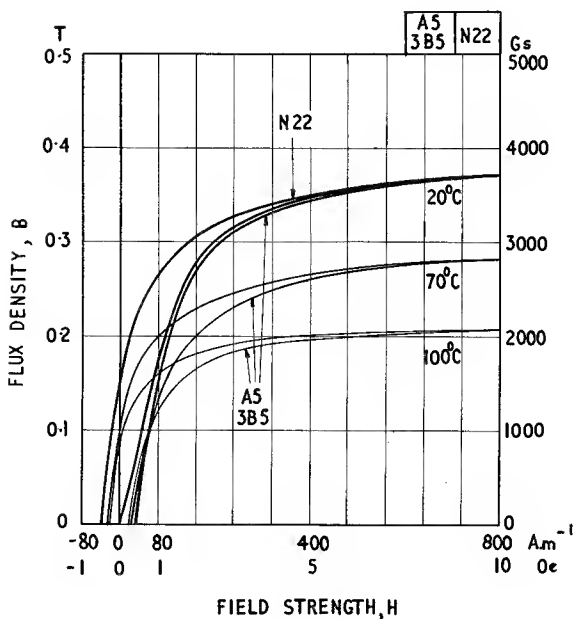


Fig. 3.1.1

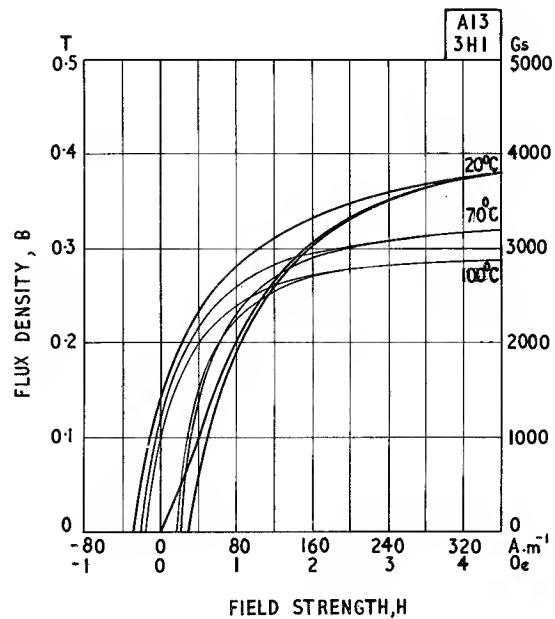


Fig. 3.1.2

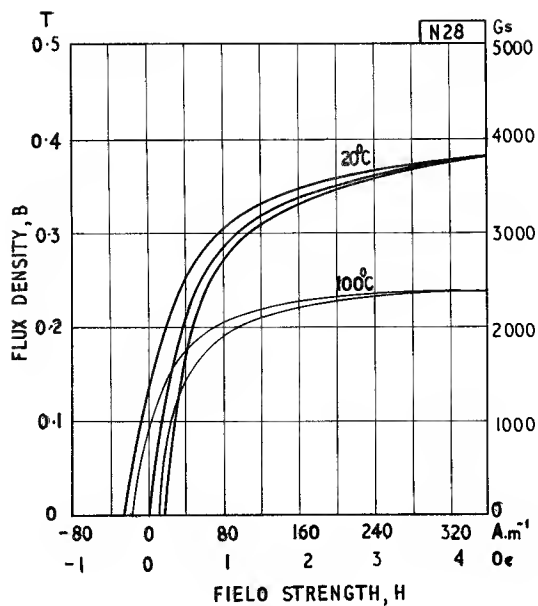


Fig. 3.1.3

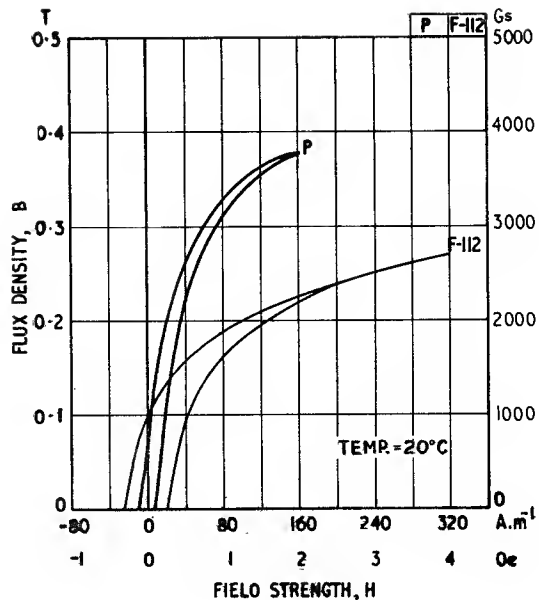


Fig. 3.1.4

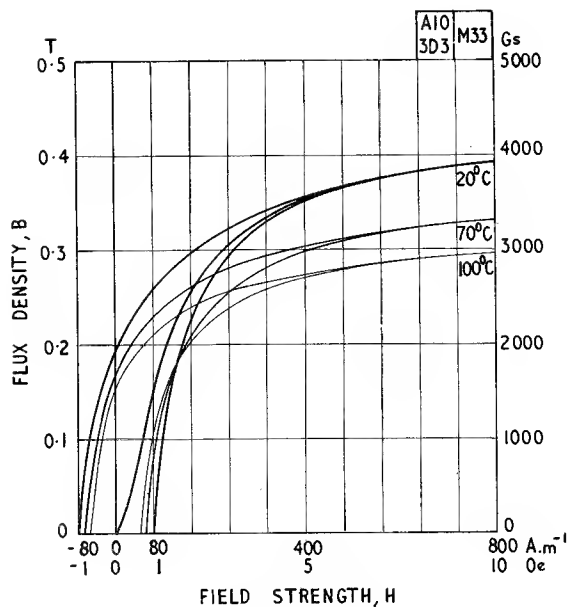


Fig. 3.1.5

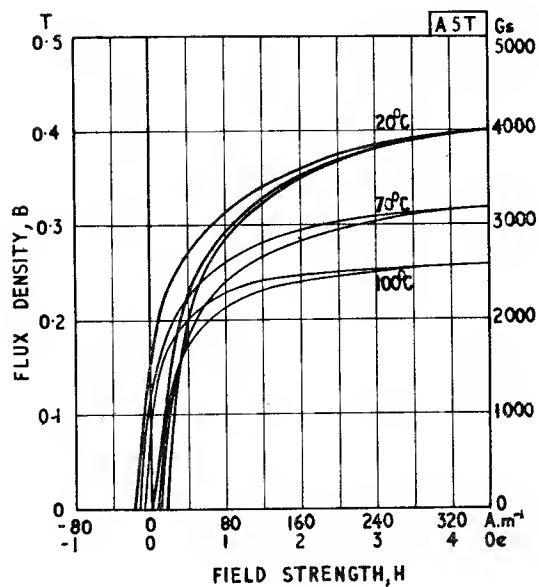


Fig. 3.1.6

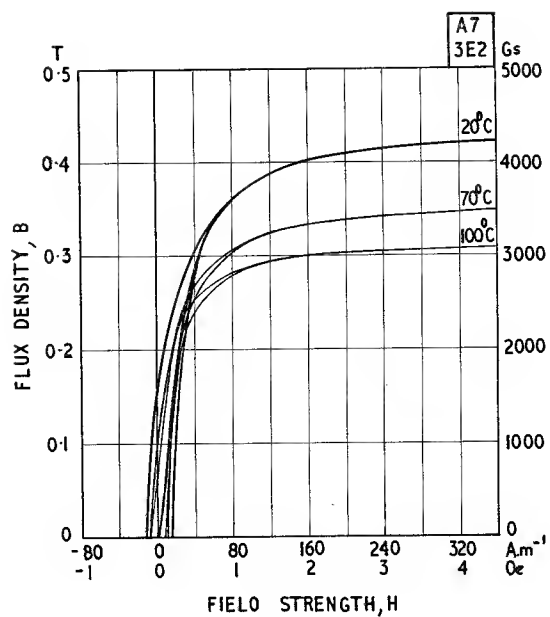


Fig. 3.1.7

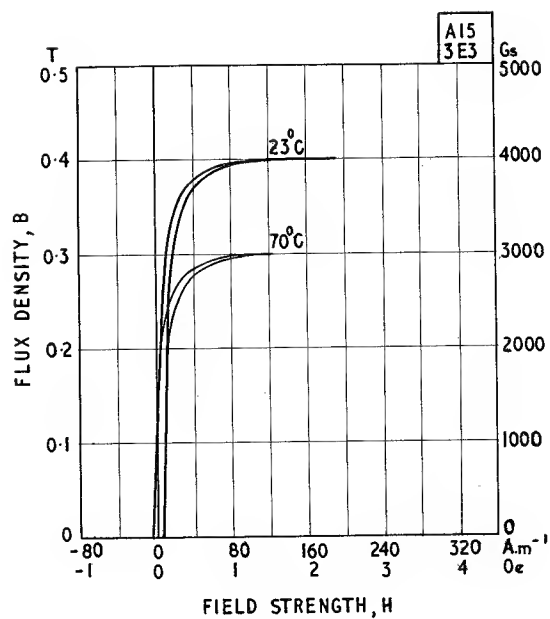


Fig. 3.1.8

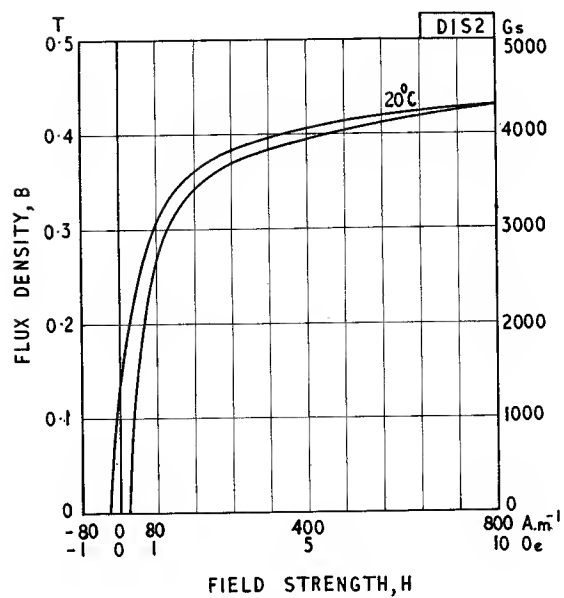


Fig. 3.1.9

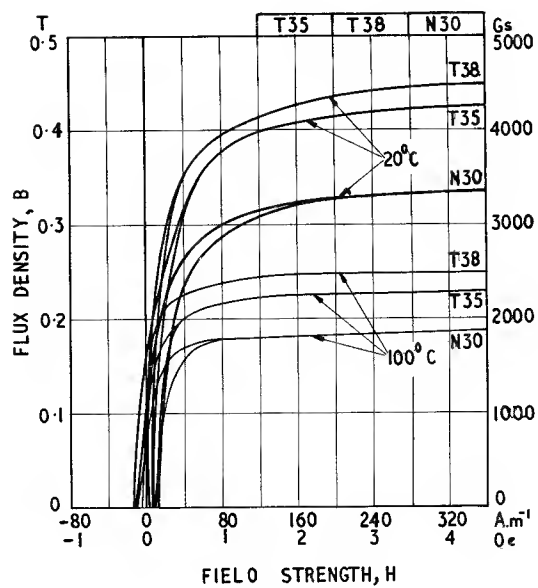


Fig. 3.1.10

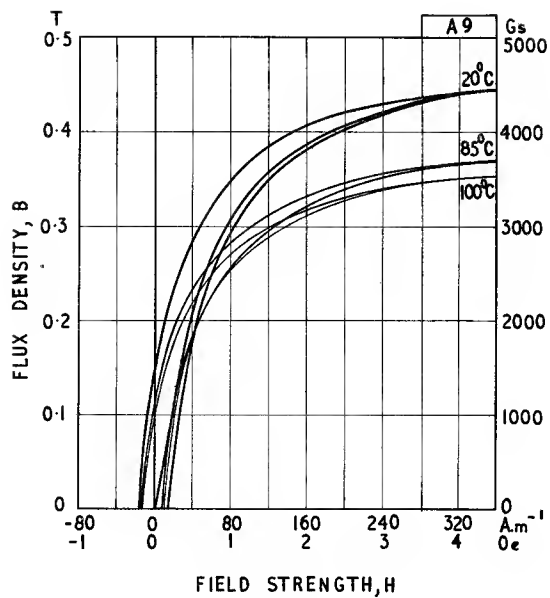


Fig. 3.1.11

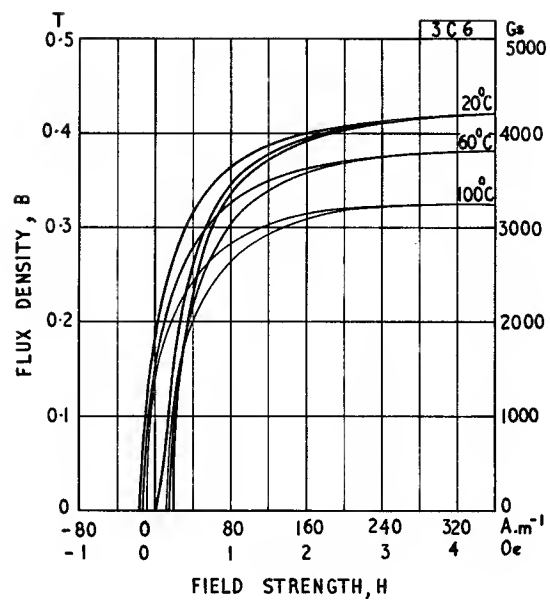


Fig. 3.1.12

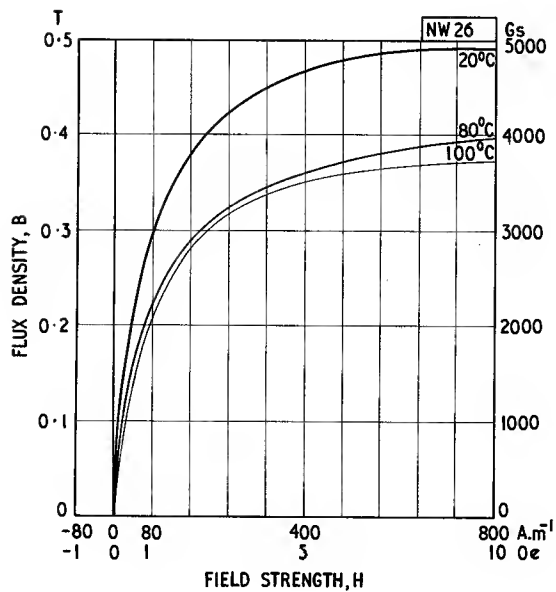


Fig. 3.1.13

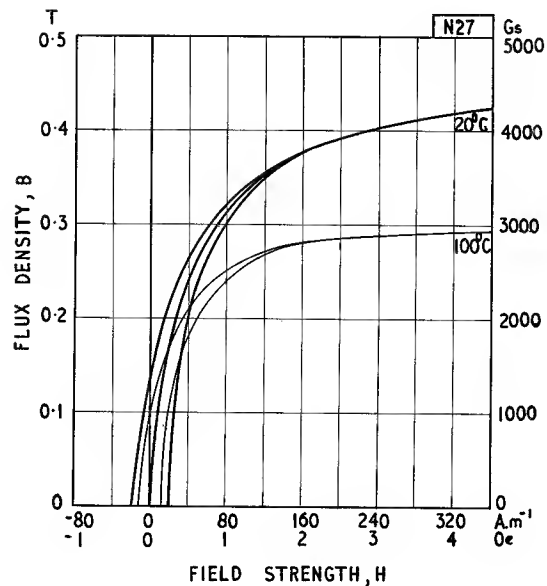


Fig. 3.1.14

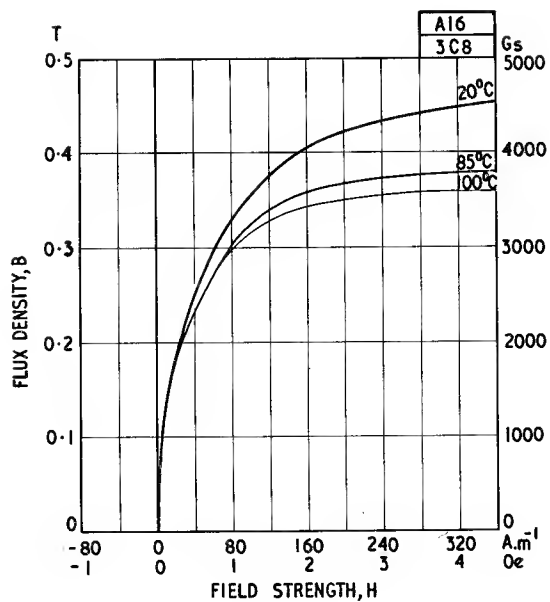


Fig. 3.1.15

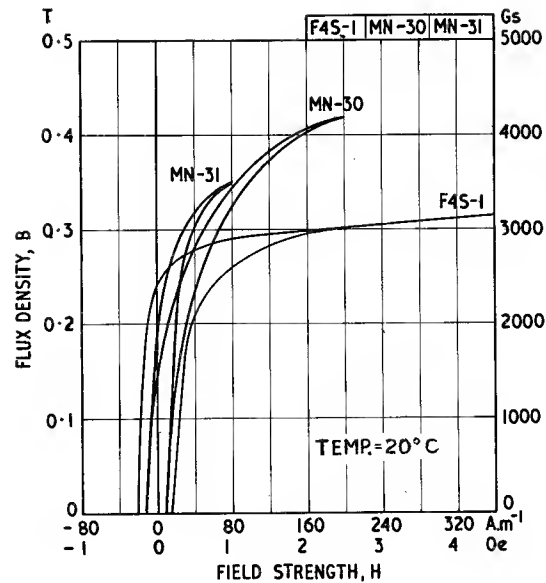


Fig. 3.1.16

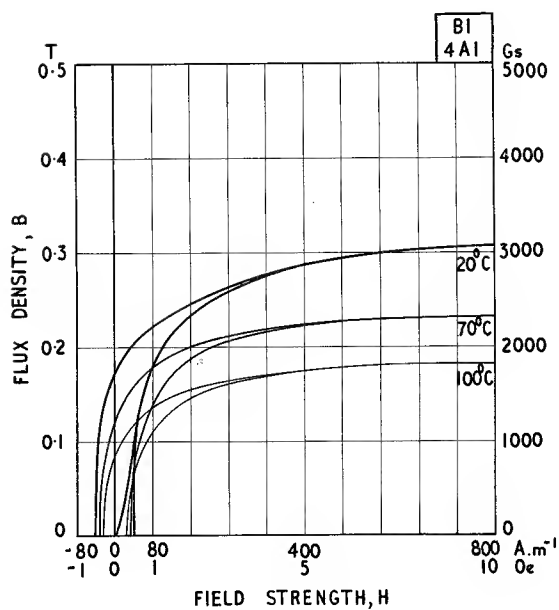


Fig. 3.1.17

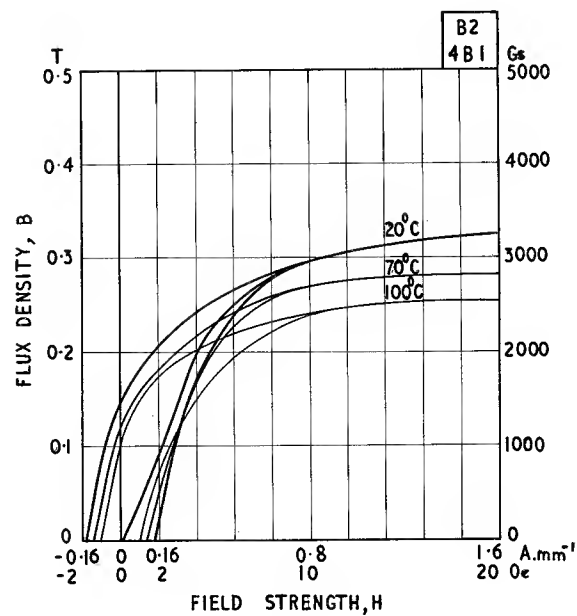


Fig. 3.1.18

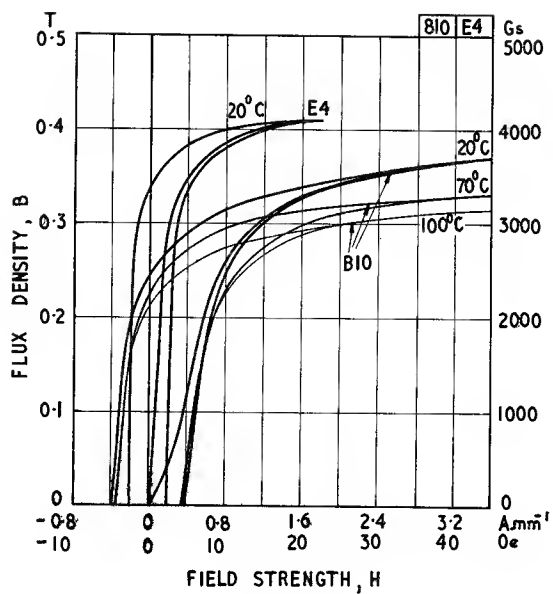


Fig. 3.1.19

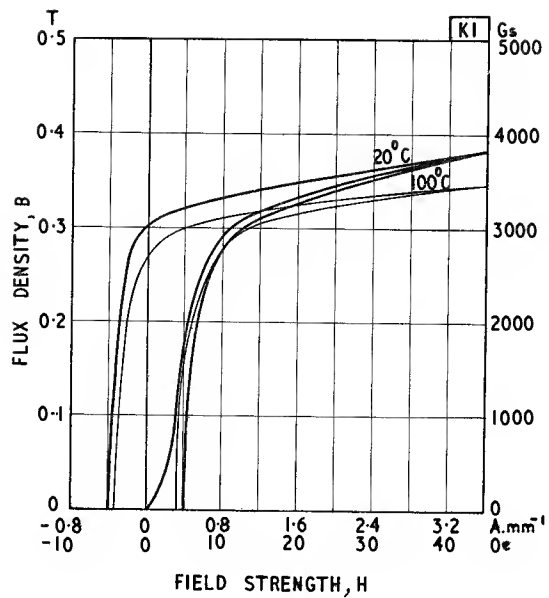


Fig. 3.1.20

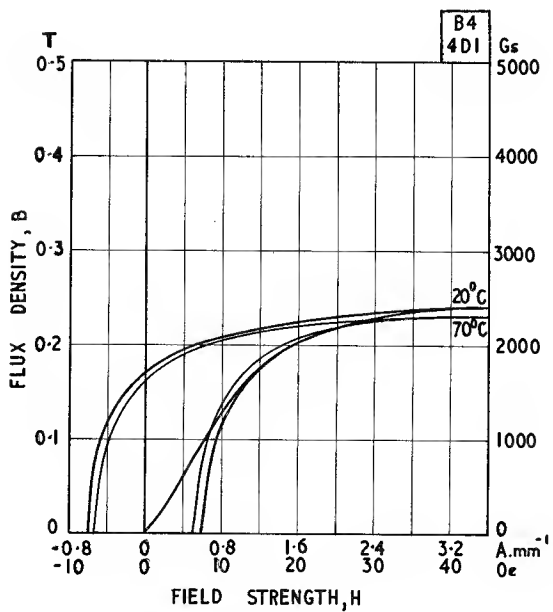


Fig. 3.1.21

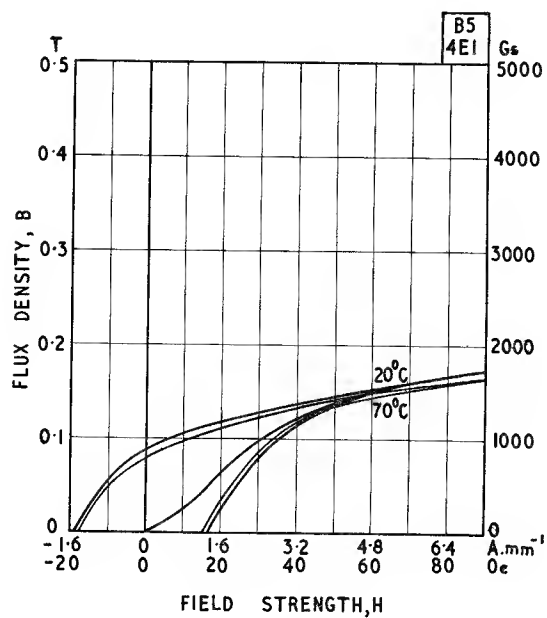


Fig. 3.1.22

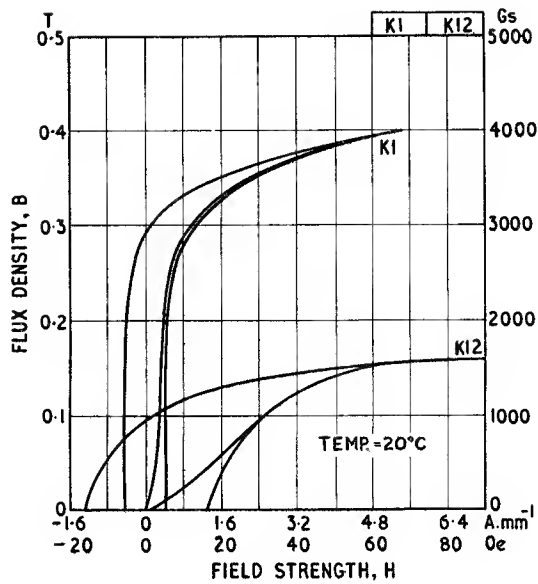


Fig. 3.1.23

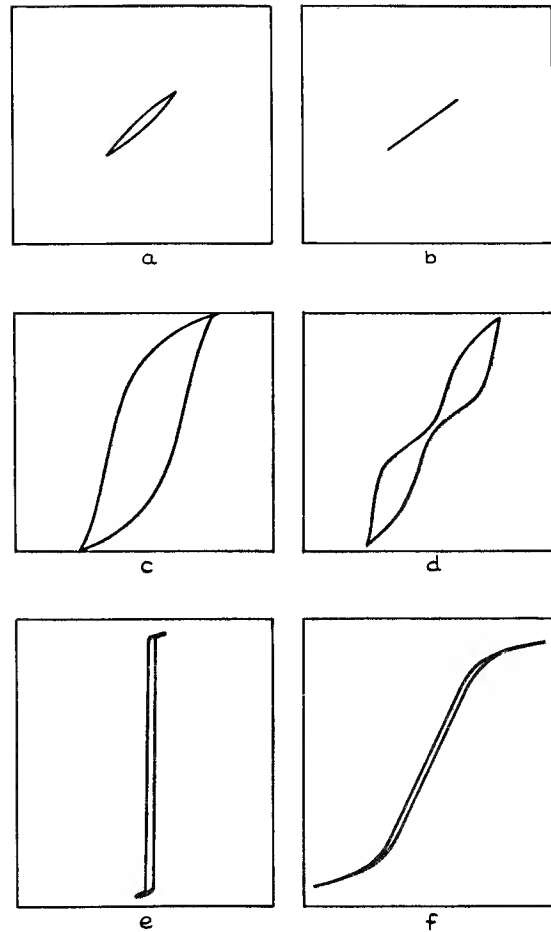


Fig. 3.1.24. B-H loops obtained by special heat treatment of nickel zinc ferrite having a small addition of cobalt. These materials have been described by Kornetzki⁶ and others.^{7,8}

Loops (a) and (c): Low and high amplitude loops for the ferrite without special treatment.

Loops (b) and (d): Corresponding loops obtained by slow cooling after sintering. The loop shows virtually no hysteresis until, at an 'opening field', a butterfly loop is obtained. This opening of the loop is irreversible.

Loops (e) and (f): Loops obtained by cooling in a magnetic field (e) parallel to measuring field and (f) perpendicular to measuring field.

Minor B-H loops Fig. 3.2

$f \rightarrow 0$ (ballistic measurement)

$\theta \approx 20^\circ\text{C}$

The graphs in these figures show the initial magnetization curves for several ferrites. Branching from these curves at various field strengths are the return B - H curves obtained when the field is reduced from those field strengths. Thus if a number of uni-directional pulses of equal field strength are applied to a core these graphs will show the corresponding value of flux density, and give an indication of the remanent flux density. The first pulse will leave the material at the appropriate remanent flux density. The second will take it, by the lower arm of the minor loop (such as the curve shown by a broken line in Fig. 3.2.1), approximately to the previous value of peak flux density. Subsequent pulses will traverse substantially the same minor loop. Thus the graphs will indicate the

total swing of flux density and the incremental permeability.

If a number of uni-directional pulses, each corresponding to a given peak value of flux density are applied to a core the minor loop that will be traversed may be estimated by finding or interpolating a minor loop having a total flux density swing equal to the applied flux density swing. This use of these graphs is explained in more detail in Chapter 8.

In Fig. 3.2.6 the permeability μ_p corresponding to the slope of the minor loop is given as a function of the total uni-directional flux density excursion.

(See also Sections 2.1 and 8.5 and Fig. 8.18)

$$\text{Permeability, } \mu_p = \frac{\Delta B}{\mu_0 \Delta H} \quad (\text{see Eqn 8.30})$$

$$\Delta B = \frac{U t_d}{NA} \quad (\text{see Eqn 8.31})$$

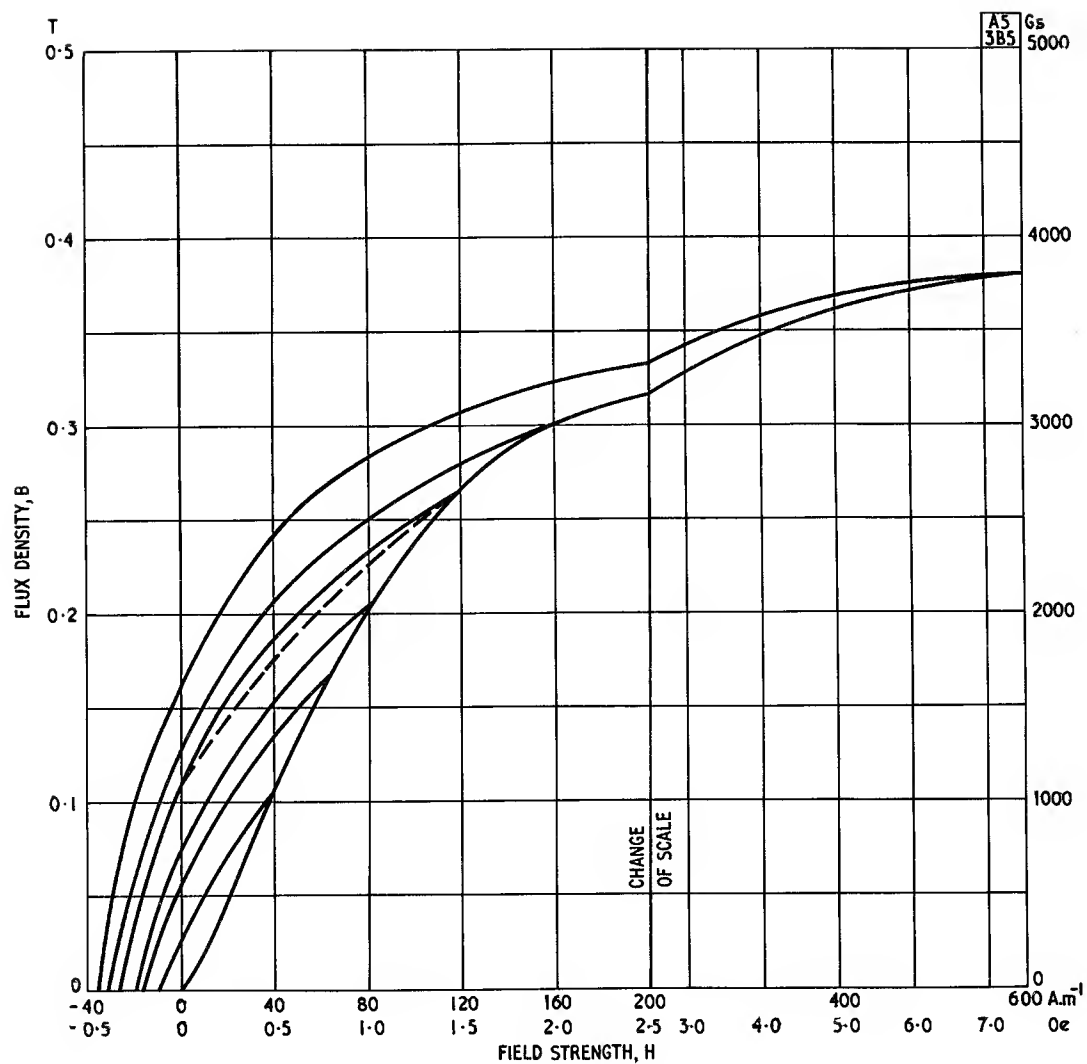


Fig. 3.2.1

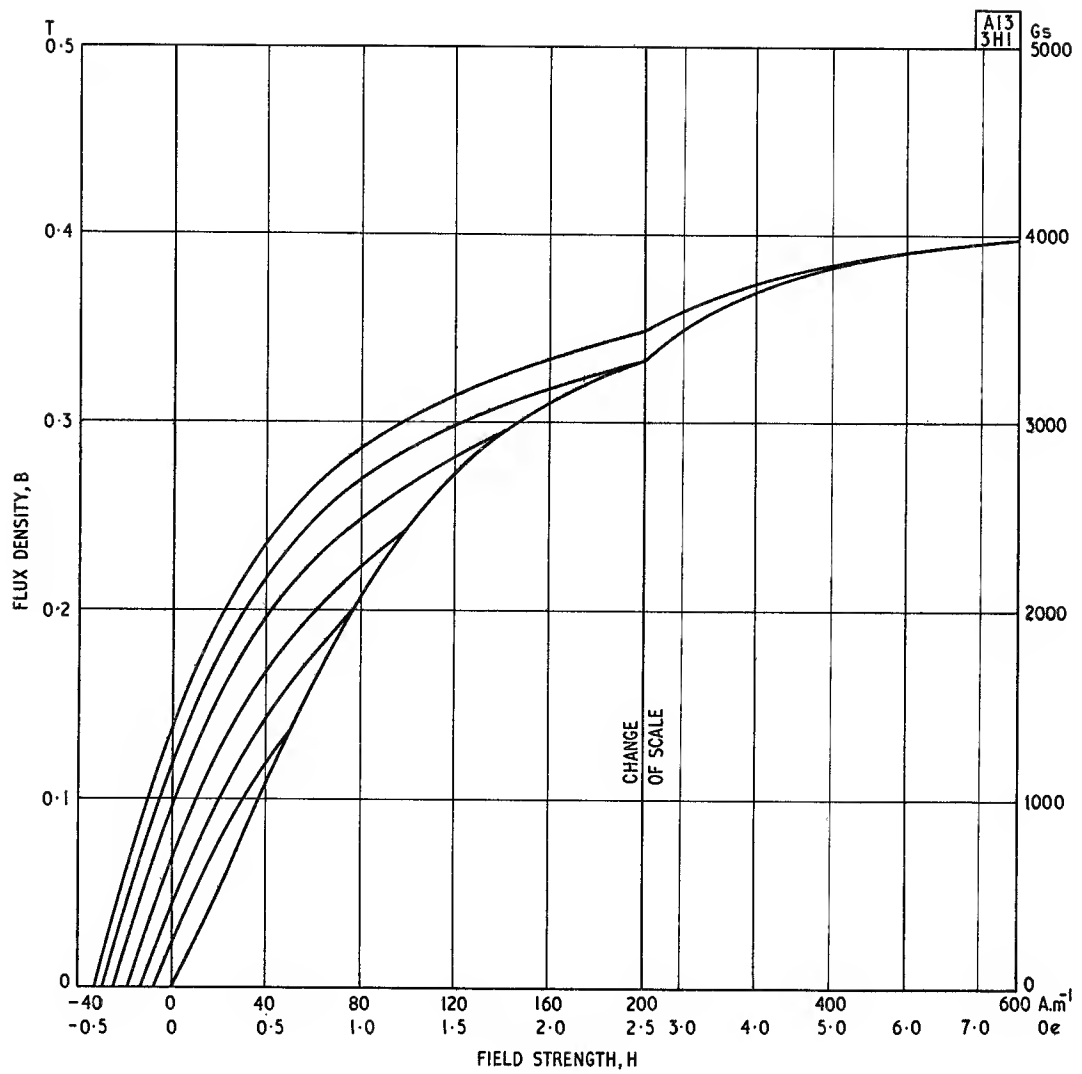


Fig. 3.2.2

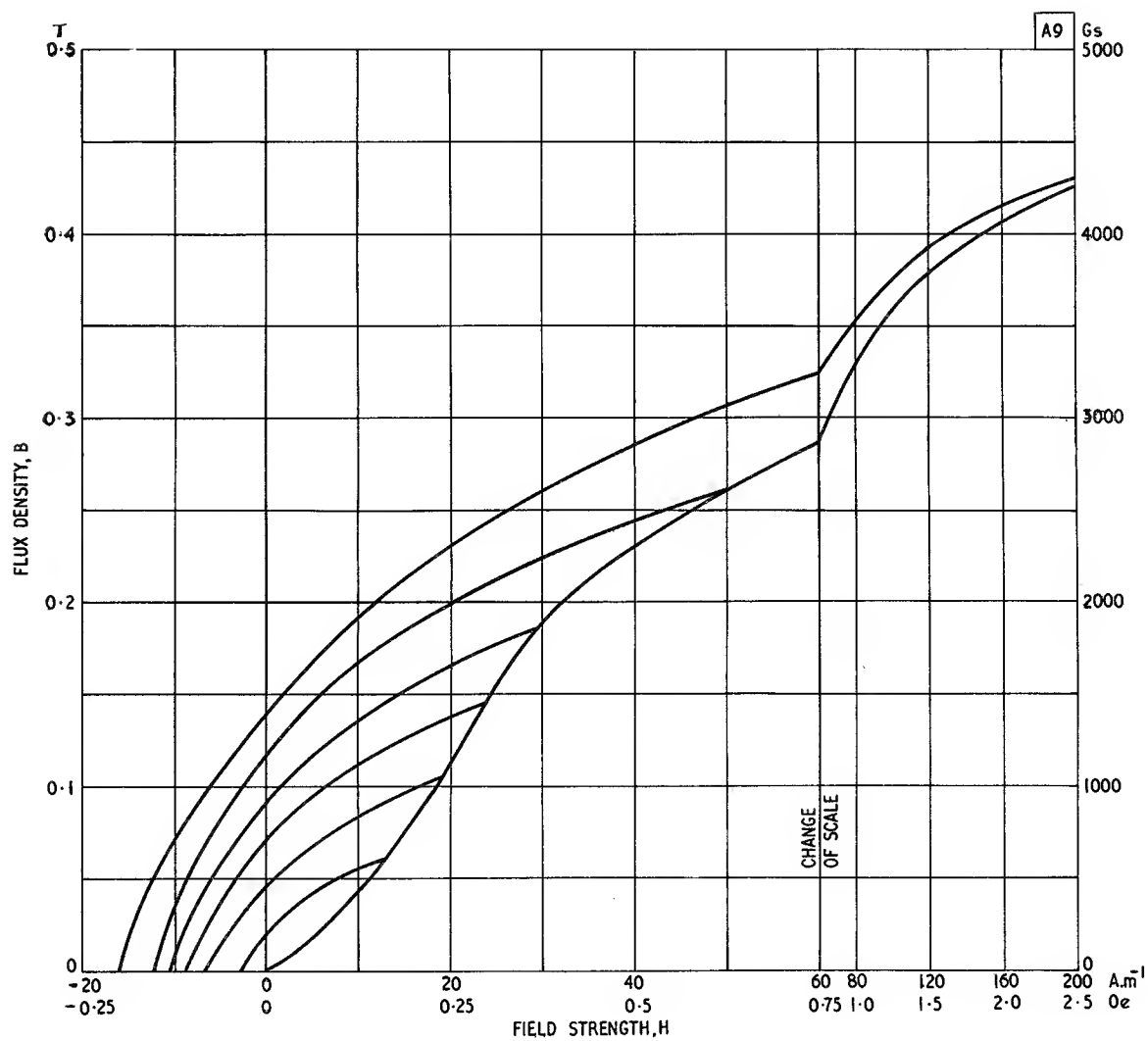


Fig. 3.2.3

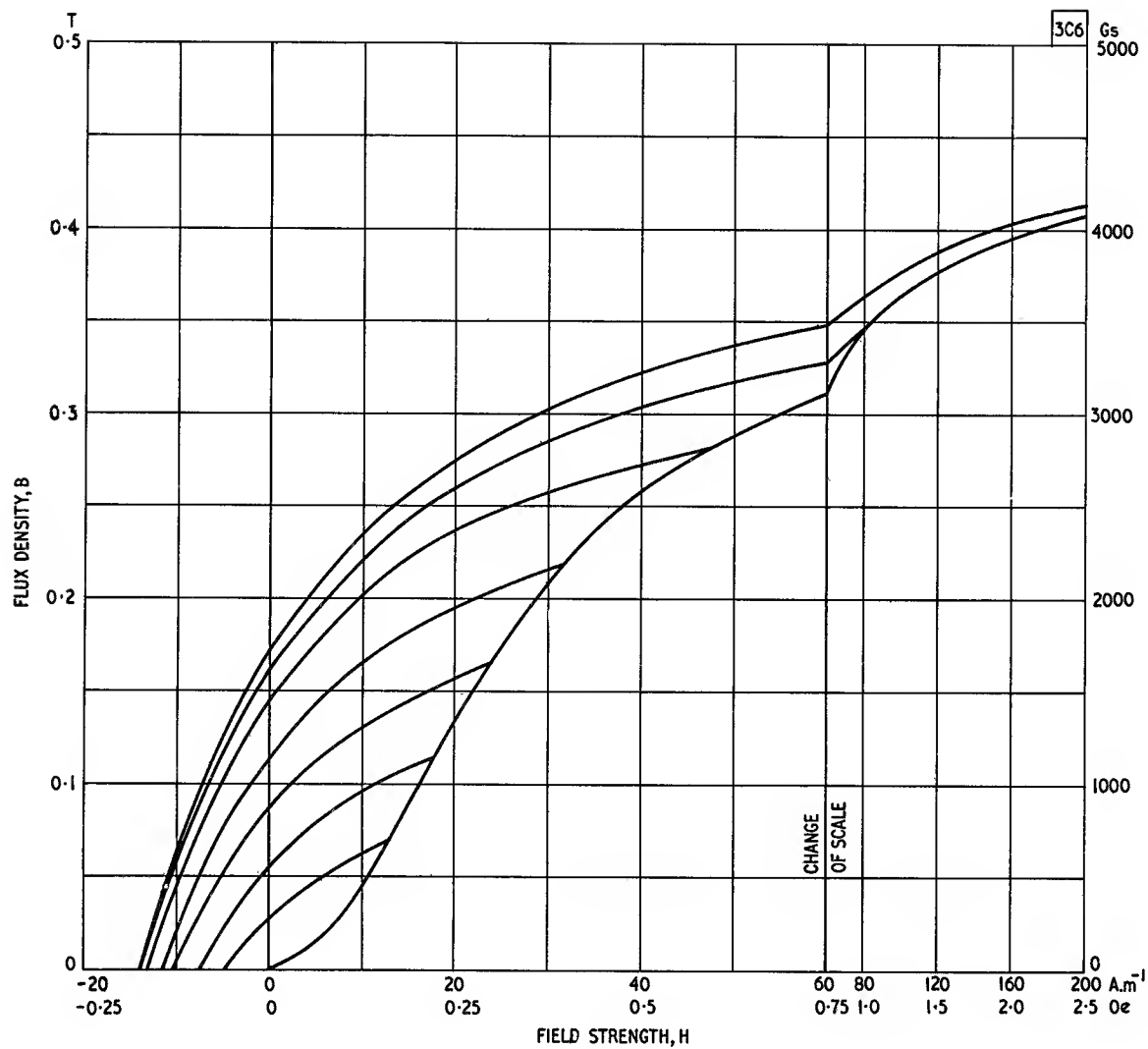


Fig. 3.2.4

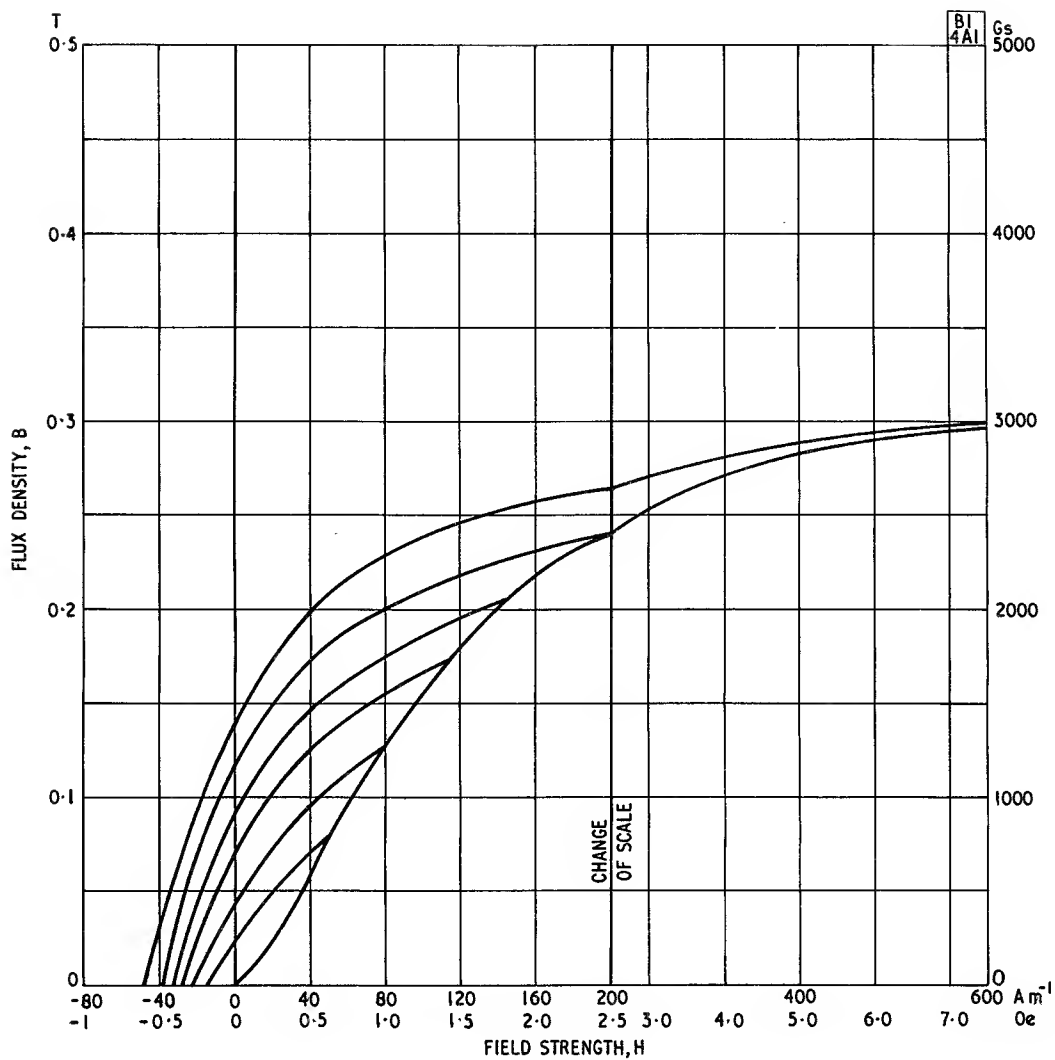


Fig. 3.2.5

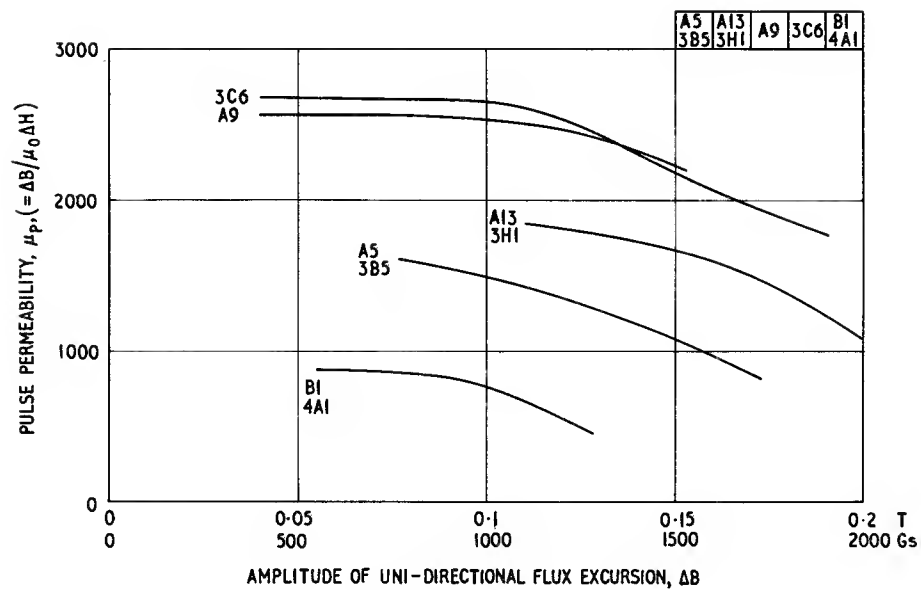


Fig. 3.2.6

Saturation flux density as a function of temperature

Fig. 3.3

$f \rightarrow 0$ (ballistic measurement)

As the temperature rises from 0°K the magnetic alignment within the domains is increasingly disturbed by thermal agitation and as a result the saturation flux density falls until, at the Curie point magnetic alignment

is completely destroyed and the material becomes para-magnetic. In manganese zinc and nickel zinc ferrites the larger the proportion of zinc the lower the Curie point. At room temperature the saturation flux density reaches a maximum at a particular proportion of zinc. This is illustrated in the first two graphs which show the B_{sat} -temperature relations for an experimental series of ferrite compositions (after Smit and Wijn⁹).

(See also Fig. 3.1.)

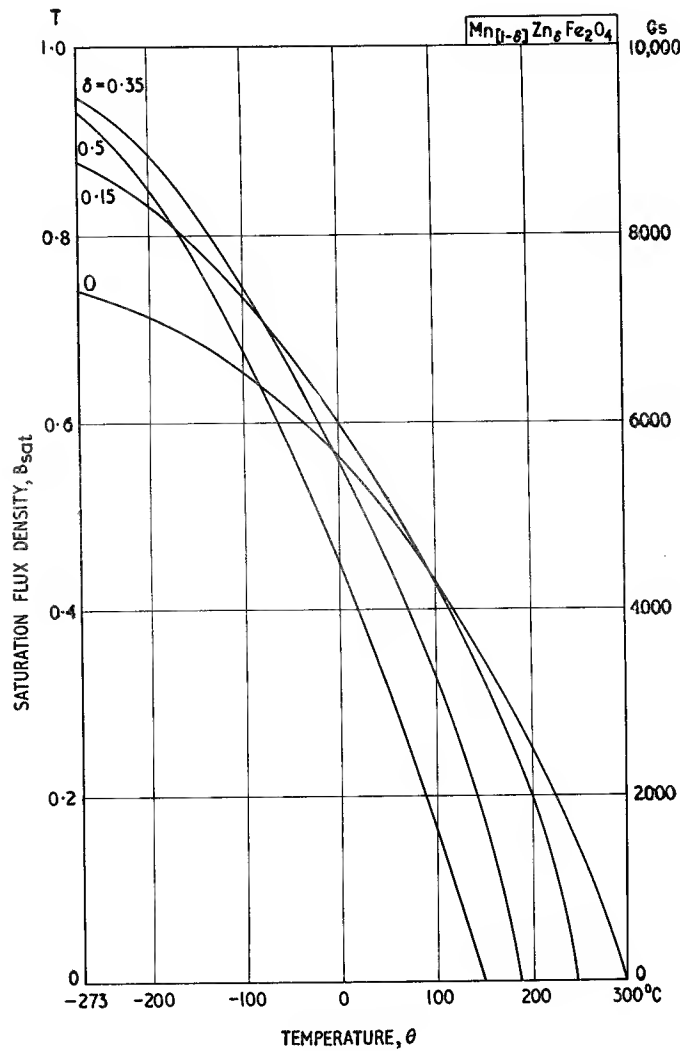


Fig. 3.3.1

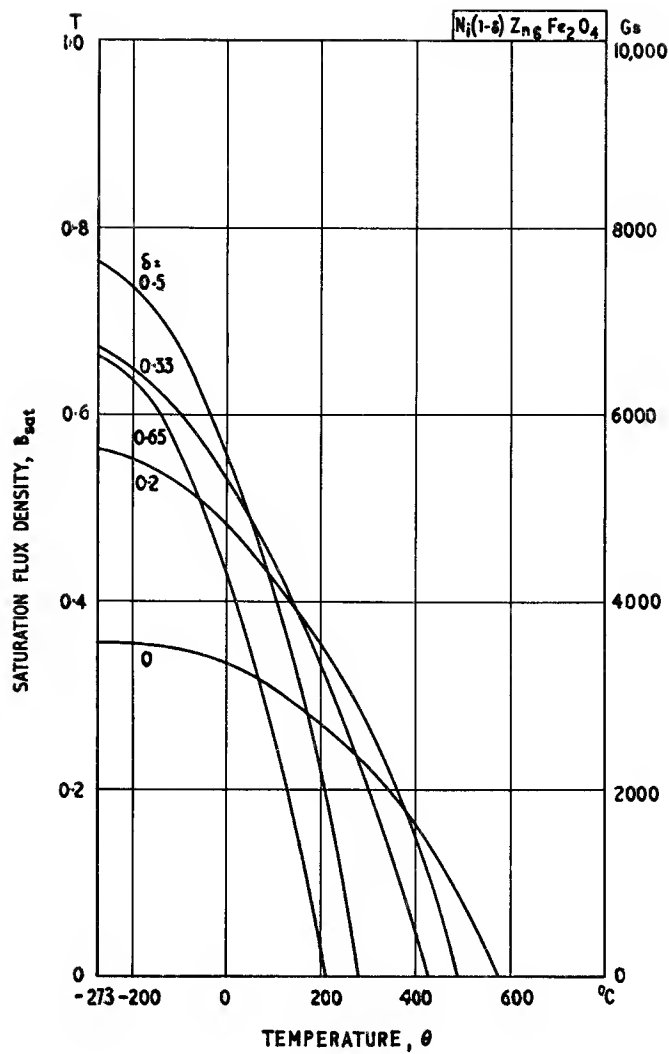


Fig. 3.3.2

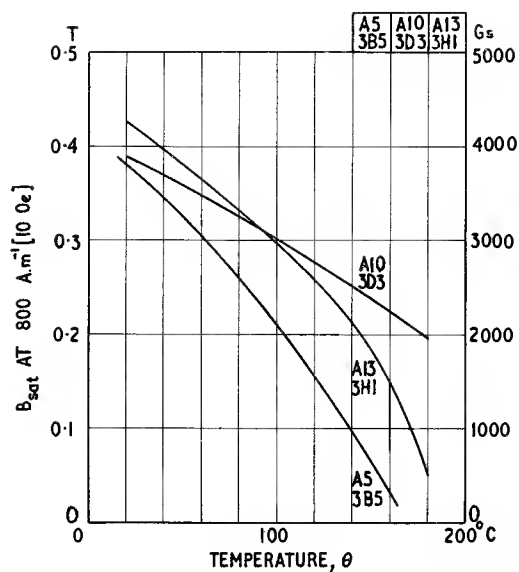


Fig. 3.3.3

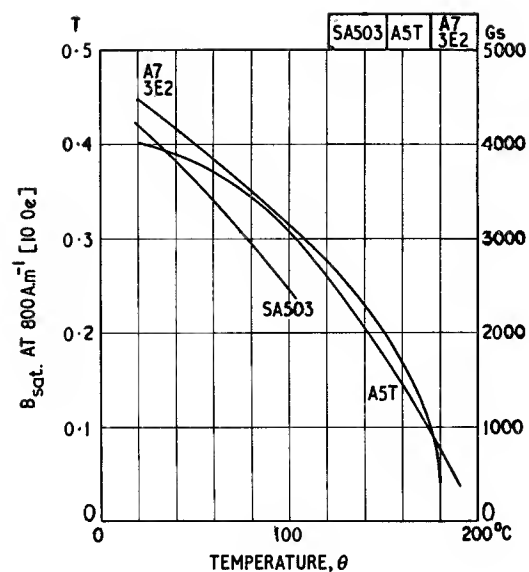


Fig. 3.3.4

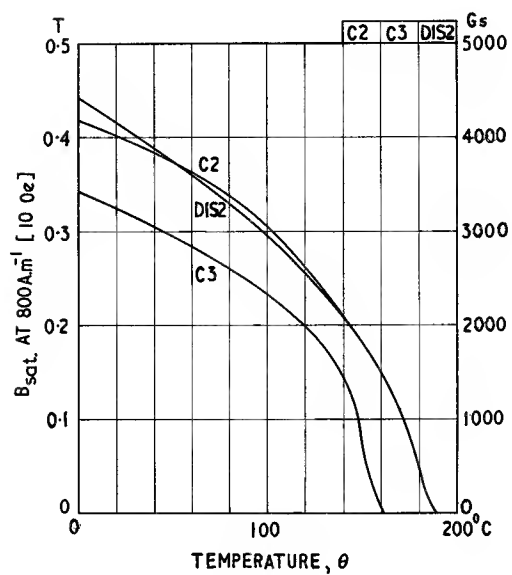


Fig. 3.3.5

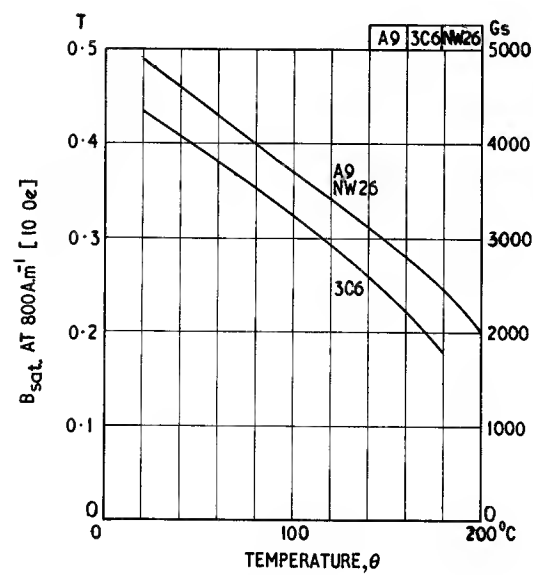


Fig. 3.3.6

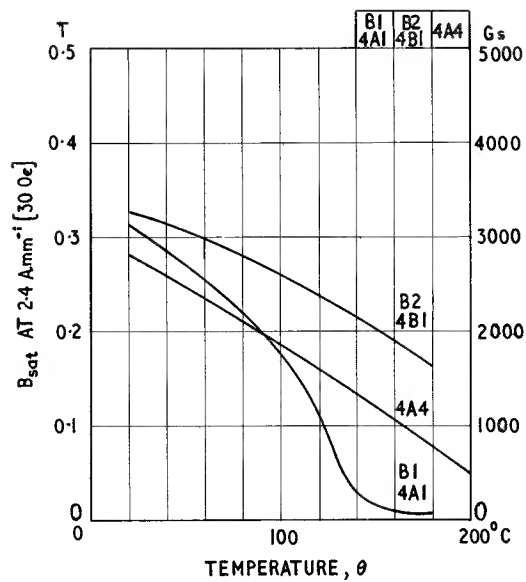


Fig. 3.3.7

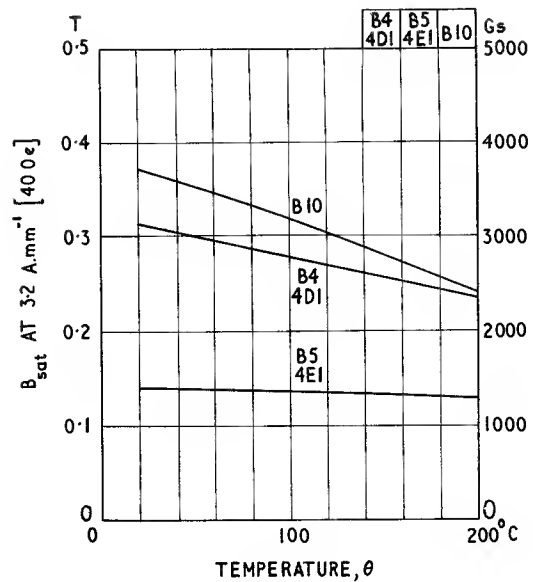


Fig. 3.3.8

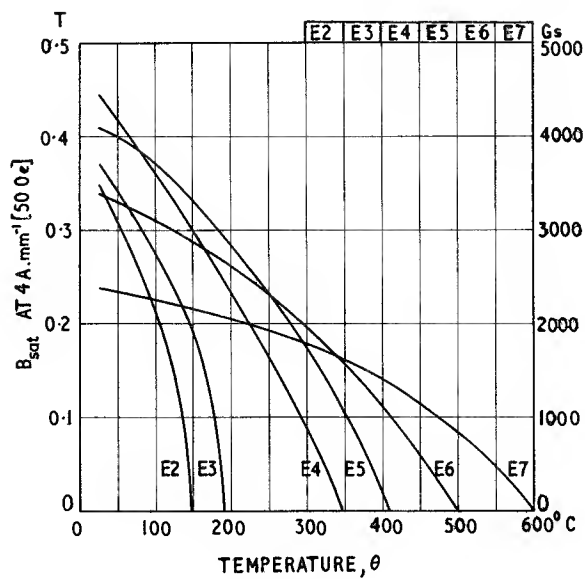


Fig. 3.3.9

Permeability as a function of high amplitude flux density
Fig. 3.4

$$f = 50 \text{ Hz}$$

$$\theta \approx 20^\circ\text{C}$$

As described in Section 2.1 the permeability rises with flux density from the initial value when the flux density is nearly zero to a maximum value corresponding to the slope of a line from the origin, tangential to the knee of the initial magnetization curve. Any further increase in \hat{B} reduces the permeability.

The graphs illustrate a wide variety of behaviour. In some grades the increase of permeability is not great but on the other hand μ_{\max}/μ_i ratios exceeding 2 may often be found, and values of μ_{\max} between 6000 and 10000 are observed.

At higher frequencies, e.g. $> 50 \text{ kHz}$, the rise in permeability may be expected to be less.

From the practical point of view these amplitude permeabilities are rarely of benefit in design work because a device that must have a given performance at high flux densities must usually operate equally well at low flux densities. The main use of these data is in checking that a given design stays within requirements over the specified range of flux densities.

(See also Section 2.1.)

$$\text{Amplitude permeability } \mu_a = \frac{\hat{B}}{\mu_o \hat{H}} \quad (\text{see Eqn 2.8})$$

$$\text{Initial permeability } \mu_i = \lim_{\hat{B} \rightarrow 0} \mu_a$$

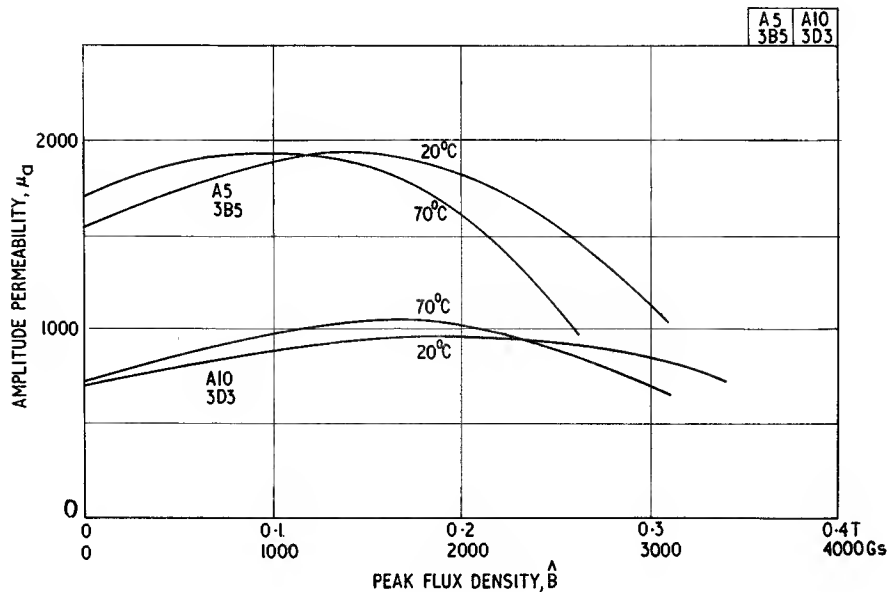


Fig. 3.4.1

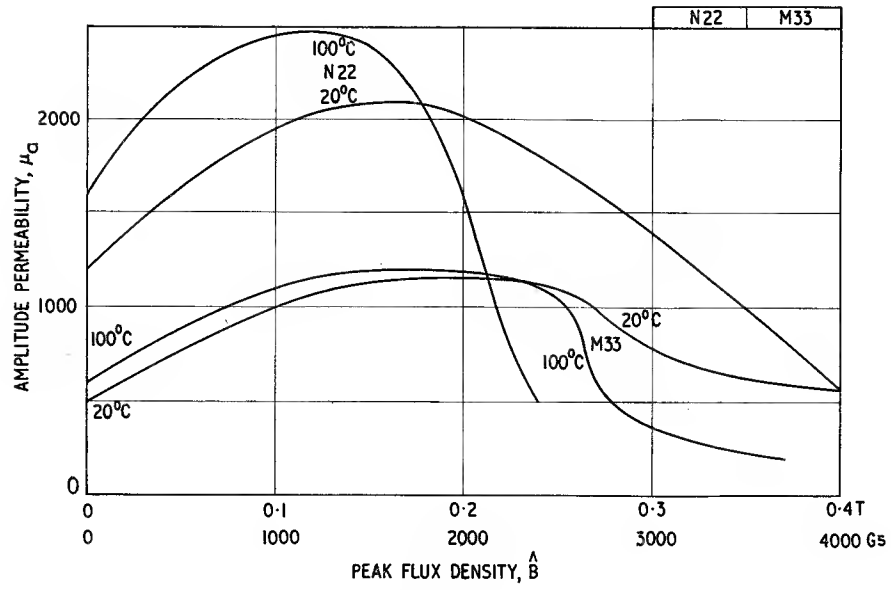


Fig. 3.4.2

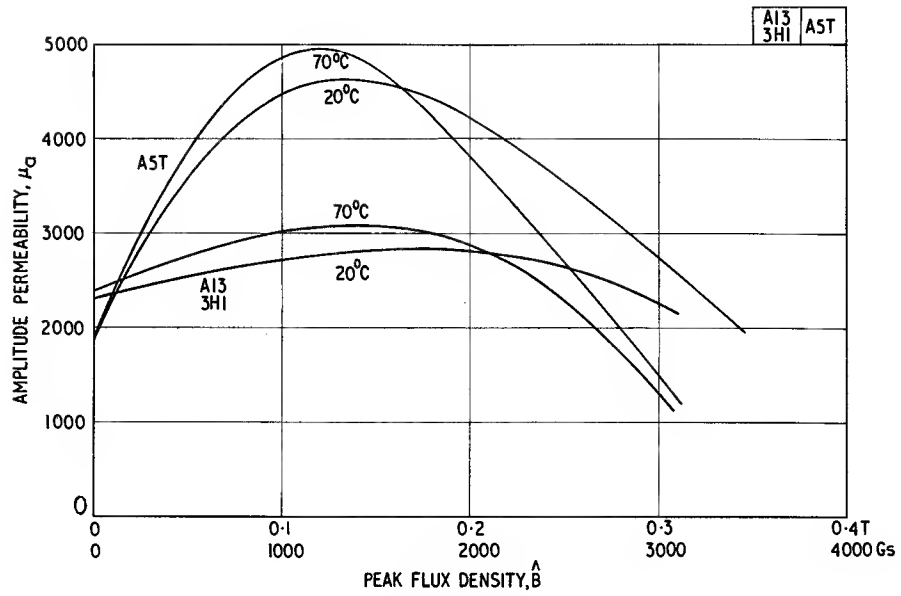


Fig. 3.4.3

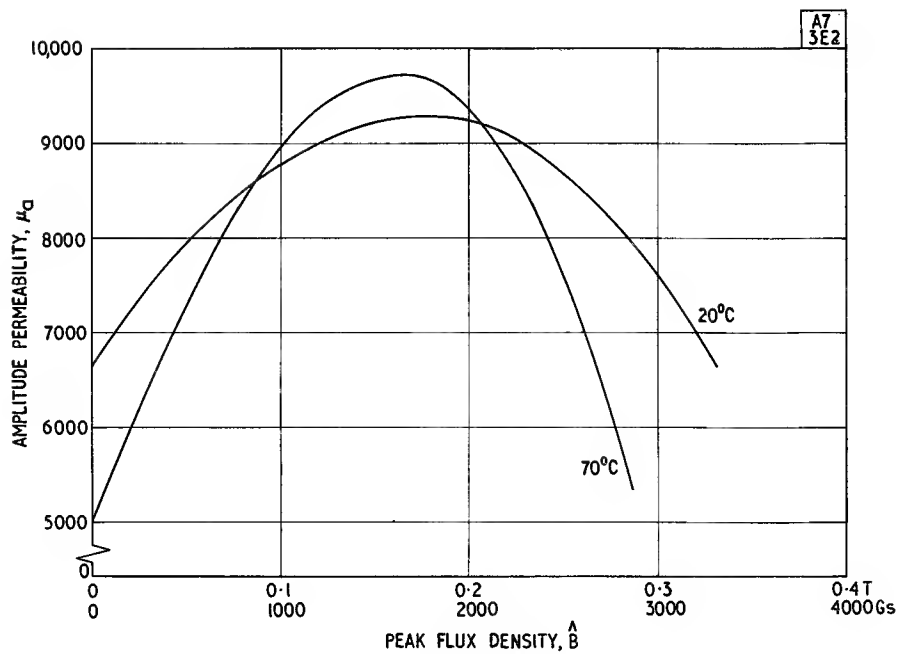


Fig. 3.4.4

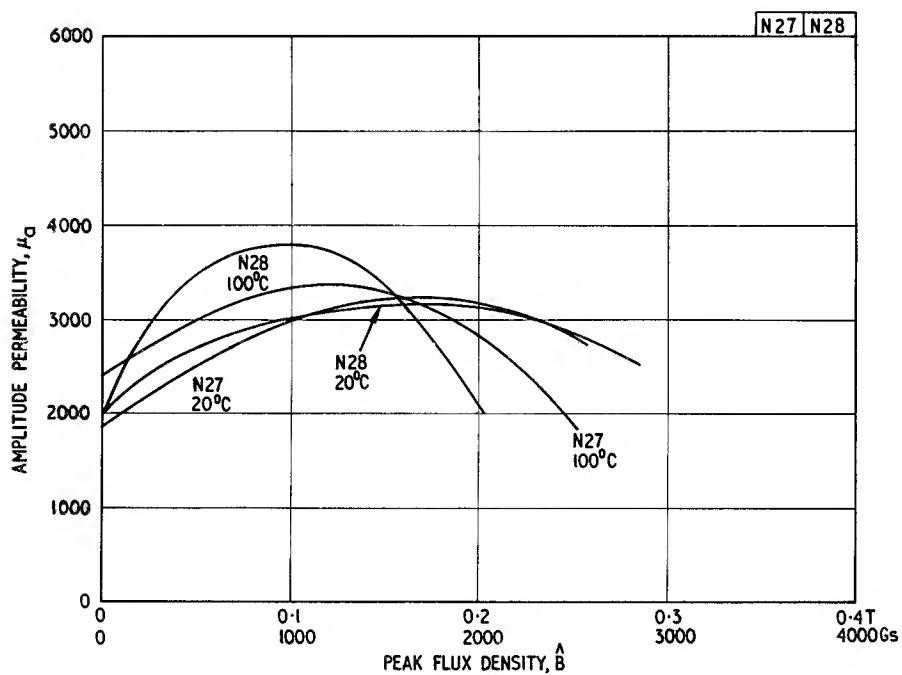


Fig. 3.4.5

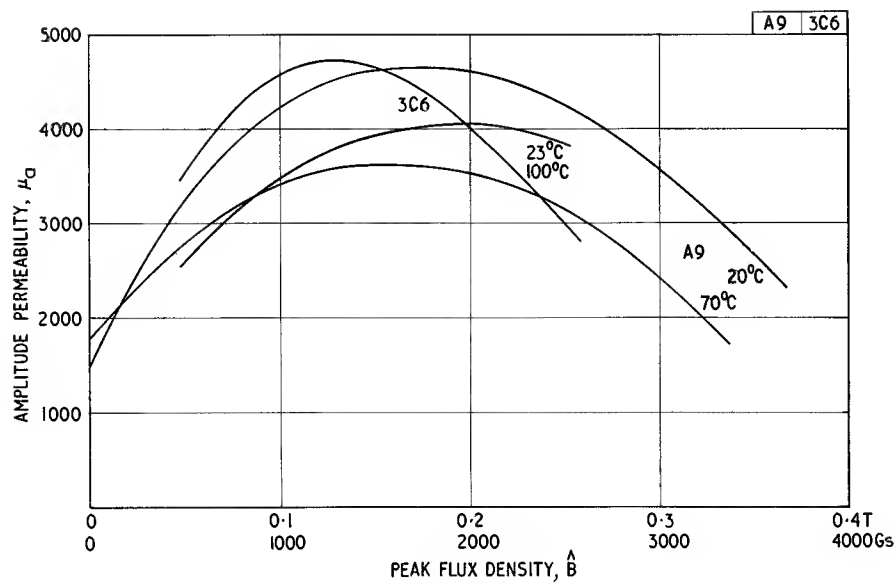


Fig. 3.4.6

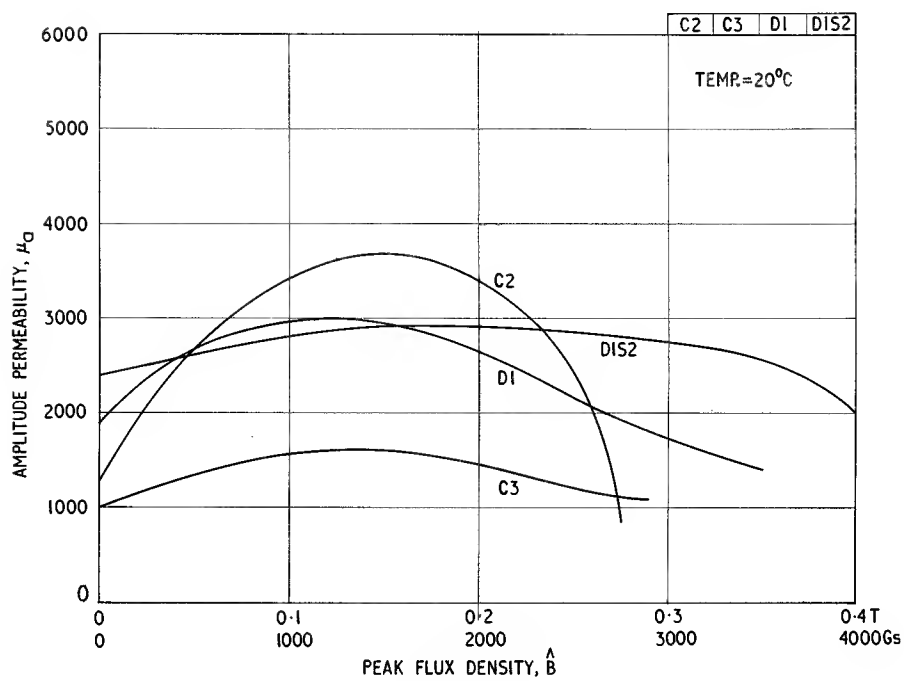


Fig. 3.4.7

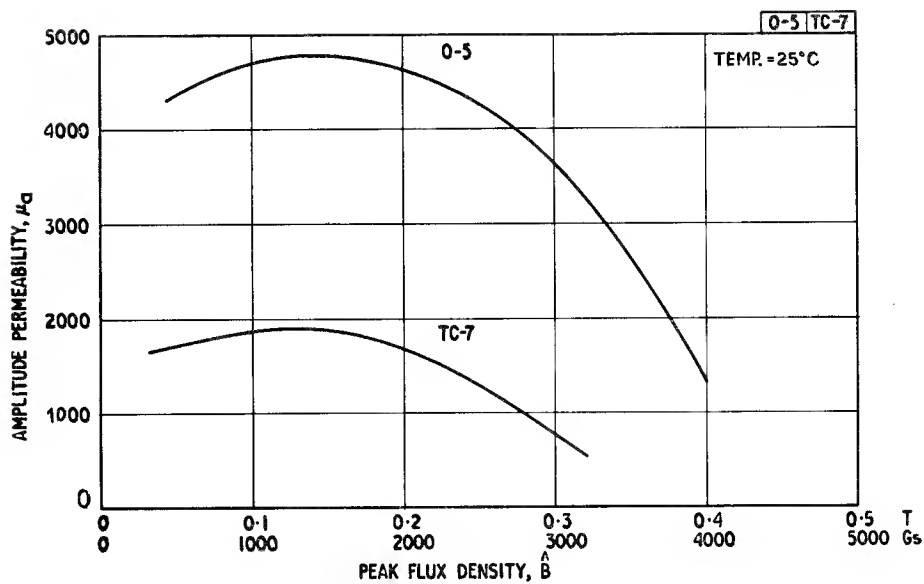


Fig. 3.4.8

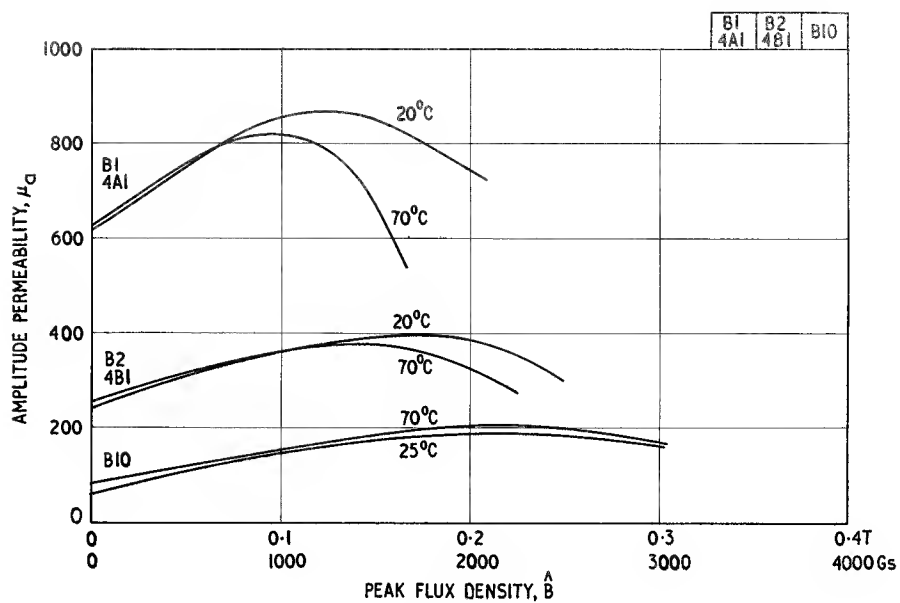


Fig. 3.4.9

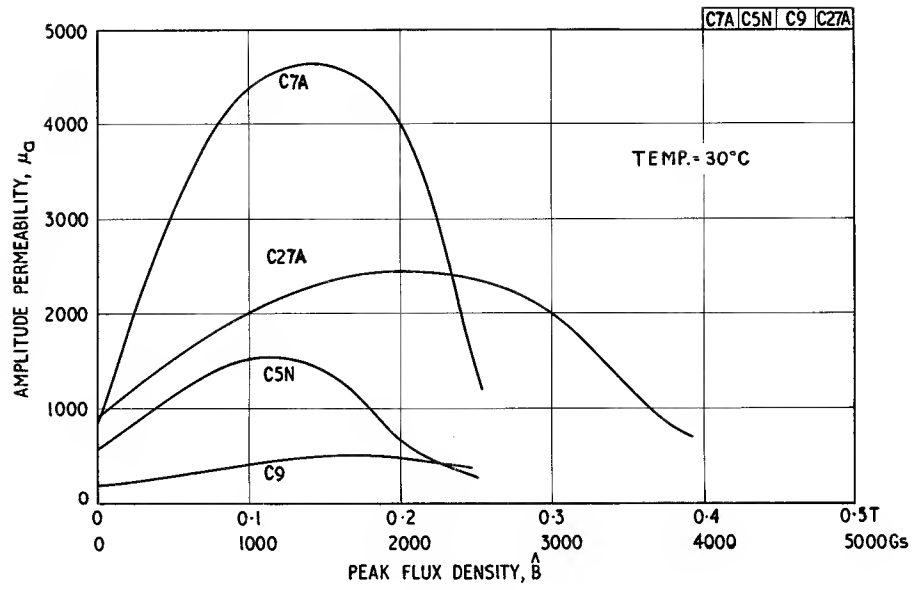


Fig. 3.4.10

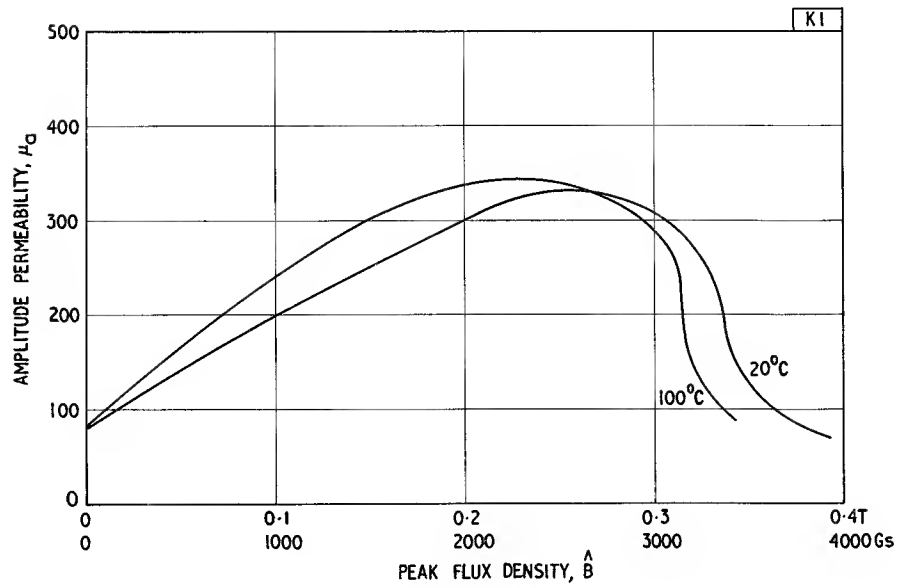


Fig. 3.4.11

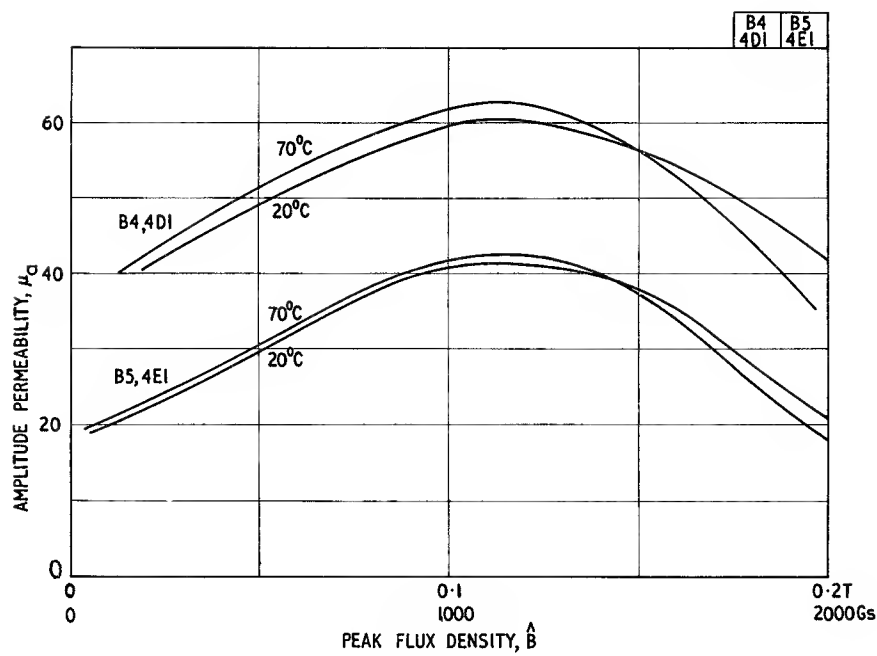


Fig. 3.4.12

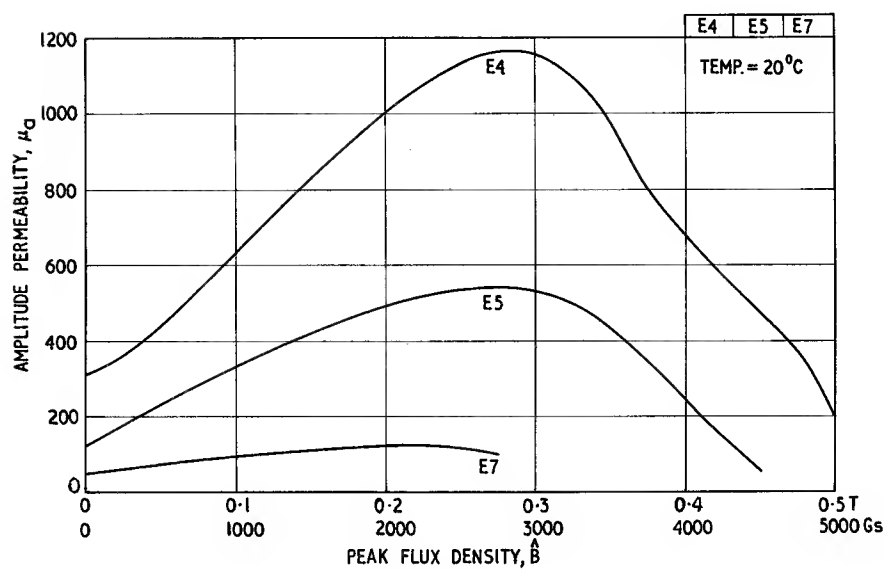


Fig. 3.4.13

Permeability as a function of low amplitude flux density

Fig. 3.5

$$f = 10 \text{ kHz}$$

$$\theta \approx 20^\circ\text{C}$$

The graphs show the rise in permeability as a function of the alternating flux density at low amplitudes. Such data are useful in estimating the stability of inductors subject to changes of low flux density.

They also give an indication of the permeability rise factor used in wave-form distortion calculations, e.g. the Raleigh coefficient ν and the Peterson coefficient a_{11} . For this purpose it is usual to work in terms of field strength rather than flux density. However, as the equations below indicate, the conversion may be readily obtained. Using the slopes of these graphs at zero flux density the values of the above coefficients are as follows:

Specimen	$d\mu/d\hat{H}$ or ν or a_{11}	
	SI units	CGS
A5	18	1440
A13	12.5	1000
A10	2.1	168
A5T	54	4310
A7	540	43400

c.f. values obtained in Fig. 3.15

(See also Sections 2.2.3, 2.2.7 and Figs. 3.15, 3.18.)

$$\left(\frac{\delta\mu}{\delta H}\right)_{dc} = \left(\frac{\delta\mu}{\delta \hat{H}}\right)_{ac} = \nu = a_{11} = \frac{\mu_0 \mu_a \delta\mu}{\delta \hat{B}} \quad (\text{see Eqn 2.30})$$

where μ_a is the amplitude permeability at flux density \hat{B}
 $\mu_a \rightarrow \mu_i$ when $\hat{B} \rightarrow 0$

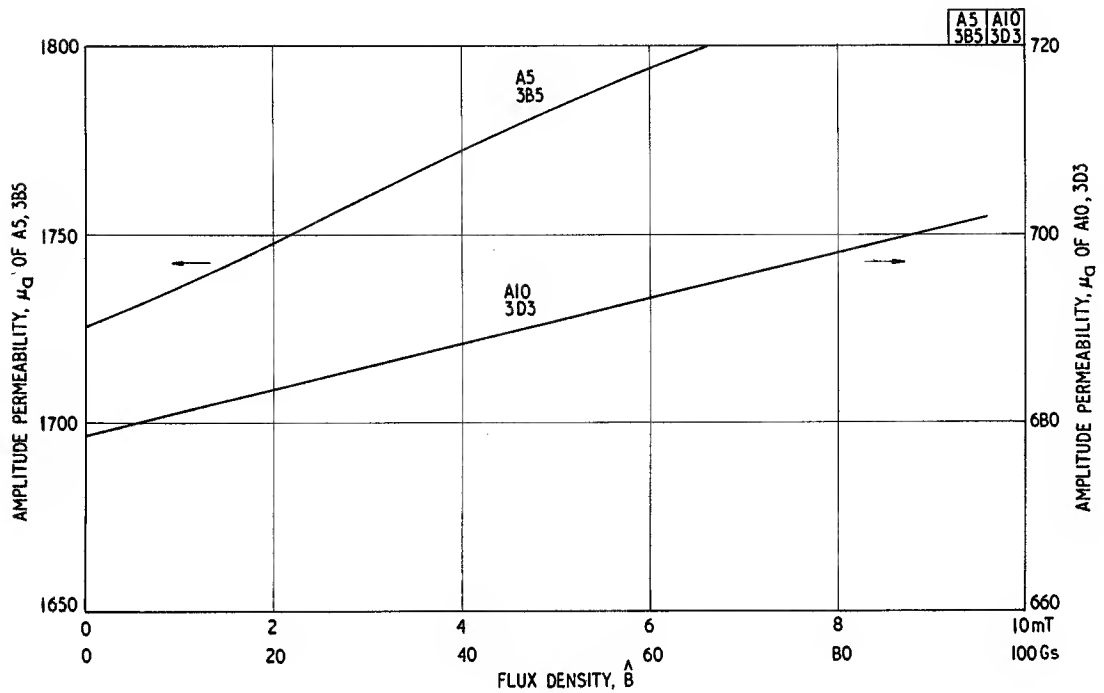


Fig. 3.5.1

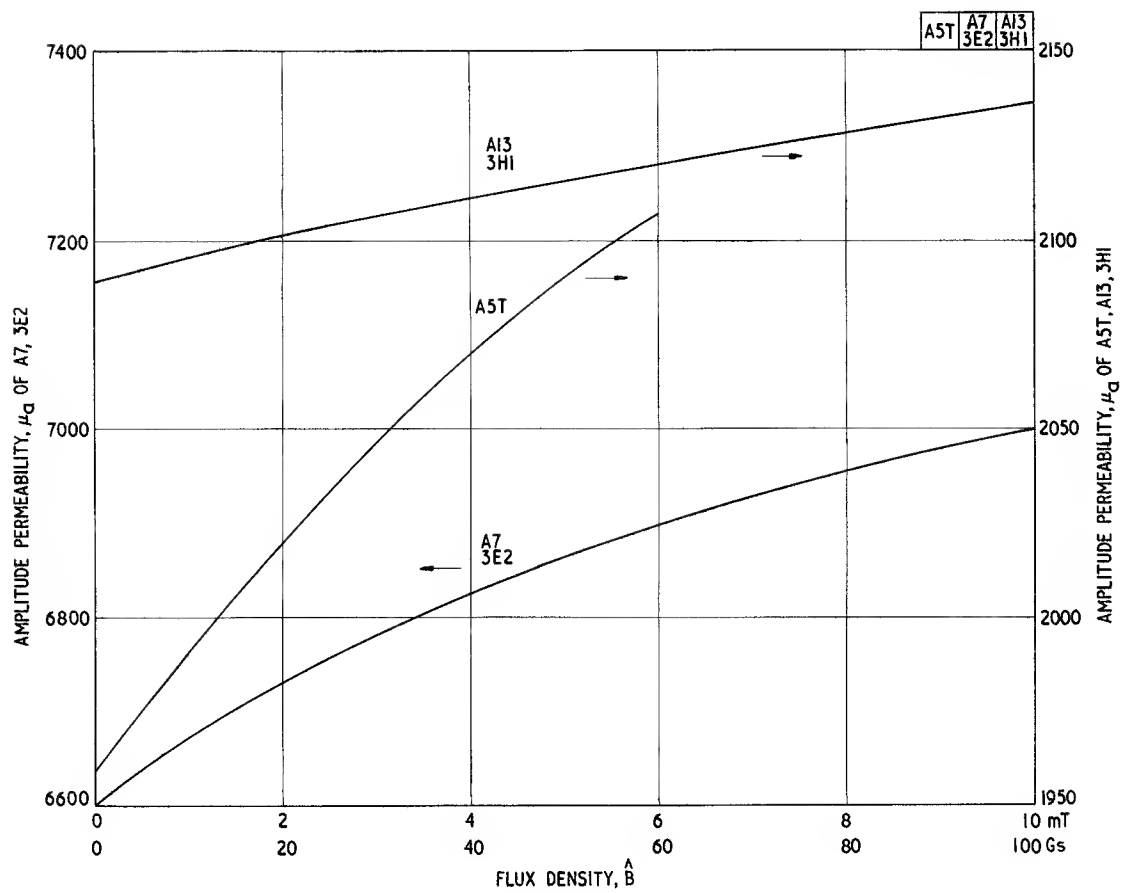


Fig. 3.5.2

Incremental permeability as a function of steady field strength Fig. 3.6

$$f = 5 \text{ kHz}$$

The permeability of a material measured with an alternating field in the presence of a superimposed steady field is referred to as the incremental permeability, μ_A . Apart from a possible small initial increase it becomes progressively less as the steady field is increased. If an air gap is introduced into the magnetic circuit there are two effects: in the absence of a steady field the effective permeability is reduced (see Eqn 4.25), and the reluctance of the magnetic path to the steady field is increased and this reduces the superimposed flux density. The overall result of the introduction of an air gap is that the value of μ_A is reduced at the lower values of the steady field but it is increased when the applied steady field exceeds a certain value depending on the ratio of gap length to magnetic path length, l_g/l_e . If the incremental permeability is measured as a function of steady field strength with a number of different gap lengths a family of curves is obtained. Each curve emerges above the others over a limited range of applied field strength indicating that for a given field strength there is a particular air gap ratio that will give the maximum effective incremental permeability.

These curves are useful in predicting the effect of

superimposed d.c. on a given design but they cannot easily be used for designing inductors or transformers carrying d.c. This is because until the effective μ_A is known it is not possible to estimate the number of turns for a required inductance; until the number of turns is known the applied d.c. ampere turns cannot be calculated and so the optimum effective μ_A is not known. This problem is solved by deriving from these graphs others called Hanna curves. These are presented in Fig. 3.7.

The present graphs have been obtained at both very low alternating flux density and also at a relatively high value; some indication of the temperature dependence is also given. Before the measurement of μ_A for a given air gap ratio the core was demagnetized and measurements were then made at successively increasing values of field strength. If in practice a core is brought to a particular value of steady field strength from a higher value, hysteresis effects may cause the results to depart a little from those given. However at the higher gap ratios hysteresis effects will normally be negligible.

(See also Sections 4.2.2, 6.2.1.)

$$\mu_e = \frac{C_1}{l_g/A_g + C_1/\mu} \quad (\text{see Eqn 4.25})$$

$$\mu_A = \Delta B/\mu_e \Delta H \quad (\text{see Eqn 2.8})$$

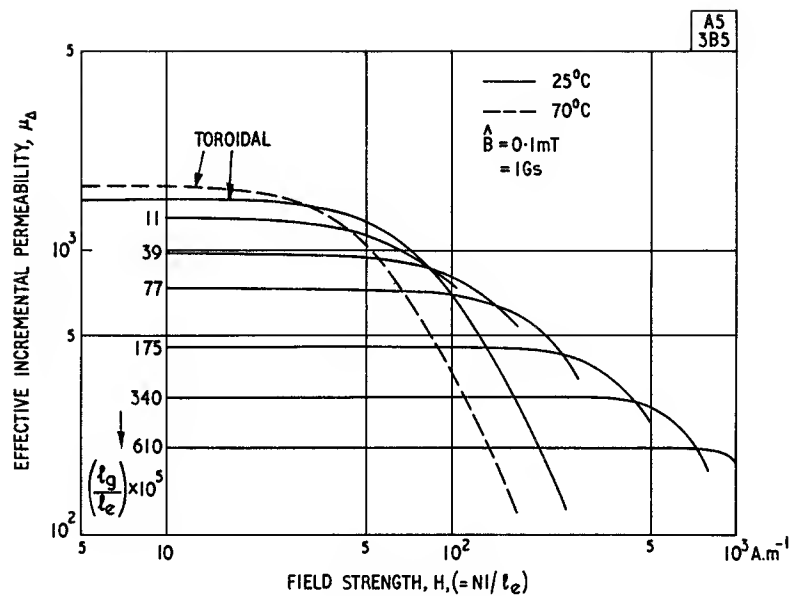


Fig. 3.6.1(a)

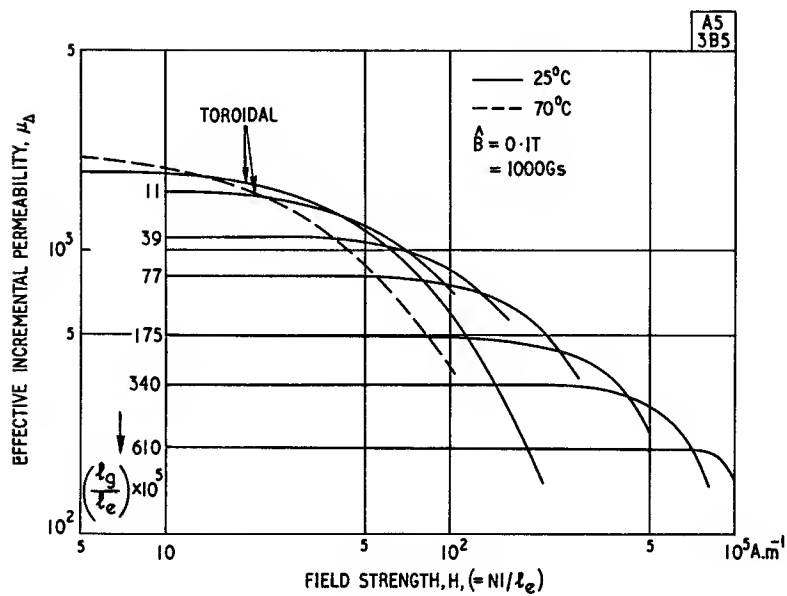


Fig. 3.6.1(b)

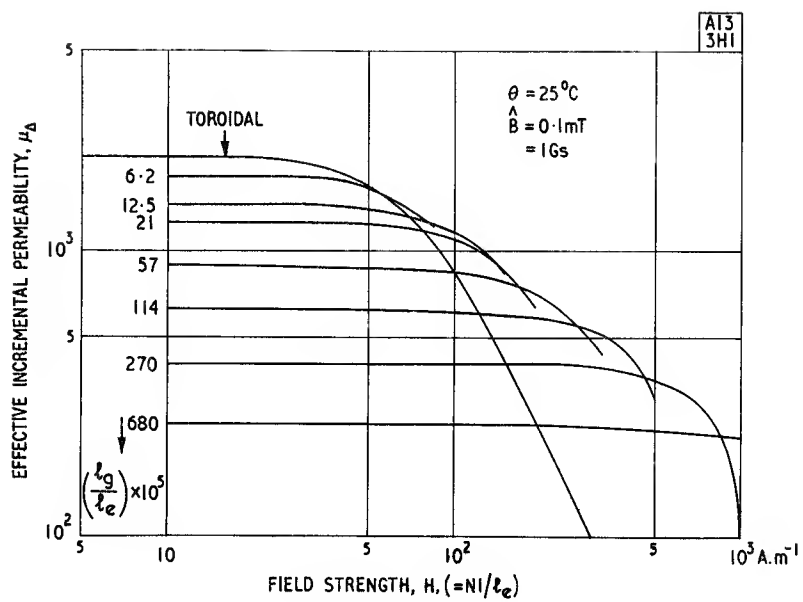


Fig. 3.6.2(a)

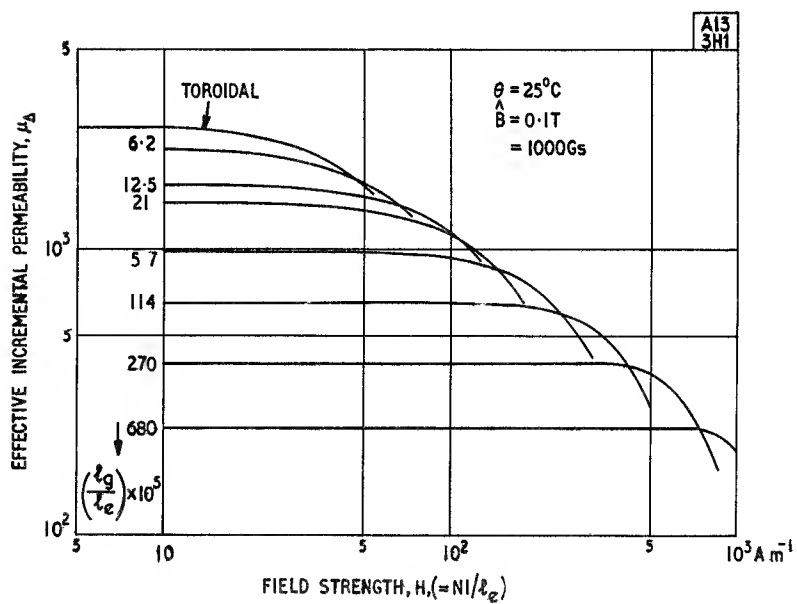


Fig. 3.6.2(b)

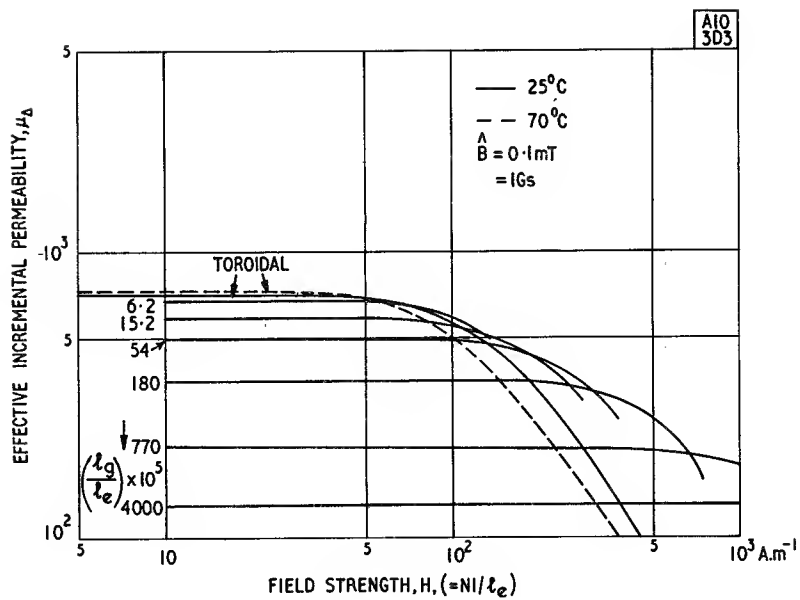


Fig. 3.6.3(a)

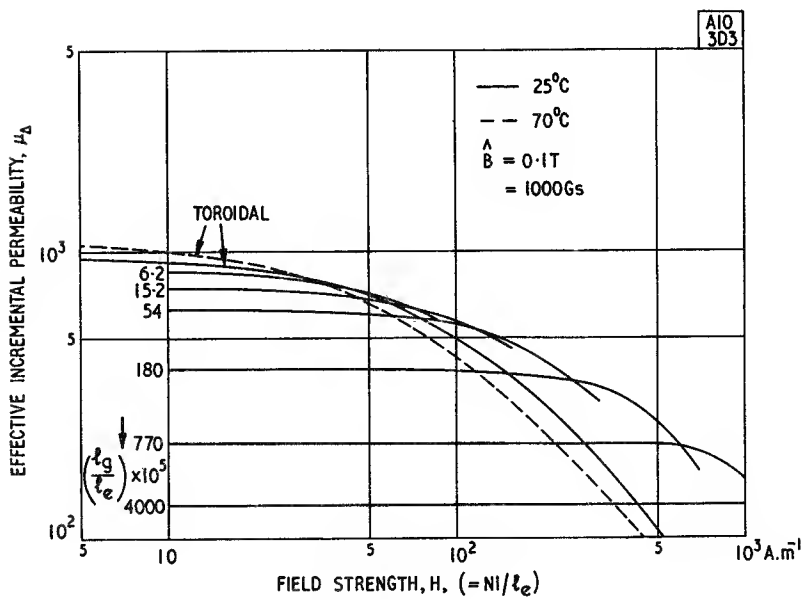


Fig. 3.6.3(b)

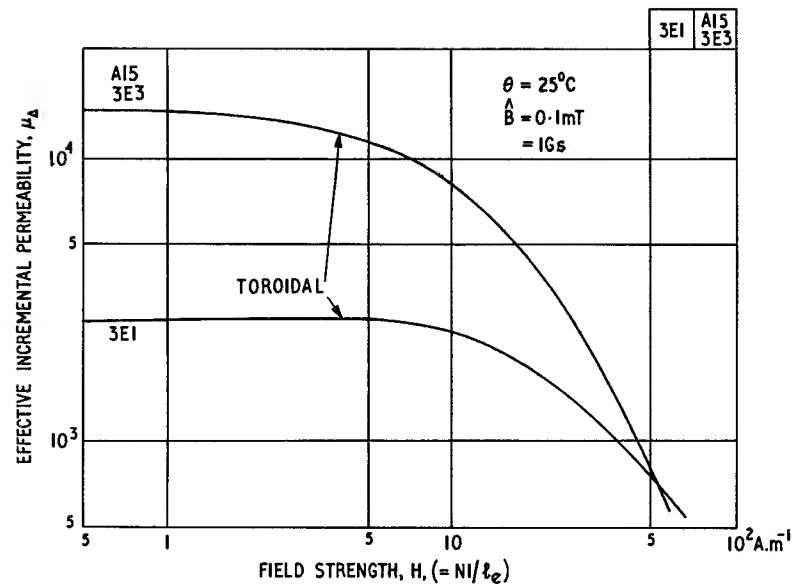


Fig. 3.6.4

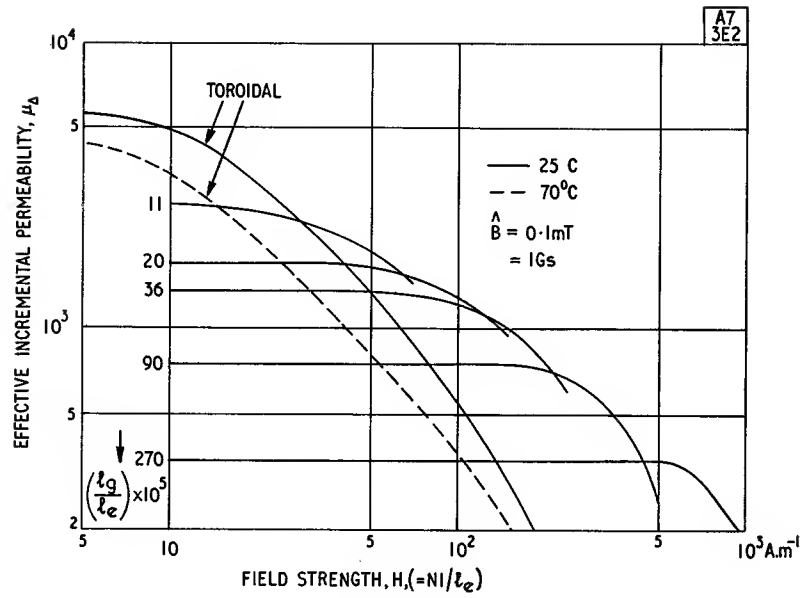


Fig. 3.6.5(a)

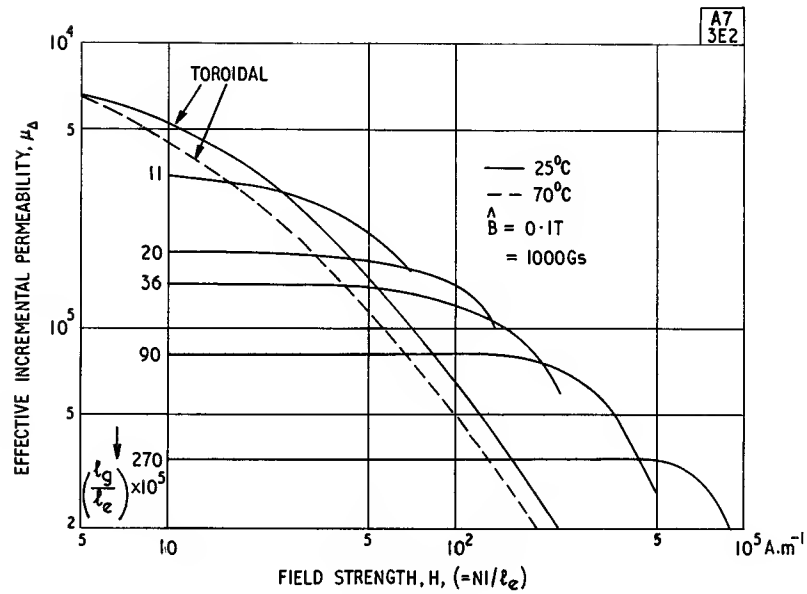


Fig. 3.6.5(b)

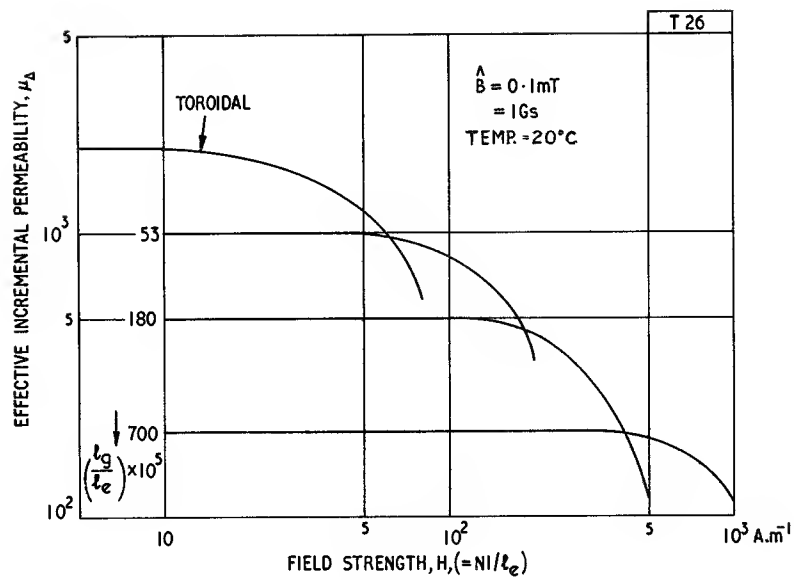


Fig. 3.6.6

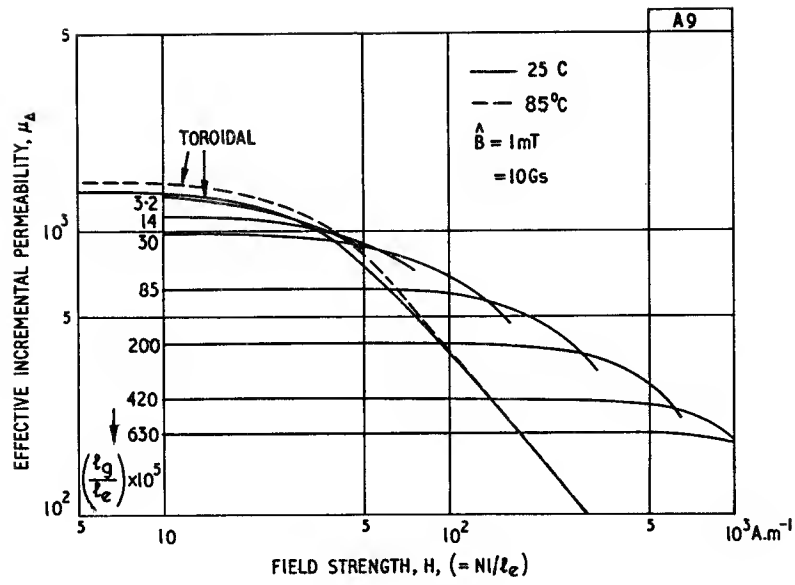


Fig. 3.6.7(a)

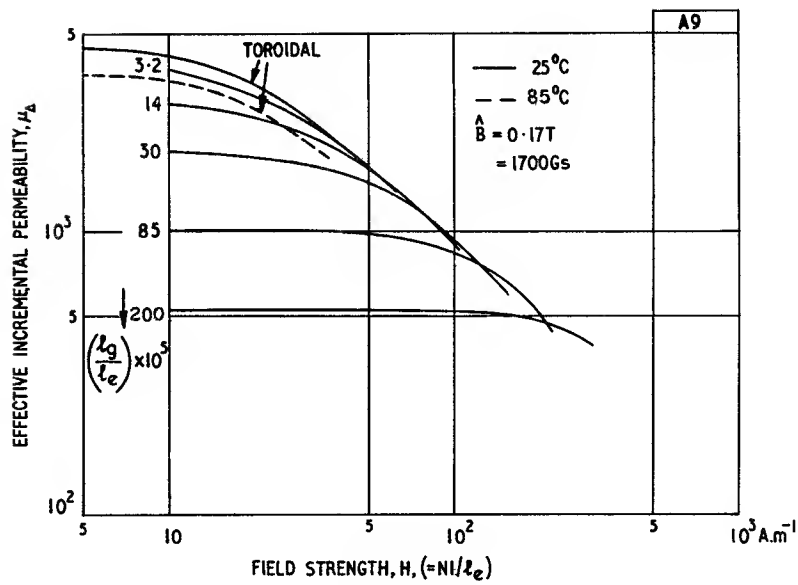


Fig. 3.6.7(b)

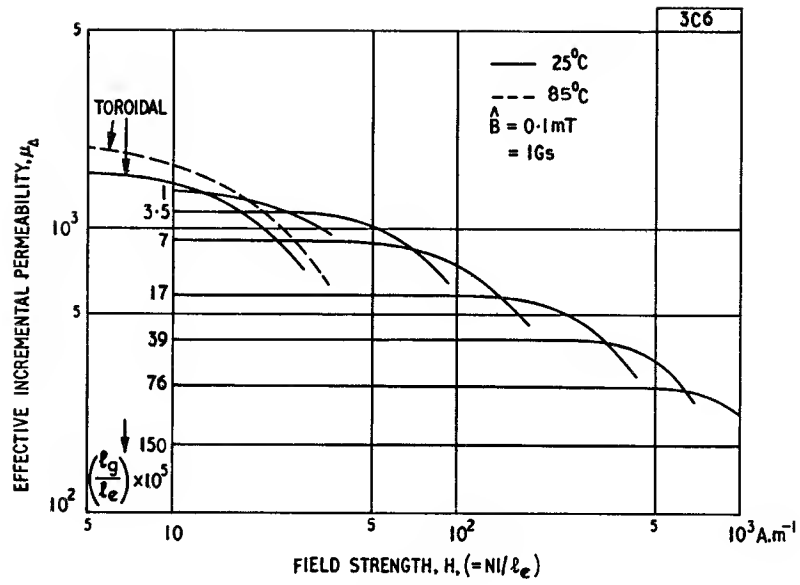


Fig. 3.6.8(a)

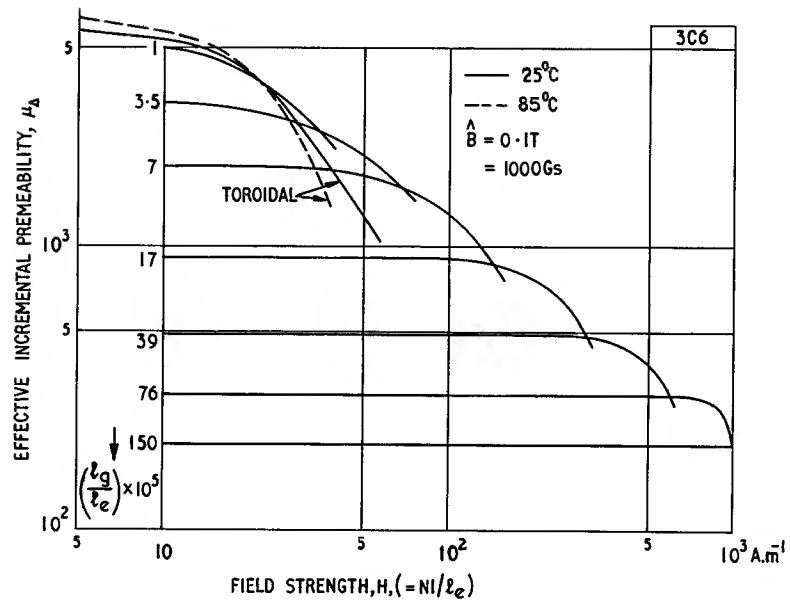


Fig. 3.6.8(b)

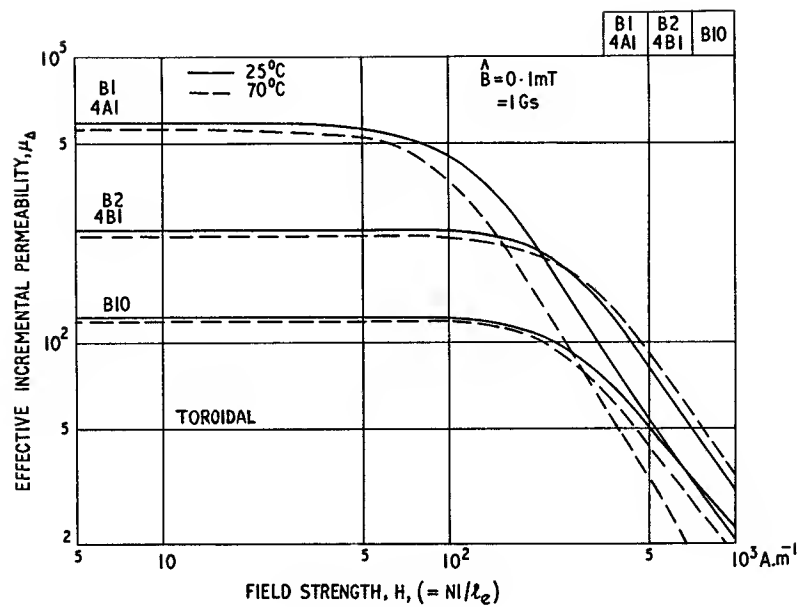


Fig. 3.6.9

Hanna curves Fig. 3.7

$$f = 5 \text{ kHz}$$

In the introduction to the preceding figure (μ_A v. steady field strength) it was observed that the usefulness of such graphs was confined to predicting the behaviour of a given design rather than preparing an original design. For convenience in the design of inductors and transformers carrying direct current the data are best presented in the form of Hanna curves.¹⁰ From the experimental data the parameter LI^2/V_e is calculated as a function of NI/l_e for each gap ratio. L is the inductance of N turns on the particular core used in the measurement, l_e and V_e are its magnetic length and volume and I is the direct current. It was shown by Hanna that the relation between these quantities is independent of the core geometry provided the cross section is constant and it may in practice be used quite generally. The curve for each given air gap ratio has a region in which it is above all the other curves; it is usual to draw a single envelope curve and mark along its length a scale of optimum air gap ratios.

To use the composite curve, the parameter LI^2/V_e is calculated from the value of the inductance required at a given direct current through a winding on a given core. From the curve the corresponding value of NI/l_e is found. Since I and l_e are known the value of N may be obtained. The point at which the calculated value of LI^2/V_e intersects the curve will give the air gap ratio that must be used to meet the requirements. This will

be the optimum design. It should be remembered that in most cases, e.g. E cores or U cores, the air gap so calculated is normally provided by means of spacers. Since there will be two spacers in the magnetic path each spacer thickness is half the required air gap.

The graphs of Fig. 3.7 show Hanna curves for a representative selection of ferrites, the majority measured at room temperature and at an elevated temperature. In a number of cases curves are shown for both low amplitudes and high amplitudes of alternating flux density. The curves for the nickel zinc ferrites are not true Hanna curves because data were available only for the ungapped core, however they have been included because in a limited way they are useful. Some indication of gapped performance may be obtained by analogy with the curves for the manganese zinc ferrites by extrapolating the lower part of the curve upwards, ignoring the falling off at the knee.

In the derivation, l_e and V_e are used as though they referred to an ideal core shape, i.e. a radially thin toroid. In the case of a practical core the effective length and volume may be used without much error. Where a core has a particularly non-uniform cross-section it may be preferable to determine experimentally a special curve for it, expressing LI^2 as a function of NI with spacer thickness as a parameter so that the core geometry does not figure in either the preparation or the practical use of the curve (see Fig. 7.11).

(See also Section 7.3.1, p. 253)

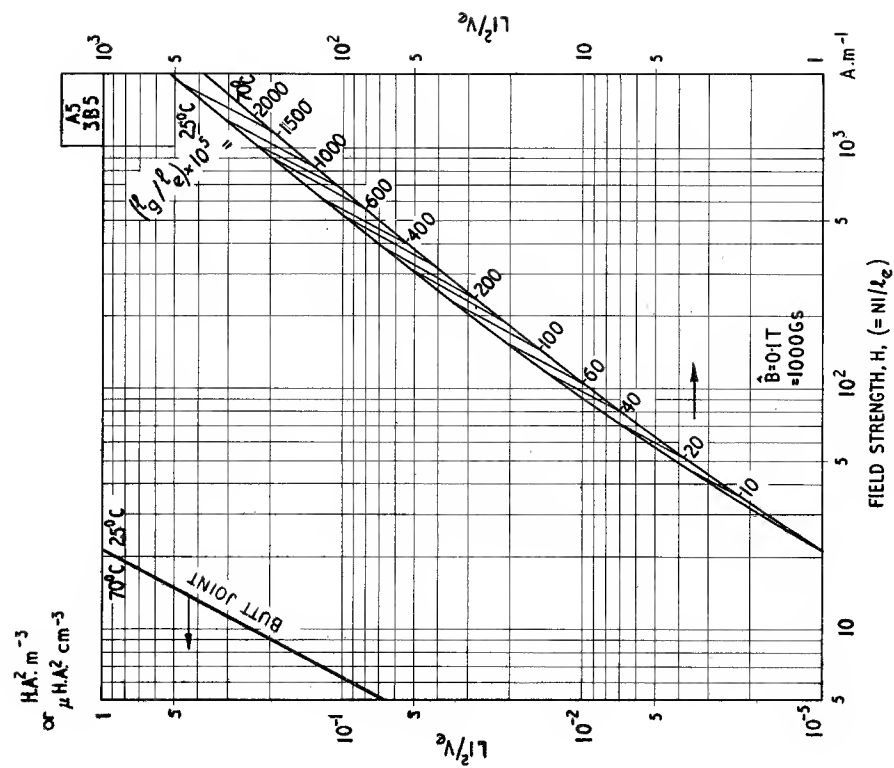


Fig. 3.7.1(b)

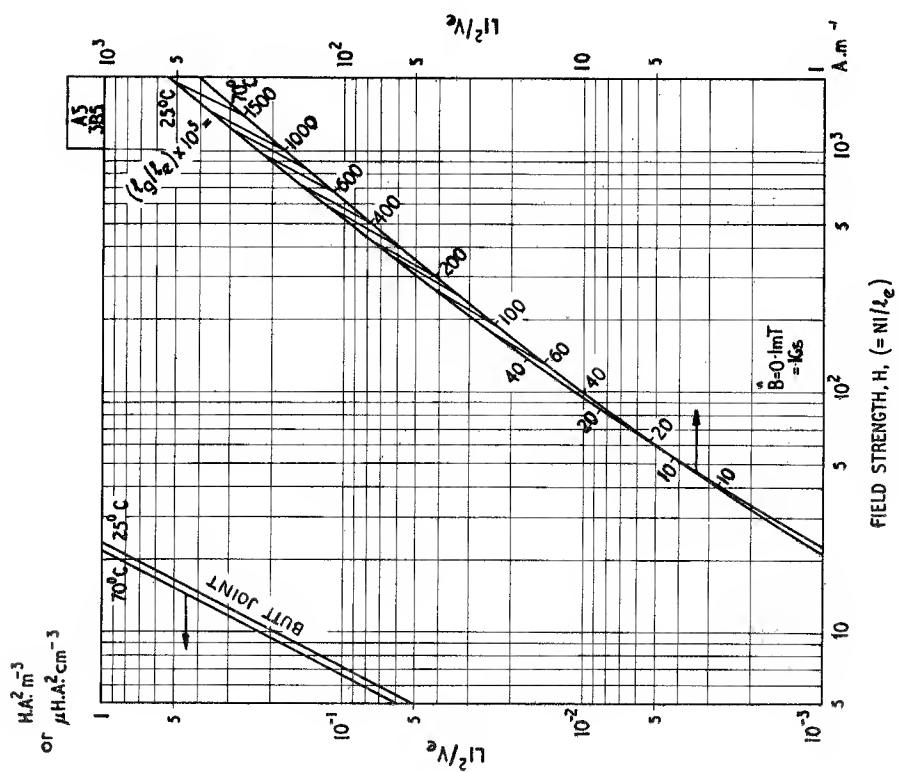


Fig. 3.7.1(a)

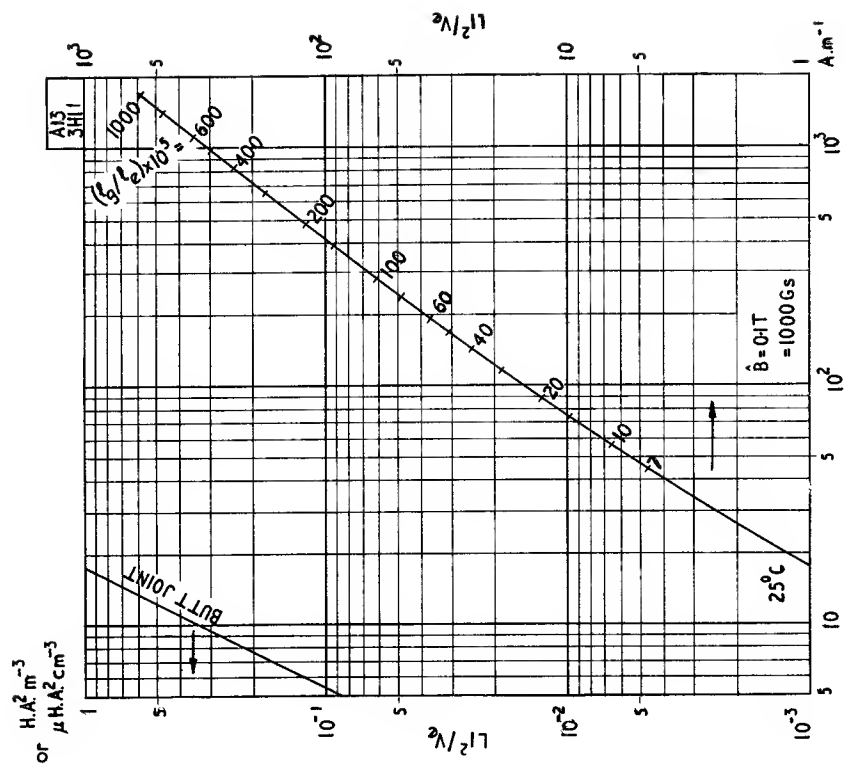
FIELD STRENGTH, H , ($= NI/L_e$)

Fig. 3.7.2(b)

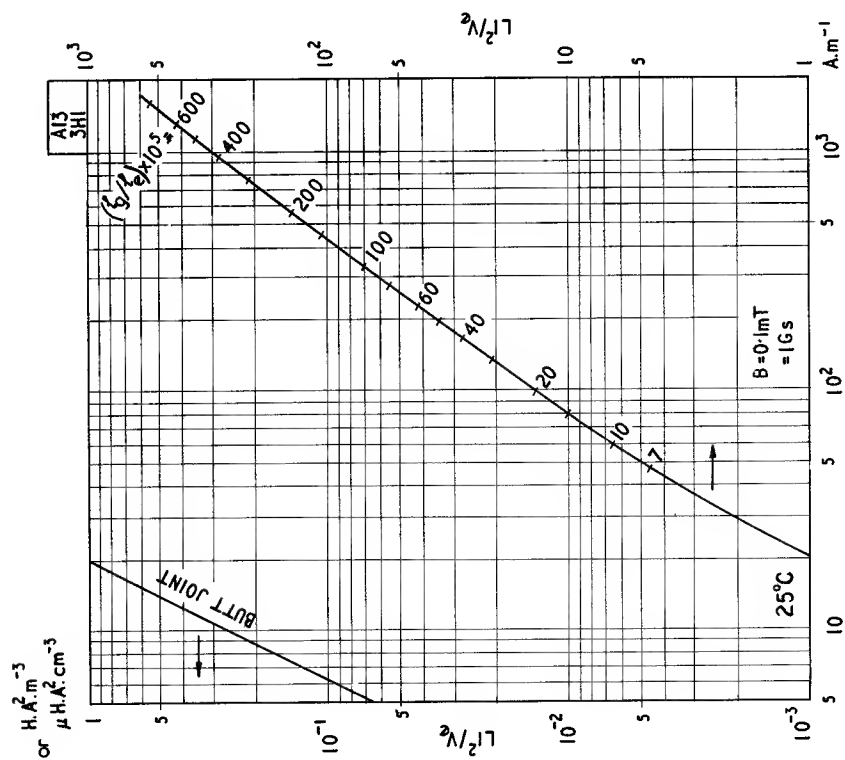
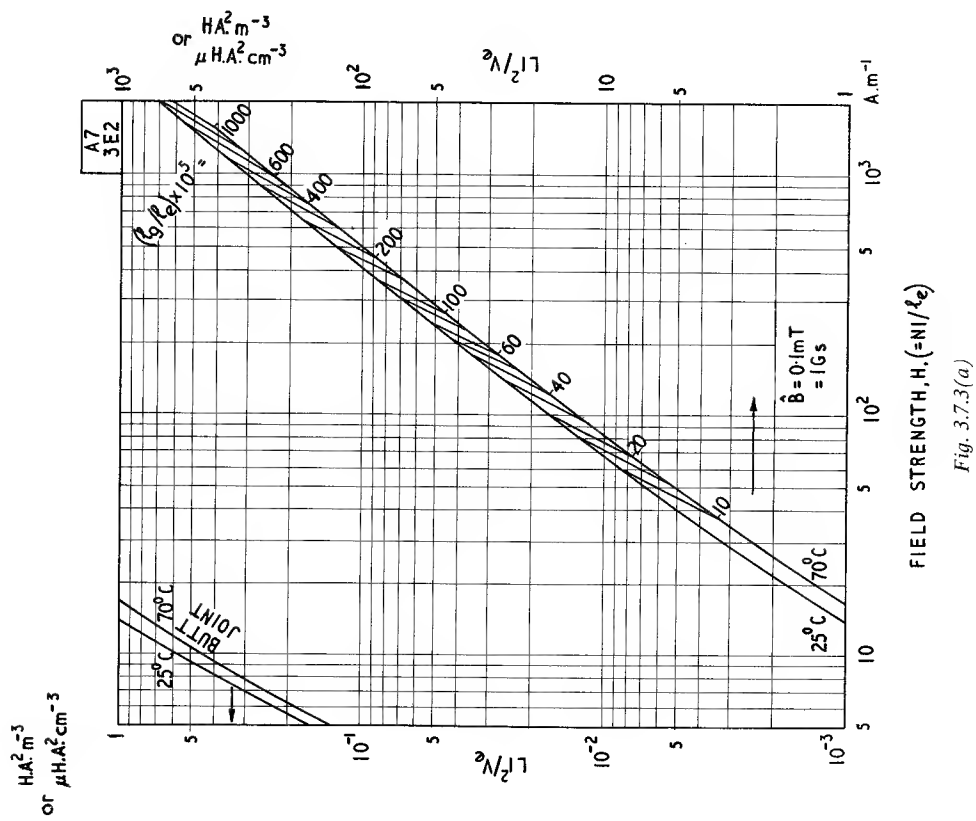
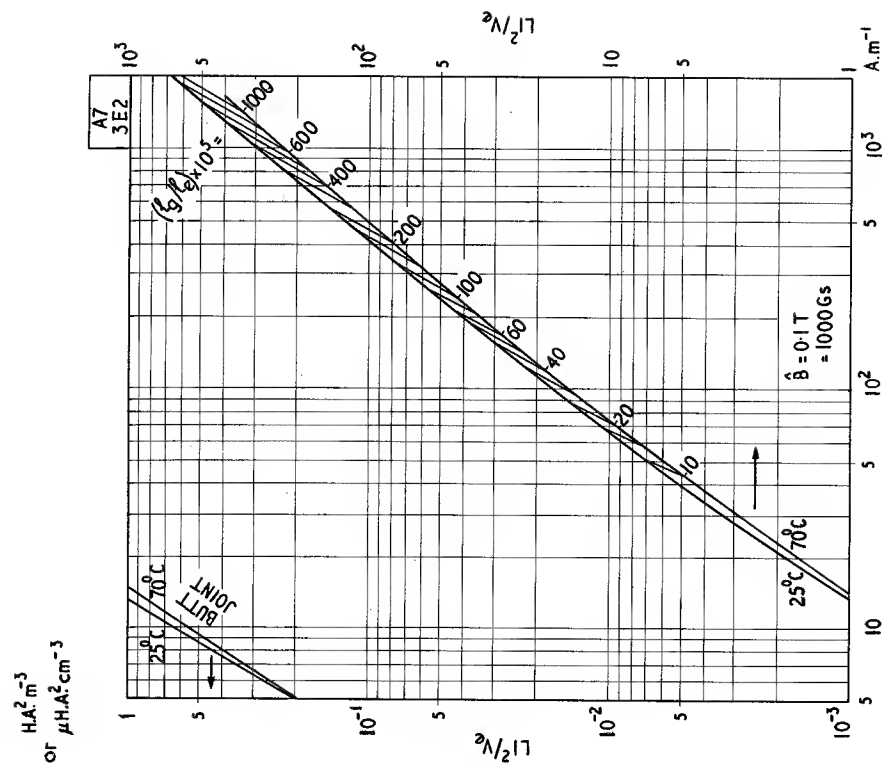
FIELD STRENGTH, H , ($= NI/L_e$)

Fig. 3.7.2(a)



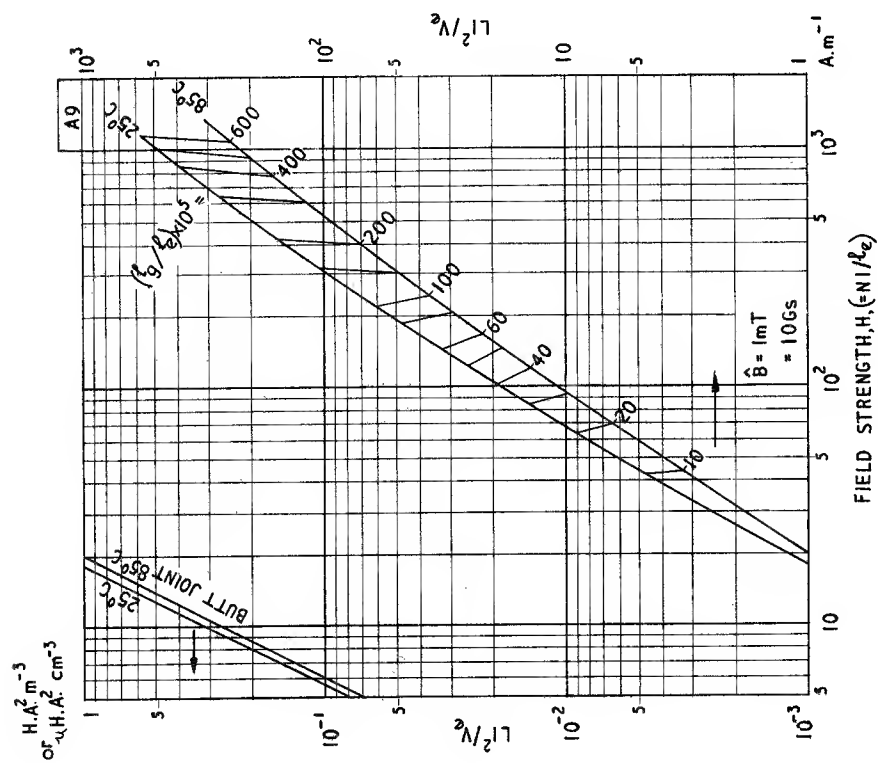


Fig. 3.7.4(a)

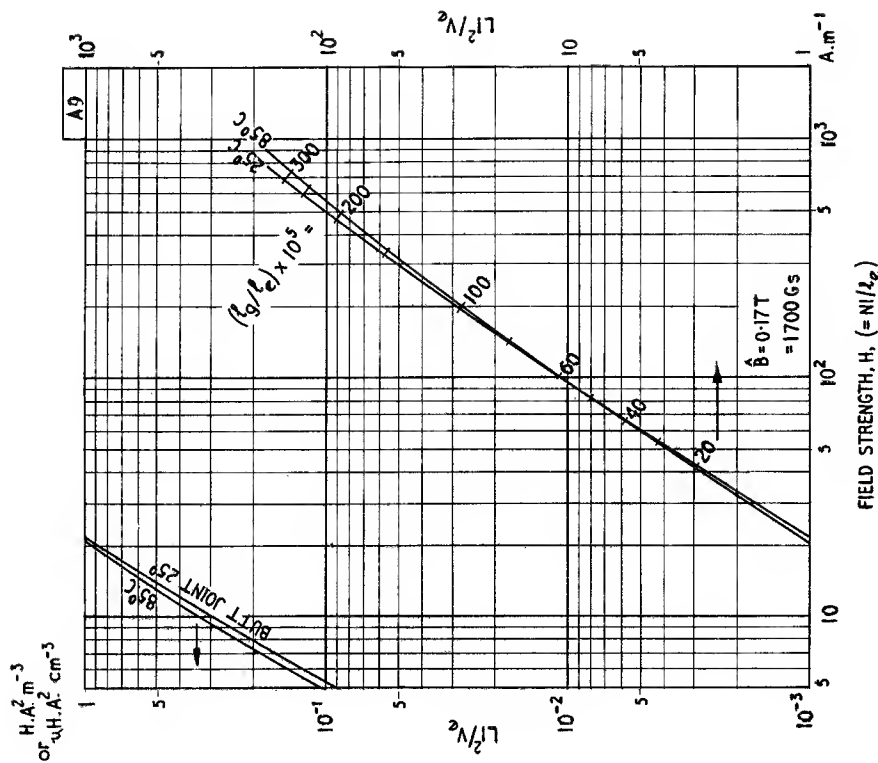


Fig. 3.7.4(b)

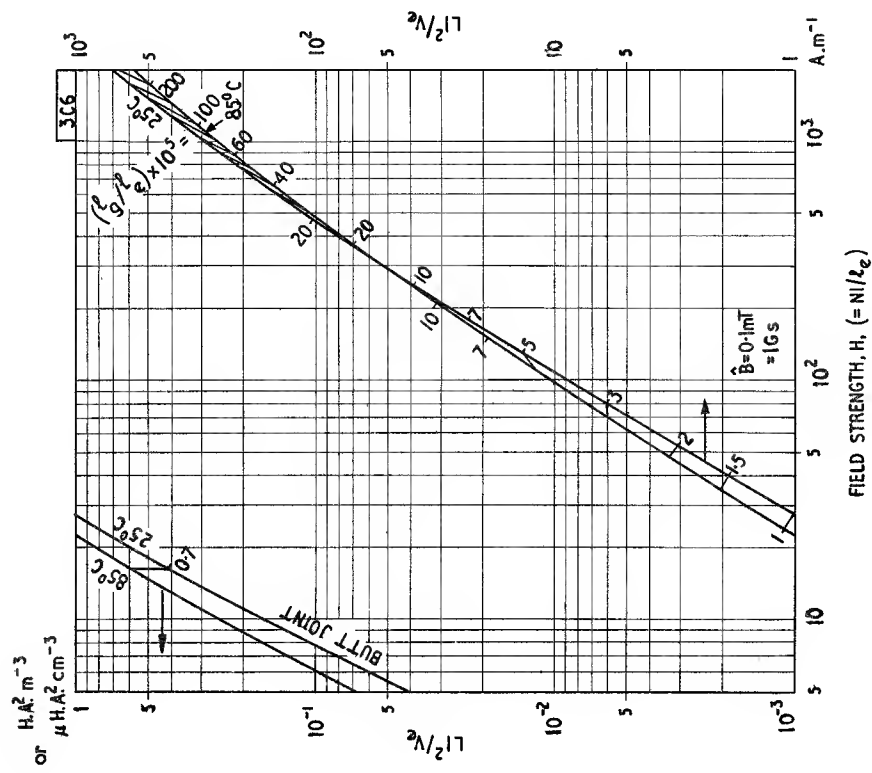


Fig. 3.7.5(a)

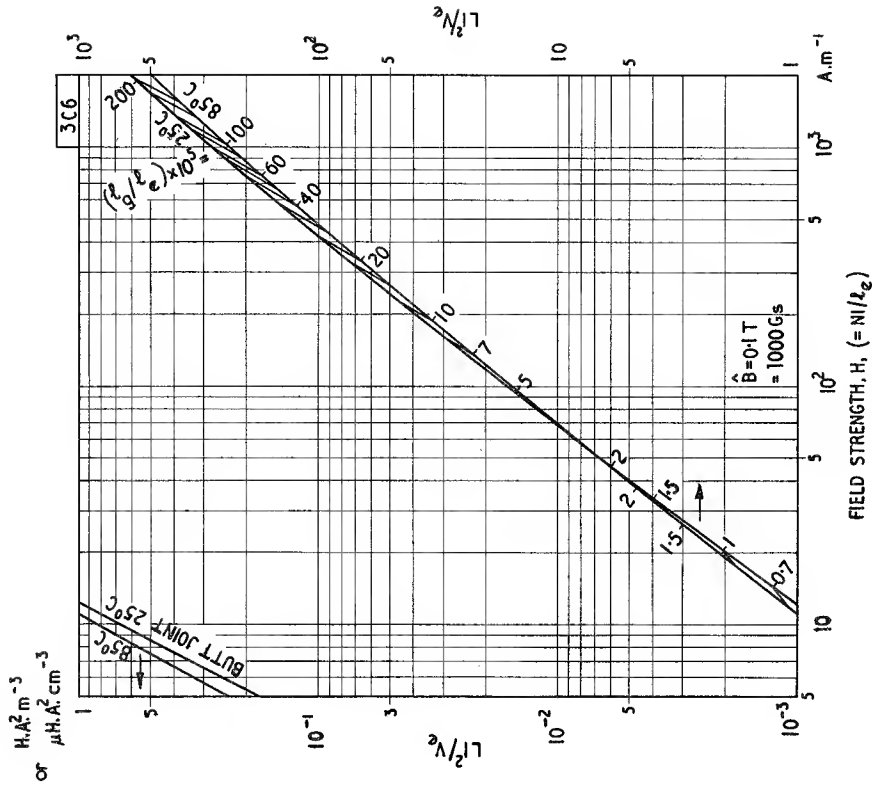


Fig. 3.7.5(b)

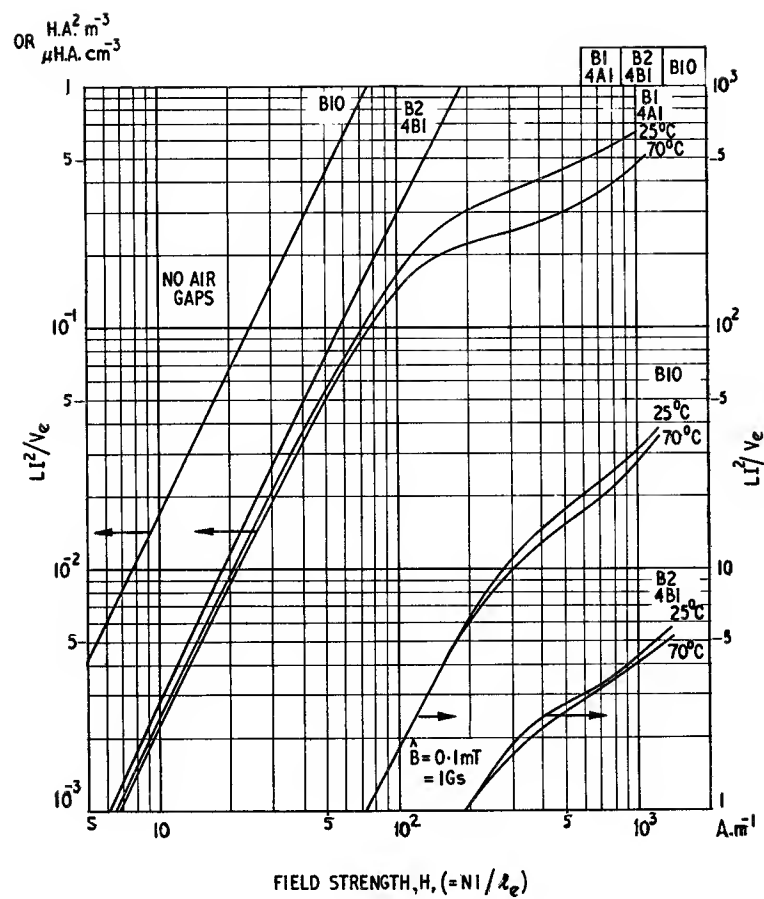


Fig. 3.7.6

Initial permeability as a function of temperature Fig. 3.8

$f = \text{low}$

$\hat{B} = \text{low}$

As the temperature is raised from a low value, the initial permeability of a ferrite normally rises until it peaks just below the Curie point and then drops rather abruptly towards unity at the Curie point. There is often evidence of a secondary peak near or below room temperature. It is believed that this is normally due to a small excess of ferrous ions which, having a large positive crystalline anisotropy, cause the overall crystalline anisotropy to go through zero at a particular temperature, the anisotropy due to the remaining cations being small, negative and diminishing with increasing temperature. This effect is sometimes utilized to control the temperature coefficient of permeability over a limited range, e.g. see A13 and 3B7 in Fig. 3.8.4. Other ions, e.g. cobalt, can have a similar effect and are sometimes introduced in small quantities for this purpose.

In measuring the temperature coefficient care must be taken to avoid time effects. Obviously sufficient time must be allowed for the specimen to achieve a stable and uniform temperature. When this has been done there will in general remain a time change of permeability resulting from the thermal disturbance as described in the introduction to Fig. 3.10. If this is ignored the temperature change will appear to have an irreversible component

and the measurements will be unreliable. The difficulty may be avoided by allowing sufficient time, e.g. 1 h, after the specimen has reached the required uniform temperature; the time-change will usually have become negligible by that time. Another method that has been proposed is to subject the specimen to an alternating field diminishing rapidly from saturation to zero at a fixed time, e.g. 10 min before any measurement. Such a process is described in more detail in the introduction to Fig. 3.10. This treatment removes the effect of the thermal disturbance and replaces it with a controlled disturbance. However, if the time-dependence of the permeability due to this disturbance is itself temperature dependent errors will again be introduced. The most reliable method is to change the temperature and let the specimen remain at the new temperature until the permeability is constant.

The first two graphs show the effect of zinc content on the permeability/temperature relation (after Smit and Wijn¹¹). As the zinc content becomes larger the Curie temperature falls and the room-temperature permeability increases. The manganese zinc ferrites, which are the subject of the first graph, contain a small amount of ferrous ions and show the characteristic secondary peak. (See also Sections 2.2.2, 4.2.2 and 5.5.2.)

$$\text{Temperature coefficient} = \Delta\mu_i/\mu_i\Delta\theta \quad (\text{see Eqn 2.20})$$

$$\text{Temperature factor} = \Delta\mu_i/\mu_i^2\Delta\theta \quad (\text{see Eqn 2.23})$$

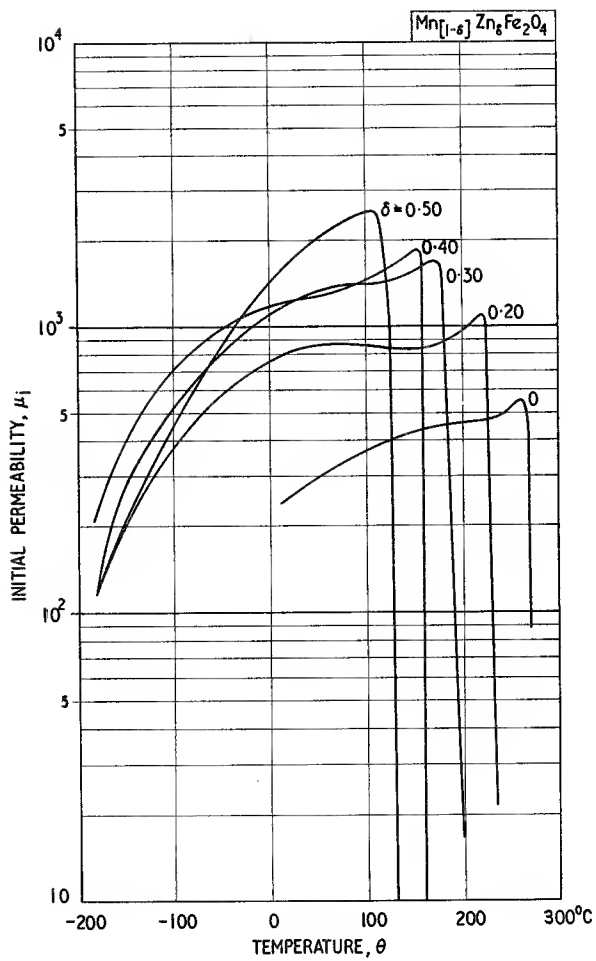


Fig. 3.8.1

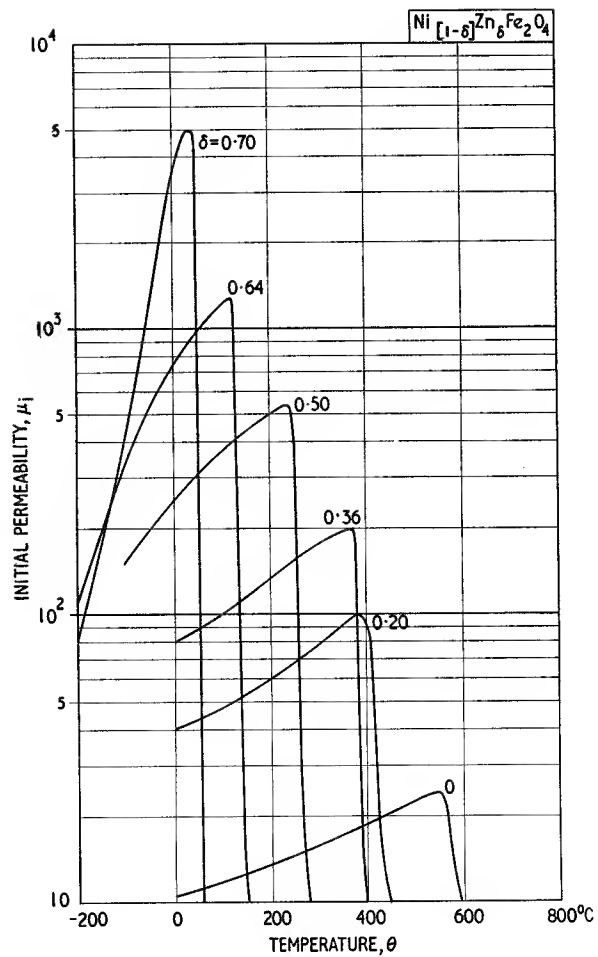


Fig. 3.8.2

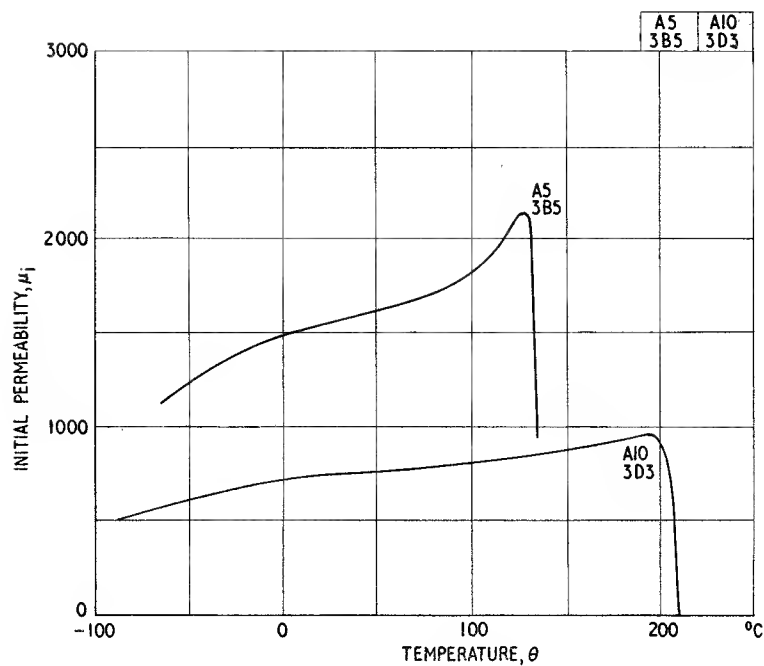


Fig. 3.8.3

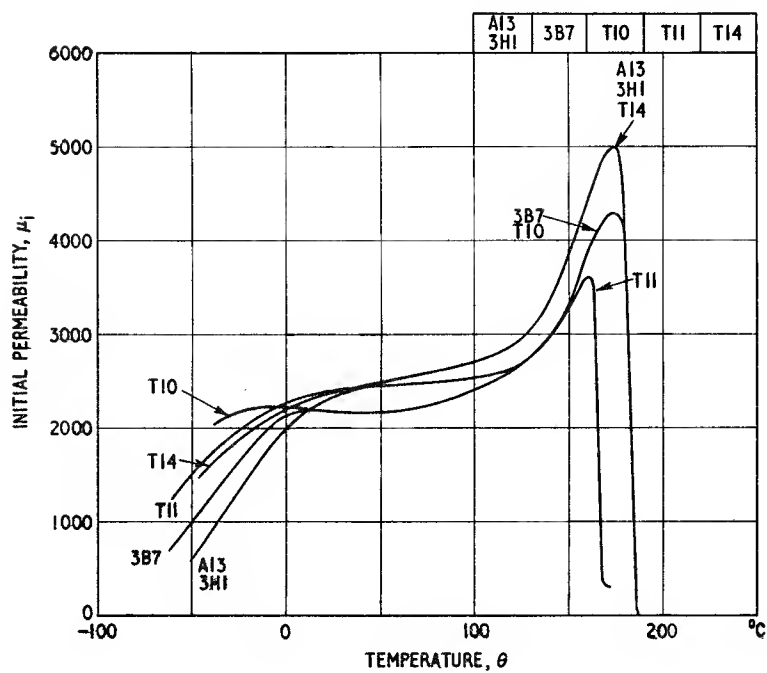


Fig. 3.8.4

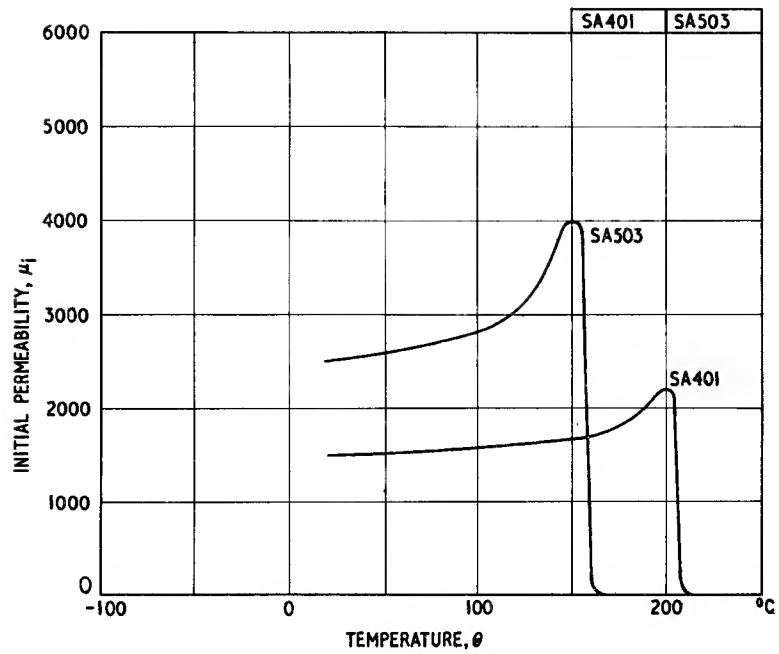


Fig. 3.8.5

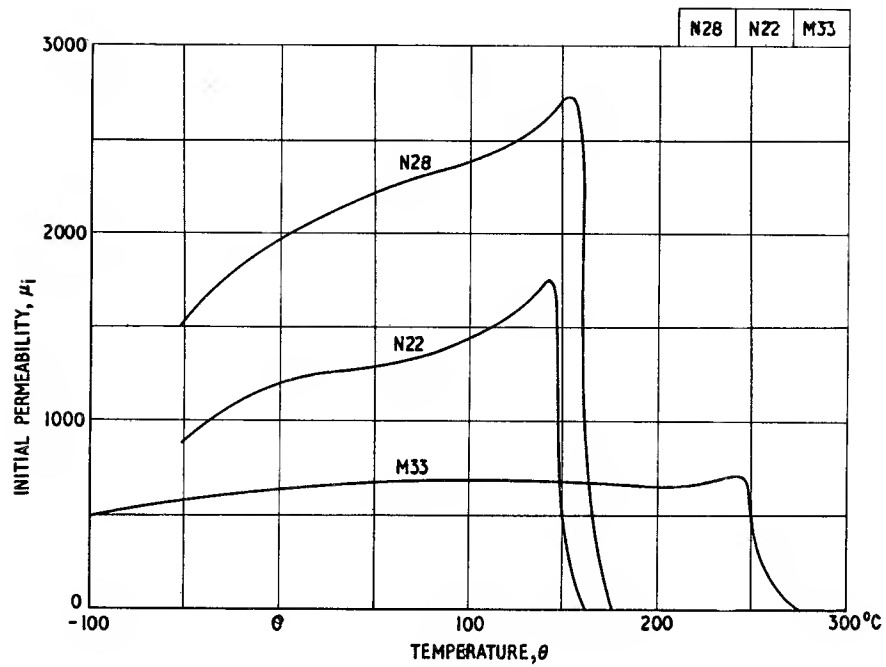


Fig. 3.8.6

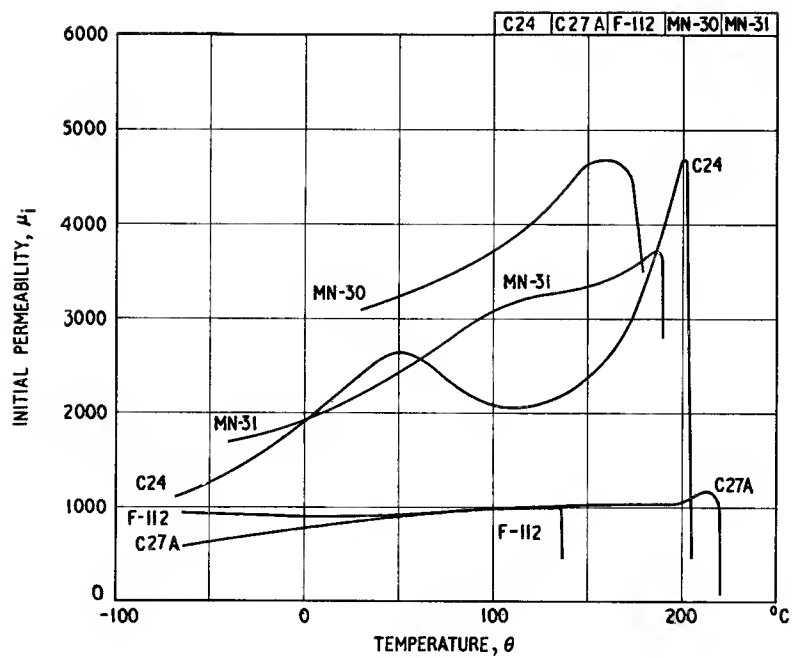


Fig. 3.8.7

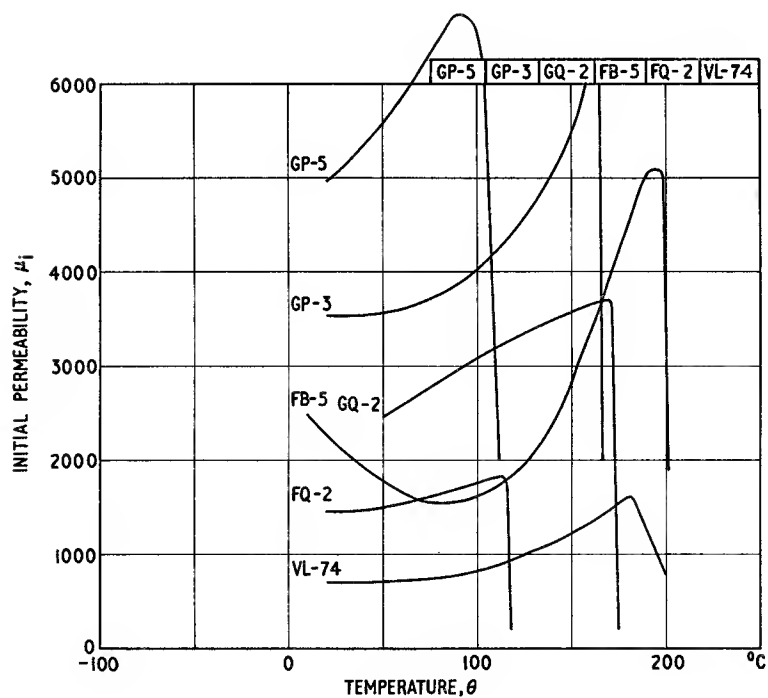


Fig. 3.8.8

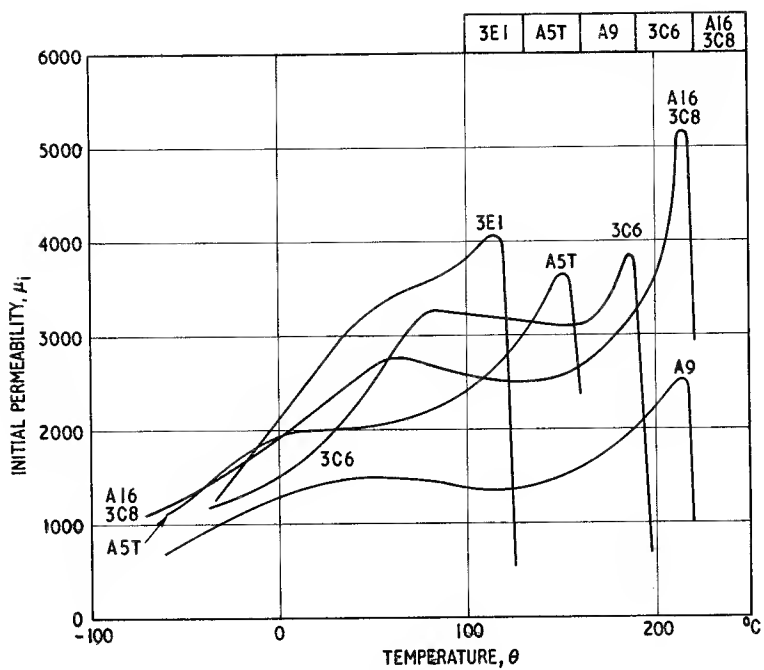


Fig. 3.8.9

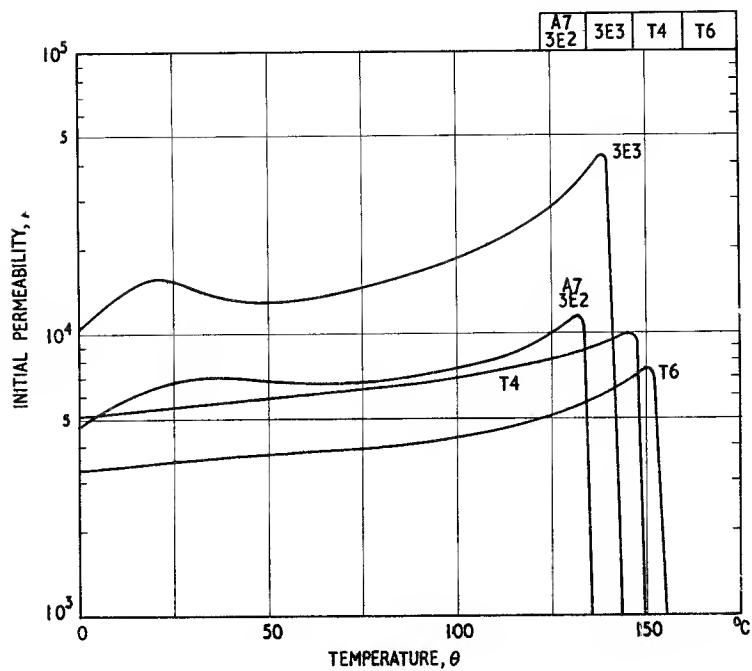


Fig. 3.8.10

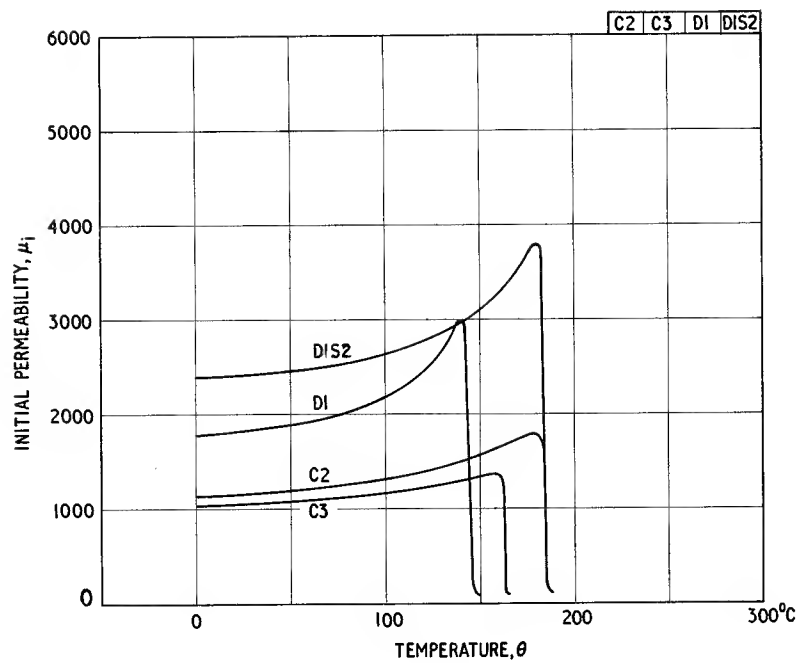


Fig. 3.8.11

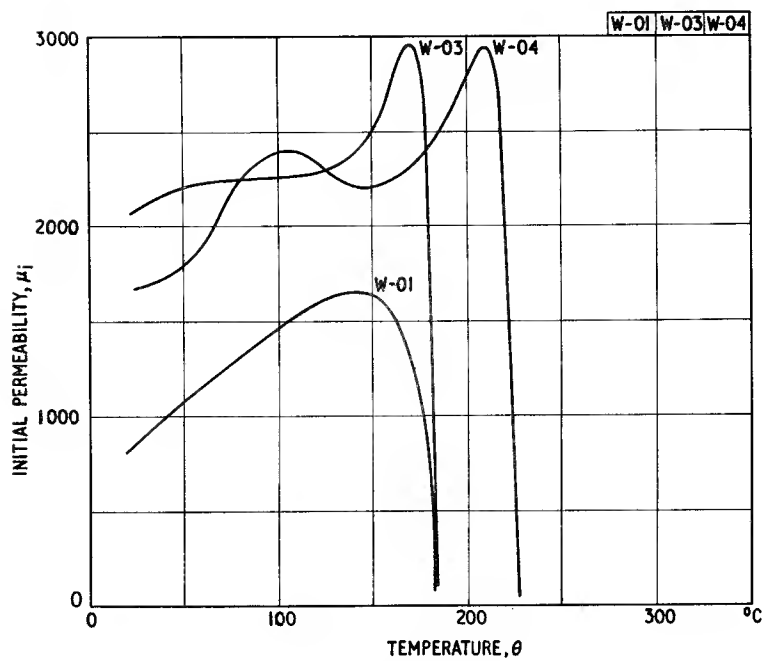


Fig. 3.8.12

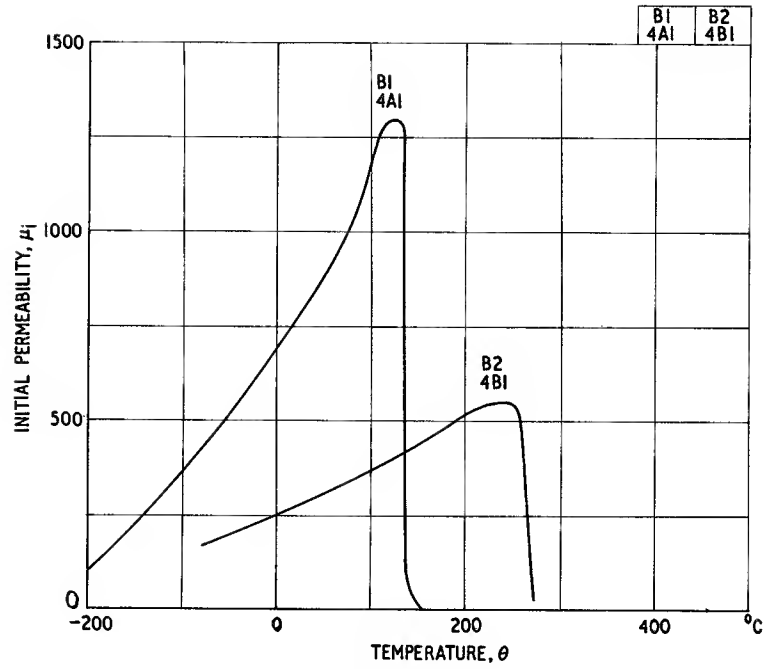


Fig. 3.8.13

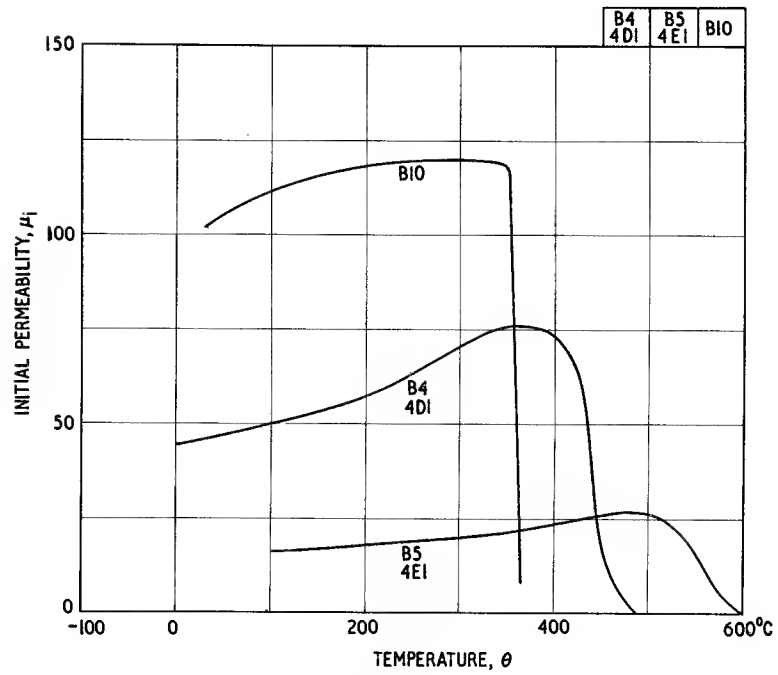


Fig. 3.8.14

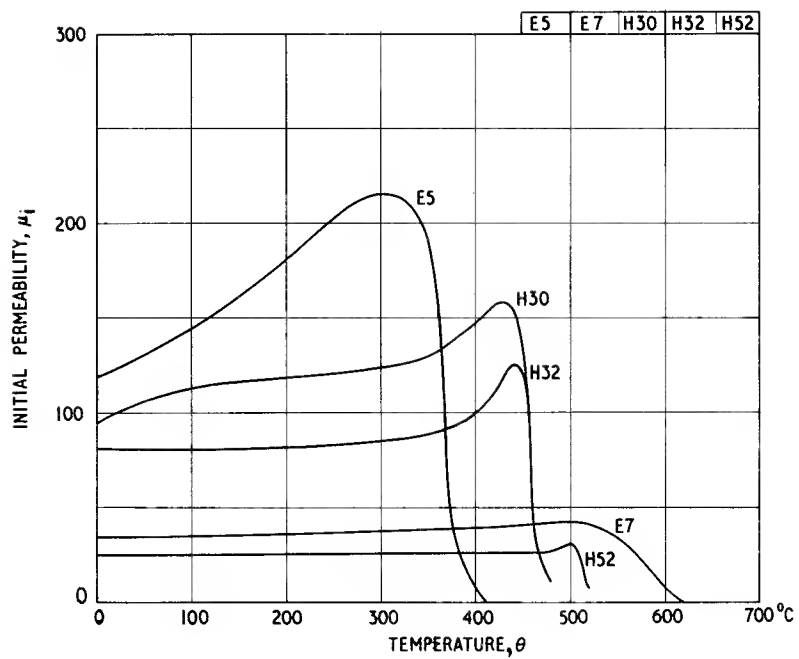


Fig. 3.8.15

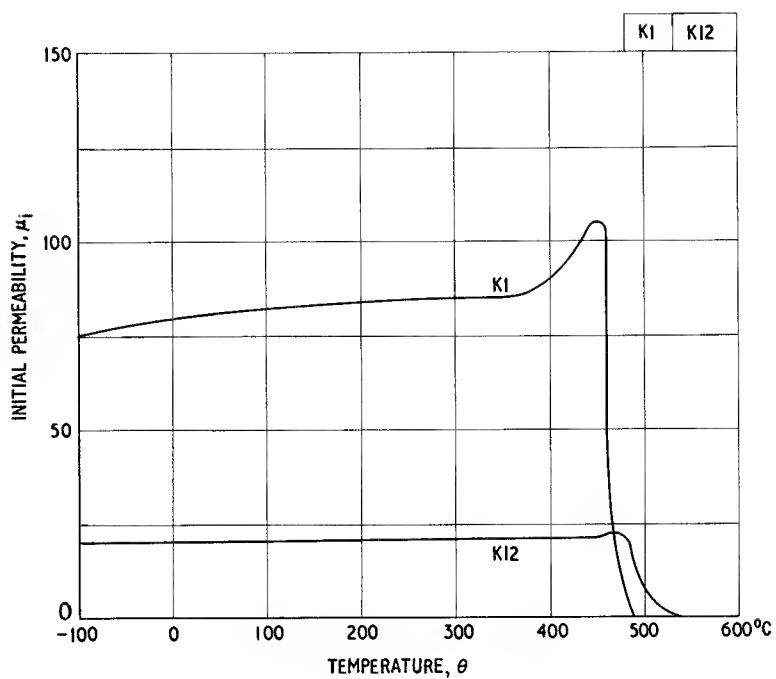


Fig. 3.8.16

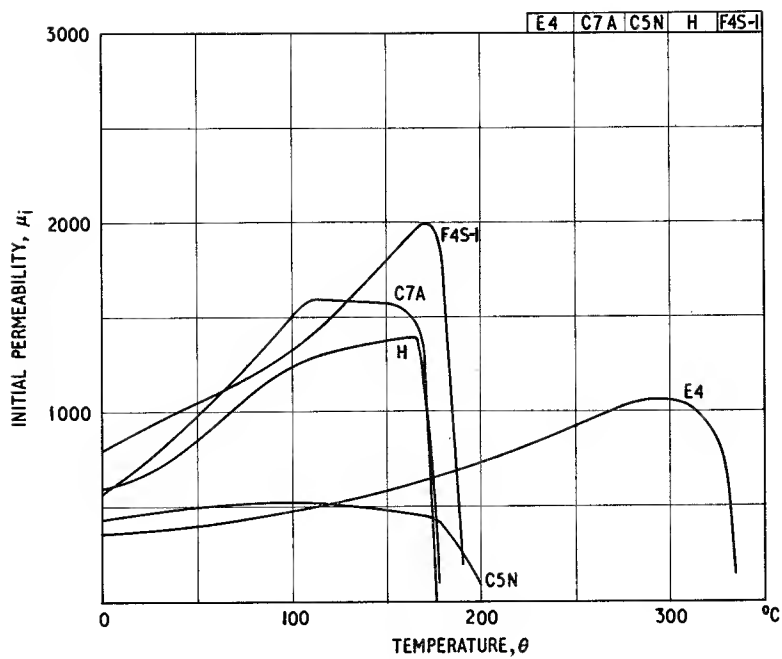


Fig. 3.8.17

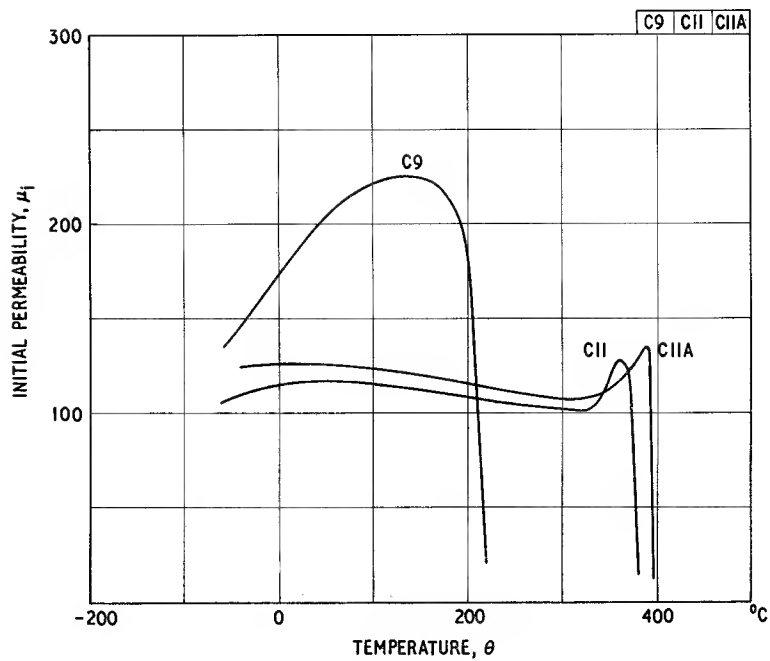


Fig. 3.8.18

Incremental permeability as a function of temperature with steady field strength as a parameter Fig. 3.9

$$f = 5 \text{ kHz}$$

$$B = 0.1 \text{ mT (1 Gs)}$$

It has been seen in the previous figure that the temperature coefficient of initial permeability is normally positive unless there is a pronounced secondary peak in the curve. However the incremental permeability is governed to some extent by the saturation flux density, e.g. referring to Fig. 3.1.1 it may be deduced that the incremental permeability at a field strength of 80 A.m^{-1} would fall as the temperature rises from 20°C to 100°C simply due to the diminishing B - H loop (see also Fig. 6.3). So it is to be expected that as the steady field strength is increased

the temperature coefficient of the incremental permeability will decrease and become negative. The graphs that follow illustrate the behaviour of some ferrites that might find application in transducers.

The effect of a steady field is to reduce the primary peak of the permeability/temperature curve that occurs just below the Curie point. As the steady field is increased this peak moves towards the lower temperatures and the whole curve is lowered. Over a small range of temperature, which depends on the value of the steady field strength, the temperature coefficient is approximately zero. The first and last graphs show secondary peaks in the region of room temperature. The steady field appears to suppress these peaks less than the primary peaks.

(See also Section 6.2.2.)

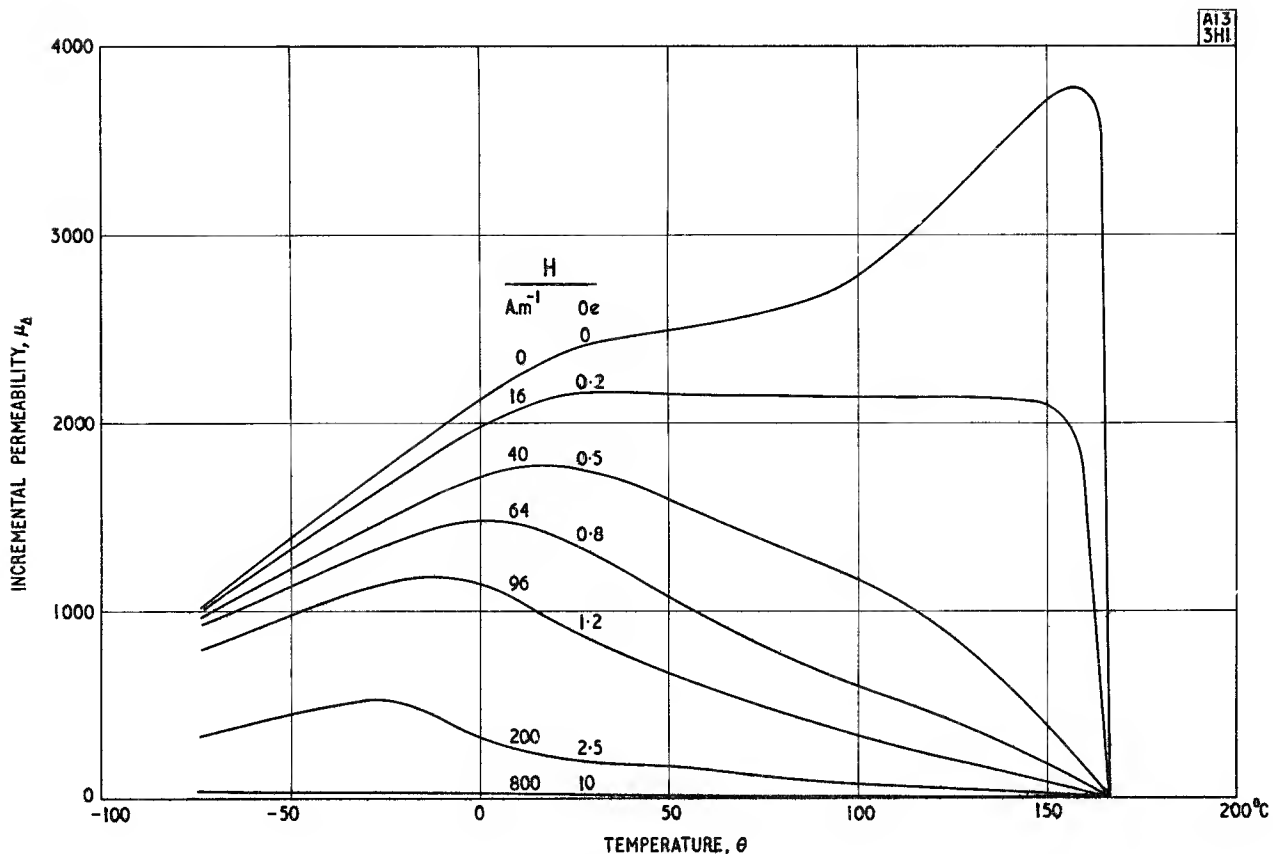


Fig. 3.9.1

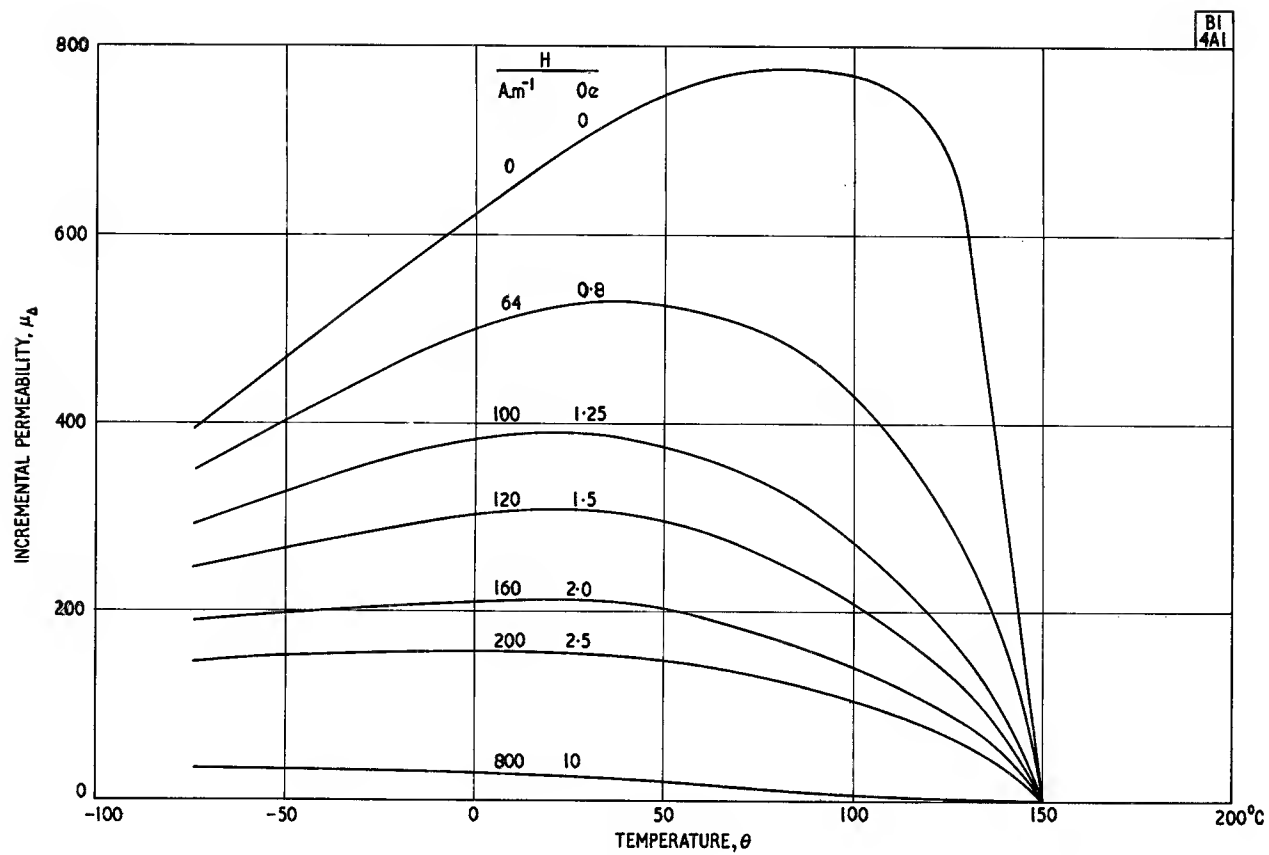


Fig. 3.9.2

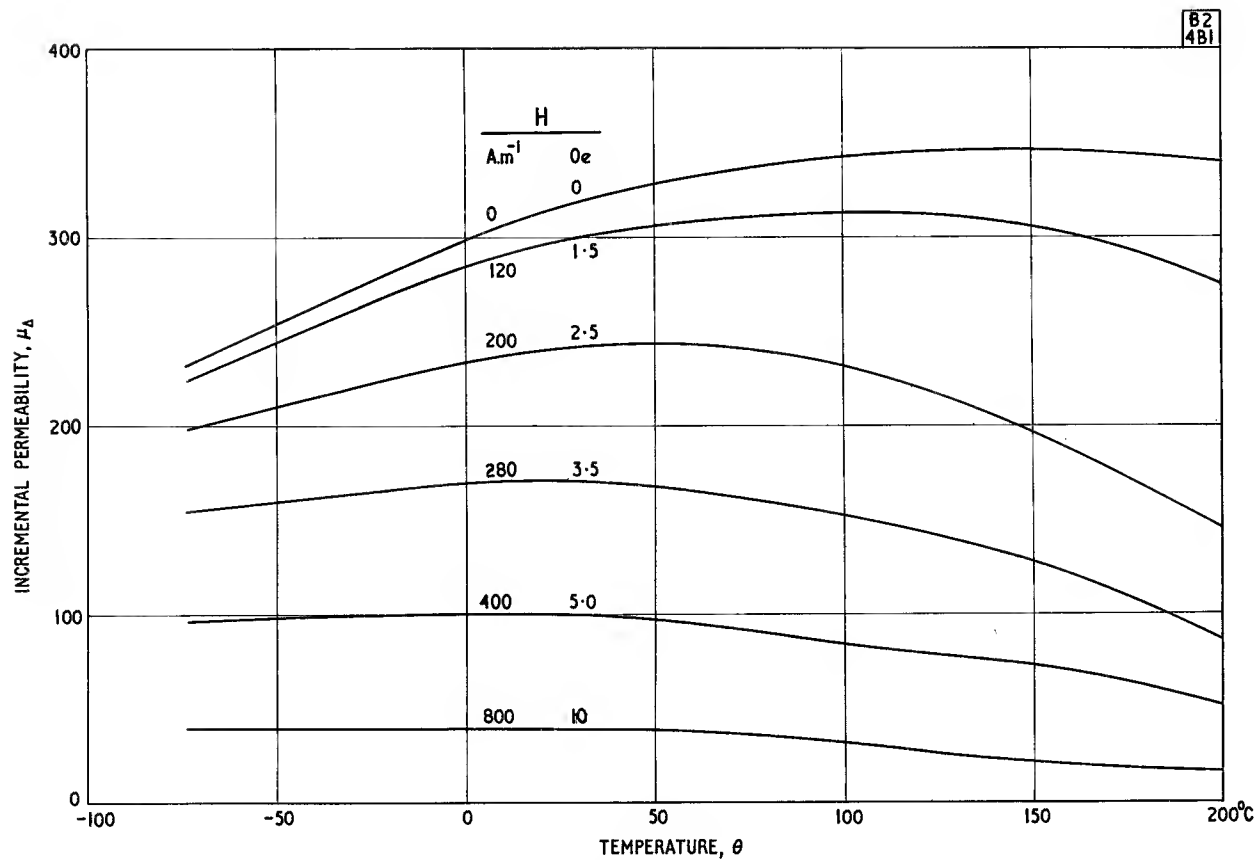


Fig. 3.9.3

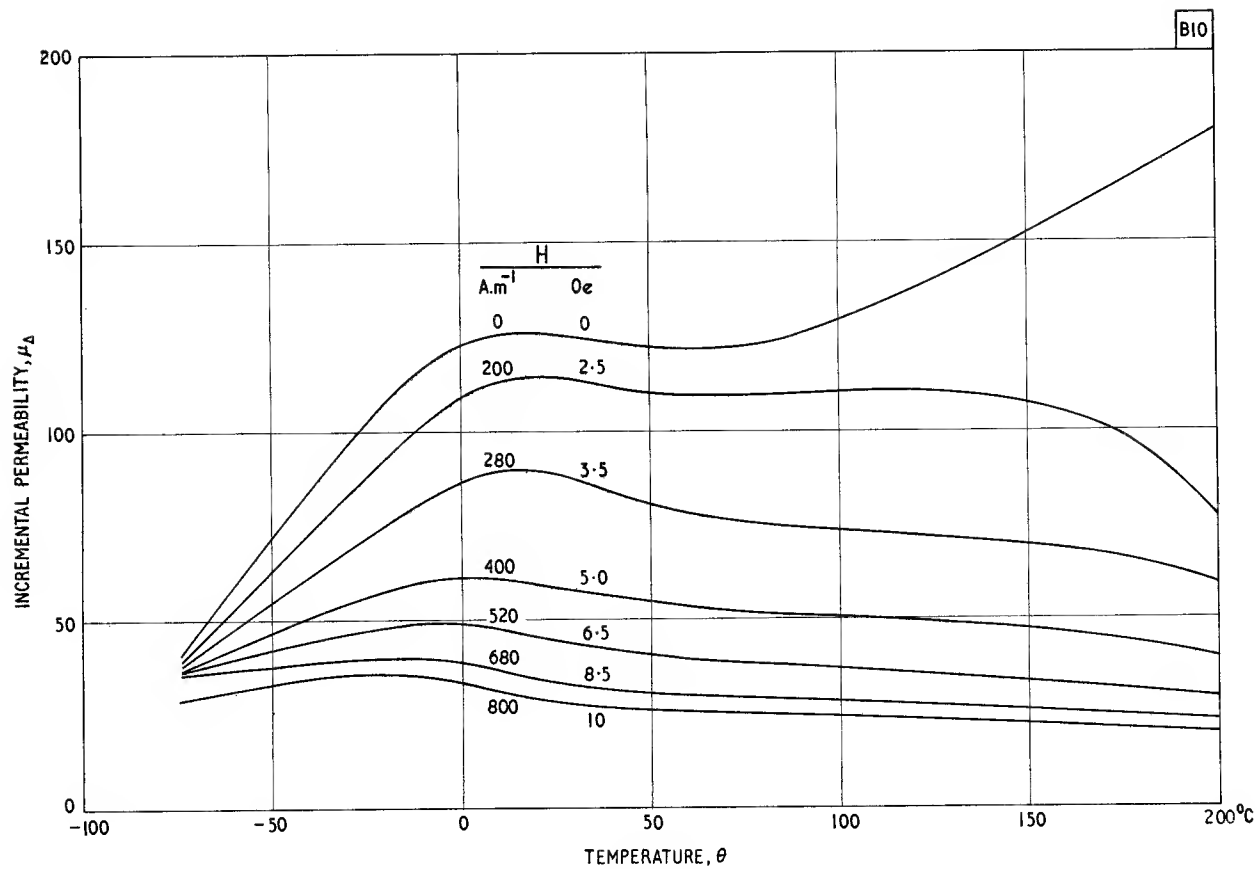


Fig. 3.9.4

Disaccommodation Fig. 3.10

$$f = 5 \text{ kHz}$$

$$\hat{B} = 0.1 \text{ mT } (< 1 \text{ Gs})$$

If a magnetic material is given a disturbance, which may be magnetic, thermal or mechanical, the permeability observed immediately after the cessation of the disturbance is normally found to be raised to an unstable value from which it returns, as a function of time, to its undisturbed or stable value. This phenomenon has been called time-change of permeability but is usually referred to as disaccommodation. The process is repeatable indefinitely and in this sense it is different from ageing, which is a permanent change with time and which is not generally observed in ferrites at normal operating temperatures.

There are a number of possible mechanisms of disaccommodation in ferrites and they all depend on migratory processes within the lattice. These processes often involve the anisotropic or preferred distribution of ferrous ions and/or cation vacancies over the four octahedral sublattices of the spinel structure. The preference for a particular sublattice depends on the direction of the domain magnetization and, therefore, on the position of the domain walls. The distribution tends to fix, and be fixed by, the location of the domain walls, giving rise to a more stable or lower permeability state. After the disturbance the vacancies and domain walls are no longer in a mutually low energy state (therefore the initial permeability is higher) but the lower energy state is progressively approached as the ferrous ions and/or vacancies migrate to the new preferred sites conditioned by the new domain wall positions. In other words the disturbed domain wall, having taken up a new position, sinks slowly into an energy trough at that position, losing mobility and reducing domain wall contribution to the permeability as it does so. The rate at which the vacancies are redistributed or diffuse depends very much on the temperature, shorter time constants being observed at the higher temperatures. If the permeability is measured with a large amplitude signal it is clear that domains will be constantly jumping to new positions and disaccommodation will not be observed; the maximum disaccommodation is observed at vanishingly small measuring amplitudes.

Perhaps the most fundamental disturbance is an excursion of the temperature of the material above the Curie point and back again. As this is rather a lengthy process it is not a very convenient basis for a quantitative method of measuring disaccommodation. Instead, a disturbance procedure similar to an a.c. demagnetization is usually preferred; it is particularly suitable for measurements on manganese zinc ferrites. On the other hand it is not suitable for field sensitive materials, such as those

described in Fig. 3.1.24; these suffer permanent change of properties due to high fields and so the Curie point method is perhaps the only means by which their disaccommodation may be assessed.

The a.c. field method consists of subjecting the material to a saturating alternating field for a few periods and then the amplitude is reduced progressively from just above the knee of the B - H loop to zero. Excessive saturation should be avoided because this may cause heating of the core by the winding. An exponential decay of field is convenient and effective; a frequency of about 100 Hz and a time constant of about 0.08 s has been found to give reproducible results. Using such a standard disturbance the time-change of permeability may be measured (at constant temperature) and materials compared. It should be remembered when using disaccommodation data that the test disturbance is artificial and as such is unlikely to occur, for instance, during the manufacture and life of a filter inductor. However, investigations have shown¹² that the time-change following the test disturbance is similar in form and magnitude to that following a temperature change to which a ferrite-cored component may be subjected, e.g. a 50°C step.

The graphs show, for various grades of ferrite and at various temperatures, the time-change of initial permeability following the test disturbance. It may be seen that, measured over the interval from 1 min to 24 h after the test disturbance, the initial permeability of inductor ferrites at room temperature may typically decrease between 0.5 and 2.5%.

For convenience the relation is usually taken to be proportional to the logarithm of time, and based on this assumption there are several standard methods of expressing the disaccommodation numerically. The original method, which is still sometimes used, is to express the disaccommodation, D , simply as the percentage decrease of permeability between 1 min and 24 h after the test disturbance (demagnetizing procedure). This is often called the 24 h disaccommodation. More recently time intervals of 10 min and 100 min have come into use.

As shown in Section 4.2.2, any change in initial permeability is diluted in its effect on a gapped core by the ratio μ_e/μ_i . Thus, for a given μ_e , a higher value of μ_i will result in a lower value of effective disaccommodation in a gapped core. This consideration gives rise to the concept of normalized disaccommodation or disaccommodation factor, D.F., which is defined as D/μ_i . This is the parameter which characterizes the time variability of a material, since a higher value of disaccommodation is permissible provided the μ_i is proportionately higher, so that the effective value in a gapped core is unchanged:

$$\text{effective disaccommodation} = \frac{D}{\mu_i} \times \mu_e = (\text{D.F.}) \times \mu_e$$

It may be noted that the ratio 24 h/1 min equals 1440 and that if the graph were a straight line the 1 min–24 h change would be repeated in a further 1440 d, i.e. about $4\frac{1}{2}$ y.

The IEC (TC51) has recently recommended that the D.F. be expressed as:

$$\frac{(\mu_1 - \mu_2)}{\mu_1^2 \log_{10} \frac{t_2}{t_1}}$$

where the suffices refer to the first and second measurement and t is the appropriate time interval after the test disturbance. If the graph is a straight line then the same value of D.F. will be obtained whatever values of t_1 and t_2 are chosen. If $t_2/t_1 = 10$ then the logarithm is unity while if $t_1 = 1$ min and $t_2 = 24$ h the logarithm is 3.16, so to convert 24 h D.F. values as previously expressed to values corresponding to the proposed IEC expression, the previous values must be divided by 3.16.

Returning to the experimental results it is clear that the graphs are not quite straight lines but, at least over the early period, tend to droop below the tangent drawn at $t = 1$ min. The true form of the variation and its nature has been described in the literature. The error in taking the long-term disaccommodation as proportional to the 24 h value on a log time basis is not large. For the ferrites referred to in this figure it is seen that with increasing temperature the variation with time increases.

It has been observed previously that a thermal disturbance such as a rise in temperature (well below the Curie temperature) will cause a variation with time similar in form to that just described. The implications of this in relation to the measurement of temperature coefficient have been mentioned in the introduction to Fig. 3.8. Either sufficient time must be allowed at each temperature so that the rate of time-change of permeability becomes negligible, or a test disturbance (demagnetization procedure) must be applied to remove the past history of time-change and replace it with a prescribed time-change, the measurement being performed at a fixed

interval, say 10 min, after the test disturbance. This works quite well over small temperature ranges but it follows from the temperature dependence of disaccommodation that it cannot hold over a wide range. The first method, i.e. allowing sufficient time for thermal disaccommodation to become negligible, is probably the more reliable.

In any accurate measurement of permeability or inductance the possibility of time change due to previous disturbance should be taken into account and sufficient recovery time allowed. Apart from its effect on the accuracy of measurements, the principal importance of disaccommodation is in the design of high stability inductors used in wave filters as described in Chapter 5. (See also Sections 2.2.2, 4.2.2, 5.5.2.)

Using the 1 min–24 h method:

$$D = \frac{\mu_1 - \mu_2}{\mu_1} \quad \text{usually expressed in per cent}$$

$$\text{Disaccom. factor} = \frac{D}{\mu_1} = \frac{\mu_1 - \mu_2}{\mu_1^2} \quad \begin{array}{l} \text{(see Eqn 2.27)} \\ \text{(see Eqn 2.28)} \end{array}$$

where μ_1 is the permeability 1 min after test disturbance
 μ_2 is the permeability 24 h after test disturbance

Following the IEC recommendation:

$$D = \frac{\mu_1 - \mu_2}{\mu_1 \log_{10} \frac{t_2}{t_1}}$$

$$\text{Disaccom. factor} = \frac{D}{\mu_1} = \frac{\mu_1 - \mu_2}{\mu_1^2 \log_{10} \frac{t_2}{t_1}} \quad \text{(see Eqn 2.29)}$$

where μ_1 is the permeability at time t_1 after the test disturbance

μ_2 is the permeability at time t_2 after the test disturbance

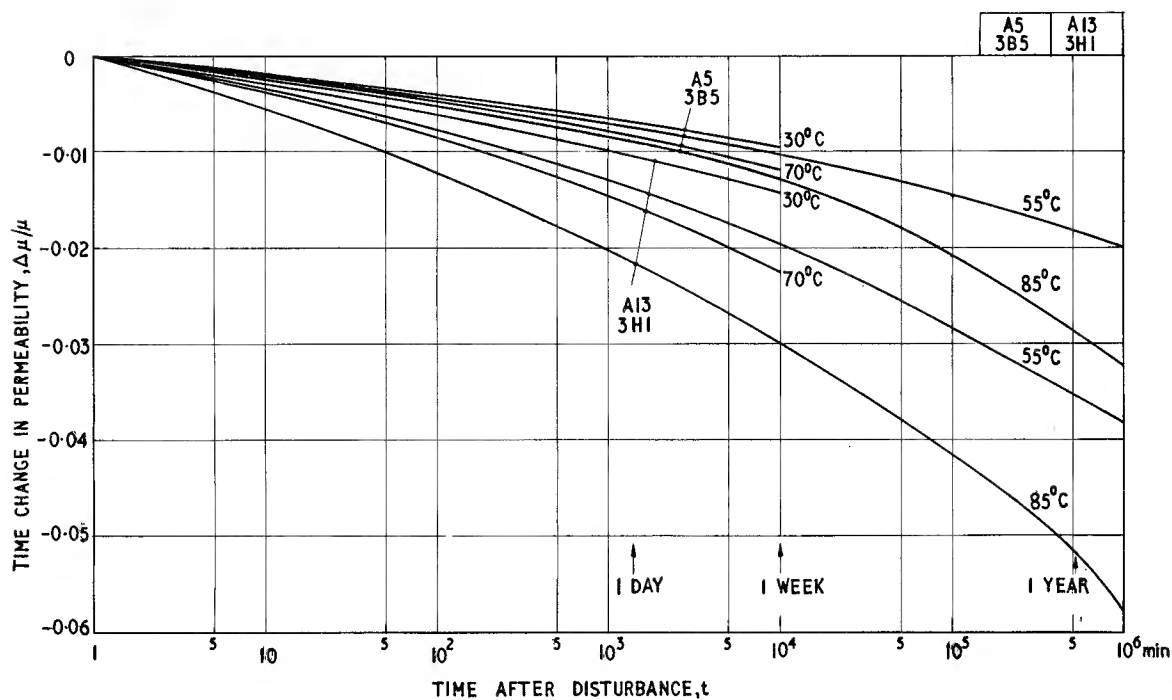


Fig. 3.10.1

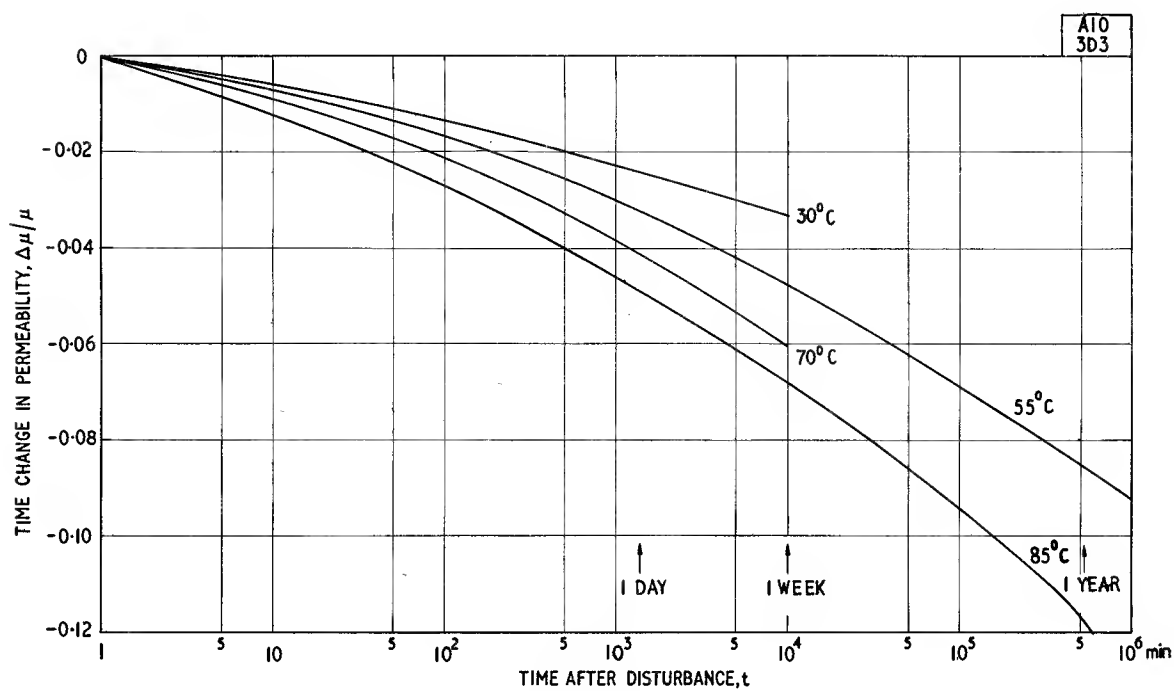


Fig. 3.10.2

Complex initial permeability spectrum Fig. 3.11

$$B < 0.1 \text{ mT (1 Gs)}$$

$$\theta \approx 20^\circ\text{C}$$

In Section 2.2.1 the well-known concept of complex permeability is introduced. The real and imaginary components represent reactive and loss terms respectively and may be expressed as series components (μ'_s, μ''_s) or parallel components (μ'_p, μ''_p).

The graphs in this figure show the components of the complex initial permeability (i.e. permeability measured with $B \rightarrow 0$) as functions of frequency. For each group of materials the series components are given first and the succeeding graph shows the corresponding parallel components. It often happens that the designer requires the product of the angular frequency and the permeability components. This may be readily obtained by placing a 45° graticule in the appropriate position on the permeability curves; the new graticule may then be scaled in terms of $\omega\mu'_s$ and $\omega\mu''_s$ or $\omega\mu'_p$ and $\omega\mu''_p$. This has been done for each of the graphs in this figure; it should be used in conjunction with the normal frequency scale.

The general form of these relations may be seen by referring to the first pair of graphs as an example. These illustrate the complex permeability of a group of manganese zinc ferrites. The measurements have been made in such a way that the loss due to macroscopic eddy currents and phenomena associated with dimensional resonance (see Section 2.2.4) have been eliminated. It is seen that at low frequencies the real part of the initial permeability, μ'_s , is about 2000 for A13 and about 500 for A10. As the frequency rises, each curve remains level at first and then rises to a shallow peak before falling rapidly to relatively low values. The loss component, μ''_s , rises to a pronounced peak as μ'_s falls. In high permeability ferrites this dispersion is principally due to the ferrimagnetic resonance¹³ (spin precession resonance). In a magnetically saturated ferrite this occurs as a sharp resonance at microwave frequencies; in the absence of an externally applied static field there is a distribution of domain magnetizations and the precession resonance is rather broad. Domain wall motion may, in general, also contribute to the magnetization process, so wall resonance or relaxation may contribute to μ'_s and μ''_s in this region.¹⁴

Snoek¹⁵ observed that the frequency of ferrimagnetic resonance varies inversely as the initial permeability. He gave the following relation:

$$f_{\text{res}} = \frac{\gamma M_{\text{sat}}}{3\pi(\mu_i - 1)} \quad \text{Hz} \quad (3.2)$$

where f_{res} = frequency at which μ''_s is maximum, Hz

$$\gamma = \text{gyromagnetic ratio} \approx 0.22 \times 10^6 \text{ (rad.s}^{-1}\text{).A}^{-1}\text{.m}$$

$$M_{\text{sat}} = \text{saturation magnetization in A.m}^{-1}$$

$$\mu_i = \text{initial permeability, i.e. } \lim_{f \rightarrow 0} \mu'_s$$

$$\therefore f_{\text{res}} = 23.4 \times 10^3 \frac{M_{\text{sat}}}{(\mu_i - 1)} \quad \text{Hz} \quad (3.3)$$

The saturation magnetization in most cubic ferrites lies between 250×10^3 and $350 \times 10^3 \text{ A.m}^{-1}$ (250 and 350 Gs). Therefore if M_{sat} is given a mean value of 300×10^3 the ferrimagnetic resonance frequency may be estimated with reasonable accuracy for any value of initial permeability. This treatment is rather over-simplified; for a fuller discussion the references should be consulted.

The useful frequency range of a ferrite is limited by the onset of ferrimagnetic resonance, either because the permeability begins to fall or, at a somewhat lower frequency, the losses rise steeply. The maximum frequency for which the ferrite has usefully low loss may be taken as a fraction, e.g. $1/6$, of f_{res} depending on the limit of $\tan \delta$, that is chosen. In illustration, ferrite grade B10 in Fig. 3.11.4 has $\mu_i = 120$ and therefore the calculated value of f_{res} is about 60 MHz compared with a measured value of about 50 MHz. For this ferrite $\tan \delta_r = 0.01$ at about 7.5 MHz, i.e. at about $0.15 f_{\text{res}}$.

The applications of high permeability manganese zinc ferrites are usually confined to the lower frequency region, e.g. less than about 2 MHz, although it will be seen below that this is not necessarily the case in transformer applications.

Reading the curves against the 45° graticule, the $\omega\mu'_s$ product rises at first in proportion to the frequency and then it either peaks or becomes almost independent of frequency.

The corresponding parallel components are shown in the second of each pair of graphs. The resonance dispersion is of course still apparent but μ'_p does not fall so rapidly with frequency. The products with ω are more revealing because, for a winding on a core, $\omega\mu'_p$ is proportional to the parallel reactance, and $\omega\mu''_p$ is proportional to the parallel resistance, arising from the core properties. These values are of importance in transformer design. It is seen that $\omega\mu''_p$ ($\propto R_p$) peaks at relatively low frequency and then becomes almost constant with frequency. The product $\omega\mu'_p$ ($\propto \omega L_p$) rises with frequency and, except for the highest permeability material, the rising characteristic extends to frequencies beyond 100 MHz. It is for this reason that a ferrite-cored

$$(3.2) f_{\text{res}} = \frac{4\gamma M_{\text{sat}}}{3(\mu - 1)} \quad \text{Hz}$$

$$(3.3) f_{\text{res}} \approx 23.4 \times 10^6 \frac{M_{\text{sat}}}{\mu - 1} \quad \text{Hz}$$

transformer, having sufficient shunt impedance at the lower end of the pass band, will not usually suffer extra attenuation due to the core at higher frequencies unless it is particularly sensitive to changes of R_p .

The nickel zinc ferrites behave in a similar way. It is interesting to note that in general their values of $\omega\mu'_p$ ($\propto \omega L_p$) remain lower than corresponding values of the manganese zinc ferrites even up to 100 MHz; the advantage of the higher frequency of the resonance being offset by the lower initial permeability.

(See also Sections 2.2.1, 7.3.1, 7.4.1.)

Series impedance in terms of complex permeability:

$$\left. \begin{aligned} Z &= j\omega L_s + R_s = j\omega L_o(\mu'_s - j\mu''_s) \\ \omega L_s &= \omega L_o\mu'_s \\ R_s &= \omega L_o\mu''_s \\ \text{and } \tan \delta_m &= \frac{R_s}{\omega L_s} = \frac{\mu''_s}{\mu'_s} \end{aligned} \right\} \begin{array}{l} \text{(see Eqns} \\ \text{2.15, 2.16)} \end{array}$$

Parallel impedance and admittance in terms of complex permeability:

$$\left. \begin{aligned} Y &= \frac{1}{j\omega L_p} + \frac{1}{R_p} = \frac{1}{j\omega L_o} \left(\frac{1}{\mu'_p} - \frac{1}{j\mu''_p} \right) \\ \omega L_p &= \omega L_o\mu'_p \\ R_p &= \omega L_o\mu''_p \end{aligned} \right\} \begin{array}{l} \text{(see Eqns.} \\ \text{2.17, 2.18)} \end{array}$$

$$\text{and } \tan \delta_m = \frac{\omega L_p}{R_p} = \frac{\mu'_p}{\mu''_p}$$

Conversion:

$$\left. \begin{aligned} \mu'_p &= \mu'_s(1 + \tan^2 \delta_m) \\ \mu''_p &= \mu''_s(1 + 1/\tan^2 \delta_m) \end{aligned} \right\} \begin{array}{l} \text{(see Eqn 2.19)} \end{array}$$

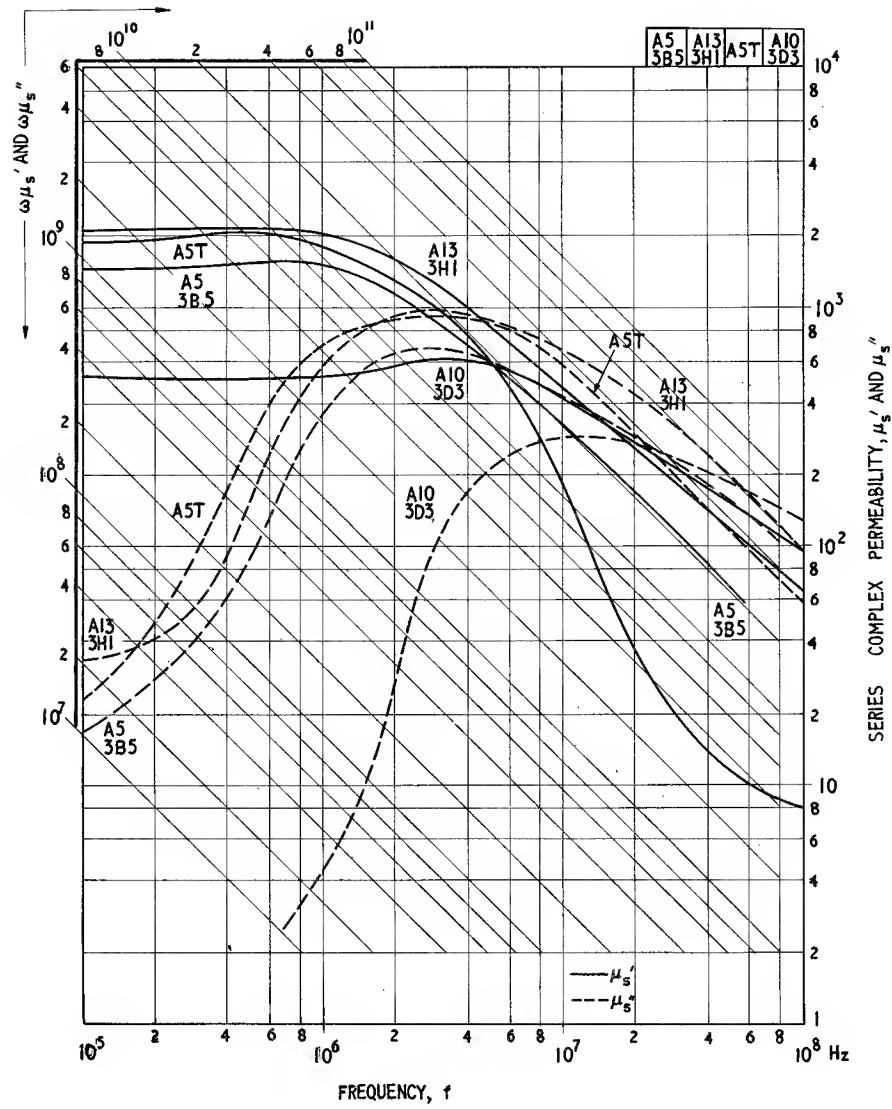


Fig. 3.11.1(a)

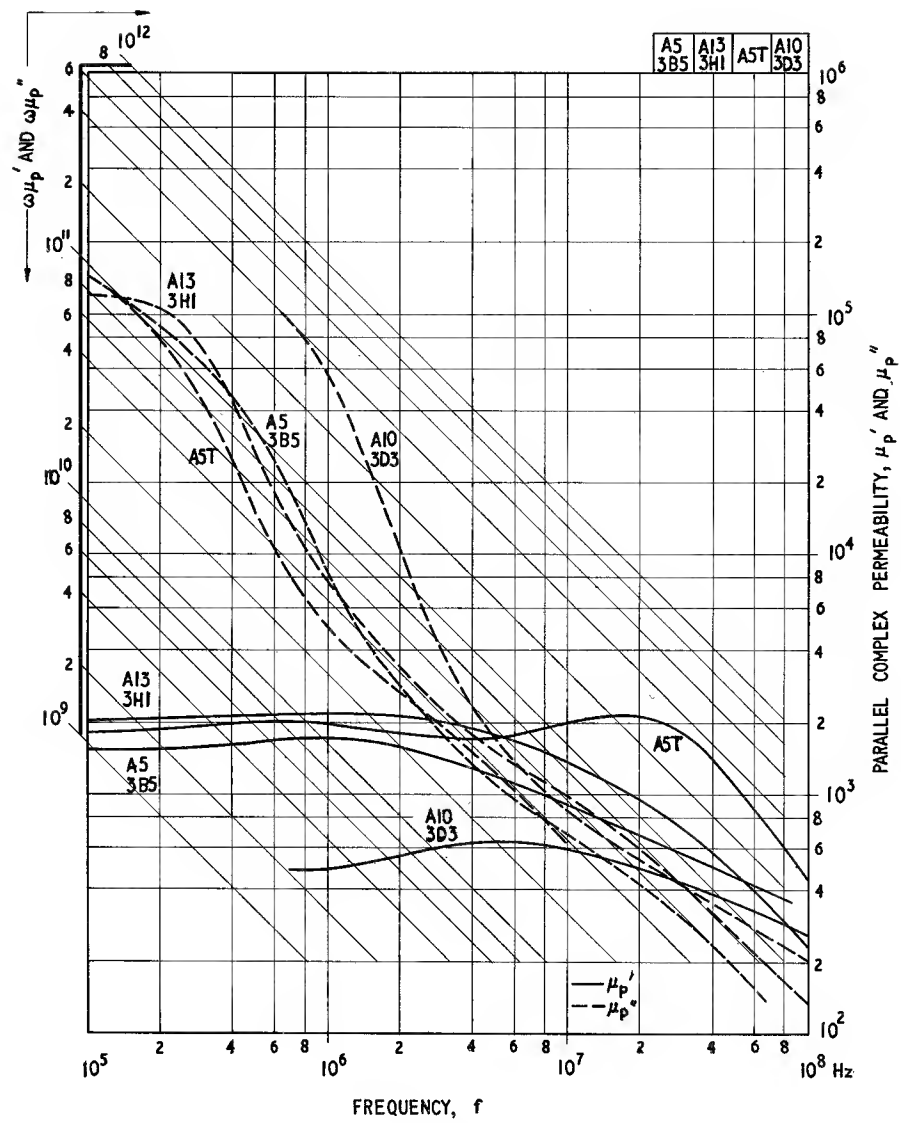


Fig. 3.11.1(b)

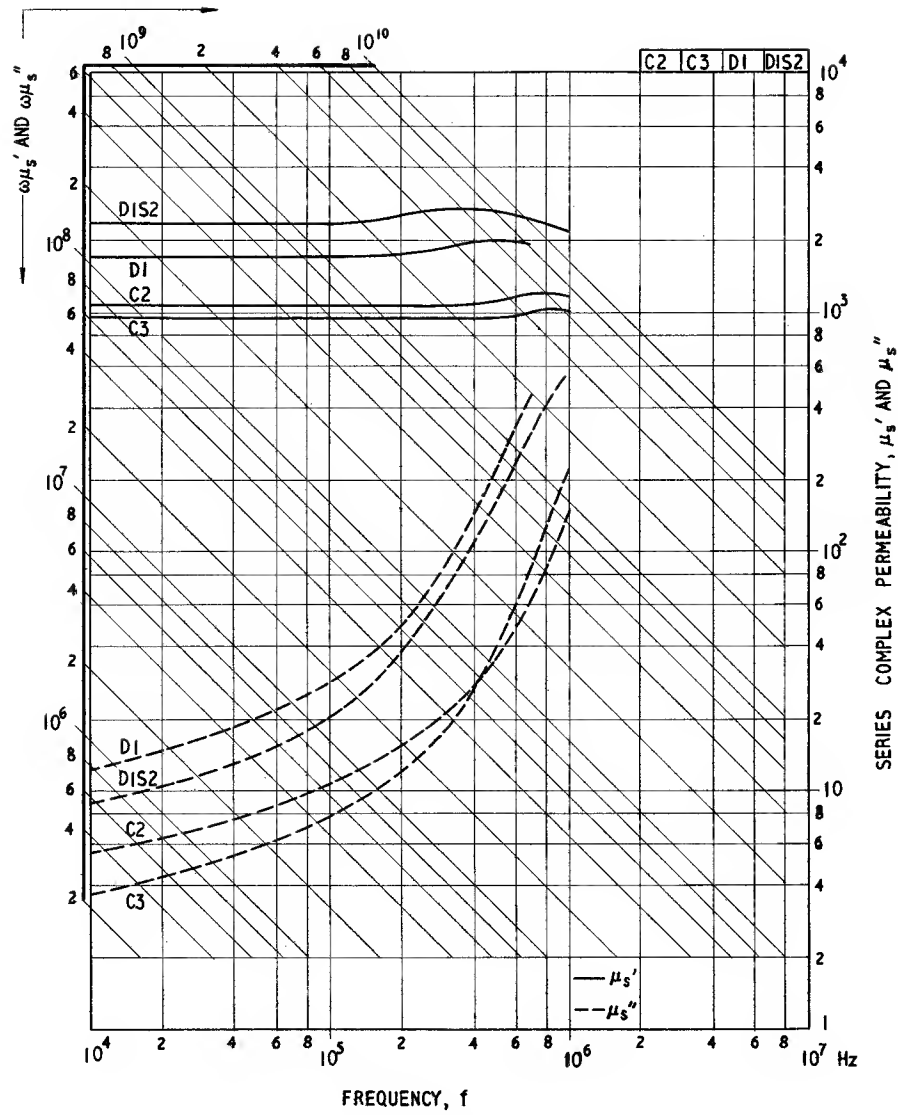


Fig. 3.11.2(a)

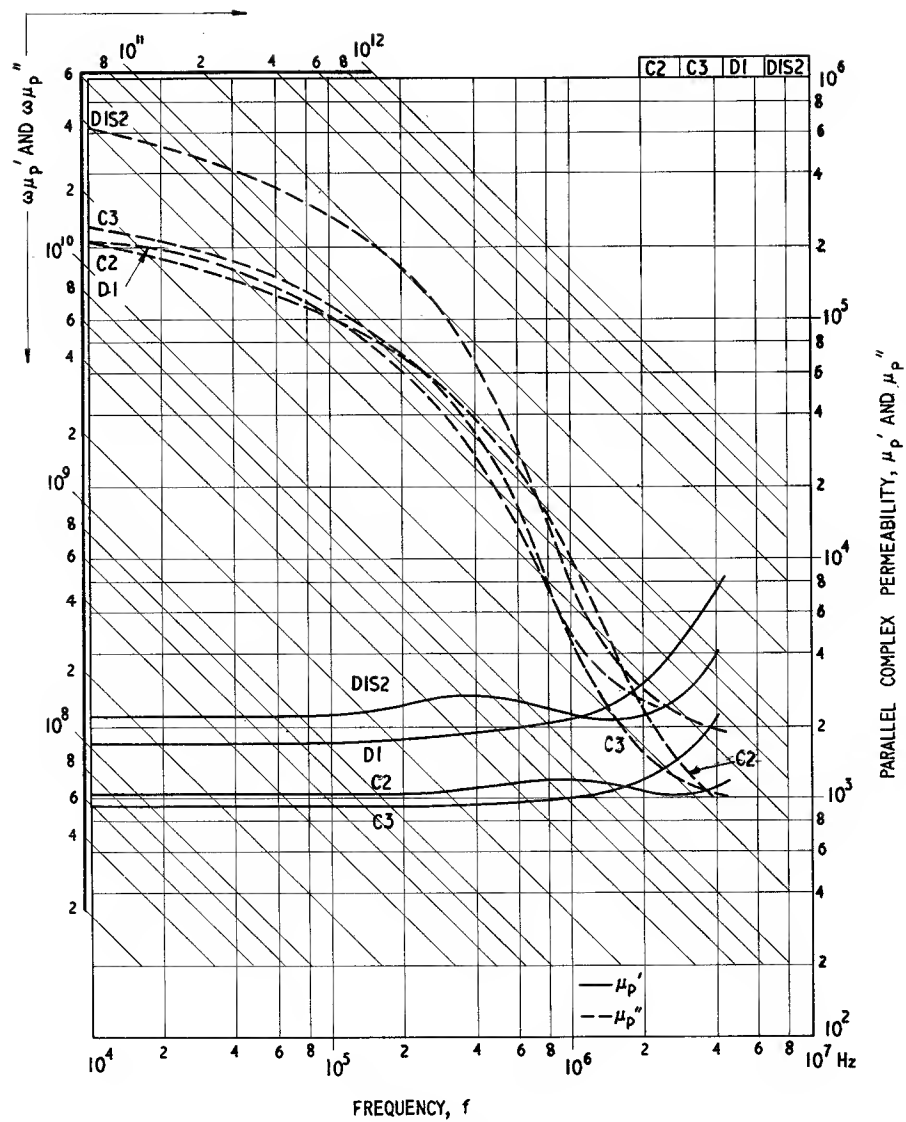


Fig. 3.11.2(b)

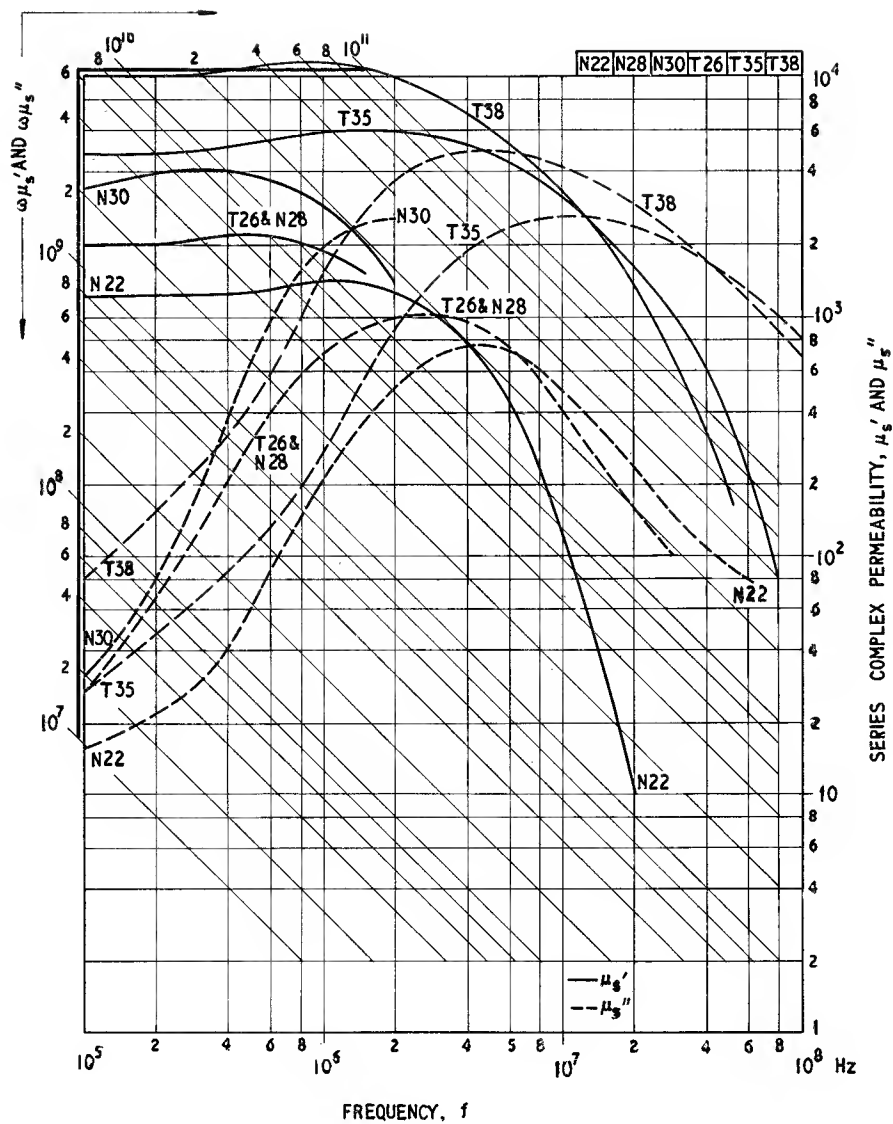


Fig. 3.11.3(a)

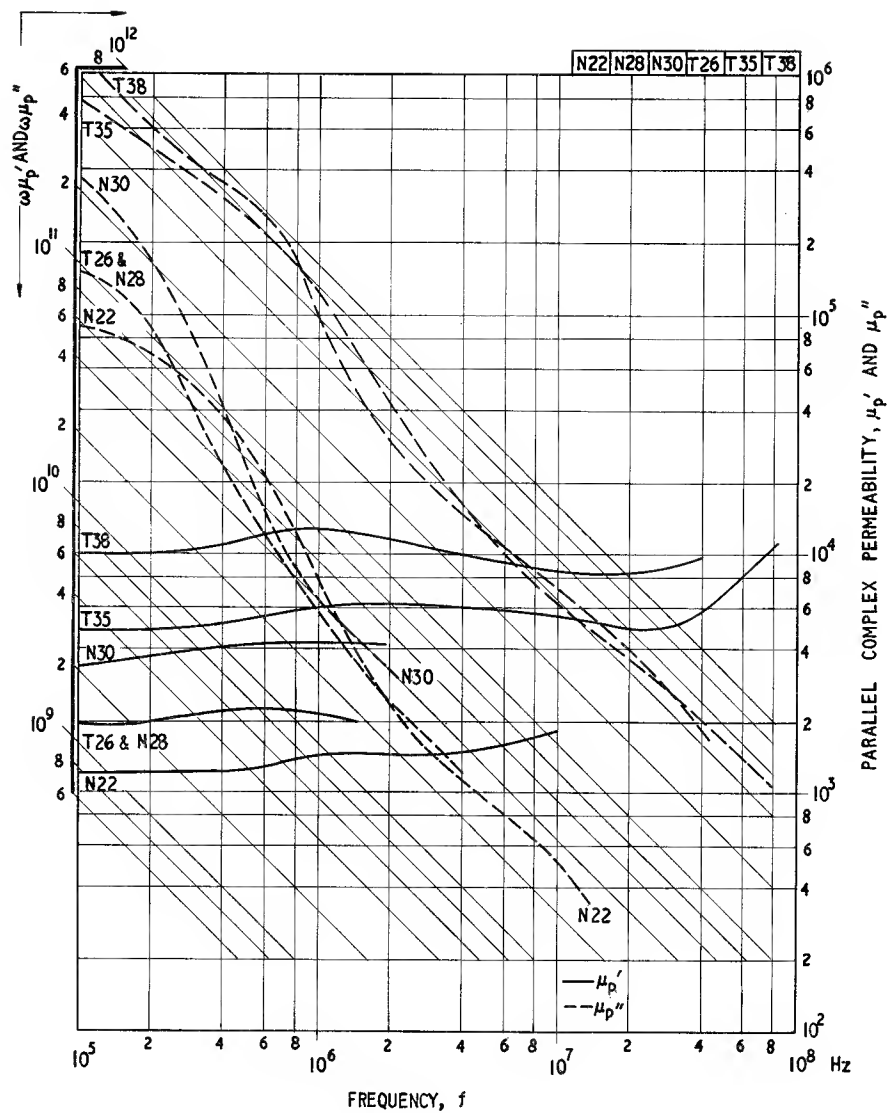


Fig. 3.11.3(b)

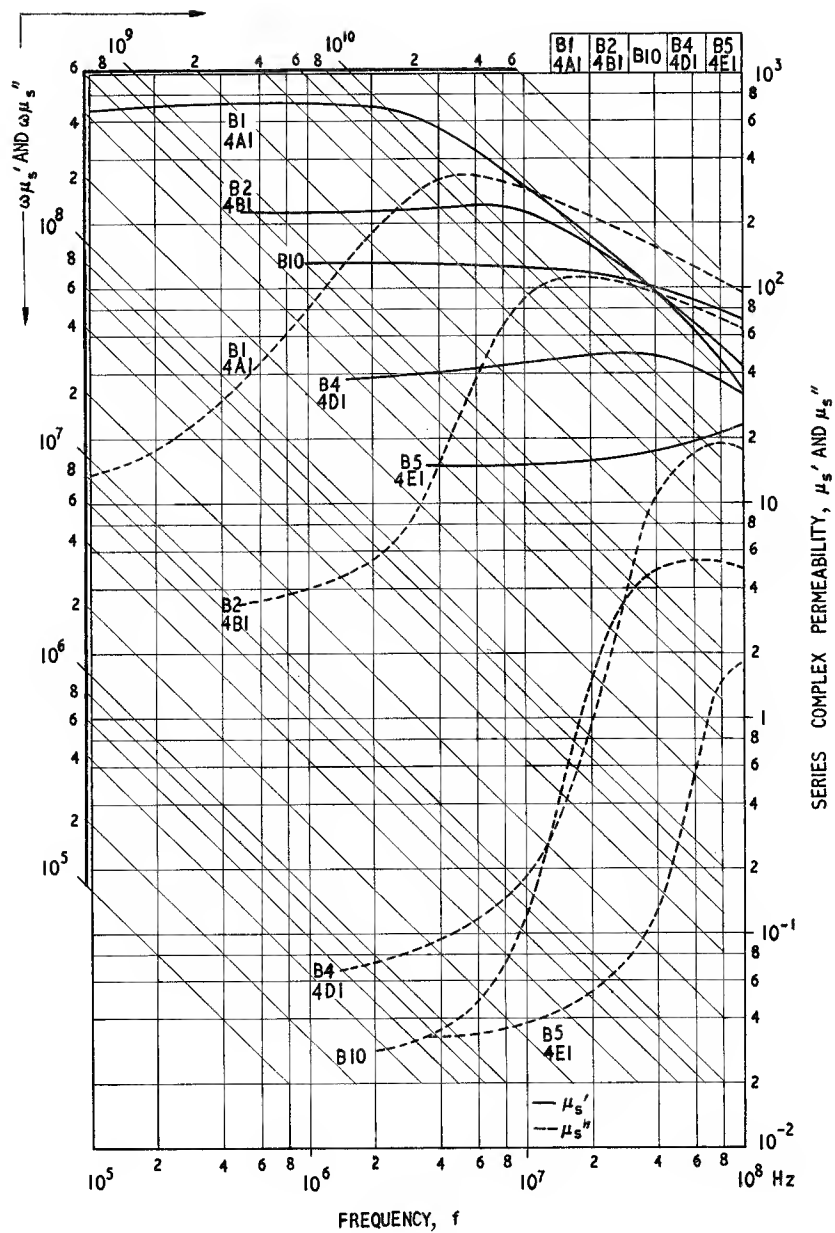


Fig. 3.11.4(a)

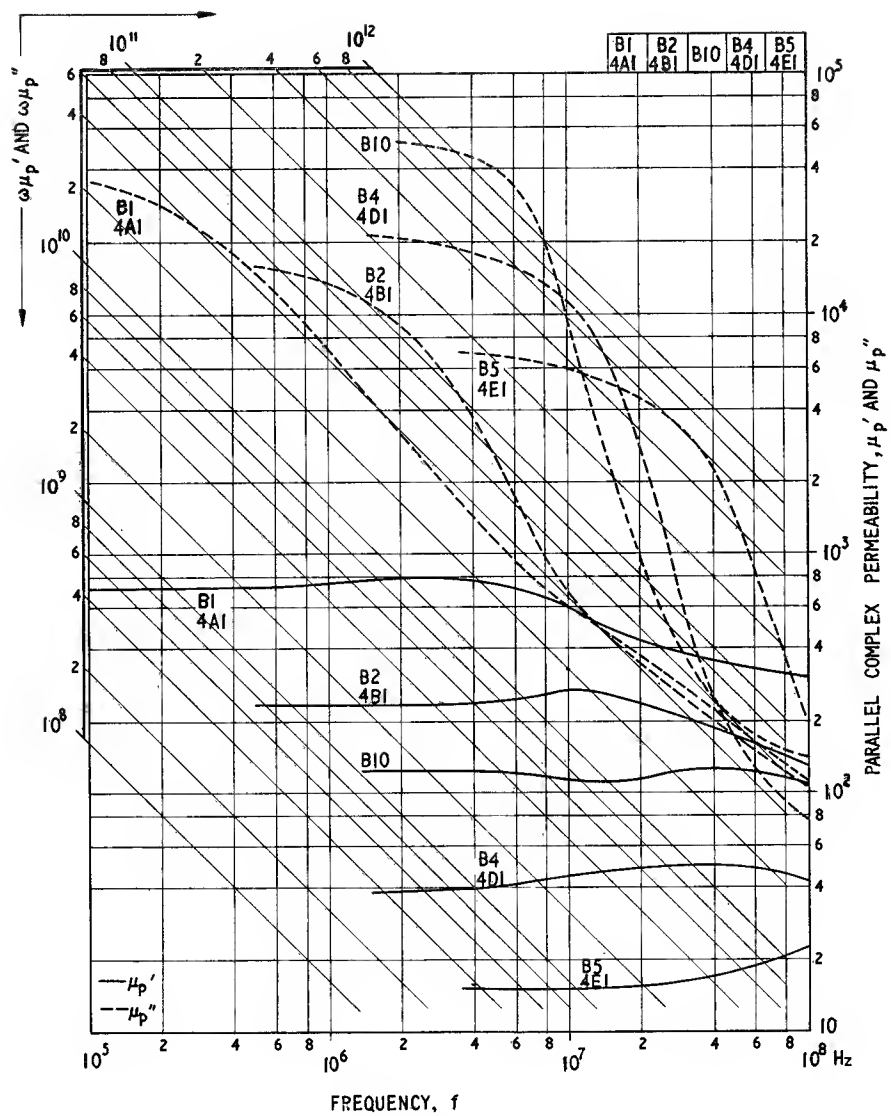


Fig. 3.114(b)

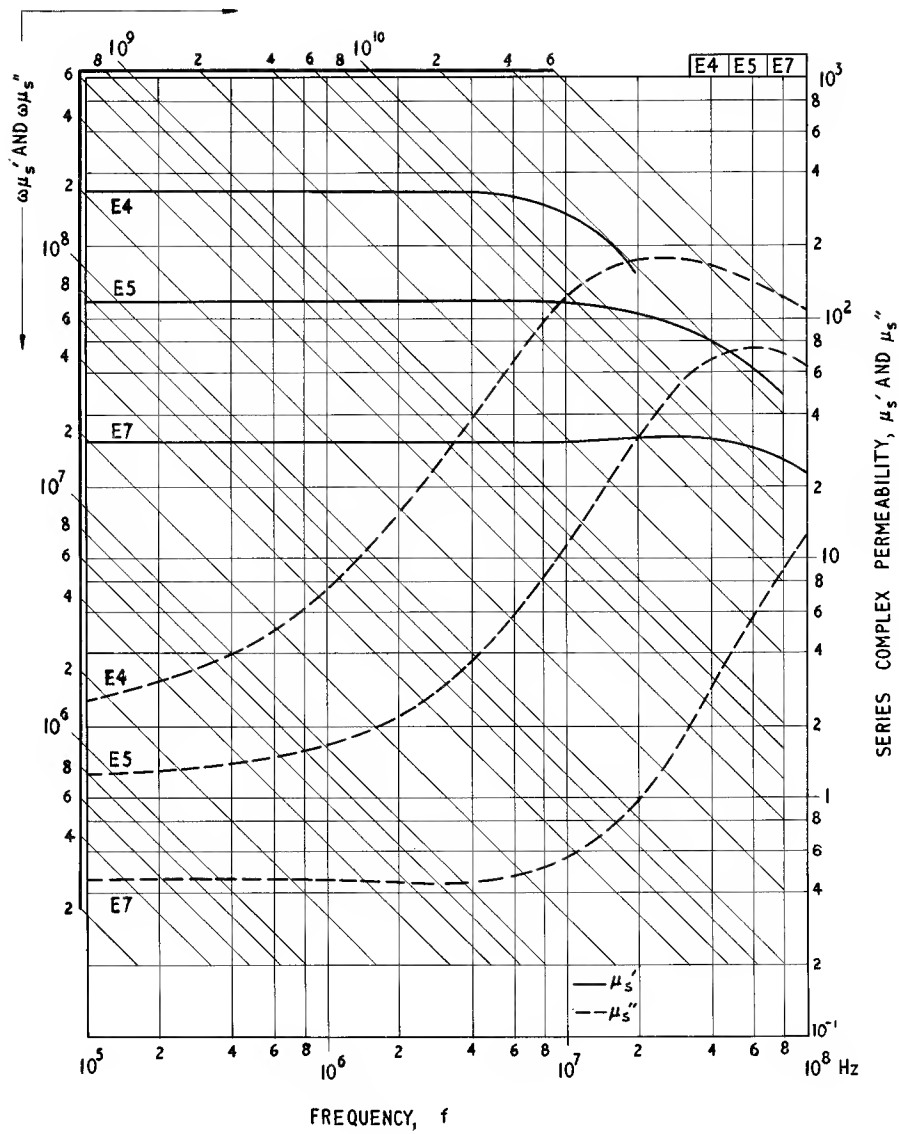


Fig. 3.11.5(a)

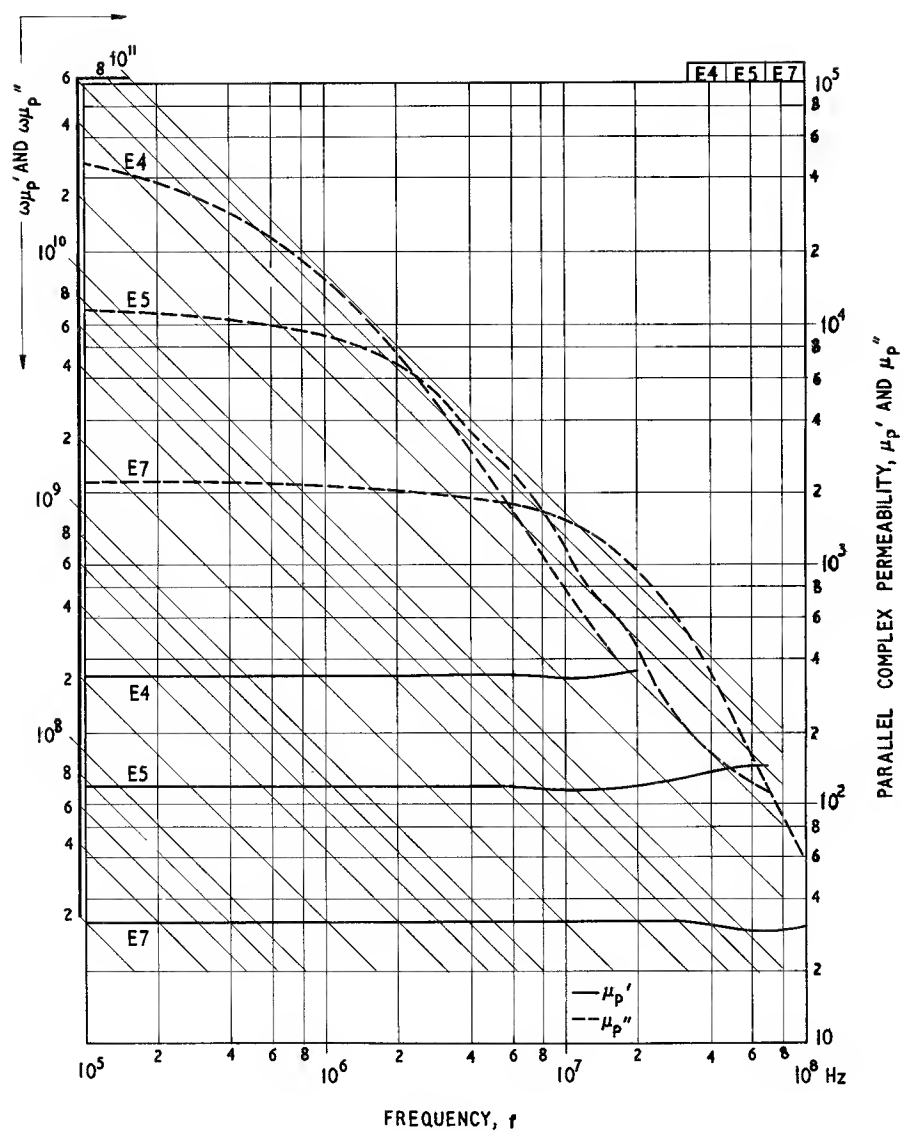


Fig. 3.11.5(b)

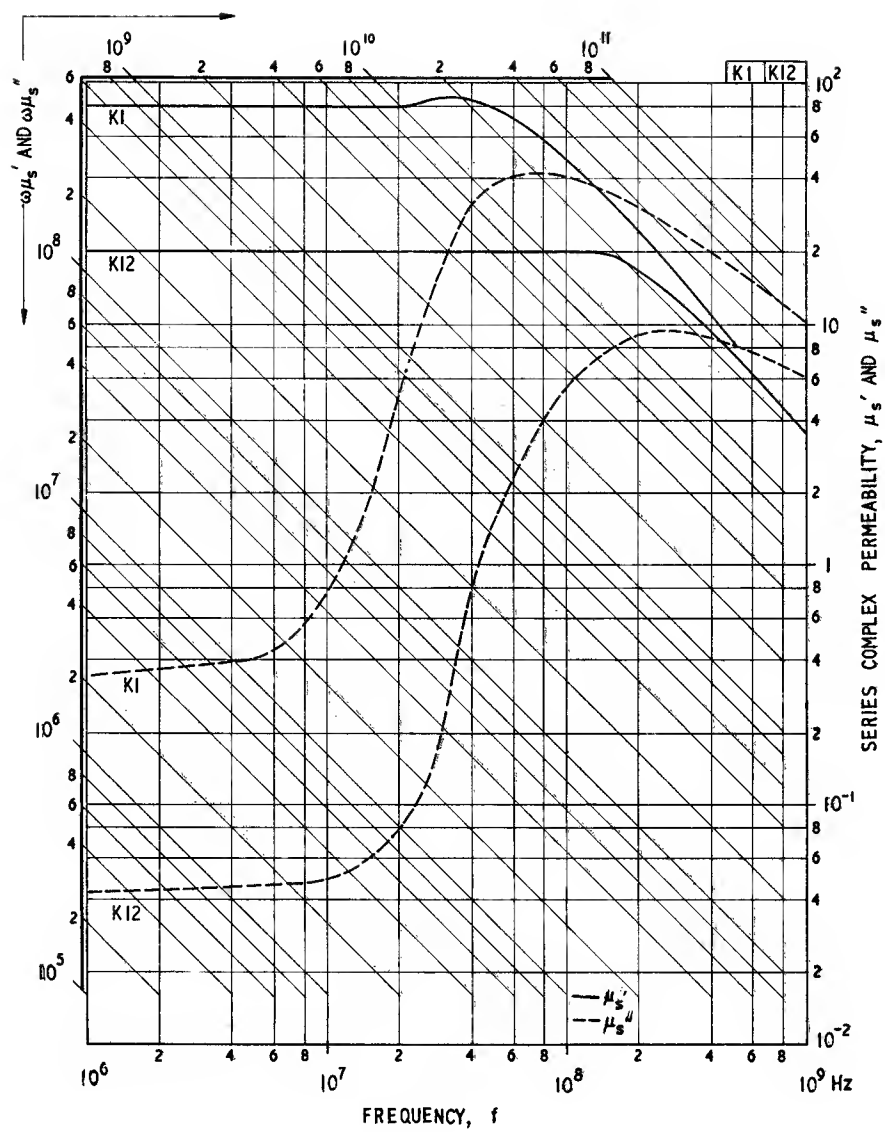


Fig. 3.11.6(a)

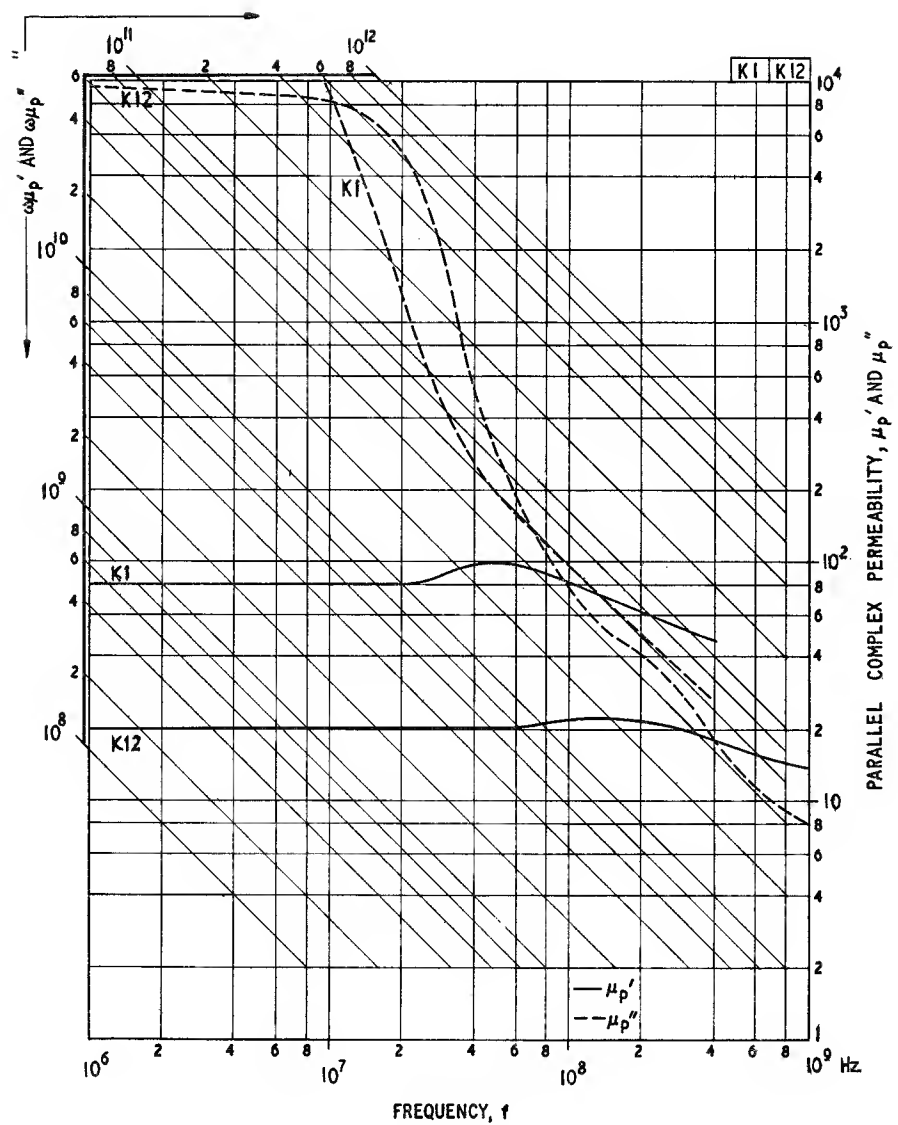


Fig. 3.11.6(b)

Residual loss factor spectrum Fig. 3.12 $B < 0.1 \text{ mT}$ (1Gs) $\theta \approx 20^\circ\text{C}$

The residual loss factor $(\tan \delta_r)/\mu_i$ is usually the principal loss parameter at low flux densities. For a given value of effective permeability μ_e , the inductor using a core material having the lowest $\tan \delta_r/\mu_i$ will have the lowest core loss (neglecting the core conductivity). The low frequency residual loss tangent, $\tan \delta_r$, does not vary much between the various grades of soft ferrites; the values for the nickel zinc ferrites usually lie between 0.002 and 0.02 while for manganese zinc ferrites a smaller range, 0.002 to 0.004, includes most low loss grades. This being so, $\tan \delta_r/\mu_i$ may in principle be lowered by increasing the initial permeability. However, as mentioned in the introduction to Fig. 3.11, the higher the permeability the lower is the frequency of the ferrimagnetic resonance dispersion. This may be seen clearly in the graphs of the present figure where the ferrites having the lower loss factors tend to cut off at the lower frequencies. Using residual loss factor as a criterion, the first graph shows that, of the grades referred to, A13 ($\mu_i \approx 2000$) is best up to about 300 kHz, where grade A10, due to its lower permeability ($\mu_i \approx 500$) and the attendant higher cut-off frequency, emerges as a better material.

Fig. 3.12.9 shows that grade A10 is overtaken by the nickel zinc ferrite grade B2 ($\mu_i \approx 250$) at about 2 MHz, and so on. In this way each ferrite may have a frequency

range in which it has the lowest loss factor and would therefore be the best choice for the core of a low loss inductor. Of course, some materials, e.g. grade A1, are superseded at all frequencies by other grades. Such materials may be of early development, or they may have special characteristics such as higher B_{sat} or lower cost which gives them a particular field of application.

At frequencies well below the ferrimagnetic resonance the residual loss is believed to arise at least in part from thermally activated domain wall movements.

(See also Sections 2.2.1, 2.2.5, 4.2.3, 5.7.5.)

$$\frac{\tan \delta_r}{\mu_i} = \omega L_o G \quad (\text{see Eqn 4.45})$$

where $L_o = \mu_o N^2 / C_1$

G = residual loss conductance

(thus loss factor is proportional to the residual loss conductance measured across a winding of N turns on a core of given core factor C_1)

$$\frac{(\tan \delta_r)_{\text{gapped}}}{\mu_e} \approx \frac{\tan \delta_r}{\mu_i}$$

$$\text{and } (\tan \delta_r)_{\text{gapped}} \approx \mu_e \left(\frac{\tan \delta_r}{\mu_i} \right) \quad (\text{See Eqns 2.58, 4.49})$$

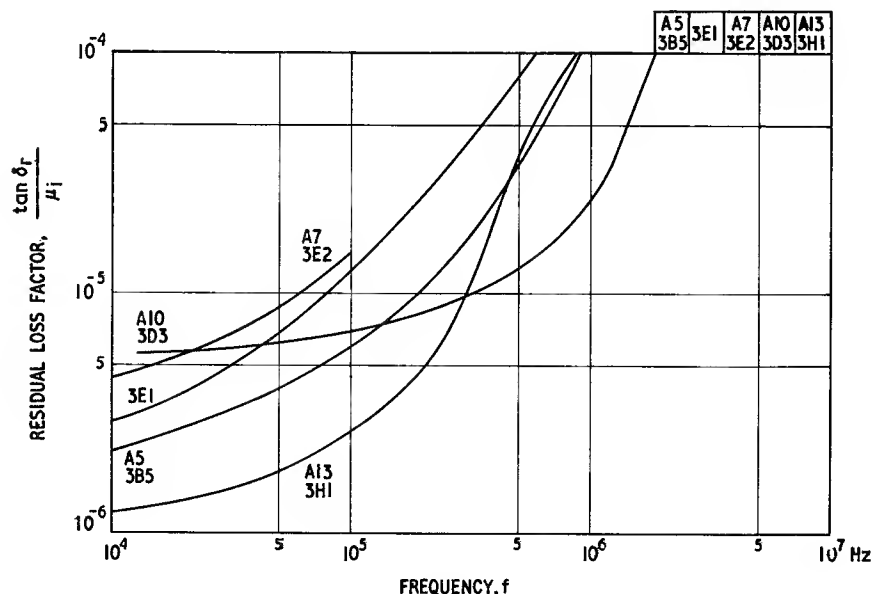


Fig. 3.12.1

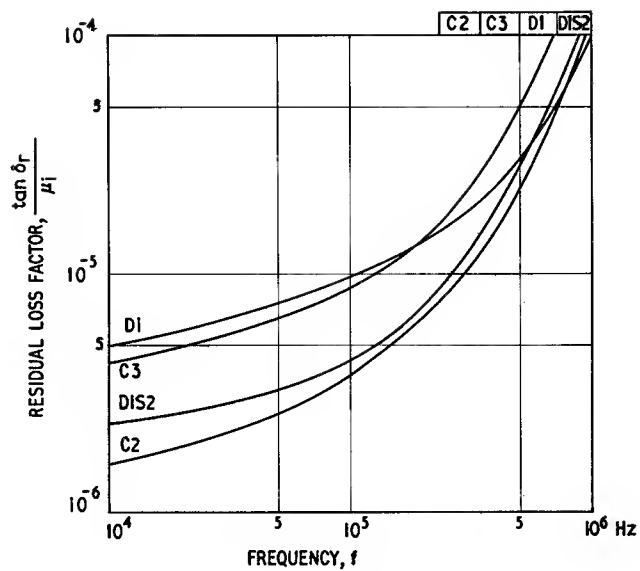


Fig. 3.12.2

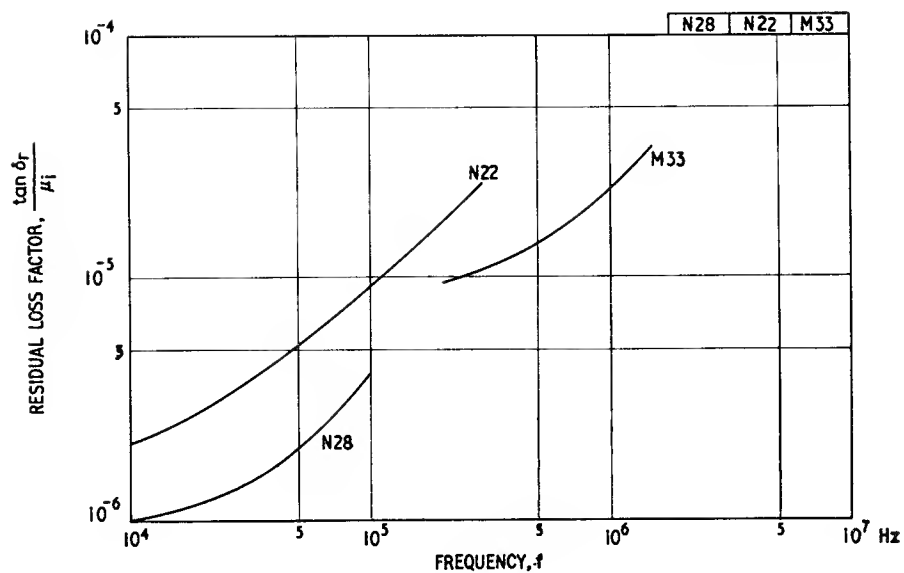


Fig. 3.12.3

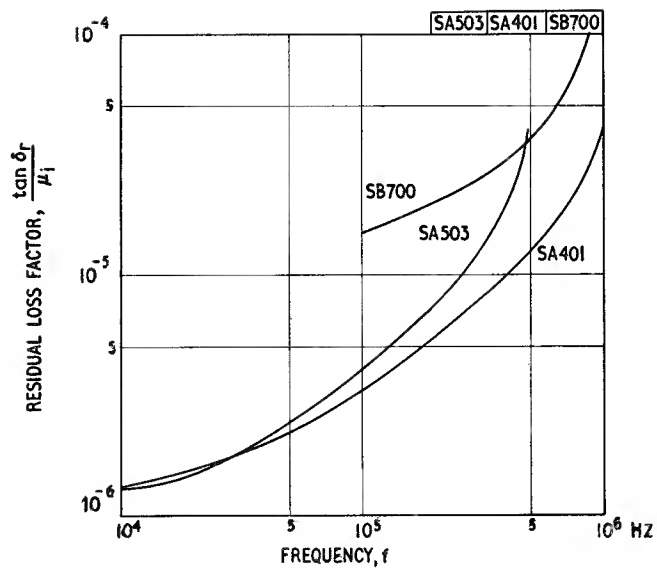


Fig. 3.12.4

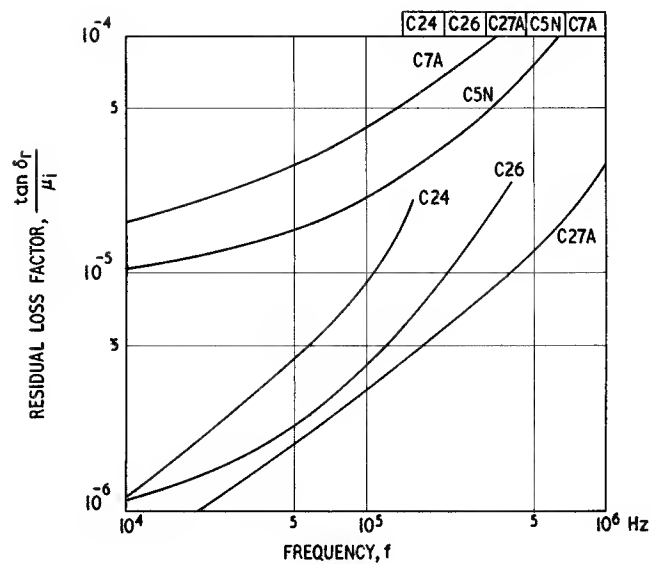


Fig. 3.12.5

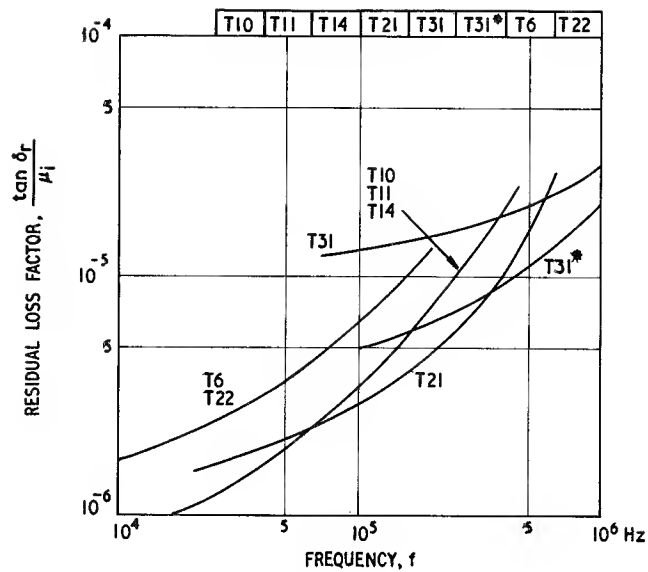


Fig. 3.12.6

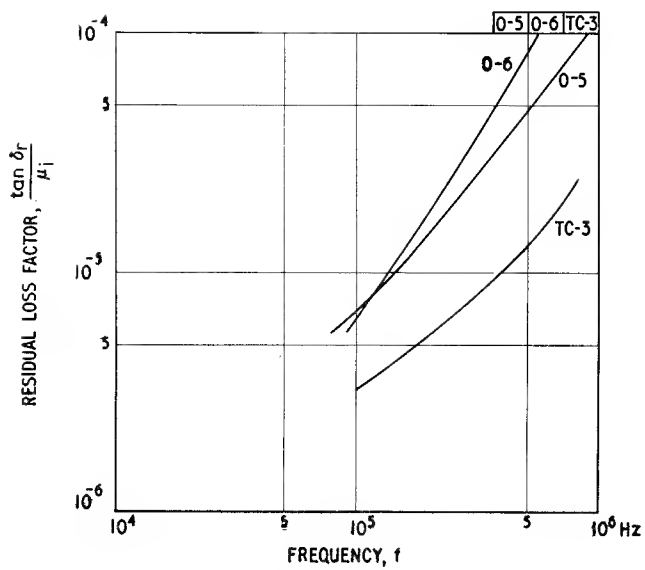


Fig. 3.12.7

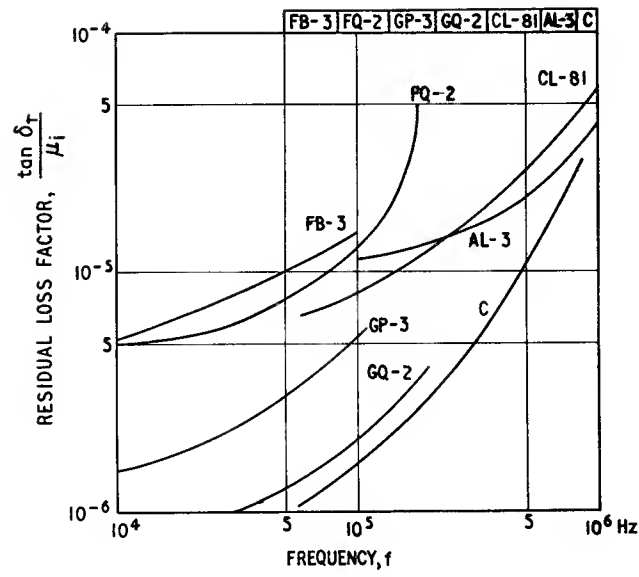


Fig. 3.12.8

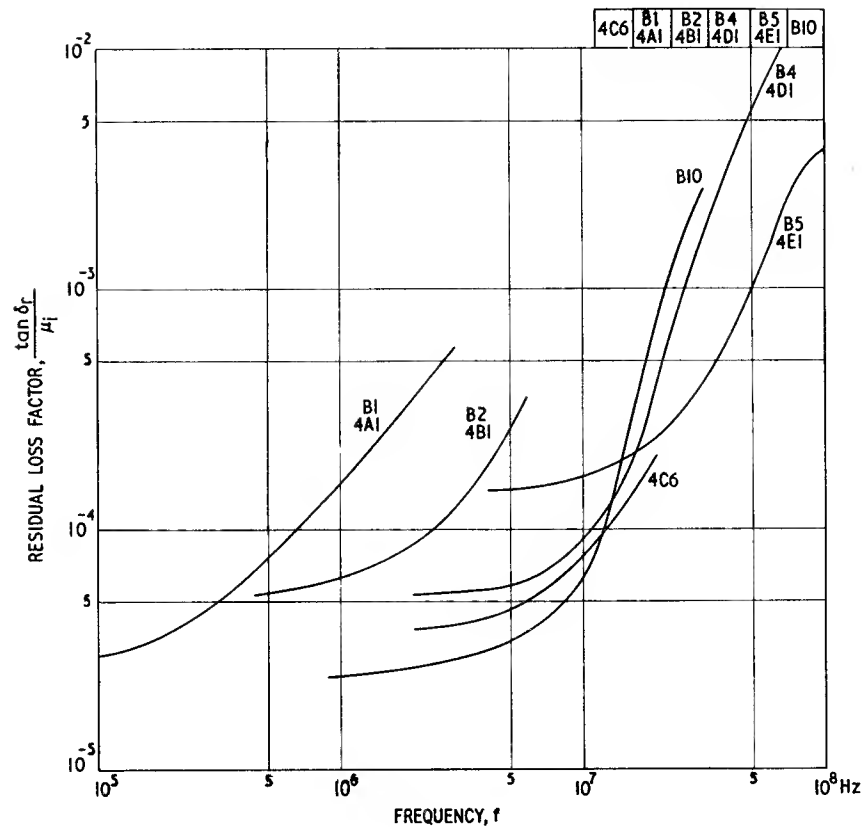


Fig. 3.12.9

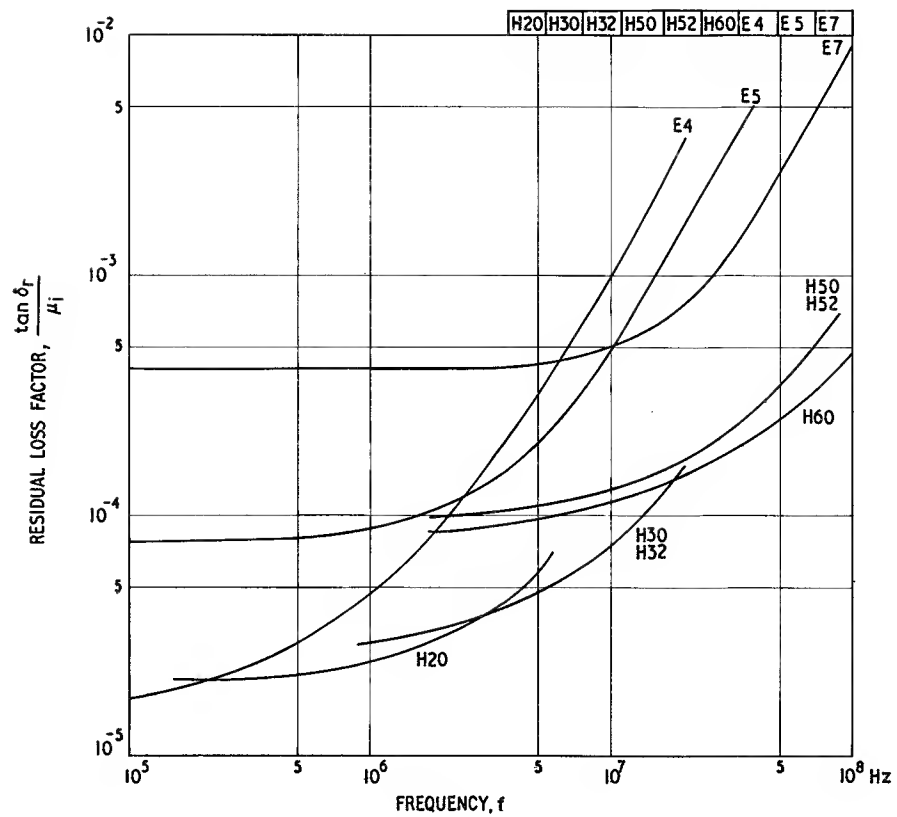


Fig. 3.12.10

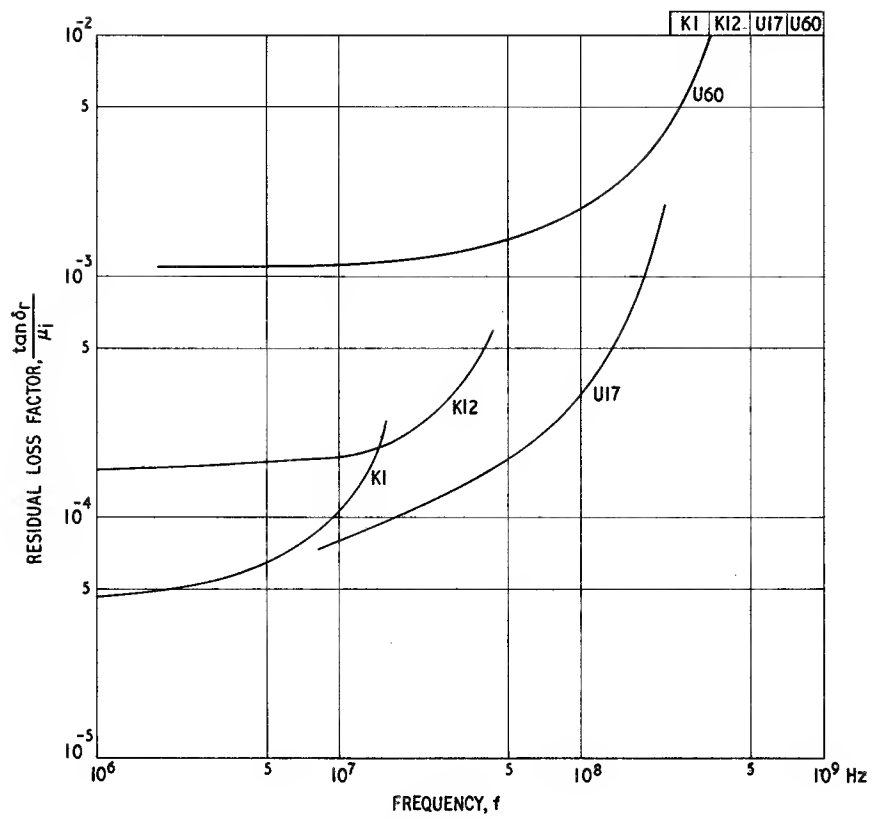


Fig. 3.12.11

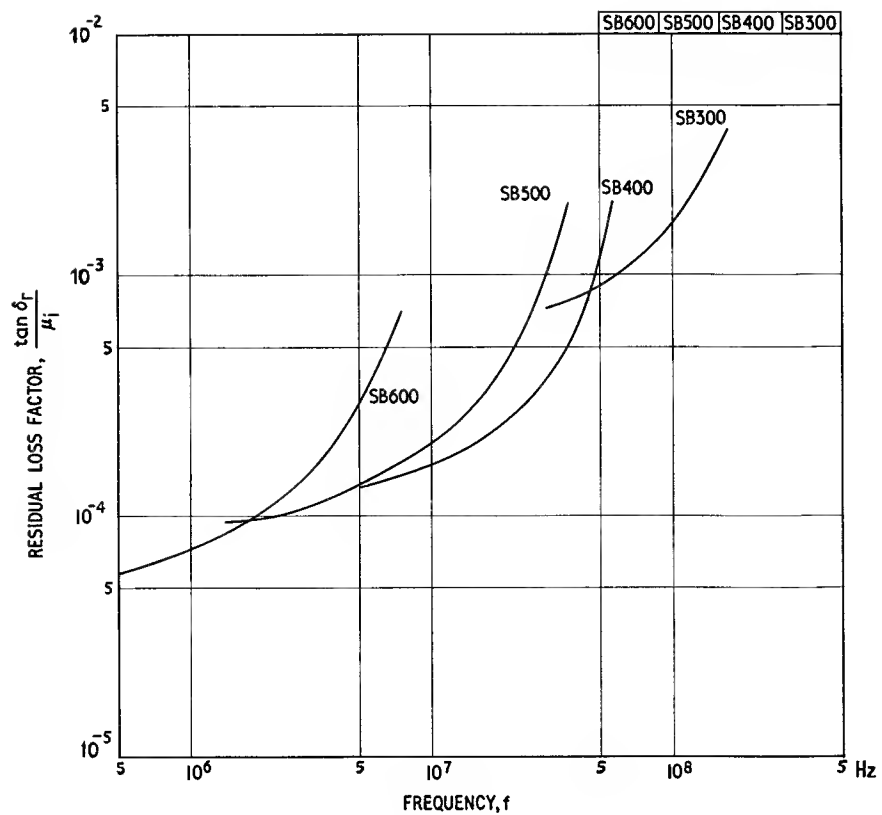


Fig. 3.12.12

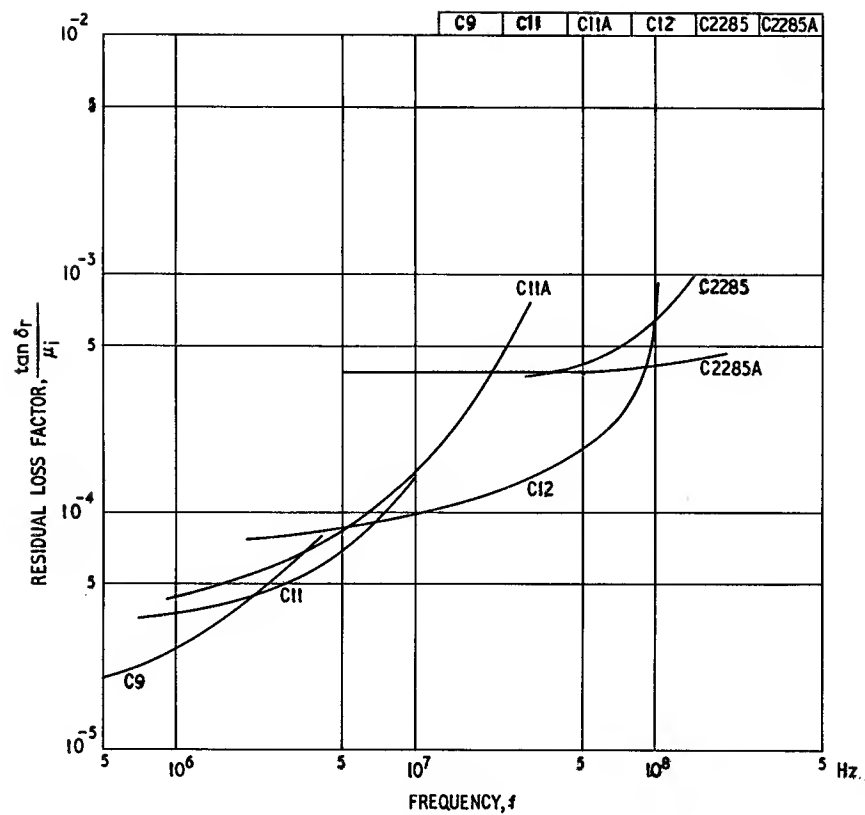


Fig. 3.12.13

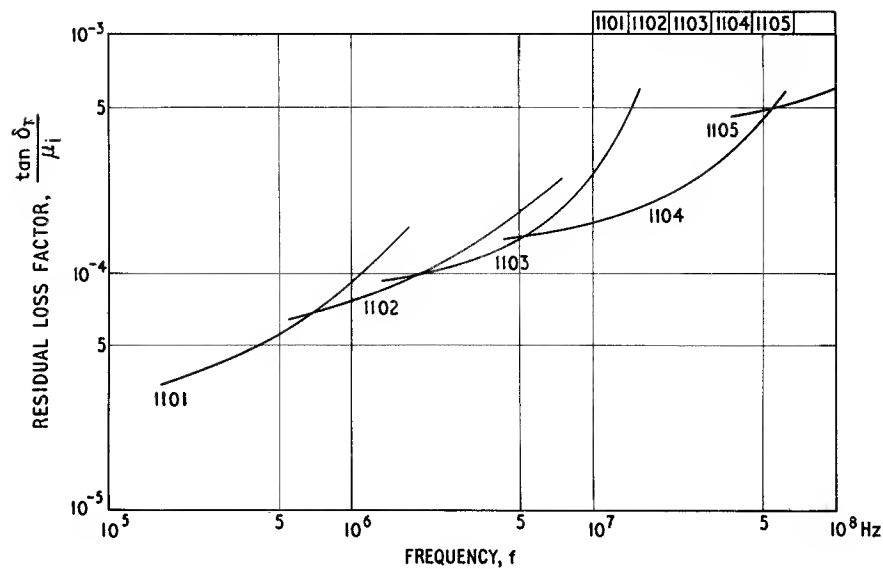


Fig. 3.12.14

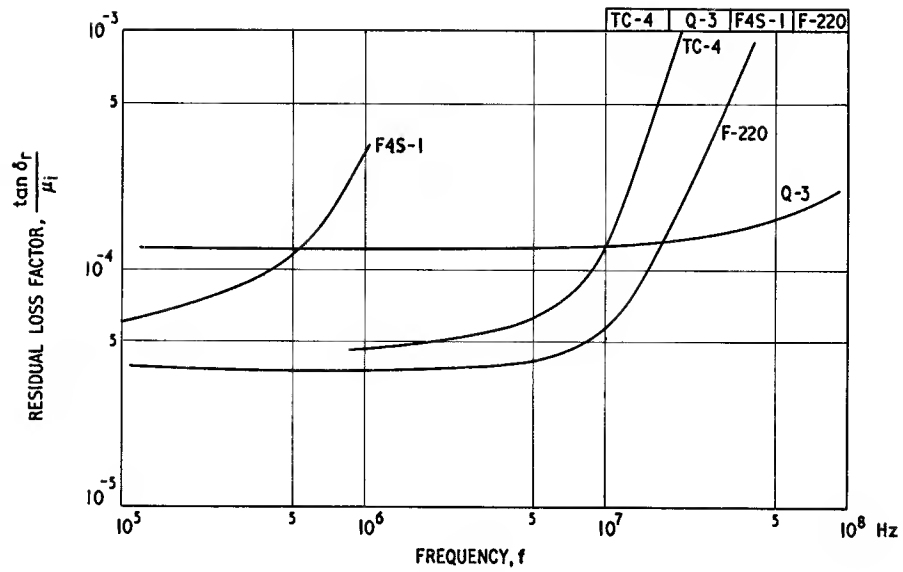


Fig. 3.12.15

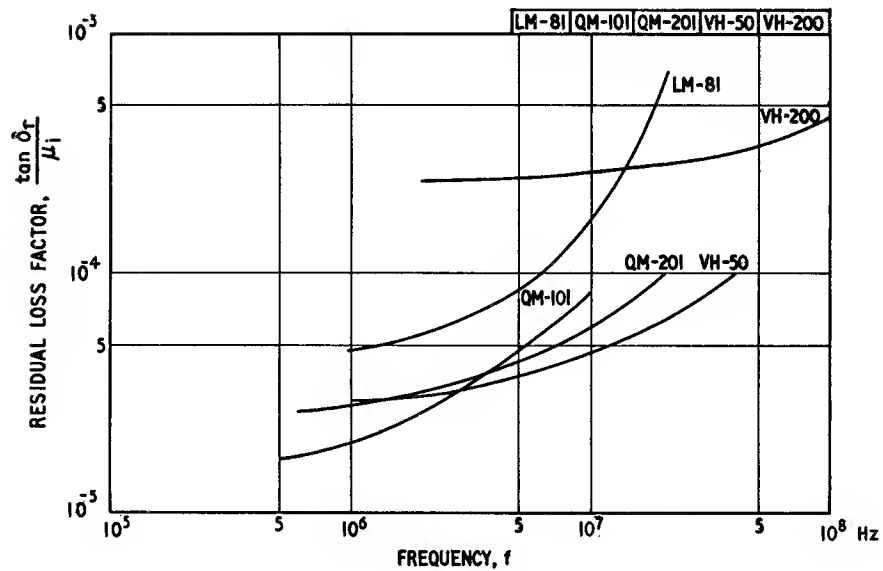


Fig. 3.12.16

Residual loss factor as a function of temperature
Fig. 3.13

$$\hat{B} < 0.1 \text{ mT (1 Gs)}$$

The dependence of $(\tan \delta_r)/\mu_i$ on temperature at various frequencies is shown in these graphs for a number of ferrites.

The graphs for the manganese zinc ferrites show minima in the vicinity of room temperature. The general shape may be partly explained in terms of the increase of μ_i with temperature. Referring to Fig. 3.12.1 it is seen that the $(\tan \delta_r)/\mu_i$ —frequency curve for high permeability A13 crosses that for lower permeability A10; the reason for this cross-over is explained in the introduction to that figure. In the region of the graph remote from the upward dispersion of the curves, an increase in μ_i reduces $(\tan \delta_r)/\mu_i$ whereas in the vicinity of the dispersion the reverse is true because an increase in μ_i lowers the dispersion frequency. Returning to the present figure, the initial

permeability is relatively low at low temperatures so, assuming that it rises with temperature, the loss factor will correspondingly fall as the temperature rises from low values. As the temperature, and permeability, continue to rise the loss factor eventually starts to rise due to the lowering of the dispersion frequency.

In the measurements made to obtain the first three graphs, and probably the others also, care was taken to eliminate error due to eddy current loss in the core. In a practical core at the higher frequencies some loss might be present due to eddy currents circulating in the core and this would be inversely proportional to the resistivity. Since the resistivity falls rapidly with temperature it is to be expected that the total loss factor due to both residual and eddy current losses would tend to be tilted upwards, relative to the present curves, at the higher temperature and the minimum would tend to be at a somewhat lower temperature.

(See also Figs. 3.8 and 3.12.)

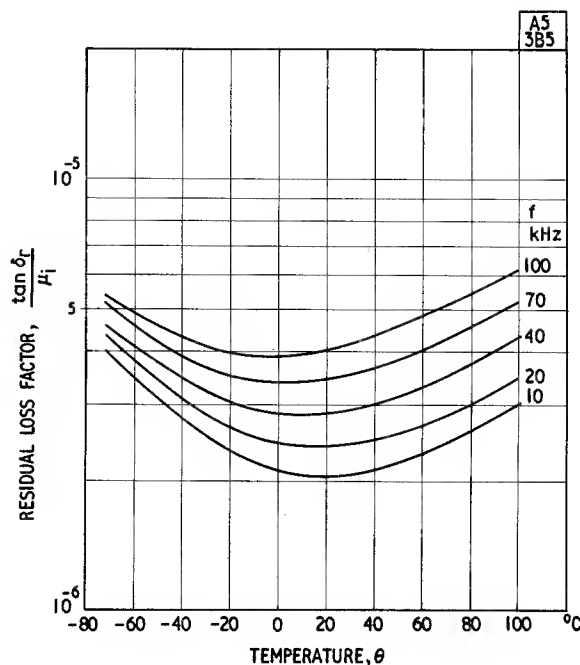


Fig. 3. 13.1

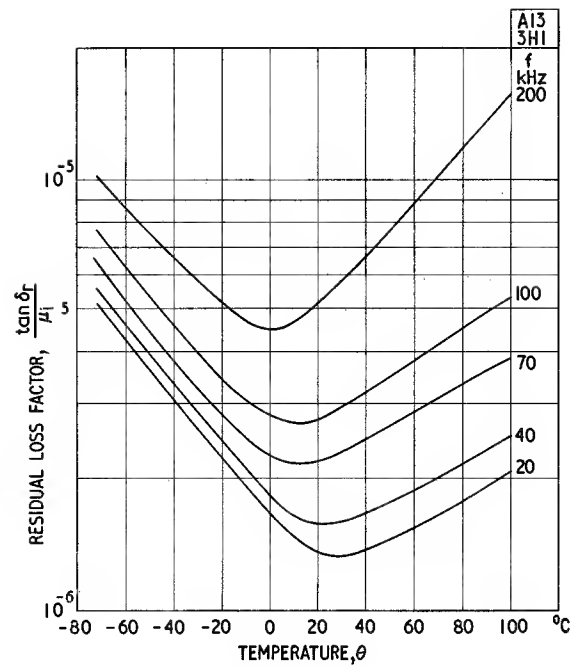


Fig. 3.13.2

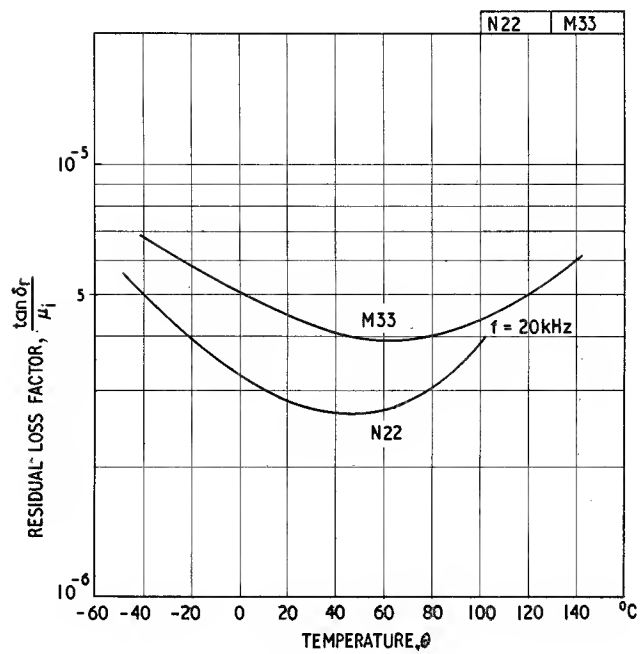


Fig. 13.3

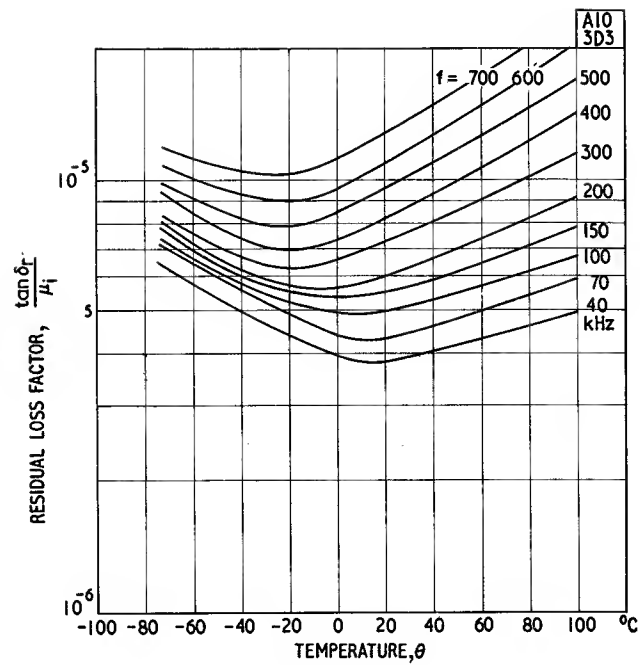


Fig. 3.13.4

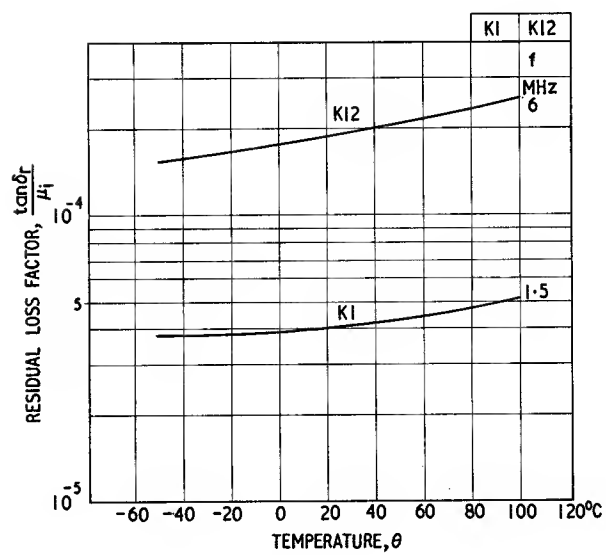


Fig. 3.13.5

Residual loss tangent as a function of frequency with superimposed steady field as a parameter Fig. 3.14

$$\hat{B} < 0.1 \text{ mT (1 Gs)}$$

$$\theta \approx 20^\circ\text{C}$$

These graphs show the influence of a steady magnetic field on the residual loss tangent, the steady field and the measuring field being parallel. At high frequencies the loss is associated, at least in part, with the ferrimagnetic resonance. The frequency of this resonance, i.e. the frequency at which μ''_s reaches a maximum value, is increased when a polarizing field is applied. This reduces the loss at any given frequency immediately below the cut-off region. The basic residual loss, extending over the

lower part of the spectrum, is believed to arise largely from thermally activated domain wall movements. Since a polarizing field reduces the number of domain walls the residual loss is decreased. Therefore the overall effect of a steady field is to move the curves towards the R.H. bottom corner of the graph.

Since the permeability also decreases when a steady field is applied the variation of residual loss factor ($\tan \delta_r$)/ μ depends on whether $\tan \delta_r$ or μ decreases at the greater rate. In fact $\tan \delta_r$ usually decreases at the greater rate at low values of the steady field so that $\tan \delta_r/\mu$ initially falls; at higher fields the situation is reversed.

(See also Figs. 3.6, 3.12 and Section 6.2.3.)

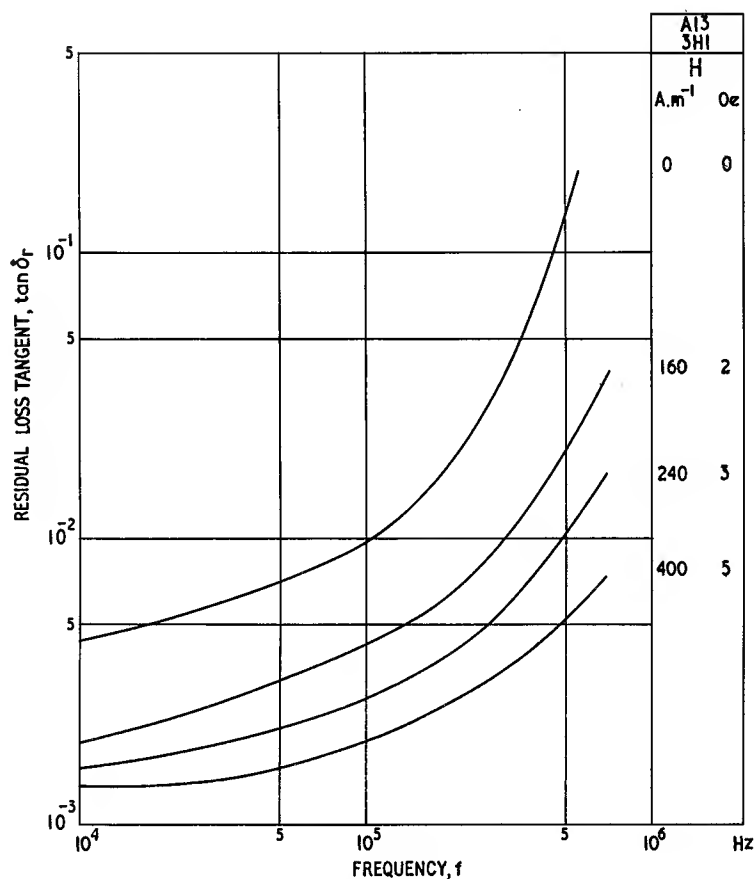


Fig. 3.14.1

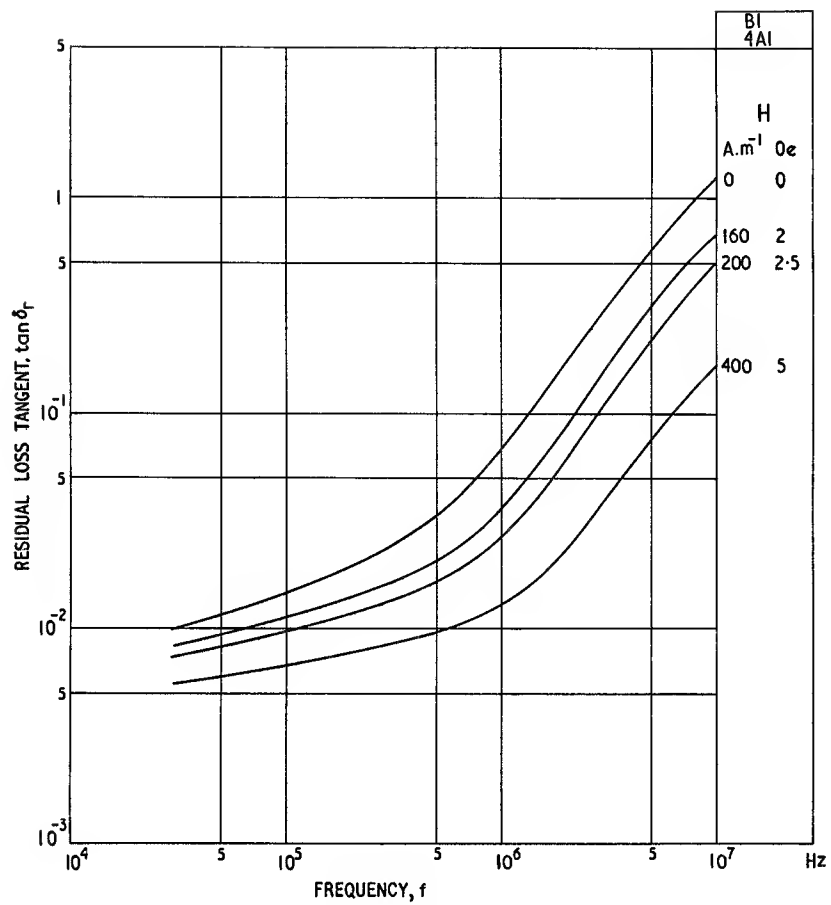


Fig. 3.14.2

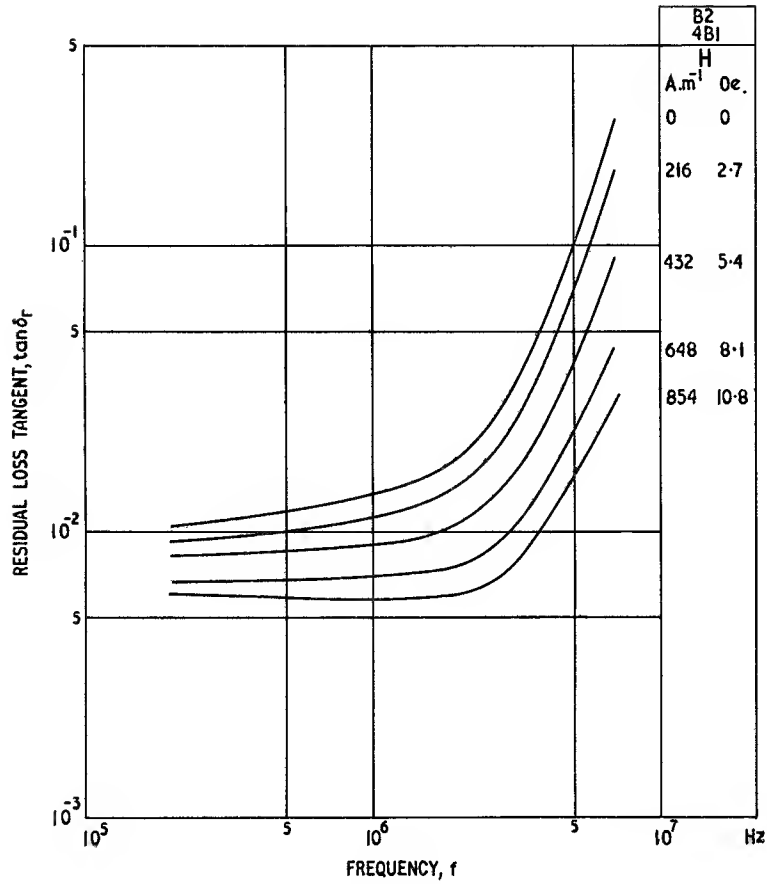


Fig. 3.14.3

Hysteresis loss factor as a function of flux density
Fig. 3.15

$$f = 10 \text{ kHz}$$

$$\theta \approx 20^\circ \text{C}$$

In the discussion of loss expressions in Section 2.2.6 it was pointed out that in practice the higher powers of f and B are usually ignored in considering the low-amplitude loss terms and as a result simple relations such as the Legg expression (Eqn 2.67) are obtained. At low frequencies and low flux densities the coefficients may be regarded as material constants, but at higher frequencies or flux densities the higher power terms become significant and are usually allowed for by making the coefficients themselves functions of frequency and flux density. In this figure the relation between the hysteresis loss factor and the flux density is shown for the same manganese zinc ferrite specimens as used for the data in Fig. 3.5. From Eqn 2.68 or Table 2.1:

$$\frac{\tan \delta_h}{\mu} = \frac{1}{2\pi} a \hat{B}$$

Thus if the hysteresis coefficient a were constant the hysteresis loss factor would be proportional to \hat{B} . In practice the relation is not linear so, if the above equation is used in an experimental determination of a , the range of flux densities over which the slope of the curve is measured must be specified. Typical flux density ranges that may be found in test specifications are 0.5 to 1, or 1 to 2 mT, i.e. 5 to 10, or 10 to 20 Gs. In laboratory measurements the tangent at the origin may be used.

The Rayleigh and Peterson coefficients may also be obtained from these graphs. Strictly both of these coefficients relate to the hysteresis loss with field strength as the independent variable. However at very low flux densities the permeability closely approaches the initial permeability and Eqns 2.35 and 2.39 may be used to obtain these coefficients. Using the tangent of the curves at the origin, the values of the various coefficients have been obtained for each of the specimens referred to in this figure. (Table 3.6)

These results may be compared with those derived

from the variation in permeability with amplitude in Fig. 3.5. It is seen that there is a rough correspondence between the respective values of v . In the Rayleigh relation the permeability rise and the hysteresis loss are both dependent on the value of a single constant v .

The significance of the hysteresis coefficients in the calculation of hysteresis loss, third harmonic distortion and third order intermodulation products is discussed in detail in Chapter 2.

From the loss point of view the hysteresis loss tangent is a particularly useful parameter when determining the extra dissipation, or the degradation of Q -factor, occurring in an inductor when it is being operated at a flux density that is not vanishingly small. It is shown in Section 4.2.3 that if a core has a material loss factor $(\tan \delta)/\mu$ at a given frequency and flux density, arising from any origin then, when it is gapped to an effective permeability μ_e and operated at the same frequency and flux density, the effective loss tangent will be $\mu_e \times (\tan \delta)/\mu$. Thus the curves of this figure may be used directly for any gapped core provided the effective peak flux density \hat{B}_e is known and the frequency is not too high. The dependence of $(\tan \delta_h)/\mu$ on frequency is shown in the next figure. (See also Sections 2.2.3, 2.2.6, 4.2.3, Table 2.1, Figs. 3.5, 3.16, 3.17 and 3.18.)

$$\frac{\tan \delta_h}{\mu_a} = \frac{4v\hat{B}}{3\pi\mu_0\mu_a^3} \quad (\text{see Eqn 2.35})$$

$$= \frac{8a_{02}\hat{B}}{3\pi\mu_0\mu_a^3} \quad (\text{see Eqn 2.39})$$

$$\text{as } \hat{B} \rightarrow 0, \mu_a \rightarrow \mu_i$$

$$\frac{\tan \delta_h}{\mu} = \frac{a\hat{B}}{2\pi} \quad (\text{see Eqns 2.68 and 4.51})$$

$$(\tan \delta_h)_{\text{gapped}} = \mu_e \left(\frac{\tan \delta_h}{\mu} \right) \quad (\text{see Eqn 4.49})$$

$$\frac{E_{3a}}{E_a} = 0.6 \tan \delta_h \quad (\text{see Eqn 2.78})$$

for a material operating in the Rayleigh region.

Table 3.6

Specimen	μ_i	Rayleigh coefficient v	Peterson coefficient a_{02}		Legg coefficient a	
		(SI units)	(SI units)	(CGS)	(SI units)	(CGS)
A5	1720	19	9.5	760	0.8×10^{-2}	0.8×10^{-6}
A13	2090	15.4	7.7	616	0.35×10^{-2}	0.35×10^{-6}
A10	690	1.6	0.8	64	1.0×10^{-2}	1.0×10^{-6}
A5T	1960	52	26	2080	1.5×10^{-2}	1.5×10^{-6}
A7	5160	530	265	21200	0.8×10^{-2}	0.8×10^{-6}

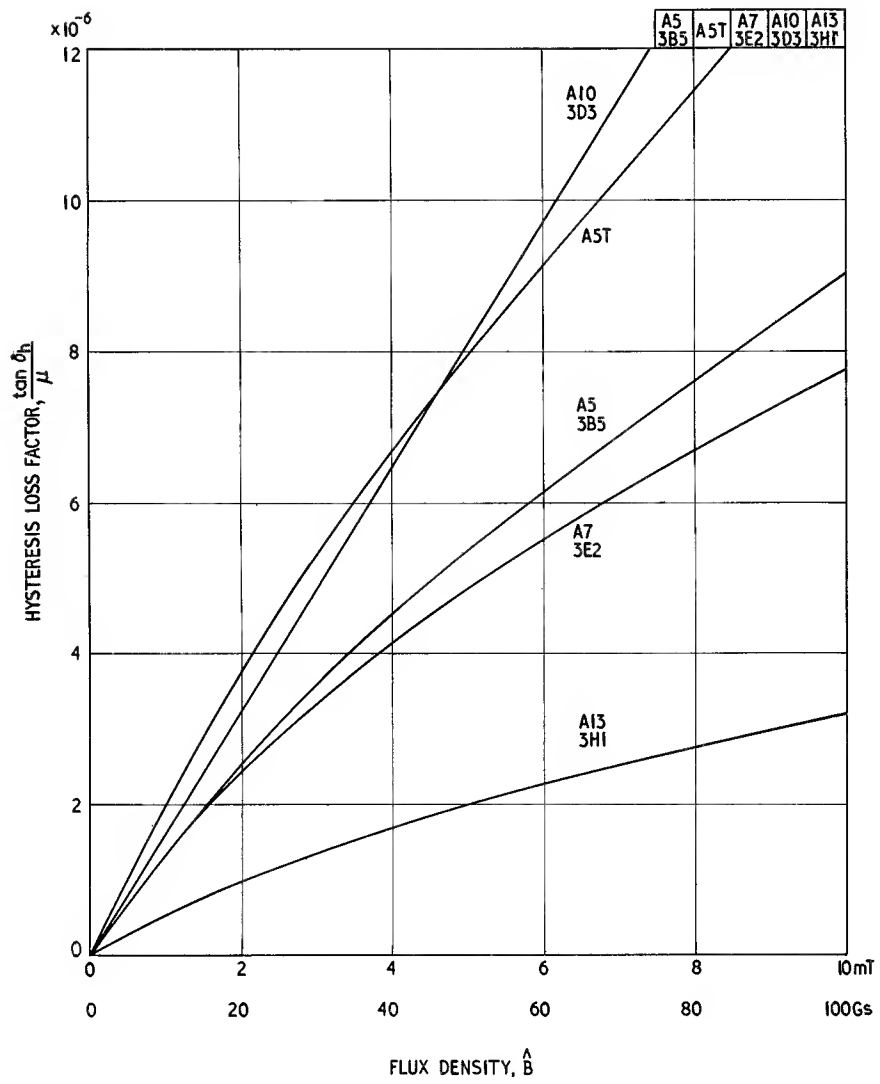
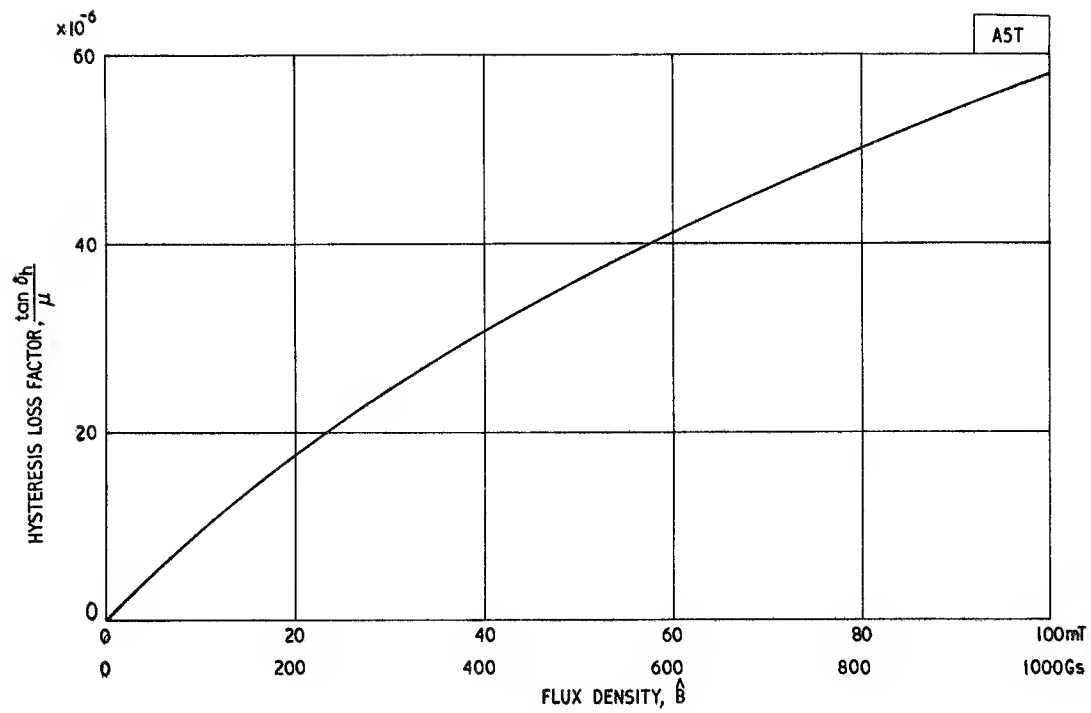


Fig. 3.15.1

*Fig. 3.15.2*

Hysteresis loss factor as a function of frequency Fig. 3.16

$$\hat{B} = 1 \text{ mT (10 Gs)}$$

$$\theta \approx 20^\circ\text{C}$$

In considering the shape of the curves in this figure it is necessary to have a clear definition of the dependent variable. At low frequencies and at low flux densities it may be seen from Section 2.2.6 that:

$$\frac{\tan \delta_h}{\mu} = \frac{a\hat{B}}{2\pi}$$

where a is the Legg hysteresis coefficient

Eqns 4.52 and 4.53 are expressions that are relevant to measuring a on an admittance bridge.

It follows that:

$$\frac{\tan \delta_h}{\mu} = \frac{\hat{B}\omega^2 N^3 \mu_0}{\sqrt{2}C_2} \times \frac{\Delta G}{\Delta U}$$

Thus at a given frequency and flux density the hysteresis loss factor is proportional to the quotient of the increase in conductance and the increase of voltage producing it. At low frequencies this increase of conductance is undoubtedly the result of simple hysteresis loss, i.e. due to irreversible domain wall movements, but at higher frequencies it may be caused by other magnetic loss processes. In particular, as the ferrimagnetic resonance is approached a part of the total loss is due to the damping

of this resonance and it is possible that level dependent components of this damping contribute to the change in conductance. It is interesting to speculate at this stage whether such contributions increase the magnetic intermodulation. Some light is thrown on this question by the data on intermodulation magnetic distortion given in Fig. 3.18.

Summing up, although it is convenient to refer to this variable as the hysteresis loss factor it must be recognized that this may be a misnomer at the higher frequencies.

Some evidence of a contribution from a ferrimagnetic resonance process is apparent in the figure. It is seen that the loss factor of the highest permeability material, A7, rises at a relatively low frequency while that of the lowest permeability material shown, A5, rises at a higher frequency. The specimens used for these measurements were identical with those for which data are given in Figs. 3.5, 3.15 and 3.18.

(See also Sections 2.2.3, 2.2.6, 4.2.3, Figs. 3.5, 3.12, 3.15 and 3.18.)

$$\frac{\tan \delta_h}{\mu} = \frac{a\hat{B}}{2\pi} = \frac{4\pi\hat{B}}{3\pi\mu_0\mu^3} \quad (\text{see Eqns 2.68, 2.35})$$

$$a = \sqrt{2\pi} \cdot \frac{\mu_0\omega^2 N^3}{C_2} \cdot \frac{\Delta G}{\Delta U} \quad (\text{see Eqn 4.52})$$

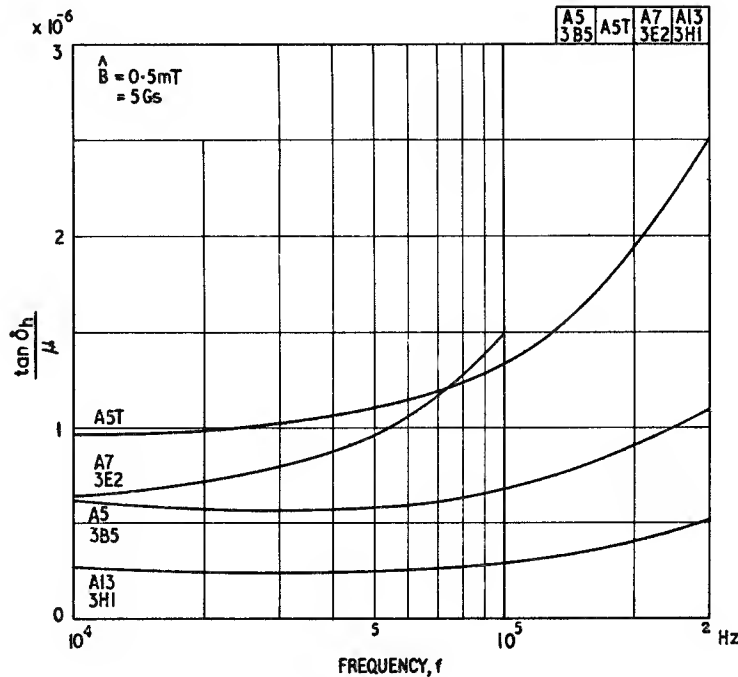


Fig. 3.16.1

Hysteresis loss factor as a function of temperature

Fig. 3.17

$$f = 10 \text{ kHz}$$

$$\hat{B} = 1 \text{ mT (10 Gs)}$$

This figure shows results obtained on three manganese zinc ferrites. It is interesting to note that each curve has a

minimum coinciding approximately with the temperature at which the secondary peak occurs in the permeability/temperature relation. It is at this temperature that the crystalline anisotropy goes through zero, so some connection between the hysteresis process and the crystalline anisotropy is apparent.

(See also Fig. 3.8)

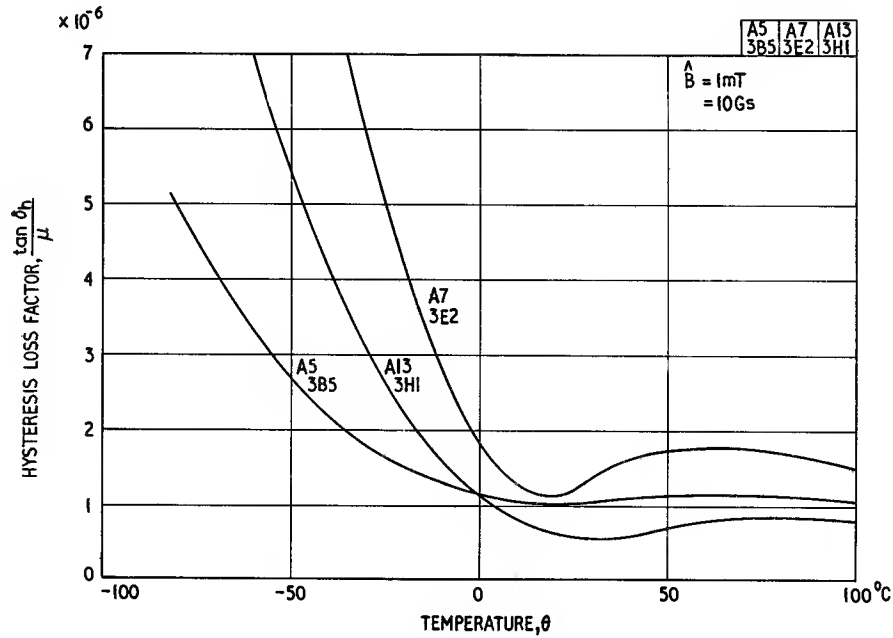


Fig. 3.17.1

Magnetic distortion Fig. 3.18

$$\hat{B} = 0.5 \text{ mT (5 Gs)}$$

$$\theta \approx 20^\circ\text{C}$$

The graphs in this figure show the variation of the magnetic distortion with frequency for a number of typical ferrites. With the exception of those for B10, the measured results, shown by the full lines, were obtained on the actual toroidal specimens used to obtain the data for Figs. 3.5, 3.15 and 3.16. The results refer to the distortion e.m.f. (open-circuit voltage) due to a sinusoidal current, and are expressed in decibels relative to the voltage of the applied signals. The abscissa represents the fundamental frequency or the mean of the applied frequencies.

The third harmonic was measured by passing the signal through a low pass filter and applying it to a winding on the specimen through a relatively high inductance coil. The e.m.f. across the winding on the specimen was applied through another high inductance coil to a high pass filter and thence to a wave-analyser. The filters and inductances were composed of air-cored coils to prevent spurious distortion. The low pass filter was designed to suppress the distortion from the source and the high pass filter prevented the fundamental from reaching the detector. A number of pairs of filters and inductors were needed.

For the intermodulation measurements,¹⁶ two independent signals were applied to the winding on the specimen via a bridge network which was adjusted to prevent coupling between the sources. Each amplitude was equivalent to 0.5 mT (5 Gs). The frequencies, f_a and f_b , were chosen to be on either side of a nominal frequency and removed from it by about 20%. The nominal frequency is represented along the abscissa. Again the specimen was separated from the source and detector impedances by high inductance air-cored coils and a simple filter was used to prevent the applied signals reaching the wave-analyser.

It has been seen in Chapter 2 that the distortion products depend on one or both of the Peterson (or similar) coefficients, e.g. a_{11} and a_{02} . Fig. 3.5 shows μ as a function of \hat{B} from which a_{11} , at a particular frequency, may be calculated using Eqn 2.37. The value of a_{11} calculated from this and similar graphs falls with frequency, reaching about half of its low-frequency value by about 300 kHz. Fig. 3.16 shows the variation of hysteresis loss factor with frequency; from these data the

coefficient a_{02} may be calculated using Eqn 2.39. Since a_{02} is proportional to $(\tan \delta_h)/\mu$ it follows that a_{02} is a rising function of frequency for these specimens.

From Eqn 2.78 the relative amplitude of the third harmonic may be calculated and from the appropriate equations in Table 2.2 the relative amplitudes of the sum and difference products may be obtained. The starting data are the Peterson coefficients obtained from Figs. 3.5 and 3.15 and similar graphs obtained at other frequencies. The results are shown as broken curves in the following graphs. Whereas the measured difference products show reasonable agreement with theory the sum products show a discrepancy of about 5 to 10 dB at the lower frequencies. However the separation of the measured third order summation product curve from the third harmonic curve is in reasonable agreement with theoretical prediction; from the equations quoted below the third harmonic amplitude should be 4.6 dB below that of the summation product.

As the frequency rises the calculated third harmonic and sum products rise following the rise of $(\tan \delta_h)/\mu$ with frequency (Fig. 3.16) but the corresponding measured curves fall. This tends to confirm the suggestion made in the introduction to Fig. 3.16, that at the higher frequencies the measured hysteresis loss factor contains components not having their origins in the simple hysteresis phenomenon. The falling characteristics measured for the third harmonic and third order summation products tend to confirm the theory that in high permeability ferrites the domain wall movement relaxes at frequencies in the order of 100 kHz. Magnetic distortion and other hysteresis phenomena arise from the irreversible components of domain wall movement. In the case of the lower permeability ferrites, e.g. A10 and B10, the droop is not established at frequencies much below 1 MHz. No clear dispersion of the third order difference products is apparent within the range of measurements.

In view of the above observations, it would appear more reliable, when comparing materials for magnetic distortion, to use directly measured distortion data rather than measured hysteresis factors or coefficients; the theoretical relations between these parameters appear to be unreliable, particularly at the higher frequencies.

(See also Sections 2.2.3, 2.2.6, 2.2.7, 4.2.3, Table 2.2 and Figs. 3.5, 3.15, 3.16 and 3.17.)

Peterson coefficients:

$$a_{11} = d\mu_a/dH = \mu_0\mu_a d\mu_a/dB \quad (\text{see Eqn 2.37})$$

$$a_{02} = \frac{3\pi}{8} \frac{\mu_0\mu_a^2}{\hat{B}} \tan \delta_h \quad (\text{see Eqn 2.39})$$

$$\text{as } \hat{B} \rightarrow 0, \mu_a \rightarrow \mu_i$$

$$\frac{E_{2a+b}}{E_a} = \frac{128}{15\pi^2} \frac{a_{02}\hat{B}_a}{\mu_0\mu^2} = 1.019 \tan \delta_h \quad (\text{see Table 2.2})$$

$$\frac{E_{2a-b}}{E_a} = \frac{16}{15\pi} \frac{a_{02}\hat{B}_a}{\mu_0\mu^2} \sqrt{\left(\frac{a_{11}}{a_{02}}\right)^2 + \left(\frac{8}{3\pi}\right)^2} \quad (\text{see Table 2.2})$$

Product amplitudes

$$\frac{E_{3a}}{E_a} = \frac{8}{5\pi} \frac{a_{02}\hat{B}_a}{\mu_0\mu^2} = 0.6 \tan \delta_h \quad (\text{see Eqn 2.78})$$

$$= 0.869 \tan \delta_h \text{ if } \frac{a_{11}}{a_{02}} = 2$$

\hat{B}_a is the flux density of the applied signal of frequency f_a .

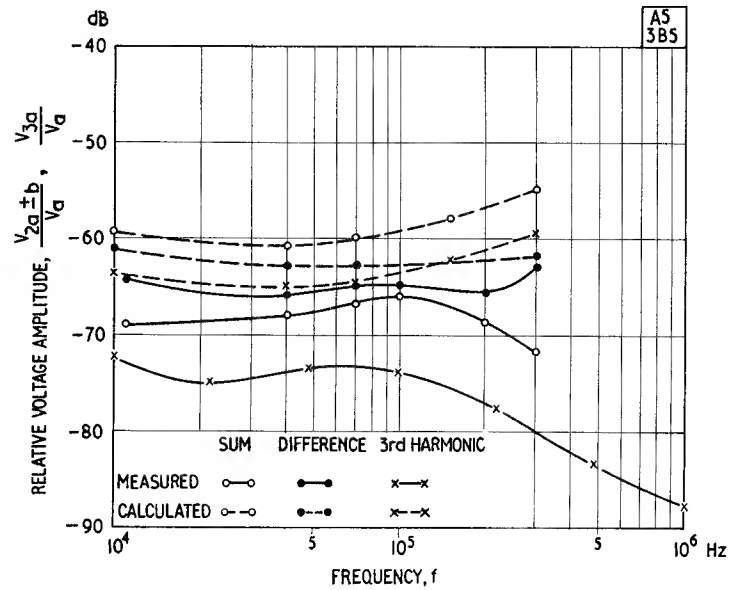


Fig. 3.18.1

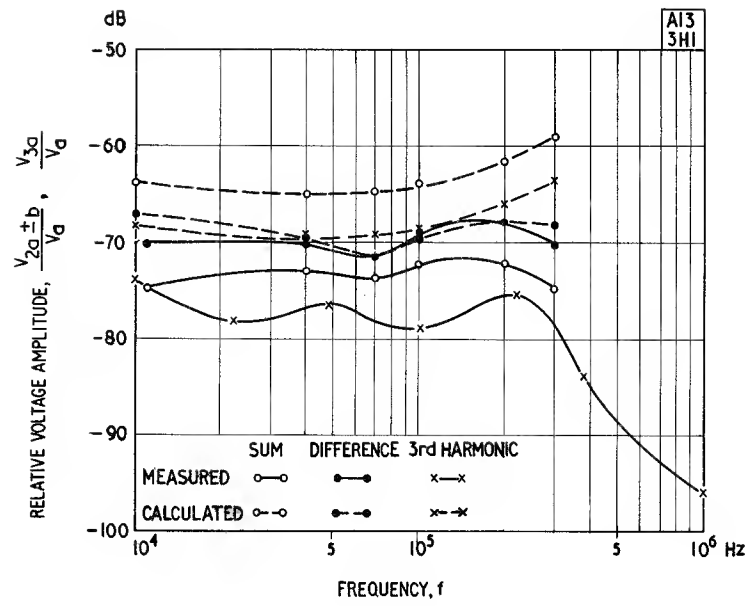


Fig. 3.18.2

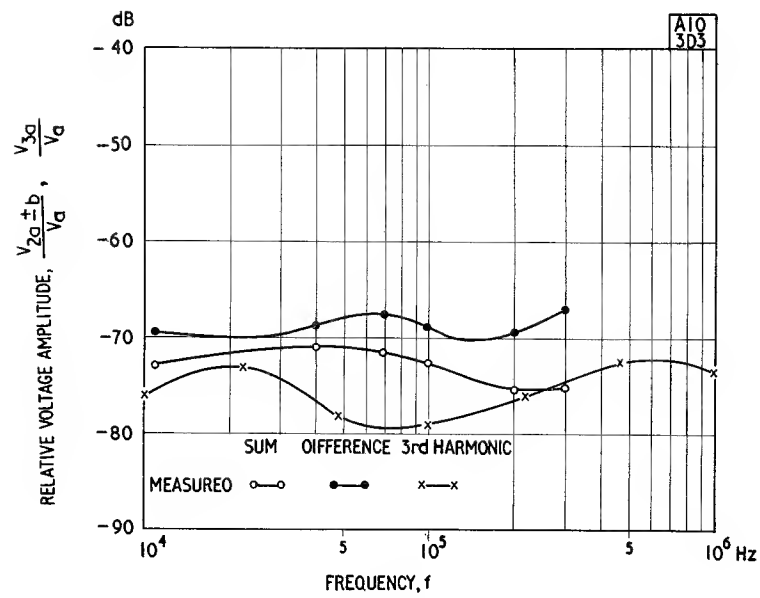


Fig. 3.18.3

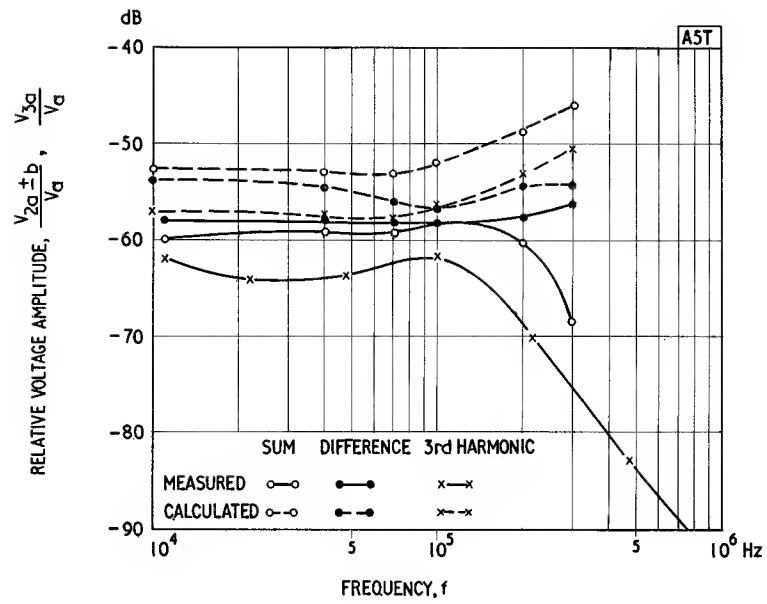


Fig. 3.18.4

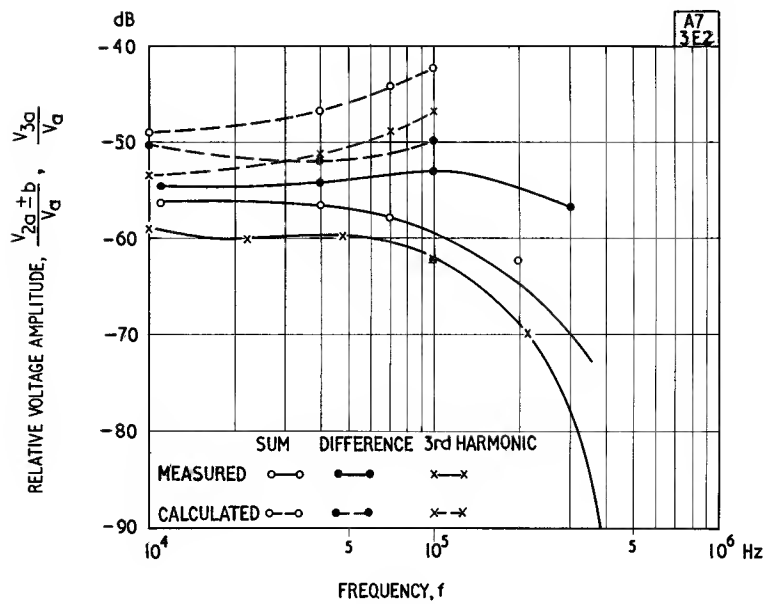


Fig. 3.18.5

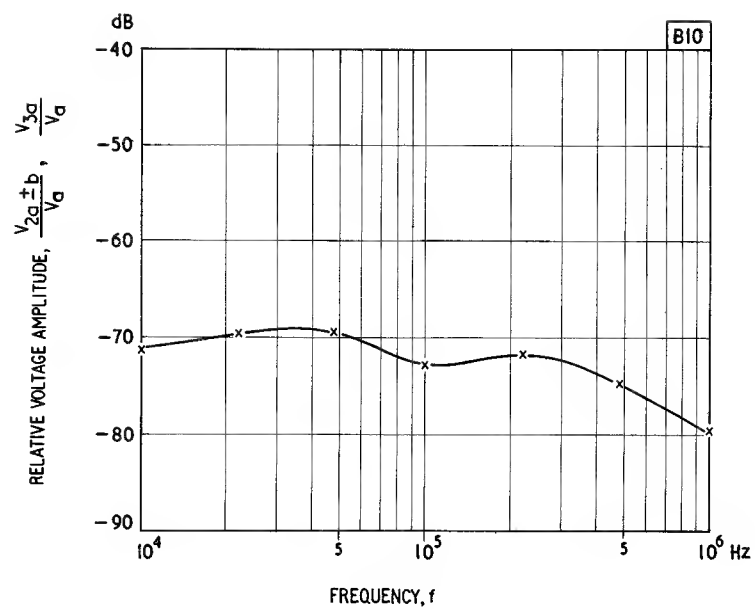


Fig. 3.18.6

Power loss as a function of frequency at high flux densities
Fig. 3.19.

The graphs in this figure show the variation of the power loss (volume) density, P_m , with frequency at a number of high flux densities within the working range. As far as possible, loss due to eddy currents in the bulk of the core has been eliminated from these results so they are applicable to a general core. If a given core has large cross sections then the possibility of extra loss due to these eddy currents must be considered, and an additional calculation must be made as indicated in Section 2.2.4.

For the manganese zinc ferrites the power loss is approximately proportional to frequency except at the lower flux densities where the residual loss, i.e. the loss expressed by $(\tan \delta_r)/\mu$ in Fig. 3.12, plays a significant part in the total and causes an increase in slope. Thus whatever the behaviour of the low amplitude hysteresis loss factor with frequency (see Fig. 3.16), it is clear that at high flux densities the energy loss per cycle remains fairly constant up to at least 100 kHz.

The graphs for the nickel zinc ferrites do not show the same characteristic. At the higher frequencies at which these materials have an advantage, the total loss density becomes large at quite low flux densities and it increases much more than in proportion to the frequency. It may be concluded that the major loss process is connected with ferrimagnetic resonance which is being approached at these frequencies. Domain wall resonance may also play an important part.

The loss density in manganese zinc ferrites at 10kHz varies in proportion to B^n where n varies from 1.9 to 2.9

in the materials considered. The value is given on each graph. By Eqn 2.33, the hysteresis loss density, $P_h \propto \hat{B}^3/\mu_a^3$ for a magnetic material operating in the Rayleigh region. Since, in this region, μ_a does not differ by much from μ_i the specific loss varies approximately as the cube of the flux density. It is interesting that for some ferrites this cubic relation seems to hold up to quite high flux densities irrespective of the variations of μ_a . In other ferrites a square law is a better approximation. (See also Sections 2.2.3, 2.3, 9.4.4.)

Power loss density:

$$P_m \propto f \hat{B}^n \quad \text{W.m}^{-3} \quad (\text{approximately}) \quad (3.4)$$

where n is the Steinmetz exponent; the value of n at 10 kHz for each manganese zinc ferrite is given on the graphs.

Eddy current loss (extra to the losses shown in this figure):

$$P_F = \frac{(\pi \hat{B} f d)^2}{\rho \beta} \quad \text{W.m}^{-3} \quad (\text{see Eqn 2.48})$$

where $\beta = 6$ for laminations of thickness d m
 $= 16$ for a cylinder of diameter d m
 $= 20$ for a sphere of diameter d m

For a square cross-section a reasonable approximation is to put d equal to the diameter of the circle of equal area and use $\beta = 16$.

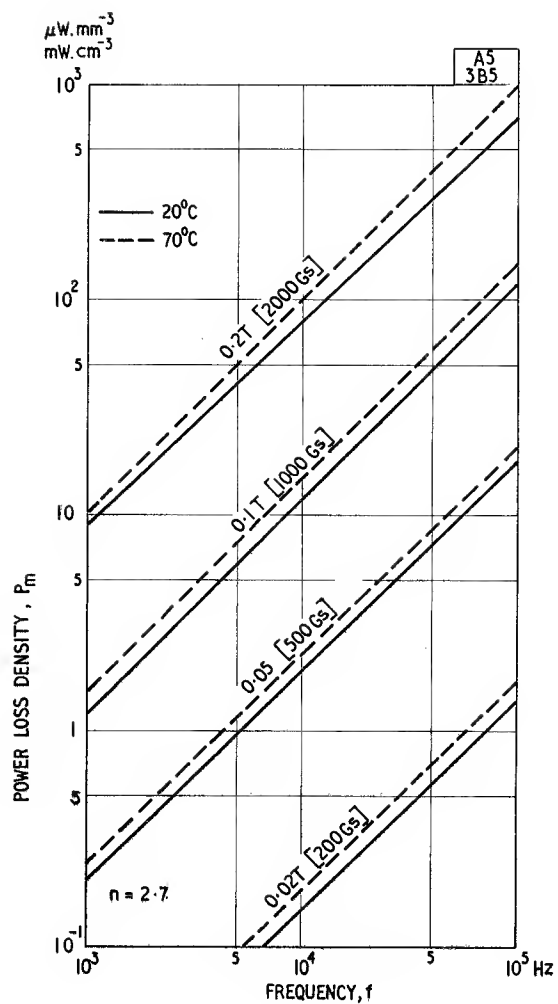


Fig. 3.19.1

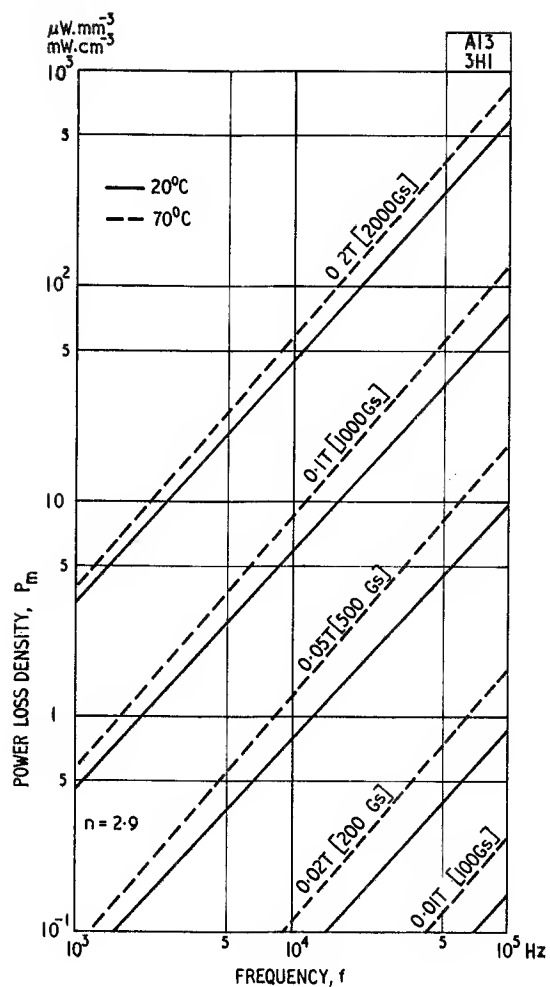


Fig. 3.19.2

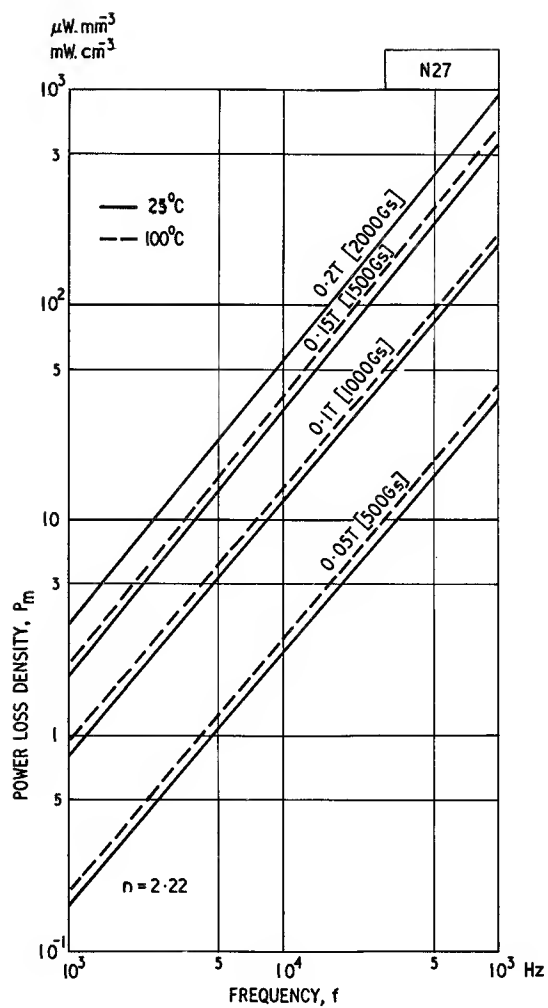


Fig. 3.19.3

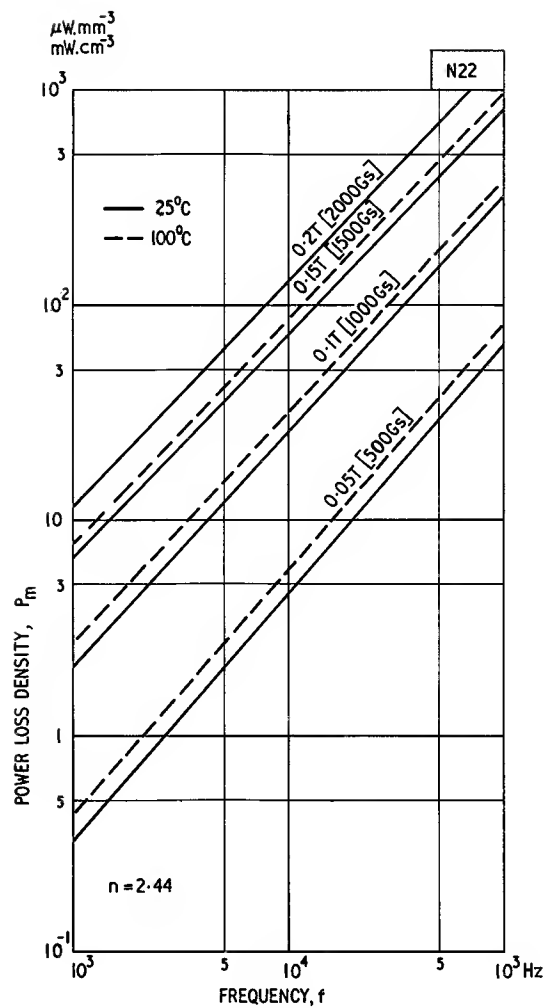


Fig. 3.19.4

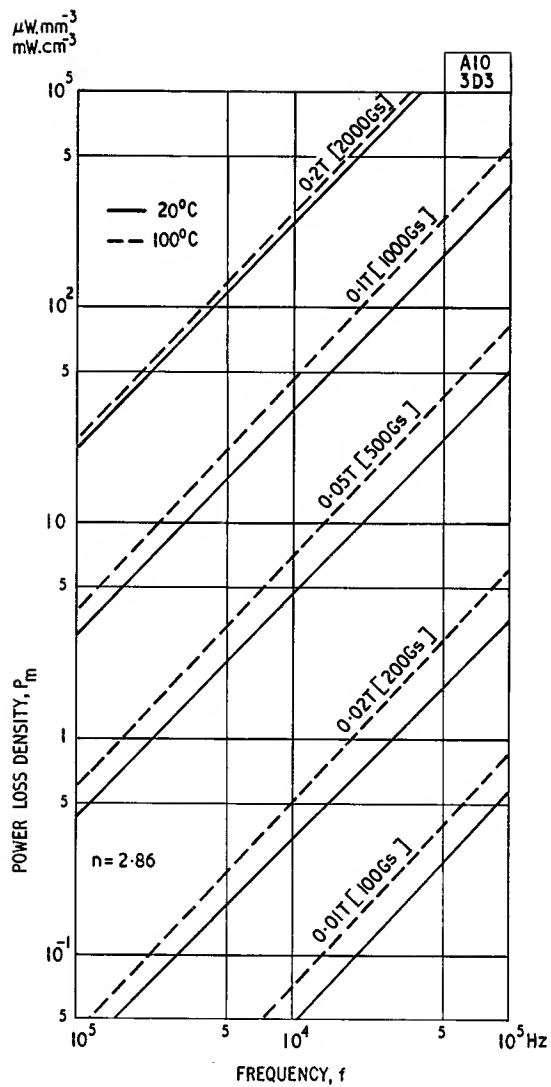


Fig. 3.19.5

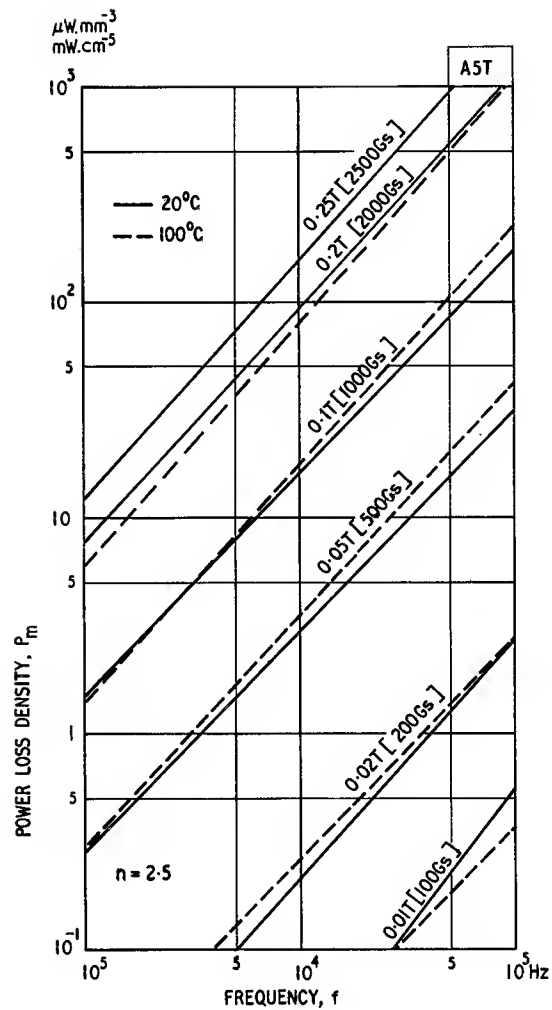


Fig. 3.19.6

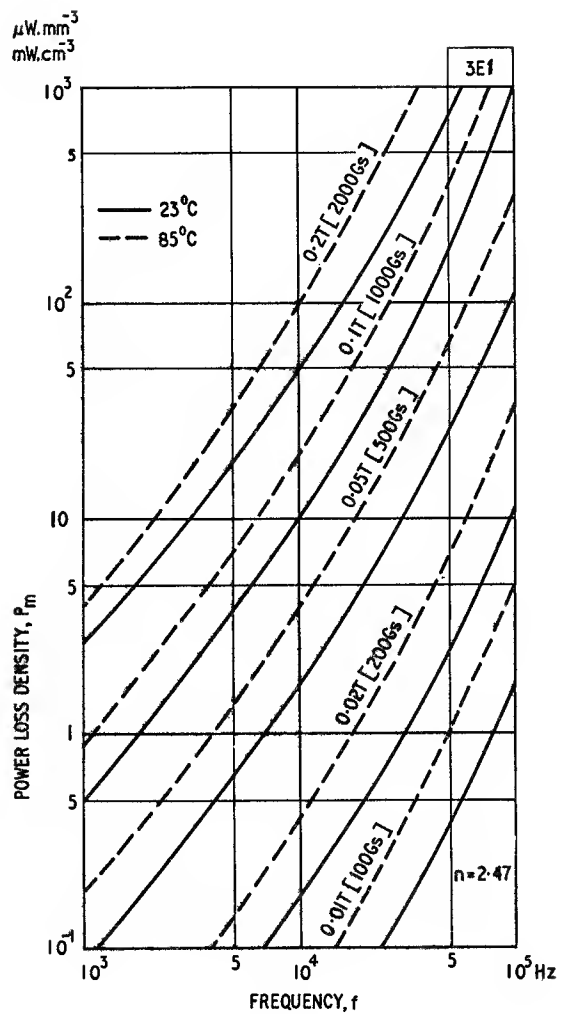


Fig. 3.19.7

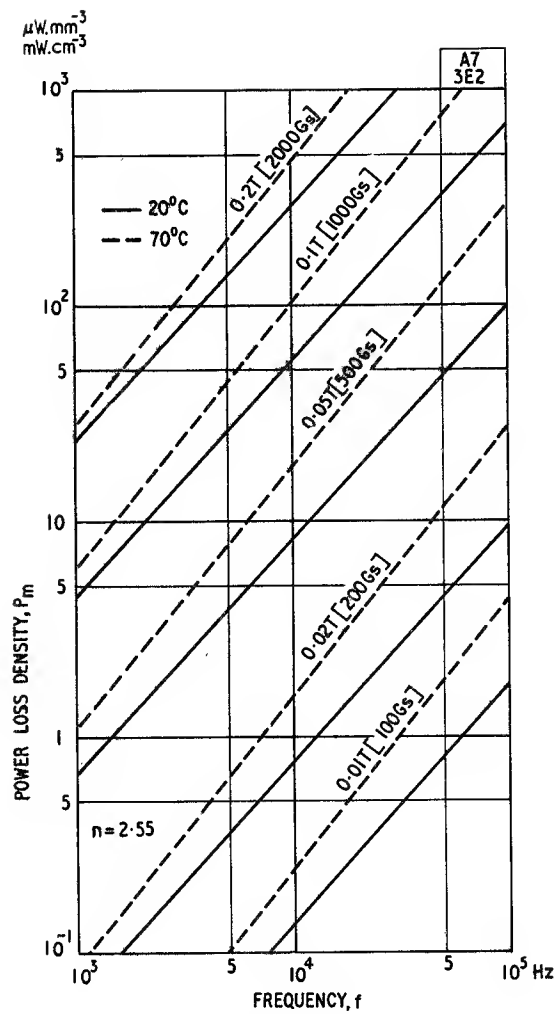


Fig. 3.19.8

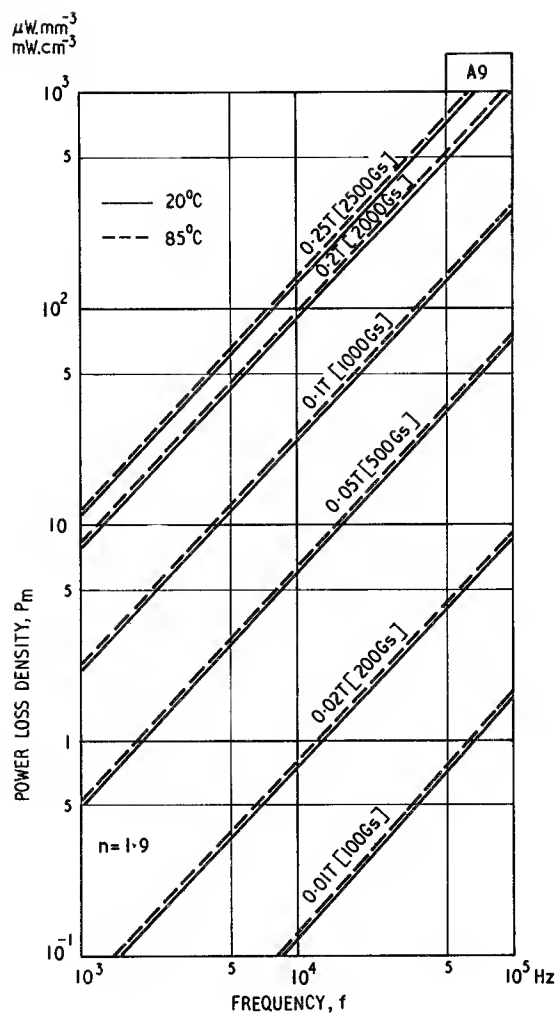


Fig. 3.19.9

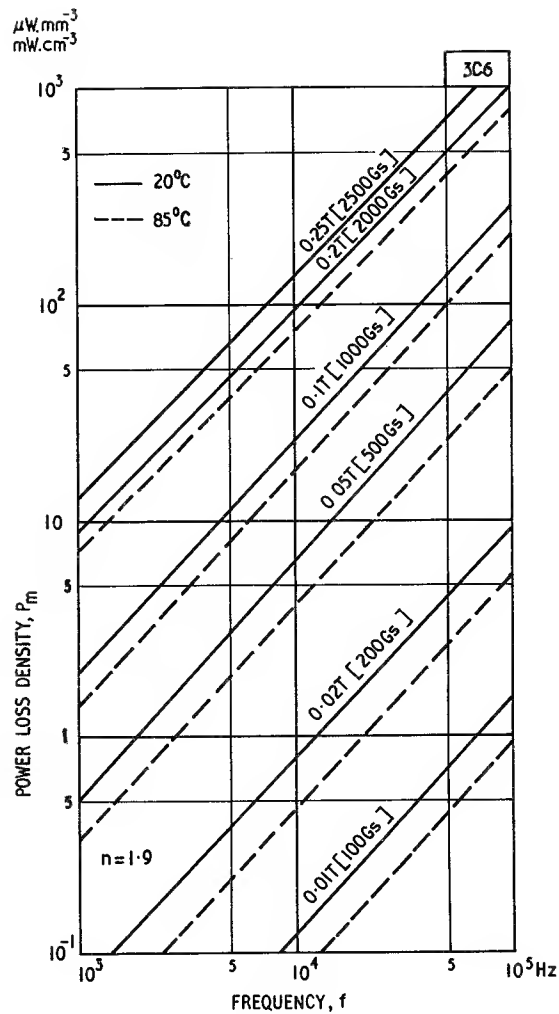


Fig. 3.19.10

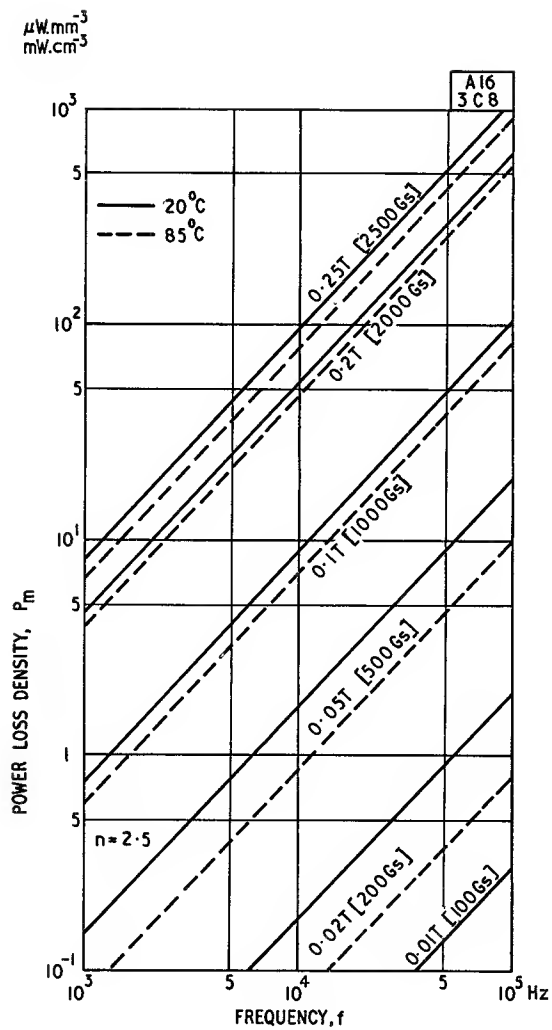


Fig. 3.19.11

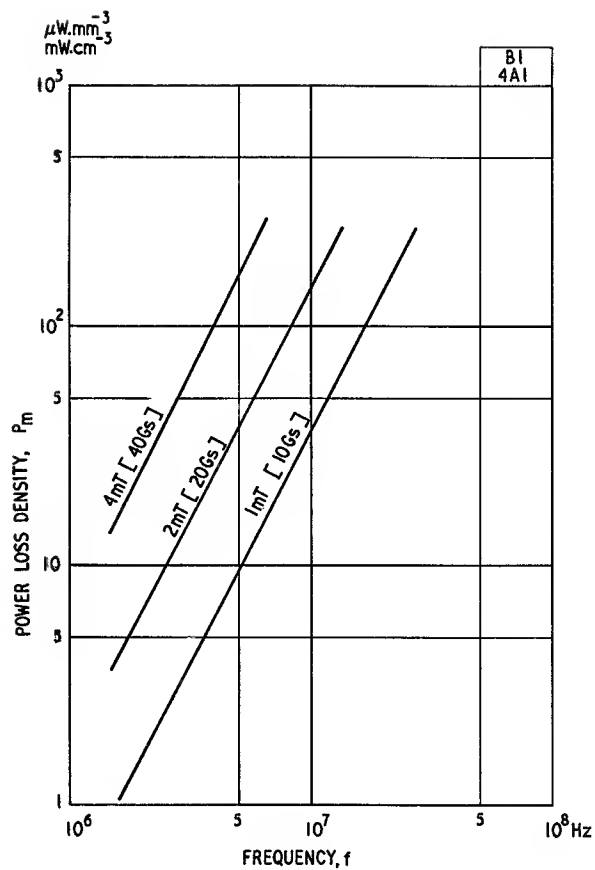


Fig. 3.19.12

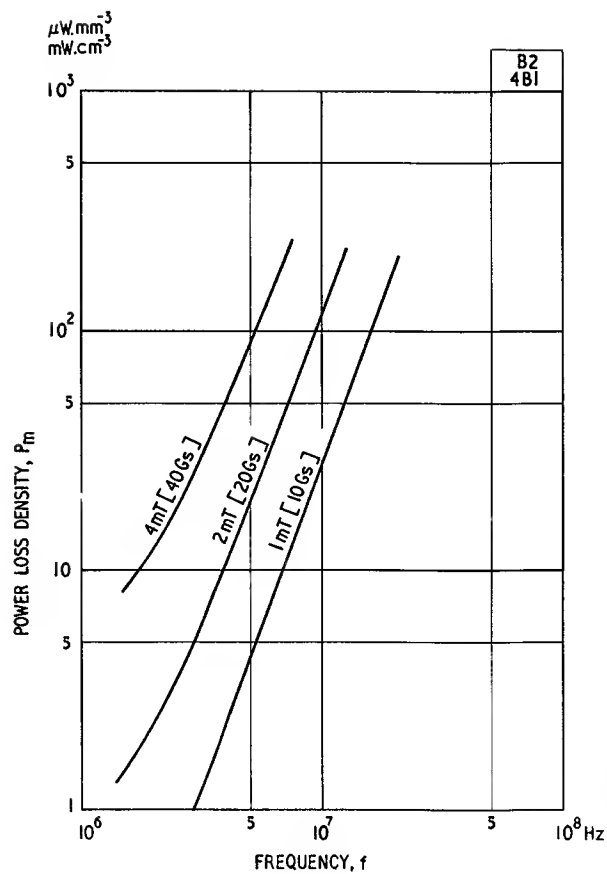


Fig. 3.19.13

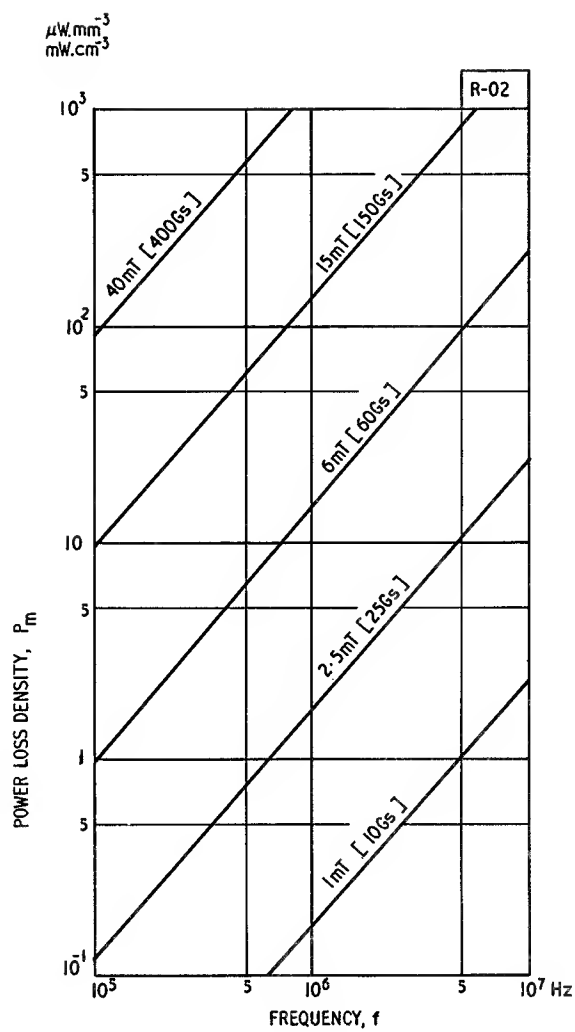


Fig. 3.19.14

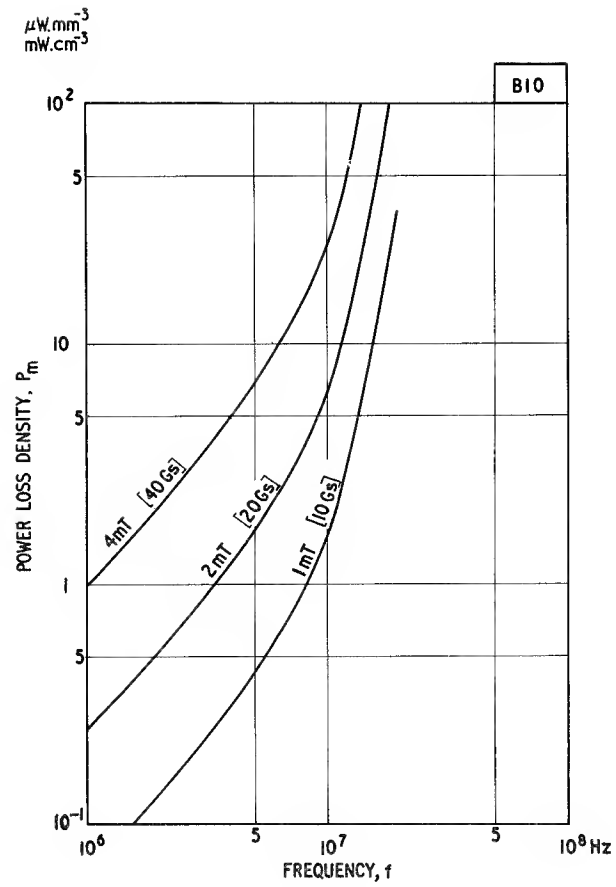


Fig. 3.19.15

Resistivity as a function of temperature Fig. 3.20

$$f \rightarrow 0$$

At room temperature most manganese zinc ferrites have resistivities between about 0.01 and $10 \Omega\cdot\text{m}$ (1 and $1000 \Omega\cdot\text{cm}$); nickel zinc ferrites normally have much higher values, e.g. $> 10^3 \Omega\cdot\text{m}$ ($10^5 \Omega\cdot\text{cm}$). As ferrites are semiconductors the resistivity falls with rising temperature.

The graphs in this figure show the d.c. resistivity as a function of temperature for a number of grades of ferrite. It is seen that over the temperature range -70 to $+100^\circ\text{C}$ the resistivity of manganese zinc ferrites falls by a ratio that is between 30 and 100 ; the corresponding figures for nickel zinc ferrites are $10^3 - 10^4$.

Only polycrystalline ferrites are considered, so the bulk resistivity arises from a combination of the crystallite resistivity and the resistivity of the crystallite boundaries.

The boundary resistivity is much greater than that of the crystallite so the boundaries have the greatest influence on the d.c. resistivity.

The resistivity ρ at an absolute temperature T is given by:

$$\rho = \rho_\infty \exp(E_p/kT) \quad (3.5)$$

where ρ_∞ is the resistivity extrapolated to $T = \infty$

E_p is the activation energy

k is Boltzmann's constant

If E_p is to be expressed in electron-volts

$$k = 8.62 \times 10^{-5} \text{ eV}^\circ\text{K}^{-1}.$$

From this equation, E_p has been derived for each curve, or in some cases a region of a curve, and the value has been placed against the curve to which it applies.

(See also Section 2.2.4 and Figs. 3.21 and 3.22.)

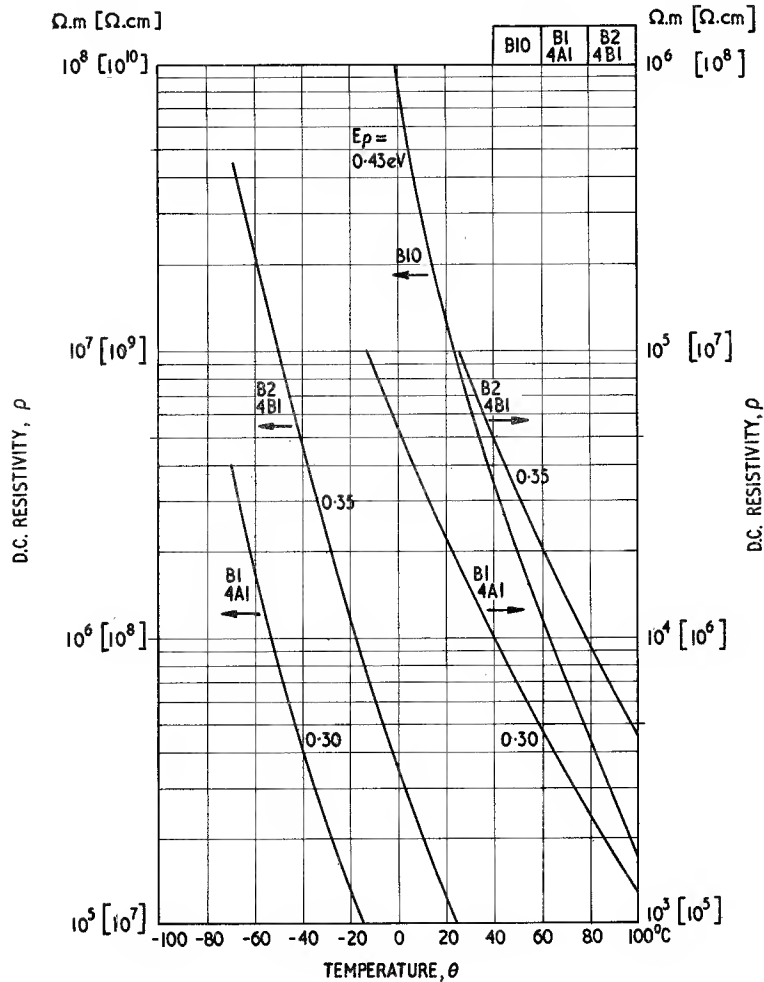


Fig. 3.20.1

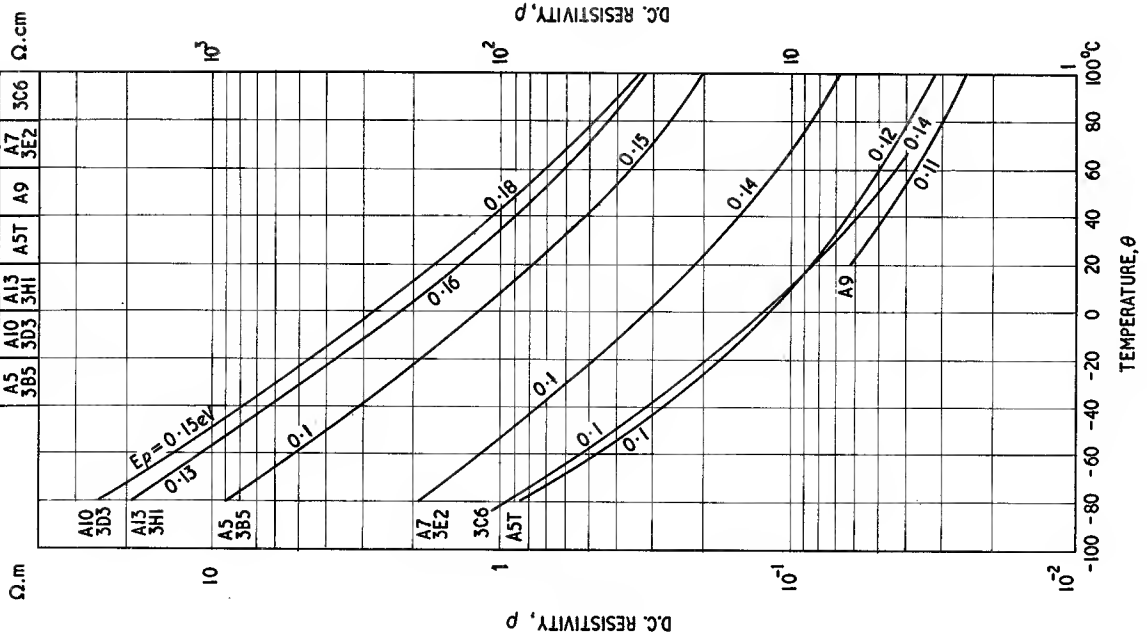


Fig. 3.20.2

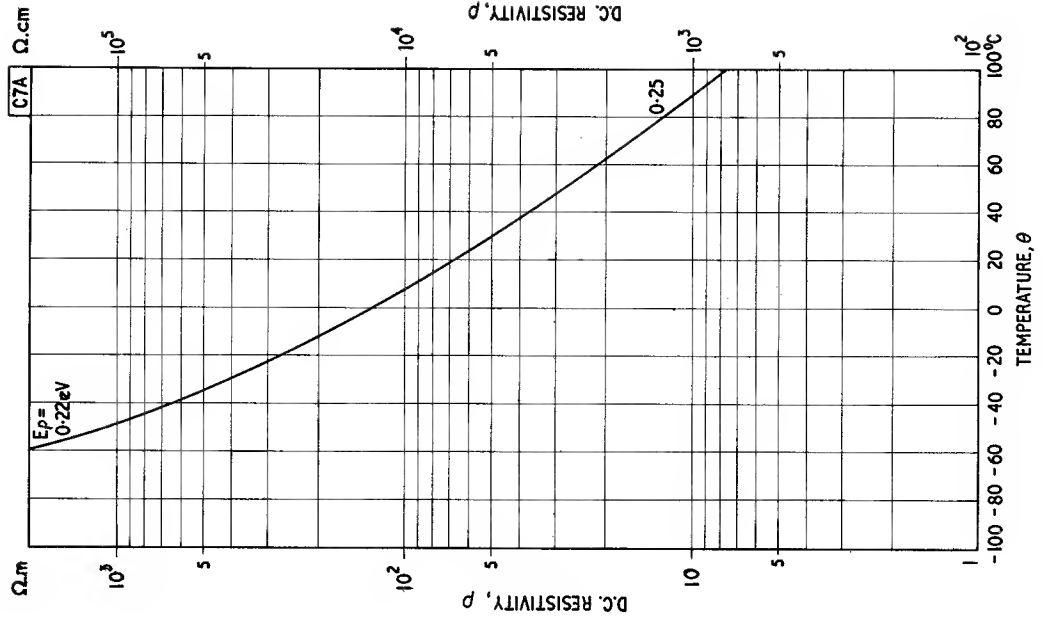


Fig. 3.20.3

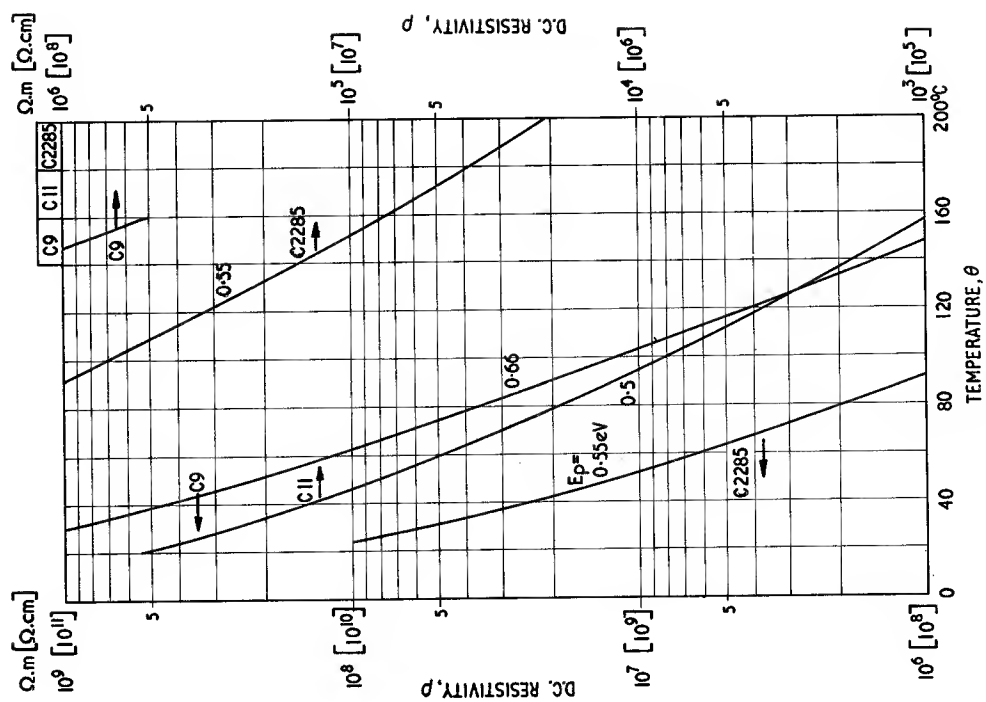


Fig. 3.20.4

Resistivity and permittivity as functions of frequency
Fig. 3.21

$$\theta \approx 25^\circ\text{C}$$

As the frequency rises from a low value the bulk resistivity, ρ , and permittivity, ϵ , of a polycrystalline ferrite stay constant at first and then fall to become asymptotic to lower values at high frequencies. This variation has the characteristic of a relaxation and is attributable to the granular structure of ferrites, in which crystallites are separated by boundaries having much higher resistivity than the crystallites. Thus the structure behaves as a compound dielectric and in Section 2.2.4 the theoretical characteristics of such a structure have been considered.

For manganese zinc ferrites typical values are:

$$\begin{aligned} \text{The relative boundary thickness, } \alpha, & 10^{-4} \\ \text{crystallite resistivity, } \rho_1, & 10^{-3} \Omega\text{.m} \\ & (0.1 \Omega\text{.cm}) \\ \text{boundary resistivity, } \rho_2, & 10^4 \Omega\text{.m} \\ & (10^6 \Omega\text{.cm}) \\ \left. \begin{array}{l} \text{crystallite permittivity, } \epsilon_1, \\ \text{boundary permittivity, } \epsilon_2, \end{array} \right\} & 10 \end{aligned}$$

Thus the bulk properties at low frequency are

$$\rho \rightarrow 1.0 \Omega\text{.m} (100 \Omega\text{.cm})$$

$$\epsilon \rightarrow 10^5$$

at high frequency $\rho \rightarrow 10^{-3} \Omega\text{.m} (0.1 \Omega\text{.cm})$

$$\epsilon \rightarrow 10$$

The relaxation time, calculated from Eqn 2.47 is $8.85 \times 10^{-10}\text{s}$ giving a relaxation frequency of 180 MHz.

For nickel zinc ferrites typical values are:

$$\begin{aligned} \text{The relative boundary thickness } \alpha, & 0.3 \times 10^{-2} \\ \text{crystallite resistivity, } \rho_1, & 30 \Omega\text{.m} \\ & (3 \times 10^3 \Omega\text{.cm}) \end{aligned}$$

$$\begin{aligned} \text{boundary resistivity, } \rho_2 & 33 \times 10^6 \text{ to} \\ & 3 \times 10^7 \Omega\text{.m} \\ & (3 \times 10^8 \text{ to} \\ & 3 \times 10^9 \Omega\text{.cm}) \end{aligned}$$

$$\left. \begin{array}{l} \text{crystallite permittivity, } \epsilon_1, \\ \text{boundary permittivity, } \epsilon_2, \end{array} \right\} 10$$

Thus at low frequency $\rho \rightarrow 10^4 \text{ to } 10^5 \Omega\text{.m} (10^6 \text{ to } 10^7 \Omega\text{.cm})$

$$\epsilon \rightarrow 3 \times 10^3$$

at high frequency $\rho \rightarrow 30 \Omega\text{.m} (3 \times 10^3 \Omega\text{.cm})$

$$\epsilon \rightarrow 10$$

The corresponding relaxation time is $8.8 \times 10^{-7}\text{s}$ and the relaxation frequency is 180 kHz.

The experimental results do not support the simple theory very well. Perhaps the dielectric cannot be adequately represented by the diagram in Fig. 2.5. (See also Section 2.2.4 and Figs. 2.5 and 3.20.)

The shunt capacitance, C_p , and resistance, R_p , of a block of material having resistivity ρ and permittivity ϵ are given by:

$$\begin{aligned} C_p &= \epsilon_0 \epsilon A / l & \text{F} \\ R_p &= \rho l / A & \Omega \end{aligned} \quad (\text{see Eqn 2.43})$$

where $\epsilon_0 = 8.854 \times 10^{-12} \text{F.m}^{-1}$

For two-layer dielectric, or crystallite and boundary:

$$\left. \begin{array}{l} \text{when } f \rightarrow 0 \quad \left. \begin{array}{l} \rho \rightarrow \alpha \rho_2 \\ \epsilon \rightarrow \epsilon_2 / \alpha \end{array} \right\} \\ \text{when } f \rightarrow \infty \quad \left. \begin{array}{l} \rho \rightarrow \rho_1 \\ \epsilon \rightarrow \epsilon_1 \end{array} \right\} \end{array} \right\} \quad (\text{see Eqn 2.46})$$

$$\tau = \epsilon_0 \frac{\epsilon_1 + \epsilon_2 / \alpha}{1 / \rho_1 + 1 / \alpha \rho_2} \quad (\text{see Eqn 2.47})$$

where the suffix 1 refers to the crystallite and 2 refers to the boundary.

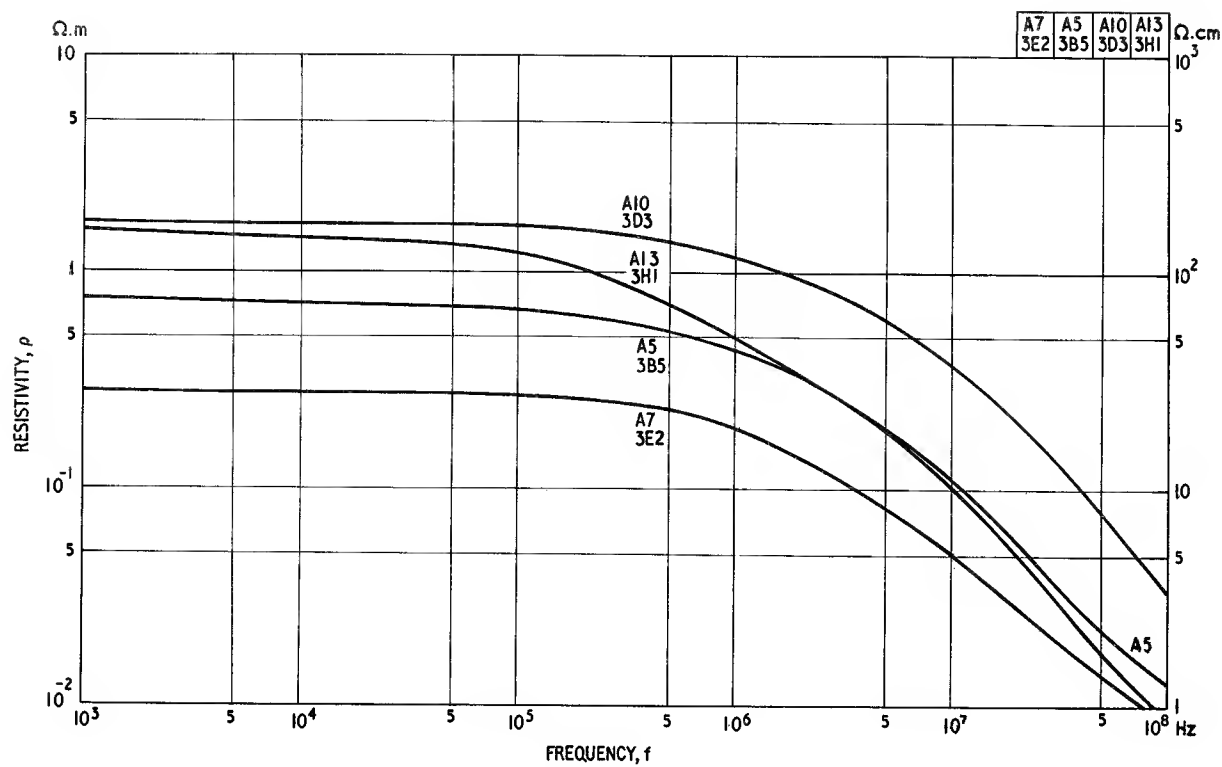


Fig. 3.21.1(a)

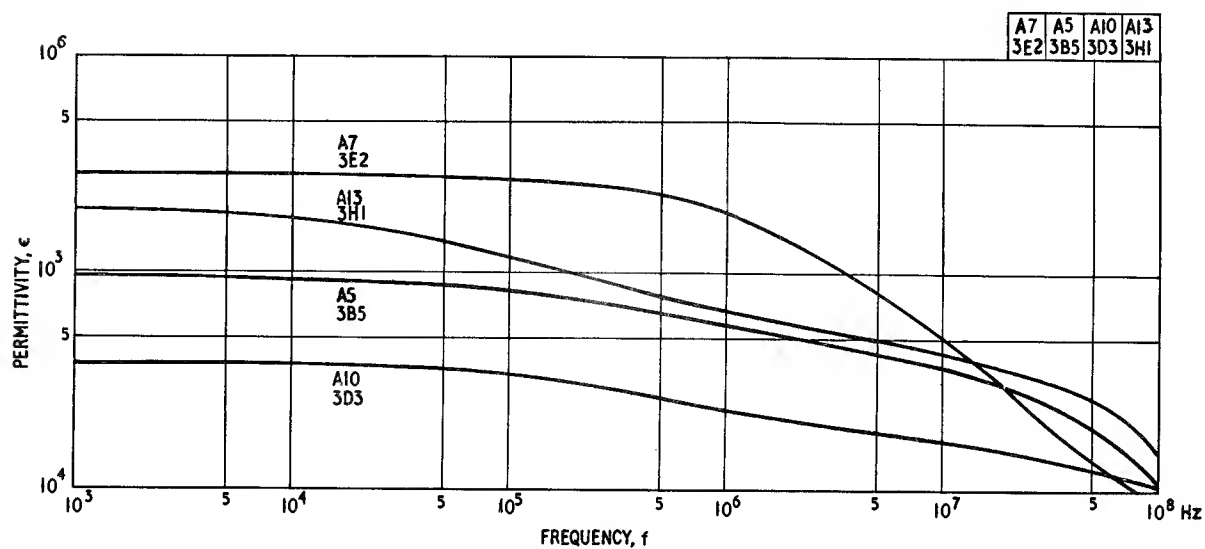


Fig. 3.21.1(b)

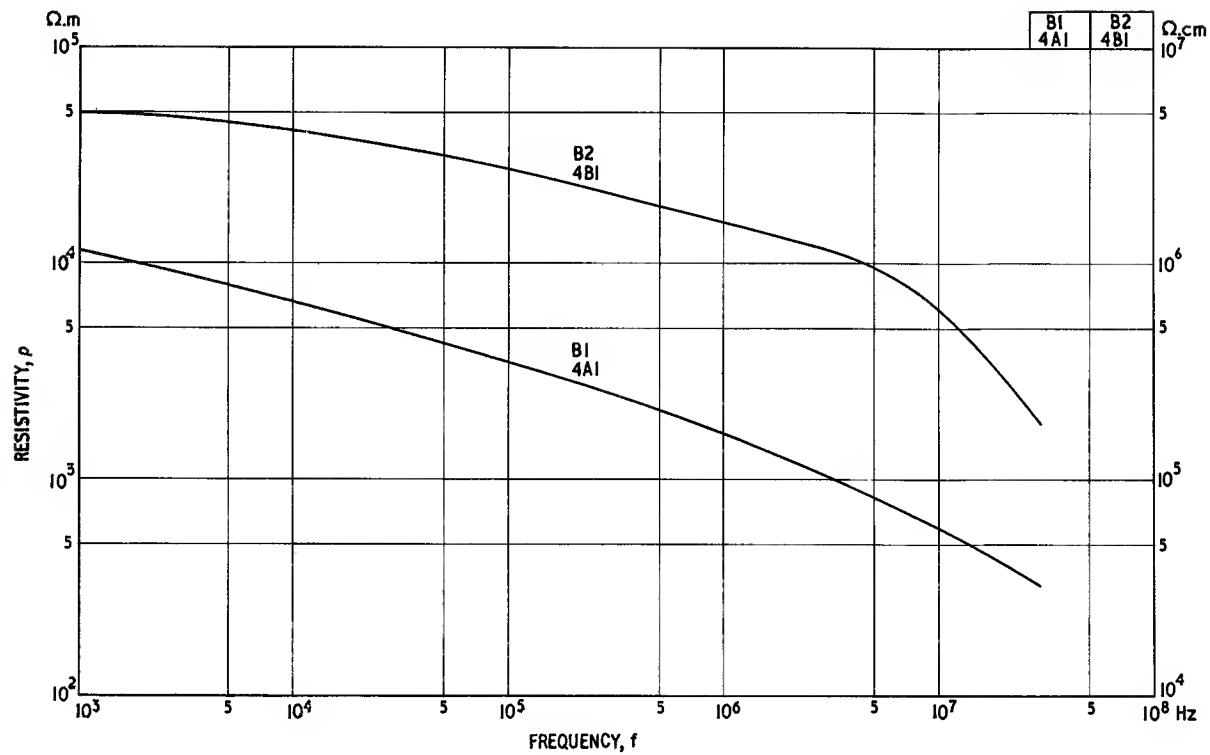


Fig. 3.21.2(a)

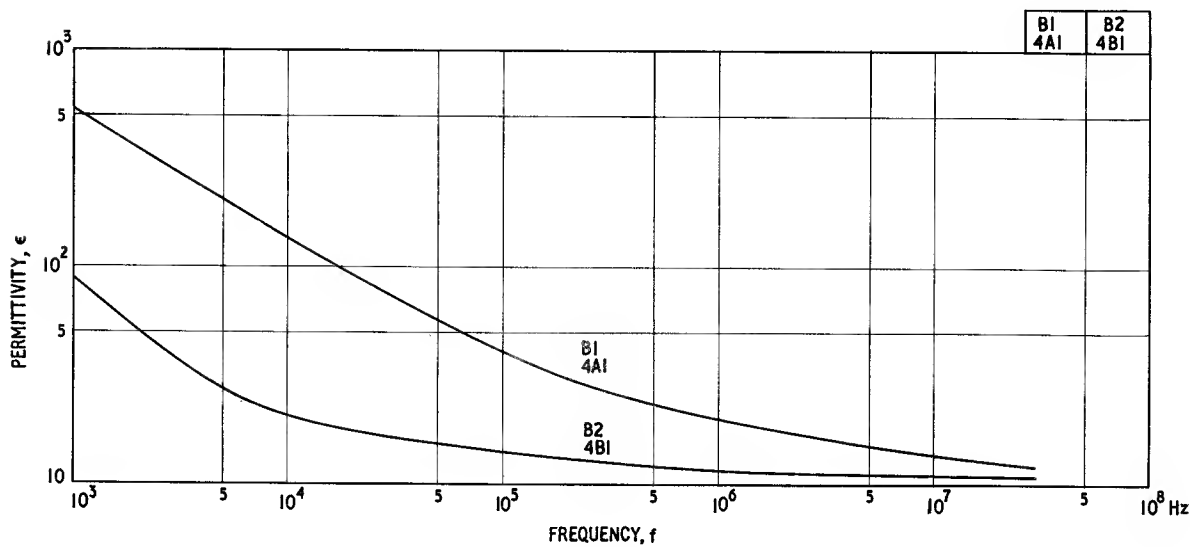


Fig. 3.21.2(b)

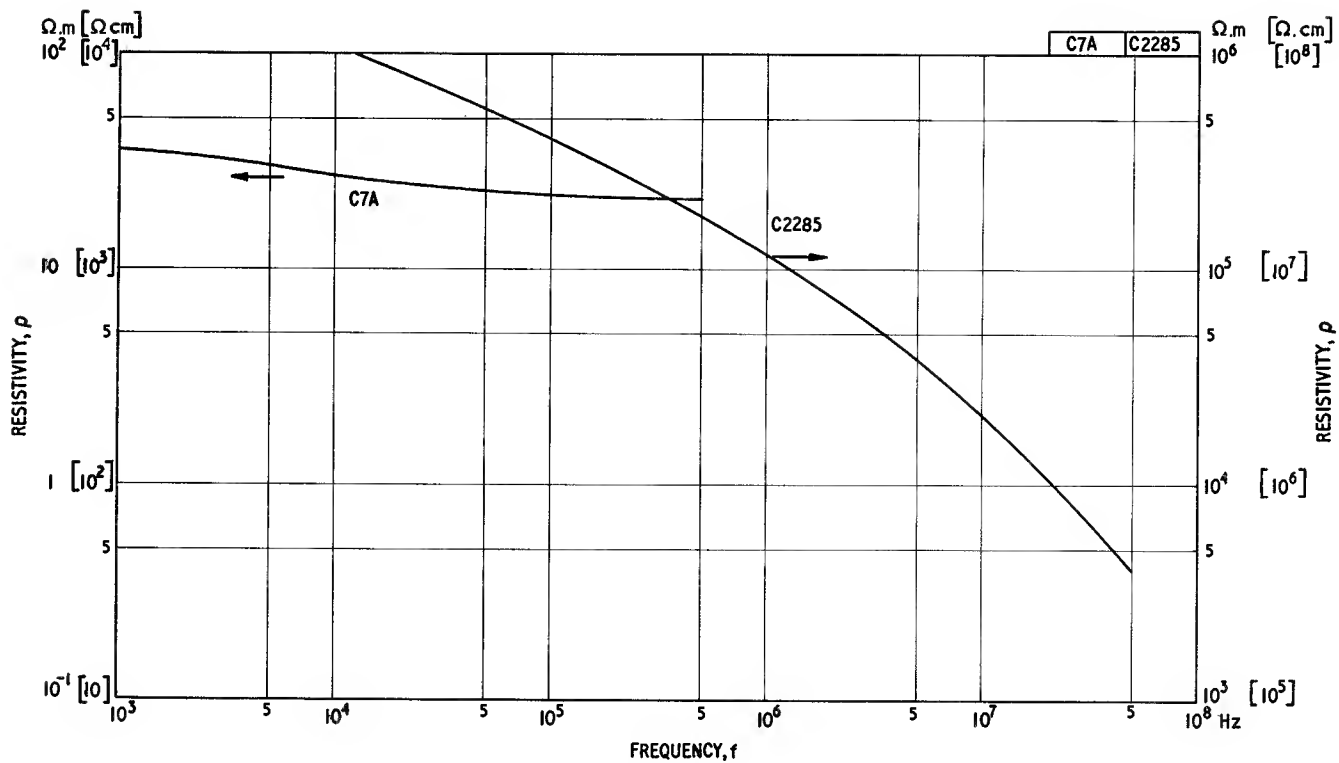


Fig. 3.21.3(a)

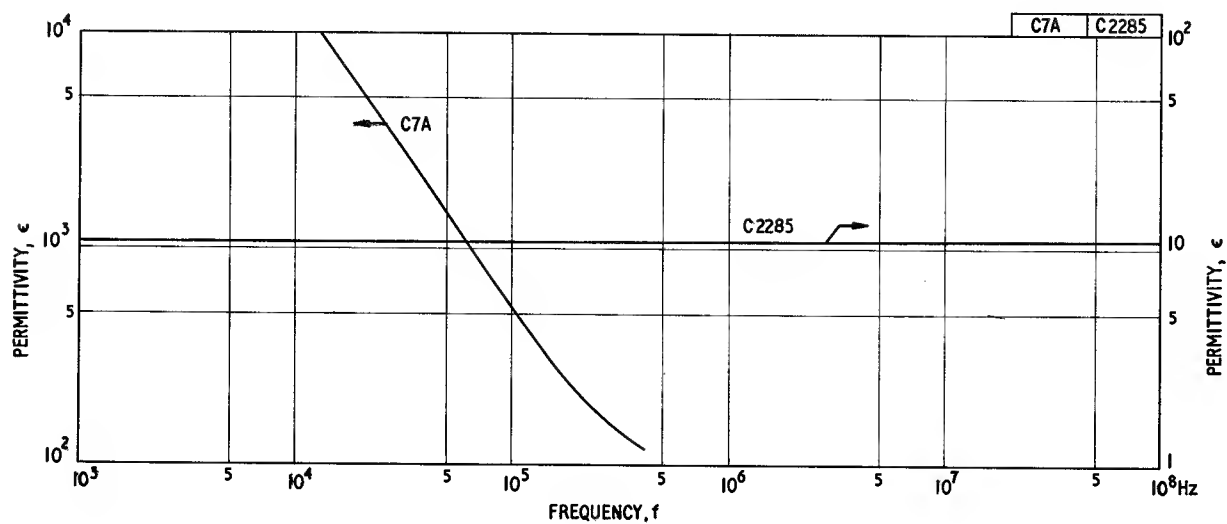


Fig. 3.21.3(b)

High frequency resistivity and permittivity as functions of temperature Fig. 3.22

$$f = 1 \text{ MHz}$$

This figure shows the resistivity and permittivity of a number of typical manganese zinc and nickel zinc ferrites

measured against temperature. As at low frequencies (see Fig. 3.20) the resistivity falls with temperature. The permittivity generally increases slowly with temperature over the range considered.

(See also Section 2.2.4 and Figs. 2.5, 3.20 and 3.21.)

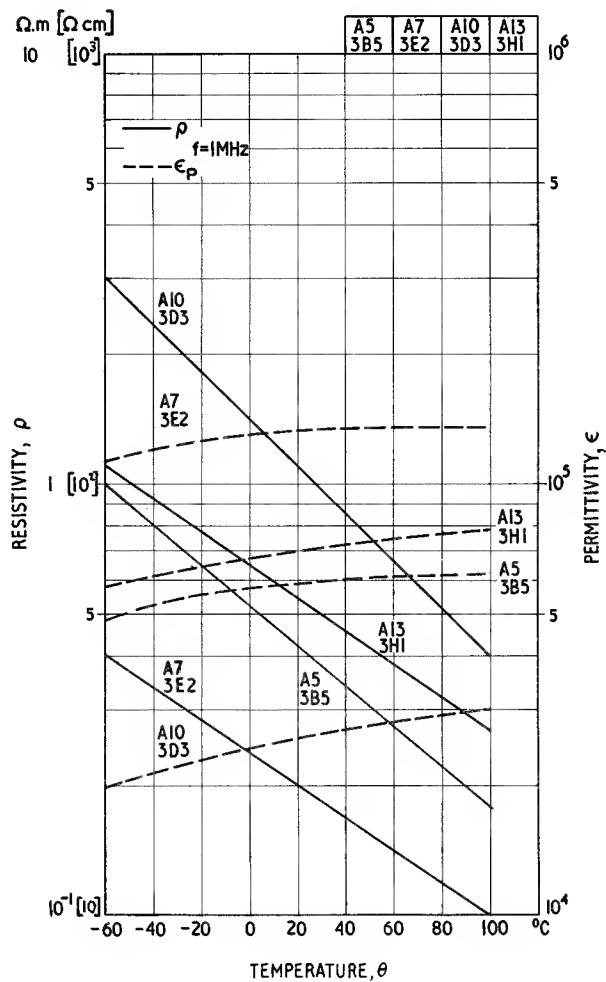


Fig. 3.22.1

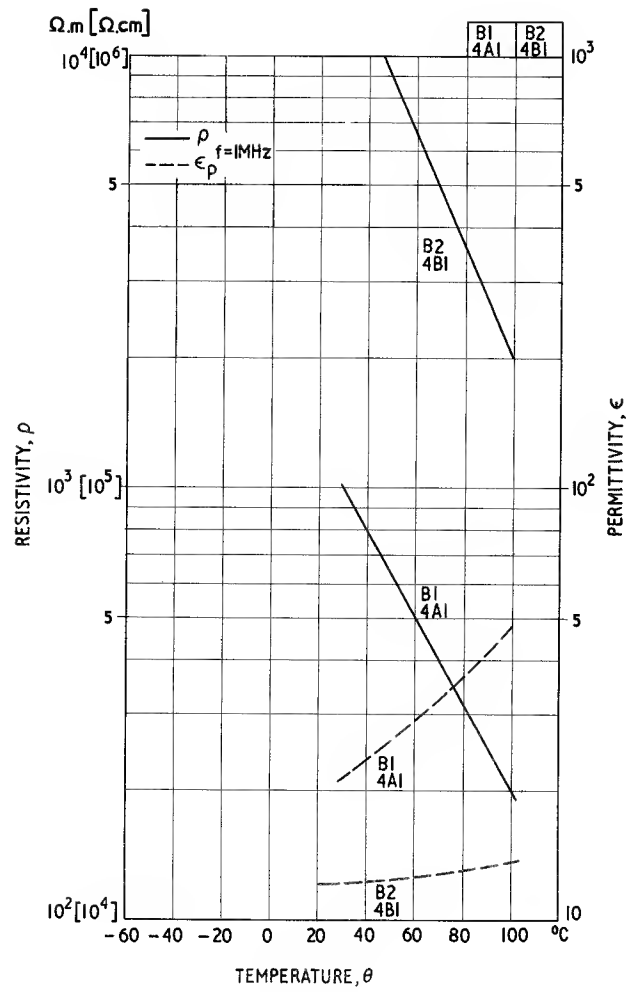


Fig. 3.22.2

Static magnetostriction Fig. 3.23

$$\theta \approx 20^\circ\text{C}$$

This figure shows the magnetostriction, i.e. the fractional change of length, as a function of steady field strength. Toroidal specimens were used and they were demagnetized before each measurement was made.

The manganese zinc ferrites, A7, A9 and A13 have very low magnetostriction; the saturation values are less than 10^{-6} and may be positive or negative. The curves show that the saturation value may be much smaller than the value at lower field strengths and indeed sign reversal has been observed on some specimens.

The range of nickel zinc ferrites is represented by the

high permeability grade B1 and, at the other extreme, the low permeability grade B5 (nickel ferrite). For these ferrites the saturation magnetostriction is relatively large and negative; the saturation magnetostrictions for the other nickel zinc grades may be expected to lie in intermediate positions depending on the nickel/zinc ratio (e.g. the curve for B10).

These static magnetostriction curves are somewhat analogous to the initial $B-H$ curve; they may be useful for predicting the steady-state situation but, for alternating (vibratory) conditions, data on the dynamic magnetostriction are required.¹⁷ Pursuing the analogy, the dynamic magnetostriction corresponds to the incremental permeability and cannot be deduced very well from the static curves.

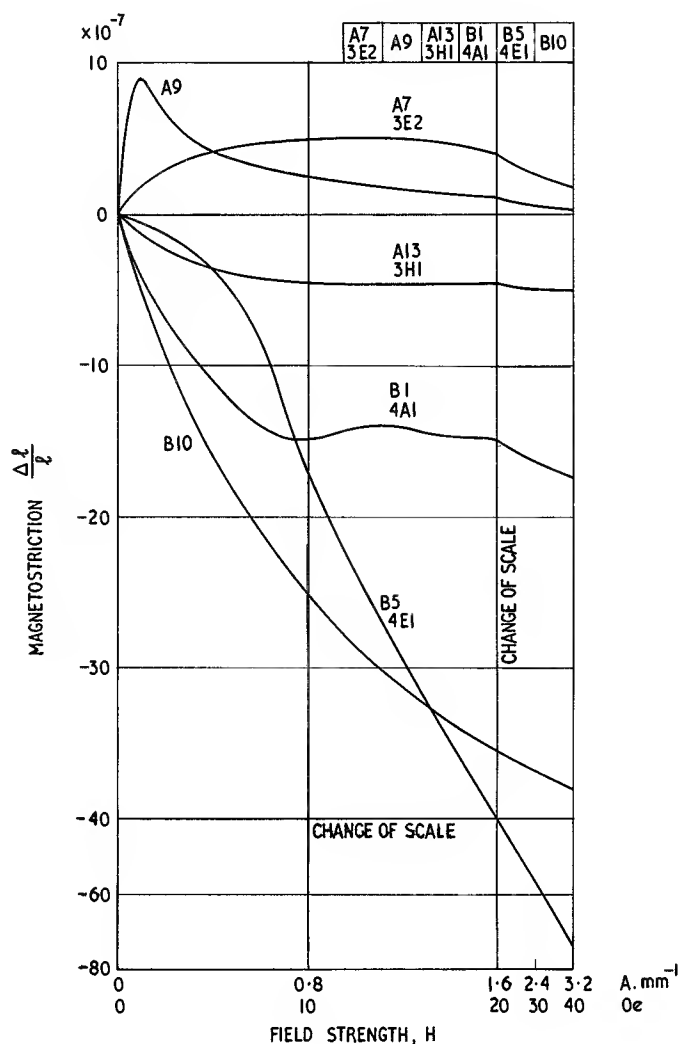


Fig. 3.23.1

Initial permeability as a function of stress Fig. 3.24

$$f \approx 1 \text{ kHz}$$

$$\theta \approx 20^\circ\text{C}$$

Components using ferrite cores are often assembled with clips or clamps that set up a stress in the ferrite. It is therefore useful to have data showing the influence of mechanical stress on the initial permeability. This figure shows such data for a number of typical ferrites.

It is notable that a large change of permeability may be produced by quite a moderate stress. In the case of the manganese zinc ferrites this may at first sight seem inconsistent with the very low magnetostriction observed

in the previous figure. High permeability depends on the total anisotropy being small and one of the components of this total is the stress anisotropy which equals the product of the stress and the magnetostriction. If the other components, e.g. magnetocrystalline anisotropy, are very small, the stress anisotropy will predominate and it will have a controlling influence on the permeability. Changes in externally applied stress will then produce large changes of permeability. It has been shown¹⁸ that if the magnetostriction is negative a small externally applied compressive stress will usually raise the permeability and vice versa. Large stresses, compressive or tensile invariably lower the permeability.

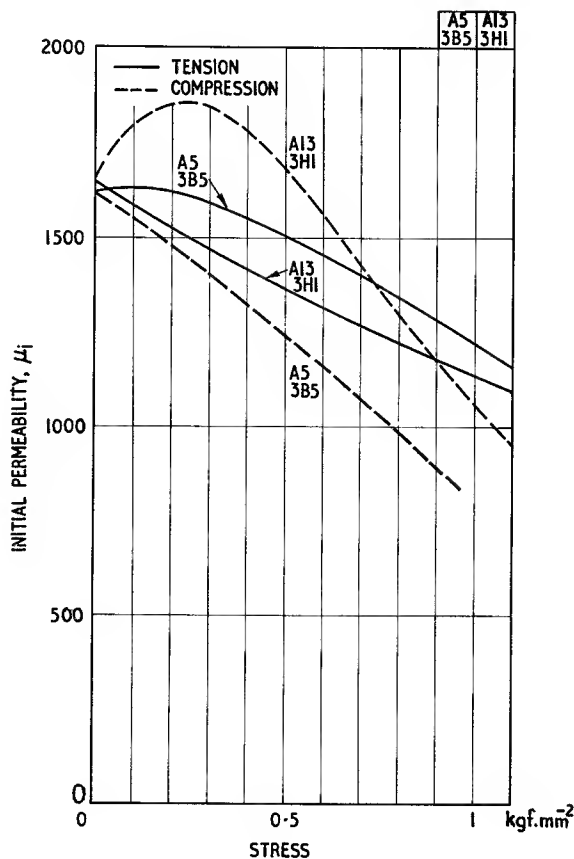


Fig. 3.24.1

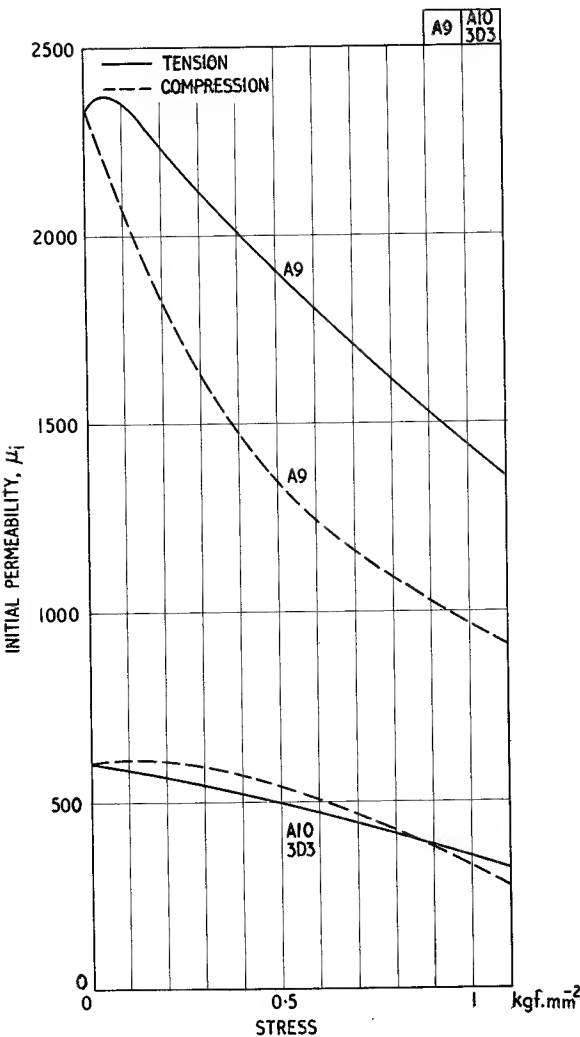


Fig. 3.24.2

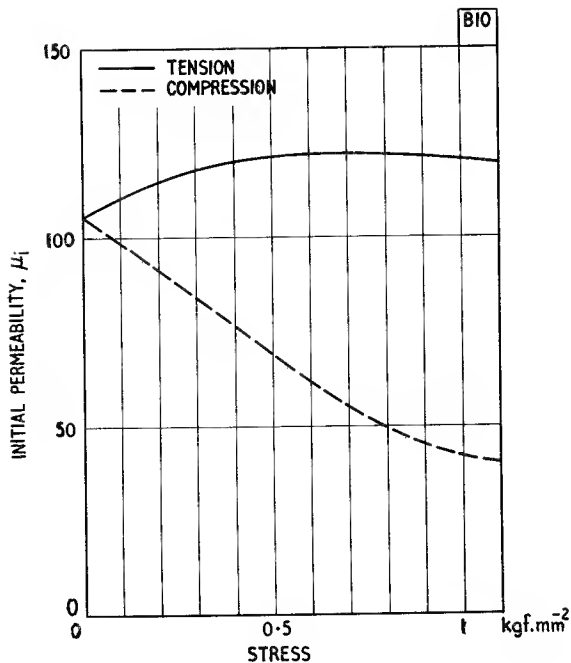


Fig. 3.24.3

REFERENCES AND BIBLIOGRAPHY

Section 3.3.

1. STUITS, A. L., VERVEEL, J. and PELOSCHKE, H. P., 'Dense ferrites and their applications', *Trans. I.E.E.E., Commun. Electron.*, no. 75, 726, (1964).
2. SELLWOOD, D., (Kingston Technical College), private communication.
3. WEIL, L. and BOCHIROL, L., 'Mesure du module d'Young des ferrites', *C.R. Acad. Sci., Paris*, **232**, 1807, (1951).
4. NISHIKAWA, T. *et al.*, 'Mechanical properties of ferrites', *Natn. tech. Rep.*, **10**, Part 1, 305, Part 2, 477, (1964).
5. BEKKER, YA. M., 'Some features of the thermal resistance of ferrites', *Soviet Phys. solid St.*, **7**, 1240, (1965).
6. VERHAEGHE, J. L., ROBBRECHT, G. G. and BRUYNOOGHE, W. M., 'On the specific heat of Mn-Zn and Ni-Zn ferrite between 20°C and 350°C', *Appl. scient. Res., B*, **8**, 128, (1960).

Fig. 3.1.

6. KORNETZKI, M., 'Die Hystereseverluste von Ferriten mit anomaler Magnetisierungsschleife', *Z. angew. Phys.*, **10**, 368, (1958).
7. ECKERT, O., 'Ferrite with constricted loops and thermal magnetic treatment', *Proc. Instn elect. Engrs*, **104**, B, 428, (1957).
8. MICHALOWSKI, L., 'The influence of the anisotropy constant on the perminvar effect in ferrites', *Physica Stat. Sol.*, **8**, 543, (1965).
- EDWARDS, G. W. and GLAISTER, R. M., 'Cobalt-ferrous ferrite with re-entrant hysteresis loop', *Trans. I.E.E.E., Mag* **2**, 696, (1966).
- KOSHKIN, L. I. and STRYGIN, YU. F., 'Magnetic anisotropy in polycrystalline ferrites, induced by electrothermal treatment', *Soviet Phys. solid St.*, **8**, 380, (1966).

Fig. 3.3.

9. SMIT, J. and WIJN, H. P. J., *Ferrites*, Sec. 32.2, Philips Technical Library, Eindhoven, (1959).

Fig. 3.7.

10. HANNA, C. R., 'Design of reactances and transformers which carry direct current', *J. Am. Inst. elect. Engrs*, **46**, 128, (1927).
- LEGG, V. E., 'Optimum air gap for various magnetic materials in cores of coils subject to superposed direct current', *Trans. Am. Inst. elect. Engrs*, **64**, 709, (1945).

Fig. 3.8.

11. SMIT, J. and WIJN, H. P. J., *Ferrites*, Sec. 48.1, Philips Technical Library, Eindhoven, (1959).

Fig. 3.10.

12. SNELLING, E. C., 'Disaccommodation and its relation to the stability of inductors having manganese zinc ferrite cores', *Mullard tech. Commun.*, **6**, 207, (1962).
- WIJN, H. P. J. and VAN DER HEIDE, H., 'A Richter type after-effect in ferrites containing ferrous and ferric ions', *Revs. mod Phys.*, **25**, 98, (1953).
- KRUPICKA, S. and GERBER, R., 'A contribution to studying the mechanism of permeability disaccommodation in ferrites', *Czech J. Phys.*, **10**, 158, (1960).
- KAMPEZYK, W. and ROESPEL, G., 'Some mechanisms governing the permeability versus time of ferrite cores', *Siemens Rev.*, **31**, 312, (1964).
- BRAGINSKI, A., 'Magnetic after-effects in iron-rich

ferrites containing vacancies', *Physica Stat. Sol.*, **11**, 603, (1965).

- NAKAJIMA, S., 'Lessening disaccommodation in MnZn ferrites', *Fujitsu sci. tech. J.*, **1**, 215, (1965).
- OKADA, T. and AKASHI, T., 'Richter type after effect in manganese zinc ferrite', *J. phys. Soc., Japan*, **20**, 639, (1965).
- RASMUSSEN, A. L., 'Disaccommodation of magnetic spectra of two MnZn ferrites', *Bur. Stand J. Res.*, **69A**, 181, (1965).

Fig. 3.11.

13. BLOEMBERGEN, N., 'Magnetic resonance in ferrites', *Proc. Inst. Radio Engrs*, **44**, 1259, (1956).
14. RADO, G. T., 'Magnetic spectra of ferrites', *Rev. mod. Phys.*, **25**, 81, (1953).
15. SNOEK, J. L., 'Dispersion and absorption in magnetic ferrites at frequencies above 1 Mc/s', *Physica Amsterdam*, **14**, 207, (1948).
- POLDER, D., 'On the theory of ferromagnetic resonance', *Phil. Mag.*, **40**, 99, (1949).
- BROESE VAN GROENOU, A., BONGERS, P. F. and STUITS, A. L., 'Magnetism, crystal chemistry and microstructure of spinel ferrites', *Mater. Sci. and Engng.*, Jan., (1969).

Fig. 3.14

- ANGEL, Y., 'Comportement des ferrites dans des champs magnetiques croises', *Acta electron.* **7**, Part 1, 7, Part 2, 119, (1963).

Fig. 3.18.

16. SNELLING, E. C., 'Magnetic intermodulation in manganese zinc ferrites', *Instn. elect. Engrs, Conference Pub. no. 12*, 34-1, (1965).
- KÖHLER, J. W. L., 'Non-linear distortion phenomena of magnetic origin', *Philips tech. Rev.*, **2**, 193, (1937).

Fig. 3.20.

- KOMAR, A. P. and KLIVSHIN, V. V., 'Temperature dependence of the electrical resistivity of ferrites', *Izv. Akad. Nauk SSSR, Ser. fiz.*, (Bull. Acad. Sci. USSR., Phys.), **18**, 400, (1954).
- BRÔZ, J., 'A study of the electrical conductivity of MnZn ferrite', *Czech. J. Phys.*, **6**, 321, (1956).
- VAN UITERT, L. G., 'Dielectric properties of and conductivity in ferrites', *Proc. Inst. Radio Engrs*, **44**, 1294, (1956).
- PARKER, R., GRIFFITHS, B. A. and ELWELL, D., 'The effect of cobalt substitution on electrical conduction in nickel ferrite', *Br. J. appl. Phys.*, **17**, 1269, (1966).

Fig. 3.21

- KRÖTZSCH, M., 'Über die Niederfrequenzdispersion der Dielektrizitätskonstanten und der elektrischen Leitfähigkeit polykristalliner Ferrite', *Physica Stat. Sol.*, **6**, 479, (1964).
- SATO, H. and WANATABE, M., 'Dielectric properties of ferrites', *Electronics Commun. Japan*, **48**, 92, (1965).

Fig. 3.23

17. VAN DER BURGT, C. M., 'Piezomagnetic ferrites', *Electronic Tech.*, **37**, 330, (1960).
- BOZORTH, R. M., TILDEN, E. F. and WILLIAMS, A. J., 'Anisotropy and magnetostriction of some ferrites', *Phys. Rev.*, **99**, 1788, (1955).

OHTA, K. and KOBAYASHI, N., 'Magnetostriction constants of Mn-Zn-Fe ferrites', *Jap J. appl. Phys.*, **3**, 576, (1964).

Fig. 3.24.

SMIT, J. and WIJN, H. P. J., *Ferrites*, Sec. 49.2, Philips Technical Library, Eindhoven, (1959).

General

KORNETZKI, M., 'Meßergebnisse an hochpermeablen Ferritkern', *Z. angew. Phys.*, **3**, 5, (1951).

WIJN, H. P. J. and WENT, J. J., 'The magnetization process in ferrites', *Physica*, **17**, 976, (1951).

KAMPCZYK, W., 'Einige Eigenschaften und Anwendungen hochpermeabler Ferrite', *Siemens-Z.*, **34**, 90, (1960).

AKASHI, T., 'Improvements of MnZn ferrites: Neferrite', *N.E.C. Res. Dev. (Japan)*, no. 2, 1, (Sept. 1961).

OHTA, K., 'Magnetocrystalline anisotropy and magnetic permeability of Mn-Zn-Fe ferrites', *J. phys. Soc Japan*, **18**, 685, (1963).

TAIMUTY, S. I. and MILLS, J. S., 'The effects of radiation on ferrites', *Trans. I.E.E.E., Commun. and Electron*, **66**, 305, (1963).

'New ferrite materials', *Jap. Electron*, **5**, no. 2, 21, (1964).

MIZUSHIMA, M., 'Magnetic properties of cobalt-substituted Ni-Zn ferrites', *Jap. J. appl. Phys*, **3**, 82, (1964).

ROSS, E. V., HANKE, I. and MOSER, E., 'Mangan-Zink-Ferrite mit Anfangspermeabilitäten bis über 20 000 und ihr Gefüge', *Z. angew. Phys.*, **17**, 504, (1964).

SNELLING, E. C., 'The properties of ferrites in relation to their application', *Proc. Br. Ceram. Soc.*, **2**, 151, (1964).

Magnetic Circuit Theory

4.1. INTRODUCTION

The foregoing chapters have been concerned principally with the intrinsic properties of ferrite materials. These properties have been expressed mainly in terms of the electrical impedance of an ideal winding on an ideal core shape, i.e. a uniform toroid having small radial thickness. For such a core it may be assumed that the field strength is uniform, and the magnetic path length and cross-sectional area equal the mean circumference and physical cross-sectional area respectively. It is now necessary to consider the magnetic properties of more practical core shapes and, as far as possible, to relate these to the properties of the material.

Before these relations are considered the underlying assumptions must be emphasized. In all the expressions relating core properties to material properties it is assumed that the ferrite, on a macroscopic scale, is homogeneous and isotropic. It is also assumed that any arbitrary core made of a particular grade of ferrite will have the same intrinsic properties as an ideal toroid made of the same material. These assumptions are seldom completely valid; the more complicated the form of the practical core the greater is the discrepancy likely to be. The reason is that in the manufacture of a simple toroid it is possible to make the pressed density fairly uniform throughout the core volume and to control

accurately the sintering conditions in the immediate vicinity of the core. The properties of the ferrite are sensitive to both pressed density and firing conditions. When the same powder is pressed into a more complicated shape, e.g. a half pot core, it is more difficult to ensure uniformity either in density or exposure to kiln conditions. Differences will also result if the cores have very different cross-sectional areas. For these reasons the performance of a particular core shape may differ from that predicted from the relations that are derived in this chapter. In addition some of these relations involve approximations which may add to the discrepancy.

To avoid these difficulties the present tendency is for manufacturers to state the performance of a given core in terms of the core properties; data on materials are given mainly as a guide. For example, the performance of a transformer core is better specified in terms of the minimum inductance that will be obtained for a given number of turns (i.e. a property of the particular core) than in terms of minimum initial permeability (a material property). On the other hand a designer mainly interested in predicting the performance of a new or proposed ferrite core must have access to the intrinsic properties of the ferrite, such as those given in Chapter 3. He is not, however, concerned at this stage with the performance limits of the core and therefore some discrepancies

between predicted and realized performance are usually not too serious.

Provided the limitations are recognized, the relations that follow provide a useful and reasonably accurate approach to the design of magnetic devices.

4.2. CLOSED MAGNETIC CORES

4.2.1. The effective dimensions of a core

When considering a uniform toroid having a very small radial thickness it is possible to speak of its magnetic length, l , cross-sectional area, A , and volume, V , without ambiguity. If however the cross-section is not small or uniform, the effect of the core geometry on the core properties is more complicated. The problem is to find the effective dimensions, l_e , A_e and V_e , which would define a hypothetical toroid having the same properties as the non-uniform core. Once this has been done, these effective dimensions may be used to calculate the performance of the non-uniform core just as though it were an ideal toroid. It is however necessary to limit this concept to low flux densities where the material may be assumed to obey approximately the Rayleigh or Peterson relations.

The first approach is rigorous but is limited in its practical application. The line integral of the field strength along an elementary path enclosing a winding of N turns carrying a current I is

$$\oint H ds = NI \quad A \quad (4.1)$$

For an elementary path of length l the line integral equals Hl where H is the total field strength. A practical closed magnetic path may be regarded as a bundle of elementary paths in parallel, each elementary path being a tube of magnetic flux, i.e. containing a uniform flux $d\Phi$ but varying in cross-sectional area dA in accordance with the contour of the main body of the core.

Then $d\Phi = \mu_0 \mu H dA = (\mu_0 \mu NI dA)/l$

$$\text{and} \quad \Phi = \mu_0 NI \int \frac{\mu dA}{l} \quad \text{Wb} \quad (4.2)$$

the integral being the sum of all the elementary areas across any section, each element being multiplied by the permeability of the elementary circuit and divided by its length. Thus it is in the nature of a parallel integration.

From the Peterson relation (Eqn 2.37) the permeability depends on the field strength. Ignoring the higher powers of H this expression for μ may be substituted in Eqn 4.2.

$$\Phi = \mu_0 NI \left\{ a_{10} \int \frac{dA}{l} + a_{11} NI \int \frac{dA}{l^2} \right\} \quad \text{Wb.}$$

The flux in an equivalent ideal toroid having dimensions l_e and A_e is

$$\begin{aligned} \Phi &= \mu_0 NI \mu \frac{A_e}{l_e} \\ &= \mu_0 NI \left\{ a_{10} \frac{A_e}{l_e} + a_{11} NI \frac{A_e}{l_e^2} \right\} \quad \text{Wb.} \end{aligned}$$

For equivalence these two fluxes will be equal so, by equating coefficients, the following identities are obtained

$$\left. \begin{aligned} \frac{A_e}{l_e} &= \int \frac{dA}{l} \\ \frac{A_e}{l_e^2} &= \int \frac{dA}{l^2} \end{aligned} \right\} \quad (4.3)$$

These results may be corroborated by use of Peterson's loss expression (Eqn 2.38). The hysteresis loss per cycle in an elementary magnetic path is given by

$$\begin{aligned} W_h &= \frac{8}{3} \mu_0 a_{02} \bar{H}^3 l dA \\ &= \frac{8}{3} \mu_0 a_{02} (NI)^3 \frac{dA}{l^2} \\ \therefore \text{Total loss} &= \frac{8}{3} \mu_0 a_{02} (NI)^3 \int \frac{dA}{l^2} \quad \text{J. cycle}^{-1} \\ &= \frac{8}{3} \mu_0 a_{02} (NI)^3 \frac{A_e}{l_e^2} \end{aligned}$$

for the equivalent toroid.

The integrations expressed in Eqns 4.3 are practicable only when a simple expression for l may be obtained in terms of the position of the element of area, dA . Such a

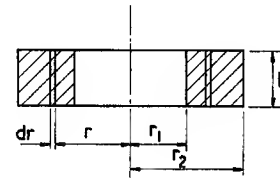


Fig. 4.1. Dimensions of a toroid

case is a radially thick toroid of rectangular cross-section having inner and outer radii r_1 and r_2 respectively and an axial thickness h , see Fig. 4.1.

Then $dA = h dr$ and $l = 2\pi r$

$$(4.1) \quad \oint H ds = \frac{4\pi NI}{10} \quad A$$

$$(4.2) \quad \Phi = \frac{4\pi NI}{10} \int \frac{\mu dA}{l} \quad \text{Mx}$$

$$\therefore \frac{A_e}{l_e} = \int_{r_1}^{r_2} \frac{h dr}{2\pi r} = \frac{h \log_e \frac{r_2}{r_1}}{2\pi}$$

$$\text{and } \frac{A_e}{l_e^2} = \int_{r_1}^{r_2} \frac{h dr}{4\pi^2 r^2} = \frac{h}{4\pi^2} (1/r_1 - 1/r_2)$$

$$\text{Hence } A_e = \frac{h \log_e^2(r_2/r_1)}{1/r_1 - 1/r_2} \quad \text{m}^2 \quad (4.4)$$

$$l_e = \frac{2\pi \log_e(r_2/r_1)}{1/r_1 - 1/r_2} \quad \text{m} \quad (4.5)$$

and the effective volume

$$V_e = A_e l_e = \frac{2\pi h \log_e^3(r_2/r_1)}{(1/r_1 - 1/r_2)^2} \quad \text{m}^3 \quad (4.6)$$

In practice an alternative approach¹ depending on integration along the magnetic path is often more useful, if less exact. It is necessary to assume that, within the region of low flux densities being considered, the variation of permeability with field strength may be ignored.

As before $NI = \oint H ds$

$$= \frac{\Phi}{\mu_0} \oint \frac{ds}{\mu A}$$

$$\therefore \Phi = \frac{\mu_0 NI}{\oint \frac{ds}{\mu A}} \quad \text{Wb.} \quad (4.7)$$

The line integral is, of course, the reluctance of the magnetic path. If μ is uniform the reluctance is usually written

$$\frac{1}{\mu} \Sigma l/A$$

The reluctance of the equivalent ideal toroid is $\frac{l_e}{\mu A_e}$

$$\text{Therefore } \frac{l_e}{A_e} = \Sigma l/A \quad (4.8)$$

i.e. a series summation of elements of path length measured along the mean magnetic path, divided by the corresponding areas. This summation is sometimes called the core factor C_1 .

To obtain separate expressions for l_e and A_e use may be made of another factor, namely l/A^2 . This arises naturally when the hysteresis loss is integrated along the

mean magnetic path. The hysteresis loss per cycle is given by

$$\begin{aligned} W_h &= \frac{8}{3} \mu_0 a_{02} \oint \hat{H}^3 A ds \\ &= \frac{8}{3} \frac{a_{02}}{\mu_0^2 \mu^3} \oint \hat{B}^3 A ds \\ &= \frac{8}{3} \frac{a_{02} \Phi^3}{\mu_0^2 \mu^3} \oint \frac{ds}{A^2} \quad \text{J. cycle}^{-1} \\ &= \frac{8}{3} \frac{a_{02} \Phi^3}{\mu_0^2 \mu^3} \frac{l_e}{A_e^2} \quad (4.9) \end{aligned}$$

for the equivalent ideal toroid.

The line integral is usually written $\Sigma l/A^2$ and referred to as the core factor C_2

$$\text{Thus } \frac{l_e}{A_e^2} = \Sigma \frac{l}{A^2} \quad (4.10)$$

Combining this with Eqn 4.8

$$A_e = \frac{\Sigma l/A}{\Sigma l/A^2} = \frac{C_1}{C_2} \quad (4.11)$$

$$l_e = \frac{(\Sigma l/A)^2}{\Sigma l/A^2} = \frac{(C_1)^2}{C_2} \quad (4.12)$$

$$\text{and } V_e = A_e l_e = \frac{(\Sigma l/A)^3}{(\Sigma l/A^2)^2} = \frac{(C_1)^3}{(C_2)^2} \quad (4.13)$$

These expressions are in common use for calculating the effective dimensions of an arbitrary core. However, the results must be rather approximate because the calculation assumes that the mean magnetic path is known and that it is possible to assign an effective area to each element of it. In practice the mean path is usually taken to coincide with a surface, perpendicular to the plane of the flux path, which divides the cross-section of the core into two equal areas. However, it is clear from the more exact treatment of the radially thick toroid that the actual mean magnetic path lies somewhat inside this approximate path.

A recent IEC publication lists standard formulae for calculating core factors and effective dimensions for a number of widely used shapes.² These standard formulae, whilst not being theoretically accurate for the reasons just explained, do ensure that a common yardstick is used when calculating the properties of a core from electrical measurements on an associated winding. Fig. 4.2 sets out the calculation of the core factors for a simple core shape. This example illustrates typical

$$(4.7) \quad \Phi = \frac{4\pi NI}{10 \oint \frac{ds}{\mu A}} \quad \text{Mx}$$

$$(4.9) \quad W_h = \frac{2}{3\pi} \frac{a_{02} \Phi^3 10^{-7}}{\mu^3} \frac{l_e}{A_e^2} \quad \text{J. cycle}^{-1}$$

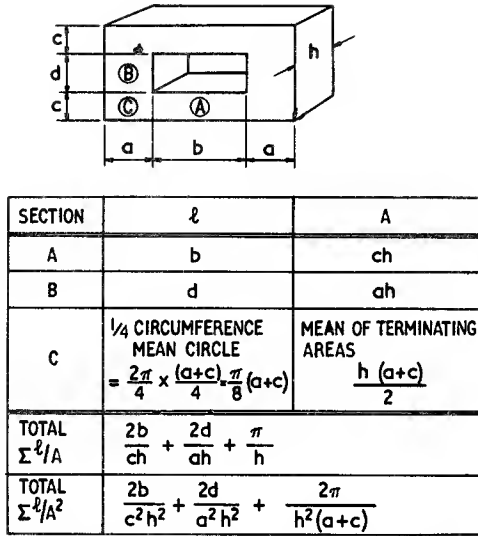


Fig. 4.2. Example of core factor calculation showing typical approximations

approximations that have to be made to deal with difficult sections, e.g. corners (see also Appendix B).

Within the limits of the assumptions, the use of the effective dimensions will simplify calculations involving reluctance and hysteresis loss of a non-uniform magnetic core. In particular they give rise to an effective flux density, B_e . From Eqn 4.9 the hysteresis loss per cycle in a core of non-uniform cross-section is given by

$$W_h = \frac{8}{3} \frac{a_{02} \hat{\Phi}^3}{\mu_0^2 \mu^3 A_e^3} V_e$$

$$= \frac{8}{3} \frac{a_{02} \hat{B}_e^3 V_e}{\mu_0^2 \mu^3} \quad \text{J.cycle}^{-1} \quad (4.14)$$

$$\text{where } \hat{B}_e = \hat{\Phi}/A_e \quad (4.15)$$

It follows from Eqn 2.13 that

$$E = \frac{\omega \hat{B}_e A_e N}{\sqrt{2}} \quad \text{V} \quad (4.16)$$

The inductance of a winding on such a core is

$$(4.14) \quad W_h = \frac{2}{3\pi} \frac{a_{02} \hat{B}_e^3 V_e}{\mu^3} \times 10^{-7} \quad \text{J.cycle}^{-1}$$

$$(4.16) \quad E = \frac{\omega \hat{B}_e A_e N}{\sqrt{2}} \times 10^{-8} \quad \text{V}$$

$$L = \frac{N\hat{\Phi}}{\hat{I}} = \frac{\mu_0 N^2}{\Sigma \frac{l}{\mu A}} \quad \text{H} \quad (4.17)$$

from Eqn 4.7.

$$\therefore L = \mu_0 \mu N^2 A_e / l_e = \mu_0 \mu N^2 / C_1 \quad \text{H} \quad (4.18)$$

Thus the inductance is calculated for the equivalent ideal toroid having the same material permeability.

4.2.2. The effect of an air gap on core reluctance and effective permeability

Air gaps are introduced into magnetic cores for a variety of reasons. In the design of a permanent magnet, for instance, an air gap is essential to make the stored magnetic energy accessible. An inductor usually has an air gap to dilute unwanted effects of the core material and, by proper choice of gap length, to improve the overall performance. In a choke or transformer carrying d.c. an optimum air gap will ensure that the maximum inductance is obtained for a given number of turns. In this section the effect of the air gap will be studied in relation to the core reluctance and effective permeability. The effect on losses will be considered in the following section.

The air gap or gaps may be regarded as a section of length l_g , cross-sectional area A_g and unity relative permeability in a generalized core having a reluctance as expressed in Eqn 4.7. This equation may be written as

$$\Phi = \frac{\mu_0 NI}{\frac{l_g}{A_g} + \Sigma \frac{l_m}{\mu A_m}} \quad \text{Wb} \quad (4.19)$$

where the subscript m refers to the magnetic core.

Although this equation is general it is usually restricted in its use to cores having air gap lengths that are small compared with the dimensions of the core cross-section adjacent to the gap. Only under these conditions is the fringing flux a small proportion of the total flux and is it possible to estimate a value for the effective area of the gap. Eqn 4.19 may be written

$$(4.17) \quad L = \frac{N\hat{\Phi}}{\hat{I}} \times 10^{-8} = \frac{4\pi N^2}{\Sigma \frac{l}{\mu A}} \times 10^{-9} \quad \text{H}$$

$$(4.18) \quad L = \frac{4\pi \mu N^2 A_e}{l_e} \times 10^{-9} = \frac{4\pi \mu N^2}{C_1} \times 10^{-9} \quad \text{H}$$

$$(4.19) \quad \Phi = \frac{4\pi NI}{10 \left\{ \frac{l_g}{A_g} + \frac{l_m}{\mu A_m} \right\}} \quad \text{Mx}$$

$$\Phi = \frac{\mu_0 NI}{\frac{l_g}{A_g} + \frac{l_e - l_g}{\mu A_e}} \quad \text{Wb} \quad (4.20)$$

where l_e is the total effective magnetic path length, as before.

By analogy with the derivation of Eqn 4.17.

$$L = \frac{\mu_0 N^2}{\frac{l_g}{A_g} + \frac{l_e - l_g}{\mu A_e}} \quad \text{H} \quad (4.21)$$

If the gap length is small compared with the total magnetic path length this equation reduces to

$$L = \frac{\mu_0 N^2}{\frac{l_g}{A_g} + \frac{C_1}{\mu}} \quad \text{H} \quad (4.22)$$

Assuming that the material permeability is not affected by the air gap (as it would be if the core were subjected to a steady field, see Fig. 3.6) it is seen that the effect of an air gap is to reduce the inductance. Thus the core behaves as though it had a reduced permeability, referred to as the effective permeability, μ_e :

$$L = \frac{\mu_0 \mu_e N^2 A_e}{l_e} \quad \text{H} \quad (4.23)$$

Combining Eqns 4.21 and 4.23.

$$\mu_e = \frac{l_e/A_e}{\frac{l_g}{A_g} + \frac{l_e - l_g}{\mu A_e}} \quad (4.24)$$

Again if $l_g \ll l_e$ this simplifies to

$$\mu_e = \frac{C_1}{\frac{l_g}{A_g} + \frac{C_1}{\mu}} \quad (4.25)$$

If the permeability of the material is high and the gap length is not too small then l_g/A_g may be large compared with C_1/μ . Then, if A_g may be taken approximately equal to A_e , μ_e approaches l_e/l_g , i.e. it becomes largely dependent on the gap ratio and relatively independent of the material permeability.

Developing the more exact expression, Eqn 4.24, and putting $A_g = A_e$

$$\frac{l_e}{\mu_e} = \frac{l_e - l_g}{\mu} + l_g$$

$$\therefore \mu_e = \frac{l_e}{\frac{l_e - l_g}{\mu} + l_g} \quad (4.26)$$

from which

$$\frac{\mu}{\mu_e} = \frac{\mu}{l_e} \left(\frac{l_e - l_g}{\mu} + l_g \right)$$

$$= 1 + \frac{l_g(\mu - 1)}{l_e}$$

$$\therefore \frac{l_g}{l_e} = \left(\frac{\mu}{\mu_e} - 1 \right) / (\mu - 1)$$

which may be rearranged to give

$$1 - \frac{l_g}{l_e} = \frac{\mu(\mu_e - 1)}{\mu_e(\mu - 1)} \quad (4.27)$$

This relation is useful in the analysis of the effect of the gap on the stability and the loss of cores. If the gap is small compared with the dimensions of the cross-section then A_g may be taken as equal to the area of the core face forming the gap. However, as the gap length increases the value of A_g becomes larger due to the fringing flux. This effect reduces the reluctance of the gap and results in a higher value of μ_e than that predicted by Eqns 4.24 or 4.25. Any attempt to analyse the problem on a general basis is complicated by the fact that, as the gap becomes larger, the fringing or leakage flux becomes dependent not only on the gap geometry but also on that of the winding and the rest of the magnetic circuit.

The method of conformal transformations may be used to obtain an expression for the reluctance of the air gap. Astle³ has shown that the effect of the fringing flux is to increase the effective semi-width of the gap (e.g. the radius in the case of a circular pole face) by

$$(0.241 + \frac{1}{\pi} \log_e b_a/l_g) l_g$$

where b_a is the total inside length of the limb containing the air gap (e.g. for a pot core b_a equals the width of the winding space). Eqn 4.25 may now be modified to allow for fringing flux:

$$(4.20) \quad \Phi = \frac{4\pi NI}{10 \left\{ \frac{l_g}{A_g} + \frac{l_e - l_g}{\mu A_e} \right\}} \quad \text{Mx}$$

$$(4.21) \quad L = \frac{4\pi N^2 10^{-9}}{\frac{l_g}{A_g} + \frac{l_e - l_g}{\mu A_e}} \quad \text{H}$$

$$(4.22) \quad L = \frac{4\pi N^2 10^{-9}}{\frac{l_g}{A_g} + \frac{C_1}{\mu}} \quad \text{H}$$

$$(4.23) \quad L = \frac{4\pi \mu_e N^2 A_e 10^{-9}}{l_e} \quad \text{H}$$

$$\mu_e = \frac{C_1}{\frac{1}{\frac{A}{l_g} + (0.241 + \frac{1}{\pi} \log_e \frac{b_a}{l_g})P} + \frac{C_1}{\mu}} \quad (4.28)$$

where A is the actual area of the pole face and P is the length of the pole face perimeter, e.g. the circumference for a circular pole face. Eqn 4.28 is accurate provided l_g is much less than the width of the air gap, and provided b_a/l_g is larger than about 5. Calculations based upon this formula have given values for the effective permeability of pot cores accurate to within 2% over wide ranges of gap length.

One of the principal benefits of an air gap is that any changes in the value of the material permeability are reduced in their effect on the inductance of a winding on the core. From Eqn 4.24

$$\begin{aligned} \frac{d\mu_e}{d\mu} &= \frac{\frac{l_e}{A_e} \frac{l_e - l_g}{\mu^2 A_e}}{\left(\frac{l_g}{A_g} + \frac{l_e - l_g}{\mu A_e}\right)^2} = \frac{\mu_e^2}{\mu^2} (1 - l_g/l_e) \\ &= \frac{\mu_e^2}{\mu^2} \cdot \frac{\mu(\mu_e - 1)}{\mu_e(\mu - 1)} \quad \text{from Eqn 4.27} \end{aligned}$$

$$\therefore \frac{d\mu_e}{d\mu} = \frac{\mu_e(\mu_e - 1)}{\mu(\mu - 1)} \quad (4.29)$$

$$\text{or } \frac{d\mu_e}{\mu_e} = \frac{d\mu}{\mu} \cdot \frac{(\mu_e - 1)}{(\mu - 1)} \quad (4.30)$$

Thus the fractional change in the effective permeability is smaller by a factor $(\mu_e - 1)/(\mu - 1)$ than the change $d\mu/\mu$

that produces it. The factor $(\mu_e - 1)/(\mu - 1)$ is called the dilution ratio. In practice μ_e and μ are usually much greater than unity so the dilution ratio becomes μ_e/μ . Then

$$\frac{d\mu_e}{\mu_e} = \frac{d\mu}{\mu} \cdot \frac{\mu_e}{\mu} \quad (4.31)$$

The cause of the change of material permeability may be a temperature change, a time effect, mechanical pressure, magnetic polarization, etc. The first two causes give rise to the factors mentioned in Section 2.2.2.

1. Temperature Factor

If the temperature coefficient of permeability is $\frac{\Delta\mu}{\mu\Delta\theta}$ then the temperature coefficient of effective permeability is, from Eqn 4.31

$$\frac{\Delta\mu_e}{\mu_e\Delta\theta} = \frac{\Delta\mu}{\mu\Delta\theta} \frac{\mu_e}{\mu} = \frac{\Delta\mu}{\mu^2\Delta\theta} \mu_e \quad (4.32)$$

$\Delta\mu/\mu^2\Delta\theta$ is called the Temperature Factor. It is a material property which when multiplied by μ_e gives the temperature coefficient of the gapped core.

2. Instability factor

By the same approach the instability of permeability defined by Eqn 2.25 gives rise to an instability factor $(\mu_1 - \mu_2)/\mu_1^2$ which when multiplied by μ_e gives a measure of the instability of the gapped core.

Considering now the B - H relation of a given core, the effect of an air gap is to change the horizontal scale so that the loop is less inclined relative to the horizontal, and this is consistent with a reduction of the effective permeability. This effect is referred to as the shearing of the

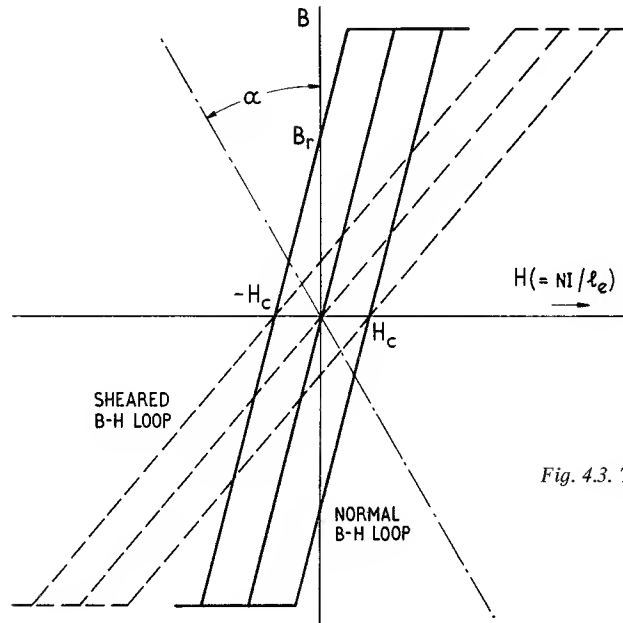


Fig. 4.3. The shearing of an idealized B - H loop due to an air gap

B - H relation and applies to both the initial magnetization curve and the hysteresis loop. It is illustrated in Fig. 4.3 by reference to an idealized loop.

In the analysis that follows it will be assumed that the core is of uniform cross section. The B - H loop, to be representative of a material, must refer to such a core otherwise the flux density would depend on the particular cross section chosen for the measurement. For a continuous uniform core, having the idealized B - H loop shown in Fig. 4.3, the initial magnetization curve is given, below saturation, by

$$(B)_0 = \frac{\mu_0 \mu (NI)_0}{l_e} \quad \text{T} \quad (4.33)$$

where the suffix denotes the zero gap condition. The corresponding two arms of the B - H loop may be expressed by

$$(B)_0 = \mu_0 \mu \left(\frac{(NI)_0}{l_e} \pm H_c \right) \quad \text{T} \quad (4.34)$$

where H_c is the coercivity, and the left-hand and right-hand limbs of the loop are represented by taking the positive and negative sign respectively.

If now an air gap of length l_g ($\ll l_e$) and effective area A_g is introduced it follows from Eqn 4.20 that the magnetization curve is given by

$$B = \frac{\mu_0 NI}{A_e \left(\frac{l_g}{A_g} + \frac{l_e}{\mu A_e} \right)} = \frac{\mu_0 \mu NI}{l_e \left(\frac{\mu A_e l_g}{A_g l_e} + 1 \right)} \quad \text{T} \quad (4.35)$$

and for the corresponding loop:

$$B = \frac{\mu_0 \mu}{\frac{\mu A_e l_g}{A_g l_e} + 1} \left(\frac{NI}{l_e} \pm H_c \right) \quad \text{T} \quad (4.36)$$

(when $B = 0$ the total $NI/l_e = \pm H_c$ since the m.m.f. across the gap must be zero.)

The field strengths for equal flux densities, with and without air gap, may be obtained from these equations.

For the initial magnetization curve the sheared value of the field strength is

$$H = \frac{NI}{l_e} = \frac{(NI)_0}{l_e} \left(1 + \frac{\mu A_e l_g}{A_g l_e} \right) \quad \text{A.m}^{-1} \quad (4.37)$$

and the corresponding value on the loop is

$$H = \frac{NI}{l_e} = \frac{(NI)_0}{l_e} \pm H_c \left(1 + \frac{\mu A_e l_g}{A_g l_e} \right) \mp H_c \quad \text{A.m}^{-1} \quad (4.38)$$

Thus if the flux density is to remain unchanged when an air gap is introduced, the field strength on the initial magnetization curve must be increased by a factor $(1 + \mu A_e l_g / A_g l_e)$; the extra field strength being required to overcome the gap reluctance. This result applies equally well to a practical B - H loop, in which case μ is replaced by the amplitude permeability. A B - H loop may be graphically sheared by calculating new values of NI/l_e from Eqn 4.38 for a number of values of B . A simpler method is to draw an inclined B -axis as shown by the chain dotted line in Fig. 4.3. The tangent of the angle α is clearly the ratio of the extra field strength to the corresponding flux density i.e.

$$\tan \alpha = \frac{(NI)_0}{l_e} \frac{\mu A_e l_g}{A_g l_e} \frac{1}{B} = \frac{A_e l_g}{\mu_0 A_g l_e} \quad (4.39)$$

This new B -axis having been constructed, the values for the sheared loop may be read off from the original loop, the B scale remaining unchanged in the vertical direction and the H values being measured off horizontally from the new B -axis in terms of the unchanged H scale.

Apart from the reduction of effective permeability it is clear from Fig. 4.3 that the presence of an air gap reduces the remanence

4.2.3. Magnetic losses

In this section the core is assumed to have a general shape characterized by core factors C_1 and C_2 or effective dimensions l_e , A_e and V_e (see Eqn 4.8 to 4.13). The core

$$(4.33) \quad (B)_0 = \frac{4\pi \mu (NI)_0}{10 l_e} \quad \text{Gs}$$

$$(4.34) \quad (B)_0 = \mu \left(\frac{4\pi (NI)_0}{10 l_e} \pm H_c \right) \quad \text{Gs}$$

$$(4.35) \quad B = \frac{4\pi NI}{10 A_e \left(\frac{l_g}{A_g} + \frac{l_e}{\mu A_e} \right)} = \frac{4\pi \mu NI}{10 l_e \left(\frac{\mu A_e l_g}{A_g l_e} + 1 \right)} \quad \text{Gs}$$

$$(4.36) \quad B = \frac{\mu}{\frac{\mu A_e l_g}{A_g l_e} + 1} \left(\frac{4\pi NI}{10 l_e} \pm H_c \right) \quad \text{Gs}$$

$$(4.37) \quad H = \frac{4\pi NI}{10 l_e} = \frac{4\pi (NI)_0}{10 l_e} \left(1 + \frac{\mu A_e l_g}{A_g l_e} \right) \quad \text{Oe}$$

$$(4.38) \quad H = \frac{4\pi NI}{10 l_e} = \left(\frac{4\pi (NI)_0}{10 l_e} \pm H_c \right) \left(1 + \frac{\mu A_e l_g}{A_g l_e} \right) \mp H_c \quad \text{Oe}$$

$$(4.39) \quad \tan \alpha = \frac{4\pi (NI)_0}{10 l_e} \cdot \frac{\mu A_e l_g}{A_g l_e} \frac{1}{B} = \frac{A_e l_g}{A_g l_e}$$

is also assumed to be operated at low amplitude such that the Raleigh relations apply, to have uniform permeability and to have losses that may be expressed by a relation having the form of Eqn 2.61.

If secondary effects such as changes of temperature may be ignored then the total loss in watts per unit volume of material is a function only of the frequency and flux density (or the field strength applying to a particular element). If these are constant then the dissipation of the core, i.e. the power that it draws from the circuit, is constant. It is very useful to keep this principle in mind when considering the loss expressions for a general core.

There are two fundamental ways of expressing the losses of a core in terms of circuit elements. They are

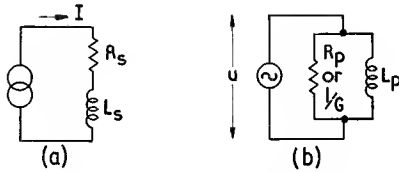


Fig. 4.4. Series and parallel representations of core loss

illustrated in Fig. 4.4. The first is in terms of current and a series impedance and the second is in terms of voltage and parallel impedance or admittance.

In the first case the magnetizing current and therefore the total applied field strength are the reference parameters and the loss is expressed in terms of series resistance, i.e. the core loss is $I^2 R_s$. While this is convenient in certain instances, difficulties arise when considering the influence of an air gap because the relation between the flux density and the current involves the effective permeability, and thus the current and the frequency do not alone define the conditions in the core. For example, consider the Legg hysteresis term from Eqn 2.67

$$\frac{R_h}{\mu f L} = a \hat{B}_e$$

It follows from Eqn 2.58 that for a gapped core of general shape:

$$\frac{R_h}{\mu_e f L} = a \hat{B}_e$$

$$\therefore R_h = a \mu_e f L \hat{B}_e = \sqrt{2} a \mu_0 \mu_e^2 f L N I / l_e$$

Substituting for N from Eqn 4.23

$$R_h = a I f \sqrt{\left[\frac{2 \mu_0 \mu_e^3 L^3}{V_e} \right]} \quad \Omega \quad (4.40)$$

$$(4.40) \quad R_h = a I f \sqrt{\left(\frac{8 \pi \mu_e^3 L^3 10^7}{V_e} \right)} \quad \Omega$$

Thus when the series loss resistance is expressed in terms of a material hysteresis loss coefficient the relation is somewhat unwieldy and, due to uncertainty in practice of the value of μ_e , the relation may be unreliable. For this reason the measurement of R_h on a gapped core may not be an accurate indication of the material hysteresis coefficient. However, it is by definition a direct measure of the hysteresis loss contribution of the gapped core (i.e. the component property) and it is often used for this purpose. More generally it gives rise to a well-known hysteresis factor which is defined as

$$F_h = \frac{R_h}{I f L^{3/2}} \quad (4.41)$$

Inasmuch as the hysteresis coefficient a is a constant, this factor is constant for a given core having a given effective permeability. From it, the hysteresis resistance may be calculated for particular values of current, frequency and inductance. So for a general core

$$\tan \delta_h = \frac{R_h}{2 \pi f L} = \frac{F_h I \sqrt{L}}{2 \pi} \quad (4.42)$$

A recent IEC recommendation⁴ has a similar factor:

$$\tan \delta_h = \eta I^2 \sqrt{L} \quad (4.43)$$

Thus the series impedance, or current, approach is suitable for expressing the hysteresis properties of gapped cores.

Turning to the alternative method, the reference parameter is voltage or the corresponding flux density. It is convenient now to repeat the derivation of Eqn 2.56 in terms of a general core. If a loss-free winding having N turns is placed on a general magnetic core and an alternating voltage U is applied, a power loss $P = U^2 G$ will be observed, where G is the conductance appearing across the winding due to the magnetic loss in the core. The induced e.m.f., the frequency and the flux density are related by Eqn. 4.16. If the loss tangent is much less than unity the induced e.m.f. will approximately equal the applied voltage, so

$$U = \frac{\omega \hat{B}_e A_e N}{\sqrt{2}} \quad V \quad (4.44)$$

Thus for a given effective core cross-sectional area and number of turns, the voltage and frequency determine the effective flux density.

The loss tangent due to the magnetic core is

$$\tan \delta_m = \frac{\omega L_p}{R_p} = \omega L_p G$$

$$(4.44) \quad U = \frac{\omega \hat{B}_e A_e N}{\sqrt{2}} \cdot 10^{-8} \quad V$$

Since $\tan \delta_m \ll 1$, the distinction between series and parallel inductance may be dropped (see Eqn 2.19).

Substituting $L_p = \mu_o \mu N^2 A_e / l_e$

$$\tan \delta_m = \omega \mu_o \mu N^2 A_e G / l_e \quad (4.45)$$

Putting $G = P_m A_e l_e / U^2$,

where P_m is the power loss density corresponding to a flux density \hat{B}_e ,

$$\tan \delta_m = \frac{\mu_o \mu}{\pi f \hat{B}_e^2} P_m \quad (4.46)$$

The effect of introducing an air gap may now be considered. An air gap of length l_g introduced into a core having a total magnetic length l_e reduces the volume by a factor $(1 - l_g/l_e)$. If the frequency and flux density (applied voltage) are unchanged so that the power loss (volume) density is constant, the total power loss will also be reduced in the ratio $(1 - l_g/l_e)$. Therefore the conductance due to the gapped core

$$\begin{aligned} &= (\text{power loss})/U^2 = \frac{P}{U^2} (1 - l_g/l_e) \\ &= G \frac{\mu(\mu_e - 1)}{\mu_e(\mu - 1)} \quad \Omega^{-1} \quad (4.47) \end{aligned}$$

by substitution from Eqn 4.27. Thus the conductance is reduced from the ungapped value by the ratio of the gapped to the ungapped volumes. The new loss tangent is therefore given by

$$\begin{aligned} (\tan \delta_m)_{\text{gapped}} &= \omega L \frac{\mu_e}{\mu} \times G \frac{\mu(\mu_e - 1)}{\mu_e(\mu - 1)} = \omega LG \frac{(\mu_e - 1)}{(\mu - 1)} \\ \text{or } \frac{(\tan \delta_m)_{\text{gapped}}}{(\mu_e - 1)} &= \frac{\tan \delta_m}{(\mu - 1)} \quad (4.48) \end{aligned}$$

These expressions are referred to as loss factors. Because μ_e and μ are usually much greater than unity, the above equation is usually approximated to

$$\frac{(\tan \delta)_{\text{gapped}}}{\mu_e} = \frac{\tan \delta}{\mu} \quad (4.49)$$

The subscript m has been dropped in this general equation because clearly the loss tangent need not be due to the total loss; it may be due to any specific form of loss. From Eqns 2.68 and 4.49 the loss tangent for a core, gapped or ungapped, may be expressed in terms of the Legg coefficients

$$(4.45) \quad \tan \delta_m = \frac{4\pi\omega\mu N^2 A_e G}{l_e} \times 10^{-9}$$

$$(4.46) \quad \tan \delta_m = \frac{4\mu P_m 10^7}{f \hat{B}_e^2}$$

$$\tan \delta_m = \frac{\mu_e}{2\pi} (a \hat{B}_e + ef + c) \quad (4.50)$$

The effective flux density is now used because the core shape is no longer restricted to the ideal. If the core is ungapped, $\mu_e = \mu$.

Considering first the hysteresis component

$$\tan \delta_h = \frac{\mu_e a \hat{B}_e}{2\pi} \quad (4.51)$$

This relation gives the hysteresis loss tangent for a perfectly general core in terms of the Legg hysteresis coefficient, assuming the hysteresis power loss is proportional to B^3 and the gap is physically small. It follows that the material coefficient a may be related to the hysteresis loss conductance of a general core. Putting $\tan \delta_h = \omega LG_h$ and substituting for L and B_e from Eqns 4.23 and 4.44 the above expression gives

$$\begin{aligned} a &= \frac{\omega \mu_o N^2 A_e G_h}{l_e} \cdot \frac{2\pi A_e N \omega}{\sqrt{2U}} = \sqrt{2\pi} \cdot \frac{\mu_o \omega^2 N^3}{C_2} \cdot \frac{G_h}{U} \\ &= 55.8 \frac{\omega^2 N^3}{C_2} \cdot \frac{G_h}{U} \quad 10^{-7} \quad \text{T}^{-1} \quad (4.52) \end{aligned}$$

where U is the applied voltage. This relation may be used to measure the hysteresis coefficient of a given gapped core. In practice the voltage applied to the winding is changed by an amount ΔU and the corresponding change ΔG in the total measured conductance is noted. Then

$$\frac{G_h}{U} = \frac{\Delta G}{\Delta U} \quad (4.53)$$

This differential method eliminates those parts of the loss conductance which are due to other causes, e.g. residual loss, and which do not depend on flux density. Since magnetic materials do not, in general, obey the simple relation of Eqn 2.33, G_h is not exactly proportional to U so it is usual to make the measurement between two specified low flux densities.

There is one difficulty with this measurement. When U increases, the permeability increases slightly in accordance with the Rayleigh relation. The corresponding increase in inductance changes the value of the loss conductance due to the other losses, e.g. the copper loss. The copper loss conductance equals $R_{dc}/\omega^2 L^2$ so the measured change in conductance will be partly due to an increase of hysteresis loss and partly due to a decrease of

$$(4.52) \quad a = 55.8 \frac{\omega^2 N^3}{C_2} \cdot \frac{G_h}{U} 10^{-17} \quad \text{Gs}^{-1}$$

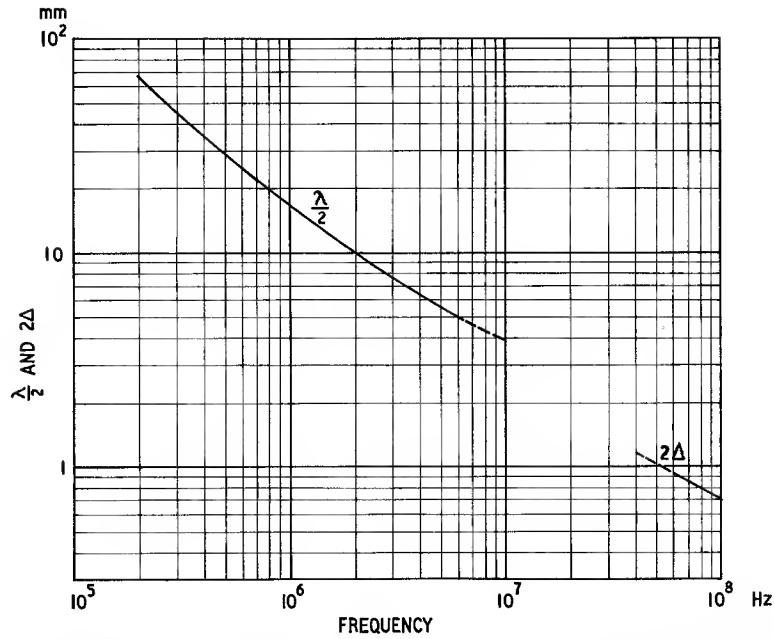


Fig. 4.5. Dimensional resonance and skin effect in manganese zinc ferrite. To avoid dimensional resonance or skin effect at a given frequency, the least cross sectional dimension of the core must be less than $\lambda/2$ or 2Δ at that frequency

copper loss. The residual loss and the eddy current copper loss may also have some effect. If a Rayleigh material is assumed, it may be shown that the resultant error will be less than 5% if the overall Q factor is greater than 100. This is usually the case.

Summarizing, the series hysteresis resistance or the hysteresis loss factor is often used to express the hysteresis of particular cores, whereas the use of the Legg coefficient or $\tan \delta_h$ expressed in terms of \hat{B}_e is a more flexible means of relating the hysteresis of the material to the hysteresis properties of a particular core.

The remaining two loss terms in Eqn 4.50 do not depend on the value of the flux density (assuming the change of μ_e with amplitude is negligible) so the question of the current or voltage approach does not arise. From Eqn 2.61 the loss factor due to eddy currents in the core, $(\tan \delta_F)/\mu$, is given by

$$\frac{\tan \delta_F}{\mu} = \frac{\pi \mu_0 d^2 f}{\rho \beta} = \frac{(\tan \delta_F)_{\text{gapped}}}{\mu_e}$$

from Eqn 4.49

So, in general,

$$\tan \delta_F = \frac{\pi \mu_0 \mu_e d^2 f}{\rho \beta} \quad (4.54)$$

$$(4.54) \quad \tan \delta_F = \frac{4\pi^2 \mu_e d^2 f}{\rho \beta} 10^{-9}$$

For cores of more complicated shape than those covered by Eqn 2.48 the factor corresponding to d^2/β must be calculated from first principles.

At high frequencies or with large cross sections dimensional resonance or skin effect may occur. The basic phenomena have been described in Chapter 2 but as they are essentially properties of a specific core the more practical aspects may be considered here.

For most practical purposes these phenomena are confined to the high permeability, fairly low resistivity ferrites such as manganese zinc ferrite. In nickel zinc ferrites the permeability is relatively low so dimensional resonance can only occur at frequencies beyond the normal range of application.

From Eqn 2.51, the half wavelength corresponding to dimensional resonance has been calculated as a function of frequency for ferrite A5 using data given in Figs. 3.11 and 3.21. The result is shown in Fig. 4.5. The curve is stopped in the frequency region where $\tan \delta_m \cdot \tan \delta_d \rightarrow 1$. The same figure shows the double penetration depth 2Δ (see Eqn 2.52) which applies over the frequency range for which the loss tangent product is much greater than unity. So if it is proposed to use a manganese zinc core in the frequency range where dimensional resonance may occur then the least cross-sectional dimension should be much less than $\lambda/2$ if dimensional resonance is

to be avoided. On the other hand if the frequency is in the skin effect range the least cross-sectional dimension should be much less than 2Δ if it is wished to avoid skin effect, with its attendant loss of permeability. Strictly these curves apply only to an infinite plate of material, but in practice they may be used for estimating the possibility of dimensional resonance and skin effect in a practical core.

Fig. 2.6 shows the complex permeability and permittivity components as functions of frequency in the region of dimensional resonance calculated by Brockman *et al*⁵ for a typical manganese zinc ferrite. It may be observed that while μ'_s goes to zero, the impedance of a winding on such a core (proportional to $\sqrt{[\mu_s'^2 + \mu_s''^2]}$) does not. In fact the impedance stays fairly constant in the vicinity of resonance, but the phase angle rotates.

For most manganese zinc ferrites, μ_s falls rapidly with frequency between about 1 and 10 MHz due to the ferrimagnetic resonance. So any dimensional resonance that might occur at frequencies above a few MHz merges with this ferrimagnetic resonance. Although dimensional resonance could have a serious effect on transformer and inductor performance, in practice it rarely does so. At higher frequencies smaller cores are normally used and at frequencies above a few MHz it is usual to change over to nickel zinc ferrite cores to avoid the ferrimagnetic resonance dispersion that occurs in manganese zinc ferrites at these frequencies. These two reasons tend to make the avoidance of dimensional resonance automatic. Therefore it is in the design of devices requiring large manganese zinc ferrite cores at frequencies between about 100 kHz and 5 MHz that the possibility of dimensional resonance should be checked (see also Section 7.3.1 p. 253.) Skin effect in ferrites is even rarer; it would only occur in manganese zinc ferrite cores at frequencies greater than about 50 MHz.

An air gap which reduces the permeability to an effective value, μ_e , will increase the frequency of dimensional resonance. For a loss-free medium the frequency is increased by the ratio $(\mu/\mu_e)^{1/2}$ since in this case μ_e must be substituted for μ in Eqn 2.50.

Dimensional resonance is troublesome mainly when one is measuring the complex permeability or permittivity of high permeability ferrites at frequencies higher than 1 MHz. The most practical way of avoiding error due to this phenomenon is to ensure that the least cross-sectional dimension of the specimen, measured perpendicularly to the field, is made much smaller than the half-wavelength given by Fig. 4.5.

Moving on from eddy current effects, the last of the loss components in Eqn 4.50 is the residual loss. The nature of this loss has been discussed briefly in the introduction to Fig. 3.12. As a material property it is usually expressed by the residual loss factor, $(\tan \delta_r)/\mu$,

as a function of frequency. For a gapped core, it follows from Eqns 2.68 and 4.50 that

$$(\tan \delta_r)_{\text{gapped}} = \left(\frac{\tan \delta_r}{\mu} \right) \mu_e \quad (4.55)$$

This is the simplest of the losses to calculate. Provided the material properties are constant, the residual loss tangent is independent of the size and shape of the core and depends only on the material parameter and the effective permeability.

Since, for a given core, $\tan \delta_F$ and $\tan \delta_r$ are functions only of frequency they are often lumped together and designated $\tan \delta_{r+F}$ in specifications for particular ferrite cores.

Finally the problem of calculating the high amplitude losses in a general core may be briefly considered. It is seen from Fig. 3.19 that the power loss (volume) density may be expressed by

$$P_m = kf\hat{B}^n \quad (4.56)$$

where n lies between about 2 and 3 for most manganese zinc ferrites. For a general core, having varying cross section, the total flux must be calculated using the induction formula, Eqn 2.13, in which $\hat{B}A$ is replaced by Φ . It must be remembered that Eqn 2.13 is only valid for sinusoidal e.m.f.'s; if the waveform departs substantially from a sine wave then Eqn 2.12 must be used. Further, if the total loss is large so that the total loss tangent is not small compared to unity, the e.m.f. will not equal the applied voltage. Having calculated the total flux, the flux density in any section of the core may be obtained by dividing by the particular cross-sectional area. For each section a power loss density may be obtained from the calculated flux density and Fig. 3.19. The total power loss is then the sum of $P_m \times \text{volume}$ for each section. If eddy current loss is appreciable this must be added separately using Eqn 2.48 for each section.

4.2.4. Distortion and intermodulation

In Chapter 2 the generation of wave form distortion and intermodulation products in a magnetic material is studied. The analysis assumes that the material has a Rayleigh or Peterson parabolic loop and that the core is of an ideal shape. The results are derived by calculating the amplitude distortion products in the flux density when a sinusoidal field strength is applied. In this section the way in which these results may be applied to a general core will be briefly considered.

The effect of an air gap may be inferred from Eqn 4.49. Applying this, for example, to Eqn 2.78, the e.m.f. distortion ratio for a gapped core is

$$\frac{E_{3a}}{E_a} = 0.6 (\tan \delta_h)_{\text{gapped}} = 0.6 \tan \delta_h \frac{\mu_e}{\mu} \quad (4.57)$$

This may be derived more convincingly by considering the derivation of Eqn 2.78 and replacing the Peterson coefficient, which depends on μ , by the Legg coefficient, which does not. Using the relation given in Table 2.1, Eqn 2.76 becomes

$$\hat{B}_{3a} = \frac{a}{2\pi} \frac{\mu_0^2 \mu^3 \hat{H}_a^2}{5}$$

If the magnetic circuit has an effective permeability μ_e , then this may be substituted for μ . It then follows that

$$\begin{aligned} \frac{\hat{B}_{3a}}{\hat{B}_a} &= \frac{a}{2\pi} \frac{\mu_e \hat{B}_a}{5} \\ \text{or } \frac{\hat{E}_{3a}}{\hat{E}_a} &= \frac{a \mu \hat{B}_a}{5} \cdot \frac{\mu_e}{2\pi \mu} \\ &= 0.6 \tan \delta_h \frac{\mu_e}{\mu} \quad \text{from Eqn 2.68} \end{aligned}$$

The other intermodulation amplitude ratios expressed in terms of $\tan \delta_h$ in Table 2.2 may be similarly converted.

The derivation of the relative magnitudes of the distortion and intermodulation e.m.f.s in Section 2.2.7 was based on the assumption that the current wave is sinusoidal. However, the magnitude of the distortion e.m.f.

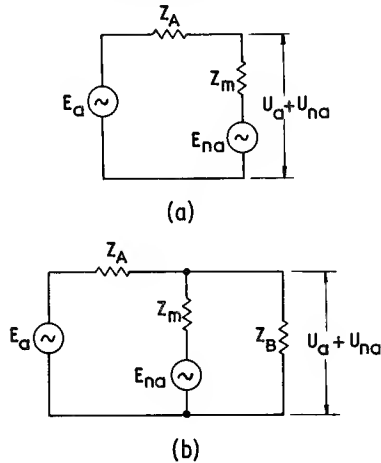


Fig. 4.6. Distortion voltage across the terminals of a loaded inductor or transformer

will be substantially the same even if the applied voltage waveform is sinusoidal, for although, the resulting current waveform will be non-sinusoidal, the amount of distortion considered in an analysis confined to the Rayleigh region is so small that the error in neglecting it will be of second order.

Referring to Fig. 4.6(a), Z_m represents the impedance due to the magnetic material and it has in series with it a distortion generator, E_{na} , where n represents the order of the distortion product. The impedance Z_A represents

the source impedance, the winding resistance being assumed negligible. If $Z_A \rightarrow \infty$, the situation is in accordance with the analysis in Section 2.2.7. The sinusoidal source generator, E_a , will drive a sinusoidal current at frequency f_a through the inductor and the full distortion e.m.f. will appear across the inductor terminals together with the fundamental voltage, U_a . Therefore the distortion ratio $E_{na}/U_a = U_{na}/U_a$ may be measured across the terminals of the inductor.

If Z_A is not infinite, the distortion generator will not have an open-circuit and a distortion current, I_{na} , will flow.

$$I_{na} = \frac{E_{na}}{Z_A + Z_m}$$

where Z_A and Z_m are the impedances observed at the distortion frequency.

Assuming that the amplitude of the fundamental e.m.f. across the inductor is unchanged and the winding resistance is negligible, the distortion voltage ratio across the terminals will be

$$\begin{aligned} \frac{U_{na}}{U_a} &= \frac{E_{na} - I_{na} Z_m}{U_a} \\ &= \frac{E_{na}}{U_a} \frac{Z_a}{Z_A + Z_m} \end{aligned} \quad (4.58)$$

If, as in the low frequency equivalent circuit of a transformer (see Fig. 7.3), there is also a load impedance, the circuit appears as in Fig. 4.6(b). In this case

$$\frac{U_{na}}{U_a} = \frac{E_{na}}{U_a} \frac{Z}{Z + Z_m} \quad (4.59)$$

where $Z = Z_A Z_B / (Z_A + Z_B)$, all impedances corresponding to the distortion frequency.

In a well designed transformer Z_m is usually much greater than Z at the distortion frequencies so the distortion voltage ratio will be much less than the distortion e.m.f. ratio.

4.3. OPEN MAGNETIC CORES

4.3.1. General

The magnetic cores considered so far have had either no air gaps or air gaps so small that the flux could be assumed approximately constant round the magnetic path, i.e. the lines of flux leave the magnetic material mainly at the surfaces forming the air gap. When the gap becomes an appreciable fraction of the total magnetic path length, the greater reluctance of the gap causes the flux to leave the magnetic material before crossing the ends of the core which form the gap and the flux is not constant within the core. This invalidates the foregoing treatment and calls

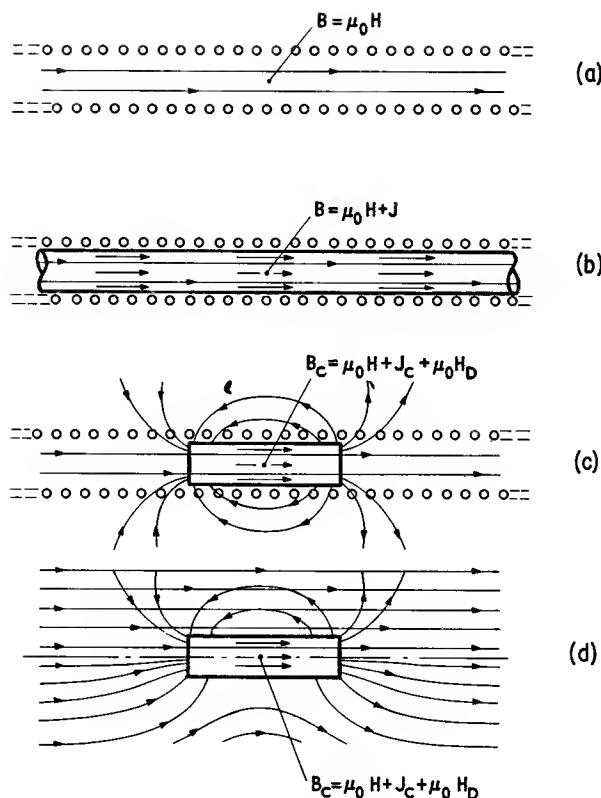


Fig. 4.7. Magnetic flux associated with: (a) a very long air-cored solenoid; (b) a very long solenoid enclosing a very long ferromagnetic cylinder; (c) a very long solenoid enclosing a short cylindrical core; (d) a short cylindrical core immersed in a uniform magnetic field. (upper half: component fields, lower half: resultant field)

for an approach which takes this fringing or leakage flux into account.

The most common form of ferrite core having an air gap large enough to cause appreciable leakage flux is a simple cylindrical or rod core and this section will be mainly concerned with this shape.

Fig. 4.7(a) represents an infinitely long solenoid containing no magnetic material. The solenoid carries a current I so the internal field strength is NI/l . The flux density inside the solenoid, represented by the long arrows, is $B = \mu_0 H$ and the flux density at all points outside is zero.

The next diagram (b) shows the same solenoid containing a very long magnetic core. In addition to the

applied field H there is now a field due to the alignment of the magnetic moments of the atomic currents. In a ferromagnetic or ferrimagnetic material the net effect of these atomic currents is to enhance the applied field giving rise to an increased flux density represented by the short arrows. The total flux density in the solenoid is now

$$B = \mu_0 H + J \quad \text{T} \quad (4.60)$$

where J is the magnetic polarization or intrinsic magnetic flux density in tesla (weber. m^{-2}), see Section 2.1. The exterior flux density is still zero because the fields due to the atomic currents cancel at all points outside the core.

If all but a short centre section of the core is removed it is clear that the total field acting in the remaining section will be diminished, since the atomic fields of the removed portions no longer contribute, (see Fig. 4.7c). This reduction may be considered to be due to a reverse or demagnetizing field which has neutralized the atomic fields that were previously there. The moments of the atomic currents no longer cancel in their effect outside the solenoid and so an exterior or leakage field exists. Within the remaining portion of the cylindrical core the resultant field will, in general, vary from a maximum in the centre to a minimum at the ends. This may be regarded as due to a non-uniform distribution of the demagnetizing field. In the special case of the remaining portion being an ellipsoid the internal field and flux density are constant, and the demagnetizing field is constant.

The demagnetizing field at the centre of the core may be expressed as

$$H_D = -NJ_c/\mu_0 = -NM_c \quad \text{A.m}^{-1} \quad (4.61)$$

where J_c is the magnetic polarization at the centre of the core and N is called the demagnetizing factor. This factor is considered in more detail later. The flux density in the centre of the core is now given by

$$B_c = \mu_0 H + J_c + \mu_0 H_D \quad (4.62)$$

$$= J_c + \mu_0 \left(H - \frac{NJ_c}{\mu_0} \right) \quad \text{T} \quad (4.63)$$

from 4.61

$$\therefore \frac{B_c - J_c}{J_c} = \frac{\mu_0 H_c}{B_c - \mu_0 H_c} = \frac{\mu_0 H}{B_c - \mu_0 H_c} - N$$

$$(4.60) \quad B = H + 4\pi M \quad \text{Gs}$$

where M is the intensity of magnetization or magnetic moment per cm^3

$$(4.61) \quad H_D = -NM_c \quad \text{Oe}$$

Note: $(N)_{\text{CGS}} = 4\pi(N)_{\text{SI}}$

$$(4.62) \quad B_c = H + 4\pi M_c + H_D \quad \text{Gs}$$

$$(4.63) \quad B_c = 4\pi M + H + NM_c \quad \text{Gs}$$

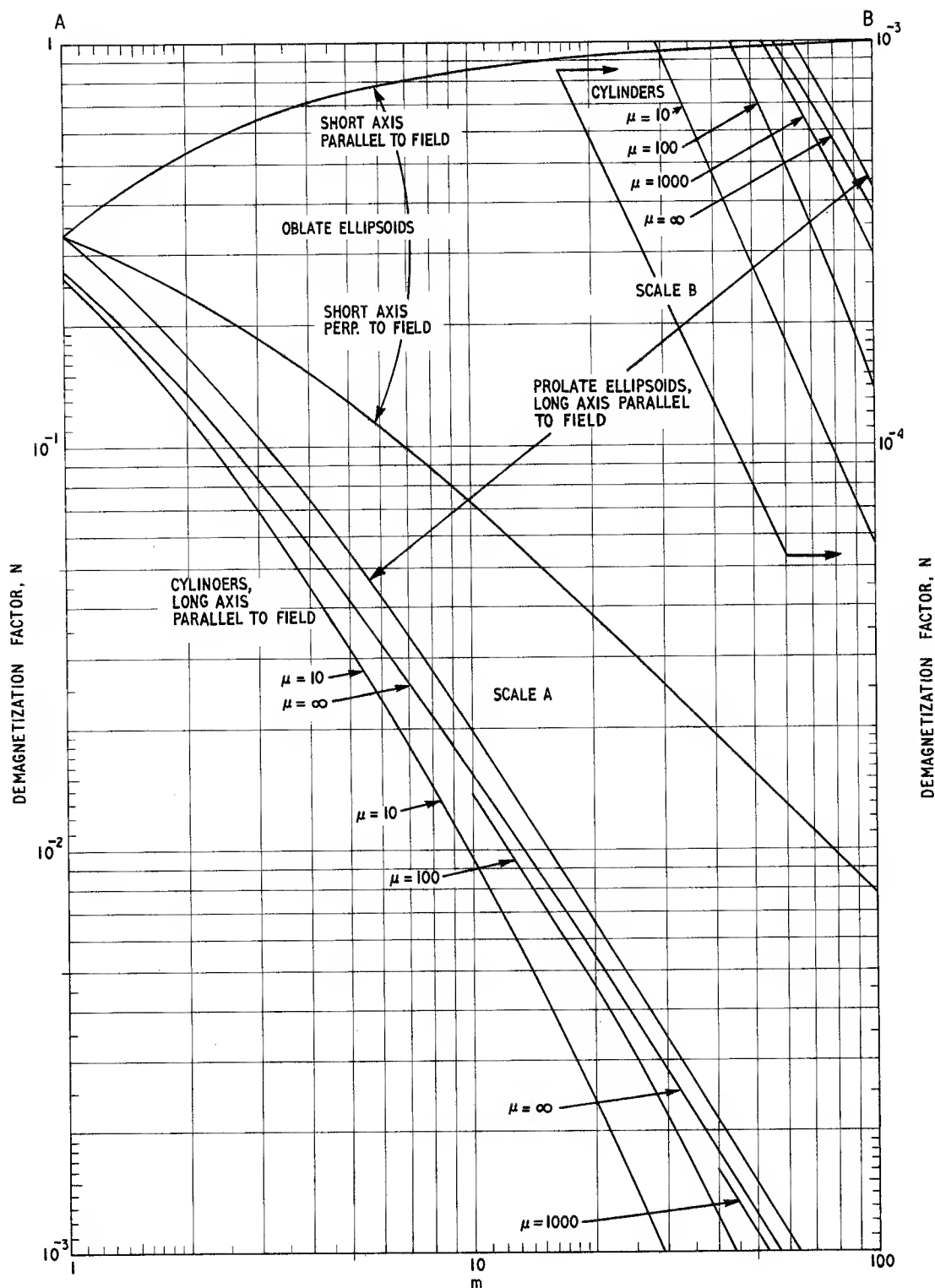


Fig. 4.8. Demagnetizing factors for ellipsoids and cylinders as functions of m ($=$ long axis/short axis for ellipsoids and length/diameter for cylinders) (After Bozorth et al.⁶) Note: The values of N are appropriate to S.I. units; $(N)_{SI} = 1/4\pi(N)_{CGS}$

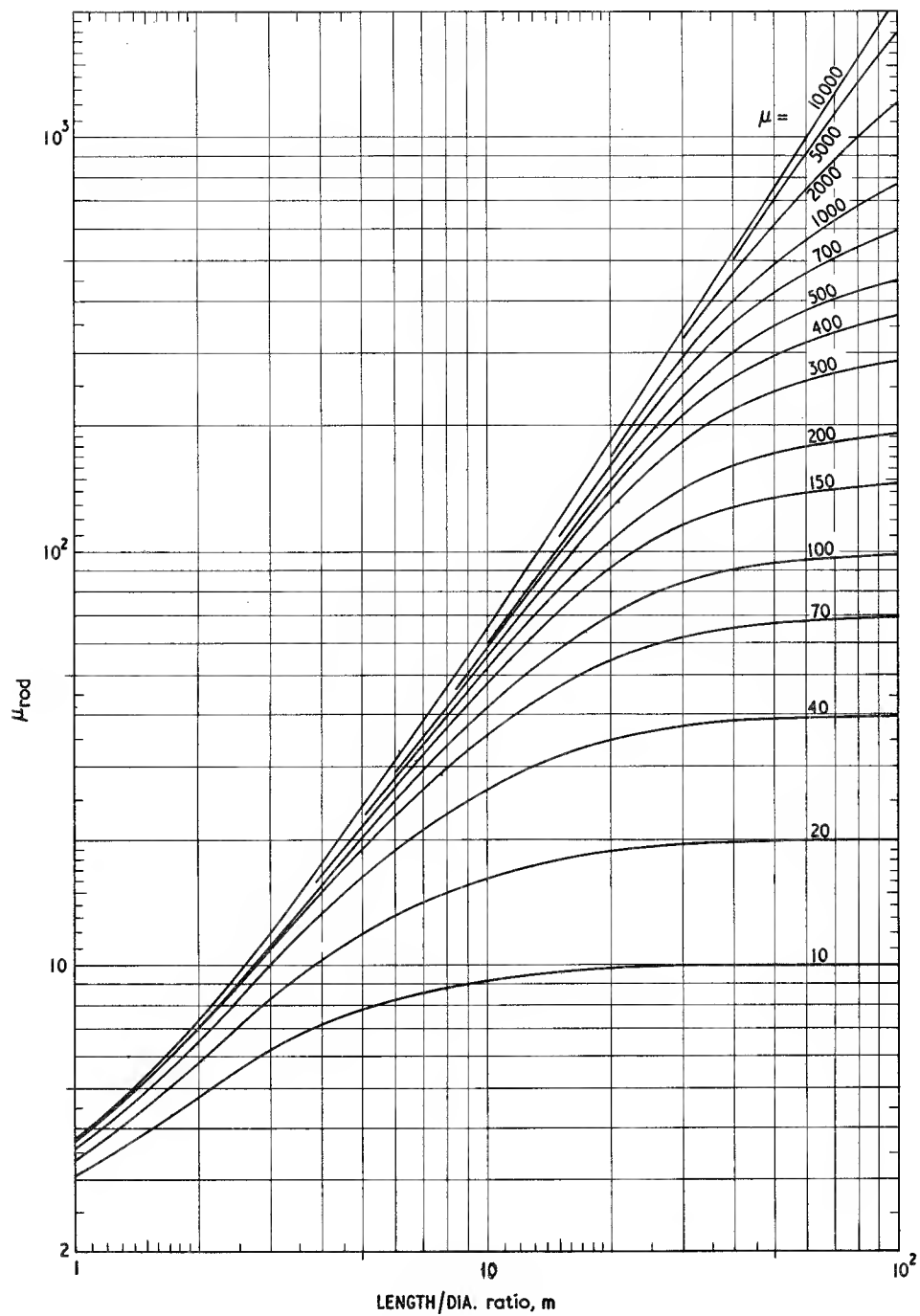


Fig. 4.9. μ_{rod} as a function of m with material permeability as a parameter

since the magnetic polarization at the centre, $J_c = B_c - \mu_0 H_c$ from Eqn 4.60, where $H_c (= H - NJ_c/\mu_0)$ is the actual field strength at the centre of the rod. The permeability of the material is $\mu = B_c/\mu_0 H_c$, while the overall permeability is denoted by μ_{rod} and is defined by $\mu_{rod} = B_c/\mu_0 H$ (H being the applied field).

Simplifying the above equation

$$\frac{1}{\mu - 1} = \frac{1}{\mu_{rod}} \left(\frac{1}{1 - 1/\mu} \right) - N \quad (4.64)$$

Since μ is nearly always much greater than unity, this equation simplifies to

$$\frac{1}{\mu} \approx \frac{1}{\mu_{rod}} - N \quad (4.65)$$

So far μ_{rod} has been defined as the ratio of the flux density at the centre of the cylindrical core in Fig. 4.7(c) to the flux density in the centre of the solenoid in Fig. 4.7(a). If, instead of being enclosed by a long close-fitting solenoid, the short cylindrical core were introduced into a relatively large region in which there existed, before the presence of the core, a uniform field H , then the situation would be similar to that depicted in Fig. 4.7(c) except that the field, H , would no longer be confined to the interior of the solenoid but would occupy the whole region. It would combine with the leakage field to give a resultant field distribution as shown in Fig. 4.7(d). The upper part of this figure shows the component fields while the lower half shows the resultant field. The value of μ_{rod} derived above may now be given an additional definition; it is the ratio of the flux density at the centre of a cylindrical core aligned in a uniform field, to the flux density existing there in the absence of the core. μ_{rod} thus differs from μ_c , the latter referring to a gapped core in which the total flux does not vary significantly along the magnetic path length.

The value of the demagnetizing factor N depends on the geometry of the core and to a lesser extent on its permeability. Fig. 4.8 gives values for cylinders and ellipsoids of revolution. These have been calculated from formulae derived in the literature.^{6,7,8} It will be noted that the demagnetization factors of the ellipsoids do not depend on the material permeability. For any body, the sum of the demagnetization factors, relating to three orthogonal axes of that body, is unity. Thus all the ellipsoid demagnetizing factors approach 1/3 as the ellipsoid shape approaches that of a sphere. The demagnetization factors of the cylinders depend on both the dimensional ratio, m (which in this case equals length/diameter), and also on the material permeability.

Using some of these data in Eqn 4.65, μ_{rod} has been calculated as a function of length/diameter ratio for cylinders, with the material permeability as a parameter. The results are shown in Fig. 4.9. This graph shows that when the material permeability is low, the value of μ_{rod} is asymptotic to the material permeability as the rod becomes more slender. This is because the demagnetizing factor becomes very small; from another point of view it could be said that the effective air gap becomes very small. When the material permeability is high the demagnetizing factor or the effective air gap does not become negligible within the practical range of slenderness considered. Even so, the graph shows that rod permeabilities of up to 200 may easily be obtained with practical ferrite rods.

If the ferrite core is a tube having the same material permeability and the same outside dimensions as a rod, then μ_{rod} will be the same, i.e. the flux density in the ferrite half way between the ends of the tube will be $\mu_0 \cdot \mu_{rod}$ times the field strength which would exist there in the absence of core. However, the total flux passing through the centre portion of the core would be less than that for a solid rod by the ratio of the cross-sectional areas.

4.3.2. Flux distribution along a cylinder immersed in a uniform magnetic field

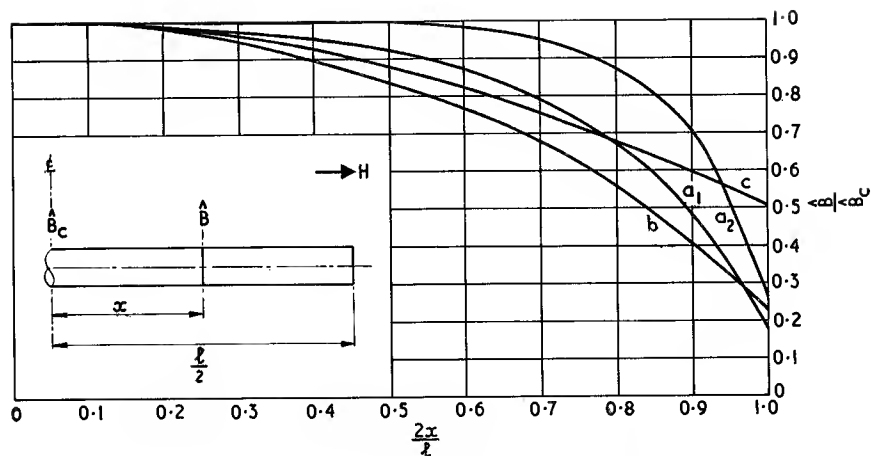
It has been seen that when a short cylindrical core is immersed in a uniform field, the flux density varies along the length. The distribution depends on the dimensional ratio of the core and on the permeability. It has been calculated by Warmuth⁸ for cores of infinite permeability.

Fig. 4.10(a) shows the measured distribution for a number of cylinders representing typical combinations of permeability and dimensional ratio. Three types of distribution may be distinguished:

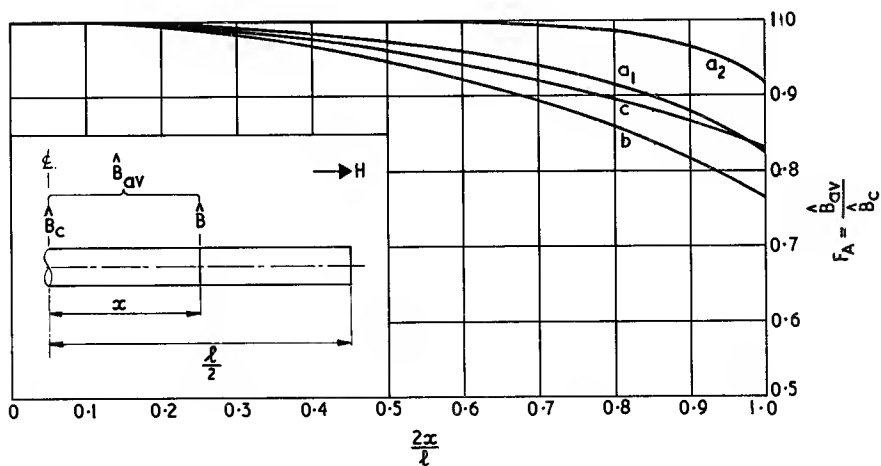
- (a) Magnetically long cylinders, i.e. m large enough to make $\mu_{rod} \rightarrow \mu$. This gives a rather flattened curve which falls to a low value at the ends of the rod. The lower the material permeability or the higher the value of m the flatter the distribution.
- (b) Intermediate cylinders, i.e. m such that μ_{rod} is less than, say, 0.8μ . An approximately parabolic distribution is obtained. This distribution is similar to that calculated by Warmuth for a cylinder of infinite permeability. If the rod is geometrically short, i.e. such that $m \rightarrow 3$ or less, then the next result applies even if $\mu_{rod} \rightarrow \mu$.
- (c) Geometrically short cylinders, i.e. where $m \rightarrow 1$. This distribution is approximately parabolic but is shallower than in (b) i.e. it gives a relatively high

$$(4.64) \quad \frac{1}{\mu - 1} = \frac{1}{\mu_{rod}} \left(\frac{1}{1 - 1/\mu} \right) - \frac{N}{4\pi}$$

$$(4.65) \quad \frac{1}{\mu} \approx \frac{1}{\mu_{rod}} - \frac{N}{4\pi}$$



(a) Flux density distribution as a function of fractional distance from centre



(b) E.m.f. averaging factor, F_A , as a function of the averaging length, centrally located

Fig. 4.10. Distribution of flux density measured along various types of ferrite cylinders immersed in a uniform field

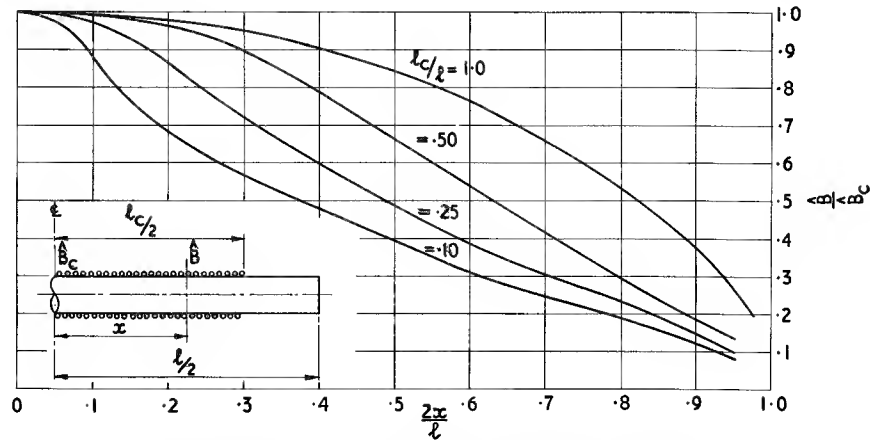
	m	μ_i	μ_{rod}	Remarks
a_1	80	50	49.5	$\left\{ \begin{array}{l} \text{Magnetically long,} \\ \mu_{rod} \rightarrow \mu_i \end{array} \right.$
a_2	80	180	172	
b	10	1000	62	intermediate
	15	1000	114	
c	3	50–1000	10.5–12	$\left\{ \begin{array}{l} \text{Physically short} \\ \text{i.e. } m < 5 \end{array} \right.$

value of flux density at the ends of the rod. In the limit as $m \rightarrow 0$ clearly the flux density will become uniform along the axis.

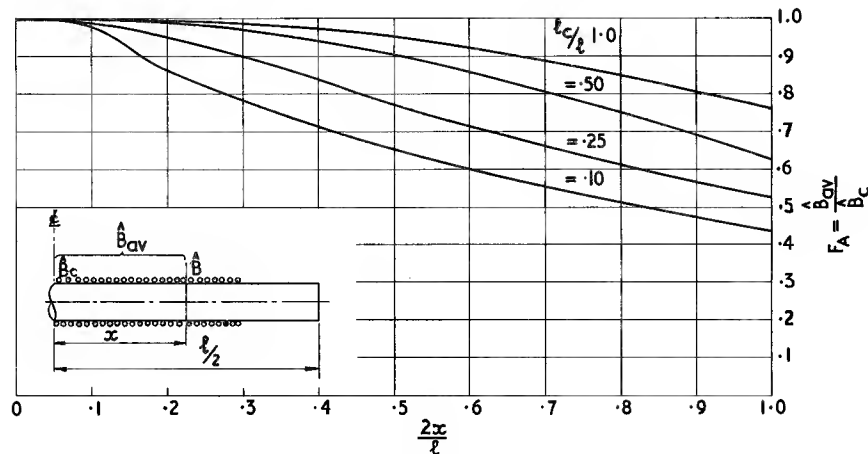
Any actual example may be identified by its value of μ and m as corresponding to, or lying between these types. When the field becomes very large the cylinder may approach saturation at the centre and the permeability may vary from a low value at the centre to a high value at the ends. This tends to make the flux density more uniform over the centre region and the distribution approaches that of (a) above.

A short coil placed in the centre of a rod, will have an

e.m.f., E_c , induced in it corresponding to the central flux density \hat{B}_c . If the length of the coil is now increased without altering the number of turns the e.m.f. will fall since it will correspond to the average flux density in the part of the rod covered by the coil. The ratio of this e.m.f. to the centre e.m.f., $E/E_c = \hat{B}$ averaged over the length of coil divided by \hat{B}_c . This ratio is called the e.m.f. averaging factor, F_A . This factor is given in Fig. 4.10(b) as a function of the fraction of the rod covered by the coil, for the three distributions distinguished above. From this graph the approximate value of F_A may be found for any type of ferrite cylinder immersed in a uniform field.



(a) Flux distribution as a function of fractional distance from centre



(b) E.m.f. averaging factor, F_A , as a function of the averaging length, centrally heated

Fig. 4.11. Distribution of flux density measured along a ferrite cylinder energized by a central solenoid, the parameter being the fraction of the cylinder covered by the solenoid. The result is almost independent of μ_{rod}

4.3.3. Flux distribution along a cylinder energized by a winding

Another type of flux distribution of importance is that resulting from an energized winding embracing all or part of the cylinder. This distribution is not very dependent on the permeability of the ferrite or on the dimensional ratio m . It is however strongly dependent on the fraction of the rod covered by the winding. Some measured distributions are shown in Fig. 4.11(a). It is seen that if the winding covers the whole of the cylinder the flux density distribution is similar to that for a cylinder of high permeability material immersed in a uniform magnetic field (see Fig. 4.10 curve *b*). As the winding becomes shorter the flux density falls away more steeply from its central value.

Fig. 4.11(b) shows the averaging factors $F_A = \hat{B}_{av}/\hat{B}_c$ for each distribution; they correspond to the curves of Fig. 4.10(b) for field-immersed cylinders. The curves of Figs. 4.11 enable the flux linkage with a winding or between windings to be estimated and also provide a basis for estimating core losses due to a current in an energizing winding.

4.3.4. The inductance of a winding having a cylindrical core

If L_a denotes the inductance of a winding having no magnetic core and L is the inductance of the same winding when embracing a magnetic core then, by definition,

$$\frac{L}{L_a} = \mu_{\text{coil}} \quad (4.66)$$

Sometimes this is called the inductance ratio or the apparent permeability. Both L and μ_{coil} are important parameters in the design of inductors having cylindrical cores.

Direct calculation of μ_{coil} is difficult since it depends on the geometry of the winding and the core and to some extent on the core permeability. A simpler approach has been adopted here; it applies only to centrally placed windings.

If a magnetically long cylinder, of cross sectional area A , is covered along its whole length, l , with a winding of N turns, it approximates to a magnetic circuit having a small gap and an effective permeability, μ_{rod} . Therefore the inductance is given by

$$L = \mu_{\text{rod}} \frac{N^2 A}{l} \quad \text{H}$$

If the winding does not equal the length of the cylinder but is nevertheless centrally placed, the inductance will be modified because of the changed flux distribution along the axis. It has been seen in Fig. 4.11 that the flux distribution is very nearly independent of μ_{rod} ; it depends almost solely on the ratio of winding length to rod length l_w/l . It follows that in the special case of $l_w/l = 1$ the flux distribution is also independent of μ_{rod} . Therefore the above equation holds for fully wound cylinders of almost any dimensional ratio. If the cylinder is not fully wound the inductance is altered by an amount depending only on l_w/l . Therefore

$$L \propto \mu_{\text{rod}} \frac{N^2 A}{l}$$

the constant of proportionality depending only on l_w/l . To test this theory, the constant of proportionality was measured as a function of l_w/l for a wide variety of ferrite cylinders; the initial permeabilities ranged from 15 to 1000 and the dimensional ratios, m , ranged from 3 to 18. The results are enclosed by the shaded area of Fig. 4.12. Further measurements were made to show that, within reason, these results do not depend on the radial thickness of the winding. This graph may be used to estimate the inductance of a wide variety of rod-cored inductors; if a mean curve is used the error will be less than about 12%.

To obtain μ_{coil} it only remains to calculate the air cored inductance, L_a , of the winding. This may be done readily by reference to Section 11.5 where general design data is given. Eqn 4.66 then gives μ_{coil} .

4.3.5. Magnetic losses

The low level loss in a cylindrical core⁹ may in principle be calculated from the general Eqn 2.56

$$P_m = \frac{\pi f \hat{B}^2}{\mu_0} \cdot \frac{\tan \delta_m}{\mu} \quad \text{W.m}^{-3} \quad (4.67)$$

This expression may be applied to each element of length and the total loss is

$$P = \frac{2\pi f A}{\mu_0} \int_0^{l/2} \hat{B}^2 \frac{\tan \delta_m}{\mu} dx \quad \text{W} \quad (4.68)$$

where x is the distance from the centre (see Fig. 4.10)

If the hysteresis loss predominates and the Rayleigh relations apply then $(\tan \delta_m)/\mu$ is proportional to B (see Eqn 2.35). If eddy current loss is the only loss considered then $(\tan \delta_m)/\mu$ is a constant depending on the diameter of the rod and its resistivity, (see Eqn 2.49).

$$(4.67) \quad P_m = \frac{f \hat{B}^2 10^{-7}}{4} \frac{\tan \delta_m}{\mu} \quad \text{W.cm}^{-3}$$

$$(4.68) \quad P = \frac{f A 10^{-7}}{2} \int_0^{l/2} \hat{B}^2 \frac{\tan \delta_m}{\mu} dx \quad \text{W}$$

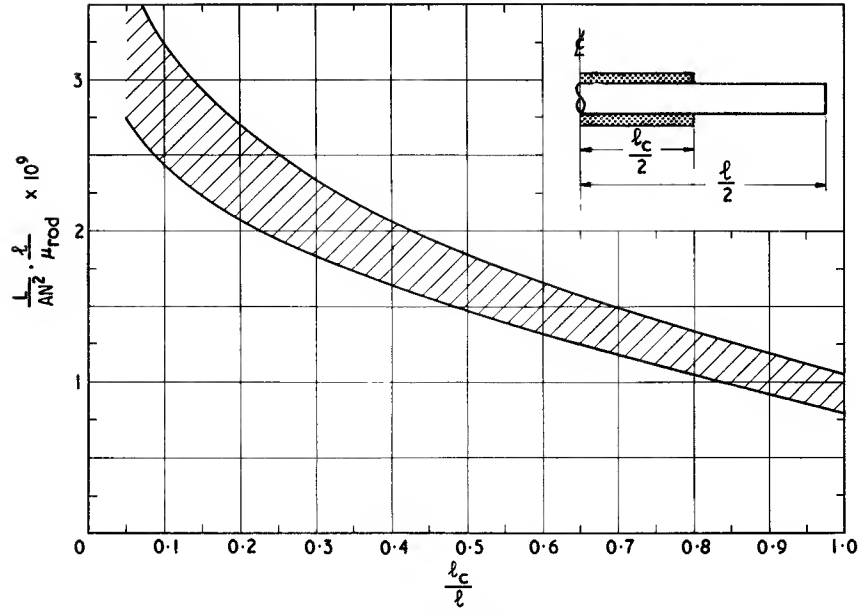


Fig. 4.12. $L/AN^2\mu_{rod}$ as a function of l_c/l . The results for a wide variety of ferrite rods are contained within the shaded area, (dimensions in mm, L in H)

If only residual loss is considered then $(\tan \delta_m)/\mu$ is a material parameter which is a function of frequency. Where more than one loss must be taken into account the corresponding loss factors must be summed for each element.

As in the case of any other magnetic circuit, the losses in a cylinder of magnetic material may be expressed in terms of the tangent of the resulting loss angle, δ , measured at the terminals of a winding embracing the core. This parameter will be designated $(\tan \delta_m)_{rod}$ to distinguish it from the corresponding material parameter. If a voltage, U , is applied to the winding, the resultant core loss may be represented as a conductance, G , in parallel with the winding. Then $P = U^2G$. If the inductance of the winding is L the effective core loss angle is given by

$$(\tan \delta_m)_{rod} = \omega LG = \omega L \frac{P}{U^2} \quad (4.69)$$

From the e.m.f. equation, assuming that the overall loss angle is small,

$$U^2 = \frac{(\omega \hat{B}_{av} AN)^2}{2}$$

where \hat{B}_{av} is the peak flux density averaged over the length of the winding. Combining this with Eqns 4.68 and 4.69

$$(\tan \delta_m)_{rod} = \frac{2L}{\mu_0 AN^2 \hat{B}_{av}^2} \int_0^{1/2} \hat{B}^2 \frac{\tan \delta_m}{\mu} dx \quad (4.70)$$

This equation may be applied to the general case of a cylinder of magnetic material surrounded over all or part of its length by a winding carrying an alternating current. The distribution of flux density along the cylinder depends on the fraction of the cylinder covered by the winding. This has been discussed in Section 4.3.3. If the distribution is known, together with the relation between $(\tan \delta)/\mu$ and \hat{B} , then the integral may be evaluated. At low flux densities $(\tan \delta_m)/\mu$ is virtually independent of \hat{B} and may be removed from the integral. Given the distribution of \hat{B} and the fraction of the cylinder covered by the winding the value \hat{B}_{av} may be readily deduced. The remaining factor L/AN^2 is a function of the cylinder and winding geometry and empirical data have been given in the previous section.

Two limiting cases will now be considered. The first is a long cylinder covered by a winding of equal length. If it is assumed that the distribution of \hat{B} is parabolic and that \hat{B} reaches zero at the ends of the rod (see Fig. 4.10a), then Eqn 4.70 may be evaluated. The flux density at distance x from the centre is

$$\hat{B} = \hat{B}_c \left(1 - \frac{4x^2}{l^2}\right)$$

$$(4.70) \quad (\tan \delta_m)_{rod} = \frac{L10^9}{2\pi AN^2 \hat{B}_{av}^2} \int_0^{1/2} \hat{B}^2 \frac{\tan \delta_m}{\mu} dx$$

If this expression is integrated over the half rod length it is found that the average value of the flux density is

$$\hat{B}_{av} = \frac{2}{3} \hat{B}_c$$

$$\therefore \hat{B}_{av}^2 = \frac{4}{9} \hat{B}_c^2 \quad (4.71)$$

If \hat{B}^2 is similarly integrated the result is

$$\int_0^{l/2} \hat{B}^2 dx = \frac{8}{15} \hat{B}_c^2 l \quad (4.72)$$

Using these results in Eqn 4.70 and assuming that $(\tan \delta_m)/\mu$ is constant

$$(\tan \delta_m)_{rod} = \frac{IL}{\mu_0 AN^2} \cdot \frac{6}{5} \cdot \frac{\tan \delta_m}{\mu} \quad (4.73)$$

This is probably the most practical form of expression for the effective loss tangent of a fully wound cylinder. The approximate value of L/AN^2 may be obtained from Fig. 4.12 (note: the dimensions in the present discussion are in m, in Fig. 4.12 they are in mm). If the inductance is put in terms of μ_{coil} an interesting analogy results; assuming the winding is a long close-fitting solenoid,

$$L = \mu_0 \mu_{coil} \frac{AN^2}{l}$$

Therefore, Eqn 4.73 becomes

$$(\tan \delta_m)_{rod} = \frac{6}{5} \frac{\tan \delta_m}{\mu} \mu_{coil} \approx \frac{\tan \delta_m}{\mu} \mu_{coil} \quad (4.74)$$

This is similar in form to the result for a toroid having a small air gap, see Eqn 4.49.

If the winding is not close-fitting or if the cylinder has a central hole a simple modification is required. It is assumed that the actual cross-sectional area of the ferrite cylinder or tube is A and the effective aperture of the winding is A_N . If A_N is not very much greater than A it will be seen that the general Eqn 4.70 will still apply; for the same value of A the flux linking the winding will to a close approximation be unchanged and the flux distribution will be as before. However, in deriving Eqn 4.74 the expression for L must now use A_N instead of A . Therefore this equation for the effective loss tangent must become

$$(\tan \delta_m)_{rod} \approx \frac{A_N}{A} \frac{\tan \delta_m}{\mu} \mu_{coil} \quad (4.75)$$

The other limiting case is that of a very short winding

on a long cylinder. Fig. 4.11(a) shows a typical distribution of flux density. By graphical integration it has been found that the average value of \hat{B}^2 is $0.22 \hat{B}_c^2$. Because the winding is short the flux density may be taken as constant over its length, therefore $\hat{B}_{av} = \hat{B}_c$. Putting these results in Eqn 4.70

$$(\tan \delta_m)_{rod} = \frac{IL}{\mu_0 AN^2} \cdot 0.22 \frac{\tan \delta_m}{\mu} \quad (4.76)$$

In this case there is no simple approximation for L/AN^2 ; for any given cylindrical core a value may be obtained from Fig. 4.12.

Finally attention may be drawn to the evaluation of losses in a cylinder operating at higher levels. At the higher flux densities the core loss is usually expressed in terms of the power loss in watts per unit volume as a function of flux density and frequency. If the flux distribution is known or may be estimated from the foregoing data then the total loss in watts may be obtained by graphical integration of the loss density along the length of the cylinder.

4.3.6. Temperature coefficient

The temperature coefficient of inductance of a gapped core having an effective permeability μ_e follows from Eqn 4.32

$$\frac{\Delta L}{L \Delta \theta} = \frac{\Delta \mu}{\mu^2 \Delta \theta} \times \mu_e$$

The factor $\Delta \mu / \mu^2 \Delta \theta$ is called the Temperature Factor (T.F.) and is a material parameter. In the particular case of a cylindrical core⁹ μ_e may, without great error, be replaced by μ_{coil} (see Section 4.3.4).

$$\text{So Temp. Coeff.} = \text{Temp. Factor} \times \mu_{coil} \quad (4.77)$$

Thus if a winding on a cylindrical ferrite core has $\mu_{coil} = 20$ and the T.F. of the ferrite is $10 \times 10^{-6} \text{ } ^\circ\text{C}^{-1}$ then the T.C. will be 200 ppm/ $^\circ\text{C}$.

REFERENCES AND BIBLIOGRAPHY

Section 4.2.1.

1. OLSEN, E., *Applied magnetism, a study in quantities*, Philips Technical Library, Eindhoven, (1966).
2. 'Calculation of the effective parameters of magnetic piece parts', *International Electrotechnical Commission, Publication 205*, Geneva, (1966).
3. ASTLE, B., private communication.

$$(4.73) \quad (\tan \delta_m)_{rod} = \frac{IL10^9}{4\pi AN^2} \cdot \frac{6}{5} \cdot \frac{\tan \delta_m}{\mu}$$

$$(4.76) \quad (\tan \delta_m)_{rod} = \frac{IL10^9}{4\pi AN^2} \cdot 0.22 \frac{\tan \delta_m}{\mu}$$

Section 4.2.2.

KORNETZKI, M., 'Die Wechselfeldverluste in gescherten-magnetischen Kernen', *Frequenz*, **6**, 313, (1952).

Section 4.2.3.

4. 'General classification of ferromagnetic oxide materials and definitions of terms', *International Electrotechnical Commission, Publication 125*, Geneva, (1961), Amend. no. 1, (1965).
5. BROCKMAN, F. G., DOWLING, P. H. and STENECK, W. G., 'Dimensional effects resulting from a high dielectric constant found in a ferromagnetic ferrite', *Phys. Rev.*, **77**, 85, (1950).

Section 4.2.4.

PARTRIDGE, N., 'Harmonic distortion in audio-frequency

transformers', *Wireless Engr.*, **19**, Part 1, 394, Part 2, 451, (1942).

Section 4.3.1.

6. BOZORTH, R. M. and CHAPIN, D. M., 'Demagnetizing factors of rods', *J. appl. Phys.*, **13**, 320, (1942).
7. STÄBLEIN, F. and SCHLECHTWEG, H., 'Über den Entmagnetisierungsfaktor zylindrischer Stäbe', *Z. Phys.*, **95**, 630, (1935).
8. WARMUTH, K., 'Über den ballistischen Entmagnetisierungsfaktor zylindrischer Stäbe', *Arch. Elektrotech.*, **33**, 747, (1939), and, **41**, 242, (1954).

Sections 4.3.5. and 4.3.6.

9. VAN SUCHTELEN, H., 'Ferrocube aerial rods', *Electron. appl. Bull.*, **13**, 88, (1952).

Inductors

5.1. INTRODUCTION

Inductors are used as elements in frequency-selective circuits in a wide variety of electronic equipment, ranging from telephony^{1, 2} to domestic radio^{3, 4} and television. The performance requirements vary accordingly, but it is in filters for carrier telephony equipment that the most exacting applications are to be found. In a typical carrier telephony terminal there may be several hundred filters and equalizers on a single rack.^{5, 6} Because inductors constitute such a large proportion of the cost and volume of such equipment it follows that a high order of performance is required. The high quality inductor has therefore been evolved mainly to meet the needs of the telephone industry. Current practice is for such inductors to use ferrite cores and it is with this class of inductor that the present chapter is concerned. Other classes of inductor, generally having less stringent requirements, are covered by the general treatment. For example, inductors for radio and television receivers are usually air-cored or have simple cylindrical cores; although they are outside the present scope, much of this chapter and Chapter 10 is relevant to their design.

Before considering the theory and practice of inductor design in detail it may be useful to survey the requirements of a high-quality inductor. The basic requirement of the network designer is usually an inductance-capacitance

combination which, ideally, resonates at the correct frequency irrespective of time or environmental conditions, which has negligible energy loss and which involves the smallest possible volume and cost. The capacitor is by no means a perfect partner in this alliance and its properties must be taken into account when considering the design of the inductor.

The requirements of the network may be translated into the following general inductor requirements:

- (a) an inductance value which, once adjusted, is substantially constant at a given temperature during the service life of the equipment
- (b) a temperature coefficient of inductance that is within close limits about an appropriate nominal value
- (c) very low electrical and magnetic losses
- (d) small cost and volume.

Before considering the problems of satisfying these requirements it will be useful to amplify them and make them more specific.

Inductance

The network calculation usually yields precise inductances and capacitances. The capacitors are usually supplied having nominal values equal to the required

values; the tolerance is normally small, e.g. $\pm 2\%$. The inductor is designed to have a nominal inductance that is also equal to the required value but it must, in accordance with current practice, be adjustable so that the correct LC product may be obtained. The adjustment range must be adequate, i.e. it must at least equal the sum of the tolerances for which it must compensate. These are typically $\pm 2\%$ for the capacitor, $\pm 1\%$ for stray capacitance, an allowance for the effect of winding geometry and the integral increments in the number of turns, and the tolerance on the effective permeability of the inductor. An adjustment range of $\pm 7\%$ is typical. Within this range the resolution of adjustment must be such that the resonant frequency may be set to an accuracy of about ± 100 ppm.

The values of the inductor and capacitor will in general change as functions of temperature, time, etc. These unwanted changes are called variability. To some extent the variability of the inductor may be reduced by increasing the air gap to lower the effective permeability (see Section 4.2.2). Perhaps the least difficult aspect of variability is the temperature coefficient. From the circuit point of view it is the total change of the LC product over a given temperature range that is important; the temperature coefficient of the LC product may typically be limited to 0 ± 100 ppm/ $^{\circ}\text{C}$ although in more severe cases the tolerance may be half this value. Typical limits for the temperature coefficient of inductance might be $+50$ to $+150$ ppm/ $^{\circ}\text{C}$ but again smaller tolerances are often required.

A typical requirement for the long-term constancy of the LC product is that it should not change by more than $\pm 0.1\%$ over a service life of twenty years. The corresponding limit for inductance drift might be ± 500 ppm/ $^{\circ}\text{C}$.

Q-factor

A high Q -factor for a given volume is nearly always desirable because this enables a better network (e.g. a filter with a lower pass-band insertion loss or a sharper cut-off characteristic) to be made from a given number of inductors or alternatively a given attenuation/frequency characteristic to be obtained with fewer inductors. At the higher frequencies, i.e. greater than a few tens of kHz, the inductor is usually designed to have the maximum Q -factor at a given frequency and in a given volume. At lower frequencies it is not usually possible to achieve maximum Q -factor without an unreasonable increase of variability. This is because a maximum Q -factor would require a high value of effective permeability in order to achieve a balance between the winding and core losses. Thus high Q -factor and low variability are often incompatible requirements; they are also to

some extent interchangeable. If the Q -factor is made high at the expense of stability then a sharp cut-off or resonance may be obtained but a sufficiently large margin or guard-band must be provided to allow for frequency drift. In such a case, the high Q -factor may to some extent be wasted, and a similar overall performance might be obtained using a larger air gap which, although it would result in a lower Q -factor, would give increased stability; the cut-off frequency or resonance will be less sharp but a smaller guard-band will be needed.

Q -factors currently specified for inductors range from 50 at frequencies below 300 Hz, through values of 500 to 1000 at 100 kHz, falling to the region of 200 at 20 MHz.

Hysteresis effects

The effects of hysteresis are, of course, required to be as small as possible. Usually filter inductors are operated at very low amplitudes and the loss contribution due to hysteresis is negligible (however this is not always true when making measurements of inductor Q -factor and precautions must be taken to ensure that the measuring voltage corresponds to a sufficiently low flux density). Other effects of hysteresis are the increase of inductance with amplitude and the introduction of waveform distortion. The former effect is not usually serious at the flux densities normally employed, but again care must be taken that the amplitude used during inductance adjustment is not too high or an erroneous inductance value will be obtained. Usually the most important effect of hysteresis is waveform distortion which gives rise to the generation of harmonics and intermodulation products. These may be particularly troublesome where a large difference in power levels exists between two separate signals in the same circuit, e.g. at the common connections of two-wire line filters. In such a case an inductor may need to have a hysteresis factor of less than 0.1 (see Eqn 4.41); in contrast a value of 8 is typical of the more usual design of filter inductors.

Miscellaneous

It is usually required that the magnetic coupling between adjacent inductors shall be very small. Precise requirements cannot be stated but it appears that a voltage ratio of between 50 and 70 dB measured between equal windings on adjacent inductors normally is acceptable.

Among the features that facilitate the design and construction of inductors are the following; an adequate range of sizes and effective permeabilities, simple provision for windings and lead-out wires, and simple but effective means of assembly, terminating and mounting.

5.2. FORM OF CORE

Until the introduction of ferrites, the inductors used in telecommunication equipment used almost exclusively the various grades of powdered iron, or nickel iron, cores. Because of the low bulk permeability, adequate magnetic isolation between adjacent inductors could be achieved only by the use of toroidal cores. Such cores

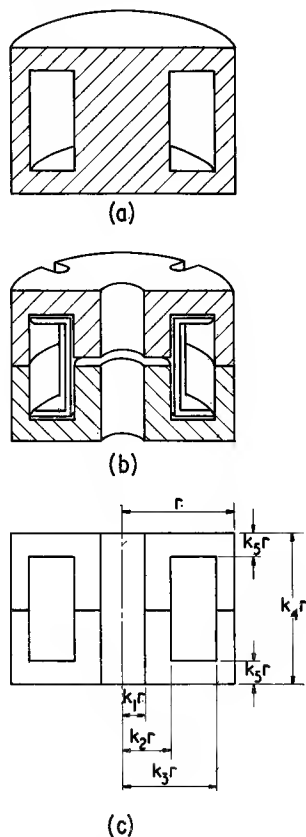


Fig. 5.1. The geometry of a ferrite pot core: (a) basic shape, (b) a practical design, (c) symbols used in analysis

present some winding and adjustment problems. When ferrites, which have relatively high permeabilities, were introduced on a commercial scale it became possible to make magnetic circuits of more convenient shape whilst maintaining a high degree of magnetic screening. One of the most successful of the forms of ferrite core so far developed for inductors is shown in Fig. 5.1(a). It is called a pot core and is essentially a cylinder of ferrite having an enclosed annular space for the winding. In practice this basic shape is modified in detail; a typical

core is shown in Fig. 5.1(b). It usually consists of two similar half pot cores having the mating surfaces finely ground to ensure a stable magnetic joint of low reluctance. An air gap is usually provided by grinding back one or both of the centre core faces. Slots or holes are provided in the outer wall so that the terminal leads of the winding may be brought out and it is usual to provide a central hole to facilitate adjustment of the inductance. There are, of course, other forms of ferrite inductor core. One, which has been derived from the pot core, is included in Plate 5.1. This is an X-core and because of its adequate provision for terminations it is used mainly for inductors or transformers having many connections.

Before considering the best design of an inductor on a given core the main considerations in the design of the core itself will be discussed briefly in the light of the requirements noted at the beginning of this chapter.

A high Q -factor implies a low magnetic loss in the ferrite and also that the shape of the core utilizes the core material to the best advantage. Assuming a given ferrite material, the problem is to find the proportions of the core that will give the highest performance. The criterion of performance may vary from one application to another but over a wide range of inductances and frequencies it is true that the core which can contain a winding giving the lowest ratio of d.c. resistance to inductance has the best over-all performance (see Section 5.7.8). In the following analysis the simple pot core shape is assumed and the optimum proportions of the core are derived according to the above criterion.

Using the symbols defined in Fig. 5.1(c) the ratio of the d.c. winding resistance to the inductance, R_{dc}/L , may be expressed in terms of the core proportions k_1 to k_5 . The inductance of N turns on a pot core with an effective permeability μ_e is (see Eqn 4.23):

$$L = \frac{\mu_0 \mu_e N^2}{C_1} \quad \text{H} \quad (5.1)$$

where C_1 is the core factor and is defined after Eqn 4.8. The resistance of the same winding, assumed to be wound with copper conductor having resistivity ρ_c , is given (see Eqn 11.11) by

$$R_{dc} = \frac{\rho_c N^2 l_w}{A_a F_a} \quad \Omega \quad (5.2)$$

where l_w is the mean turn length $= \pi r(k_2 + k_3)$

A_a is the window area $= r^2(k_4 - k_2)(k_4 - 2k_5)$ (see Fig. 11.1)

F_a is the overall copper factor

$$= \frac{\text{total copper cross section}}{A_a}$$

The winding is assumed to fill a hypothetical coil former so that the overall copper factor may be con-

$$(5.1) \quad L = \frac{4\pi\mu_e N^2}{C_1} \times 10^{-9} \quad \text{H}$$

sidered to be independent of the core proportions. It is also assumed that the spaces between the core and the inner and outer surfaces of the winding are equal.

$$\text{Then } \frac{R_{dc}}{L} = \frac{\pi \rho_c (k_2 + k_3)}{F_a r (k_3 - k_2) (k_4 - 2k_5) \mu_0 \mu_e} \frac{C_1}{\Omega \cdot H^{-1}} \quad (5.3)$$

where the core factor C_1 is a function of k_1 to k_5 and may be calculated by analogy with Fig. 4.2. An example of such a calculation is given in Appendix B. If $(C_1)_1$ denotes the core factor for a core of the same proportions but of unit radius then since the dimensions of C_1 are $[\text{length}]^{-1}$

$$C_1 = \frac{(C_1)_1}{r}$$

\therefore Eqn. 5.3 becomes

$$\frac{R_{dc}}{L} = \frac{\pi \rho_c}{F_a \mu_0 \mu_e r^2 (k_3 - k_2) (k_4 - 2k_5)} (C_1)_1 \quad \Omega \cdot H^{-1} \quad (5.4)$$

For a given set of core proportions, i.e. a given set of values for k_1 to k_5 , R_{dc}/L will vary inversely as the square of the linear dimensions since r^2 is in the denominator. The effect of size may be removed by multiplying through by $V_T^{2/3}$ where V_T is the overall volume i.e. $\pi r^3 k_4$:

$$\frac{R_{dc} V_T^{2/3}}{L} = \frac{\pi \rho_c}{F_a \mu_0 \mu_e (k_3 - k_2) (k_4 - 2k_5)} (\pi k_4)^{2/3} (C_1)_1 \quad \Omega \cdot H^{-1} \quad (5.5)$$

This expression may be minimized with respect to the proportionality factors, k_2, \dots, k_5 , remembering that $(C_1)_1$ is a function of these factors. Thus the proportions for optimum utilization of a given volume may be found. An alternative approach would be to fix the height and diameter arbitrarily and to calculate the remaining proportions. It should be noted that k_1 , the normalized radius of the central hole, is not a variable in this problem. Its value should ideally be zero but in practice the smallest value consistent with an adequate means of adjustment must be chosen.

Table 5.1 shows the results obtained using two arbitrary values of k_1

These proportions may be modified slightly in practice. The provision of slots for the lead-out wires will result in a small correction. Again, as the minimum value of

R_{dc}/L obtained by the variation of any one proportion is rather shallow, it is possible to shift the proportions marginally away from optimum to obtain some other advantage. For example, if the centre core radius is increased by 5% this might result in only 1% degradation in R_{dc}/L , but the centre core cross-sectional area increases by at least 10% and this will produce a significant improvement in the hysteresis factor. Alternatively, for a small pot core to be used mainly at the higher frequencies, it might be decided to reduce the centre core diameter

Table 5.1. POT CORE PROPORTIONS FOR MINIMUM R_{dc}/L
(SEE FIG. 5.1.(c))

k_1	k_2	k_3	k_4	k_5
0	0.390	0.840	1.30	0.226
0.210	0.442	0.854	1.17	0.206

slightly to obtain a better spacing of the winding from the core. Whatever approach is adopted Eqn 5.5 provides a means of assessing the effect of changes of core proportions on R_{dc}/L for a fully wound coil.

The actual dimensions as distinct from the proportions depend on the sizes chosen. Table 5.2 gives the approximate diameters and heights of two standard ranges of pot cores each having approximately logarithmic progression of diameters, volumes and values of R_{dc}/L . The derived parameters (Section 4.2.1) are also given.

5.3. AIR GAP AND THE CALCULATION OF INDUCTANCE

The effect of an air gap on core properties in general is discussed in Section 4.2.2. In practice the air gap in an inductor core is provided during manufacture. Originally it was common for a given size of pot core to be available with a number of standard air gap lengths. This was inappropriate because the designer is not directly interested in gap length but rather in the effect of the air gap. It is now common practice for the gap to be adjusted to give one of a series of standard values of effective permeability or, alternatively, standard values of some factor relating inductance and number of turns.

The effective permeability, μ_e , is defined in the derivation of Eqn 4.23. It is subsequently shown that this is a property on which much of the core performance depends,

$$(5.3) \quad \frac{R_{dc}}{L} = \frac{\rho_c (k_2 + k_3)}{F_a r (k_3 - k_2) (k_4 - 2k_5)} \frac{C_1 10^9}{4 \mu_e} \quad \Omega \cdot H^{-1}$$

$$(5.4) \quad \frac{R_{dc}}{L} = \frac{\rho_c 10^9}{4 F_a \mu_e r^2 (k_3 - k_2) (k_4 - 2k_5)} (C_1)_1 \quad \Omega \cdot H^{-1}$$

$$(5.5) \quad \frac{R_{dc} V_T^{2/3}}{L} = \frac{\rho_c 10^9}{4 F_a \mu_e (k_3 - k_2) (k_4 - 2k_5)} (\pi k_4)^{2/3} (C_1)_1 \quad \Omega \cdot H^{-1}$$

Table 5.2. STANDARD POT CORE RANGES

The table gives the principal physical dimensions together with approximate core factors, effective dimensions and values of R_{dc}/L . Allowance has been made for slots; four in those pot cores having dimensions of 14mm or larger and two in the smaller cores.

MULLARD 'VINKOR' RANGE			In accordance with BS 4061, range 1					
Nominal Overall Dimensions		Overall Volume	Core factors		Effective dimensions			
			$C_1 = \Sigma l/A$	$C_2 = \Sigma l/A^2$	$l_e = C_1^2/C_2$	$A_e = C_1/C_2$	$V_e = C_1^3/C_2^2$	R_{dc}/L^*
Dia.	Height							
mm	mm	mm ³	mm ⁻¹	mm ⁻³	mm	mm ²	mm ³	Ω/H
10.0	6.8	0.534×10^3	1.02	77.3×10^{-3}	13.4	13.2	0.177×10^3	1029
12.0	7.8	0.882×10^3	0.800	40.0×10^{-3}	16.0	20.0	0.321×10^3	696
14.0	9.0	1.38×10^3	0.720	27.8×10^{-3}	18.7	25.9	0.484×10^3	564
18.0	11.2	2.85×10^3	0.558	12.6×10^{-3}	24.7	44.3	1.09×10^3	346
22.5	13.6	4.94×10^3	0.425	5.88×10^{-3}	30.7	72.3	2.22×10^3	228
25.4	16.0	8.11×10^3	0.364	3.64×10^{-3}	36.4	99.9	3.63×10^3	162
29.5	18.8	12.8×10^3	0.283	1.88×10^{-3}	43.2	153	6.59×10^3	119
35.5	22.8	22.6×10^3	0.236	1.06×10^{-3}	52.5	223	11.7×10^3	79.4
45.0	29.2	46.4×10^3	0.187	0.518×10^{-3}	67.5	361	24.3×10^3	47.2

I.E.C. RANGE			In accordance with IEC Publication 133 and BS 4061, range 2					
Nominal Overall Dimensions		Overall Volume	Core factors		Effective dimensions			R_{dc}/L^*
			$C_p = \Sigma l/A$	$C_2 = \Sigma l/A^2$	$l_e = C_1^2/C_2$	$A_e = C_1/C_2$	$V_e = C_1^3/C_2^2$	
Dia.	Height							
mm	mm	mm ³	mm ⁻¹	mm ⁻³	mm	mm ²	mm ³	Ω/H
9.2	5.25	0.349×10^3	1.24	123×10^{-3}	12.5	10.1	0.126×10^3	1390
11.1	6.5	0.628×10^3	0.956	59.0×10^{-3}	15.5	16.2	0.251×10^3	898
14.05	8.35	1.29×10^3	0.794	31.9×10^{-3}	19.9	24.9	0.496×10^3	548
18.0	10.55	2.68×10^3	0.623	14.8×10^{-3}	26.2	42.0	1.10×10^3	338
21.6	13.4	4.91×10^3	0.519	8.45×10^{-3}	31.9	61.4	1.96×10^3	230
25.5	16.1	8.22×10^3	0.416	4.53×10^{-3}	38.2	91.9	3.51×10^3	165
30.0	18.8	13.3×10^3	0.343	2.58×10^{-3}	45.7	133	6.09×10^3	116
35.5	21.7	21.5×10^3	0.275	1.42×10^{-3}	53.6	194	10.4×10^3	82.2
41.2	29.4	39.2×10^3	0.265	1.01×10^{-3}	69.2	262	18.1×10^3	51.5
			(= 2.65cm ⁻¹)	(= 1.01cm ⁻³)				

*Calculated according to Eqn 5.3, putting $\rho_e = 1.694 \times 10^{-8} \Omega\text{m}$, $\mu_e = 100$ and $F_s = 0.3$.

e.g. the temperature coefficient and the residual loss factor are proportional to μ_e . If therefore a range of pot cores of various sizes are available with effective permeabilities taken from a series of standard values, the inductor design is simplified because the designer may readily translate a trial design from one size of core to another in the range and expect to find the same values of μ_e available. A logarithmic progression of preferred numbers is often used.

There are in common use two factors relating the inductance to the number of turns on a given core. The turns factor, α , is the number of turns required to obtain a given inductance, usually 1 mH.

$$\text{Since } L = \frac{\mu_o \mu_e N^2}{C_1} \times 10^3 \quad \text{mH}$$

$$N = \sqrt{\left[\frac{C_1 L 10^{-3}}{\mu_o \mu_e} \right]}$$

Therefore by the definition of α

$$N = \alpha \sqrt{L} \quad (5.6)$$

where L is in millihenries

If C_1 is in mm^{-1}

$$\alpha = \sqrt{\left[\frac{C_1}{\mu_o \mu_e} \right]} \text{ turns for 1 mH} \quad (5.7)$$

$$(5.7) \quad \alpha = 10^3 \sqrt{\left[\frac{C_1}{4\pi \mu_e} \right]} \text{ turns for 1 mH}$$

where C_1 is in cm^{-1}

The alternative factor is the inductance factor, A_L . This is the inductance in nanohenries per turn² on a given core i.e.

$$L = A_L N^2 \quad (5.8)$$

where L is in henries $\times 10^{-9}$

Thus $L = A_L N^2 10^{-9} \quad \text{H}$

$$= \frac{\mu_0 \mu_e N^2}{C_1}$$

If C_1 is in mm^{-1} then

$$A_L = \frac{\mu_0 \mu_e 10^6}{C_1} \quad \text{nH for 1 turn} \quad (5.9)$$

It follows that since

$$L = \frac{N^2}{\alpha^2} \times 10^{-3} = A_L N^2 \times 10^{-9} \quad \text{H}$$

$$\alpha = \frac{10^3}{\sqrt{A_L}} \quad (5.10)$$

It should be noted that whereas α and A_L are susceptible to precise measurement and may therefore be stated within given limits, the value of μ_e may only be deduced, in practice, from a knowledge of α or A_L and a somewhat arbitrary calculation of the core factor C_1 . Therefore the true value of μ_e is not generally known for a core such as a pot core in which the geometry of the flux path is complicated. A nominal value is quoted and this is calculated from a value of C_1 obtained according to a standard formula such as that shown in Appendix B. In practice, however, the nominal value of μ_e is sufficiently reliable to enable the performance of a gapped core to be estimated from the material parameters with reasonable accuracy.

As stated above, some manufacturers use standard values of μ_e . Others use standard values of turns factor or inductance factor, notably the latter. This approach is useful when the main emphasis of the inductor design is on calculating the number of turns and specifying the inductance. However, the value of A_L or α does not characterize the pot core as usefully as the value of μ_e .

Where a means of inductance adjustment is to be provided the air gap length is sometimes chosen so that the standard value of μ_e or A_L is obtained at the centre of the range of adjustment. Alternatively it may refer to the pot core without the adjuster.

Considering tolerances, the absolute grinding accuracy obtained when the air gap is introduced during manufacture is not dependent on the gap length. Therefore a

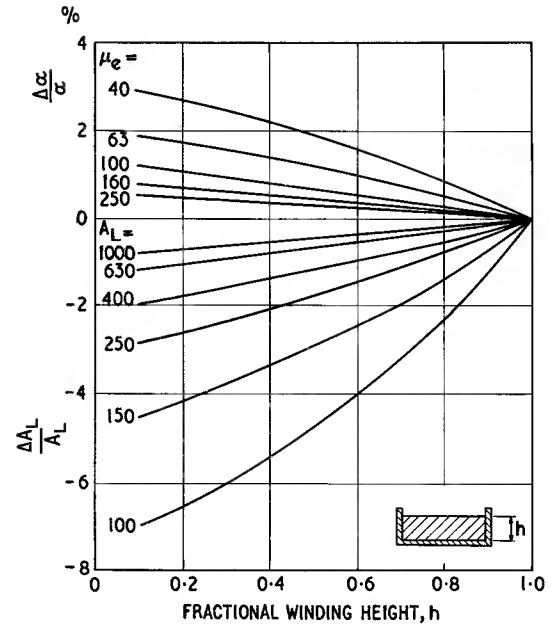


Fig. 5.2. Dependence of α and A_L on winding height for a 25 mm pot core

better fractional tolerance on length is obtainable for large air gaps, i.e. low effective permeabilities, than for small air gaps. Typical tolerances on α range from $\pm 1\%$ for $\mu_e = 40$ to $\pm 2\%$ for $\mu_e = 250$. The corresponding tolerances for μ_e or A_L would be twice these values.

The value of α or A_L measured on a given pot core depends to some extent on the disposition of the winding in the winding space. Reasonably reproducible results may be obtained if the coil former is wound full. Fig. 5.2 illustrates typical variations of α and A_L values with winding height. The specified values of α or A_L usually relate to a winding specially defined for the purpose of testing. Ref. 7 considers the case of fractional turns.

5.4. INDUCTANCE ADJUSTMENT

A variety of methods have been used in the past for adjusting the inductance of the pot core inductor and even a larger variety of methods have been proposed. There are now virtually only two basic methods in current practice. One is to shape the centre cores asymmetrically; a possible geometry is shown in Fig. 5.3(a). If one half of the core is rotated relative to the other half a change of effective permeability occurs. This

$$(5.9) \quad A_L = \frac{4\pi\mu_e}{C_1} \quad \text{nH for 1 turn}$$

where C_1 is in cm^{-1}

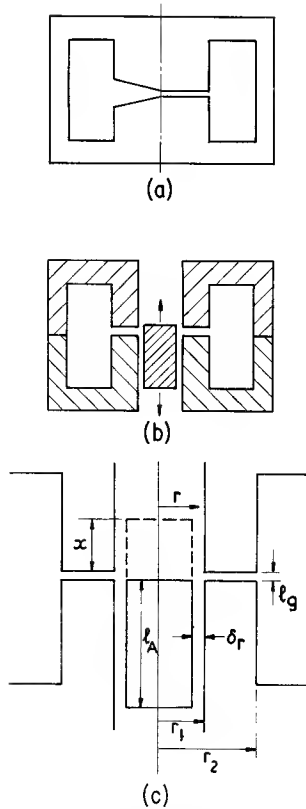


Fig. 5.3. Ferrite pot core adjustment: (a) adjustment by chamfered centre core; (b) adjustment by magnetic shunt; (c) symbols used in analysis of magnetic shunt

method depends on the redistribution of the fringing field; if the flux lines were all parallel to the axis no change would be obtained as the mean length and geometric cross-section of the air gap are unchanged. The disadvantage of this method is that the inductance must be set before the assembly of the pot core is finally secured and mounted with the rest of the circuit, and subsequent adjustment is difficult. The other method is far more widely used so it will now be described in some detail with reference to Fig. 5.3(b) and (c).

A cylindrical magnetic core is introduced into a central hole so that it partially shunts the air gap. If the axial position is varied the effective reluctance of the air gap is changed and with it the inductance of a winding on the pot core.

A simplified analysis will indicate the salient features of the method. It is assumed that the reluctance of the cylinder is negligible compared with the air gap surrounding it (in practice this is true if its permeability is greater than about 100). It is also assumed that the main air gap length l_g is so small that it is negligible compared with length l_A of the shunt, and that fringing in the absence of the shunt is zero so that the magnetic area of the air gap is $A_g = \pi(r_2^2 - r_1^2)$

\therefore Reluctance of the air gap without the shunt

$$= \frac{l_g}{A_g} \quad (5.11)$$

The reluctance in parallel with this when the shunt is in the position shown by the broken line, i.e. a distance x beyond the main air gap is:

$$\frac{\delta r}{2\pi r x} + \frac{\delta r}{2\pi r (l_A - x)}$$

(where δr is the path length of the radial gap between the shunt and the hole, and r is the mean radius of this gap).

$$\text{Therefore this shunt reluctance} = \frac{\delta r}{2\pi r} \cdot \frac{l_A}{x(l_A - x)} \quad (5.12)$$

It should be noted that this varies from ∞ when $x = 0$, through a minimum when $x = l_A/2$ (as may be shown by differentiation) to ∞ again when $x = l_A$

The minimum value is

$$\frac{\delta r}{2\pi r} \cdot \frac{4}{l_A} \quad (5.13)$$

The smaller this value is, the larger will be the total adjustment range, assuming a given value for l_g and assuming that the shunt starts from the all-out position. Thus to increase the adjustment range δr should be small and r and l_A should be large. The total air gap reluctance is obtained from the parallel combination of the reluctances given by Eqns 5.11 and 5.12, i.e.

$$\frac{\frac{\delta r l_A}{2\pi r x (l_A - x)} \times \frac{l_g}{A_g}}{\frac{\delta r l_A}{2\pi r x (l_A - x)} + \frac{l_g}{A_g}} = \frac{\delta r l_A l_g}{\delta r l_A A_g + 2\pi r x l_g (l_A - x)}$$

From Eqn 4.25, the resultant effective permeability is given by

$$\mu_e = C_1 \times \left[C_1/\mu + \frac{\delta r l_A l_g}{\delta r l_A A_g + 2\pi r x l_g (l_A - x)} \right]^{-1} \quad (5.14)$$

and the extreme values are

$$\left. \begin{aligned} (\mu_e)_{\min} &= \frac{C_1}{C_1/\mu + l_g/A_g} \quad \text{and} \\ (\mu_e)_{\max} &= \frac{C_1}{C_1/\mu + l_g/(A_g + \pi r l_g l_A/2\delta r)} \end{aligned} \right\}$$

Fig. 5.4 shows the change of effective permeability as a function of x calculated from the Eqn 5.14 assuming a typical pot core. The corresponding curve measured on the same pot core is also given. The divergence at the lower end is due to the fact that the shunt begins to reduce the effective air gap before it has crossed the lower boundary of the actual air gap. This fringing effect is ignored in the analysis. If it is desired to allow for the

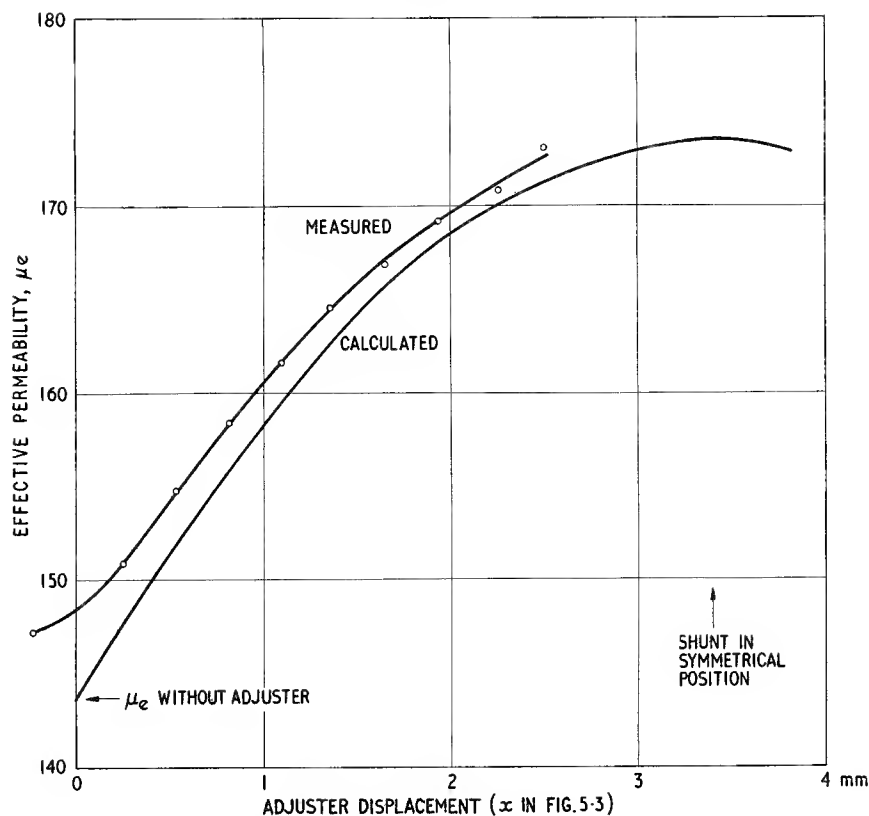


Fig. 5.4. Calculated and measured adjustment curves for a 25 mm pot core having nominal $\mu_e = 160$

effect of a low permeability shunt then its effective reluctance may be added to Eqn 5.12. This reluctance will be approximately of the form $kl_A/\mu A_A$ where l_A , μ and A_A refer to the shunt and k is a factor, less than 1, to allow for the non-uniform flux distribution in the shunt.

The adjustment range obtained with a given shunt in a given pot core depends on the length of the main air gap; the larger the air gap the greater the adjustment range (see Eqn 5.14). When the effective permeability is high, i.e. the main air gap is small it is sometimes difficult to achieve a sufficient adjustment range. For this reason it is desirable to make the radial clearance between the shunt and the pot core as small as possible and the length of the shunt as long as possible. Increasing the permeability of the shunt does not help because, as stated earlier, when it exceeds about 100 the reluctance of the shunt itself becomes negligible. At the other extreme, a low effective permeability may result in a larger adjustment range than the minimum required. This in itself is not an undesirable feature. However, it is accompanied by an increase of the maximum slope for the adjustment curve and if this is allowed to become too large the stability of inductance with temperature and

time will suffer. Accordingly it is usual to limit the maximum slope. This may conveniently be done by using a shunt of very low permeability or by increasing the radial clearance.

In the introduction to this chapter, reference was made to the minimum range of adjustment needed to ensure that the required LC product may be obtained, allowing reasonable manufacturing tolerances on parameters affecting the LC product. A typical minimum range is 14% (total) made up as follows: $\pm 3\%$ for the tolerance of A_L , $\pm 2\%$ for the tolerance of the resonating capacitor and $\pm 2\%$ margin for miscellaneous contributions such as stray capacitance. It was noted in Section 5.3 that the tolerance of μ_e depends on its value, the higher the value of μ_e the larger the tolerance. This effect aggravates the difficulty of obtaining sufficient adjustment range with the higher μ_e values; even where variability is not a limiting factor lack of adjustment range will normally prevent the use of high effective permeabilities, e.g. 400, for inductor cores.

The number of turns required on a winding to give any nominal inductance will, in general, be non-integral when calculated from the nominal α or A_L value. The nearest integral number of turns will give an in-

ductance that differs from the required value and this difference must also be taken up by the adjuster. Normally this is a negligibly small amount, but for low inductances requiring relatively few turns the possible difference will be appreciable and extra adjustment range will be necessary if gaps in the range of attainable inductances are to be avoided; e.g. if the required inductance lies mid-way between values given by 9 and 10 turns respectively, an extra margin of about $\pm 10\%$ is necessary. Low inductances are required mainly at high frequencies and at these frequencies low effective permeabilities are used to obtain optimum Q -factors. The low μ_e values are usually accompanied by large adjustment ranges, so to some extent the extra margin occurs naturally. For very low inductances, the gaps between integral turn values may only be bridged by having available several pot cores with closely spaced effective permeabilities. These permeabilities are chosen so that the corresponding net adjustment ranges just overlap thus providing, in effect, a very wide range of adjustable inductance obtainable with a given number of turns.

Fig. 5.5 shows three typical adjusting arrangements. In the first the shunt is in the form of a tube carried on a resilient plastic carrier. This carrier is an easy sliding fit in the hole. When rotated by a screwdriver engaged with the slot at the top of the carrier the shunt moves axially along the stud. The latter has a fine thread which gives good adjustment accuracy. There is no prepared thread in the plastic; the thread form is impressed by that of the stud. This arrangement gives a shake-proof adjustment that is free of backlash. In manufacture the plastic carrier is injection moulded with the tube located in the mould so that the surface of the tube is held concentric with the axis of the plug. This results in concentric rotation in use and enables δr to be made very small.

The next arrangement illustrated consists of a tube carried by a plastic screw. Usually the screw has a prepared thread but sometimes it makes its own thread when it is screwed into the threaded bush. In some variations the tube is merely cemented into position on the screw. This is simple but if the tube has an eccen-

tric bore then the rotation becomes eccentric. Alternatively the tube may have the screw injection moulded through it in a similar way to the first design. A disadvantage of this example is that the position of the tube relative to the gap depends on a length of unsupported plastic and if this is dimensionally unstable inductance instability will result.

In the third example a threaded cylindrical shunt is used and this cuts its own thread into a plastic sleeve which lines the hole. Here again the position of the shunt depends on a length of unsupported plastic. The design is simple and the action is concentric but the interposition of the sleeve between the threaded shunt and the pot core prevents the value of δr from being made very small.

In practice all three methods, and other similar ones, can give satisfactory results.

5.5. CONSTANCY OF INDUCTANCE

5.5.1. General

In the introduction to this chapter it was observed that constancy of the LC product is one of the most important requirements of a resonant circuit. The change of inductance (and capacitance) with time should be made as small as possible and the change of inductance with temperature should, ideally, balance exactly any corresponding change in capacitance.

These changes in inductance are sometimes referred to as variability. The variability may originate in the ferrite or it may be due to the non-ferrite parts of the inductor. In either case it may be reversible, e.g. a function of temperature, or irreversible, e.g. drift with time.

It is not too difficult to make a ferrite-cored inductor with a fairly small variability, i.e. having a temperature coefficient of inductance which is within 50 ppm/ $^{\circ}\text{C}$ of the required value and a long-term drift of less than 0.1%. However if a performance substantially better than this is required great care must be taken in the

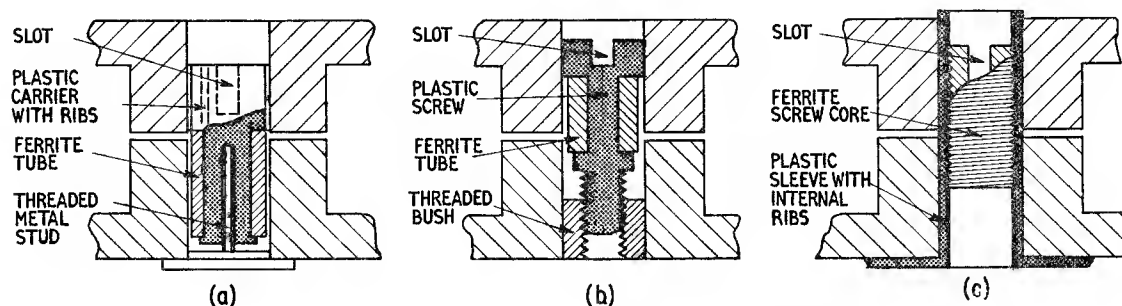


Fig. 5.5. Typical adjusters using the principle of the magnetic shunt

design and construction of the inductor assembly. There are many factors which contribute small changes of inductance and they are difficult to diagnose and remedy. Much work has been done on this subject and as a result appreciable reductions in inductance variability have been obtained. Indeed, it is now possible to make *LC* circuits with a sufficiently high performance to use them in networks which previously could only be realised with crystal resonators.

In this section the main factors affecting inductance variability will be considered and some typical experimental results will be shown.

5.5.2. Variability due to the ferrite

The contribution of the ferrite material to the variability of inductance depends on the constancy of the material permeability. The methods of expressing the variability of a magnetic core have been considered in Sections 2.2.2 and 4.2.2. In general the permeability may vary reversibly or irreversibly with temperature and it may vary with time, flux density, frequency, polarizing field strength and mechanical stress. The characteristics of some of these variations have been described in Chapter 3. In ferrites intended for high quality inductors the unwanted variations of permeability are kept to a minimum by manufacturing control.

In a ferrite-cored inductor, any change in the value of the material permeability will be reduced in its effect on the inductance by the dilution ratio, μ_e/μ_i , as shown by Eqn 4.31. Although several aspects of inductor design are influenced by the choice of μ_e it often happens, particularly at low frequency, that the value is governed mainly by the inductance constancy requirements.

The permeability is a function of temperature and provided the rate of temperature change is not too great, and other disturbances are avoided, this function may be regarded as reversible. In Fig. 3.8 there are a variety of $\mu-\theta$ graphs. In general these are not linear but they are usually taken to be so over a restricted temperature range. As described in Section 4.2.2 the temperature dependence of permeability is normally expressed as a temperature factor, T.F. This is the average material temperature coefficient, T.C., obtained from measurements at each end of the temperature range, divided by the material permeability, see Eqn 4.32. The temperature coefficient of an ideal gapped core made of the same material is $(\text{T.F.}) \times \mu_e$. The T.F. will have a nominal value and limits, and the corresponding nominal value and limits of the effective temperature coefficient may in principle be reduced or adjusted by the appropriate choice of μ_e .

Ferrite inductors are often resonated with polystyrene foil capacitors and the temperature coefficients of the two

components can be made to compensate partially. The T.C. of a polystyrene capacitor may range from -90 to -210 ppm/ $^{\circ}\text{C}$ although it is possible to obtain closer limits, e.g. -115 to -145 ppm/ $^{\circ}\text{C}$. A ferrite pot core intended to be used with such a capacitor might have $(\text{T.F.}) = (1 \pm 0.5) \times 10^{-6}/^{\circ}\text{C}$; if it had $\mu_e = 100$, the corresponding limits of T.C. would be $+50$ and $+150$ ppm/ $^{\circ}\text{C}$. The corresponding limits of T.C. for the *LC* product using the smaller tolerance capacitor would be -95 and $+35$ ppm/ $^{\circ}\text{C}$ and the limits on the temperature coefficient of resonant frequency would be -47.5 and $+17.5$ ppm/ $^{\circ}\text{C}$. If this tolerance is not acceptable then the nominal and limit values of the material T.F. must be specified more closely to improve the compensation.

Another type of capacitor often used is the silvered mica capacitor. This has a small temperature coefficient; typical limits are zero and $+30$ ppm/ $^{\circ}\text{C}$. In this case a ferrite core having a $(\text{T.F.}) = 0 \pm 0.5 \times 10^{-6}/^{\circ}\text{C}$ might be selected, and if $\mu_e = 100$ the corresponding inductor T.C. would have the limits 0 ± 50 ppm/ $^{\circ}\text{C}$. Proceeding as before the corresponding temperature coefficient limits for the resonant frequency would be -25 and $+40$ ppm/ $^{\circ}\text{C}$. Again some improvement would be obtained if the nominal and limit values of the material T.F. could be more closely specified to improve the compensation.

Often it is more difficult to obtain a suitable nominal T.F. value than to reduce the tolerance. If the nominal compensation cannot then be improved by adjusting the effective permeability (perhaps due to loss considerations) then special T.C. compensating ceramic capacitors may be used. These have high values of positive or negative T.C. and constitute a small but appropriate fraction of the total resonating capacitance, the rest being made up of low-loss polystyrene or silvered mica capacitors. Even so, the ferrite T.F. must have a close tolerance if the overall T.C. of resonant frequency is to be within close limits.

Control of temperature factor is a major consideration in ferrite pot core manufacture. As manufacturing and control techniques improve it will become possible to specify nominal T.F. values more freely and to narrow the tolerances. The ultimate goal might be to manufacture inductor cores having T.F. values that correspond to the standard μ_e values to which the cores are to be gapped, so that an inductor core would have the same nominal temperature coefficient whichever standard μ_e value is used, i.e., $(\text{T.F.}) \times \mu_e = \text{constant}$.

The above discussion assumes that the permeability is an approximately linear function of temperature. As the slope of the function is made to approach zero at a particular temperature the curvature becomes pronounced (e.g. see Fig. 3.8.4). When there is considerable departure from linearity the concept of temperature coefficient is more difficult to apply. One approach is to divide the temperature range into zones within which the slope of the μ -temperature curve is within stated limits.

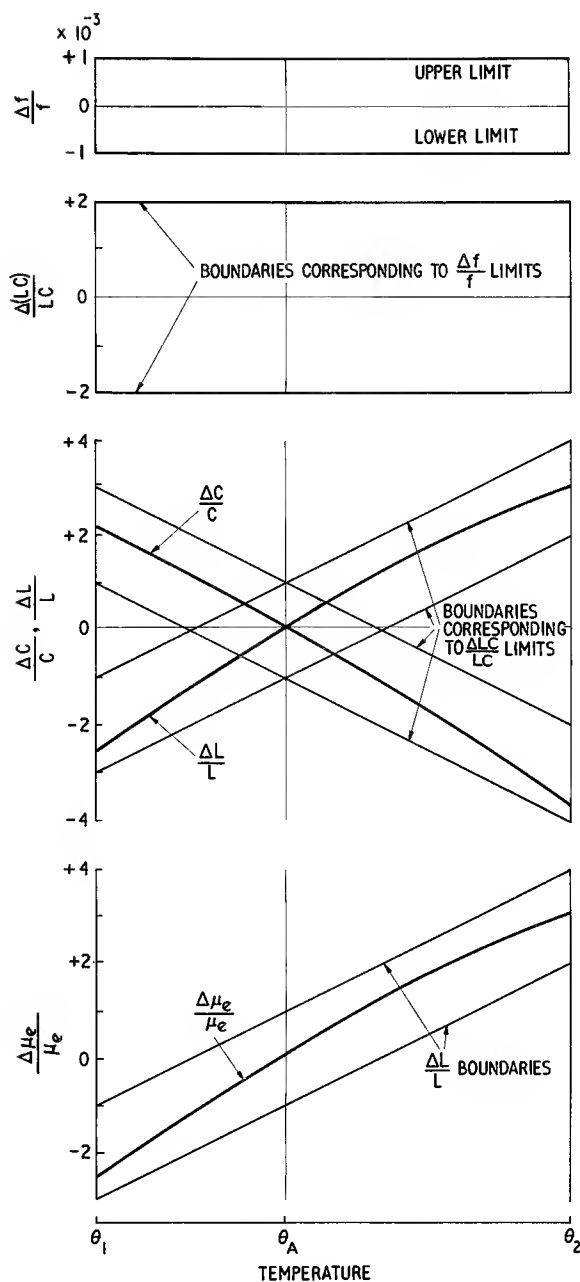


Fig. 5.6. Typical boundaries of temperature dependence of an LC circuit and its components. θ_A is the temperature at which the LC product is adjusted to the correct value

For more specific requirements it is perhaps better to consider graphical areas, bounded on each side by the temperature limits and at the top and bottom by lines defining the permissible limits of the temperature-dependent parameter. The basic parameter is resonant frequency. From such a representation the boundaries of the corresponding LC product area may be obtained and this may be split into areas defining the permissible limits of change of the inductance and capacitance values. In this way an unambiguous specification of temperature dependence of permeability may be derived. Fig. 5.6 illustrates this approach.

The next most important contribution of the material permeability to inductance variability is the time variation or disaccommodation.⁸ This phenomenon has already been considered in some detail (see Sections 2.2.2 and 4.2.2 and Fig. 3.10). Although time variation may be caused by any magnetic, thermal or mechanical disturbance, in the normal applications of telephony inductors the most common disturbance during assembly and subsequent service is temperature change. The permeability will rise above the stable value during the temperature disturbance and then when the temperature change ceases, it will return to the stable value appropriate to that temperature approximately in proportion to the logarithm of time. The effect is that a small overshoot on the permeability-time curve occurs when the temperature is raised from one steady value to another. The extent of this overshoot depends on the disaccommodation value of the material and the rate and magnitude of the temperature change. A temperature change of 50°C might produce a permeability overshoot of 1–2% in an ungapped core and, at constant temperature, a stable permeability would be substantially restored in about 24 h. The overshoot in a gapped core would be reduced by the dilution ratio. Under conditions of small irregular temperature excursions, such as might occur during service, the overall effect would be to raise the average permeability by an amount which would be quite small compared with the variations due to the temperature coefficient. Indeed natural temperature fluctuations prevent the permeability from ever approaching closely to the ultimate stable value. An obvious precaution during the manufacture of inductors is to ensure that an adequate interval (e.g. between one and three days) is left between any process involving a large temperature excursion or mechanical stress (e.g. impregnation, cementing or encapsulation) and the final process of inductance adjustment.

Other possible contributions to the inductance variability associated with permeability changes arise from changes of amplitude and the superposition of a steady magnetic field. Provided the effective flux density is not too high its influence on the inductance may be deduced from the graphs in Fig. 3.5, using the dilution ratio

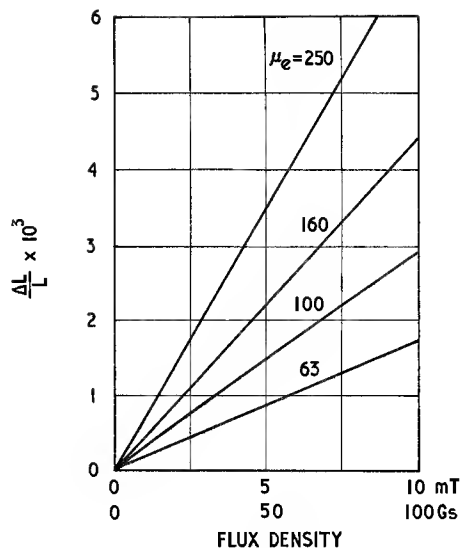


Fig. 5.7. Change in inductance as a function of flux density; typical curves for a 25 mm pot core

μ_e/μ (See Eqn 4.31). If the effective flux density is low, e.g. less than 1 mT (10 Gs), the variations in amplitude will normally have negligible effect. Fig. 5.7 shows the variation of inductance as a function of flux density for some typical pot cores. The effect of amplitude is more often encountered during test measurements than during operation. A filter may work at very low amplitudes where variation of inductance due to this cause is negligible, but during measurement of inductance or of the insertion-loss characteristic the signal level may be quite high and may result in erroneous measurements or adjustments.

The variation of μ_e due to a steady magnetic field (polarizing ampere turns) is not so easily deduced from the material properties and it is better for it to be measured on the pot core being considered. Fig. 5.8 gives some typical results. As far as possible d.c. polarization in high quality inductors should be avoided if stability is important.

Mechanical stress is another factor that must sometimes be taken into account. The ferrite core is often stressed during assembly either by design or accident and if this stress is excessive a substantial change in initial permeability will result. Fig. 3.24 gives some typical results. Stress also changes the slope of the μ - θ curve and so influences the T.C. of inductance. It may be concluded that mechanical stress should be kept to a minimum and where it is unavoidable it should be constant.

The initial permeabilities of inductor ferrites do not vary significantly with frequency within the frequency range for which the material may be used in low loss applications. This may be seen in Fig. 3.11 where the dispersion in μ'_s is shown to coincide with the large increase in residual loss. For this reason, and because the inductance is finally adjusted at the operating frequency, the influence of frequency may be ignored.

5.5.3. Contribution of the non-ferrite parts—construction and assembly

The variability of inductance arising from causes other than the variation of the material permeability is now considered. Many contributory causes are possible. Their main effect is to produce a drift or irreversible

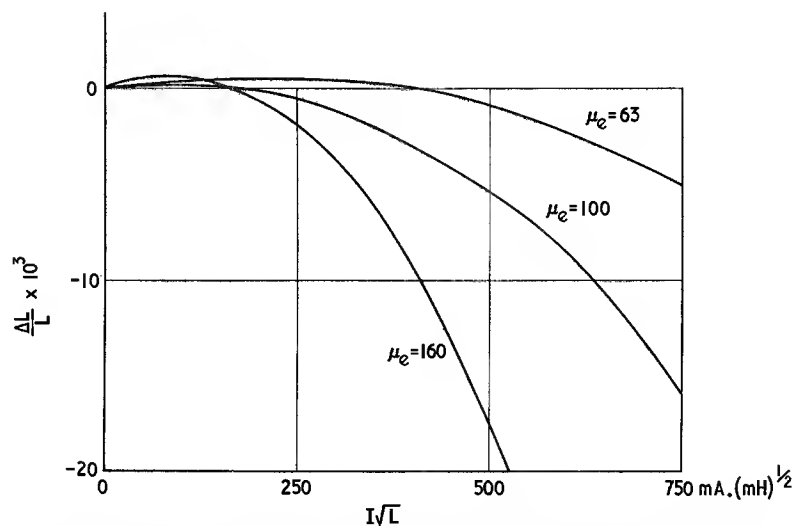


Fig. 5.8. Change in inductance of a 25 mm pot core as a function of the steady magnetic field, the field being expressed in terms of current and inductance

change of inductance; in most cases the reversible change, i.e. contribution to the temperature coefficient, is small but it will be seen that there are one or two notable exceptions to this.

The most important general category is the change of inductance due to changes in the effective reluctance of the total air gap, and again there are many possible mechanisms. The central air gap may change in length due to strain in the ferrite. Clearly pressure near the centre of the pot core faces will produce strains tending to close the central air gap. To avoid this it is essential to apply any clamping or fastening pressure around the periphery of the pot core so that only simple compression is produced. Another possible source of strain is the differential linear expansion between the ferrite and other members that might be cemented or otherwise attached to the core. A marked reduction of temperature coefficient of inductance may result from a tag board which is firmly cemented to a core face and therefore causes convex distortion of the face as the temperature rises. The direct effect of stress on the initial permeability has been mentioned in the previous section.

If the halves of the ferrite core are clamped together or fastened to a tag or pin board by a force distributed around the periphery, the value of this force must be carefully chosen. If it is very small, the effective air gap at the mating surfaces will be appreciable in spite of the fact that these surfaces are given a finely ground finish during manufacture. As the force increases the surfaces are brought into more intimate contact and the resultant air gap becomes small and stable. If the force is further increased a point is reached at which the reduction of initial permeability due to stress becomes significant and the inductance begins to decrease. It is probably best to limit the force to a value well below this point. Changes of force due to thermal expansion or creepage in the clamping parts should be avoided and of course the mating surfaces should be perfectly clean.

An alternative method of fastening the core halves together is to cement them at the mating surfaces. The general method and the precautions to be taken are discussed in Section 1.4.2. If the thickness of the adhesive is too great its thermal expansion will affect the T.C. of the inductance. More serious is the effect of creep, which may be observed on cemented joints in general. If the joint is clamped during curing and then released it will tend to expand with time; on the other hand an increase of pressure will cause the joint to contract. However, if the cementing process is done with care and the above-mentioned precautions are observed, a stable and inexpensive assembly may be obtained.

It has been seen that a typical adjuster is designed to adjust the inductance over a range of about $\pm 10\%$. From the moment the adjustment is completed, the adjuster should not contribute to further inductance change

during the service life of the inductor. The adjuster should therefore be carefully designed to make it insensitive to shock, vibration and temperature variations. In particular, steps must be taken to avoid changes of adjuster position due to thermal expansion and creep of parts, particularly those made of organic materials.

Unwanted inductance change may also result from movement of the winding. If the whole coil former is free to move about inside the core, the resulting variation of inductance is easily demonstrated. It is therefore good practice to prevent this movement either by cementing the coil former to one half of the core or by inserting a resilient packing. There is some evidence that the thermal expansion of the winding can influence the T.C. of inductance and this effect depends on the winding geometry.

Finally, processes such as encapsulation could obviously give rise to stresses producing variability of inductance. If such protection is essential the precautions given in Section 1.4.3 should be observed.

5.5.4. Overall inductance variability

Of the processes of inductance variability considered in the foregoing sections, those which are reversible with temperature will combine to give an overall temperature coefficient of inductance. This will in general be somewhat different from $(T.F.) \times \mu_e$ due mainly to the contribution of the non-ferrite parts, and it must be one of the objects of a good inductor construction to make this discrepancy as small as possible. However, only in the most exacting applications is this aspect of variability serious.

Similarly all the irreversible processes will combine to give an inductance drift with time. Most irreversible processes may be accelerated by temperature cycling. Therefore, when a high order of inductance constancy is required it is advisable to subject the inductor, before final adjustment, to a number of temperature cycles beyond the range of temperatures to which it will be exposed in service. This will have the effect of relieving stresses and making the residual changes reversible with temperature. If the inductor is to be a part of a network it would perhaps be better to temperature cycle the whole assembly as this would have a similarly advantageous effect on other network components. There is of course one irreversible effect which is not reduced but rather induced by thermal disturbance, i.e. disaccommodation. The previous advice still applies; after thermal disturbance there should be an adequate time allowed for the disaccommodation to become negligible before the final inductance adjustment is made.

Inductance variability, both the reversible part and the long-term drift, may be studied experimentally by

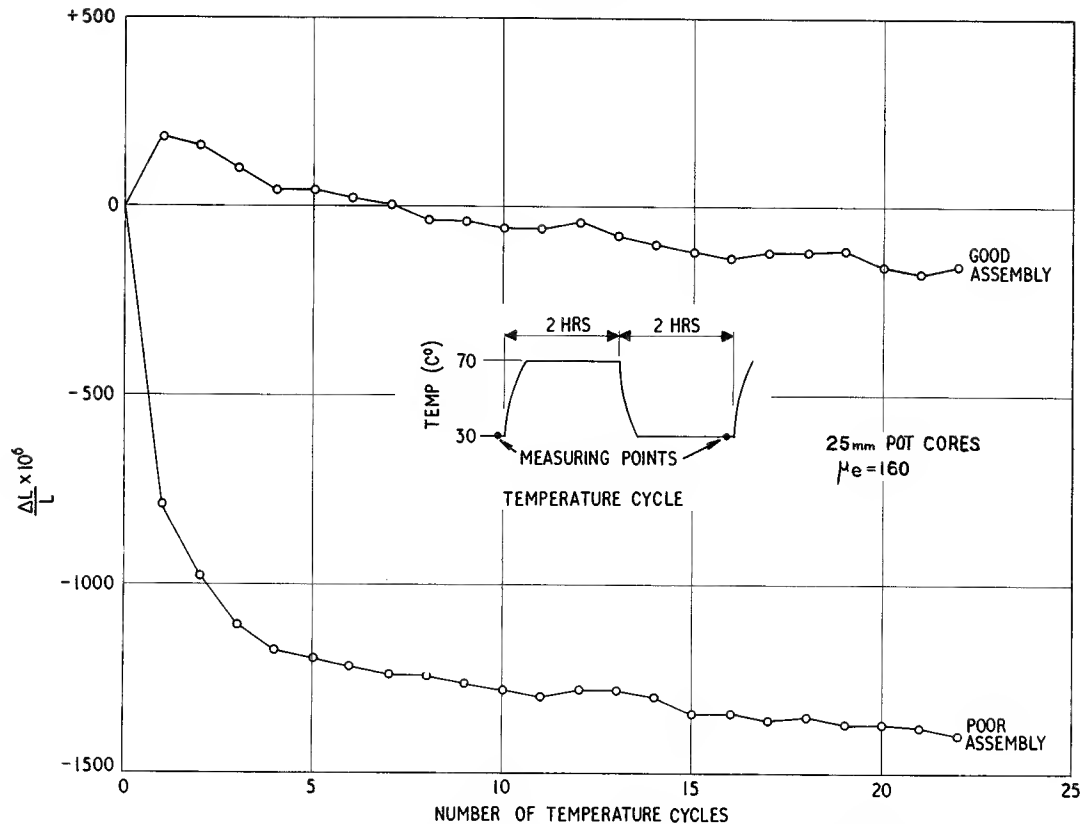


Fig. 5.9. Measured inductance drifts on typical ferrite pot cores (without adjusters). The half pot cores were cemented together with epoxy resin and the assemblies were subjected to a series of dry temperature cycles. The results illustrate good and poor examples

subjecting an inductor to a series of temperature cycles.⁹ After allowing adequate time for acclimatization at the upper and lower temperature of each cycle, the inductance is accurately measured and the results are presented graphically. Fig. 5.9 shows the results of actual measurements on typical ferrite pot cores cemented together with epoxy resin; it illustrates good and poor examples. In the latter example most of the drift occurs during the first few cycles and is due to creep of the cemented joint. Had this specimen been given five stabilizing cycles before the test its subsequent drift would have been comparable with the good example.

5.6. SELF CAPACITANCE

The analysis of the self capacitance of a winding is given in Section 11.6. It is sufficient here to discuss only the practical aspects of the subject as they affect inductor design.

The self capacitance of a single section, multi-layer, winding consists of the three components¹⁰ illustrated

in Fig. 5.10(a). If the number of layers is large, C_c is the direct capacitance between the first layer and the core (assuming the core may be regarded as an electrode) and C_b is the direct capacitance between the top surface of the winding and the core. C_a is the value of a hypothetical capacitance appearing across the winding and is equivalent to the distributed capacitances between turns and between layers. In practice the contribution of the inter-turn capacitance is usually negligible, so from item 5 of Table 11.3

$$C_a = \frac{4 C_l (p-1)}{3p^2} \quad (5.15)$$

where C_l is the direct capacitance between adjacent layers when they are considered as forming a series of parallel plate capacitors, and p is the number of layers, assumed identical.

In Section 11.6 methods for calculating the three components of the self capacitance of a practical winding are given. Table 5.3 gives typical values of C_a and C_c for full, unimpregnated, single-section windings on ferrite pot cores. The values of C_b depend strongly on the fullness of

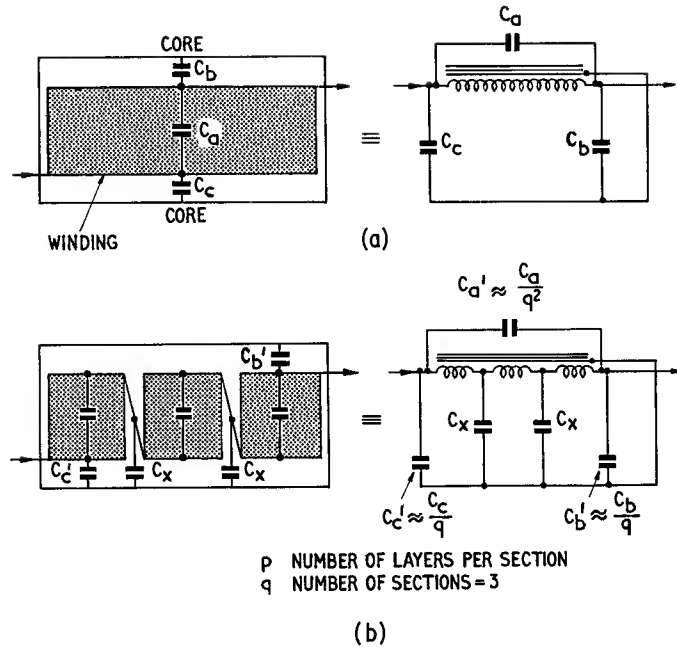


Fig. 5.10. Representation of winding self capacitances for: (a) a single section winding, (b) a three section winding

the winding and are therefore too uncertain to quote. Wax impregnation of a winding will increase C_a by 15 to 30%; the increase in C_c will be smaller unless the whole inductor is impregnated.

If the core is not, in effect, connected to either end of the winding, then the total self-capacitance is

$$C_s = C_a + \frac{C_b C_c}{C_b + C_c} \quad (5.16)$$

Inductors are often used in this way, with the cores floating with respect to the circuit, if the minimum self

capacitance is required. However it is often convenient, or necessary, to connect the core to one end of the winding. This, in effect, short circuits one of the end capacitances and puts the other directly in parallel with C_a . Experience suggests that the outer end capacitance C_b is generally the larger and is certainly the less predictable of the end capacitances so it is usually recommended that if a connection must be made, the core should be connected to the finish of the winding.

The loss tangent of the self capacitance depends, in practice, mainly on the conductor insulation, although

Table 5.3. TYPICAL VALUES OF COMPONENT SELF CAPACITANCES FOR FULL, UNIMPREGNATED, SINGLE-SECTION WINDINGS ON THE FERRITE POT CORES QUOTED IN THE UPPER PART OF TABLE 5.2.

Pot core dia.	Typical values of C_a in pF				Typical values of C_b in pF			
	Enamelled copper wire (fine covering)		Bunched conductors		Thin f coil formers		Thick coil formers	
	Copper dia.		Overall dia.		Overall conductor diameter			
	<0.15mm (0.006")	≥0.15mm (0.006")	<0.25mm (0.01")	≥0.25mm (0.01")	<0.15mm (0.006")	≥0.15mm (0.006")	<0.15mm (0.006")	≥0.15mm (0.006")
10.0	7.5	7.5	4.5	5.5	6	5	—	—
12.0	8.5	8.5	5	7	7	6	—	—
14.0	10.5	10.5	6	8.5	9	8	4.5	4
18.0	14	15	8	11	13	11	7	6
21.5	18	19	10	14	16	14	9	8
25.4	20	22	12	17	19	16	11	10
29.5	27	30	16	23	24	20	15	13
35.5	31	35	18	28	28	24	17	15
45.0	39	44	23	35	35	30	18	16

the material of the coil former may make a small contribution. For a dry unimpregnated winding of enamelled copper wire the loss tangent of the self capacitance would be typically 0.01 to 0.02. For a winding of bunched conductors the loss tangent of the self capacitance depends very much on the textile covering. The following loss tangents are typical: natural silk, 0.015; polypropylene fibre, 0.003; rayon, 0.035.

The effect of impregnation depends on the material used; good quality wax will not increase the loss tangent very much, whereas some varnishes have very high loss factors and would certainly reduce the overall Q -factor of the inductor at the high frequencies. Impregnation is not normally used as a means of protecting inductors intended to have high Q -factors at high frequencies. However some protection is required, for moisture in the winding will certainly cause the loss tangent of the self capacitance to be excessively high. The preferred practice is to seal hermetically the whole network into a container from which all water vapour has been removed.

The most effective way of reducing the self capacitance of a winding is to divide it into sections wound side-by-side. Fig. 5.10(b) illustrates a three section winding in comparison with the single section winding. Item 6 in Table 11.3 gives an expression for C_a for various multi-section windings (it also gives an expression for the value of C_b that will be obtained if the start of the winding is connected to the core or an adjacent screen and there is no capacitance from the top of the winding).

Sectioning reduces C_a in two ways; C_l is divided by the number of sections, q , (ignoring the inevitable wastage of winding space due to the separation of the sections), and the number of layers, p , is multiplied by q . Thus from Eqn 5.15, C_a is divided approximately by q^2 .

The end capacitances are clearly divided approximately by q . There are in addition capacitances from the intersection positions, denoted by C_x . These are each equal to $C'_b + C'_c$. If one end of the winding is connected to the core then these capacitances are transformed across the terminals of the winding in accordance with the usual transformation ratio, i.e. in the arrangement illustrated in Fig. 5.10(b) the additional shunt self capacitance is $C_x(1/9 + 4/9)$. If the core is floating the situation is more complicated. The star mesh consisting of one of the capacitances, C_x , and the two parts into which it divides the winding may be transposed into the equivalent delta mesh. The result of this transposition is that each of the capacitances, C_x , is equivalent to additional end capacitances, adding to C'_b and C'_c , and a negative capacitance in parallel with C'_a .

At frequencies above a few MHz very low values of self capacitance are essential. Usually the inductance values are quite small so relatively few turns are required. Under these circumstances a single layer winding gives the best results. The self capacitance of a single layer

winding depends almost only on the overall dimensions; Fig. 11.16 provides a means of estimating this self capacitance assuming that the capacitance to core may be neglected.

Self capacitance introduces loss and possibly variability in proportion to its magnitude relative to the total resonating capacitance. Thus at low frequencies it will normally have negligible effect but at high frequencies where resonating capacitances are small, self capacitance is a major design consideration and should be made as small as possible.

5.7. Q-FACTOR

5.7.1. General

The Q -factor requirements of an inductor and their relation to the need for inductance constancy are briefly discussed in Section 5.1. In the design of an inductor the following features are, in principle, independent variables; choice of ferrite material, size of core, effective permeability and form of winding. Usually some of these features are determined by considerations other than Q -factor, e.g. availability may dictate the grade of ferrite, the equipment construction may influence the choice of core size, and variability or hysteresis specifications will impose a maximum value of μ_e . Within such boundaries an inductor must usually be designed to have the maximum possible Q -factor; a lower limit will often be specified.

The Q -factor is the reciprocal of the total loss tangent, $\tan \delta_{\text{tot}}$. Provided $\tan \delta_{\text{tot}} \ll 1$ it may be taken as equal to the sum of all the partial or contributory loss tangents corresponding to the various origins of loss. For this reason it is convenient to work in terms of loss tangents

$$\frac{1}{Q} = \tan \delta_{\text{tot}} = \Sigma \tan \delta \quad (5.17)$$

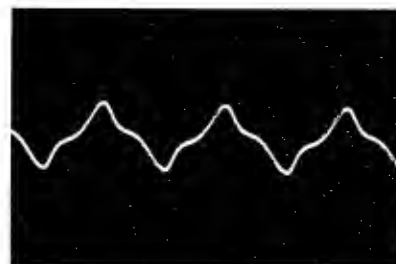
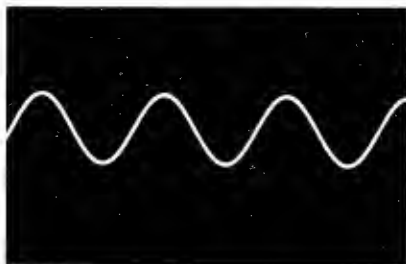
The design problem therefore is to calculate the contributory loss tangents and to minimize the total. The following sections first consider these loss factors separately and then in combination. Finally the overall Q -factor is considered in relation to frequency, inductance, type of winding conductor, and the effective permeability of the core.

5.7.2. Loss due to the d.c. winding resistance

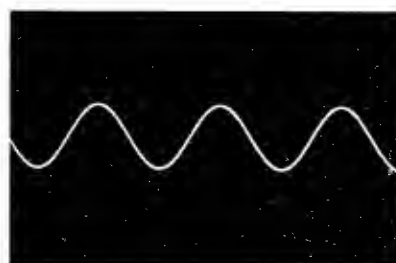
If R_{dc} is the d.c. resistance of a winding and L is the inductance, then the corresponding loss tangent is

$$\tan \delta_{dc} = R_{dc}/\omega L \quad (5.18)$$

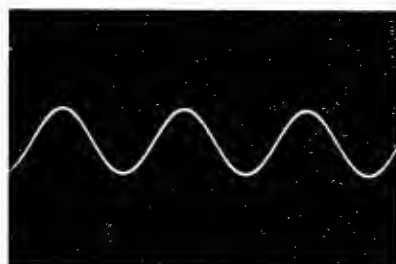
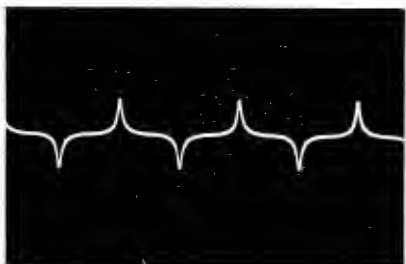
CURRENT
AND
FIELD STRENGTH



FLUX



E.M.F.



(a)
SINUSOIDAL CURRENT

(b)
SINUSOIDAL E.M.F.

Plate 2.1. High-amplitude waveform distortion in magnetic materials. The oscillograms show current (and field strength), flux and e.m.f. for (a) sinusoidal current and (b) sinusoidal e.m.f.

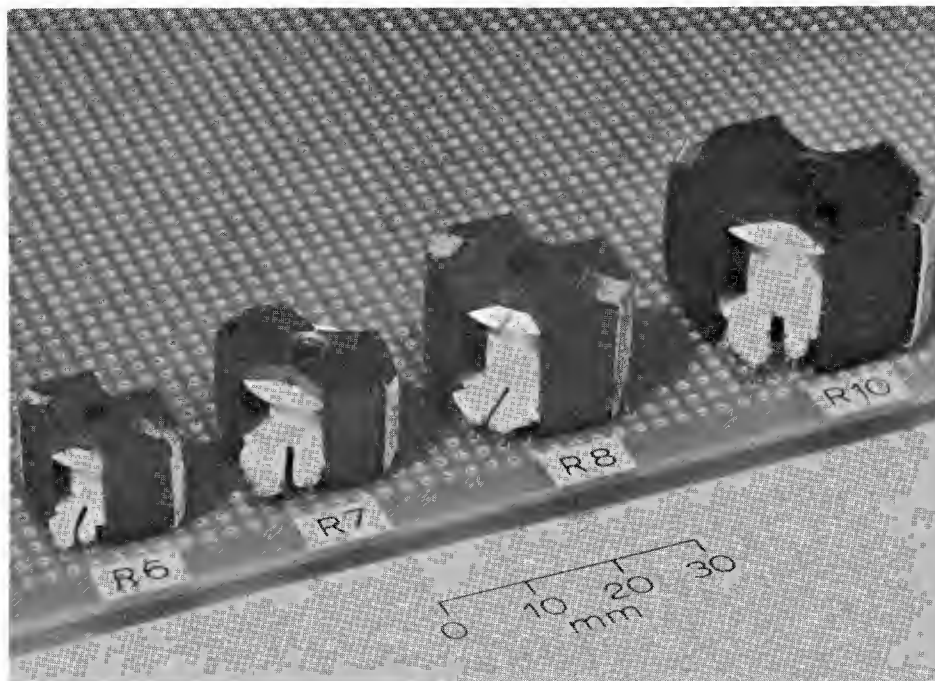


Plate 5.1. Recently developed inductor assemblies designed for use on printed circuit boards. (Courtesy: Mullard Ltd. (R7, R10) and N.V. Philips (R6, R8))

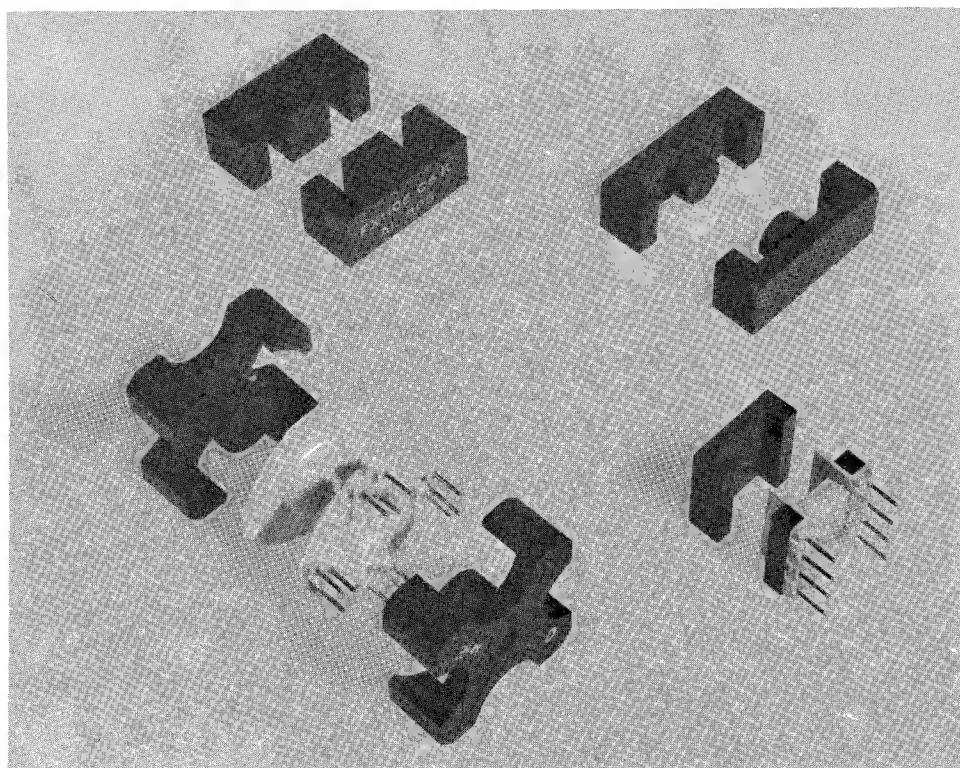
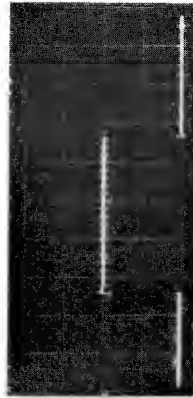
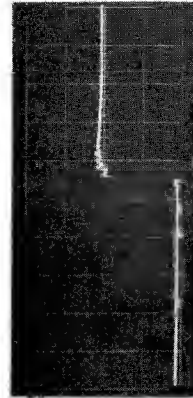
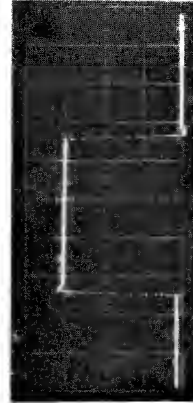


Plate 7.1. Some ferrite transformer core shapes

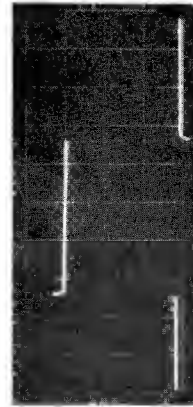
TIME
SCALE
1 DIV. =



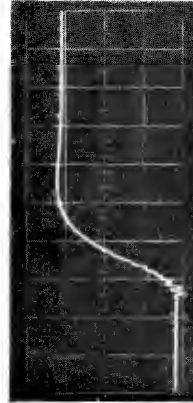
WHOLE
PULSE



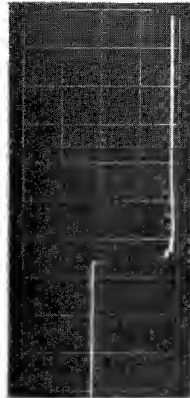
LEADING
EDGE



1 μ s



50ns



TRAILING
EDGE



50ns

APPLIED PULSE

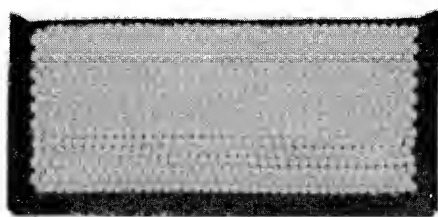
PULSE ACROSS LOAD
(NORMAL)

PULSE ACROSS LOAD
(EXT. CAP. REMOVED)

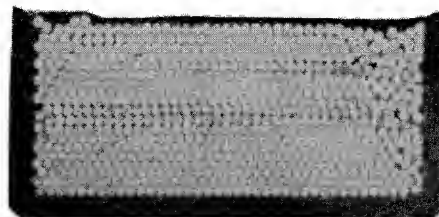
Plate 8.1. Oscillograms showing the performance of
the example pulse transformer (see section 8.6.2)

Net distortion.

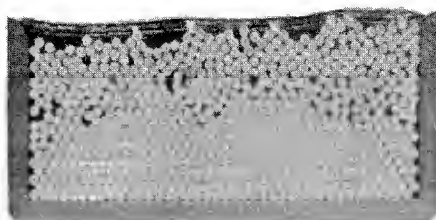
Rise time	62ns	30ns
Overshoot	4%	6%
Droop	1.5%	1.5%
Fall time	60ns	30ns
Backswing	4%	6%



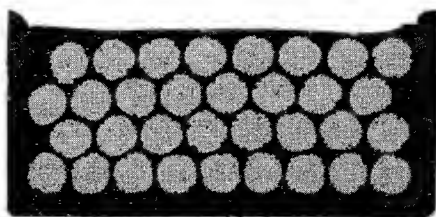
(a)



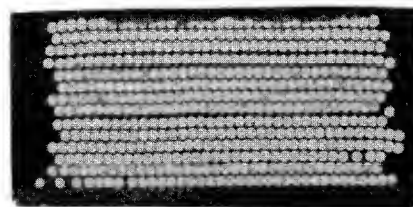
(b)



(c)



(d)



(e)

Plate 11.1. Cross-sections of some actual windings.
Nominal winding area dimensions = $9.18 \times 4.0 = 36.72 \text{ mm}^2$

Type of winding	Conductor	Turns	F_w	F_p
(a) Layer wound, hand traverse	0.0076 in (0.193 mm) fine enamelled	740	0.59	0.93
(b) Layer wound, machine traverse	0.0076 in (0.193 mm) fine enamelled	733	0.58	0.92
(c) Random wound by hand	0.0076 in (0.193 mm) fine enamelled	690	0.55	0.87
(d) Layer wound by hand	81×0.0028 in (0.0711 mm) SSC bunched conductors	32	0.28	0.87
(e) Interleaved and layer wound by hand	0.0076 in (0.193 mm) fine enamelled	490	0.39	0.61

F_w and F_p are based on nominal overall conductor diameter except for F_p in (d) where conductor was appreciably oversize

At a given frequency this factor depends primarily on the geometry of the core. The influence of the core shape on the ratio R_{dc}/L has been analysed in Section 5.2. If the core size and shape are fixed then this ratio depends mainly on the effective permeability, and the fullness of the winding. When the loss due to d.c. winding resistance is important the winding should occupy as much of the available space as possible. From Eqns 5.2, 5.6 and 5.8

$$R_{dc} = \frac{\rho_c N^2 l_w}{A_a F_a} \quad \Omega$$

$$\text{and} \quad L = \frac{N^2}{\alpha^2} \times 10^{-3} = N^2 A_L 10^{-9} \quad \text{H}$$

$$\therefore \tan \delta_{dc} = \frac{\rho_c l_w \alpha^2 10^3}{\omega A_a F_a} = \frac{\rho_c l_w 10^9}{\omega A_a F_a A_L} \quad (5.19)$$

Section 11.2 considers the relation between the window area A_a , the actual available winding space, the type of conductor and the overall copper factor F_a . Calculation of $\tan \delta_{dc}$ from Eqn 5.19 inevitably involves some judgement of copper factor, since this will depend on the type of winding and the margin that must be allowed if over-full windings are to be avoided. A more direct calculation is possible if, for the coil formers being used, there are reliable tables giving the number of turns for a reasonably full winding, and the corresponding resistance, for a range of conductor sizes and types. Such tables are usually based on experimentally determined copper factors. From the required inductance value, the number of turns may be calculated and, from the winding tables, the most suitable conductor diameter may be found. The d.c. resistance may be obtained directly from the tables or, if the actual number of turns required differs appreciably from the number corresponding to the most suitable conductor diameter, the d.c. resistance may be found by proportion.

The reciprocal of $\tan \delta_{dc}$ is the Q -factor due to the d.c. winding resistance. It is usually impracticable to obtain high Q -factors at low frequencies because (1) in this region $\tan \delta_{dc}$ ($= R_{dc}/\omega L$) is almost the only loss contribution so the Q -factor is proportional to f , and (2) R_{dc}/L can only be decreased significantly by using larger cores or larger effective permeabilities. Economics limit core size, and the need for inductance constancy or adequate adjustment range limits the value of μ_e .

5.7.3. Loss due to eddy currents in the winding conductors

As the frequency increases additional losses occur in the windings due to eddy currents induced in the conductors by the magnetic fields within the winding. These eddy current phenomena are considered in detail in Section 11.4 where graphs may be found which express the func-

tions necessary in the calculation of the eddy current losses.

In the design of inductors both skin effect and proximity effect need to be considered. Both effects depend on the ratio of conductor diameter, d , to penetration depth, Δ .

Skin effect is the tendency for the alternating current to flow near the surface of the conductor. It is due to eddy currents in the conductor which arise from the magnetic field associated with the current in the conductor itself (see Fig. 11.4). It causes the resistance to increase by an amount, R_{se} , above the d.c. value. Therefore the a.c. resistance due to skin effect may be expressed by

$$R_{ac} = R_{dc} + R_{se} = R_{dc}(1 + F) \quad \Omega$$

where F is the skin effect factor. It is given as a function of d/Δ in Fig. 11.5; Δ may be obtained from Table 11.2 or Fig. 11.6.

The combined loss tangent, $\tan \delta_{ac}$, may be obtained by putting R_{ac} in place of R_{dc} in Eqn 5.18. Alternatively the skin effect loss tangent, $\tan \delta_{se}$, may be calculated separately from

$$\tan \delta_{se} = \frac{R_{dc} F}{\omega L} \quad (5.20)$$

As stated in Section 11.4.2, F is proportional to f^2 at low values of d/Δ , so at low frequencies $\tan \delta_{se}$ is proportional to f . It reaches a maximum when $d/\Delta \approx 6$. At higher values of d/Δ , F becomes approximately proportional to $f^{\frac{1}{2}}$ so that $\tan \delta_{se}$ approaches proportionality to $f^{-\frac{1}{2}}$ at higher frequencies.

In most inductor designs the skin effect loss is small compared with other losses. If solid conductors are used, then at low frequencies $\tan \delta_{se}$ is very small while at frequencies for which $\tan \delta_{se}$ is near maximum, proximity effect will usually be very much larger than the skin effect. With bunched conductors, i.e. conductors formed as a rope of insulated strands, the skin effect is usually very much reduced. A simply twisted bunch of insulated strands would have the same skin effect as a solid conductor having the same copper cross-section. However, measurements have shown that most bunched conductors behave as though the strands weave between the outer surface and the centre thus preventing skin effect by ensuring a uniform current distribution. This arises because bunched conductors are usually made by twisting together groups of strands which have, in turn, been twisted together. Thus most bunched conductors behave as though the strands are almost perfectly transposed, so the skin effect is negligible.

The major cause of eddy current loss in inductor windings is proximity effect. This is the effect of the magnetic field of the winding as a whole. In most cases this field is substantially perpendicular to the axis of the conductor at any point. Eddy currents flow and return

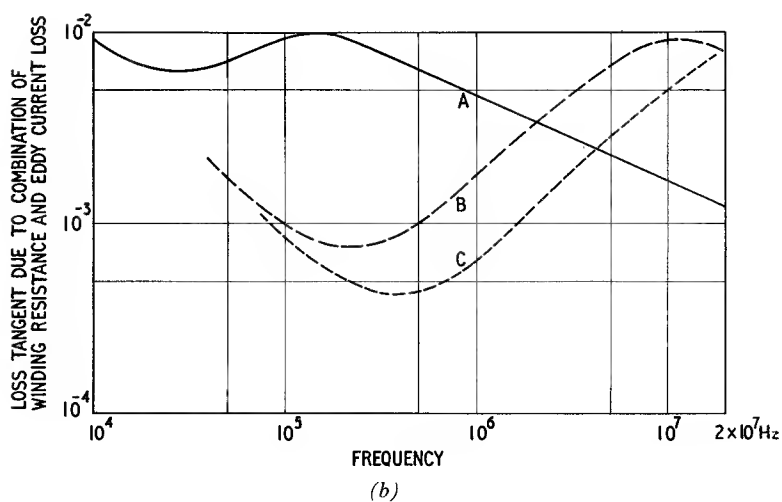
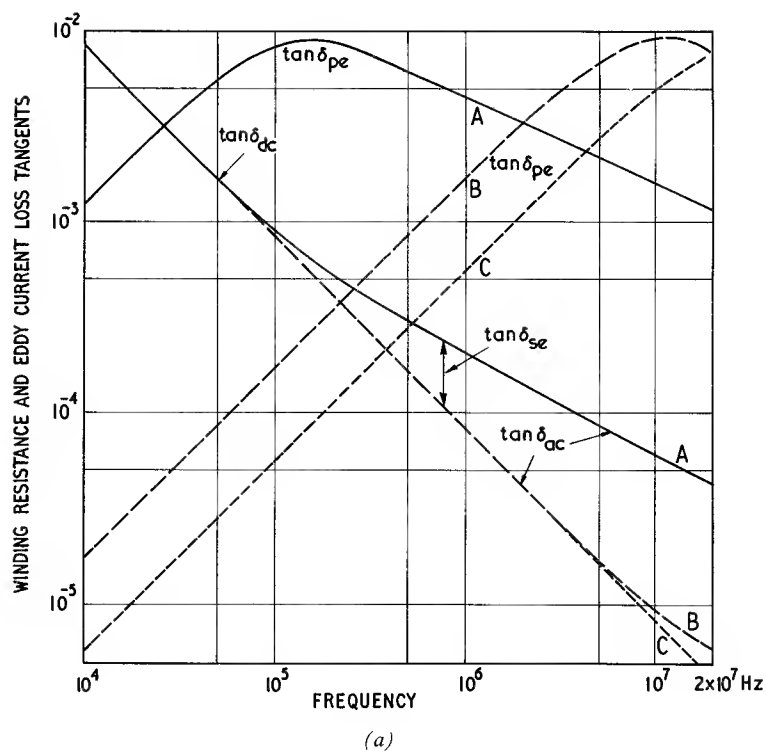


Fig. 5.11. Winding resistance and eddy current loss tangents as functions of frequency for three particular windings: (a) component loss tangents; (b) combined loss tangents.

Inductor details:

18 mm core, $\mu_e = 100$, $k_e = 5.1 \times 10^{-6}$

Number of turns = 19, inductance = $82 \mu\text{H}$

Winding A: 0.6 mm solid conductor

B: 74×0.07 mm bunched conductor

C: 225×0.04 mm bunched conductor

Equal conductor
cross-sectional areas:
 $R_{dc} = 41.6 \text{ m}\Omega$

Note: Bunched conductor assumed to be perfectly transposed

typical pot core. The windings have equal numbers of turns and the copper cross-sectional areas are equal so that the inductance and d.c. resistance are the same for each. Winding *A* has a solid conductor while windings *B* and *C* have bunched conductors of different strand diameter. Fig. 5.11(a) shows the component loss tangents. It has been assumed that the bunched conductors are perfectly transposed, i.e. the only skin effect and proximity effect is that occurring in the individual strands. It is seen that the skin effect causes the loss tangent to rise above the $R_d/\omega L$ line at high frequencies but even for the solid conductor the contribution is small compared with that of the proximity effect. For bunched conductors the skin effect in the strands is quite negligible. The proximity effect loss tangent has a maximum at the frequency which corresponds to $d/\Delta \approx 3.5$. It is clear that for the solid conductor at the higher frequencies $\tan \delta_{pe} \propto f^{-\frac{1}{2}}$ and in consequence it ultimately falls below the value of $\tan \delta_{pe}$ for the bunched conductors. Fig. 5.11(b) shows the total loss tangent due to winding resistance and eddy current losses. The advantage of bunched conductors for the middle frequency range is illustrated and the superiority of solid conductor at the higher frequencies may be seen.

5.7.4. Loss due to stray capacitance

The nature of the stray capacitances associated with an inductor winding has been discussed in Section 5.6 and a table of typical values is given. The effect of the stray capacitance on the loss tangent of an inductor will now be considered. It is assumed that the stray capacitances may be regarded as a single self capacitance, C_s , connected in parallel with the winding. This self-capacitance may contribute to the total loss tangent in two ways. The first arises simply from the loss angle associated with C_s and is referred to as dielectric loss and the second is called shunt capacitance loss and arises in certain circumstances due to circulating currents in the LC_s circuit. Each loss will now briefly be considered.

Dielectric loss

If the loss angle of the self capacitance is δ_d then the corresponding loss conductance appearing in parallel with the inductance is

$$G_s = \omega C_s \tan \delta_d \quad (5.22)$$

(note: for practical purposes $\tan \delta_d$ equals the power factor, $\cos \phi$, of the self capacitance.)

This loss contributes a loss tangent, $\tan \delta_{cp}$, to the overall loss tangent of the inductor:

$$\left. \begin{aligned} \tan \delta_{cp} &= \omega L G_s = \omega^2 L C_s \tan \delta_d \\ &= \frac{C_s}{C_{res}} \tan \delta_d \end{aligned} \right\} \quad (5.23)$$

where C_{res} is the total capacitance required to resonate the inductance L at the frequency $\omega/2\pi$, i.e. $C_{res} = 1/\omega^2 L$.

Normally $\omega^2 L C_s \ll 1$, i.e. the inductor will not be near self-resonance at its design frequency. If, however, a specification calls for a high inductance at a high frequency then self resonance may be approached and the degradation of Q -factor due to the dielectric loss would become appreciable. In the limit $\tan \delta_{cp}$ would equal $\tan \delta_d$.

The value of $\tan \delta_d$ depends on the dielectrics associated with the self capacitance; typical values are quoted in Section 5.6. As an example of the effect of dielectric loss, an inductor with the following properties may be considered

$$Q\text{-factor without dielectric loss} = 500$$

$$\tan \delta_d = 0.01$$

$$C_s/C_{res} = 0.04$$

By Eqn 5.23

$$\tan \delta_{cp} = 0.04 \times 0.01 = 0.0004$$

\therefore the Q -factor including this dielectric loss is given by

$$\frac{1}{1/500 + 0.0004} = 417$$

Loss due to circulating currents in self capacitance

This occurs in a series resonant circuit when the inductor is shunted by a self capacitance. The equivalent circuit is shown in Fig. 5.12; R represents the loss associated

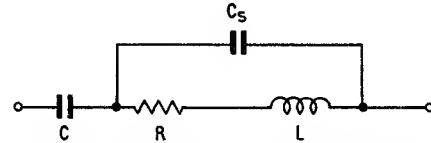


Fig. 5.12. Equivalent circuit to illustrate the loss due to circulating currents in the self capacitance

with the inductor and C_s is at this stage considered loss-free. The impedance in series with the resonating capacitance, C , is

$$\frac{R + j\omega L}{j\omega C_s \{R + j(\omega L - 1/\omega C_s)\}} \approx R(1 + 2\omega^2 L C_s) + j\omega L(1 + \omega^2 L C_s)^* \quad (5.24)$$

*Proof

The impedance of the parallel circuit in Fig. 5.12 is

$$\begin{aligned} Z &= (R + j\omega L) / j\omega C_s \{R + j(\omega L - 1/\omega C_s)\} \\ &= \frac{R + j\omega L(1 - \omega^2 L C_s - C_s R^2/L)}{(1 - \omega^2 L C_s)^2 + \omega^2 C_s^2 R^2} \end{aligned}$$

cont.

This assumes that $R/\omega L$ and $(\omega^2 LC_s)^2$ are negligible compared with unity, i.e. that the inductor Q -factor is reasonably high and that the inductance is far from self-resonance. Both of these conditions are normally satisfied in practice. The real part of this expression represents the series loss resistance and this is greater than R by an amount $2R\omega^2 LC_s$. Since the Q -factor of the inductor is more readily estimated than the value of R , this increase in loss resistance is more conveniently expressed as $2\omega^3 L^2 C_s / Q$, i.e. the loss tangent of the inductor is increased by $2\omega^2 LC_s / Q$ or $2C_s / C_{res} Q$.

If the dielectric loss of the self capacitance, $\tan \delta_d$, is also taken into account, by including a resistance in series with the capacitance, an expression corresponding to Eqn 5.24 may be obtained in which the real part is

$$R + (2/Q + \tan \delta_d) \omega^3 L^2 C_s \quad (5.25)$$

assuming $\tan \delta_d \ll 1$

Thus the total loss factor, $\tan \delta_{cs}$, due to self capacitance in a series circuit is given by

$$\left. \begin{aligned} \tan \delta_{cs} &= (2/Q + \tan \delta_d) \omega^2 LC_s^\dagger \\ &= (2 \tan \delta_L + \tan \delta_d) C_s / C_{res} \end{aligned} \right\} \quad (5.26)$$

where Q and $\tan \delta_L$ refer to the inductor.

Using again the example illustrating dielectric loss which was quoted above but this time assuming a series-connected circuit:

$$\begin{aligned} \tan \delta_{cs} &= (2 \times 0.002 + 0.01) \times 0.04 \\ &= 0.00056 \end{aligned}$$

$$\therefore Q_{tot} = 390$$

Let $\omega^2 LC_s \ll 1$ so that $(\omega^2 LC_s)^2$ is negligible compared with 1 and let $R/\omega L$ be negligible compared with 1. Now $\omega^2 C_s^2 R^2 = (\omega^2 LC_s)^2 R^2 / \omega^2 L^2$ and this is negligible compared with $\omega^2 LC_s$. Then

$$\begin{aligned} Z &\approx \{R + j\omega L(1 - \omega^2 LC_s - C_s R^2 / L)\} (1 + 2\omega^2 LC_s) \\ &\approx R(1 + 2\omega^2 LC_s) + j\omega L(1 - \omega^2 LC_s - C_s R^2 / L + 2\omega^2 LC_s \\ &\quad - 2\omega^4 L^2 C_s^2 - 2\omega^2 C_s^2 R^2) \end{aligned}$$

The last two terms are negligible and so is $C_s R^2 / L$ since this equals $\omega^2 LC_s \times R^2 / \omega^2 L^2$

$$\therefore Z \approx R(1 + 2\omega^2 LC_s) + j\omega L(1 + \omega^2 LC_s)$$

[†]This result also follows from Eqns 5.24 and 5.23. The increase in resistance due to C_s when this is loss-free is $2R\omega^2 LC_s$. Therefore the loss factor due to this is $\tan \delta_{cs} = 2\omega C_s R$. If now C_s has a loss factor $\tan \delta_d$ then from Eqn 5.23 the combined loss factor due to C_s is

$$\begin{aligned} \tan \delta_{cs} &= 2\omega C_s R + \frac{C_s}{C_{res}} \tan \delta_d \\ &= (2/Q + \tan \delta_d) C_s / C_{res} \\ &\text{since } C_{res} = 1/\omega^2 L \end{aligned}$$

Here the major degradation is from the dielectric loss; however had the Q -factor of the inductor been 200 then the two contributions would have been equal.

5.7.5. Core losses

In Chapter 4 the relations between the intrinsic properties of the ferrite material and the properties of a given core of general shape were considered. The concepts of core factors, the effective dimensions of a core and the effective flux density were introduced. Using these principles the contribution of the core loss to the total loss tangent of an inductor may be calculated from the material properties (e.g. see Eqns 4.49 and 4.50).

It was, however, observed that this approach, while useful for analysis, is limited in practical usefulness because the actual material properties in a given core of intricate shape cannot be accurately known or controlled except by destructive testing. It is therefore common practice to specify the core properties explicitly in terms of parameters measured on the core and controlled during manufacture. This makes the calculation of the core loss contribution very straightforward.

The residual loss tangent of a gapped core at a given frequency is given approximately by

$$\tan \delta_r = \mu_e \left(\frac{\tan \delta_r}{\mu} \right) = \mu_e (\omega L_o G) \quad (5.27)$$

where $\left(\frac{\tan \delta_r}{\mu} \right)$

is the residual loss factor measured on the ungapped core (see Eqns 4.49, 2.18 and 2.14).

Similarly the eddy current core loss tangent is given by

$$\tan \delta_F = \text{const.} f \mu_e \quad (5.28)$$

(see Eqn 4.54)

Since both of these loss tangents are functions of frequency and are proportional to μ_e they are almost inseparable in a given core. It is usual to specify, at a given frequency or frequencies, the sum of these loss tangents, i.e. $\tan \delta_{r+F}$. Thus the value of the core loss contribution at very low amplitudes is available directly for the particular core type and effective permeability being considered.

The hysteresis loss may be expressed in a variety of ways and these have been considered in Sections 2.2.6 and 4.2.3. Three commonly used methods will be quoted here by way of illustration. Some manufacturers specify a hysteresis factor such as F_h (see Eqn 4.41 also η_i in Eqn 4.43). The hysteresis factor is a normalized representation of the series hysteresis loss resistance and is therefore essentially a core parameter. From the expression for F_h

$$\left. \begin{aligned} \frac{R_h}{L} &= F_h I \sqrt{L} \quad \Omega \cdot H^{-1} \\ \text{or } \tan \delta_h &= \frac{F_h I \sqrt{L}}{2\pi} \quad (= \eta_i \hat{I} \sqrt{L}) \end{aligned} \right\} \quad (5.29)$$

Alternatively a hysteresis coefficient (material parameter) may be specified, e.g. the Legg hysteresis coefficient, a (see Eqn 4.51) or η_B (see Eqn 2.74). Then

$$\tan \delta_h = \frac{\mu_e a \hat{B}_e}{2\pi} \quad (= \mu_e \eta_B \hat{B}_e) \quad (5.30)$$

Since the hysteresis factors or coefficients are not constant with amplitude, the flux density must also be specified. Another approach is to specify the value of $\tan \delta_h$ at a given flux density for a particular core having a stated effective permeability.

Whichever method is used the required value of hys-

teresis loss tangent is readily obtained, whether it is required for its contribution to the total loss tangent or, in another context, to enable the waveform distortion to be estimated.

5.7.6. The combined loss tangents

The total loss tangent is the sum of all the contributory loss tangents set out in the foregoing sections. Table 5.5 summarizes the expressions.

The loss tangent due to the d.c. winding resistance is inversely proportional to f while other loss tangents are approximately proportional to f or f^2 . It follows that, other parameters being constant, there will be a frequency at which the total loss tangent is a minimum. Similarly some loss tangents are proportional to μ_e while others

Table 5.5. SUMMARY OF LOSS EXPRESSIONS FOR INDUCTORS

Since the loss tangents are dimensionless the expressions apply equally to SI units and CGS units: the constants k_e , k_E and a have the dimensions [time].[length]⁻⁴, [time].[length]⁻⁴. [henries] and [flux density]⁻¹ respectively and must be expressed in appropriate units.

Loss tangent due to:	Symbol	Expression	Eqn. No.	Page No.
D.C. resistance	$\tan \delta_{dc}$	$\frac{R_{dc}}{\omega L} =$	5.18	208
		$\frac{\rho_c I_w \alpha^2 10^3}{\omega A_a F_a} = \frac{\rho_c I_w 10^9}{\omega A_a F_a A_L}$	5.19	209
Skin effect	$\tan \delta_{se}$	$\frac{R_{dc} F}{\omega L}$	5.20	209
Proximity effect	$\tan \delta_{pe}$	$\frac{k_e f N n d^4 G_r}{\mu_e} = \frac{k_E f N n d^4 G_r}{A_L}$	5.21	210
Dielectric loss in self capacitance (parallel resonant circuit only)	$\tan \delta_{cp}$	$\omega^2 L C_s \tan \delta_d = \frac{C_s}{C_{res}} \tan \delta_d$	5.23	212
Circulating currents in self capacitance (series resonant circuit only)	$\tan \delta_{cs}$	$(2/Q + \tan \delta_d) \omega^2 L C_s$ $= (2 \tan \delta_L + \tan \delta_d) \frac{C_s}{C_{res}}$	5.26	213
Residual loss in core	$\tan \delta_r$	$\mu_e \left(\frac{\tan \delta_r}{\mu} \right) \left. \vphantom{\frac{\tan \delta_r}{\mu}} \right\} \tan \delta_{r+F}$	5.27	213
Eddy current loss in core	$\tan \delta_F$	$\text{const. } f \cdot \mu_e \left. \vphantom{\text{const. } f \cdot \mu_e} \right\} \tan \delta_{r+F}$	5.28	213
Hysteresis loss in core	$\tan \delta_h$	$\frac{F_h I \sqrt{L}}{2\pi} (= \eta_i \hat{I} \sqrt{L})$	5.29	214
		$= \frac{\mu_e a \hat{B}_e}{2\pi} (= \mu_e \eta_B \hat{B}_e)$	5.30	214

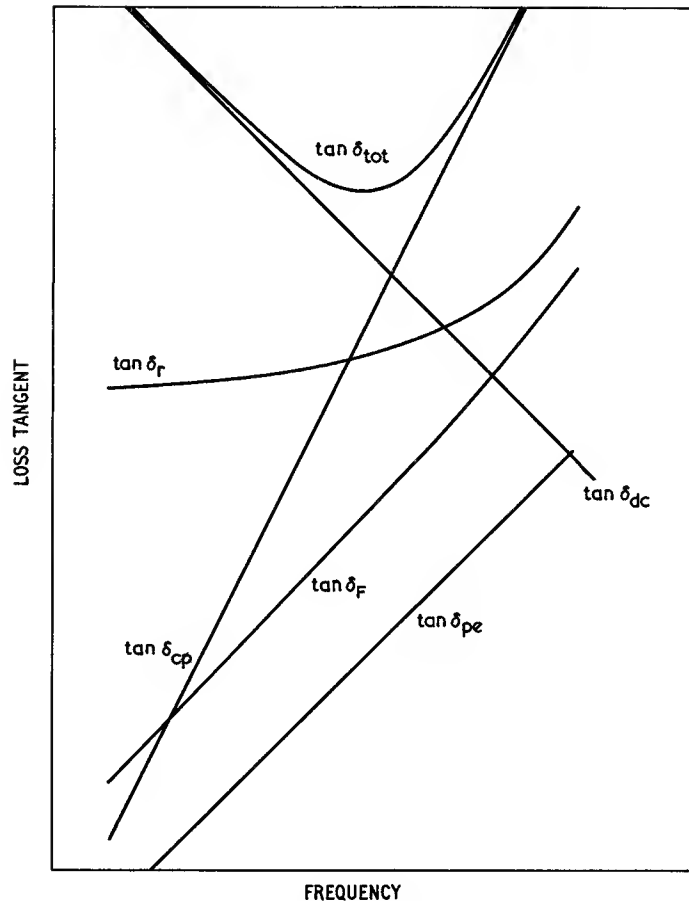


Fig. 5.13. Typical variation of contributory loss tangents with frequency

are inversely proportional. Thus at a given frequency, other parameters being constant, there will be a particular value of μ_e for which $\tan \delta_{\text{tot}}$ will be a minimum.

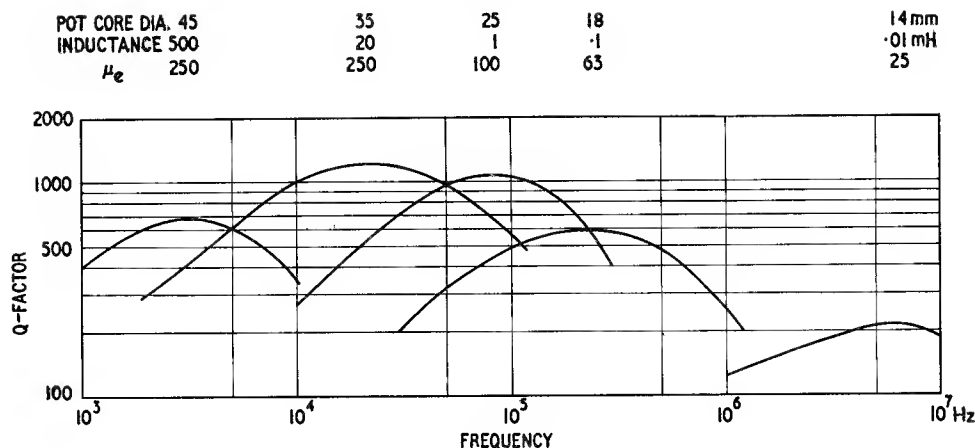
Fig. 5.13 shows a typical variation of the contributory loss tangents with frequency for an arbitrary inductor design. The upper curve is the total loss tangent. At low frequencies the total loss tangent is due almost entirely to the d.c. resistance of the winding. As the frequency rises this contribution falls and, in the vicinity of minimum total loss, it is exceeded by one of the rising losses. The relative magnitude of the contributory loss tangents at any frequency depends on the inductor design. At the higher frequencies the total loss tangent may be dominated by the loss due to the proximity effect, the self capacitance or the core.

In this and the following sections the hysteresis loss contribution has been ignored. This is because inductors for telephony filters normally operate at very low amplitudes. Moreover, the inclusion of hysteresis loss in a general way complicates the presentation because it adds another independent variable; if the amplitude is

not negligible it might have any value. Allowance for hysteresis loss is easily made; the value of $\tan \delta_h$ appropriate to the particular design has only to be added to the otherwise total loss tangent or $1/Q$.

5.7.7. The presentation of Q -factors

It is common practice to present the Q -factor of an inductor as a function of frequency. Such a curve will give some information about the performance attainable with a given core type but since it will depend very much on the inductance, the type of wire and the winding geometry, many Q -curves would be required if the possible performance is to be adequately described. Fig. 5.14 shows some typical Q -curves. At the lower frequencies, where the winding resistance loss predominates, high Q -factors may be achieved only with large cores and/or high effective permeabilities. Since variability requirements usually set an upper limit to the effective permeability, it is seldom that a pot core can be used to attain its

Fig. 5.14. Some typical Q -curves

maximum possible Q -factor at low frequencies. At frequencies between about 40 kHz and 200 kHz the optimum effective permeability with respect to Q -factor matches the variability requirements quite well and the maximum Q -factors may be exploited. At higher frequencies the residual core loss factors are rising (see Fig. 3.12) and this causes a reduction in the maximum Q -factors.

Q -curves are often obtained by measurements made on representative inductors. A glance at Table 5.5 will show that the results of such measurements depend on many parameters, e.g. copper factor, conductor diameter, core loss, and these will have manufacturing tolerances. In order to ensure that the measured results are typical, average values of these parameters must be used or one must take the average of measurements made on many samples representing the spread of all the parameters. The alternative is calculation.

Calculation based on the expressions given in Table 5.5 is quite straightforward provided reliable values of certain parameters are available. Such parameters are F_a , k_e , C_s and $\tan \delta_d$; they must usually be determined experimentally and it may be necessary to express the results as functions of conductor diameter, winding geometry or effective permeability. As these parameters are basic to many possible calculations great care in their determination is justifiable. Other parameters, such as conductor diameter and core loss, have known limits and their values may be carefully chosen to be nominal or typical. Given accurate data, calculations based on the loss tangent expressions will provide reliable Q -curves. In general they will represent the typical performance of an inductor more accurately than a few measurements on a random sample.

Individual Q -curves, however obtained, are of limited value as a guide to an inductor designer. To be useful, a Q -curve must represent a core type, effective permeability, inductance and type of conductor corresponding to the

designer's requirements. There are a large number of combinations. The solution is to compute the Q -curves for a wide range of possibilities and express the results in the form of Q -contours on inductance-frequency co-ordinates.^{11, 12} This form was described by Welsby¹³ as a means of representing measured results; it is particularly valuable for the display of a large set of computed Q -factors.

A typical Q -chart showing a set of Q -contours is illustrated in Fig. 5.15. Such a chart is computed for a particular pot core with a certain effective permeability and some assumption must be made about the winding, e.g. the type of conductor, the type of coil former and how full it is wound. If the calculation is based on a full winding, with an appropriate copper factor to allow for practical considerations, then a particular conductor diameter will determine the number of turns and the corresponding inductance. The R.H. and L.H. scales represent these parameters in the correct relation. A horizontal line at any inductance will intersect the Q -contours to give the Q -factor as a function of frequency for that inductance.

For each core type and effective permeability, several Q -charts may be prepared representing different types of conductor, solid and bunched. In this way a set of Q -charts may be built up representing the performance of all inductors falling within the boundaries of the computation. Such charts make the design of an inductor a relatively simple matter of inspection and choice, and they also provide a valuable indication of the influence of the design parameters on the Q -factor.

5.7.8. The effect of design parameters on Q -factor

Fig. 5.15 is an actual computed Q -chart for a 25 mm pot core having an effective permeability of 160 and a full

winding of solid, enamel covered conductor. In this and the following Q -chart the hysteresis loss is assumed to be negligible, and the loss due to the circulating currents in the self capacitance has been omitted as these charts are intended to represent only the performance of inductors in parallel resonant circuits.

Fig. 5.16 gives the contributory loss tangents as functions of frequency corresponding to three inductance values from Fig. 5.15.

Fig. 5.16(a) is for a high inductance value. The winding has many turns of fine wire. Only two of the loss tangents are of importance, that due to d.c. winding resistance at low frequencies and that due to dielectric loss in the self capacitance at high frequencies. The emphasis of the latter

loss is not the result of high self capacitance but due to the high inductance leading to the approach of self-resonance at a fairly low frequency (see Eqn 5.23).

Fig. 5.16(b) is for a medium inductance value approximately corresponding to the peak of the Q -surface. The maximum Q -factor is determined mainly by the d.c. winding loss and the proximity effect loss, while the value of the high frequency Q -factor is again due mainly to the dielectric loss.

Fig. 5.16(c) is for a low inductance. Again the maximum Q -factor depends principally on the d.c. winding resistance and the proximity effect. The curvature of the latter function, due to G_r in Eqn 5.21 falling below unity, is very marked. It causes a distortion of the $\tan \delta_{\text{tot}}$ curve

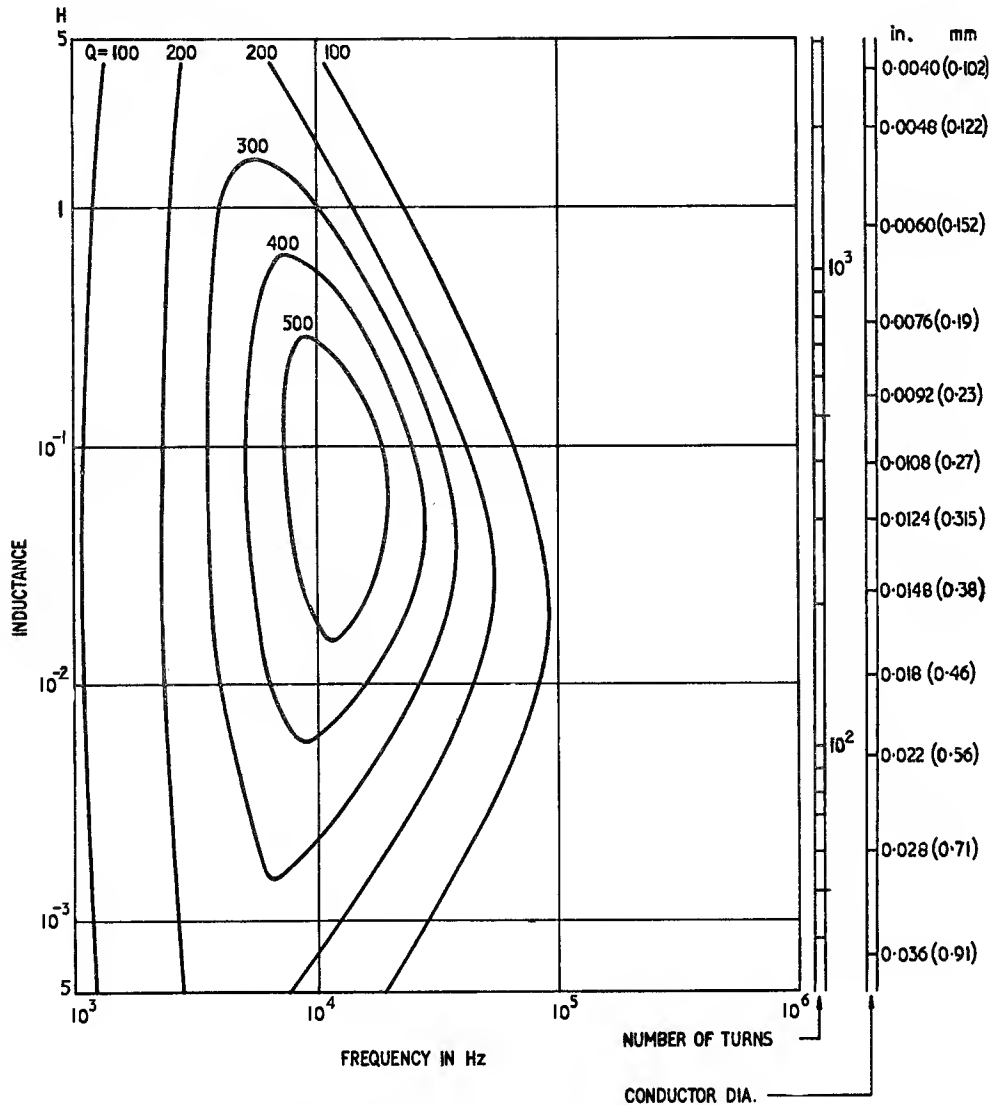
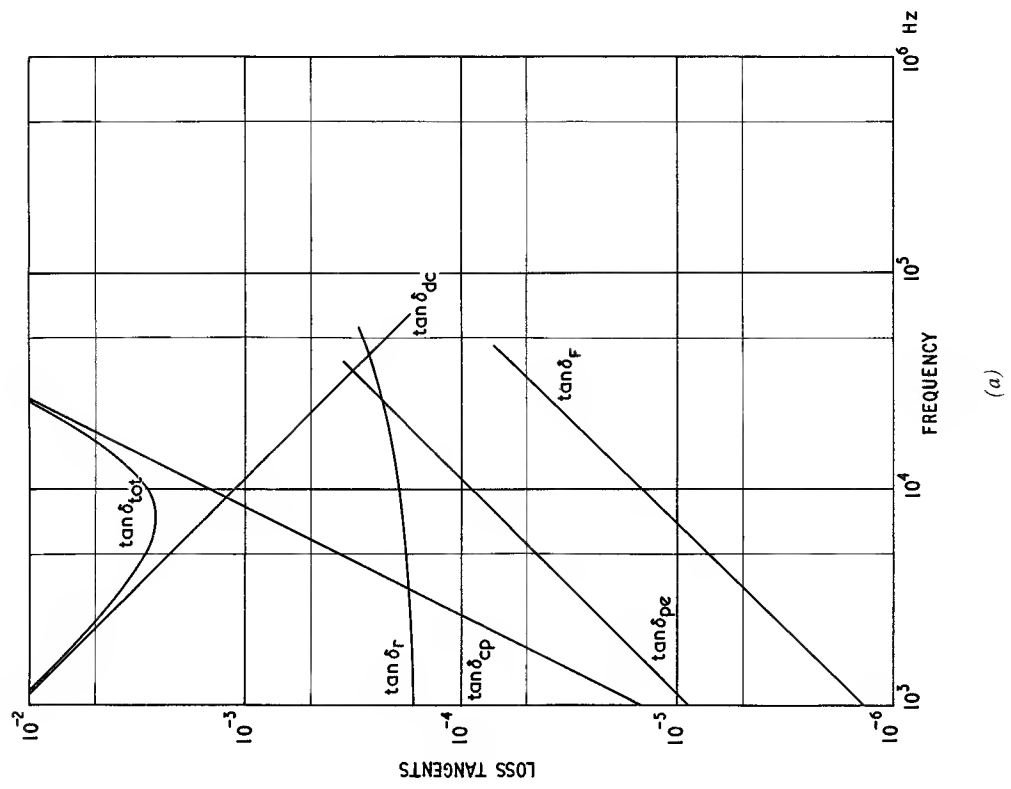
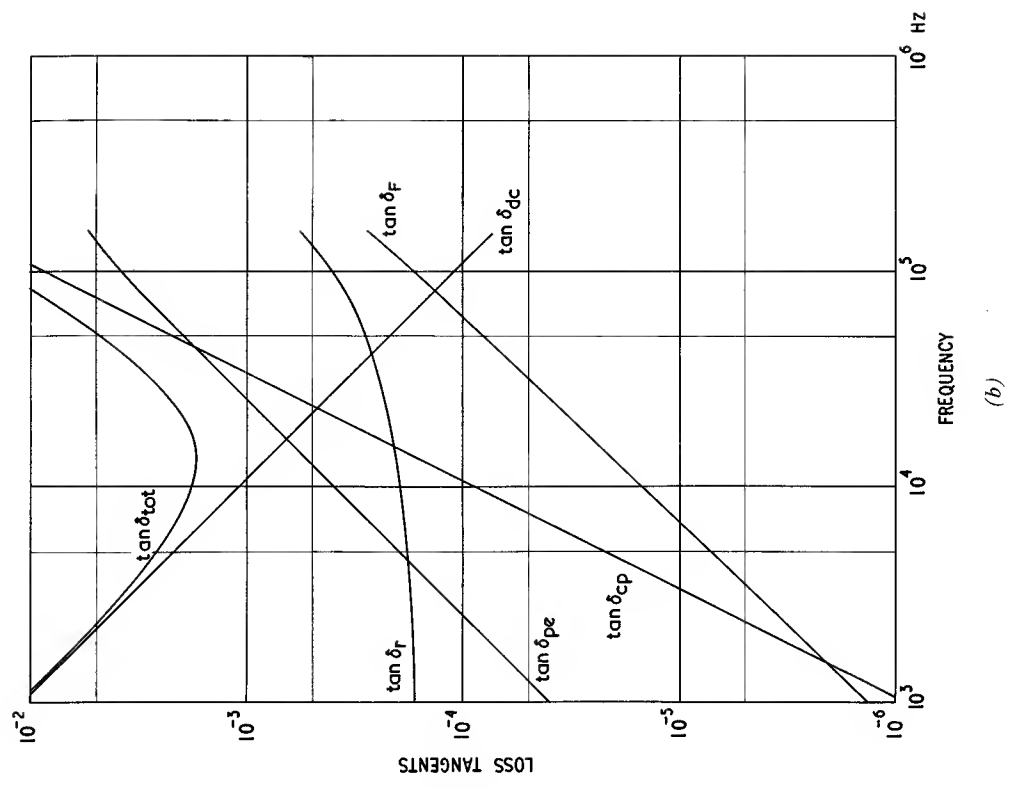


Fig. 5.15. Q -chart for a 25 mm pot core, $\mu_r = 160$, fully wound with solid conductor, (contribution of $\tan \delta_{\text{cs}}$ and $\tan \delta_{\text{h}}$ omitted)



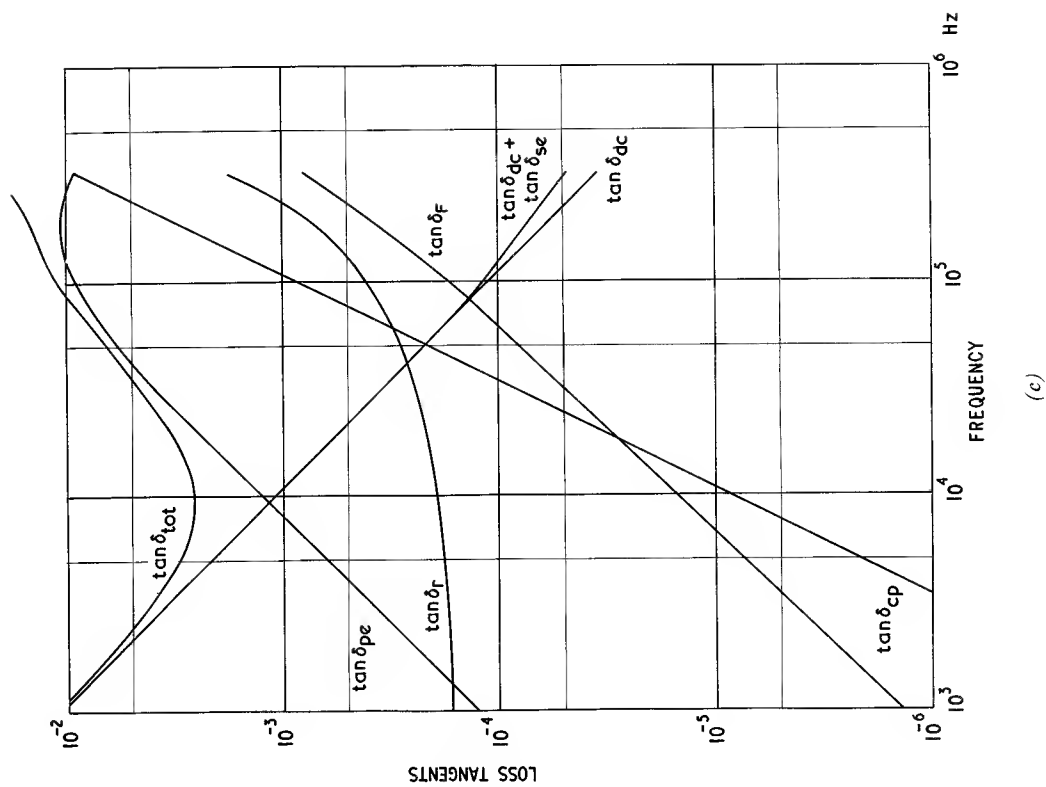


Fig. 5.16. Contributory loss tangents at three sections of Fig. 5.15.

(a) at $L = 0.85$ H, 1240 turns of 0.0006 in (0.152 mm) dia. solid wire

(b) at $L = 50$ mH, 303 turns of 0.0124 in (0.315 mm) dia. solid wire

(c) at $L = 5.1$ mH, 96 turns of 0.022 in (0.56 mm) dia. solid wire

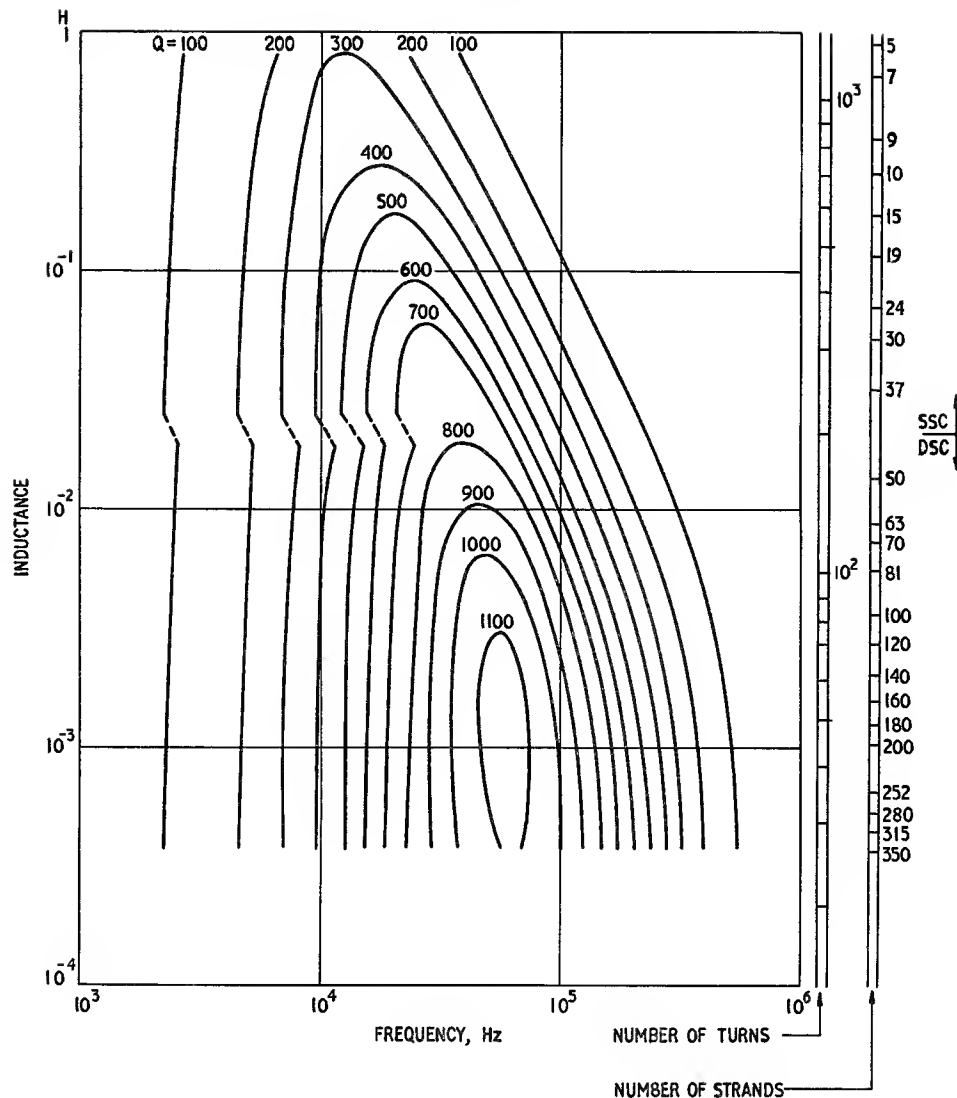


Fig. 5.17. Q -chart for a 25 mm pot core, $\mu_e = 160$, fully wound with bunched conductor having strand diameter = 0.0016 in (0.04 mm). Contribution of $\tan \delta_{cs}$ and $\tan \delta_h$ omitted

and results in the dielectric loss rising to predominance at high frequencies.

As a result of this analysis the reason for the shape of this particular Q -surface becomes apparent. The L.H. side is determined by the d.c. winding resistance. Because the copper factor is not very sensitive to the number of turns, R_{dc}/L and $\tan \delta_{dc}$ are also insensitive. This is apparent in the graphs of Fig. 5.16, and is the reason why the L.H. contours of Fig. 5.15 are almost parallel with the L axis. The top R.H. slope of the surface is due to the high inductance values emphasizing the dielectric loss of the self capacitance, while the lower R.H. slopes depend on the proximity effect. Skin effect has negligible effect over the range of this analysis. The peak of the

surface depends mainly on d.c. winding resistance and proximity effect. It is clear, therefore, that with $\mu_e = 160$ the core loss is hardly contributing to the total loss and higher Q -factors could be attained with higher values of effective permeability. Variability or the need for sufficient adjustment range usually sets a limit to the increase in μ_e under these circumstances.

Fig. 5.17 shows another computed Q -chart. It is for the same 25 mm pot core and the same effective permeability (160) but this time it is for a full winding of bunched conductors consisting of insulated strands of 0.0016 in (0.04 mm) diameter. The number of strands determines the overall diameter and therefore determines the number of turns and the inductance. Compared with

the previous Q -chart, it is seen that the use of bunched conductors has resulted in the region of maximum Q -factor moving to a higher frequency and lower inductance; the maximum value of Q -factor is much higher. The discontinuity at the L.H. side is due to the abrupt change of copper factor as the conductor covering changes from single silk, SSC, to double silk, DSC.

Fig. 5.18 gives the contributory loss tangents as functions of frequency, again corresponding to three inductance values from the Q -chart. The following general observations may be made. The poorer copper factor of bunched conductors has appreciably raised the position of the $\tan \delta_{ac}$ line, but stranding has made proximity effect negligible over the whole range. The relative contribution of eddy current losses in the core is also apparent; it is only significant over a narrow frequency range where the residual loss is beginning to increase rapidly with frequency.

Fig. 5.18(a) is for an inductance corresponding approximately to that of Fig. 5.16(b). The total loss depends mainly on d.c. winding resistance and dielectric loss in the self capacitance while the residual loss in the core significantly affects the minimum value.

Fig. 5.18(b) is for an inductance that is typical of the values used at about 100 kHz. Core loss and dielectric loss join the d.c. winding loss to form the total loss curve.

Fig. 5.18(c) is for a low inductance. Here the dielectric loss has become negligible over most of the frequency range and the total loss curve depends mainly on the d.c. winding loss and the core loss.

Returning to the Q -chart in Fig. 5.17, the L.H. side is again dependent mainly on d.c. winding losses. In this region the Q -factors are less than the corresponding ones in the Q -chart for solid conductors because windings of bunched conductors have smaller copper factors. Again the slope at the top R.H. side of the surface is due to dielectric loss in the self capacitance. The higher contours and the slope at the bottom R.H. side depend mainly on the core loss.

An increase in effective permeability will lower the winding loss and increase the core loss so that the peak of the surface will move to lower frequencies. A decrease in effective permeability will tend to have the reverse effect but because the core loss rises rapidly at frequencies above about 100 kHz the maximum Q -factors will be decreased. To get the best Q -factors at higher frequencies it would be necessary to use a lower permeability grade of ferrite; the residual loss factor would be greater at low frequencies but the frequency at which it would begin to rise rapidly would be higher, see Fig. 3.12.

A decrease in pot core size would increase the d.c. winding loss tangent for the same effective permeability. This would tend to increase the frequency at which the peak occurs but rising core loss would depress its height.

This type of analysis could be extended to different

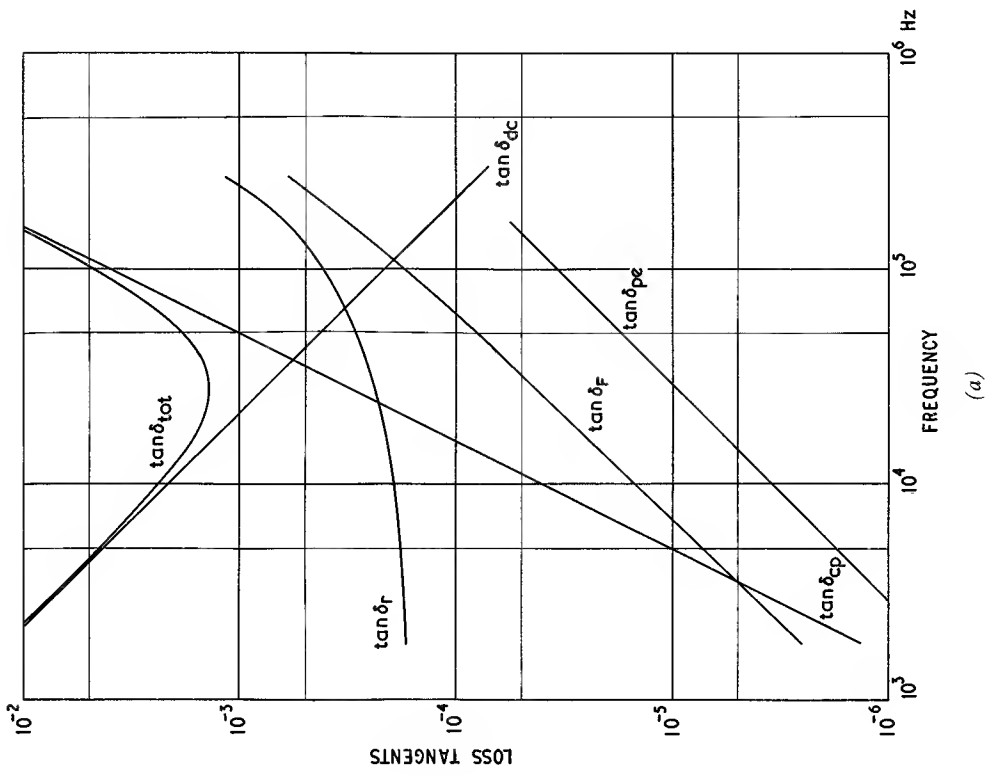
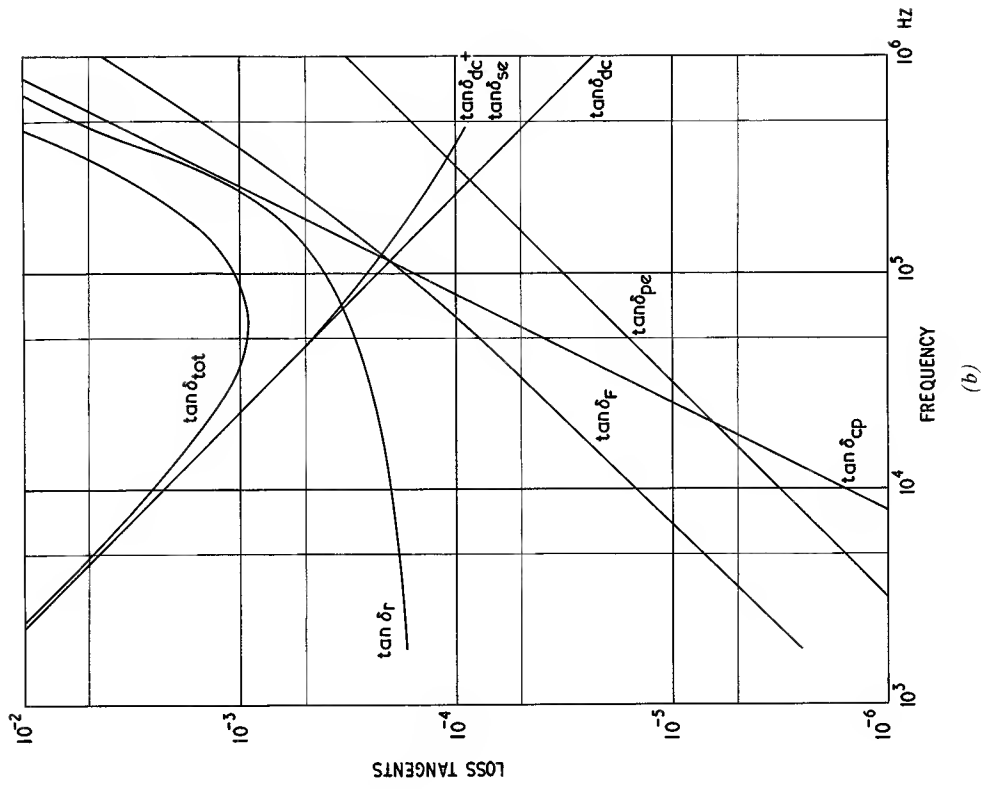
winding configurations, e.g. sectioned windings, and could provide Q -charts which allow for the hysteresis loss corresponding to a particular amplitude or Q -charts representing lower limits of performance. At high frequencies, e.g. 2 to 20 MHz, the highest Q -factors are obtained with windings that occupy only a fraction of the available space, thus the relation between conductor diameter and inductance is lost. In this case it is possible to compute a Q -chart in which each point represents the highest Q -factor obtainable over a range of conductor sizes and types, i.e. the surface is the envelope of many possible surfaces. The optimum conductor size and type may be indicated by an overlaid set of curves.¹⁴

5.8 WAVEFORM DISTORTION AND INTERMODULATION

The way in which waveform distortion and intermodulation arise in a magnetic material is considered in Section 2.2.7 and the results of some analyses are given in terms of the flux density and the Peterson coefficients. The relation between the Peterson coefficients and other hysteresis coefficients and factors are given in Table 2.1 and Eqns 4.42 and 4.43. It is observed that direct measurement of third harmonic and third order intermodulation products is a more reliable guide than the use of hysteresis coefficients. Graphs giving such data are given in Fig. 3.18. In Section 4.2.4 the effect of practical considerations such as an air gap and the external electric circuit are discussed. It is shown that the relative amplitude of the third harmonic is reduced from its value for an ungapped toroid by the dilution ratio μ_c/μ , the flux density amplitude being assumed constant.

In practice it is difficult to predict the magnitude of the distortion or intermodulation products that a given inductor in a filter network may produce at the terminals of an equipment, even when adequate magnetic data is available. This is because the amplitude of the signal e.m.f. across the inductor is not normally known and it is difficult to evaluate the relevant impedances and attenuations. Thus in this aspect of inductor specification and design, experience based on measurements plays an important part. Filter designers usually work in terms of a core hysteresis parameter such as the hysteresis factor F_h . If a previous filter network gave a known intermodulation performance with a certain value of hysteresis factor then the hysteresis factors required to meet a different specification may be deduced, approximately, from equations given in Section 4.2.4. However it seems that it would be simpler to work directly in terms of $\tan \delta_h$.

Intermodulation is most troublesome when large differences in amplitude exist between two separate signals in one circuit, e.g. at the junction of a pair of two-wire line filters where the send signal may be at a level of



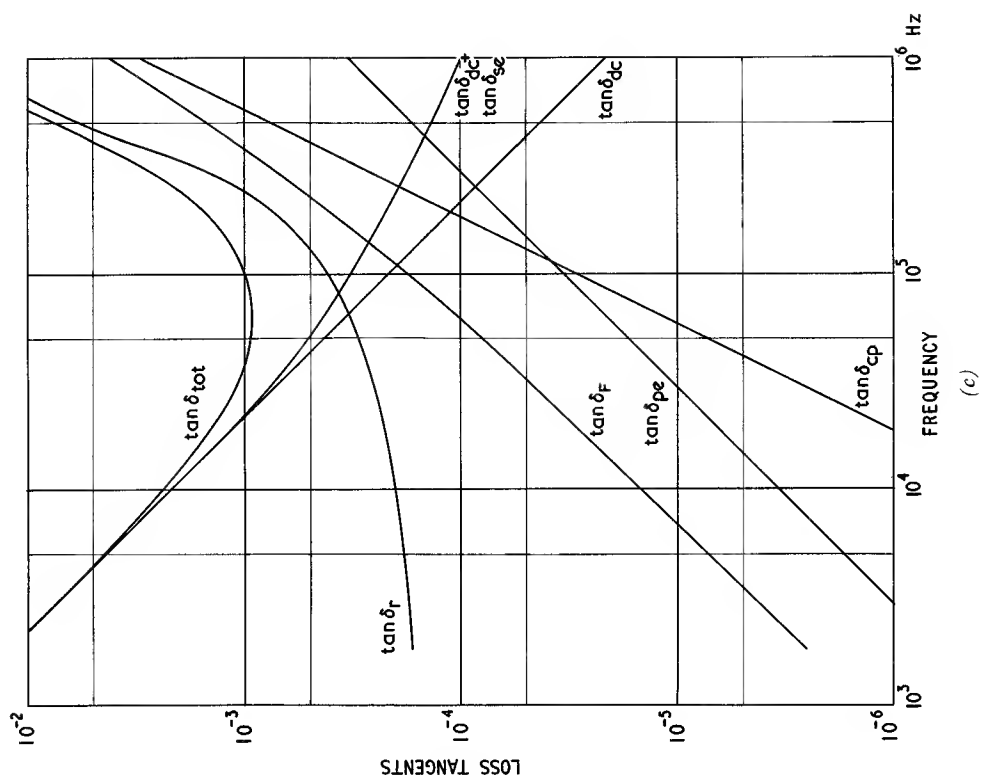


Fig. 5.18. Contributory loss tangents at three sections of Fig. 5.17
 (a) at $L = 53$ mH, 309 turns of 30×0.0016 in (0.04 mm) dia. bunched conductor
 (b) at $L = 2.1$ mH, 62 turns of 140×0.0016 in (0.04 mm) dia. bunched conductor
 (c) at $L = 0.37$ mH, 26 turns of 350×0.0016 in (0.04 mm) dia. bunched conductor

+17 dB and the receive signal may be at a level 60 dB lower than this. The intermodulation products would typically be required to be 60 dB below the receive signal, i.e. -120 dB with respect to the send signal that generates them. A typical specification for the inductors at the common ends of the filter would require hysteresis factors (F_h) of about 0.1 compared with 4 to 30 obtained on normal ferrite inductor cores. Low values of F_h are obtained by using very large air gaps or even removing the centre core entirely.

5.9 FUTURE DEVELOPMENTS

There is always a need to reduce volume and cost of inductors for a given overall performance. A reduction of the residual core loss factor, $(\tan \delta_r)/\mu$, will permit the use of higher effective permeabilities, and this in turn will allow a given d.c. winding resistance loss tangent, $R_{dc}/\omega L$, to be achieved in a smaller volume. The higher effective permeabilities will emphasize the problems of variability; in particular it will be necessary to narrow the limits of the temperature factor and control more closely the drift of inductance with time. As cores get smaller hysteresis effects may become important so that the hysteresis coefficients may have to be reduced.

Small cores will make it more important to obtain a good utilization of the winding space. It may be profitable to use self-supported windings and dispense with coil formers. Economic arrangements must be found for terminating the windings and this will influence the configuration of the core; square pot cores, X cores and butterfly-shaped cores have already been proposed. Finally, size reduction will make necessary a critical re-examination of the means of adjusting the resonant circuit.

Some of these guiding principles have recently been applied in the development of ferrite core assemblies specifically designed for equipment using printed circuit boards. Plate 5.1 shows four sizes; the numeral in the identifying code indicates the length of the side of the square occupied by the assembly, expressed in printed circuit modules, i.e. 2.54 mm or 0.1 in.

REFERENCES AND BIBLIOGRAPHY

Section 5.1.

1. BÉLUS, R., CAGNAT, G., ROCH, R., PIERROT, A. and BORY, F., 'Les bobines de charge', *Câbles Transm.*, **15**, 319, (1961).
2. FRENNING, J. and RAUB, W., 'Loading equipment', *Ericsson Rev.*, **40**, 126, (1963).
3. 'Ferroxcube in I.F. transformers for F.M.', *Matronics*, no. 3, 48, (1953).
4. 'Inductance and inductors', *Electronics*, **35**, no. 18, 72, (1962).

5. SNELLING, E. C., 'Ferrite cores for carrier-telephony equipment', *Proc. Instn. elect. Engrs*, **109**, Part B, Suppl. 21, 234, (1962).
6. HANSEN, H. N., 'Modern carrier telephone systems', *Philips tech. Rev.*, **26**, 206, (1965).

Section 5.3.

7. LONGHURST, C. E., 'Performance of coils with fractional turns when used with Vinkor assemblies', *Mullard tech. Commun.*, **6**, 183, (1962).

Section 5.5.2.

8. SNELLING, E. C., 'Disaccommodation and its relation to the stability of inductors having manganese zinc ferrite cores', *Mullard tech. Commun.*, **6**, 207, (1962).

Section 5.5.4.

9. NEWCOMB, C. V. and SNELLING, E. C., 'Analysis of variability in ferrite cored inductors', *Philips tech. Rev.*, **28**, 184, (1967).

Section 5.6.

10. LONGHURST, C. E., 'Stray capacitances of coils wound on Mullard Vinkor pot-core assemblies', *Mullard tech. Commun.*, **5**, 218, (1961).

Section 5.7.

- 'Calculating coils in ferroxcube pot cores', *Matronics*, no. 4, 53, (1953).
- SCHULTE, R. J., 'Q calculations for high frequency inductors', *Tele-tech and Electron. Ind.*, **15**, no. 7, 45, (1956).

Section 5.7.7.

11. MEYER, R. and SIRILLE, R., 'Essais de présentation des caractéristiques principales d'un pot en ferrite', *Onde élect.*, **42**, 638, (1962).
12. SNELLING, E. C., See general.
13. WELSBY, V. G., See general.

Section 5.7.8

14. Mullard Technical Handbook, 6.

General

- MACFADYEN, K. A., *Small transformers and inductors*, Chapman and Hall Ltd., London, (1954).
- VAN SUCHTELEN, H., 'Tolerances and temperature coefficient of coils with ferroxcube slugs', *Electron Applic. Bull.*, **14**, 27, (1953).
- STEWART, C., 'Measurement of the quality factor of inductor cores', *Trans. Am. Inst. elect. Engrs*, **73**, Part 1, Commun.
- ARRAZAU, J., 'Détermination des bobinages utilisant des pots fermés ferroxcube', *Onde élect.*, **36**, 252, (1956).
- DUNCAN, R. S. and STONE, H. A., 'A survey of the applications of ferrites in inductor design', *Proc. Inst. Radio Engrs*, **44**, 4, (1956).
- WELSBY, V. G., *The theory and design of inductance coils*, Macdonald and Co. (Publishers) Ltd., London, 2nd Edition, (1960).
- BORY, B. F., 'The behaviour of ferrite cores used in inductor coils', *Proc. Instn. elect. Engrs*, **109**, Part B, Suppl. 21, 202, (1961).
- PARENT, M., 'Comportement des circuits magnétiques en ferrite doux', *Onde élect.*, **43**, 540, (1963).
- SNELLING, E. C., 'Ferrite cored inductors and transformers', *Mullard tech. Commun.*, **9**, 30, (1966).

High Frequency Transducers

6.1. INTRODUCTION

Because the relation between the flux density and the field strength in a magnetic material is essentially non-linear it follows that the permeability depends on the magnitude of the field strength. In Section 2.1 the main features of the B - H loop are described and it is seen that a number of different permeabilities may be distinguished. Of these it is the incremental or reversible permeability that is of interest in transducer design. Fig. 3.6 shows the incremental permeability as a function of field strength for simple magnetic circuits composed of typical ferrites. It is seen that in the absence of an air gap the incremental permeability varies from a value equal to the initial permeability when the superimposed steady field is small, to a value approaching unity when the steady field is large enough to saturate the material.

This phenomenon has long been used as a means of controlling current at power frequencies. In its simplest form the current is controlled by a choke, the reactance of which may be varied by passing a direct current through a separate control winding. More elaborate forms of control by this method are described in the literature on magnetic amplifiers.

The extension of the method to high frequency circuits was described in 1938¹ but the limitations of the available

high frequency core materials prevented its practical use. Laminated cores gave a large range of control but the losses were too high, whereas powdered iron cores which had relatively low H.F. losses were unsatisfactory because of the small range over which it was possible to vary the permeability.

When ferrites became available these difficulties were greatly reduced. Ferrites have low losses and relatively high permeabilities which can be readily varied with a polarizing field. With these materials came the possibility of controlling the inductance in H.F. circuits electrically, remotely and automatically.^{2, 3} A wide variety of applications have been described. They include:

1. Remote tuning of receivers, e.g. manually in communication receivers or electronically in panoramic receivers,⁴
2. Remote or automatic antenna matching (or tuning),⁵
3. Automatic frequency control,
4. Frequency modulation in F.M. generators, frequency sweep generators and telemetering systems,⁶
5. H.F. switching and attenuation,⁷
6. Variable coupling transformers,
7. Variable frequency filters,⁸
8. Control of frequency in particle accelerators such as synchrotrons,^{9, 10}
9. Television raster correction.¹¹

6.2. GENERAL MODE OF OPERATION

6.2.1. The magnetic circuits

The basic magnetic and electrical circuits are shown schematically in Fig. 6.1. The H.F. core is situated between the poles of a magnetic yoke. Usually the H.F. core and the yoke are separate items but in some designs they may be formed from the same piece or pieces of ferrite. A control winding on the yoke applies a field to the H.F. core. The associated flux divides equally between the two sides of this core. The signal winding, the inductance of which it is proposed to control, is wound on the H.F. core in two series-aiding halves, one on each side. This arrangement is used to avoid magnetic coupling between the H.F. winding and the windings on the yoke; the flux linkages between the yoke and the two halves of the H.F. winding ideally cancel. A high degree of isolation is essential because otherwise the impedance associated with the control winding would be reflected into the H.F. circuit giving rise to additional losses and self capacitance. The bias winding is not always necessary; it permits the H.F. core to be set to a selected working point on the B - H curve, but sometimes the mean current in the control winding has the appropriate value. In some designs bias is achieved by means of a permanent magnet; this reduces the operating power. Practical arrangements will be discussed later in this section.

The operation may be explained qualitatively with reference to Fig. 6.2. In (a) a typical relation between the ampere-turns applied to the yoke and flux in the yoke is shown. If the steady or bias m.m.f. is represented by $(NI)_b$ and the control m.m.f. is varied over a total excursion $\Delta(N_1I_1)$ then the flux, Φ , in the yoke varies over the range $\Delta\Phi$. Assuming no leakage flux, the sum of the control fluxes in the two arms of the H.F. core equals the flux in the yoke. If the subscript 1 refers to the yoke and 2 refers to either of the side limbs, the following simplified analysis of the control conditions may be written:

$$B_2 = \frac{B_1 A_1}{2 A_2} \quad (6.1)$$

$$N_1 I_1 = \frac{\Phi}{\mu_0} \left[\frac{l_1}{\mu_1 A_1} + \frac{l_2}{2 \mu_2 A_2} \right] \quad \text{A} \quad (6.2)$$

where N_1 is the number of turns on the control winding

$$N_1 I_1 = \frac{B_1 A_1}{\mu_0} \left[\frac{l_1}{\mu_1 A_1} + \frac{l_2}{2 \mu_2 A_2} \right]$$

$$\therefore B_2 = \frac{\mu_0 N_1 I_1}{\frac{2 l_1 A_2}{\mu_1 A_1} + \frac{l_2}{\mu_2}} \quad \text{T} \quad (6.3)$$

This relation is of limited usefulness because (1) it ignores the reluctance of the horizontal branches of the H.F. core, (2) μ_2 is a function of B_2 and (3) the permeability of the H.F. core varies along the local magnetic path length so there is no simple relation between B_2 and the effective incremental permeability of the H.F. core. However in practice it is often sufficient to estimate the limiting conditions. When the control current is small the H.F. core has a permeability that is near the initial (unpolarized) permeability. As the control current increases and the H.F. core progresses towards saturation, the yoke reluctance, in an efficient device, should become negligible. Eqn 6.3 then reduces to

$$B_2 = \frac{\mu_0 \mu_2 N_1 I_1}{l_2} \quad \text{T}$$

$$\text{or } H_2 = \frac{B_2}{\mu_0 \mu_2} = \frac{N_1 I_1}{l_2} \quad \text{A.m}^{-1} \quad (6.4)$$

So far only the control magnetic circuit has been considered. Fig. 6.2(b) shows the corresponding conditions in the H.F. core. Such a diagram requires careful interpretation. An H.F. signal corresponding to a field strength excursion ΔH_s acting around the H.F. magnetic circuit will produce a corresponding flux density ΔB_s . The effective incremental permeability will be complicated by the varying degree of polarization round the H.F. magnetic circuit. Further, ΔH_s and ΔB_s refer to a different magnetic circuit to that which determines the steady or control conditions. Indeed, the major loop drawn in this diagram cannot refer directly to the H.F. magnetic circuit as such but only to those parts of it influenced by the control field. And the conditions in these depend to some extent on the conditions in the yoke.

To obtain a qualitative picture of the operation these difficulties may be ignored. The steady field strength may be regarded as being controlled over the extent of the major loop, and the minor H.F. loop will change its slope successively as shown. Thus the effective incremental permeability ($= \Delta B_s / \mu_0 \Delta H_s$) of the H.F. core may be

$$(6.2) \quad N_1 I_1 = \frac{10 \Phi}{4 \pi} \left(\frac{l_1}{\mu_1 A_1} + \frac{l_2}{2 \mu_2 A_2} \right) \quad \text{A}$$

$$(6.3) \quad B_2 = \frac{0.4 \pi N_1 I_1}{\frac{2 l_1 A_2}{\mu_1 A_1} + \frac{l_2}{\mu_2}} \quad \text{Gs}$$

$$(6.4) \quad H_2 = \frac{B_2}{\mu_2} = \frac{0.4 \pi N_1 I_1}{l_2} \quad \text{Oe}$$

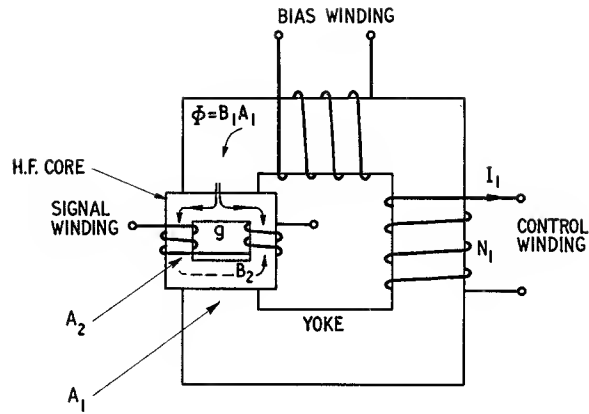


Fig. 6.1. Schematic diagram of a transducer

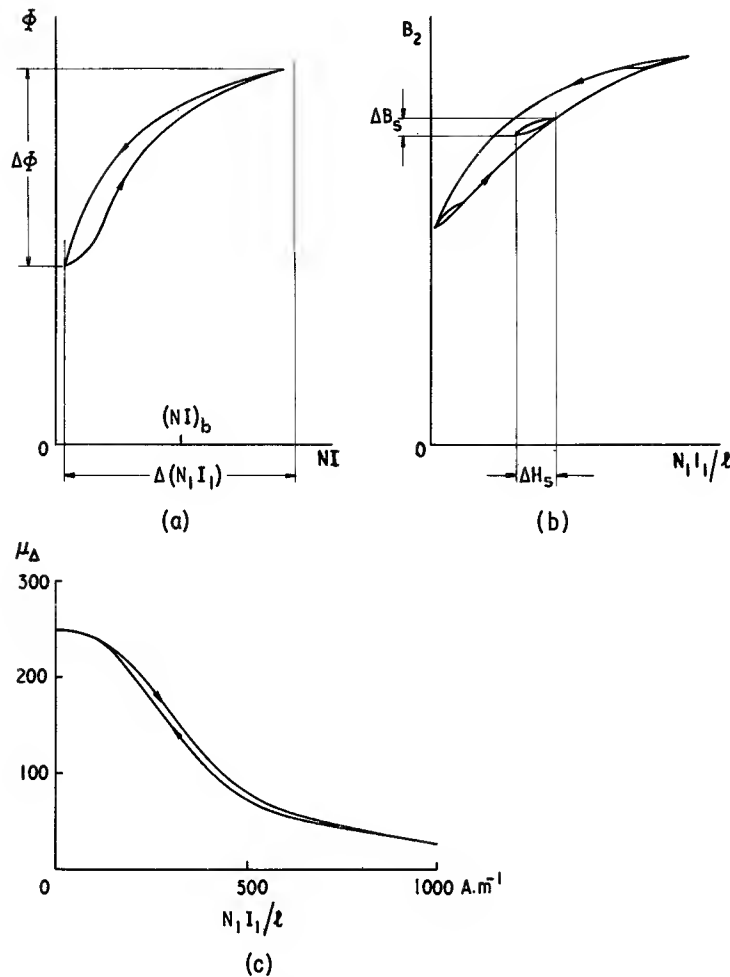


Fig. 6.2. Curves illustrating the operation of a transducer. (a) The relation between the control flux and the control m.m.f. (b) The relation between the flux density and field in the H.F. core due to currents in the signal winding as a function of the operating point of the H.F. core. (c) The incremental permeability of a typical H.F. core as a function of the control field strength

varied and the inductance of the signal winding will vary accordingly. Fig. 6.2(c) shows a typical relation between μ_A and $N_1 I_1 / l$. Within the limitations mentioned above the quantitative relation for a particular core may be estimated from the graphs showing μ_A as a function of $N I / l$ for the (ungapped) material. Such graphs are shown in Fig. 3.6. When the control current (plus the bias current, if any) approaches zero the effective incremental permeability of the H.F. core will approach the initial permeability and the inductance of a winding on that core may be calculated. When the control current is sufficient to saturate the vertical limb of the H.F. core the effective incremental permeability will approach unity. However, the shape of the curve in Fig. 6.2(c) and the curves in Fig. 3.6 suggests that the extra inductance range obtainable from complete saturation is not worth the large increase in control current that is necessary.

So far the hysteresis effects illustrated in Fig. 6.2 have not been introduced into the discussion. The hysteresis shown by the composite control magnetic circuit, Fig. 6.2(a), is partly due to the yoke and partly due to the H.F. core. Often the H.F. core is made of nickel zinc ferrite which may have a large amount of magnetic hysteresis. The overall hysteresis may be minimized by making the yoke of low hysteresis material such as manganese zinc ferrite. Other methods depend on the electronic regulation of the control current and will be briefly mentioned later. The control magnetic circuit hysteresis is reflected in the effective $B-H$ curve of the H.F. magnetic circuit, Fig. 6.2(b), and the incremental permeability becomes a two-valued function of $N_1 I_1 / l$, Fig. 6.2(c).

6.2.2. Temperature dependence

An important consideration in the design of a transducer is the variation of temperature coefficient of inductance of the signal inductor as the control range is traversed. Fig. 6.3 shows the $B-H$ relation at two temperatures. Assuming the temperature coefficient of the initial permeability is positive the curve for the higher temperature will have the greater slope at the origin. However, at the higher temperature the material will saturate at a lower flux density so the two curves will cross. If the slope of the curve is taken as a rough indication of the magnitude of the incremental flux density then it is clear that at H_1 the temperature coefficient is positive, at H_3 it is negative and at H_2 it has an average value of zero.

In Fig. 3.9 the incremental permeability of a number of ferrites is shown as a function of temperature for increasing values of polarizing field. The polarizing field depresses the permeability and also lowers the temperature at which it peaks. Thus if it is required to have a zero temperature dependence at a particular temperature

the appropriate static field strength will be the value that places the peak at that temperature.

Sometimes magnetic polarization has been used for the express purpose of reducing the temperature coefficient of an inductor but usually this phenomenon is merely a by-product of operation of a transducer. If the required

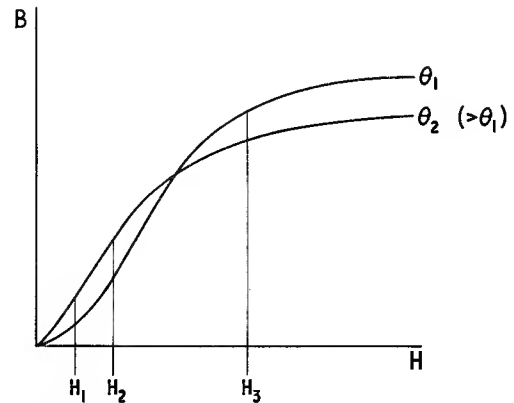


Fig. 6.3. Typical $B-H$ curves at two different temperatures illustrating the way in which the temperature dependence varies with H .

range of control is small, e.g. where a substantially linear inductance variation is required, then it is usually possible to arrange that the average temperature coefficient approaches zero over the control range. More often a large range of control is desired and any reduction of temperature dependence is incidental.

6.2.3. Core loss

The application of an external magnetic field increases the internal magnetic anisotropy and this moves the ferrimagnetic resonance to higher frequencies. In addition, the steady field reduces the number of domain walls in the material and this tends to reduce phenomena associated with domain wall movement, e.g. hysteresis loss and to some extent residual loss (see the caption to Fig. 3.12). Thus there will be a general lowering of the $\tan \delta$ curve as the steady field is increased. Experimental results are shown in Fig. 3.14.

In estimating the total loss of an inductor having an ungapped core the loss contribution from the core is represented by the core loss tangent. It is seen that this progressively falls as the steady field is increased. Therefore it is to be expected that the Q -factor of the H.F. inductor will rise as the field is increased, and in practice this is found to be true. However, at the same time as the core loss is decreasing the permeability and inductance are decreasing so that the winding loss tangent ($= R_{AC} / \omega L$)

increases. This causes the Q -factor to peak at an intermediate value of polarizing field and then to fall as the field is further increased. If however the inductor is resonated with a fixed capacitance, C , the resonant frequency will increase as the inductance falls; the winding loss tangent is then given by $R_{AC}\sqrt{C/L}$. Often this loss is negligible in H.F. transducers.

The behaviour of the loss factor, $(\tan \delta)/\mu$, which is the usual criterion of core quality, may also be mentioned here although it is not very relevant to the design unless the H.F. core is gapped. Since both numerator and denominator of this factor decrease with increasing steady field the overall effect depends on which decreases at the greater rate. At the higher frequencies $\tan \delta$ initially has the greater rate of decrease and the loss factor decreases as the field rises. When it reaches an intermediate value the rate of decrease of μ becomes larger; the loss factor then shows a minimum. (See also Fig. 3.14.)

6.2.4. General

The overall performance of a H.F. transducer is often expressed in graphical form, e.g. as in Fig. 6.4. Such graphs show the frequency at which the signal inductor resonates with a given capacitor, as a function of control current; the Q -factors are indicated at intervals along the curve.

In choosing the best ferrite for the signal core account must be taken of the required range of inductance control, the operating frequency range and the required Q -factors. Temperature coefficient and hysteresis may also be important. Factors affecting the choice of ferrite are discussed at the end of Section 6.4.

Throughout the foregoing discussion it has been assumed that the polarizing field is as far as possible directed along the same magnetic axis as the H.F. field and all the data relate to this mode of operation. It is quite

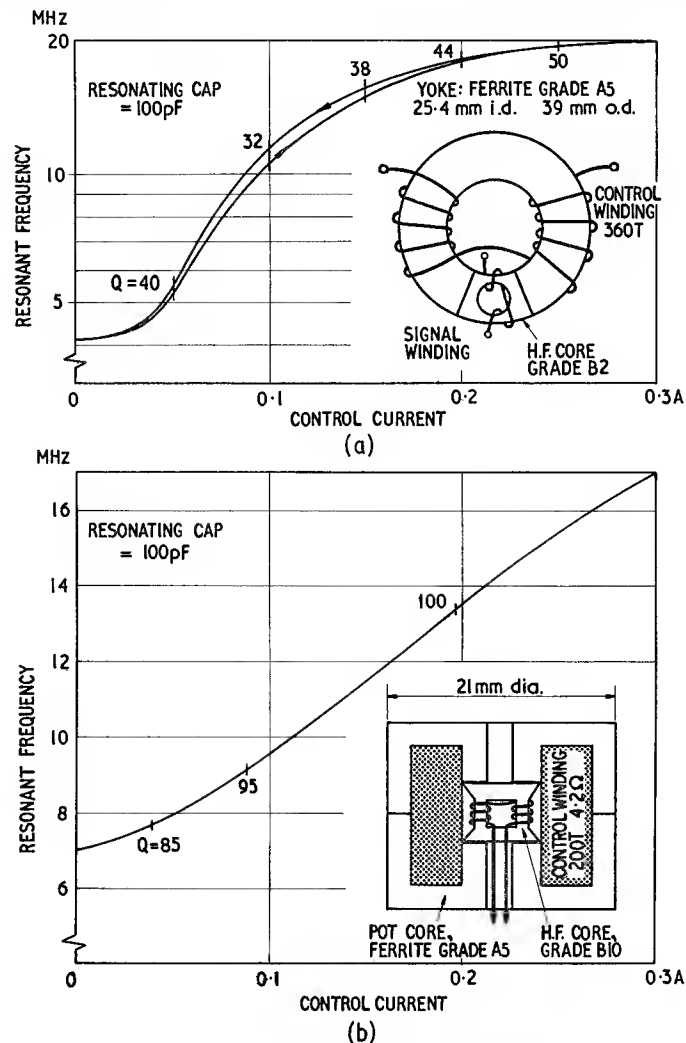


Fig. 6.4. The construction and performance of two experimental transducers

possible to make a transducer in which the static field is everywhere perpendicular to the H.F. field. The behaviour, while similar to the parallel case, is generally inferior; in particular the range of inductance control is usually smaller.

6.3 APPLICATIONS AND PERFORMANCE

The basic characteristics described in the previous section may now be put into their proper context by reference to practical examples drawn from the literature and elsewhere. The examples have been chosen to illustrate the wide range of applications and to give data on the performance that may be expected.

6.3.1. Experimental models

The author and some colleagues¹² have investigated a number of ferrites and configurations to assess their suitability as cores for transducers to operate at frequencies between 3 and 25 MHz. Fig. 6.4 shows some of the results obtained. The most interesting configuration was the 'picture frame' core made of nickel zinc ferrite placed between the recessed centre poles of an otherwise standard ferrite pot core. The control winding is in the position of the normal pot core winding and because the pot core is designed to make efficient use of the winding space a good sensitivity was achieved. In the example illustrated the signal inductor was resonated with a capacitance of 100 pF and the resonant frequency was variable from 7 to 17 MHz with a Q -factor of about 100. The maximum control winding power was 0.4W and the overall diameter was 21 mm.

6.3.2. Antenna tuning

The most obvious application is the remote or automatic tuning of R.F. circuits in communication systems. Newhall, Gomard and Ainlay⁵ have described the use of a transducer for the remote adjustment of the antenna matching circuit in a 12W marine transmitter operating in the 2 to 4 MHz band. Fig. 6.5 shows the practical construction, the performance and the basic circuit in which it was used.

The signal inductor uses a ferrite pot core and is mounted between the poles of a silicon iron yoke which carries the control windings. Copper foil is placed between the ferrite and the poles to prevent the H.F. flux from entering the iron and thereby increasing the loss in the signal inductor. The coaxial cable from the antenna is connected to the tank circuit (T) through a wide-band

ferrite-cored transformer.

The tank circuit is tuned with the circuit broken at A , the milliammeter indicating the resonance by a minimum in the current. The circuit is then restored, and if the secondary circuit is reactive the transmitter will be letuned. The direct current to the transducer control winding, L_C , is then varied by means of a rheostat until the H.F. inductor, L_A , has the correct value to tune the antenna and the secondary circuit becomes resistive. The correct adjustment is indicated by the restoration of tank circuit resonance, the tank capacitance not entering into this adjustment. The radio frequency chokes (R.F.C.) isolate the control circuit from the radio frequency while the capacitors C_1 and C_2 block the d.c. from the R.F. circuits. The diode limits the back-e.m.f. developing across the control winding when the d.c. is switched off. The thermistor, V , is arranged to compensate the temperature coefficient of the signal inductor L_A through the medium of the control current.

It is obviously possible to make this adjustment automatic by linking the control current adjustment to the tank circuit tuning.

6.3.3. Control of a synchrotron field

This application concerns the control of the frequency of the accelerating field in a proton synchrotron. As the protons accelerate they are held in an orbital track by the increasing intensity of the transverse magnetic field. Because the track radius is constant the accelerating field must increase in frequency to keep step with the speed of revolution. For a particular device described by Pressman and Blewett⁹ the range of control required is 343 to 4181 kHz (1 : 12.2) with 0.3% stability.

The construction chosen was a ferrite toroid with a slot cut in the side to receive the H.F. winding. Fig. 6.6 shows the arrangement and the performance achieved. By winding the H.F. inductor in two halves, one on each limb formed by the slot, coupling between the H.F. and control winding is avoided. The core and H.F. winding were enclosed in an annular box which carried the toroidal control winding. It was necessary to pump oil at constant temperature through the box in order to achieve the necessary temperature stability.

6.3.4. Dynamic raster correction in colour television

In colour television it is necessary to design the deflection coils to give optimum spot quality and such a design gives rise to some pin cushion distortion of the raster, see Fig. 6.7(a). This distortion may be corrected by modulating the line-scanning current with a parabolic waveform at the same frequency as the field (or frame)

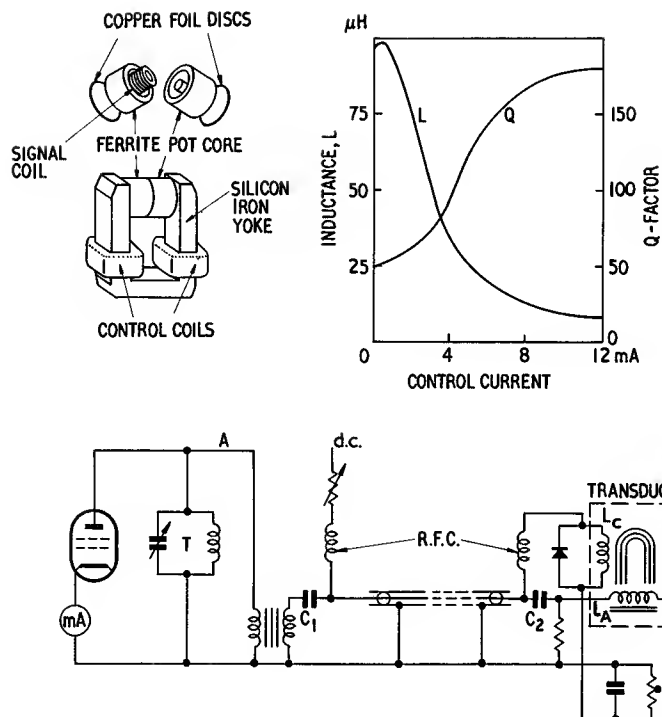


Fig. 6.5. The construction, performance and circuit of a remotely controlled antenna matching system. (After Newhall et al⁵)

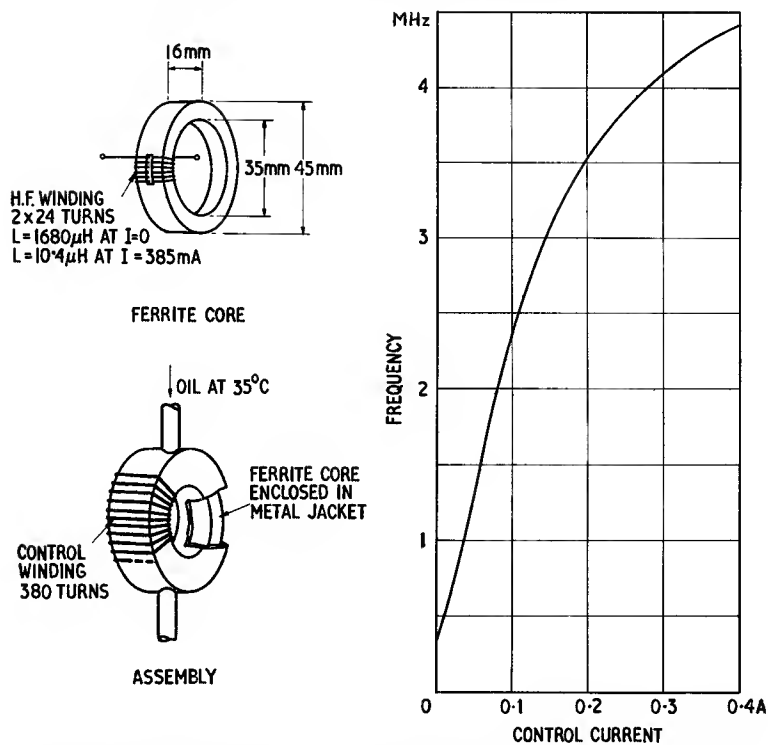


Fig. 6.6. The construction and performance of a transducer controlling the frequency of the accelerating field in a proton synchrotron. (Courtesy of Pressman et al⁹)

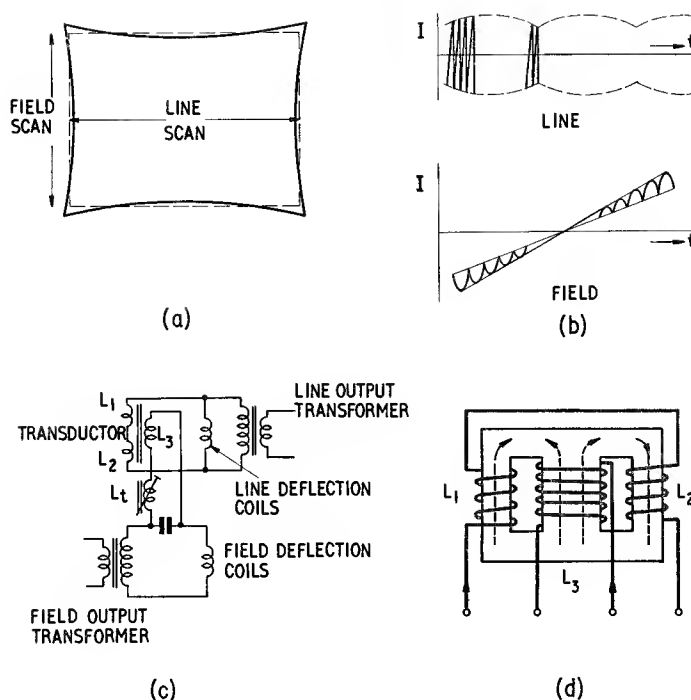


Fig. 6.7. Dynamic raster correction in colour television. (a) Pin cushion raster distortion, (b) Corrective modulation of the line and field waveforms, (c) Basic correction circuit, (d) Transductor arrangement. (Courtesy of Wöbler¹¹)

scan and modulating the field-scanning current with a parabolic waveform at the line-scanning frequency, see Fig. 6.7(b).

One method of achieving this raster correction has been described by Wöbler,¹¹ it uses a transductor between the line and field deflection circuits. Fig. 6.7(c) shows a simplified circuit which illustrates the basic principles. The transductor uses a double aperture ferrite core, Fig. 6.7(d). The centre limb carries a winding which is connected in series with the field deflection coils so that the core is taken towards saturation at each end of the field scan. The two outer limbs carry windings series-connected so that, when the core is unsaturated, there is no coupling with the winding on the centre limb. Thus the impedance of the series-connected windings decreases towards each end of the line scan and, because they shunt the line deflection coils they modulate the line deflection current in the required manner.

As the field current increases towards the saturation value, the balance of flux in the core is disturbed because in one outer limb the fluxes due to the line and field current add together while in the other outer limb they are in opposition. Thus one of the outer limbs is driven further towards saturation than the other. It follows that there is a coupling between the line and field circuits

which varies from zero at the centre of the field scan to equal and opposite maxima at each end of the field scan. If the voltage due to this coupling were injected directly in series with the field deflection circuit the correction would be in the wrong sense. This is overcome by connecting a capacitor across the centre-limb winding such that it is resonated below the line frequency. The inductor L_t is introduced to control the correction required. The resultant current at line frequency provides the necessary modulation of the field scanning current.

6.3.5. Commercially available transductors

Several ranges of transductors are commercially available. An example taken from the literature of the Wiltek Inc¹³ will serve as an illustration. Fig. 6.8 shows the details of the construction and performance. The core is formed from two rings of ferrite, the control and bias winding being applied to the two rings in parallel while the signal winding is in two series halves, each embracing one ring and wound in opposite directions so that coupling with the control winding is avoided. In such a construction the inductance of the control winding varies with control current in proportion to the inductance of the signal

winding. The control winding has a nominal inductance of 6H and a d.c. resistance of 1000 Ω . The peak control current is limited to 50 mA and the R.M.S. control current is limited to 30 mA. Thus the peak control power required to achieve the maximum frequency is 2.5W and the maximum continuous control power is 0.9W.

This saturable reactor covers the A.M. broadcast band and would be applicable to swept-frequency signal generators operating in this band. It could also be used for remote tuning of a radio receiver but due to the steady control current being limited to 30 mA the range of tuning would be inadequate to cover the whole A.M. band. In either of these applications it may be desirable to use several tuned circuits operating in unison, i.e. tracking. Specially matched groups are available for this purpose.

6.4. DESIGN AND OPERATING TECHNIQUES

Because a transducer is current operated it is preferable that the impedance of the control winding should be low; resistance will absorb power from the control circuit, and inductance may lead to long time constants and resonance effects. The control winding should be supplied from a constant current (high internal impedance) source. This will ensure that the control ampere-turns are determined only by the control circuit and are not affected by any variations of control winding resistance or inductance. The resonant frequency of the control winding should be well above the maximum control current frequency.

The operating point, as previously mentioned, may be set by means of a magnet, a bias winding or by the

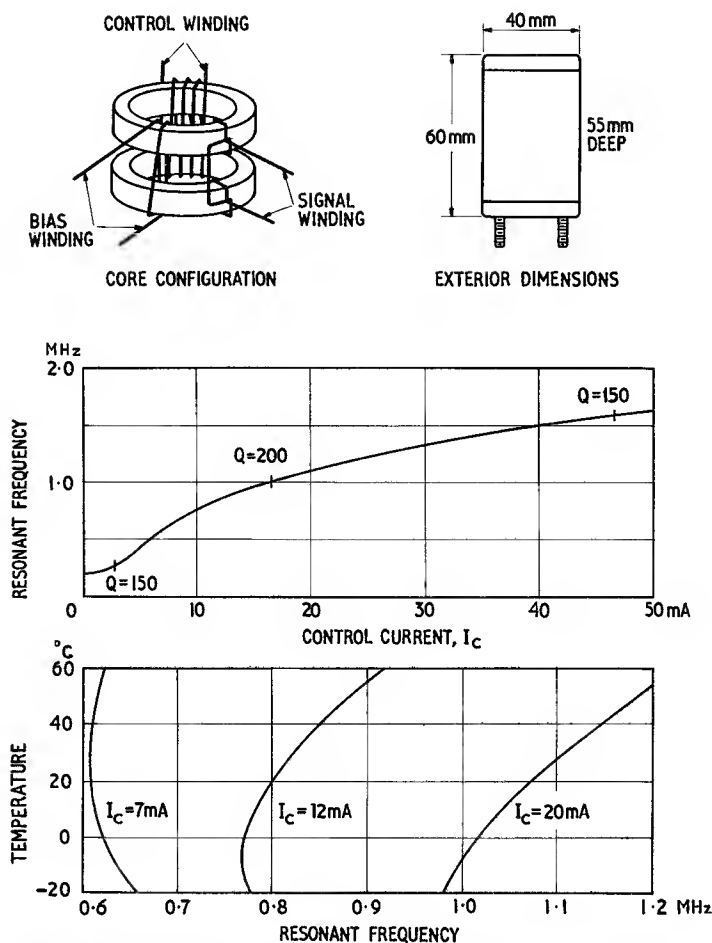


Fig. 6.8. Performance data on a typical commercially available transducer (Courtesy of Wiltek Inc ¹³)

Control winding: $L = 6H$, $R = 1000\Omega$

Peak current ≤ 50 mA

R.M.S. current ≤ 30 mA

Bias winding: $L = 0.175H$, $R = 200\Omega$

Nominal current = 10 mA

average control current. Assuming that there is no feedback in the control circuit, the choice of operating point will depend on the relative importance of control range, linearity and temperature coefficient.

If the maximum control range is required then the linearity requirement reduces merely to accommodating the control range ($\Delta(N_1 I_1)$) in Fig. 6.2(a) between saturation and the point of maximum μ_A . This latter point may, due to hysteresis, lie a little to the left of the Φ axis. The greatest inductance linearity will be obtained with a small control range centred about the point of inflection of the $\mu_A - N_1 I_1/l$ curve. A possible alternative requirement is for a linear variation of resonant frequency with control current. An approximation to this is obtainable over a limited range by choosing a working point such that μ_A is proportional to $(N_1 I_1)^{-2}$. In practice linear frequency control is more conveniently obtained by a feedback system as described later.

effective control range will be reduced. The loss tangent will also be reduced. Therefore the gapping technique may be reserved for stable, high Q -factor inductors which do not require a high sensitivity.

Another obvious technique is to enclose the device in a temperature controlled box such as an oven of the type used for crystal resonators. By this means the resonant frequency may be held to better than 500 ppm over a wide ambient temperature range. Yet another method that has been used successfully is to shunt or series connect the control or bias winding with a network comprising thermistors and resistors arranged to compensate the temperature coefficient of the H.F. core by the automatic adjustment of the working point. Since the required compensation varies over the control range (see Fig. 6.8) this method is of limited application.

There is in practice considerable difficulty in isolating the control and signal circuits. Coupling can result in a

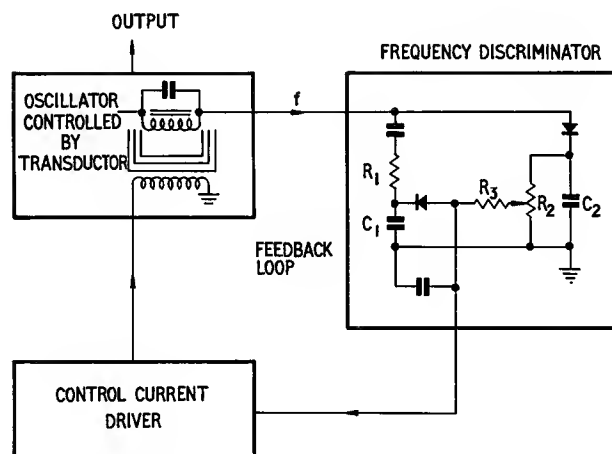


Fig. 6.9. Simplified schematic diagram of closed loop control of transductors

It was mentioned in Section 6.2.2 that the temperature coefficient of inductance depends on the working point. In practice zero temperature coefficient may be approached only if the control range is very small. If the control range is not small then the best compromise must be sought for the temperature coefficients at each end of the range, see Fig. 6.8. When no other attempt is made to reduce the temperature coefficient the fractional change of inductance may typically range from 0.01 to 2% per °C. These relatively high values arise from the use of an ungapped H.F. core. They may be reduced, as in ferrite cored inductors, by introducing an air gap (see Sections 2.2.2, 4.2.2 and 5.5.2). This should be done in such a way that the gap does not intercept the control flux, e.g. by placing it at g in Fig. 6.1. The control of the incremental permeability of the side limbs of the H.F. core will be unaffected but, of course, the gap will reduce the value, and the variation, of the effective permeability so the

very large decrease in Q -factor. If the control and signal windings share a common magnetic core, minor unbalances in magnetic symmetry result in appreciable coupling. If the signal core is separate as in Fig. 6.1, the H.F. field may leak into the yoke particularly if the H.F. core has air gaps near the pole faces of the yoke. The yoke material may have a very large magnetic loss at the signal frequency and so contribute to a decrease in Q -factor. A suitable copper foil screen between the signal core and the yoke will prevent this form of coupling but it will introduce some eddy current loss into the signal inductor and in addition it introduces a gap in the control magnetic circuit. The minimum thickness for such a screen may be judged from Fig. 11.6.

So far, the discussion has been concerned with the performance of ferrite transductors as isolated devices. The stability and hysteresis problems may be overcome without sacrifice of control range by using a closed loop

control circuit. Fig. 6.9 shows a very simplified block schematic diagram intended to illustrate the basic principle. The transducer controls an oscillator which has a feedback path to a frequency discriminator. This circuit is arranged to give a d.c. signal proportional to the deviation of the frequency of the oscillator from a given value. This may conveniently be done by taking a part of the available oscillator signal, passing it through an RC circuit, R_1C_1 , so that its amplitude varies with frequency, and then applying it to a detector. The magnitude of the d.c. voltage obtained is dependent on the oscillator frequency and amplitude. The other part of the oscillator output is simply rectified and applied, through a variable potentiometer, R_2 , in a series opposing connection with the frequency-sensitive d.c. voltage. The resultant voltage depends on the frequency of the oscillator, the setting of the potentiometer and the amplitude of the oscillator output. This error signal is amplified and applied to the control circuit of the transducer in such a way as to reduce the error signal. The oscillator will be automatically set to a frequency such that the error signal is zero; since this means that the two components of the error signal are equal and opposite, the setting is immune to changes of oscillator amplitude. The frequency depends only on the setting of the potentiometer so the effects of temperature and hysteresis are virtually eliminated. The circuit could easily be used to control a number of matched transducers connected in cascade. Clearly the potentiometer could be replaced by some electronic means of attenuation or gain control so that automatic control of sweep may be used.

Finally it is useful to consider the relative merits and limitations of the various grades of ferrite; Figs. 3.6, 3.9 and 3.14 show relevant properties of materials that may find application in transducer design.

The high permeability manganese zinc ferrites have the greatest sensitivities; inductance ratios of 300:1 are obtainable without excessive control fields, e.g. 200 A.m.⁻¹ provided the core may be ungapped. If excessive core loss is to be avoided the lowest frequency of the control range should not exceed about 400 kHz (e.g. see Fig. 3.14.1); it is assumed that as the control current is increased and the operating frequency rises the polarizing field will prevent any appreciable rise in loss factor. As previously stated, an air gap will raise the Q -factor, lower the temperature coefficient and restrict the control range.

At higher frequencies the choice must be confined to nickel zinc ferrites. These give rather small inductance ratios, e.g. 6:1 with 1000 A.m.⁻¹ for B10. The operating frequency range for such a ferrite would be situated between about 5 and 50 MHz. Ferrite transducers operating up to 400 MHz have been reported.

When using nickel zinc ferrites for transducers it is necessary to take simple precautions to avoid mechanical

resonance of the core. Nickel zinc ferrite has a relatively large magnetostriction so that under the influence of combined a.c. and d.c. fields mechanical resonances are likely to occur. As these resonances have many overtones the electrical performance of the transducer may be impaired by the spectrum of the motional impedance. The application of heavy mechanical damping such as varnish, immersion in oil or encapsulation in an elastomer is usually completely effective in preventing this trouble.

REFERENCES AND BIBLIOGRAPHY

Section 6.1.

1. DE KRAMOLIN, L., 'Magnetic tuning devices', *Wireless Wld.*, **42**, 160, (1938).
2. STIBER, S., 'Electronically tunable circuit elements', *Trans. Inst. Radio Engrs.*, **MIL-4**, 527, (1960).
3. KISER, J. L., 'The electrically variable inductor', *Electron. Inds.*, **20**, no. 6, 144, (1961).
4. STIBER, S., 'Remote tuning receiver has no moving parts', *Electronics*, **26**, no. 7, 186, (1953).
5. NEWHALL, E., GOMARD, P. and AINLAY, A., 'Saturable reactors as R.F. tuning elements', *Electronics*, **25**, no. 9, 112, (1952).
6. SLATER, F., 'A ferrite frequency modulator', *Marconi Instrum.*, **4**, 186, (1954).
7. JACKSON, R. C. and SIMPSON, A. W., 'A high frequency ferrimagnetic attenuator', *Electron. Engng*, **34**, 246, (1962).
8. BESKOROVAINYI, B. M., VOL'F, V. M., GORBENKO, V. S., KAROVSKII, M. L., SHOTSKII, B. I. and IUR'EV, A. A., 'Variable ferrite filters', *Radio Eng. USSR.*, **15**, no. 9, 79, (1960).
9. PRESSMAN, A. I. and BLEWETT, J. P., 'A 300- to 4,000-kilocycle electrically tuned oscillator', *Proc. Inst. Radio Engrs*, **39**, 74, (1951).
10. LOMBARDINI, P. P., SCHWARTZ, R. F. and DOVIAK, R. J., 'Measurements of the properties of various ferrites used in magnetically tuned resonant circuits in the 2.5 to 45 Mc/s region', *J. appl. Phys.*, **29**, 395, (1958).
11. WÖLBER, J., 'A saturable core reactor for raster correction in colour television receivers', *Electron. Applic.*, **26**, 43, (1965).

Section 6.3.1.

12. WHILLIER, R. T. and WHITBOURN, E. A., 'Performance of ferrite saturable reactors in the frequency range 1-40 Mc/s', unpublished report, (1962).

Section 6.3.2.

5. NEWHALL, E., *et al.*, see Section 6.1, ref. 5.

Section 6.3.3.

9. PRESSMAN, A. I., *et al.*, see Section 6.1, ref. 9.

Section 6.3.4.

11. WÖLBER, J., see Section 6.1, ref. 11.

Section 6.3.5.

13. *Track Incredutors*, technical literature by Wiltek, Inc., Wilton, Conn., U.S.A.

General

- HARVEY, R. L., GORDON, I. and BRADEN, R. A., 'The effect of a d-c magnetic field on the U.H.F. permeability and losses of some hexagonal magnetic compounds', *R.C.A. Rev.*, **22**, 648, (1961).
- BARKER, R. C., 'Nonlinear magnetics', *Electro-Technology*, **71**, no. 3, 95, (1963).
- GEYGER, W. A., *Nonlinear-magnetic control devices*, McGraw-Hill Book Company, (1964).
- STUITS, A. L., VERVEEL, J. and PELOSCHEK, H. P., 'Dense ferrites and their applications', *Trans. I.E.E.E., Commun. Electron.*, no. 75, 726, (1964).

Wide Band Transformers

7.1. INTRODUCTION

Wide band transformers are used extensively in communication systems. They may be used to match different impedances, provide accurate current or voltage ratios, provide interconnection between balanced and unbalanced circuits and to provide d.c. isolation. Because the signal power levels in a communication system are low except at the output stages most wide band transformers are not required to transmit appreciable amounts of power. On the other hand most high power transformers operate at a single frequency or over a narrow frequency band. The design procedure for such transformers is considered in Chapter 9; it differs fundamentally from the approach to wide band transformers. However, it is sometimes required to design a wide band high power transformer and then it is necessary to combine both procedures, considering the power limitations of the core and winding together with the limitations due to leakage inductance and self capacitance. In this chapter the emphasis will be on low power wide band transformers but most of the transmission relations apply to transformers of any rating.

The voltage applied to a wide band transformer is usually complex, containing energy distributed over a wide spectrum, and ideally it is required that the voltage waveform appearing across the load shall have lost

nothing by the transformation. The fractional bandwidth may be defined as the ratio f_2/f_1 where f_2 is the highest frequency to be transmitted satisfactorily and f_1 is the corresponding lowest frequency. Fig. 7.1 shows a typical transmission characteristic of a wide band transformer,

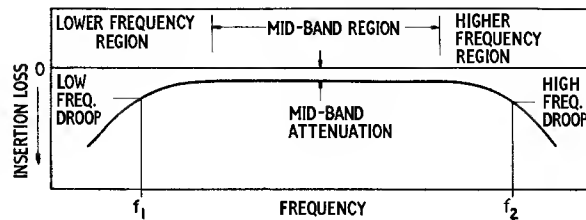


Fig. 7.1. Idealized transmission characteristic of a wide band transformer showing the main features

indicating the main features. In practice, bandwidths are rarely less than 10 and may in some applications be required to exceed 1000. Such bandwidths are possible only when the primary and secondary windings are tightly coupled; narrow bandwidth transformers such as those used in intermediate frequency amplifiers are very loosely coupled.

Pulse transformers, which are considered in the next chapter, may be regarded as a special case of a wide band transformer. The information characterizing the pulse is

usually distributed over a wide band and if an effective bandwidth may be assigned to it then the design procedures discussed in this chapter may be used. However since the avoidance of pulse distortion involves both the attenuation and phase shift characteristics it is usually better to design a pulse transformer using the pulse characteristics directly, as described in the next chapter.

7.2. THE TRANSMISSION AND REFLEXION CHARACTERISTICS IN TERMS OF THE EQUIVALENT CIRCUIT ELEMENTS

7.2.1. Some basic concepts

The relations between the equivalent circuit of a transformer and its transmission and reflexion characteristics are a special case of the more general passive network theory. Since, in the present context, the emphasis is on the application of ferrite in practical transformer design, much of the fundamental theory must be assumed. However, a summary of the basic network concepts is given in this section and, in the following sections, the essential transformer design equations and functions are presented. Derivations and a fuller treatment may be found in the standard text books.

Fig. 7.2 illustrates some basic properties of passive networks. If a source having resistance R_a is connected to a load of resistance R_b , the power in the load is given by $E_a^2 R_b / (R_a + R_b)^2$. This is a maximum when $R_a = R_b$. The maximum power in the load is called the applied power and is designated P_a .

$$P_a = \frac{E_a^2}{4 R_a} \quad \text{W} \quad (7.1)$$

If $R_a \neq R_b$, the power in R_b may be made equal to the applied power by interposing an ideal transformer as shown in Fig. 7.2(b). Since an ideal transformer has no energy losses or series reactances, the terminal voltages will equal the winding e.m.f.s. Considering the magnetic induction in the core

$$\frac{d\Phi}{dt} = \frac{U'_b}{N_1} = \frac{U_b}{N_2} \quad \text{V} \quad (7.2)$$

where Φ is the flux in the core and N_1, N_2 are the primary and secondary turns respectively

$$\therefore U_b = U'_b \frac{N_2}{N_1} = U'_b r \quad \text{V} \quad (7.3)$$

where r is the turns ratio N_2/N_1

If I_1 and I_2 are the primary and secondary currents respectively, then:

$$\begin{aligned} \text{input power} &= I_1 U'_b = \text{output power} = I_2 U_b \\ \therefore I_2 &= I_1 / r \quad \text{A} \end{aligned} \quad (7.4)$$

The input resistance

$$\frac{U'_b}{I_1} = \frac{U_b}{r} \times \frac{1}{r I_2} = \frac{R_b}{r^2} = R'_b \quad \Omega \quad (7.5)$$

where R'_b is the load resistance as it appears at the primary terminals. When the transformation ratio is such that $R_a = R'_b$, i.e. when $r = (R_b/R_a)^{1/2}$, the transformer is said to match the source and load and the power in the load equals the applied power.

If the circuit shown in (a) is broken and a linear passive 4-pole network is inserted as shown in (c), then in general the power in the load will change. The change may be expressed as the insertion loss A_i . This is the ratio, in dB, of the power in the load without the network to the power in the load when the network is inserted i.e.

$$A_e = 20 \log_{10} \left| \frac{\text{Load voltage when network is replaced by direct connexion}}{\text{Load voltage with network}} \right| \text{ dB} \quad (7.6)$$

The insertion loss may be negative, i.e. a gain; this could be the case when the 4-pole is a matching transformer, the improvement in matching more than compensating for the loss introduced by the transformer. To avoid this difficulty when expressing the attenuation of a transforming network, the following definition is adopted. The effective loss, A_e , of a network is the ratio, in dB, of the applied power to the power in the load when the network is inserted, i.e.

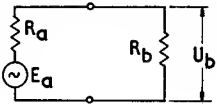
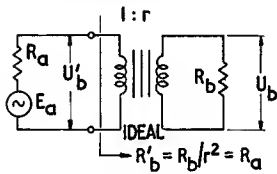
$$A_e = 20 \log_{10} \left| \frac{\text{Load voltage when network is replaced by ideal matching transformer}}{\text{Load voltage with network}} \right| \text{ dB} \quad (7.7)$$

The effective loss is normally used to describe the attenuation of a transformer since it compares it to an ideal matching transformer. If $R_a = R_b$, then the effective loss equals the insertion loss.

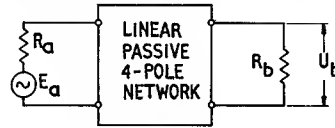
The insertion and effective losses include not only the dissipative components of the attenuation occurring within the network but also the mismatch losses occurring at its terminals. For example, mismatch between the source impedance and the input impedance of the network has the effect of reflecting a part of the applied power. This is illustrated in Fig. 7.2(d) and the following expressions are derived:

$$\text{Reflection coefficient} = \left| \frac{R_b - R_a}{R_b + R_a} \right| \quad (7.8)$$

$$(7.2) \quad \frac{d\Phi}{dt} 10^{-8} = \frac{U'_b}{N_1} = \frac{U_b}{N_2} \quad \text{V}$$

DIRECT CONNECTION OF SOURCE AND LOAD	CONNECTION OF SOURCE AND LOAD THROUGH AN IDEAL MATCHING TRANSFORMER
 $U_b = \frac{E_a R_b}{R_a + R_b}$ $\text{Power in } R_b = P_b = \frac{U_b^2}{R_b} = \frac{E_a^2 R_b}{(R_a + R_b)^2}$ <p>This is max. when $R_a = R_b$, then</p> $P_b = \frac{E_a^2}{4 R_a} = P_a, \text{ the applied power}$ <p style="text-align: center;">(a)</p>	 $U_b = \frac{r E_a}{2}$ $\text{Power in } R_b = P_b = \frac{E_a^2}{4 R_a} = P_a, \text{ the applied power}$ <p style="text-align: center;">(b)</p>

SOURCE AND LOAD CONNECTED THROUGH A LINEAR PASSIVE 4-POLE

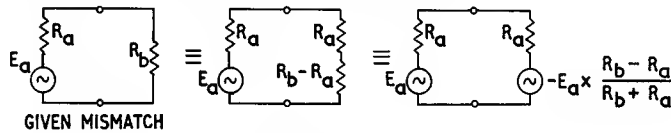


$$\text{Insertion loss of network} = A_i = 20 \log_{10} \left| \frac{U_b \text{ when network is replaced by direct connection}}{U_b \text{ with network}} \right| \quad \text{dB}$$

$$\text{Effective loss of network} = A_e = 20 \log_{10} \left| \frac{U_b \text{ when network is replaced by ideal matching transformer}}{U_b \text{ with network}} \right| \quad \text{dB}$$

(c)

MEASURE OF MISMATCH BETWEEN SOURCE AND LOAD



$$\text{Power reflected from load} = P_r = \frac{E_a^2}{4 R_a} \cdot \left(\frac{R_b - R_a}{R_b + R_a} \right)^2 \quad \text{W.} \quad \text{Reflection coefficient} = \frac{R_b - R_a}{R_b + R_a}$$

$$\text{Return loss} = A_r = 20 \log_{10} \left| \frac{R_b + R_a}{R_b - R_a} \right| \quad \text{dB. In general, } A_r = 20 \log_{10} \left| \frac{Z_b + Z_a}{Z_b - Z_a} \right| \quad \text{dB}$$

(d)

Fig. 7.2. A summary of useful expressions and definitions relating to passive networks

$$\begin{aligned} \text{Return loss} &= A_r = 10 \log_{10} \left| \frac{\text{Applied power}}{\text{Reflected power}} \right| \\ &= 10 \log_{10} \left| \frac{E_a^2}{4 R_a} \times \frac{4 R_a}{E_a^2} \left\{ \frac{R_b + R_a}{R_b - R_a} \right\}^2 \right| \\ &= 20 \log_{10} \left| \frac{R_b + R_a}{R_b - R_a} \right| \quad \text{dB} \end{aligned} \quad (7.9)$$

These expressions have been derived in terms of resistances but it may be shown that they are true also for

general impedances Z_a and Z_b in which case the expression within the modulus brackets will, in general, be complex. Return loss can, and often does, occur when there is simply a direct connection between source and load; in this case R_b is the load resistance. Generally, it is common practice to express any circuit impedance in terms of its return loss relative to a nominal or specified value.

Reflection or mismatch is often more troublesome than the attenuation and it is common to find that the return loss requirement in a wide band transformer specification

is more severe than that for insertion loss.

If the inserted network has no dissipation, i.e. it contains only pure reactances, then the attenuation must be due entirely to reflection and there will be a relation between the return loss and the effective loss. Of the applied power P_a let a proportion, P_r , be reflected, the remainder $(P_a - P_r)$ being transmitted into the load. The power in the load is

$$P_b = P_a - P_r$$

$$\text{but } \frac{P_a}{P_b} = \text{antilog}_{10} \frac{A_e}{10} \quad \text{and} \quad \frac{P_a}{P_r} = \text{antilog}_{10} \frac{A_r}{10}$$

$$\therefore \frac{1}{\text{antilog}_{10} \frac{A_e}{10}} = 1 - \frac{1}{\text{antilog}_{10} \frac{A_r}{10}} \quad (7.10)$$

This relation is true for any passive dissipationless network connected between any source and load. If the source and load impedances are equal then the relation concerns only the network. On the other hand the network may be a direct connection of unequal source and load impedances in which case the relation refers only to the effective loss and return loss between source and load. In general both forms of mismatch may be present. The alternative ordinate scales of Figs. 7.7 and 7.8 are nomograms for the above relation.

7.2.2. The equivalent circuit of a transformer

The foregoing summary refers to the general linear passive 4-pole network. The present section is concerned with a particular form of such a network, namely, the equivalent circuit of a transformer. The usual form of this circuit, inasmuch as it may be represented by lumped components, is shown in Fig. 7.3 in which the physical significance of each of the components is indicated. All the components that normally belong to the secondary side of the transformer have been transferred to the primary side and carry a prime to indicate this. Direct capacitive coupling between the primary and secondary circuits would cause the higher frequency signals to by-pass the transformer and this should be avoided; usually this capacitive coupling is eliminated by inserting an electrostatic screen between the windings. The actual transformation is provided by the ideal transformer shown at the R.H.S. of the diagram. In most of the discussion that follows, this ideal transformer will be ignored and attention will be confined to the equivalent circuit referred to the primary side. This is inserted between the source resistance R_a and the reflected load resistance R'_b . The attenuation of this equivalent circuit or of part of it may, in this context, be expressed as insertion loss. In most of the following discussion it is this insertion loss that will be referred to. This will avoid

any ambiguity which might arise when the transformer does not provide nominal impedance matching.

Referring to Fig. 7.1, the transmission characteristic of a wide band transformer may be divided into three parts, namely, the lower frequency region, the mid-band region, and the higher frequency region. These are usually far enough apart on a frequency basis to be considered

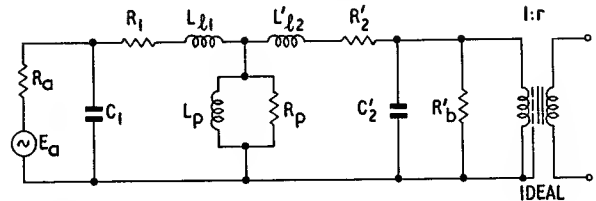


Fig. 7.3. Lumped-element equivalent circuit of a transformer
 E_a is the source e.m.f.

R_a is the source resistance

R_1 is the resistance of the primary winding

R'_2 is the resistance of the secondary winding referred to the primary side

R'_b is the load resistance referred to the primary side

R_p is the shunt resistance representing the total loss in the core
 C_1 is the effective capacitance shunting the terminals of the primary winding. This is usually the self capacitance associated with the primary winding plus any other capacitance shunting the input circuit

C'_2 is the corresponding secondary capacitance referred to the primary side

L_{l1} is the primary leakage inductance

L'_{l2} is the secondary leakage inductance referred to the primary side. Since leakage inductances are much smaller than the shunt inductance, L_p , the two leakage inductances are usually treated as one i.e. $L_l = L_{l1} + L_{l2}$

L_p is the open circuit inductance of the primary.

The direct capacitance between primary and secondary is usually eliminated by insertion of a screen as shown

separately, e.g. the factors which affect the lower frequency region usually have negligible effect in the higher frequency region and vice versa.

A typical transformer specification would state the maximum permitted effective loss at mid-band and the maximum permitted additional effective loss (or droop) at f_1 and f_2 respectively. The mid-band effective loss might be limited to about 0.5 dB and the specified maximum droop would be typically between 0.1 and 3 dB depending on the required flatness of the characteristic. If the specification includes return loss requirements, these, as previously observed, are usually more stringent than the attenuation requirements. A typical specification might set the minimum return loss to a value lying somewhere between 14 and 25 dB over all or part of the frequency band. For a dissipationless network these figures correspond to effective losses of 0.18 and 0.015 dB respectively, thus illustrating relative severity of the return loss requirements.

In certain special applications the phase shift of the load voltage due to the transformer may be specified.

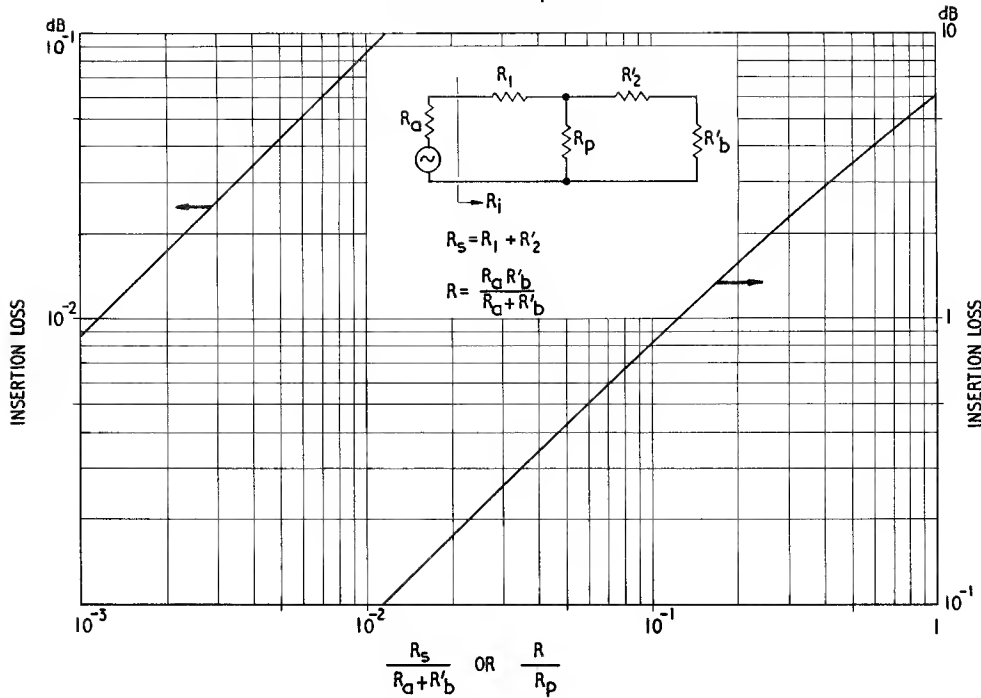


Fig. 7.4. Insertion loss due to series or shunt resistance

The three main regions of the transmission characteristic will now be considered. For each region the insertion loss, return loss and, in some cases, the phase shift will be related quantitatively to the elements of the equivalent circuit. The resulting expressions will facilitate the first stage of transformer design, i.e. to translate the specification into limit values of the equivalent circuit elements.

7.2.3. The mid-band region

For the majority of low and medium frequency transformers, and in particular those using ferrite cores, the only elements of the equivalent circuit which are likely to influence the transmission at mid-band are the winding resistances, $R_1 + R'_2 (= R_s)$, and the shunt resistance, R_p , representing the core loss. In certain circumstances the mid-band transmission of high frequency transformers may also be influenced by the shunt inductance; this possibility is considered in Section 7.4.1 and is disregarded in the present discussion.

It will be seen in Section 7.3.1, p. 253, that, for low frequency transformers having ferrite cores, the shunt loss resistance, R_p , is usually so large that it does not have a significant effect on the mid-band loss. On the other hand the effect of the winding resistance is usually negligible in the design of medium and high frequency transformers.

From Eqn 7.6 it is readily derived that the insertion loss due the series resistance is

$$A_i = 20 \log_{10} \left(1 + \frac{R_s}{R_a + R'_b} \right) \quad \text{dB} \quad (7.11)$$

while for the shunt resistance

$$A_i = 20 \log_{10} \left(1 + \frac{R}{R_p} \right) \quad \text{dB} \quad (7.12)$$

where $R_s = R_1 + R'_2$

$$R = R_a R'_b / (R_a + R'_b)$$

Fig. 7.4 represents these equations in graphical form. If both R_s and R_p are present and their individual contributions are small then the total insertion loss may be taken as the sum of the separate losses. It should be noted that if R_s significantly increases with frequency due to eddy current effects the mid-band characteristic will droop towards the upper end.

Eqn 7.9 gives the return loss of one resistance relative to another. Using this equation and referring to the diagram in Fig. 7.4 the input resistance R_i may be expressed in terms of its return loss relative to R'_b :

$$20 \log_{10} \left\{ \frac{2 + \frac{R'_b}{R_p} + \frac{R_s}{R'_b}}{\frac{R'_b}{R_p} \frac{R_s}{R'_b}} \right\} \quad \text{dB} \quad (7.13)$$

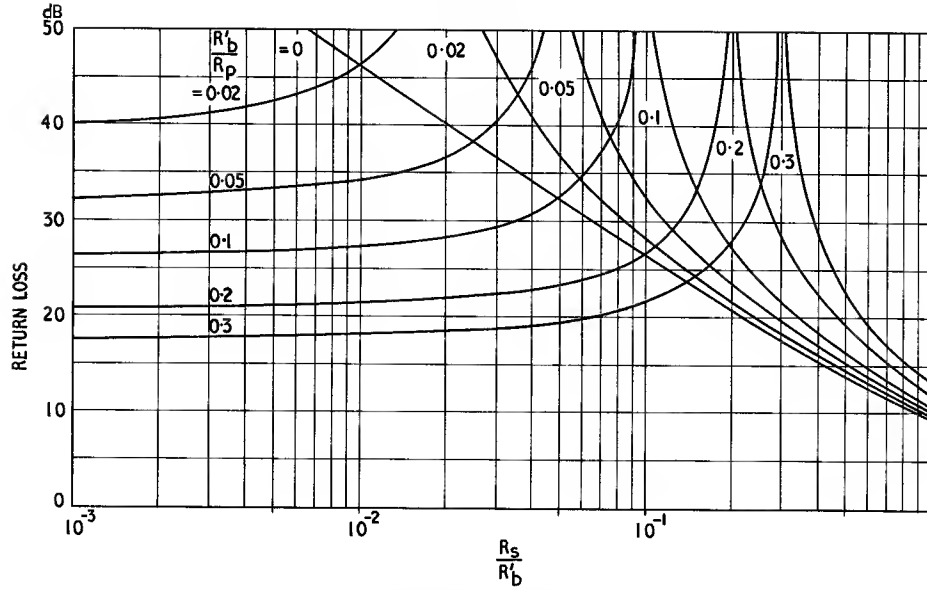


Fig. 7.5. Return loss (R_1 w.r.t. R'_b) due to any combination of series and shunt resistance

This assumes that $R_1 = R'_2$

This function is represented graphically in Fig. 7.5. If both R_s and R_p are present they compensate when $R_s/R'_b = R'_b/R_p$ and then the return loss is infinite (perfect matching). If $R_p = \infty$, the monotonic curve gives the return loss due to R_s , while if $R_s = 0$ the intercepts with the L.H. ordinate give the return loss due to R_p . An inspection of this graph suggests that it is not difficult to achieve a good mid-band return loss.

7.2.4. The lower frequency region

This is the region in the vicinity of f_1 (see Fig. 7.1). The term is relative; for a high frequency transformer f_1 might for example be in the neighbourhood of 10 MHz. In general the droop in the transmission characteristic in the lower frequency region is due to the shunt impedance. This impedance diminishes as the frequency decreases and causes a progressive increase in attenuation which is additional to the mid-band loss. In most cases the contribution of R_p to this droop is negligible; an exception arises when the flux density ($\propto f^{-1}$) is high enough to cause significant hysteresis loss and then R_p will decrease as the frequency falls. Ignoring this effect, the droop may be expressed in terms of the shunt inductance:

$$A_i = 10 \log_{10} \left\{ 1 + \left(\frac{R}{\omega L_p} \right)^2 \right\} \quad \text{dB} \quad (7.14)$$

The corresponding return loss of the input impedance relative to R'_b is

$$A_r = 10 \log_{10} \left\{ 1 + \left(\frac{2 \omega L_p}{R'_b} \right)^2 \right\} \quad \text{dB} \quad (7.15)$$

and the phase shift, ϕ , is given by

$$\tan \phi = \frac{R}{\omega L_p} \quad (7.16)$$

These three functions are expressed in Fig. 7.6, where the independent variable is $\omega L_p/R$ for insertion loss and phase shift, and $\omega L_p/R'_b$ for return loss. A limit on any of these three parameters at a given frequency will set a minimum value for L_p . This is usually the starting point for wide band transformer design.

It is possible under certain circumstances to improve the characteristic in the lower frequency region by inserting capacitance in series with the primary and/or secondary winding. This may be regarded as an analogue of the more usual practice for the higher frequency region which is considered in the next section. The technique for the lower frequency region is described in Section 7.2.6.

7.2.5. The higher frequency region—filter techniques

The transmission characteristic in the higher frequency region (i.e. in the region of f_2 in Fig. 7.1) is influenced mainly by the leakage inductance and the shunt capacitances, and their relation to R_s and R'_b . The winding resistance, if comparable to the leakage reactance or capacitive reactance, may also influence the shape of the characteristic but it is usual to assume that the winding resistance can be neglected in this respect.

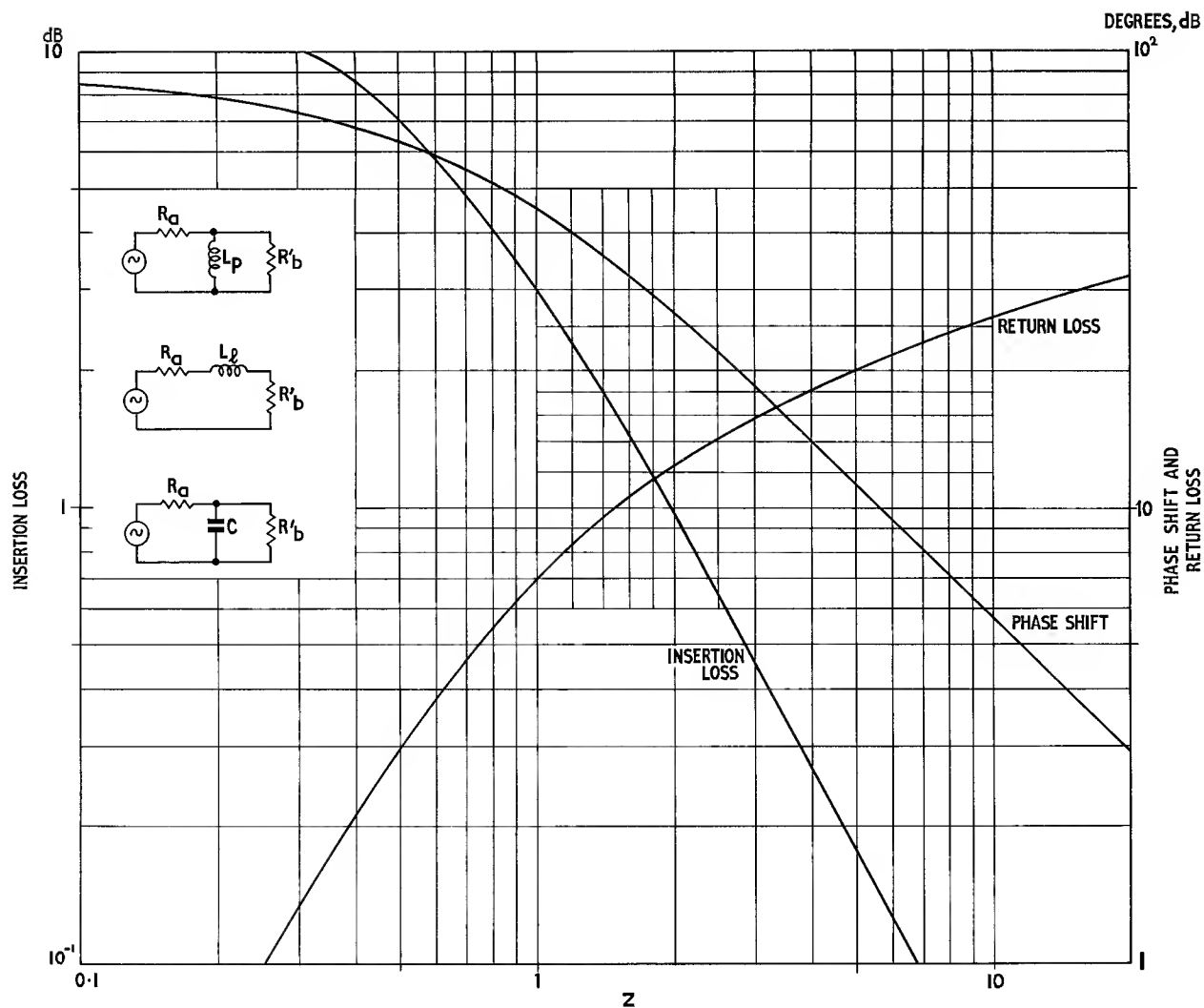


Fig. 7.6. Insertion loss, return loss and phase shift due to shunt inductance, leakage inductance or shunt capacitance taken separately

Element :	Expressions for the independent variable, z		
	L_p	L_l	C
Insertion loss	$\omega L_p/R$	$(R_a + R'_b)/\omega L_l$	$1/\omega CR$
Return loss	$\omega L_p/R'_b$	$R'_b/\omega L_l$	$1/\omega CR'_b$
Phase shift	$\omega L_p/R$	$(R_a + R'_b)/\omega L_l$	$1/\omega CR$

The phase shift due to the shunt inductance is positive (leading) and for the other two elements it is negative

It often happens that the shape of the higher frequency characteristic is determined by either the leakage inductance or the shunt capacitance acting alone; e.g. in a low impedance circuit the series leakage reactance may be appreciable while the shunting effect of the capacitance could be negligible, while for a high impedance circuit the reverse could apply. When it is required to consider the effect of either of these two reactances in isolation the following equations apply. The higher frequency droop due to leakage inductance is given by:

$$A_i = 10 \log_{10} \left(1 + \left(\frac{\omega L_l}{R_a + R'_b} \right)^2 \right) \quad \text{dB} \quad (7.17)$$

and due to shunt capacitance it is given by

$$A_i = 10 \log_{10} (1 + (\omega CR)^2) \quad \text{dB} \quad (7.18)$$

The corresponding return loss of the input impedance relative to R'_b is given by

$$A_r = 10 \log_{10} \left(1 + \left(\frac{2 R'_b}{\omega L_l} \right)^2 \right) \quad \text{dB} \quad (7.19)$$

and

$$A_r = 10 \log_{10} \left(1 + \left(\frac{2}{\omega CR_b} \right)^2 \right) \quad \text{dB} \quad (7.20)$$

and the corresponding phase shifts are given by

$$\tan \phi = - \frac{\omega L_l}{R_a + R'_b} \quad (7.21)$$

and

$$\tan \phi = -\omega CR \quad (7.22)$$

Fig. 7.6 may again be used to express these functions, the abscissa being a scale of $(R_a + R'_b)/\omega L_l$ or $1/\omega CR$ for insertion loss and phase shift, or $R'_b/\omega L_l$ or $1/\omega CR'_b$ for return loss. C is the sum of C_1 and C'_2 in Fig. 7.3; if the transformer has a turns ratio greater than about 3 only the shunt capacitance of the high impedance side is significant and $C \approx C_1$ or C'_2 depending on whether it is a step-down or a step-up transformer. This graph may be used in the early stages of design to determine maximum values of L_l and C acting individually.

At this stage experience may suggest that it will be either the leakage inductance or the stray capacitance that will limit the bandwidth, in which case the subsequent transformer design merely consists of meeting the leakage inductance or stray capacitance limit while at the same time providing adequate shunt inductance.

If, however, the performance requirements are stringent, e.g. a flat response over a wide bandwidth within a restricted volume, then it is probable that the combined effect of L_l and C will have to be considered. This is best done by synthesizing the high frequency

equivalent circuit from the performance requirements using wave filter techniques.* In this way the combined effect of L and C may often be turned to good account. The procedure may be used in reverse to analyse the response of a given equivalent circuit.

The step-up transformer will first be considered. In this case only C'_2 need be taken into account so, if the winding resistance can be neglected, the equivalent circuit is simplified to that shown in Fig. 7.7. This is a simple half-section low pass filter having a nominal impedance:

$$\left. \begin{aligned} R_o &= \sqrt{\left(\frac{L_l}{C} \right)} \quad \Omega \\ \text{and a cut-off frequency given by} \\ \omega_c &= \frac{1}{\sqrt{(L_l C)}} \quad \text{rad.s}^{-1} \end{aligned} \right\} \quad (7.23)$$

The mid-series† impedance is equal to $R_o \sqrt{[1 - (\omega/\omega_c)^2]}$, i.e. it is asymptotic to R_o at low frequencies but falls to zero at cut-off. Thus if it is desired to maintain a given degree of impedance matching over the widest possible frequency band it is better to design the filter such that the terminating resistance (R_a in this case) equals not R_o but a lower value, e.g. ρR_o , where ρ is a nominal mismatch factor and is less than unity. Similarly the mid-shunt impedance is $R_o / \sqrt{[1 - (\omega/\omega_c)^2]}$ i.e. it is asymptotic to R_o at low frequencies but rises to infinity at cut-off. In this case it is better to arrange that the terminating resistance (R'_b in practice) equals not R_o but a higher value, e.g. R_o/ρ . If the value of ρ is the same for both sides, the nominal primary and secondary mismatches will be equal and $R_a = \rho^2 R'_b$.

The effective loss of the circuit is given by

$$A_e = 10 \log_{10} \left\{ 1 + \left(\frac{\omega^2/\omega_c^2 - (1 - \rho^2)}{2\rho} \right)^2 \right\} \quad \text{dB} \quad (7.24)$$

This function is presented graphically in Fig. 7.7, with the mismatch factor ρ as a parameter. It will be noted that values of ρ greater than unity have been included. In practice only those equal to or less than unity will be considered in transformer design. The higher values may be useful in predicting the characteristic of a given transformer having arbitrary values of L_l and C . A scale of return loss has been added; this has been calculated from Eqn 7.10. It should also be noted that the graph is given in terms of effective loss, thus when the frequency approaches zero the effective loss is not zero unless $\rho = 1$, in which case $R_a = R'_b$ and the effective loss

*The approach is based on an unpublished lecture given by the late Dr. J. H. Mole.

†Half-sections may be cascaded, series element to series element and shunt to shunt. Thus the series terminals of a half-section are referred to as mid-series and the shunt terminals are mid-shunt.

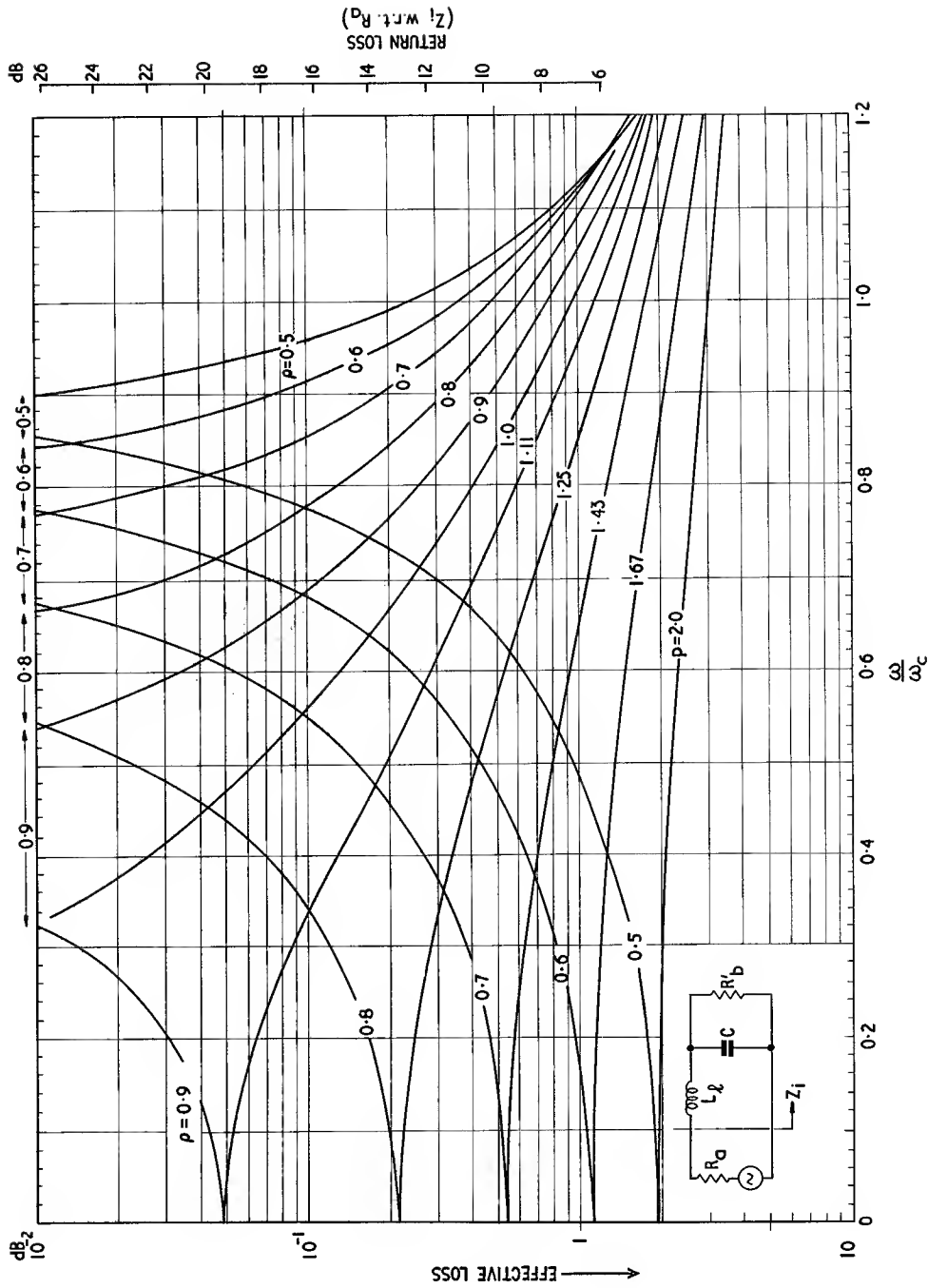


Fig. 7.7. Transformer characteristics using the half-section low pass filter technique; effective loss and return loss due to a combination of L_1 and C regarded as a half-section low pass filter with a mismatch ratio ρ

In the form shown, the graph applies to a step-up transformer in which C_1 (see Fig. 7.3) may be neglected; then

$$R_a = \rho R_o \quad R'_b = R_o/\rho \quad R_a = \rho^2 R'_b$$

$$R_o = \sqrt{\left[\frac{L_1}{C} \right]}, \quad \omega_c = \sqrt{\left[\frac{1}{L_1 C} \right]}$$

For the step-down transformer C_2 (see Fig. 7.3) may be neglected instead and C moves to the L.H.S. of L_1 . The same graph may be used but now

$$R_a = R_o/\rho \quad R'_b = \rho R_o \quad R_a = R'_b/\rho^2$$

The expressions for R_o and ω_c remain as above.

This graph may also be used for the corresponding half-section high pass filters, in which case it must be used in conjunction with Fig. 7.9

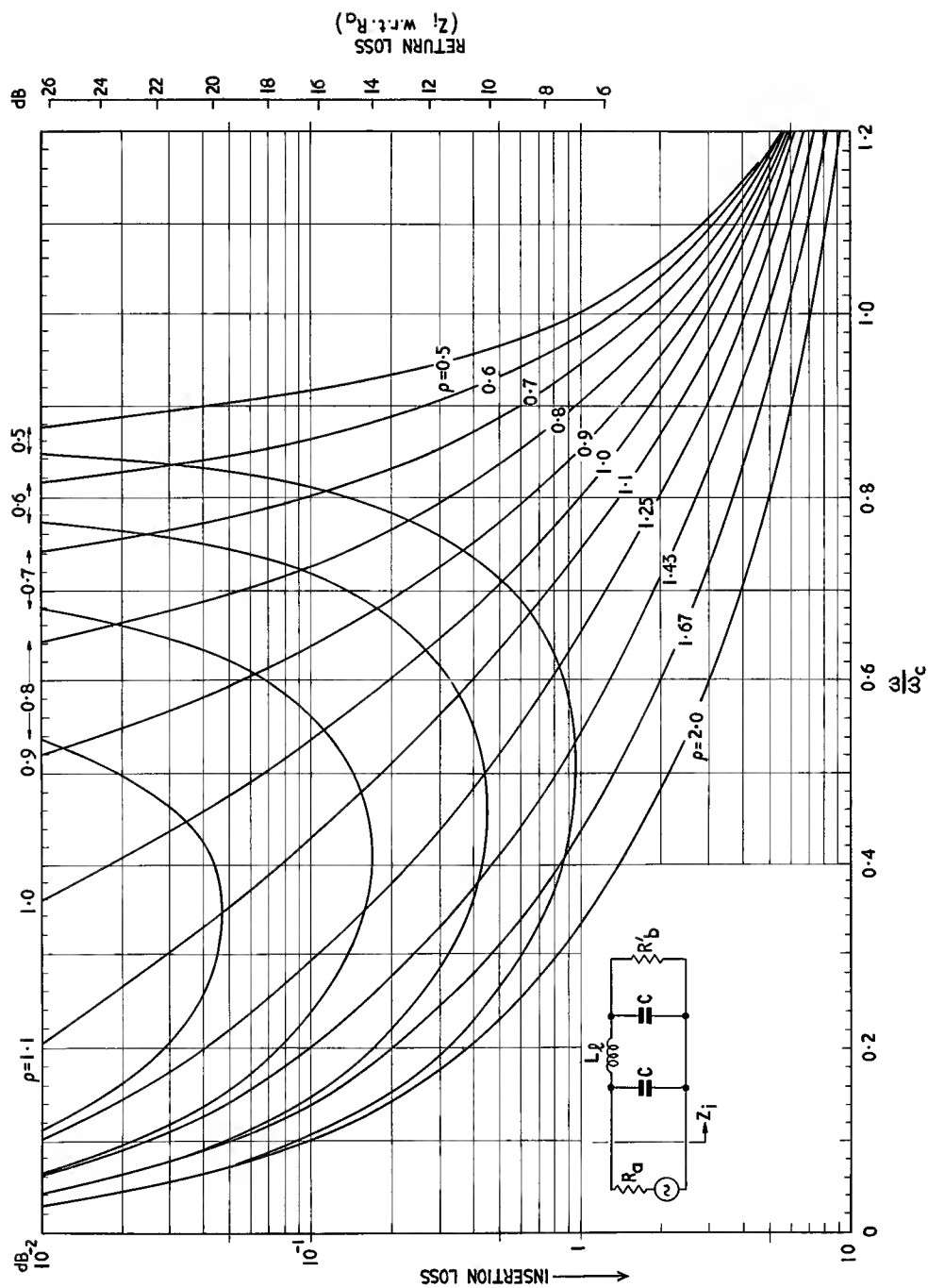


Fig. 7.8. Transformer characteristics using the full-section low pass filter technique; insertion loss and return loss due to combination of L_1 and C regarded as a full-section low pass filter with a mismatch ratio ρ

$$R_a = R'_b = R_o/\rho \quad R_o = \sqrt{\frac{L_1}{2C}} \quad \omega_c = \sqrt{\frac{2}{L_1 C}}$$

This graph may also be used for the corresponding full-section high pass filters, in which case it must be used in conjunction with Fig. 7.9

becomes equal to the insertion loss. However, the graph may easily be used for insertion loss. It may be shown that by taking the intercept at $\omega/\omega_c = 0$ as the zero insertion loss datum, the relative effective loss, positive or negative, read from the graph at other frequencies equals the insertion loss.

To obtain the shape of the response characteristic in the high frequency region, the intercept of the appropriate curve at $\omega/\omega_c = 0$ may be taken as equal to the mid-band loss. This is because the graph ignores factors affecting the response in other frequency regions, and both zero frequency and mid-band frequency may be regarded as far removed from the higher frequency region. Thus if it is required, for example, that the variation of attenuation between mid-band and f_2 should not exceed about 0.2 dB then a mismatch of $\rho = 0.8$ would be suitable and f_2 would correspond to $\omega/\omega_c = 0.84 = f_2/f_c$.

From R_a and ρ the value of R_o may be calculated, and from ω/ω_c and f_2 the value of ω_c may be obtained. Eqn 7.23 may then be used to calculate the required leakage inductance and shunt capacitance. When realizing the design it is necessary to adjust the actual values of L_l and C by adding inductance in series with the primary and shunt capacitance to the secondary winding. The practical design must allow a margin for this adjustment.

Again, R_a and ρ may be used to calculate R'_b and from this the actual turns ratio is obtained i.e. $r = (R_b/R'_b)^{1/2}$.

If the transformer has a large step-down ratio then the primary shunt capacitance will predominate and C must be moved to the other side of L_l . This does not affect the response, but now $R_a = R_o/\rho$ and $R'_b = \rho R_o$.

This mismatched filter technique is useful if the transformer must meet a severe attenuation or return loss requirement over the widest possible frequency band. If the requirement is not severe, e.g. if the permitted variation in attenuation up to f_2 is greater than 1 or 2 dB then it is usually better to use a simple design in which L_l or C is, if possible negligible and R_a equals R'_b .

If the transformer has a ratio approaching unity, the primary and secondary shunt capacitances will become comparable in magnitude. If there is a severe attenuation or return loss requirement then the full-section low pass filter technique may be used. The circuit is shown in Fig. 7.8; it consists of two half-section low pass filters connected back to back. In the present context C is simply one of a pair of mid-shunt capacitances; in the realization, C_1 and C'_2 of Fig. 7.3 must each be made equal to C . The filter section is mismatched at each end by a factor $\rho < 1$ but since both ends are mid-shunt there is no mismatch required between R_a and R'_b . This means that the attenuation may be expressed in terms of insertion loss of the equivalent circuit and this insertion loss will approach zero as $\omega \rightarrow 0$.

$$R_a = R'_b = R_o/\rho$$

$$R_o = \sqrt{\left[\frac{L_l}{2C}\right]}, \quad \omega_c = \sqrt{\left[\frac{2}{L_l C}\right]} \quad (7.25)$$

The insertion loss is given by

$$A_i = 10 \log_{10} \left\{ 1 + \left(\frac{\omega}{\rho \omega_c} \right)^2 \left(\frac{\omega^2}{\omega_c^2} - (1 - \rho^2) \right)^2 \right\} \text{ dB} \quad (7.26)$$

This function is presented graphically in Fig. 7.8, with ρ as a parameter. Again only values of ρ less than unity are relevant in the present context but larger values have been included to enable the transmission characteristic to be predicted. Again a scale of return loss has been added.

The curves may be used in a similar manner to that described above for the single section filter. If the permissible insertion loss variation is for example less than about 0.2 dB then the curve of $\rho = 0.7$ would be satisfactory. The insertion loss would increase from its mid-band value by about 0.2 dB at $\omega/\omega_c = 0.4$, then return to the mid-band value at $\omega/\omega_c = 0.715$ before increasing again by about 0.2 dB at $\omega/\omega_c = 0.83$, this frequency corresponding to f_2 .

It will be noted that if L_l and C have the same values respectively in the half-section and full-section equivalent circuits then the value of ω_c is larger by a factor of $\sqrt{2}$ in the latter case. Thus it is often advantageous to use a full-section even if the ratio of the transformer would suggest a half-section. In the practical realization the required values of L_l and C are obtained by the addition of external elements as previously mentioned.

The phase shift at cut-off, ω_c , is 90° (lagging) for the half-section and 180° for the full-section. It increases monotonically from zero to the cut-off value as the frequency rises through the pass band. The rate at which it approaches the cut-off value depends on the mismatch factor; if this is low then the phase shift rises relatively sharply.

Finally a word of caution must be added. It has been assumed that the resistance of the windings may be neglected. This is not always true. Particularly when the full-section low pass filter technique is used to extend the higher frequency region, the winding resistance, probably increased by eddy current effects, may cause the Q -factor of the circuit to be quite low. The curves given in Fig. 7.8 are calculated on the assumption that the π -network consists of pure reactances; in practice the winding resistances are included in this network. This may have the effect of suppressing the zero attenuation peak in the characteristic and causing an additional droop at the higher frequency end of the band. Thus the expected performance may not be fully realized. This effect is less pronounced in the T -network (see Section 7.2.6) and half-section versions. Here the winding resistances may be considered as being absorbed in the terminating resistances leaving the inductive and capacitive elements as pure reactances.

7.2.6. Filter techniques in the lower frequency region

The filter techniques described above apply, with a few modifications, to the lower frequency region. The corresponding simple high pass filter circuits are shown in Fig. 7.9 together with the essential equations. When considering the lower frequency region these equivalent circuits may be substituted for those in Fig. 7.7 and 7.8 respectively and the graphs will give the lower frequency response in the same way as has been described for the

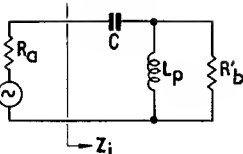
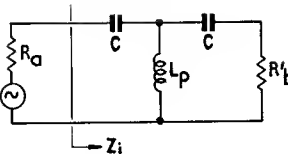
HALF SECTION	FULL SECTION
Circuit and Equations to be substituted:	
in Fig. 7.7	in Fig. 7.8
	
$R_a = \rho R_o$	$R_a = R'_b = \rho R_o$
$R'_b = R_o / \rho$	
$R_o = \sqrt{\left[\frac{L_p}{C} \right]}$	$R_o = \sqrt{\left[\frac{2L_p}{C} \right]}$
$\omega_c = \sqrt{\left[\frac{1}{L_p C} \right]}$	$\omega_c = \sqrt{\left[\frac{1}{2L_p C} \right]}$
$\frac{\omega_c}{\omega}$ to be substituted for $\frac{\omega}{\omega_c}$ as parameter of frequency scale	

Fig. 7.9. High pass filter technique in transformer design. Diagrams and equations to be substituted in Figs. 7.7 and 7.8 respectively to convert these figures to the corresponding high pass filter cases

higher frequency response except that the parameter of the frequency scale should now be ω_c/ω instead of ω/ω_c .

The required capacitance must be introduced in series with one or both windings. Obviously if there is d.c. in one of the windings, only the half-section may be used. If the permitted variation of pass band attenuation is small then for a given primary inductance the filter design extends the bandwidth. Alternatively, with the same qualification, it permits a given bandwidth to be obtained with the lowest value of primary inductance L_p . However if the permissible droop is greater than 1 or 2 dB the required characteristic is better obtained by using the simple design as this will result in a lower value of primary inductance.

The phase shift at cut-off, ω_c , is 90° (leading) for the half-section and 180° for the full-section. The remarks made in the previous section concerning rate of change of phase apply here also.

The high pass version of the filter technique does not appear to suffer the degradation due to winding resistance discussed at the end of the previous section. This is presumably because the circuit is mid-series connected to the source and load, and the winding resistances may be regarded as being absorbed by these terminations.

7.2.7. Example of the filter design technique

The following example will illustrate the filter technique outlined in the previous sections. A transformer is required to meet the following specification.

Source impedance, R_a	= 600 Ω
Load impedance, R_b	= 1200 Ω
Frequency, f_1	= 300 Hz
Effective loss at f_1	< 0.1 dB w.r.t. the mid-band loss.
Effective loss at mid-band	< 0.3 dB
Frequency, f_2	= 300 kHz
Return loss relative to source impedance	> 16 dB from f_1 to f_2

The transformation ratio is not large and the pass band requirements are quite severe. It might therefore be appropriate to use the full-section filter technique at both ends of the pass band. However as there is no margin available for any degradation of the characteristic in the region of f_2 due to the effects of winding resistance, the higher frequency characteristic will be based on a half-section filter, in which such degradation is less marked. The lower frequency region will use a full-section filter, thus the example will illustrate both techniques.

General

Turns ratio, $r = \sqrt{2}$ and $R_a = R'_b = 600 \Omega$

$$R = R_a R'_b / (R_a + R'_b) = 300 \Omega$$

$$\omega_1 = 2\pi f_1 = 1885 \text{ rad.s}^{-1}$$

$$\omega_2 = 2\pi f_2 = 1.885 \times 10^6 \text{ rad.s}^{-1}$$

Mid-band

It is assumed that the shunt resistance, R_p , due to the core loss may be neglected. From Fig. 7.4 an effective mid-band loss of less than 0.3 dB will be obtained if

$$\frac{R_s}{R_a + R'_b} < 0.035, \text{ i.e. } R_s < 42 \Omega$$

The corresponding return loss obtained from Fig. 7.5 is approximately 30 dB.

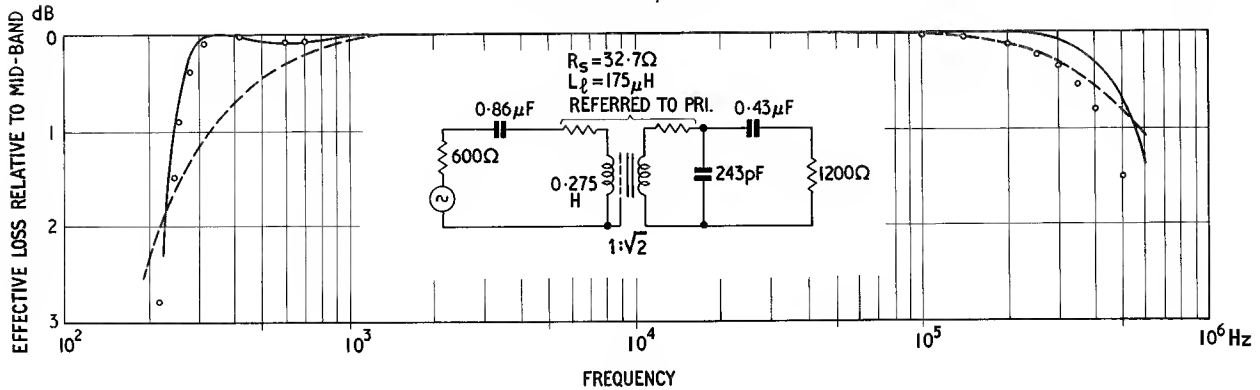


Fig. 7.10. Example of wide band transformer design using filter techniques.

- Calculated transmission characteristic
 ○○○○ Values measured on a transformer made to this design (see Sec. 7.3.2)
 - - - - - Calculated characteristic for circuit capacitances

Higher frequency region

When a half-section is used, the turns ratio does not in general equal $(R_b/R_a)^{1/2}$, i.e. there is a net mismatch.

Since the lower frequency region will use a full-section filter it follows that the actual turns ratio will in fact equal $(R_b/R_a)^{1/2}$. Therefore, referring to Fig. 7.7, ρ must equal unity for the higher frequency region. The curve for $\rho = 1$ crosses the 16 dB return loss line at $\omega/\omega_c \approx 0.55$ and falls monotonically with increasing frequency.

$$R_o = R_a/\rho = 600 = \sqrt{\left[\frac{L_t}{C}\right]}$$

$$\omega_c = 1.885 \times 10^6 / 0.55 = 3.43 \times 10^6 = \sqrt{\left[\frac{1}{L_t C}\right]}$$

$$\therefore C = 486 \text{ pF} \quad L_t = 175 \text{ } \mu\text{H}$$

N.B. The return loss due to $L_t = 175 \text{ } \mu\text{H}$ in the absence of C may be obtained from Fig. 7.6: $R_b/\omega L_t = 600/1.885 \times 175 = 1.82$.

\therefore Return loss would be 11.5 dB.

Lower frequency region

This time Fig. 7.8 is used but it is modified in accordance with the R.H.S. of Fig. 7.9. It must be remembered that the frequency scale is inverted, i.e. it must be read in terms of ω_c/ω . A curve is required such that its trough touches the 0.1 dB line (this neglects any margin for tolerances). As the frequency decreases from the value at the trough the characteristic passes through a point of zero attenuation and thereafter the attenuation increases monotonically, crossing the 0.1 dB line at a frequency which is put equal to f_1 . Between f_1 and mid-band the variation of attenuation will not exceed 0.1 dB. Inter-

polating, a curve to meet this requirement has $\rho = 0.75$ and $\omega_c/\omega = 0.77$.

$$\therefore R_o = 600/0.75 = 800 = \sqrt{\left[\frac{2L_p}{C}\right]}$$

$$\omega_c = 1885 \times 0.77 = 1450 = \sqrt{\left[\frac{1}{2L_p C}\right]}$$

$$\therefore C = 0.862 \text{ } \mu\text{F} \quad L_p = 0.275 \text{ H}$$

N.B. The effective loss due to $L_p = 0.275 \text{ H}$ if the series capacitances are not introduced is given by Fig. 7.6:

$$\omega L_p/R = 1885 \times 0.275/300 = 1.73$$

$$\therefore \text{Effective loss} = 1.25 \text{ dB}$$

Alternatively the value of L_p required to obtain the specified effective loss at 300 Hz, in the absence of the series capacitances is obtained from

$$\omega L_p/R = 6.7, \therefore L_p \approx 1 \text{ H}$$

However, in this particular example, the provision of two large-value capacitors may outweigh the advantage of the smaller inductance. A larger core may give a more satisfactory overall design.

Overall results

Fig. 7.10 shows the complete equivalent circuit with the elements referred to the appropriate sides of the transformer. The calculated attenuation characteristic is also shown. This may be compared with the characteristic (shown by the broken line) which would be obtained if none of the capacitances had been introduced. It is seen that the effect of the filter design technique is to extend the relatively flat part of the pass band by sharpening the cut-off regions.

7.3. LOW AND MEDIUM FREQUENCY WIDE BAND TRANSFORMERS

The transformers to be considered under this heading are those having the lower end of the pass band, i.e. f_1 , below a few hundred kHz. Up to these frequencies the initial permeability of suitable manganese zinc ferrites is substantially constant so the design of such transformers may proceed as for an audio frequency transformer. In general it will be necessary to use more than a few turns to obtain the required shunt inductance and the winding resistance will usually be a significant factor in the design. For these reasons it is usual to use a two-piece core embracing conventional windings on a coil former. The toroidal core is an alternative that is usually better suited to high frequency transformers where relatively few turns are required.

The foregoing sections have considered the translation of the performance specification into element values in the equivalent circuit. The next stage of the design is to realize these values as parameters of a physical transformer. The relations between these elements and the design of the core and windings will now be discussed with particular reference to ferrite cores. An example of transformer design will then be given to illustrate the procedure.

7.3.1. The practical design in terms of the element values

The contribution of the core

The transformer core, by providing a low reluctance path for the magnetic flux, ensures a high degree of coupling between primary and secondary windings. It is shown in text books on transformers that the coupling factor, k , defined as the proportion of flux due to one winding which actually links the other winding, is related to the shunt inductance and leakage inductance by the equation :

$$\frac{L_p}{L_l} = \frac{1}{2(1-k)} \quad (7.27)$$

The better the coupling, the nearer k approaches unity and the greater is the ratio L_p/L_l . Ignoring the limitations imposed by self capacitance, this ratio is proportional to the bandwidth of the transformer, a fact that follows from a consideration of Fig. 7.6. The L_p/L_l ratio and other similar parameters will be discussed in more detail in the next section. From that discussion, other things being equal, the best transformer core is the one that gives the highest value of L_p for a given number of turns.

The relation between the inductance and the parameters of the core and winding is considered in detail in Chapter 4. The essential result is in Eqn 4.23 which for convenience may be expressed here as:

$$\frac{L_p}{N^2} = \mu_0 \mu_e A_e / l_e = \frac{\mu_0 \mu_e}{C_1} \quad \text{H} \quad (7.28)$$

where C_1 is the core factor expressing the core reluctance normalized with respect to permeability (see Eqn 4.8) and μ_e is the effective permeability of the core.

For a given magnetic material, a core having a low value of C_1 will give a high inductance for a given number of turns. However C_1 , being a geometric factor, depends on the shape and size of the core and is thus related to other important design parameters such as winding resistance, leakage inductance and core volume. Thus the best value of C_1 is not necessarily the lowest.

The effective permeability, on the other hand, affects only the inductance for a given number of turns and the higher its value the better. At low audio frequencies cores of high permeability nickel iron alloy give the best performance. Strip wound toroids having permeabilities $> 100,000$ are obtainable, while conventional laminations stacks can provide effective permeabilities $> 10,000$. As the frequency increases, eddy currents within the alloy reduce the permeability and even when this reduction is combated by the use of very thin strip or laminations the permeability eventually falls below the value obtainable with ferrites. The frequency of change-over depends on the initial permeability of the alloy and its thickness, and, of course, on the effective permeability of the ferrite core under consideration. Cost and convenience are also considerations. As the effective permeability of ferrite cores is progressively increased their use extends further into the audio frequency range. Although much of this chapter applies to wide band transformers in general the core considerations will be confined to ferrite cores.

The effective permeability has been used in this discussion because ferrite transformer cores are often assembled from two or more pieces, and the residual gaps at the joints, however well the joints are made, reduce the permeability from the value intrinsic in the core material to an effective value. If the core has no gaps, e.g. a continuous toroid, then μ_e may be replaced by the material permeability, μ .

The relation between μ_e and μ is given in Eqn 4.25. In the present context, the gap length, l_g , is small so that the gap area may be taken as equal to the pole face area. Assuming a core of uniform cross-section, this expression is presented graphically in Fig. 7.11 for various gap ratios, l_g/l_e . These ratios are typical of two-part transformer

$$(7.28) \quad \frac{L_p}{N^2} = \frac{4\pi\mu_e A_e 10^{-9}}{l_e} = \frac{4\pi\mu_e 10^{-9}}{C_1} \quad \text{H}$$

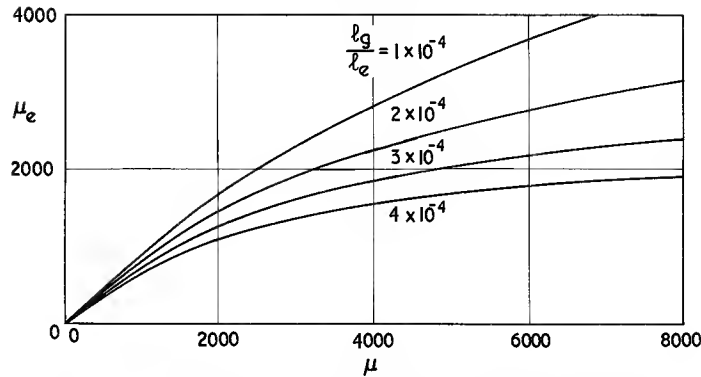


Fig. 7.11. The effective permeability as a function of material permeability for several ratios of residual gap length to magnetic path length

cores having mating surfaces that have been made smooth and flat by surface grinding. It is clear that as the material permeability is made larger the greater is the degradation due to the residual gap. The influence of this on the design of cores is discussed on page 258.

While the concept of effective permeability is useful in assessing the merit of a transformer core, a more practical parameter is the turns factor, α , or the inductance factor, A_L . These factors have already been introduced in connection with inductors (see Section 5.3). They relate the number of turns to the inductance thus:

$$N = \alpha \sqrt{L} \quad (7.29)$$

where L is in mH

and α is the number of turns required to give 1 mH,

$$\text{or } L = A_L N^2 \quad \text{nH} \quad (7.30)$$

where A_L is the inductance in nH corresponding to one turn.

It follows that these factors are related:

$$\alpha = \frac{10^3}{\sqrt{A_L}}$$

The specification for a ferrite transformer core invariably quotes a limit value of α or A_L . This value corresponds to the *initial* effective permeability, i.e. it relates to low flux density, low frequency, a butt joint and no magnetic polarization. It provides a ready means of calculating the number of turns required to give an inductance equal to or greater than a required minimum. In most simple transformer designs it does not matter by how much the shunt inductance exceeds the minimum value. However in a design involving the high pass filter technique an upper and lower limit must be placed on L_p and it is better to use a mean value of α or A_L .

If the amplitude is not small, so that there is an appreciable flux density in the core, then the permeability will be greater than the initial value (see Fig. 3.4) and a

higher inductance will be obtained. However, it is rarely possible to take advantage of this because wide band transformers, even those operating at relatively high power levels, must retain their performance characteristics down to vanishingly small amplitudes. In fact high amplitudes might result in a greater number of turns being required in order to prevent excessive core loss, an aspect considered later in this section.

For most manganese zinc ferrites the initial permeability, and therefore α and A_L , remain substantially constant up to a few hundred kHz. Fig. 3.11 shows typical permeability spectra; the higher the initial permeability the lower the frequency at which the fall of permeability occurs. As indicated at the beginning of Section 7.3 the low and medium frequency transformers at present being considered are those having f_1 within the substantially flat region of the permeability spectrum. The low frequency value of α or A_L will give a satisfactory design even if f_1 is situated at the upper extremity of the flat region and, in consequence, the pass band lies wholly in the region of permeability dispersion. This is because the shunt reactance (or impedance) is proportional to $\omega \mu_p$ and this continues to rise with frequency even when μ_p is falling due to dispersion phenomena. Therefore the pass-band characteristic is practically unaffected.

Another possible dispersion in shunt inductance may arise from dimensional resonance. This phenomenon, which has been discussed in detail in Sections 2.2.4 and 4.2.3, arises from the establishment of standing electromagnetic waves across the core section. It may occur, in practice, when a manganese zinc ferrite core of relatively large cross-section is used at medium or high frequencies, e.g. > 20 kHz. Fig. 4.5 relates the frequency of dimensional resonance to the least cross-sectional dimension of a core of typical manganese zinc ferrite. The resonant frequency is proportional to $\mu_e^{-\frac{1}{2}}$ so an air gap will move the resonance to higher frequencies. In the discussion of this phenomenon it was observed that the main effect of dimensional resonance on the impedance of the core is

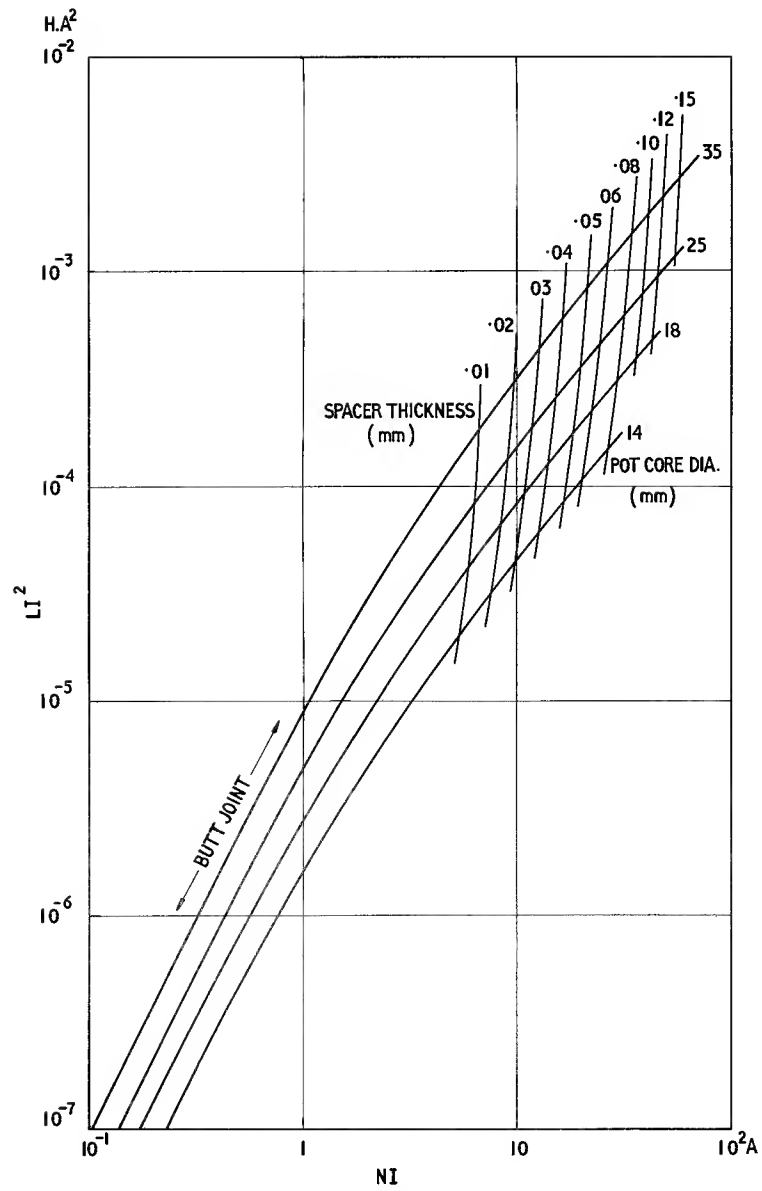


Fig. 7.12. A family of Hanna curves for the pot cores listed in Table 7.1

that the phase angle changes rapidly as a function of frequency while the modulus shows a relatively small variation. So unless it happens that the core is large enough for dimensional resonance to occur in the region of f_1 it will not normally cause any distortion of the transmission characteristic. Since the frequency of dimensional resonance increases as the core cross-section is reduced, and it is usually desirable for other reasons to use smaller cores at higher frequencies, there is a natural tendency to avoid dimensional resonance. However, if a design ever necessitates a manganese zinc core of abnormally large cross section then the possibility of dimensional resonance should be checked by reference to Fig. 4.5.

If there is to be direct current flowing in one or more of the transformer windings so that there is a net polarization, this will reduce the material permeability to its incremental value and the simple procedure of using α or A_L may no longer be used. The most convenient procedure is that due to Hanna, in which an air gap is introduced into the magnetic circuit to minimize the effect of the direct current. This method has been discussed in the introduction to Fig. 3.7 which gives Hanna curves for a variety of ferrites. The procedure is summarized here for convenience. A trial core of volume V and magnetic length l is selected. If L_p is the required inductance and I is the net polarizing current referred to the winding under consideration, then the value of $L_p I^2/V$ is calculated. Using the Hanna curves for a suitable transformer ferrite (see Table 3.1) the value of NI/l is obtained. Since I and l are known, the required number of turns, N , may be calculated. The curve is marked along its length by a scale of l_g/l and the value of this ratio at the intercept of the curve with the relevant co-ordinates enables the optimum air gap length l_g to be calculated. If the core is of non-uniform cross-section there is some uncertainty about the values to be assigned to l and V . In most cases the effective parameters l_e and V_e give reasonably accurate results. Even for pot cores these parameters are satisfactory. However when the core shape is complicated it is preferable to use a form of Hanna curve prepared specifically for the core type, if this is available. In this case the dimensional parameters of the core need not enter into the calculation. The curve gives $L_p I^2$ as a function of NI with gap or spacer thickness as a parameter. Fig. 7.12 shows a family of these curves for the transformer pot cores listed in Table 7.1.

The air gap may, of course, be introduced into most core designs by grinding back one of the limbs. Although this is done it is not a common practice because the wide

range of possible requirements makes gap standardization impracticable. So unless a large quantity of identical cores are required it is more usual to obtain the required gap by inserting a paper or mica spacer. It must be remembered that, in the general Hanna curves, l_g is the total gap length, i.e. twice the thickness of the spacer inserted between a pair of half cores.

In the foregoing, the core loss has been disregarded and in the majority of low and medium frequency transformers using ferrite cores the core loss is indeed negligible. At low amplitudes the residual loss and the eddy current loss in the core are the only possible contributions to the shunt loss resistance R_p . Considering the contributions separately, and assuming that the effect of the residual air gap is negligible, the residual loss component of R_p is given by Eqn 2.18

$$R_p = \omega L_o \mu_p'' \quad \Omega \quad (7.31)$$

$$\text{where } L_o = \frac{\mu_o N^2}{C_1} \quad \text{H}$$

and μ_p'' is the loss component of the parallel complex initial permeability; it is given as a function of frequency for a number of ferrites in Fig. 3.11.

Multiplying and dividing the above equation by μ_p'

$$R_p = \omega L_o \left(\frac{\tan \delta_r}{\mu_p'} \right) = \frac{\omega L_p}{\tan \delta_r} \quad (7.32)$$

where $(\tan \delta_r)/\mu_p'$ is for most practical purposes equal to the residual loss factor. This factor $(\tan \delta_r)/\mu$ is given as a function of frequency for a number of ferrites in Fig. 3.12.

In the frequency range under consideration, $\tan \delta_r \ll 0.1$ for most manganese zinc ferrites. R_p will therefore be much greater than ωL and the attenuation that it causes will be small compared with the droop due to ωL_p . If the core has a residual air gap such that the effective permeability is μ_e it follows from Eqns 4.49 and 7.32 that the value of R_p is unchanged.

The component of the shunt resistance due to eddy current loss in the core may be obtained from Eqn 4.54

$$R_p = \frac{\omega L_p}{\tan \delta_F} = \frac{\omega L_p \rho \beta}{\pi \mu_o \mu_e d^2 f} \quad \Omega \quad (7.33)$$

where the symbols are defined after Eqn 2.48.

This component is again negligible in most practical cases. Indeed if the frequency and core cross-sectional dimension, d , are such that the eddy current loss is significant then a check should be made (using Fig. 4.5)

$$(7.31) \quad R_p = \omega L_o \mu_p'' \quad \Omega$$

$$\text{where } L_o = \frac{4\pi N^2 10^{-9}}{C_1} \quad \text{H}$$

$$(7.33) \quad R_p = \frac{\omega L_p}{\tan \delta_F} = \frac{\omega L_p \rho \beta 10^9}{4\pi^2 \mu_e d^2 f} \quad \Omega$$

to see whether dimensional resonance may occur. Eddy current core loss and dimensional resonance are described in greater detail in Sections 2.2.4 and 4.2.3.

Finally, if the amplitude is not negligibly small there may be a hysteresis loss contribution. For a given voltage amplitude, the flux density will increase as the frequency decreases (see Eqn 4.44) and so the hysteresis loss will become greater; if it becomes significant it will contribute to the lower frequency droop. Hysteresis loss is discussed in Sections 2.2.3 and 4.2.3.

If hysteresis data are available in the form of the loss tangent, $\tan \delta_h$, or the loss factor, $(\tan \delta_h)/\mu$, then the form of Eqn 7.32 applies and the contribution to the shunt resistance is given by:

$$R_p = \omega L_o \left(\frac{\tan \delta_h}{\mu} \right) = \frac{\omega L_p}{\tan \delta_h} \quad \Omega \quad (7.34)$$

assuming that $\tan \delta_h \ll 1$.

The hysteresis loss factor is given as a function of flux density for a number of ferrites in Fig. 3.15. It is only necessary to calculate the effective flux density, \hat{B}_e , from Eqn 4.44 for a number of frequencies in the vicinity of f_1 , obtain the corresponding values of $(\tan \delta_h)/\mu$ and use these to calculate R_p . Within the Rayleigh region, $\tan \delta_h$ may also be calculated from the hysteresis coefficients or factors, see Table 2.1.

For large amplitudes, core loss density data such as given in Fig. 3.19 may be used. If at a given frequency and flux density the power loss density is P_m and the core has a volume V_c

$$\begin{aligned} U^2/R_p &= P_m V_c \\ \therefore R_p &= \frac{U^2}{P_m V_c} \end{aligned} \quad (7.35)$$

If this core loss causes a significant increase in attenuation at f_1 allowance for this must be made by increasing the inductance. In higher power transformers the hysteresis loss dominates the design. A given limit on R_p or total core loss determines P_m and hence places a limit on the flux density. For a given core operating at a given frequency and voltage, the e.m.f. Eqn 4.44, determines the minimum number of turns.

It is also possible for hysteresis to dictate the number of turns at low amplitudes. This might occur if there were a limit imposed on the permissible waveform distortion. This would limit $\tan \delta_h$ (see Section 4.2.4) and in consequence would restrict the flux density.

A final remark concerning the contribution of the core in transformer design. The transformer must usually have a satisfactory performance over a given temperature range. The permeability and losses may show appreciable variations within this range (e.g. see Figs. 3.8 and 3.19) and, since the core normally has only a residual air gap, the inductance and shunt loss resistance vary by almost the

same proportion. It is thus advisable to ensure that the design is based on the maximum α or minimum A_L , or maximum loss density, occurring within the operating temperature range.

Relations arising from the geometry of core and winding

In the design of a transformer any core may, in principle, be used to obtain a sufficient shunt inductance; it is only necessary to provide enough turns. However, it is shown in Section 11.3 that the resistance of a winding on a given core is proportional to N^2 , see Eqn 11.11. Therefore a core requiring a larger number of turns for a given inductance will give a relatively high winding resistance and this may cause excessive mid-band attenuation.

Since both the inductance, L_p and the winding resistance, R_{dc} , are proportional to N^2 , the ratio R_{dc}/L_p depends only on the effective permeability and on the geometry of the core and winding, see Eqn 11.12. This ratio may be taken as a figure of merit of a transformer core. In practice one transformer winding occupies only a fraction of the total winding space. It is shown in Section 11.3 that for a simple transformer the least total winding loss is obtained when the primary and secondary each occupy substantially half the total winding space. Therefore the resistance of the primary or secondary will be approximately twice the value that would be obtained for a full winding of the same number of turns, see Eqn 11.11. The resistance/inductance ratio for a winding occupying half the coil former, designated $(R_{dc}/L)_\frac{1}{2}$, will be twice the value given by Eqn 11.12. In terms of the core factor, A_L ;

$$(R_{dc}/L)_\frac{1}{2} = \frac{2 \rho_c l_w 10^9}{F_w A_w A_L} \quad \Omega \cdot \text{H}^{-1} \quad (7.36)$$

The mid-band and lower frequency specifications will determine limit values for $R_s (= R_1 + R_2)$ and L_p respectively. A core having

$$(R_{dc}/L)_\frac{1}{2} \leq R_1/L_p \quad (7.37)$$

will enable both specification requirements to be met. This assumes that eddy current losses in the winding are unimportant, which is usually true. However, if the transformer uses solid conductors at high frequencies and the d.c. winding resistance is near the limit, then the a.c. resistance should be checked by reference to Section 11.4.4. If the a.c. resistance is excessive, reference should be made to Section 9.5.3 where the conditions for minimum a.c. resistance are examined.

After considering the mid-band performance relative to that at the lower frequency region, the next most important performance parameter is the bandwidth. It is often the case that the higher frequency cut-off is determined by the leakage inductance alone. This is particu-

larly so when the circuit impedance is low or the transformation ratio is near unity. Under these circumstances the simple equivalent circuit will show a low maximum limit for the leakage inductance while the corresponding self capacitance limit may be so high that it clearly will not be a limiting factor in the design. When this is so the bandwidth is proportional to L_p/L_l . Indeed, it is easily shown from Fig. 7.6 that if the source is matched to the load then for a 1dB droop at both f_1 and f_2 :

$$\frac{f_2}{f_1} = \frac{L_p}{L_l} \quad (7.38)$$

Leakage inductance in transformers is considered in Section 11.7. Expressions are given which enable the leakage inductance of various winding arrangements to be calculated. A simplified expression for L_l in a transformer having two windings wound one above the other may be derived (see Eqns 11.35 and 11.37a):

$$L_l = \mu_0 N_1^2 \frac{l_w h_w}{3 b_w} \quad \text{H} \quad (7.39)$$

where l_w is the mean turn length,
 h_w is the total winding height of both windings,
 b_w is the winding breadth.

Therefore, combining this with Eqn 7.28

$$\frac{L_p}{L_l} = \frac{3 \mu_e b_w}{l_w h_w C_1} \quad (7.40a)$$

The corresponding expression for the side-by-side winding arrangement is

$$\frac{L_p}{L_l} = \frac{3 \mu_e h_w}{l_w b_w C_1} \quad (7.40b)$$

The former arrangement, in which the windings are placed one over another, is usually preferred. In this case the lowest leakage inductance is obtained by using a broad shallow winding area.

The side-by-side arrangement favours a tall narrow winding space but this leads to a larger mean turn length, l_w and increases R_{dc}/L_p .

Given an optimum core shape, the ratio L_p/L_l and hence the fractional bandwidth may be increased by increasing the effective permeability of the core. As observed in the previous section, a high effective permeability is the main attribute of a good transformer core. If the highest practical value of effective permeability has been achieved then L_p/L_l can only be further increased by reducing L_l . For a given core shape this is only possible by subdividing the windings into alternate sections of primary and secondary (see Section 11.7).

If the circuit impedance is high or the transformation ratio differs appreciably from unity, or if the pass band is towards the top of the frequency range at present under consideration, then self capacitance may limit the bandwidth at the higher frequency end. Under these circumstances the simple equivalent circuit will have an easily achievable value of L_p/L_l while the maximum limit of shunt capacitance will be low, e.g. $< 50\text{pF}$. In the present context only the self capacitance of the windings is relevant; if there is shunt capacitance associated with the source or load this must be deducted from the overall limit to obtain the limit of winding self capacitance.

The calculation of winding self capacitance is considered in Section 11.6; self capacitance expressions are tabulated for most common winding configurations. If the transformation ratio differs appreciably from unity, only the self capacitance of the higher impedance winding is significant. Direct capacitance between windings is usually eliminated by means of an electrostatic screen. When windings consist of only a few layers, the capacitance of winding to screen must be taken into account.

From Section 11.6 the winding self capacitance is largely independent of the number of turns. For a simple multilayer winding it is shown in Eqn 11.33 that

$$C_s \propto \frac{b_w l_w}{h_w} \quad (7.41)$$

where, in this case, h_w is the height of the winding under consideration (see Fig. 11.1).

Thus the best winding geometry for minimum self capacitance is a tall narrow cross-section. This is the reverse of the shallow broad winding shape required for low leakage inductance, and a low value of R_{dc}/L_p . However a tall narrow winding may be simulated in a shallow broad winding space by constructing the winding in narrow sections wound side-by-side, see expression 6 of Table 11.3 and Section 5.6.

For a simple two-winding unsectionalized transformer, Eqns 7.41 and 7.39 may be combined to give

$$L_l C_s \propto N_1^2 l_w^2 \quad (7.42)$$

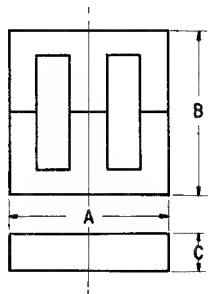
since h_w in the two equations, although different, are proportional. In Section 7.2.5 it was seen that L_l and C combine to form a low pass filter having a cut-off given by $\omega_c = (L_l C)^{-\frac{1}{2}}$. Although the upper limit of the transmission band is usually less than the theoretical cut-off frequency, the value of ω_c may be taken as an indication of the limit of high frequency performance. From the above equation:

$$\omega_c \propto \frac{1}{N_1 l_w} \quad (7.43)$$

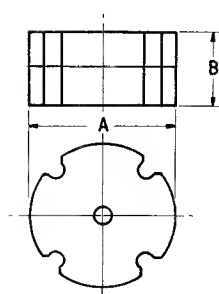
$$(7.39) \quad L_l = 4\pi 10^{-9} N_1^2 \frac{l_w h_w}{3 b_w} \quad \text{H}$$

Table 7.1. PROPERTIES OF SOME

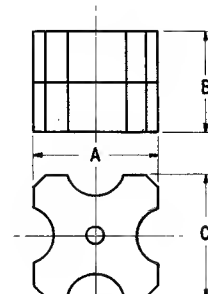
Transformer core		Overall volume of core plus winding $\text{mm}^3 \times 10^3$	Core dimensions (see sketches)			l_e mm	Dimensional parameters	
Type and size ref. $\text{mm} \times \text{mm}$	Spec. and ref. No.		breadth A mm	height B mm	thickness C mm		A_e mm^2	V_e $\text{mm}^3 \times 10^3$
<i>Double E core</i>	BS 4257 DEF 5194A	approx.	nom.	nom.	nom.	nom.	nom.	nom.
10 × 9	1 799	0.58	9.48	9.15	2.11	22.88	4.288	0.098
13 × 13	2 801	1.54	12.7	13.21	3.175	31.72	9.681	0.307
17 × 10	3 800	2.1	16.97	10.16	3.94	27.49	15.61	0.429
20 × 20	4 802	5.1	20.07	19.31	4.595	38.29	27.57	1.056
26 × 19	5 803	9.0	25.4	19.05	6.295	48.72	38.14	1.858
30 × 25	6 805	16.1	30.0	24.99	11.99	56.40	116.6	6.576
30 × 22	7 —	16.0	30.2	21.99	11.51	51.30	103.2	5.295
35 × 22	8 806	18.1	34.14	26.21	7.875	62.54	77.42	4.842
42 × 45	9 —	47	41.0	44.55	8.84	101.7	104.5	10.63
42 × 35	10 807	40	41.58	34.95	9.295	81.46	103.1	8.399
56 × 59	11 808	118	55.58	58.73	12.60	131.1	188.6	24.71
92 × 64	12 809	380	90.5	63.50	23.90	163.1	535.4	87.33
<i>Pot core</i>	BS 4061 range 1		dia.					
10 × 7	1	0.68	10.0	6.8	—	13.4	13.2	0.177
14 × 9	3	1.8	14.0	9.0	—	18.7	25.9	0.484
18 × 11	5	3.6	18.0	11.2	—	24.7	44.3	1.09
25 × 16	7	10.3	25.4	16.0	—	36.4	99.9	3.63
35 × 23	9	29	35.5	22.8	—	52.5	223	11.7
<i>X core</i>	IEC Pub. 226							
21 × 14	X22	6.2	20.9	14.2	20.9	38.0	65	2.51
24 × 15	X25	8.9	24.05	15.4	24.05	41.5	72.9	3.03
29 × 23	X30	19.8	29.0	23.3	29.0	55.8	114	6.36
34 × 28	X35	32	33.9	27.7	33.9	67.3	164	11.0
<i>H core</i>	—							
H7		0.25	9.1	4.18	6.6	17.5	3.25	0.0571
H10		0.63	10.0	5.53	11.2	22.5	7.50	0.17
H16		2.4	15.9	11.8	15.9	34.4	34.6	1.19
H20		4.1	18.5	14.1	18.5	41.2	47.0	1.93



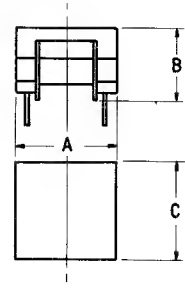
E CORE



POT CORE



X CORE



H CORE

FERRITE TRANSFORMER CORES

of the core		Dimensions of net winding space				Inductance factor A_L : inductance in nH for 1 turn	Turns factor α : turns for an inductance of 1 mH	k_3 $= \frac{2\rho_c l_w}{\mu_0 A_c A_a}$ $\Omega \cdot H^{-1}$	$\left[\frac{R_{dc}}{L} \right]_{\frac{1}{2}}$ $= \frac{2\rho_c l_w 10^9}{F_w A_w A_L}$ $\Omega \cdot H^{-1}$
C_1 $= l_e/A_e$ mm^{-1}	C_2 $= l_e/A_e^2$ mm^{-3}	breadth b_w mm	height h_w mm	area A_w $= b_w h_w$ mm^2	mean turn length l_w mm				
<i>nom.</i>	<i>nom.</i>	<i>typical</i>	<i>typical</i>	<i>typical</i>	<i>typical</i>	<i>typical limit</i>	<i>typical limit</i>	<i>typical</i>	<i>typical</i>
5.335	1.24	5.6	1.47	8.2	16	> 192	< 72.2	120 000	690
3.276	0.338	4.6	1.90	8.7	22	> 331	< 55	58 000	520
1.760	0.113	8.5	2.6	22.1	29	> 600	< 40.8	50 000	150
1.389	0.0504	7.1	2.8	19.9	32	> 886	< 33.6	29 000	120
1.277	0.0335	10.8	4.3	46.4	43	> 1060	< 30.7	17 000	59
0.4837	0.00415	13.0	3.2	41.6	59	> 2950	< 18.4	9 600	33
0.4971	0.00482	10.5	4.1	43.1	56	> 2860	< 18.7	9 700	31
0.8077	0.0104	13.5	4.3	58.1	56	> 1780	< 23.7	10 600	37
0.9728	0.00931	28.5	5.7	162	64	> 1500	< 25.8	6 000	18
0.7901	0.00766	18.4	6.7	123	64	> 1830	< 23.4	6 200	19
0.6950	0.00369	35.8	9.1	326	85	> 2100	< 21.8	3 000	8.4
0.3046	0.000569	36.5	15.1	551	151	> 4890	< 14.3	1 300	3.8
1.02	0.0773	<i>min.</i> 3.6	<i>min.</i> 1.49	<i>min.</i> 5.36	<i>nom.</i> 20.3	> 1070	< 30.6	62 000	240
0.720	0.0278	4.8	2.12	10.2	28.5	> 1690	< 24.3	34 000	110
0.558	0.0126	6.3	2.76	17.4	37.1	> 2630	< 19.5	23 000	55
0.364	0.00364	9.0	3.98	35.8	52.7	> 4270	< 15.3	9 800	23
0.236	0.00106	13.0	5.07	65.9	73.0	> 6940	< 12.0	4 800	11
0.575	0.00869	<i>min.</i> 7.3	<i>min.</i> 4.4	<i>min.</i> 32.1	<i>nom.</i> 49	> 3260	< 17.5	14 000	32
0.570	0.00782	7.5	5.7	42.8	53	> 3300	< 17.4	11 500	25
0.490	0.00430	12.8	7.35	94.1	65	> 3960	< 15.9	6 300	12
0.410	0.0025	16.1	8.1	130	77	> 4820	< 14.4	4 600	8.4
5.40	1.66	<i>min.</i> 4.2	<i>min.</i> 0.51	<i>min.</i> 2.14	<i>nom.</i> 12.1	> 700	< 37.8	360 000	550
3.0	0.40	4.9	1.09	5.34	21.2	> 1600	< 25.0	165 000	170
0.99	0.0286	8.9	1.96	17.4	37.5	> 4500	< 14.9	32 000	32
0.88	0.0187	10.4	2.66	27.7	46.4	> 5500	< 13.5	25 000	21

- Notes
1. Although every care has been taken in compiling this table the figures may not exactly agree with the article sheet of a particular manufacturer. When exact agreement is essential, the manufacturer's figures should be used.
 2. The overall volume is the volume of the least rectangular box that will just enclose the core plus winding.
 3. For cores of rectangular cross-section the quoted value of h_w is 0.8 times the actual available winding height; this allows for bowing (see Section 11.2).
 4. The core constant k_3 is the winding resistance/inductance ratio of a half winding normalized with

respect to the overall copper factor F_w , and the effective permeability, μ_e , i.e.

$$\left[\frac{R_{dc}}{L} \right]_{\frac{1}{2}} = \frac{k_3}{F_w \mu_e}$$

5. The figures in the column headed $\left[\frac{R_{dc}}{L} \right]_{\frac{1}{2}}$ have been calculated from Eqn 7.36 in which F_w is put equal to 0.56 and A_L is the listed value.
6. The electrical properties are based on the assumption that there is no air gap in the magnetic circuit except the residual gap at the mating surfaces.

i.e. for a given shunt inductance, ω_c is proportional to $\mu_c^{\frac{1}{2}}$ or $A_L^{\frac{1}{2}}$ and inversely proportional to the mean diameter of the winding. Therefore for the best high frequency performance the selected core should be the smallest that has a value of $(R_{dc}/L_p)^{\frac{1}{2}}$ adequate to ensure satisfactory mid-band and lower frequency transmission, and for that size it should have the highest possible A_L value. The winding cross-section affects ω_c only inasmuch as it affects the mean turn length. It follows that a wide shallow winding cross-section is preferable. Sectionalizing the windings either to reduce leakage inductance or self-capacitance will raise the limit of ω_c .

Form of the core

For most wide band transformer applications, the best core material is the one that provides the highest initial permeability at the lower end of the pass band, i.e. at f_1 . Of the various types of ferrite available, manganese zinc ferrite is invariably used for low and medium frequency transformer cores. As shown in Table 3.1, special high permeability grades have been developed for this application.

Most ferrite transformer cores consist of two pieces assembled together with a butt joint. The residual air gap is made as small as possible by grinding the mating surfaces so that they are flat and smooth. The magnetic properties of the transformer core and the effect of the residual gap are described earlier in this section.

Ferrite transformer cores are made in a variety of basically different shapes. For each shape it is possible to optimize the proportions to obtain the lowest value of $(R_{dc}/L)^{\frac{1}{2}}$, e.g. see Section 5.2. This is often done, but in many designs practical considerations take precedence. Most important among these are the termination requirements. Telecommunication transformers are often wound with very fine wire and may have many terminations. The geometric arrangement of the terminals must usually be compatible with the standard printed circuit grid. These considerations lead to the use of a coil former having a relatively large number of fixed terminal pins arranged in a particular pattern. The core must often be designed round the coil former. In addition, the equipment practice may set a height limitation.

The first ferrite transformer cores were made in the form of double E cores to match the standard shapes that had long been in use for metal laminations. By matching these shapes, the ferrite cores carried the attendant restriction, i.e. the core cross-section was necessarily rectangular. It was soon realized that a pressed ferrite core need not be restricted in this way and E cores with round centre legs appeared. These had the advantage that it is easier to wind a cylindrical coil, and when this is done in production a much better control may be exercised

over the leakage inductance and self-capacitance. This is particularly important if these elements are being used in a filter design technique. Plate 7.1 illustrates two forms of double E cores.

With the greater versatility of core design offered by ferrites, shapes having other special advantages were introduced. The pot core shape with proportions optimized for minimum R_{dc}/L had already been developed for inductors. The minimum R_{dc}/L and the magnetic screening provided by these cores made them attractive as transformer cores and special un-gapped, high permeability ranges were made available. The main disadvantage of the pot core is that the lead-out slots are not wide enough to accommodate a coil former having a sufficient number of fixed terminal pins.

This restriction led to the more functional approach in which the coil former is designed to have the required number of pins occupying acceptable positions on the printed circuit grid and the core is designed to have the best shape that is compatible with the coil former. Such a development is the X core shown in Plate 7.1. It may be regarded as a square pot core having, in each side, a slot wide enough to accommodate several fixed pins. Windings of the finest wire may be terminated directly (i.e. without recourse to special stranded lead-out wire) and then all the connexions may be simultaneously dip-soldered. The core may be assembled round the winding using a clamp or an adhesive and the finished transformer may be inserted into a standard printed circuit board.

The cores described so far all suffer from the appreciable degradation of permeability due to the residual air gap (see Fig. 7.11). This can only be alleviated by reducing the residual air gap reluctance, l_g/A_g . A type of core which has the reduction of l_g/A_g as the main design principle is the H core; one form of this is shown in Plate 7.1. It is essentially a U and I core but the area of contact has been increased by widening the U core and also the ends of the I core until the latter has the form of the letter H. This has the effect of increasing A_g without increasing the core cross-section embraced by the winding. In another form the magnetic circuit of the H member is completed by a rectangular frame of ferrite which mates with the two parallel limbs of the H. A lapping process is used to make the mating surfaces optically flat thus reducing l_g . As a result, such a core may efficiently use a high permeability ferrite, e.g. an H core made from ferrite having an initial permeability of 5000 would have an effective permeability of about 4500. It has a coil former that is integral with the H member, thus avoiding the waste of winding space caused by the clearances necessary with a separate coil former. Fixed pins are moulded into the coil former. This type of transformer is very suitable for small wide-band and pulse transformers.

Table 7.1 lists a number of typical transformer cores and indicates the physical dimensions, effective dimen-

sions, α and A_L values, winding dimensions and $(R_{dc}/L)_{\frac{1}{2}}$ values. In selecting a core, the choice will usually be restricted to a particular range, e.g. E cores or pot cores, etc. From the limit values of R_1 and L_p in the equivalent circuit, the maximum permissible value of R_1/L_p may be calculated. The core selected for a trial design should have a $(R_{dc}/L)_{\frac{1}{2}}$ value that does not exceed the permissible value of R_1/L_p . If the transformer has d.c. magnetization so that the design involves the Hanna procedure then clearly the $(R_{dc}/L)_{\frac{1}{2}}$ criterion cannot be used. The same is true if the transformer must have extra windings or an unusually large allowance for insulation. In such cases the trial design must be based on experience or an intelligent guess. Given adequate data the appropriate core size may be deduced quite easily.

7.3.2. An example of transformer design procedure

The design procedure depends to some extent on the requirements in the specification. The procedure outlined below includes most of the steps in the design of a normal two-winding wide band communication transformer. If there are few requirements and they are easily satisfied the more detailed steps may be omitted.

- Translate the specification into equivalent circuit element values as described in Section 7.2.
- If there is to be superimposed d.c. or if there are more than two windings the best core must be selected by experience or by trial designs. If these complications are absent, calculate R_1/L_p and choose a core having $(R_{dc}/L)_{\frac{1}{2}}$ a little less than this calculated value.
- If the windings have to carry d.c., use the Hanna curves as described in Section 7.3.1 (p. 253). If not, use α or A_L for the core and calculate the number of turns required to obtain the shunt inductance, L_p (see Eqns 7.29 and 7.30).
- From the turns ratio calculate the number of turns in the other winding(s).
- Calculate the winding area available for one of the windings; this will normally be half the total net winding area, A_w , after a deduction has been made for insulation. The conductor diameter may then be obtained as described in Section 11.2. In a similar way obtain the conductor diameter for the other winding(s).
- Calculate the winding resistances (see Section 11.3). Check that $R_1 \approx R_2/r^2$ and that $R_1 + R_2/r^2$ is less than the permitted value. If not, either a better copper factor must be obtained or a core having a lower $(R_{dc}/L)_{\frac{1}{2}}$ ratio must be used.
- Using Eqns 7.32, 7.33 and 7.34 or 7.35, the core loss may be checked to ensure that R_p is negligible over

the bandwidth. If it is excessive, more turns or a larger core or one having less loss must be used.

- Assuming the simplest winding arrangement, calculate the leakage inductance from the expression in Fig. 11.18. If the value is excessive try the effect of dividing the windings into alternately wound sections. If a sufficiently low value of L_l cannot be achieved by sectionalizing then a better core must be used, i.e. one having a higher L_p/L_l ratio; see Eqn 7.40a.
- Calculate the winding self-capacitance by the methods described in Section 11.6. If the total shunt capacitance due to source, load and windings is excessive, side-by-side sectionalizing must be tried.
- If a filter design technique is used, calculate the additional (external) inductance and capacitance that will be required.

These steps will now be exemplified by taking the transformer design already considered in Section 7.2.7 and continuing it to the practical realization.

The transformer has a ratio, secondary turns/primary turns, equal to $\sqrt{2}$. The main parameters referred to the primary (600 Ω) side are:

Open circuit inductance, $L_p = 0.275$ H

Total winding resistance, $R_1 + R_2/r^2 < 42$ Ω

Leakage inductance = 175 μ H

Secondary shunt capacitance

(referred to primary) = 486 pF

Voltage amplitudes are assumed to be small so that hysteresis may be neglected. It is also assumed that there is no direct current.

The primary and secondary windings will occupy approximately equal winding areas, so $R_1 \approx R_2'$ and therefore $R_1 < 21$ Ω . Then $R_1/L_p = 21/0.275 = 76$ $\Omega \cdot \text{H}^{-1}$. Referring to Table 7.1 suitable cores are the 26 mm double E core, the 18 mm pot core, the X22 core and the H16 core.

For the purpose of this example the pot core will be selected; it has $(R_{dc}/L)_{\frac{1}{2}} = 55$ $\Omega \cdot \text{H}^{-1}$ which is well within the requirement.

The number of turns required to ensure that the inductance is greater than the specified value may be obtained from the limit α or A_L values using Eqns 7.29 or 7.30. However in the present example L_p is a filter element and it is better to use an average value of α or A_L so that the actual value of L_p is as near as possible to the required value. Accordingly, instead of using $\alpha = 19.5$ as quoted a value of 18.5 will be used. Then the number of primary turns is given by

$$N_1 = \alpha \sqrt{L} = 18.5 \sqrt{0.275} = 307 \text{ turns.}$$

The winding cross-sectional area available for this number of turns may also be obtained from Table 7.1 either by taking approximately half of the value of A_w

or more exactly by multiplying the winding breadth by the height actually available for the primary winding. The total available height is 2.76 mm. If 0.4 mm is subtracted for the interwinding and overall insulation, the winding height available for the primary and secondary is about 1.2 mm each. Therefore the available cross-section is $6.3 \times 1.2 = 7.6 \text{ mm}^2$ for each winding. Referring to Section 11.2 and using a packing factor of 0.9 in Eqn 11.6, the maximum overall conductor diameter that may be used for the primary winding if random winding is specified is

$$d_o = \sqrt{\left[\frac{7.6 \times 0.9}{307} \right]} = 0.15 \text{ mm}$$

If wire having fine enamelled covering is to be used, Table A.1.2.1 of the appendix shows that a suitable copper diameter is 0.0048 in (0.122 mm). The preceding Table A.1.1 gives the resistance per unit length, R_c , to be $1.45 \Omega \cdot \text{m}^{-1}$. The mean turn length from Table 7.1 is 37.1 mm. Therefore the resistance of the primary winding is, from Eqn 11.9

$$R_1 = 307 \times 37.1 \times 1.45 \times 10^{-3} = 16.5 \Omega$$

This, as could be expected from the value of $(R_{dc}/L)_{\frac{1}{2}}$, is well within the limit. The corresponding calculation for the secondary is as follows:

$$N_2 = 307 \times \sqrt{2} = 434 \text{ turns}$$

$$d_o = \sqrt{\left[\frac{7.7 \times 0.9}{434} \right]} = 0.126 \text{ mm}$$

Fine enamelled wire having $d = 0.0040$ in (0.102 mm) is suitable; $R_c = 2.09 \Omega \cdot \text{m}^{-1}$

$$\therefore R_2 = 434 \times 37.1 \times 2.09 \times 10^{-3} = 33.7 \Omega$$

Referring this to the primary it becomes $R'_2 = 16.9 \Omega$, giving a total winding resistance of 33.4Ω referred to the primary side. The specification limit is 42Ω so there is an adequate margin for manufacturing tolerances.

The requirements for shunt inductance and series resistance having been satisfied, the effect of core loss may be checked. Hysteresis loss has been assumed to be negligible and the frequency is too low for eddy current loss in the core. Referring to Fig. 3.12.1 the following (pessimistic) values of $(\tan \delta_r)/\mu_i$ may be taken for the purpose of calculation: 5×10^{-6} at 10 kHz and 40×10^{-6} at 300 kHz. From Eqn 4.45

$$\frac{\tan \delta_r}{\mu_i} = \frac{\omega \mu_o N^2 A_e}{l_e R_p}$$

$$\therefore R_p = \frac{\omega \mu_o N^2 A_e}{l_e} \times \left(\frac{\mu_i}{\tan \delta_r} \right)$$

Referred to the primary side, and using the effective parameters from Table 7.1,

$$R_p = 1.43 \times 10^{-8} N_1^2 f \left(\frac{\mu_i}{\tan \delta_r} \right)$$

$$\therefore \text{ at 10 kHz } R_p = 2.7 \text{ M}\Omega$$

$$\text{and at 300 kHz } R_p = 10 \text{ M}\Omega$$

The lower of these values may be used to check the return loss by reference to Fig. 7.5. $R_s/R'_b = 33.4/600 = 0.056$ and $R'_b/R_p = 600/2.7 \times 10^6 = 2.2 \times 10^{-4}$. Clearly the core loss is so low that it may be neglected and the $R'_b/R_p = 0$ line may be used. This yields a return loss of 32 dB when $R_s/R'_b = 0.056$. Thus the mid-band return loss requirement is adequately met.

The leakage inductance must now be calculated; at first the simple winding arrangement shown in the L.H. diagram of Fig. 11.18 will be assumed. If the windings occupy all the available winding space the parameters in the leakage inductance expression given in the caption to Fig. 11.18 are as follows

$$\begin{aligned} N &= 307 & \Sigma x &\approx 2.1 \\ l_w &= 37.1 & \Sigma x_A &= 0.25 \text{ (assumed)} \\ M &= 1 \\ Y &= 6.3 \end{aligned}$$

The expression then yields $L_l = 660 \mu\text{H}$; this value is too high. However, by using the second winding arrangement shown in Fig. 11.18, i.e. a simple sandwich, the above figure may be divided by $M^2 = 4$, i.e. $L_l = 166 \mu\text{H}$. This is satisfactory; in the actual transformer it may be necessary to adjust the value obtained so that it equals the series inductance required by the filter design. Additional series inductance may be added if necessary.

It finally remains to check that the self capacitance of the windings is not excessive. For brevity only the shunt component of the self capacitance will be considered; the method will be that outlined towards the end of Section 11.6.2. The area of the mean layer is $37.1 \times 6.3 = 240 \text{ mm}^2$. There being no interleaving, the effective separation of the layers is obtained from the S_1 column of Table A.1.2.3 of Appendix A. It is 0.031 mm for 0.0048 in (0.122 mm) dia. fine enamelled wire used to wind the primary. Assuming that the effective permittivity of the dielectric is 4 and that the mean layer may be used without introducing appreciable error, the capacitance between layers is given by Eqn 11.32a

$$C_l = \frac{0.00885 \times 4 \times 240}{0.031} = 267 \text{ pF}$$

The effective number of layers, $p = 1.2/0.142 \approx 9$. Therefore the shunt element of the self capacitance, obtained from expression 5 of Table 11.3 is:

$$C_a = \frac{4 \times 267 \times 8}{3 \times 81} = 35 \text{ pF}$$

The corresponding values for the secondary are:

$$C_l = 305 \text{ pF} \quad p = 10$$

$$C_a = 37 \text{ pF}$$

These capacitances are very small compared with the filter capacitances that are required. In practice they could be neglected and external capacitors of the specified values would be used to realize the circuit.

A transformer made to this design had the following measured properties referred to the 600Ω side (the calculated values are given in brackets)

$$\text{Open circuit inductance, } L_p = 299 \text{ mH} \quad (275)$$

$$\text{Primary winding resistance, } R_1 = 15.5 \Omega \quad (16.5)$$

$$\text{Secondary winding resistance, } R'_2 = 17.2 \Omega \quad (16.9)$$

$$\text{Leakage inductance, } L_l = 160 \mu\text{H} \quad (166)$$

$$\text{Primary plus secondary self capacitance, } C_s = 106 \text{ pF} \quad (109)$$

The transmission characteristic of this transformer was measured in the circuit shown in Fig. 7.10; the plotted results are shown together with the theoretical characteristic. For comparison, the theoretical characteristic is given also for the circuit without capacitances, i.e. the characteristic that would have been obtained without recourse to filter technique (assuming L_l remains at $175 \mu\text{H}$). It is seen that the measured high frequency droop is greater than that theoretically predicted. This is due to eddy current effects increasing the winding resistance at the upper end of the band. However, the return loss at 300 kHz was found to be 16.4 dB which is in accordance with the design value. The lower frequency region is in close agreement with the theoretical curve.

7.4. HIGH FREQUENCY WIDE BAND TRANSFORMERS

Although there is no clear division of the frequency bands, high frequency transformers may be considered as those having pass bands lying wholly above about 0.1 MHz . Above this frequency the permeability of suitable transformer ferrites begins to vary significantly with frequency and the loss angle begins to rise. The higher the operating frequency the more important it becomes to regard the core impedance as a complex function of frequency; simple constants, such as α or A_L used at low frequencies, become inappropriate.

Another important distinction is that, at high frequencies, the circuit impedances are usually lower so that generally lower shunt impedances are necessary. The

required impedance may usually be obtained with few turns so, except at high powers, the winding resistance becomes a negligible factor in the design. It is no longer necessary to consider the $(R_{dc}/L)_{\frac{1}{2}}$ value of the core. Instead the main concern is that for a given shunt impedance at f_1 the leakage inductance and self capacitance shall be a minimum.

Much of the discussion concerning low and medium frequency transformers is relevant in the present context and indeed the design procedure set out in Section 7.3.2, adapted to take account of the complex permeability, could in principle be used for high frequency transformers. The object of the present section is to consider alternative approaches and techniques which are specific to the design of ferrite cored transformers intended to operate at these frequencies.

7.4.1. Contribution of the core

The shunt inductance, L_p , and the shunt resistance, R_p , see Fig. 7.3, depend directly on the core permeability and losses respectively. At low and medium frequencies the permeability may be regarded as constant and the losses are usually negligible. At high frequencies the onset of dispersion phenomena such as ferrimagnetic resonance invalidates these conditions, see Fig. 3.11, and it is better to work in terms of the parallel complex permeability.

From Eqn 2.18

$$\left. \begin{aligned} \frac{L_p}{N^2} &= \frac{\mu_0 \mu'_p}{C_1} & \text{H} \\ \frac{R_p}{N^2} &= \frac{\omega \mu_0 \mu''_p}{C_1} & \Omega \\ \text{and } \tan \delta_m &= \frac{\mu''_p}{\mu'_p} \end{aligned} \right\} \quad (7.44)$$

If the core has an air gap, the inductance is reduced in the ratio μ_0/μ'_p (see Section 4.2.2) and the shunt resistance is virtually unchanged (see Eqn 4.47). In the present context the air gap is usually negligible or entirely absent.

For a transformer to have a specified limit of insertion loss or return loss, the modulus of the shunt impedance presented by the core must not be less than a certain value, this value depending on the loss tangent. If for a given ferrite core the value of $\tan \delta_m$ at f_1 is known then a minimum permissible value of L_p or R_p may be calcu-

$$(7.44) \left\{ \begin{aligned} \frac{L_p}{N^2} &= 4\pi \mu'_p 10^{-9} / C_1 & \text{H} \\ \frac{R_p}{N^2} &= 4\pi \omega \mu''_p 10^{-9} / C_1 & \Omega \end{aligned} \right.$$

lated and the required number of turns may be obtained from Eqn 7.44. This procedure may be simplified by normalizing some of the variables and preparing a graph giving the required number of turns for a given insertion loss or return loss as a function of frequency. Such curves apply only to the ferrite material from which the complex permeability data were obtained but they may be used for any core shape. The technique is an extension of that proposed by Maurice and Minns.¹ The main steps in the preparation of the graphs will now be indicated.

The shunt impedance Z of a transformer may be expressed in terms of R_p and Q -factor thus:

$$Z = \frac{j\omega L_p R_p}{R_p + j\omega L_p} = \frac{R_p}{1 - jQ} = \frac{R_p(1 + jQ)}{1 + Q^2} \quad \Omega \quad (7.45)$$

where $Q = R_p / \omega L_p$

Applying this equation and that of Fig. 7.2(c), the insertion loss introduced when Z is connected across a 1Ω source and a 1Ω load is given by

$$\left. \begin{aligned} A_i &= 10 \log_{10} \left\{ 1 + \frac{1}{R_p} + \frac{1 + Q^2}{4 R_p^2} \right\} \\ &= 10 \log_{10} F \quad \text{dB} \end{aligned} \right\} \quad (7.46)$$

where F represents the function in the brackets.

For a given value of insertion loss, the value of F will have a particular value, e.g. F_1 . Then

$$F_1 = 1 + \frac{1}{R_p} + \frac{1 + Q^2}{4 R_p^2}$$

The solution of this quadratic equation is

$$R_p = \frac{1 + Q^2}{2\sqrt{[1 - (1 - F_1)(1 + Q^2)] - 2}} \quad \Omega \quad (7.47)$$

This gives the value of the resistive component, R_p , of impedance Z which will result in a given insertion loss, provided the value of the Q -factor is known. If the parallel components of the complex permeability have been determined for the ferrite under consideration then, at a given frequency, the Q -factor is given by

$$Q = \frac{\mu_p''}{\mu_p'}$$

and the value of R_p corresponding to N turns wound on a given core shape is

$$R_p = \frac{\omega \mu_0 \mu_p'' N^2}{C_1} \quad \Omega$$

Putting this equal to the value of R_p required to obtain

the given insertion loss (Eqn 7.47), the required number of turns may be calculated.

If the expression for R_p is normalized with respect to the core factor C_1 , by putting $C_1 = 1 \text{ mm}^{-1}$ then a fictitious number of turns, N_a , may be calculated such that when wound on a core having $C_1 = 1 \text{ mm}^{-1}$ and connected across 1Ω source and load resistances, the given insertion loss will be obtained. Thus

$$N_a^2 = \frac{R_p 10^3}{\omega \mu_0 \mu_p''} \quad (7.48)$$

Fig. 7.13 shows N_a as a function of frequency for several values of insertion loss and for two ferrites suitable for wide band high frequency transformers. In applying this graph to a practical situation where the actual core factor is C_1 and the parallel combination of source and load resistances is denoted by R , the actual number of turns required is given by

$$N = N_a \sqrt{[2 R C_1]} \quad (7.49)$$

where C_1 is in mm^{-1}

The corresponding graphs having return loss as parameter may be similarly prepared. Referring to the diagram in Fig. 7.14,

$$Z_i = \frac{Z}{1 + Z}$$

Combining this with Eqn 7.45 and the equation for return loss in Fig. 7.2d, the return loss is given by

$$\begin{aligned} A_r &= 20 \log_{10} \left| \frac{Z_i + 1}{Z_i - 1} \right| = 10 \log_{10} \left\{ 1 + \frac{4 R_p (R_p + 1)}{1 + Q^2} \right\} \\ &= 10 \log_{10} F \quad \text{dB} \end{aligned} \quad (7.50)$$

where F is now the function defined by this equation.

As before, the particular value of F corresponding to a given return loss may be denoted by F_1 and the quadratic equation involving F_1 , R_p and Q may be solved for R_p . This time

$$R_p = \frac{\sqrt{[1 - (1 - F_1)(1 + Q^2)] - 1}}{2} \quad \Omega \quad (7.51)$$

Again this may be equated to the value of R_p obtained with N_a turns on a core of the given ferrite, the core factor being unity. Fig. 7.14 shows the resulting graphs with return loss as parameter; the grades of ferrite are as before. For the practical design, Eqn 7.49 again applies.

There are several things to notice about these graphs. Clearly the best material is that which provides the given performance at the required frequency with the least value

$$(7.48) \quad N_a^2 = \frac{R_p}{4\pi\omega\mu_p''10^{-9}}$$

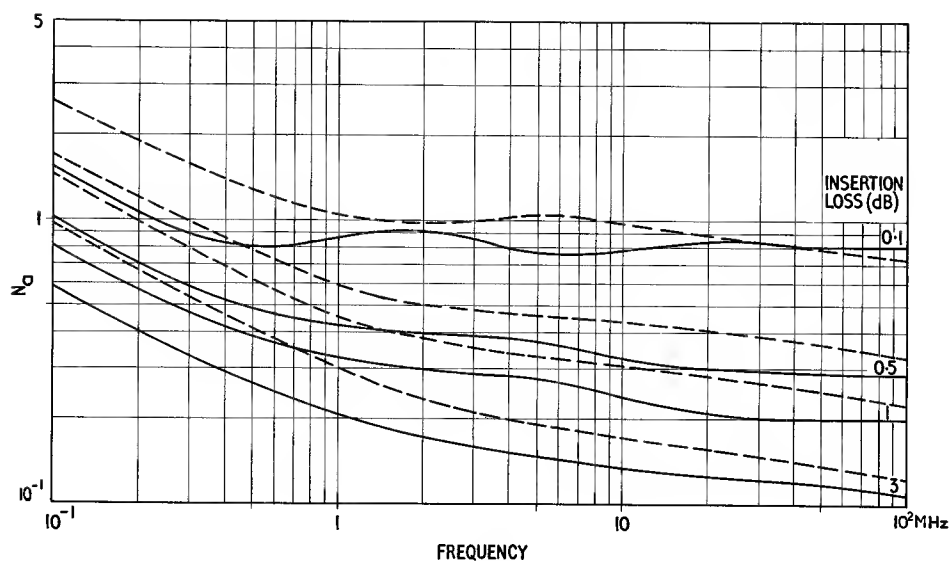


Fig. 7.13. The normalized number of turns, N_a , as a function of frequency, with insertion loss as parameter.

The number of turns in an actual design is given by $N = N_a \sqrt{[2RC_1]}$
 where $R = R_a R'_b / (R_a + R'_b)$ and C_1 is in mm^{-1}

— A HIGH PERMEABILITY MANGANESE ZINC FERRITE
 --- A HIGH PERMEABILITY NICKEL ZINC FERRITE

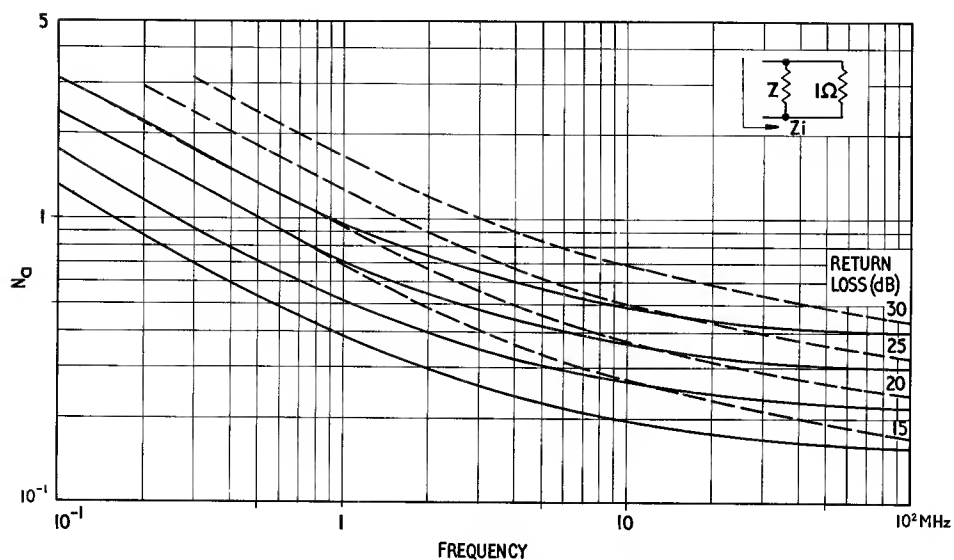


Fig. 7.14. The normalized number of turns, N_a , as a function of frequency, with return loss as parameter

of N_a . If the specification requires that the insertion loss should not exceed a given value, it is seen from Fig. 7.13 that the high permeability manganese zinc ferrite is superior up to frequencies between 1' and 10 MHz depending on the specified insertion loss. The frequency referred to is, of course, f_1 i.e. the frequency at which the transmission at the lower end of the pass band is specified. Thus if a transformer were required to have less than 1 dB attenuation between 5 and 200 MHz a manganese zinc ferrite would be the best choice. For return loss the crossover region between manganese zinc and nickel zinc ferrites is even higher; about 20 MHz.

It will be noticed that some of the curves relating to insertion loss show minima. This undulation occurs not because Z ceases to rise with frequency but rather because it changes from a mainly inductive impedance at the lower frequencies to a mainly resistive impedance at the upper end of the frequency range. If the design leads to a value of N_a in one of these troughs and this value of N_a is used to obtain the actual number of turns, the correct insertion loss will be obtained at f_1 but at higher frequencies, i.e. further into the pass band, the loss will increase to a shallow maximum. In fact, the idea of the lower frequency droop in the characteristic may have to be abandoned. A horizontal line drawn at the proposed value of N_a will indicate the variation of attenuation that will be obtained, the attenuation at any frequency being interpolated between the curves of constant insertion loss. The variation is usually not very great but in some cases it may be preferable to choose the highest value of N_a within the pass band of the transformer rather than the value at f_1 .

The complex permeability data on which these graphs are based relate to the residual loss, i.e. eddy current and hysteresis loss are not included. The remarks in Section 7.3.1 regarding eddy current loss apply equally at high frequency. If a manganese zinc ferrite core is used, dimensional resonance is a possibility. The dimensional resonant frequency is related to the cross-sectional dimension of the core in Fig. 4.5. Provided it occurs at a frequency well above f_1 it is unlikely to affect the pass band. Transformers having f_1 above 1 MHz will probably use very small cores and so avoid the effect of this resonance.

In most wide band high frequency transformers the signal levels are so small that hysteresis effects are negligible. The exceptions are the high power transformers considered in Chapter 9.

7.4.2. Relations arising from the geometry of core and winding

Before considering the particular core shapes that are suitable for high frequency transformers it will be useful

to extend the discussion begun in Section 7.3.1. In that section general relations between core performance and geometry were derived for low and medium frequency transformer cores. At high frequencies, winding resistance ceases to be a significant factor and the winding may consist of only a few turns. In this case the winding breadth and height cease to be definite. Considering only the reactive component of the shunt impedance, Eqn 7.40a yields, for an ungapped core, the proportionality

$$\frac{L_p}{L_t} \propto \frac{\mu_p}{l_w C_1} \quad (7.52)$$

It is not valid similarly to invoke Eqn 7.42 to study the factors affecting $L_t C_s$ because that equation is based on the self capacitance of a multilayer winding; in the present context the winding consists of a few turns, probably wound in a single layer against a screen. The self capacitance may be estimated from expression 1 of Table 11.3 or it may be better to use Medhurst's data (see Fig. 11.16). If the former expression is used:

$$C_s = \frac{C_m}{3} \propto b_w l_w$$

According to Medhurst C_s/l_w is a function of b_w/l_w but it is approximately constant in the region of $b_w/l_w = 1$. Thus from either consideration it is sufficient for the present purpose to conclude that the self capacitance is proportional to l_w .

The leakage inductance is proportional to $N^2 l_w$ so the factor determining the upper frequency limit of a core, i.e. $L_t C_s$, is related to the geometry by the following proportionality

$$L_t C_s \propto N^2 l_w^2 \quad (7.53)$$

These proportionalities provide a useful guide to core design or selection. From the proportionality of 7.52 it is clear that for greatest bandwidth it is desirable to use the highest available permeability and to proportion the core to minimize $l_w C_1$. From 7.53, the highest cut-off frequency will be obtained by using the highest permeability as this will result in the smallest number of turns. Given a core shape and a permeability value, $N^2 l_w^2$ appears to be independent of the core size, e.g. if the linear dimensions of cross section are increased by a factor of two this will double l_w and will increase the core area (and hence the shunt inductance) by a factor of 4; N may consequently be halved to restore the shunt inductance to the specified value. The $L_t C_s$ product is unchanged by this increase in core size. It will be seen later that for some cores the increase in L_p is less than proportional to the increase in l_w . Under these circumstances it is better to use the smallest practical core size.

In this discussion the permeability of the material has been regarded as a measure of merit and the core loss has been ignored. However in general the criteria of the

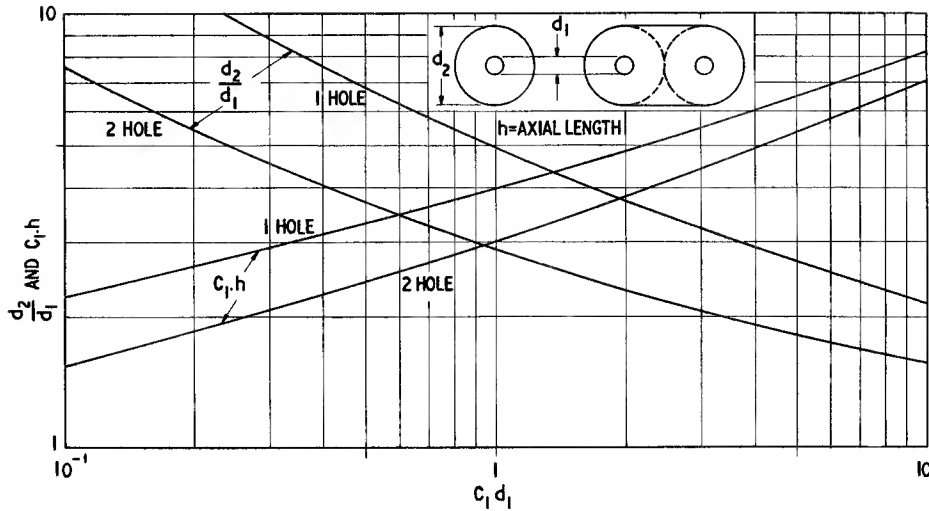


Fig. 7.15. Optimum toroidal cores for high frequency transformers

previous section do, of course, still apply, i.e. the better core material is that which yields the lower value of N_a in Fig. 7.13 or 7.14.

7.4.3. The form of the core

High frequency transformers may be designed using any of the conventional core shapes, e.g. small pot cores are often used. In such designs smallness does not necessarily confer better high frequency characteristics because, as observed above, $L_1 C_s$ tends to be independent of size. However, if the core is excessively large the required number of turns may be so small that it becomes difficult to provide the correct turns ratio. It may then be necessary to use more turns than the required minimum and this will reduce the bandwidth.

Since there tends to be few turns and the core tends to be small, the toroidal shape becomes attractive for transformers having pass bands extending to some hundreds of MHz. It is useful to consider the optimum shape following the discussion in the previous section. There it was found that for the widest bandwidth $l_w C_1$ should be a minimum. If the inner and outer diameters of the toroid are d_1 and d_2 respectively and the axial thickness is h , then assuming the turns lay flat against the core, the turn length, l_w is given by

$$l_w = d_2 - d_1 + 2h$$

The core factor, C_1 , for such a toroid is given in the derivation of Eqns 4.4 and 4.5:

$$C_1 = \frac{2\pi}{h \log_e \frac{d_2}{d_1}} \quad (7.54)$$

$$\therefore l_w = d_2 - d_1 + \frac{4\pi}{C_1 \log_e \frac{d_2}{d_1}} \quad (7.55)$$

If d_1 and C_1 are constant, l_w is a minimum when

$$C_1 d_1 = \frac{2\pi}{\frac{d_2}{d_1} \left[\log_e \frac{d_2}{d_1} \right]^2} \quad (7.56)$$

and from Eqn 7.54

$$C_1 h = \frac{2\pi}{\log_e \frac{d_2}{d_1}} \quad (7.57)$$

Fig. 7.15 shows d_2/d_1 as a function of $C_1 d_1$ obtained from Eqn 7.56 and the corresponding value of $C_1 h$ obtained from Eqn 7.57. Thus from the required value of C_1 , assuming a value of d_1 , the value of d_2 and h may be found. The value of d_1 must be as small as possible. This follows from Eqn 7.54; C_1 is equally reduced by doubling d_2 or halving d_1 but if $d_2/d_1 \gg 1$ this increase of d_2 increases l_w far more than the proportionate decrease of d_1 . The only limit to the smallness of d_1 is in the necessity to thread the windings through the hole. Since there are to be few turns and the wire diameter may be small, d_1 may in practice be in the region of 2 mm. This results in a toroid which is quite different in shape from the usual toroidal core; it is a short cylindrical core with a small axial hole, i.e. a bead.

The upper part of Table 7.2 lists some examples obtained from the graphs. It is seen that as C_1 is reduced, d_2 and the overall volume increase rapidly. The bandwidth, which is inversely proportional to $l_w C_1$, increases with volume but the rate of improvement rapidly diminishes

Table 7.2. EXAMPLES OF 1 HOLE AND 2 HOLE HIGH FREQUENCY WIDE BAND TRANSFORMER CORES HAVING OPTIMUM PROPORTIONS (SEE FIG. 7.1.5). DIMENSIONS IN MM UNITS.

1 hole core

d_1	C_1	$C_1 d_1$	$\frac{d_2}{d_1}$	$C_1 h$	d_2	h	l_w	$l_w C_1$	Overall volume
2	0.8	1.6	4.02	4.5	8.0	5.6	17.3	13.8	285
2	0.4	0.8	5.45	3.7	10.9	9.3	27.4	10.95	860
2	0.2	0.4	7.6	3.1	15.2	15.5	44.2	8.85	2800
1	0.8	0.8	5.45	3.7	5.5	4.7	13.9	11.1	111

2 hole core

2	0.8	1.6	2.45	3.5	4.9	4.37	14.5	11.6	188
2	0.4	0.8	3.1	2.8	6.2	7.0	22.4	9.0	480
2	0.2	0.4	4.02	2.25	8.04	11.3	37.7	7.55	1300
2	0.1	0.2	5.45	1.85	10.9	18.5	54.8	5.48	3900
1	0.1	0.1	7.6	1.55	7.6	15.5	44.2	4.42	1600

as the volume becomes larger. A given transmission requirement at f_1 determines L_p

$$\therefore L_p \propto \frac{N^2}{C_1} = \text{const.}$$

Substituting this in 7.53

$$L_l C_s \propto l_w^2 C_1 \quad (7.58)$$

From this proportionality and the figures in Table 7.2 it is seen that as d_2 increases $L_l C_s$ increases and the upper cut-off frequency is lowered. Thus although an increase in volume will somewhat improve the bandwidth it will move the pass band to a lower frequency. If transmission at the highest possible frequency is required then for a given value of d_1 it is better to use the smallest practicable core; the limitation being the number of turns that it is feasible to apply. The improvement resulting from reducing d_1 is demonstrated in the table. Considerable licence may be used in fixing the outside dimensions of the core since the proportions of these yield a very flat optimum.

There is a practical limit to how far C_1 and d_1 may be reduced. However, a further improvement may be obtained by using two toroids side by side as shown in the right hand diagram of Fig. 7.15; a single turn would thread both holes. In practice a single core having two holes would be used; the full line shows a possible profile. Optimum proportions may again be found. The turn length is now given by

$$l_w = 2(d_2 - d_1 + h)$$

and the core factor assuming two toroids is

$$C_1 = \frac{\pi}{h \log_e \frac{d_2}{d_1}}$$

The result is that l_w is a minimum when

$$C_1 d_1 = \frac{\pi}{\frac{d_2}{d_1} \left[\log_e \frac{d_2}{d_1} \right]^2} \quad (7.59)$$

Fig. 7.15 also gives d_2/d_1 and $C_1 h$ as functions of $C_1 d_1$ for this 2 hole core and the lower part of Table 7.2 lists several examples. The advantages of the two hole core are apparent. The above conclusions concerning core size apply also to this version. A possible disadvantage of this core is that each turn has to be threaded twice through a hole but since the number of turns is not large this is not a serious limitation.

7.4.4. The windings

In the foregoing discussion of core shape it has been assumed that factors such as the turns ratio and the winding arrangement have been constant. With conventional core shapes it is often necessary to use rather elaborate windings consisting, perhaps, of copper foil; transmission line techniques have sometimes been used to extend the bandwidth. However, with the core shapes described in the previous section the windings may be very simple. The requisite number of turns of a convenient size of enamelled copper wire may be used and no

special skill is required in the winding (or rather threading) operation.

Windings requiring few turns may give rise to problems in obtaining the correct turns ratio. Indeed the minimum number of turns may in practice be determined by the required ratio, e.g. an impedance ratio of 4 may be obtained by windings having 1 and 2 turns respectively whereas for an impedance ratio of approximately 3 the least numbers of turns are 4 and 7 respectively.

To minimize leakage inductance, the primary and secondary should be wound in close proximity. If auto transformer winding (see Section 11.7.2) is possible it will give the lowest possible leakage inductance. If not, bifilar winding using a twisted pair may be used.

If the transformer must provide a large impedance transformation, the higher impedance may result in a self capacitance limitation. The situation is made more difficult if an electrostatic screen between windings is required. These factors may prevent the use of twisted pair windings. A low value of leakage inductance may be obtained without close proximity of the windings if a closely fitting screen is used. This envelopes the core except for an annular gap to prevent a short circuit. It provides, in effect, a tight single turn coupling between primary and secondary. The windings may be placed over the screen and in the case of a single hole core may be on diametrically opposite sides of the toroid. In practice such a screen could be provided by silvering the surface of the ferrite, the annular gap being provided, for example, by subsequently grinding a chamfer at one end of the hole. The direct silvering technique can only be successfully applied to high resistivity nickel zinc ferrite; for manganese zinc ferrite an insulating barrier must first be applied so that the lower resistivity ferrite

does not short circuit the screen. If a high degree of screening is required, the winding with the fewest turns could be wound with small diameter screened or coaxial wire.

In the majority of designs, however, adequate performance may be obtained by using the simplest winding arrangement. If a nickel zinc ferrite core is used, the core resistivity is high enough for chance electrical contact between the windings and core to be ignored. However, if the lower resistivity manganese zinc ferrite is used, insulation, perhaps in the form of lacquer, must be provided.

7.4.5. An example of high frequency transformer design

Suppose a transformer is required to provide isolation and phase inversion between two 50Ω circuits, with less than 1 dB insertion loss between 100 kHz and 100 MHz.

From the list of optimum one hole cores in Table 7.2 the first will be used in this example. For this core $d_1 = 2$ mm, $d_2 = 8$ mm, $h = 5.6$ mm and $C_1 = 0.8$ mm.⁻¹

Referring to Fig. 7.13 manganese zinc ferrite is the better material at 100 kHz and the normalized number of turns required to meet the insertion loss specification is 0.8. Therefore the actual number of turns is given by Eqn 7.49 in which $R = 25\Omega$. Thus

$$N = 0.8\sqrt{[2 \times 25 \times 0.8]} \approx 5$$

therefore, allowing a margin for tolerances, each winding may consist of 6 turns.

There is no simple analytical means of estimating the performance at the upper end of the frequency band; the use of an optimum core will ensure that, within the

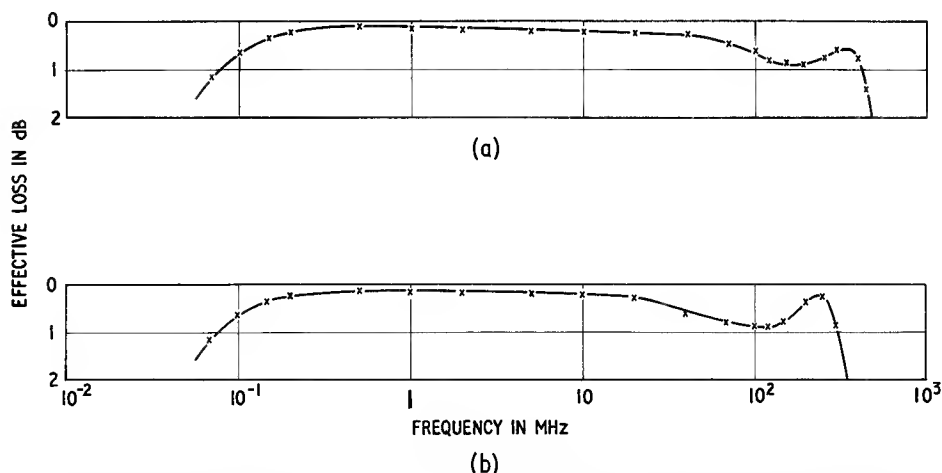


Fig. 7.16. Measured transmission characteristics of high frequency transformer examples using first core in Table 7.2. (a) Manganese zinc ferrite core, 6:6 turns bifilar wound, matching 50Ω with phase inversion; (b) Nickel zinc ferrite core, 11:11 turns bifilar wound, matching 50Ω with phase inversion

limits imposed by the core size and material, the best performance will be obtained. A transformer was made according to this design using a manganese zinc ferrite corresponding to that used in the preparation of Figs. 7.13 and 7.14. The measured transmission characteristic is shown in Fig. 7.16(a).

If, to achieve adequate insulation, it were necessary to specify a nickel zinc ferrite core then from Fig. 7.13, N_a would be raised to 1.4 and the actual number of turns would have to be raised from 6 to 10 or 11 to make the design equivalent to the previous one. A transformer was made according to this design using a nickel zinc ferrite corresponding to that quoted in Figs. 7.13 and 7.14. The measured transmission characteristic is shown in Fig. 7.16(b). It is seen that the lower permeability has had the effect of lowering the upper cut-off frequency because more turns are necessary.

REFERENCES AND BIBLIOGRAPHY

Section 7.2.

SHEA, T. E., *Transmission networks and wave filters*. Van Nostrand Company Inc., New York, (1929).

Section 7.2.5

RUDD, J. B., 'Wide-band impedance transformers', *A.W.A. tech. Rev.*, **11**, 179, (1960).

Section 7.4.

I. MAURICE, D. and MINNS, R. H., 'Very-wide band radio frequency transformers', *Wireless Engr.*, **24**, 168, (Part 1) and 209 (Part 2), (1947).

MCLEISH, C. W., 'Design procedure for very wide band R.F. transformers', *Natn. Res. Coun. Canada*, Report ERA 272, (May 1954).

O'MEARA, T. R., 'A wide-band high frequency transformer using a ferrite core', *Proc. natn. Electron. Conf.*, **10**, 778, (1954).

TALKIN, A. I. and CUNEO, J. V., 'Wide-band bulun transformer', *Rev. scient. Instrum.*, **28**, 808, (1957).

ROBERTS, W. K., 'A new wide-band bulun', *Proc. Inst. Radio Engrs*, **45**, 1628, (1957).

HUDSON, A. C., 'Wide-band transformer characteristics', *Electron Radio Engr*, **35**, 228, (1958).

RUTHROFF, C. L., 'Some broad-band transformers', *Proc. Inst. Radio Engrs*, **47**, 1337, (1959).

ELSEY, G. and JACKSON, N. C. O., 'A new approach to the design of Ferroxcube cores for wide-band H.F. transformers', *Mullard tech. Commun.*, **5**, 182, (1960).

BERG, R. S. and HOWLAND, B., 'Design of wide-band shielded toroidal r.f. transformers', *Rev. scient. Instrum.*, **32**, 864, (1961).

O'MEARA, T. R., 'A distributed-parameter approach to the high-frequency network representation of wide-band transformers', *Trans. Inst. Radio Engrs*, **CP8**, 23, (1961).

O'MEARA, T. R., 'Wide-band transformers and associated coupling networks', *Electro-Technology*, **70**, no. 3, 80, (1962).

General

LEE, R., *Electronic transformers and circuits*, John Wiley & Sons, Inc., New York, 2nd Ed., (1955).

MACFADYAN, K. A., *Small transformers and inductors*, Chapman and Hall Ltd., London, (1953).

SNELLING, E. C., 'Ferrite-cored inductors and transformers', *Mullard tech. Commun.*, **9**, 30, (1966).

GROSSNER, N. R., *Transformers for electronic circuits*, McGraw-Hill Book Company, (1967).

Pulse Transformers

8.1. INTRODUCTION

Pulse transformers, like wide band transformers, are required to transmit energy that is distributed over a wide frequency spectrum. Whereas the performance of the wide band transformer is specified in terms of this spectrum, the performance of the pulse transformer is specified in terms of its effect on the shape of a pulse of current or voltage, this shape being expressed as a function of time. The pulse shape is usually assumed to approximate to a rectangle. The transformer must transfer the pulse of energy from the primary circuit, which is often the pulse generating circuit, to the secondary, or load, circuit without excessive shape distortion. In common with other types of transformer it must of course perform one or more of the following functions:

- (a) accurate voltage or current transformation,
- (b) isolation,
- (c) reversal of polarity,
- (d) balance or unbalance to earth,
- (e) impedance matching.

It is clear that the function of a pulse transformer is similar to that of a wide band transformer. Indeed it is possible to relate pulse distortion to bandwidth; this aspect is discussed in Section 8.4. However, the most satisfactory procedure in designing a pulse transformer

is to determine the elements of the equivalent circuit from the permissible pulse distortion. It is mainly in this respect that the two transformers types differ. This chapter is therefore principally concerned with the method of determination of the equivalent circuit elements. The basic transformer concepts and the practical design to realize a given equivalent circuit are common to both types of transformer; they have been adequately covered in the previous chapter and need not be repeated.

Pulse transformers range in application from low power, e.g. use in data handling circuits, to high power, e.g. the pulsing of radar transmitters. The design of high power pulse transformers is governed largely by heat transfer considerations and the best core material is that which provides the widest excursion of flux density. In practice this implies a high saturation flux density. For this reason the iron alloys such as grain oriented silicon steel or the nickel iron alloys are usually chosen as cores for high power pulse transformers. The saturation flux density of ferrites is typically only 20% of the figure available for the best alloys. Moreover, because the Curie point of ferrites is much lower than for alloys, the saturation flux density of ferrites is appreciably reduced at the temperatures at which the higher power transformers normally operate. For these reasons ferrite cores are used only in pulse transformers intended for low or medium powers, and the scope of this chapter is restricted accordingly.

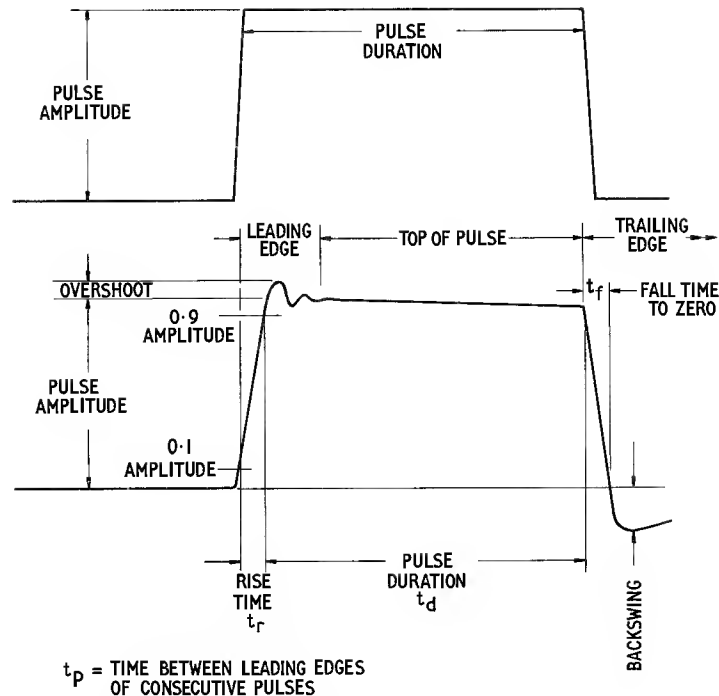


Fig. 8.1. Rectangular pulses, ideal and distorted, illustrating some of the terms used

Much of the treatment is, however, quite general.

Some useful terms and their definitions are illustrated in Fig. 8.1. In the upper part of this figure the ideal form of a rectangular or trapezoidal pulse is shown (a truly rectangular pulse is not attainable in practice because dI/dt cannot be infinite). Such pulses are usually identically repeated at regular time intervals (t_p) and the number of pulses per second (pps) is termed the Pulse Repetition Frequency (P.R.F.). If P_p is the power during the pulse then the average power is

$$P_{av} = P_p t_d / t_p \quad (8.1)$$

where t_d is the pulse duration. In high power applications t_d/t_p is very small so it is possible to achieve very high peak power without the necessity of handling high average powers. In low power applications also the ratio t_d/t_p is usually small but there are cases where it approaches 0.5 and the pulse train becomes a square wave.

When an ideal pulse is applied to the primary of a transformer, the finite reactances associated with the transformer cause the pulse appearing across the loaded secondary to be distorted. A typical secondary waveform is shown in the lower half of Fig. 8.1. A pulse transformer specification, in addition to specifying source and load impedances, turns ratios, voltages, pulse duration, etc., will define the limits of permissible pulse distortion in terms of rise time, overshoot, droop, fall time, backswing, etc. The object of the transformer design is to

achieve the required energy transformation while keeping all the elements of the transformer equivalent circuit within the limits imposed by the pulse distortion requirements.

In practice, the leading and trailing edges of the pulse usually have short durations relative to the top of the pulse. It is clear that under such circumstances these three parts of the pulse have little influence on one another and may therefore be considered separately. This principle enables the general transformer equivalent circuit, e.g. Fig. 7.3, to be simplified so that it includes only those elements which influence the part of the pulse being considered. There are two main cases, the step-up transformer in which the primary shunt capacitance may be neglected and the step-down transformer in which the secondary shunt capacitance may be neglected.

The following sections study the influence of the main elements of the equivalent circuit of the leading edge, the top of the pulse, and the trailing edge respectively. The approach and presentation are an extension of the conventional treatment to be found in the literature, e.g. Wilds.¹ It is shown how the relations so derived may be used to calculate the permissible values of these elements. After noting some relation between pulse transformer and wide band transformer design, the properties of the core material are considered with particular reference to pulse permeability. Finally some practical aspects of pulse transformer design are considered.

8.2. PULSE DISTORTION IN TERMS OF THE EQUIVALENT CIRCUIT ELEMENTS

8.2.1. The leading edge of the pulse

It is usual to suppose that the pulse applied to the primary of the transformer is a simple step function, i.e. it may be regarded as switching a source of d.c. directly across the primary terminals. In practice, of course, the pulse source will give a finite rise time, t_1 , and it may be shown that this will combine with the actual rise time, t_r , contributed by the transformer, to give an overall rise time

$$t = (t_1^2 + t_r^2)^{\frac{1}{2}}$$

If the resulting pulse is observed with an oscilloscope having a rise time, t_2 , the observed pulse will have a rise time

$$t = (t_1^2 + t_2^2 + t_r^2)^{\frac{1}{2}} \quad (8.2)$$

Knowing the value of t_1 and t_2 the necessary correction may be made.

It may be assumed that during the rise time there is negligible build-up of magnetizing current in the transformer shunt impedance, see Fig. 7.3, so this arm of the equivalent circuit may be ignored. Further, if the transformer has a reasonably large turns ratio the shunt capacitance on the low impedance side may be ignored. This means that one of two simplified equivalent circuits, Fig. 8.2, may be used depending on whether the transformer steps up or down. In this and the following

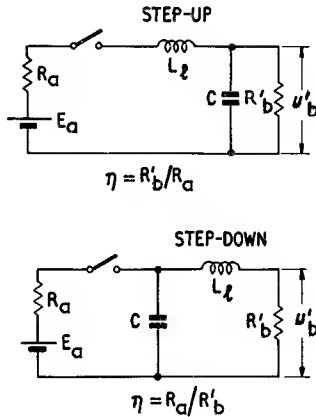


Fig. 8.2. Simplified equivalent circuit used in leading edge analysis of a step-up and step-down pulse transformer. All the elements shown are referred to the primary side; the ideal transformers have been omitted

E_a = generator e.m.f.	V
R_a = source resistance	Ω
R'_b = load resistance	Ω
L_l = leakage inductance	H
C = total shunt capacitance (transformer plus external circuit)	F
u'_b = instantaneous voltage across load	V

equivalent circuits the ideal transformer is omitted and the analysis is referred to the primary circuit.

Clearly the solution of the transient problem will yield an aperiodic result or an oscillatory result depending on the relative values of the resistive and reactive elements. The aperiodic solution for the step-up case is as follows:

$$\frac{u'_b}{E_a} = \frac{\eta}{1+\eta} [1 - \exp(-2\pi S_r \sigma_r) \{ \cosh(2\pi S_r (\sigma_r^2 - 1)^{\frac{1}{2}}) + (1 - 1/\sigma_r^2)^{-\frac{1}{2}} \sinh(2\pi S_r (\sigma_r^2 - 1)^{\frac{1}{2}}) \}] \quad (8.3)$$

where u'_b is the instantaneous load voltage referred to the primary

$$\sigma_r = a/\sqrt{b}$$

$$S_r = \frac{t\sqrt{b}}{2\pi} \quad (t = \text{time in seconds after switch has closed})$$

$$\text{and } a = \frac{1}{2} \left(\frac{R_a}{L_l} + \frac{1}{CR'_b} \right)$$

$$b = \frac{1}{L_l C} (1 + 1/\eta)$$

$$\text{where } \eta = R'_b/R_a$$

When $\sigma_r < 1$ the circuit is oscillatory and the solution becomes

$$\frac{u'_b}{E_a} = \frac{\eta}{1+\eta} [1 - \exp(-2\pi S_r \sigma_r) \{ \cos(2\pi S_r (1 - \sigma_r^2)^{\frac{1}{2}}) + (1/\sigma_r^2 - 1)^{-\frac{1}{2}} \sin(2\pi S_r (1 - \sigma_r^2)^{\frac{1}{2}}) \}] \quad (8.4)$$

where the parameters have the same meaning as given above.

For the step-down case the same result applies except that R_a and R'_b must be interchanged i.e. for step-down

$$\left. \begin{aligned} a &= \frac{1}{2} \left(\frac{R'_b}{L_l} + \frac{1}{CR_a} \right) \\ b &= \frac{1}{L_l C} (1 + 1/\eta) \end{aligned} \right\} \quad (8.5)$$

where now $\eta = R_a/R'_b$

Fig. 8.3 shows the response relative to the steady state amplitude plotted against S_r with σ_r as a parameter.

The factor S_r may be regarded as a time factor and σ_r is in effect a damping factor. Looking at these factors in more detail

$$S_r = \frac{t\sqrt{b}}{2\pi} = \frac{t}{2\pi} \left(\frac{1 + 1/\eta}{L_l C} \right)^{\frac{1}{2}} \quad (8.6)$$

$$\therefore (L_l C)^{\frac{1}{2}} = \frac{t}{2\pi S_r} (1 + 1/\eta)^{\frac{1}{2}} \quad (8.7)$$

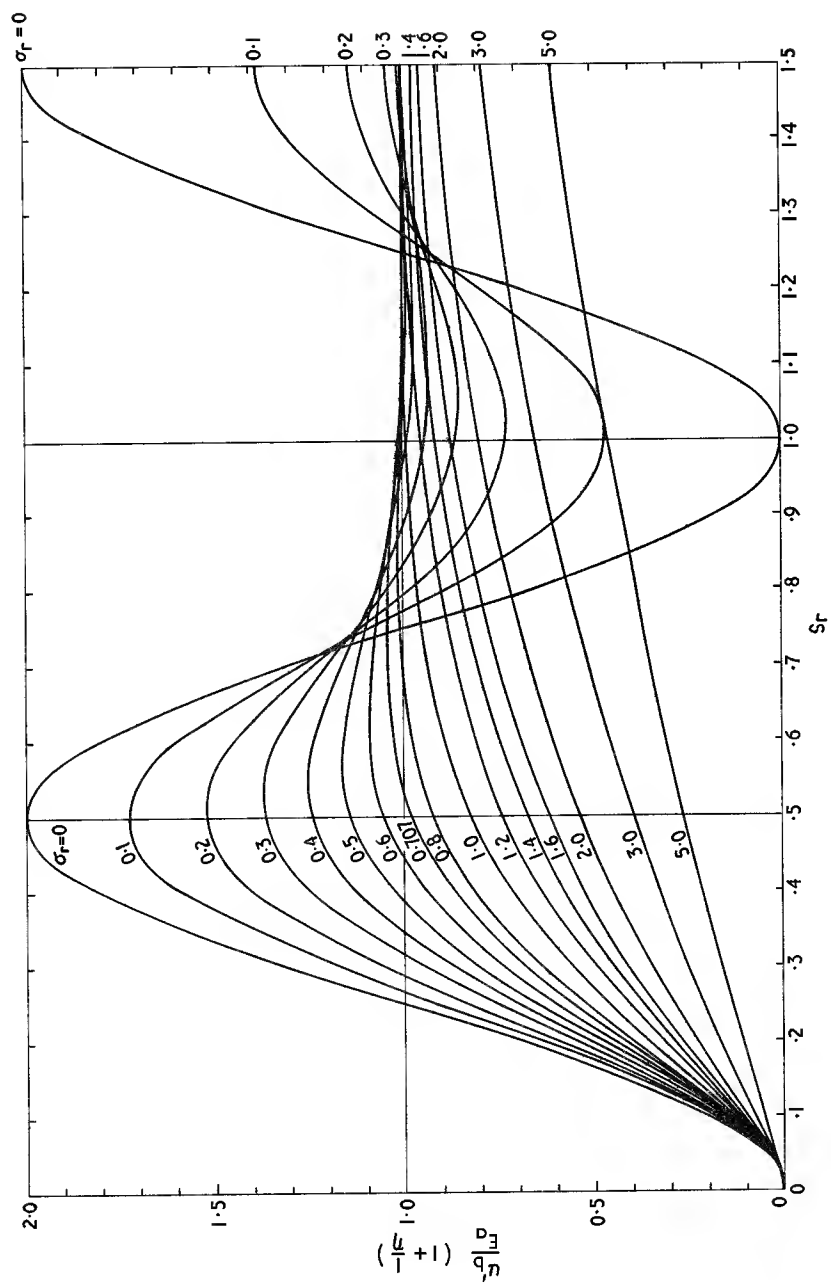


Fig. 8.3. Leading edge response: relative amplitude as a function of the time factor, S_r , with damping factor σ_r , as a parameter

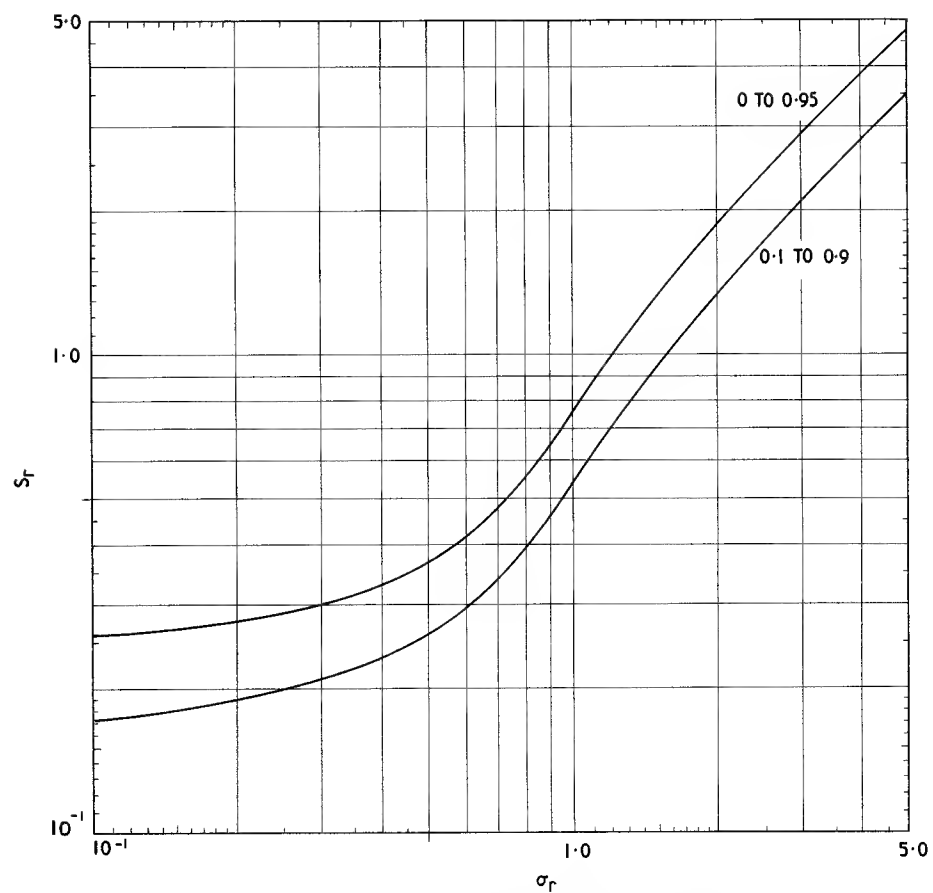


Fig. 8.4. Time factor, S_T , for the load voltage to rise between given fractions of the final amplitude, plotted as a function of σ_T . (After Wilds¹)

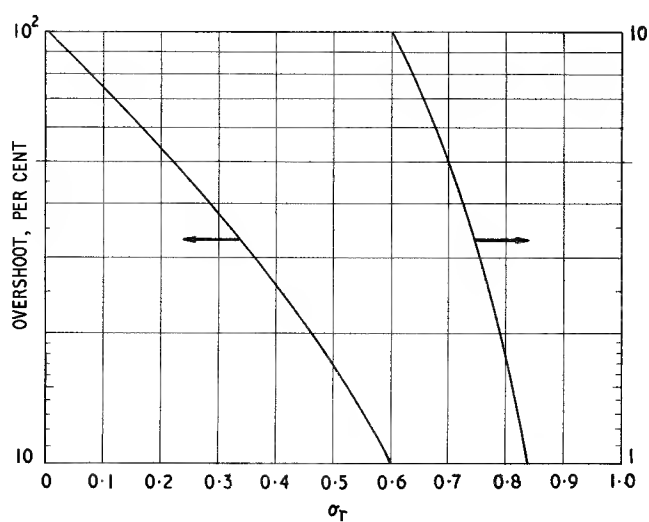


Fig. 8.5. Overshoot as a function of the damping factor, σ_T .

In Fig. 8.1 the rise time is shown as the time required for the output voltage to rise from 0.1 to 0.9 of its full amplitude. Sometimes other fractions are used. Whatever amplitude fractions are used, Fig. 8.3 enables the rise time to be obtained in terms of S_r for any given value of σ_r . Fig. 8.4 gives S_r as a function of σ_r for two specific amplitude fractions often quoted in practice, namely, 0 to 0.95 and 0.1 and 0.9. The transformer specification will require that the rise time, e.g. from 0.1 to 0.9 of full amplitude, shall be less than a certain value. This value may be substituted for t in Eqn 8.7 and S_r may be given the value obtained from Fig. 8.4 for the appropriate value of σ_r . This equation will then give the maximum value of $L_t C$.

The damping factor expression may also be manipulated² to yield information about L_t and C . For the step-up case:

$$\sigma_r = \frac{a}{\sqrt{b}} = \frac{1}{2} \left(\frac{R_a}{L_t} + \frac{1}{C R'_b} \right) \left(\frac{L_t C}{1 + 1/\eta} \right)^{\frac{1}{2}} \quad (8.8)$$

$$= \frac{1}{2} (1 + \eta)^{-\frac{1}{2}} \left[\left(\frac{\eta C R_a^2}{L_t} \right)^{\frac{1}{2}} + \left(\frac{L_t}{\eta C R_a^2} \right)^{\frac{1}{2}} \right]$$

$$\therefore \sigma_r = \frac{1}{2} (1 + \eta)^{-\frac{1}{2}} \left[\frac{1}{\sqrt{x}} + \sqrt{x} \right] \quad (8.9)$$

where $x = \frac{L_t}{R_a R'_b C}$

This quadratic equation applies also to the step-down case when the appropriate value of η is used. If the load-source mismatch factor, η , and the terminating impedances are known then the limit value of σ_r will restrict the choice

of L_t/C according to the above equation. The value of σ_r is usually limited by the overshoot requirements of the specification, e.g. if there must be no overshoot then σ_r must not be less than unity. If a certain amount of overshoot is tolerable, Fig. 8.3 will indicate the minimum value of σ_r . More conveniently Fig. 8.5 shows σ_r as a function of overshoot.

In practice the limit value of σ_r may not yield real roots to Eqn 8.9; for this reason and others to be discussed later the overshoot limit forms only one of the boundary conditions for σ_r .

Eqn 8.9 may be solved for \sqrt{x} :

$$\sqrt{x} = \sigma_r (1 + \eta)^{\frac{1}{2}} \pm (\sigma_r^2 (1 + \eta) - 1)^{\frac{1}{2}} \quad (8.10)$$

For x to be real, $\sigma_r^2 (1 + \eta)$ must be greater than unity, therefore when $\eta = 1$ (i.e. $R_a = R'_b$), $(\sigma_r)_{\min} = 0.707$. Referring to Fig. 8.3 it will be seen that a curve has been drawn for $\sigma_r = 0.707$; the corresponding overshoot is 4.5%. Therefore a transformer that perfectly matches the load to the source cannot have more than 4.5% overshoot whatever values the elements of the equivalent circuit are given. On the other hand, a designer wishing to increase the rise time at the expense of overshoot cannot go far in this direction if the transformer provides impedance matching. However, pulse transformer ratios are often fixed by the required voltage or current ratios without reference to the impedances, so the mismatched condition is more common than with wide band transformers.

Eqn 8.9 is expressed graphically in Fig. 8.6. To provide real roots, and therefore real values of L_t/C , a horizontal line drawn through the actual value of σ_r must touch or cut the curve for the appropriate value of η , i.e. the actual

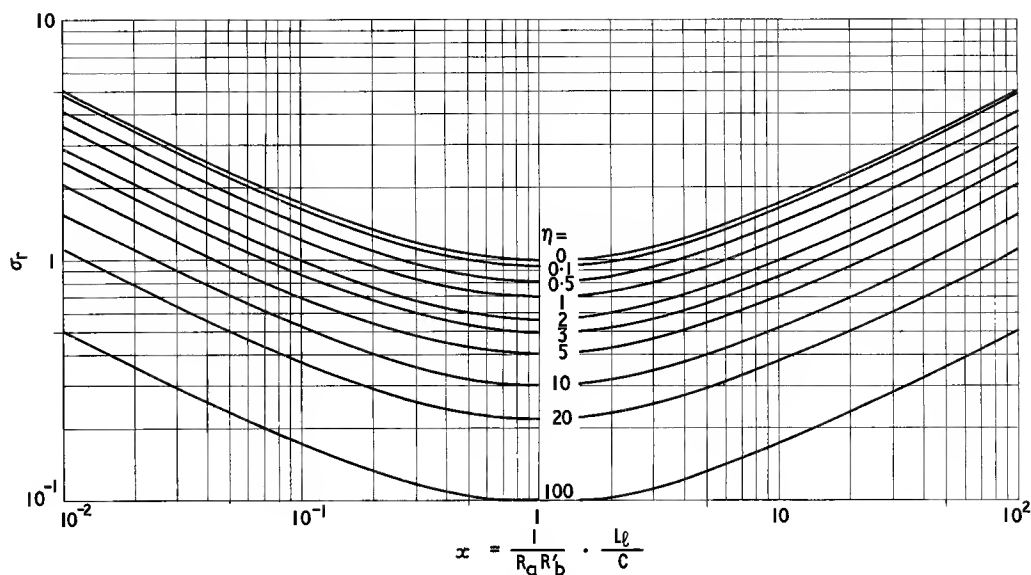


Fig. 8.6. σ_r as a function of $x \left(= \frac{1}{R_a R'_b} \cdot \frac{L_t}{C} \right)$ with the mismatch factor η as a parameter. (Courtesy of W. Postma²)

value of σ_r must be equal to or greater than the value at $x = 1$. If the minimum value of σ_r permitted by the overshoot specification equals the value at $x = 1$ on the curve for the appropriate value of η then, since σ_r may have any larger value, the roots may have any values, i.e. there is no restriction on L_l/C .

If the overshoot specification allows σ_r to be less than the value at $x = 1$ on the curve for the appropriate value of η , this must be disregarded; the minimum value of σ_r is then set by the need for real roots. The situation is then the same as in the previous paragraph, $(\sigma_r)_{\min}$ is the value at $x = 1$ and there is no restriction on L_l/C .

The other possibility is that the overshoot specification may require $(\sigma_r)_{\min}$ to exceed the value at $x = 1$ (on the curve for the appropriate value of η) by a certain amount. Since σ_r may have any value larger than $(\sigma_r)_{\min}$ it follows that in this case there are two possible zones for x (and L_l/C). This may be illustrated on Fig. 8.6 by the example $(\sigma_r)_{\min} = 0.7$, $\eta = 3$; x may be greater than 5.7 or less than 0.177.

Thus the rise time specification places a maximum limit on L_lC while the overshoot specification and/or the solution of Eqn 8.9 may place some restrictions on the value of L_l/C . The actual leakage inductance and shunt capacitance cannot be evaluated until other parts of the pulse have been considered and any further restrictions have been taken into account.

Before leaving the leading edge analysis some mention should be made of the unity-ratio transformer. This is used occasionally as an isolation or a polarity reversing transformer and a solution to the transient equations is considered to be too lengthy to be justified. The difficulty arises because primary and secondary shunt capacitances are commensurate and thus an additional element must be included in the circuit for analysis. The following procedure is similar to that proposed by Fenoglio *et al.*³

- As a first approximation the primary shunt capacitance is ignored and the rise-time and overshoot may be obtained from the solution to the step-up transformer case.
- The rise time of the voltage across the primary capacitance may be simply calculated on the assumption that it alone constitutes the load on the source.
- The total rise time may be obtained by the root of the sum of the squares relationship (see Eqn 8.2). The overshoot may be taken as approximately that obtained in (a).

8.2.2. The top of the pulse

When the pulse has attained its full amplitude and the leading edge transient has died away, the leakage inductance and shunt capacitances have little further

effect; ideally there is a constant current through the leakage inductance and a constant voltage across the capacitance. The equivalent circuit then reduces to the core impedance shunting the load impedance. Usually the core loss may be neglected so the core impedance may be regarded as due only to the open circuit inductance, L_p .

If during the pulse the inductance and the load voltage both were constant, the magnetizing current, i.e. the current in L_p , would rise linearly with time. Assuming a finite source impedance, the magnetizing current would cause a progressive fall of load voltage. This is referred to as droop, see Fig. 8.1. For a practical core, the inductance depends on the magnetizing current so strictly a transient

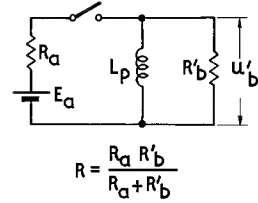


Fig. 8.7. Simplified equivalent circuit used in top of the pulse analysis of a pulse transformer. All the elements shown are referred to the primary side; the ideal transformer has been omitted.
 L_p = inductance of primary winding, H

analysis based on a constant inductance is not entirely valid. However, to avoid complication, it is usual to base the analysis on a constant inductance and when it is necessary to realize the inductance an appropriate value of permeability is taken. This will be discussed at greater length in Section 8.5.

Fig. 8.7 shows the simplified equivalent circuit, the analysis of which will enable the droop to be expressed in terms of the element values. This circuit applies to all transformation ratios. The solution is

$$\frac{u'_b}{E_a} = \frac{\eta}{1+\eta} \exp\left(-\frac{tR}{L_p}\right) \quad (8.11)$$

$$\text{where } R = \frac{R_a R'_b}{R_a + R'_b}$$

This function is plotted in Fig. 8.8. A derived function relating percentage droop to the element values is also useful. If D denotes the percentage droop at the end of a time substantially equal to t_d then

$$\frac{u'_b(1+1/\eta)}{E_a} = 1 - D/100 = \exp\left(-\frac{t_d R}{L_p}\right)$$

$$\therefore \frac{L_p}{t_d R} = -\frac{1}{\log_e(1 - D/100)} \quad (8.12)$$

Fig. 8.9 shows $L_p/t_d R$ as a function of D . From this graph the minimum value of L_p may be obtained for any specified droop and pulse duration.

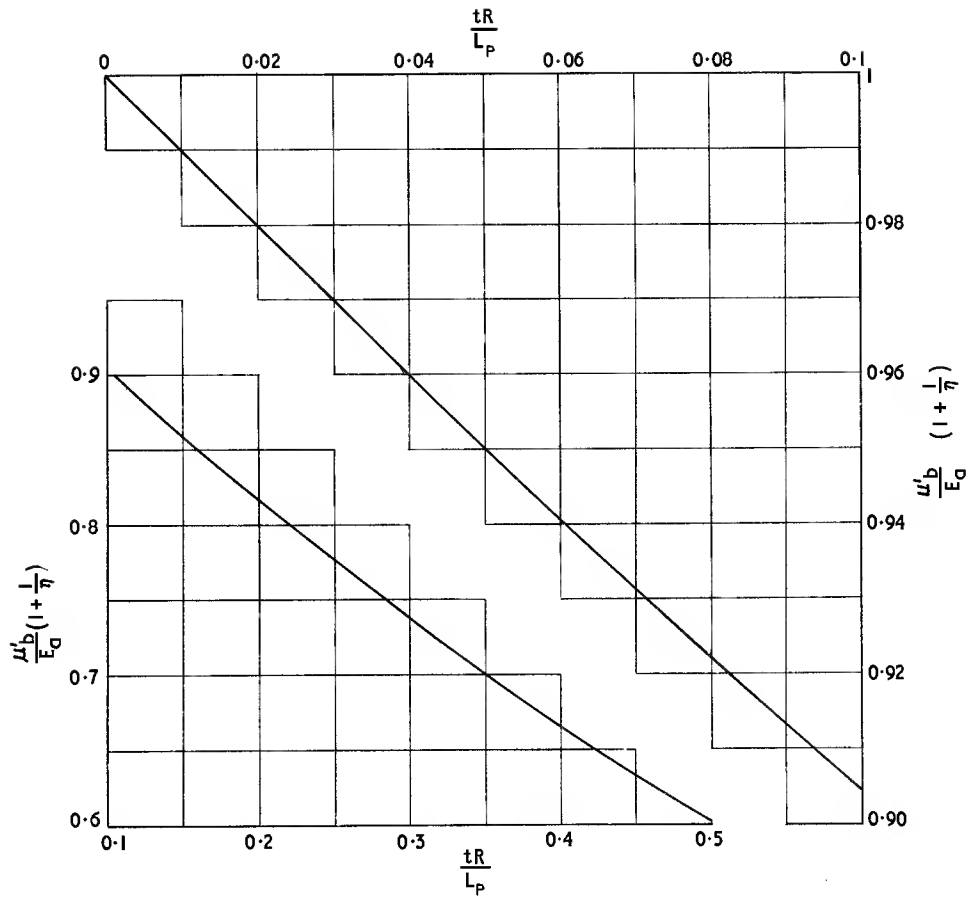


Fig. 8.8. Top of the pulse response; relative amplitude as a function of tR/L_p

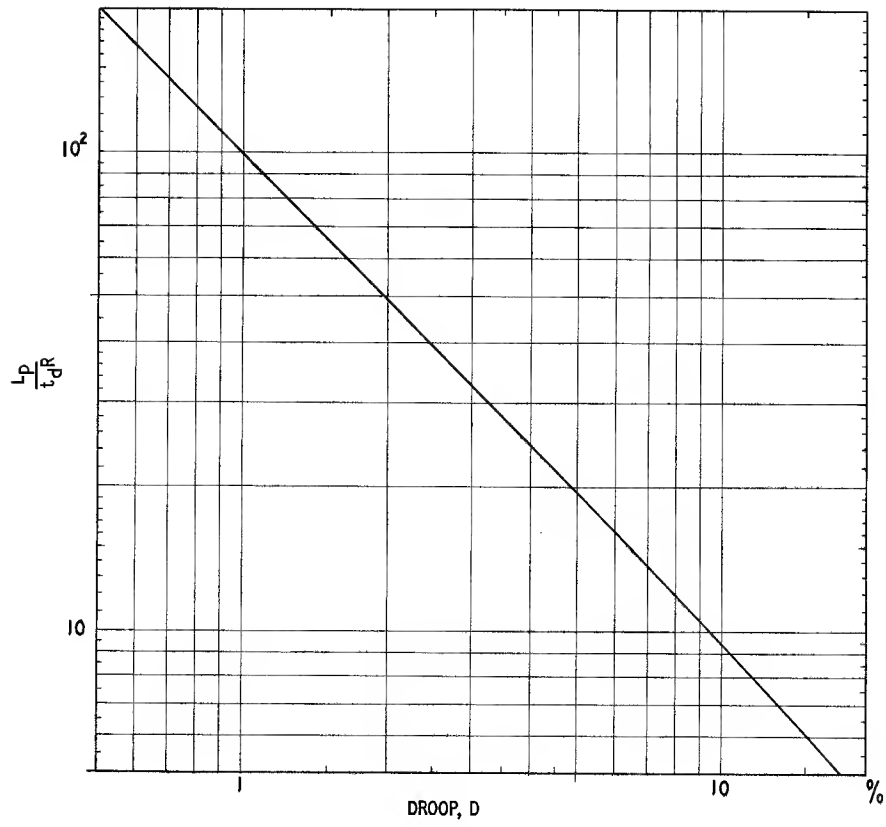


Fig. 8.9. L_p/t_dR as a function of pulse droop

8.2.3. Trailing edge of the pulse

At the end of the pulse the source voltage is removed and the energy stored in the magnetic core and the capacitances is returned to the circuit to give a trailing edge transient. If there are limitations on the shape of the trailing edge transient they may over-ride the leading edge and pulse top requirements in determining the values of the circuit elements. On the other hand it is often found that the shape of the trailing edge is of no consequence and this greatly simplifies the design.

Fig. 8.10 shows the equivalent circuit for analysis. Most references show the source as being open-circuited at the end of the pulse. While this may often be true of

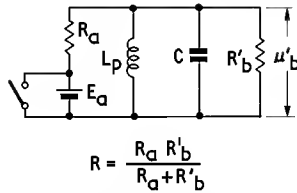


Fig. 8.10. Simplified equivalent circuit used in trailing edge analysis of pulse transformer. All the elements shown are referred to the primary side; the ideal transformer has been omitted. C = total shunt capacitance referred to primary side, in farads

high power transformers there are many cases where low power transformers remain connected to the source impedance after the end of the pulse. Therefore to make the results general the source e.m.f. is shown as short-circuited and R_a may be given the value actually remaining after the end of the pulse. So that the results have the same form as those quoted in the literature let

$$R = \frac{R_a R'_b}{R_a + R'_b} \text{ as before.}$$

The solution again assumes that the element values remain constant with time and the core loss is again neglected (the latter assumption is reasonable provided the external resistances are not disconnected; if they are, the core loss becomes the principal means of dissipating the energy). The transformation ratio has no effect on the solution. The aperiodic trailing edge transient is given by:

$$\frac{U'_b}{U'_b} = \exp(-2\pi S_f \sigma_f) \{ \cosh[2\pi S_f (\sigma_f^2 - 1)^{\frac{1}{2}}] - (1 + 2\chi)(1 - 1/\sigma_f^2)^{-\frac{1}{2}} \sinh[2\pi S_f (\sigma_f^2 - 1)^{\frac{1}{2}}] \} \quad (8.13)$$

where U'_b = voltage across load at end of pulse (referred to primary)

$$\sigma_f = a/\sqrt{b}$$

$$S_f = \frac{t\sqrt{b}}{2\pi}$$

$$\chi = \frac{t_d R}{L_p}$$

$$\text{and } a = \frac{1}{2CR}$$

$$b = \frac{1}{L_p C}$$

When $\sigma_f < 1$ the circuit is oscillatory and the trailing edge transient is given by

$$\frac{U'_b}{U'_b} = \exp(-2\pi S_f \sigma_f) \{ \cos[2\pi S_f (1 - \sigma_f^2)^{\frac{1}{2}}] - (1 + 2\chi)(1/\sigma_f^2 - 1)^{-\frac{1}{2}} \sin[2\pi S_f (1 - \sigma_f^2)^{\frac{1}{2}}] \} \quad (8.14)$$

Note that the response is relative to the load voltage at the end of the pulse. If it is required in terms of the pulse amplitude a correction must be made to allow for the droop. Normally the droop is small and this correction may be neglected.

Again S_f is a time factor

$$S_f = \frac{t\sqrt{b}}{2\pi} = \frac{t}{2\pi} (L_p C)^{-\frac{1}{2}} \quad (8.15)$$

$$\text{thus } L_p C = \left(\frac{t}{2\pi S_f} \right)^2 \quad (8.16)$$

As before σ_f may be regarded as a damping factor:

$$\sigma_f = a/\sqrt{b} = \frac{1}{2R} \left(\frac{L_p}{C} \right)^{\frac{1}{2}} \quad (8.17)$$

$$\therefore \frac{L_p}{C} = (2\sigma_f R)^2 \quad (8.18)$$

Just as, for the leading edge, S_r and σ_r yielded values for the product and quotient of L_i and C , so for the trailing edge S_f and σ_f determine the values of the product and quotient of L_p and C .

The factor χ is the ratio of the magnetizing current in the shunt inductance at the end of the pulse, to the load current.* Thus it may be regarded as an indication of the stored magnetic energy.

Figs. 8.11 to 8.15 show the trailing edge responses calculated from Eqns 8.13 and 8.14 with σ_f and χ as parameters. From these results two additional graphs may be derived. Fig. 8.16 shows the particular value of S_f for the response to fall to zero, denoted $(S_f)_0$, plotted as a function of χ with σ_f as a parameter. Fig. 8.17 shows χ plotted against σ_f with the backswing (percentage of U'_b) as a parameter. These last two graphs contain all the important information required from the actual trailing edge response curves.

*This is only true if $R_a = \infty$, otherwise the denominator is

$$E_a \left/ \frac{R_a R'_b}{R_a + R'_b} \right.$$

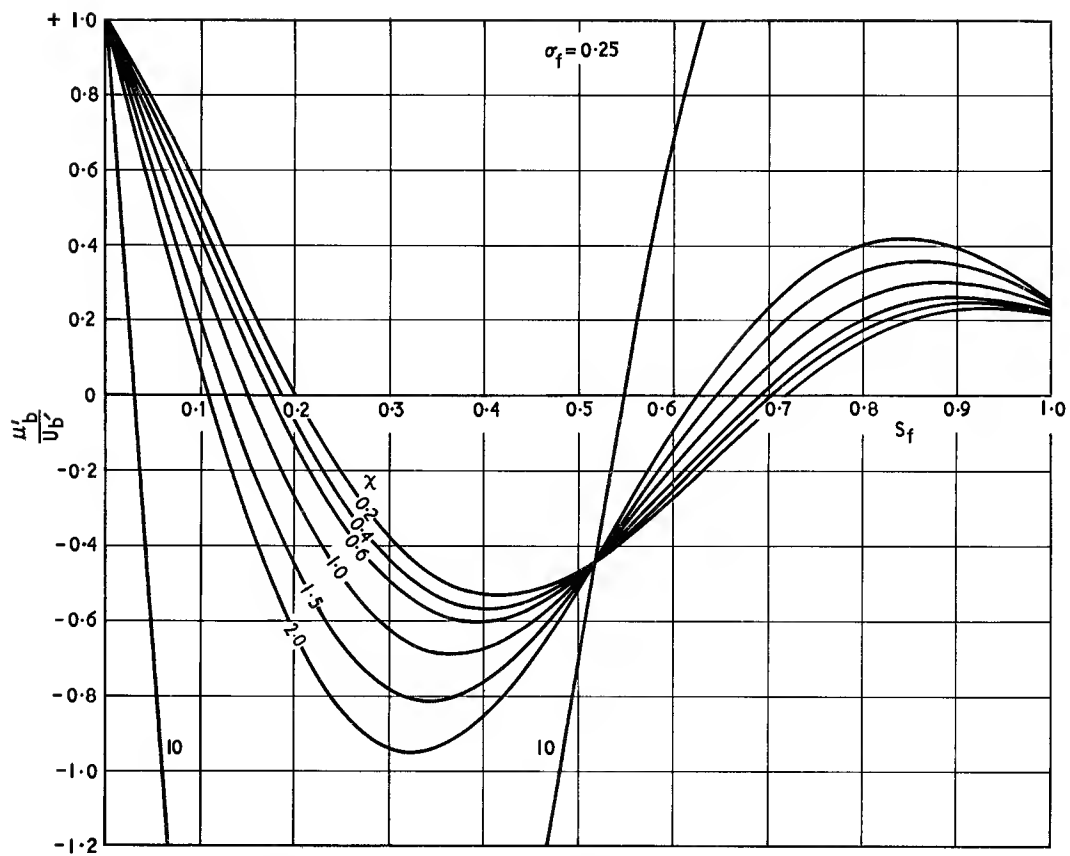


Fig. 8.11. Trailing edge response; relative amplitude as a function of the time factor, S_f , with $\sigma_f = 0.25$ and χ as parameter

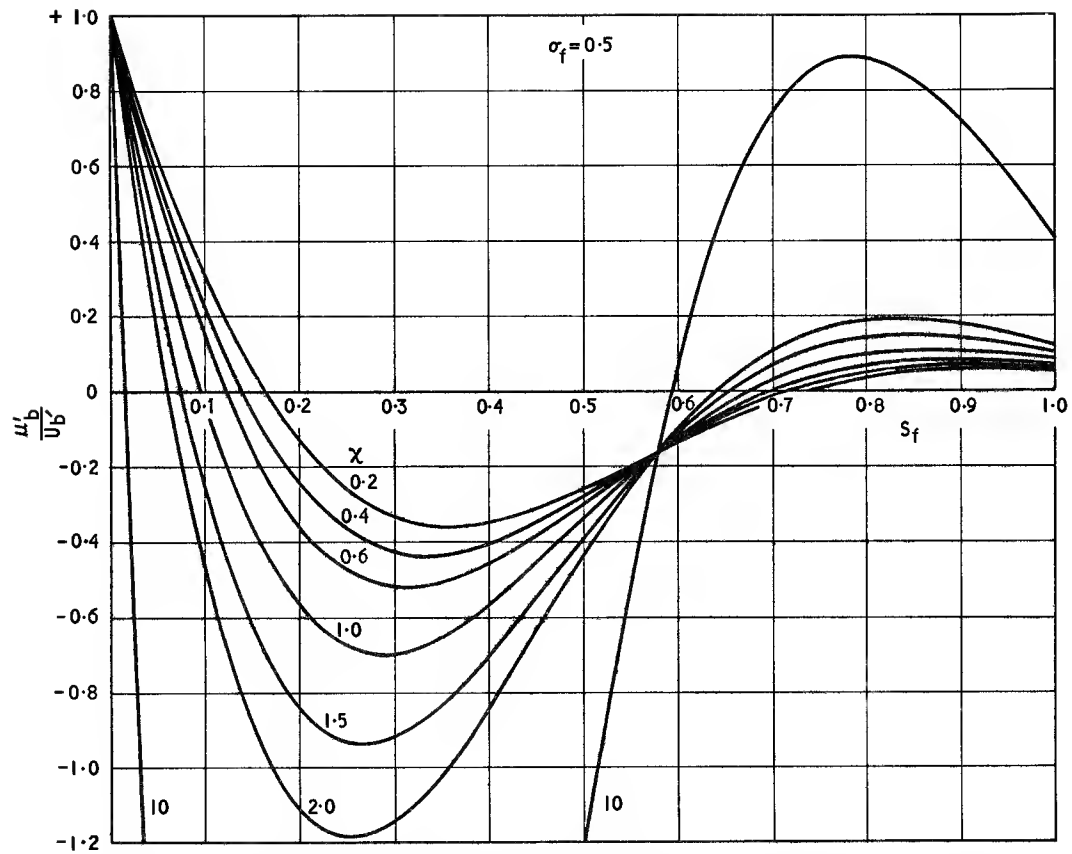


Fig. 8.12. Trailing edge response; relative amplitude as a function of the time factor, S_f , with $\sigma_f = 0.5$ and χ as parameter

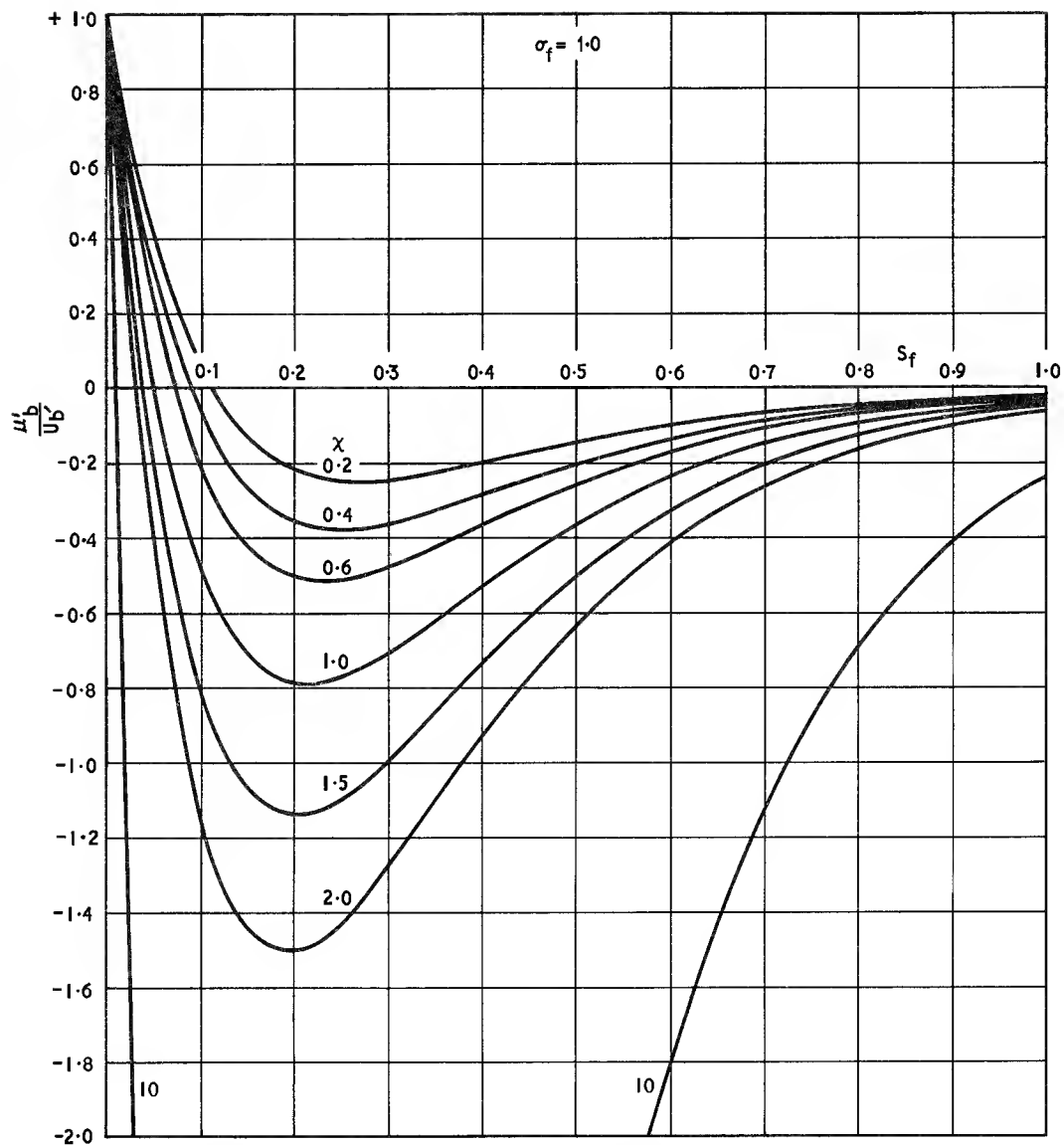


Fig. 8.13. Trailing edge response; relative amplitude as a function of the time factor, S_f , with $\sigma_f = 1.0$ and χ as parameter

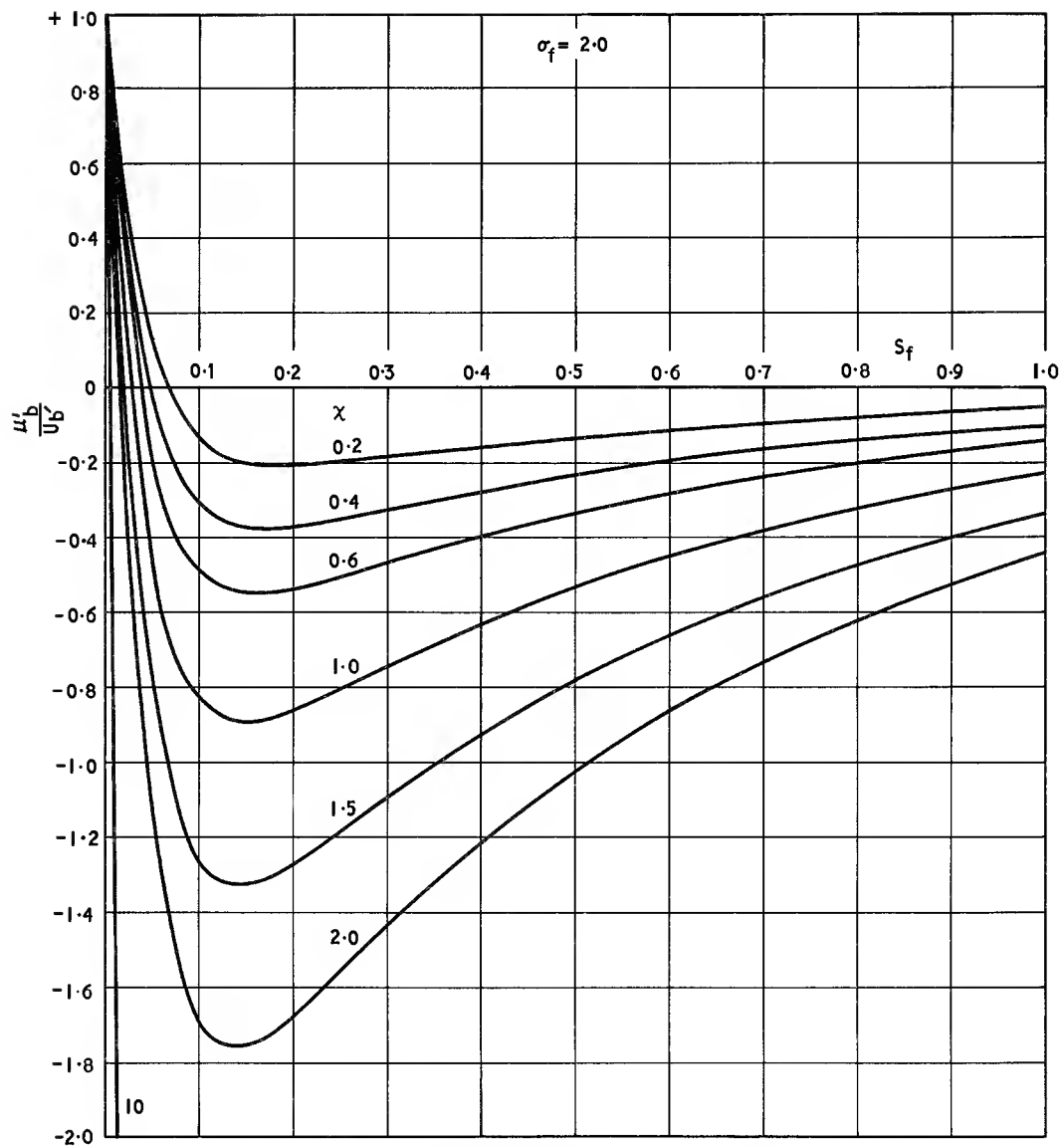


Fig. 8.14. Trailing edge response; relative amplitude as a function of the time factor, S_f , with $\sigma_f = 2.0$ and χ as parameters

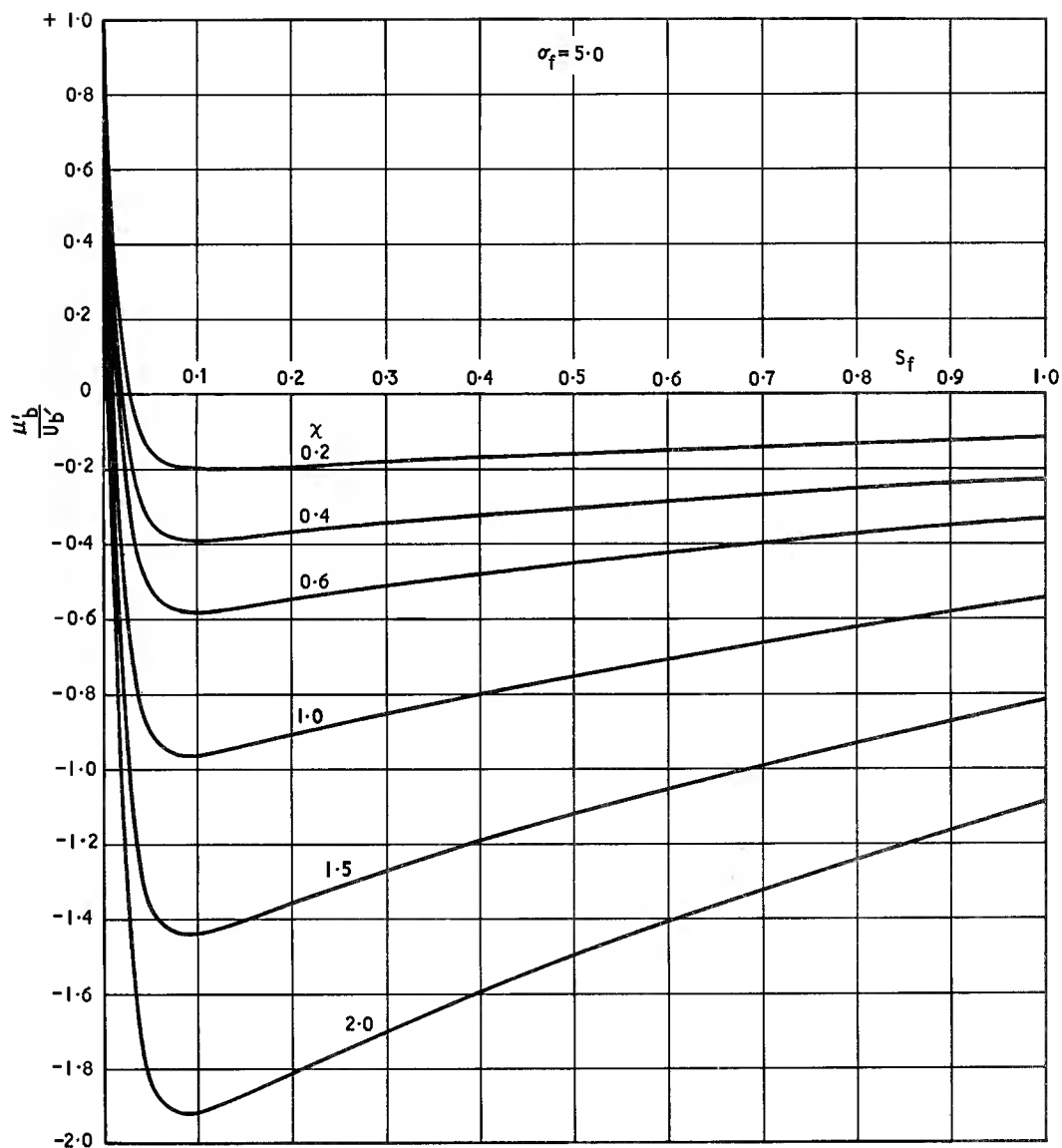


Fig. 8.15. Trailing edge response; relative amplitude as a function of the time factor, S_f , with $\sigma_f = 5.0$ and χ as parameter

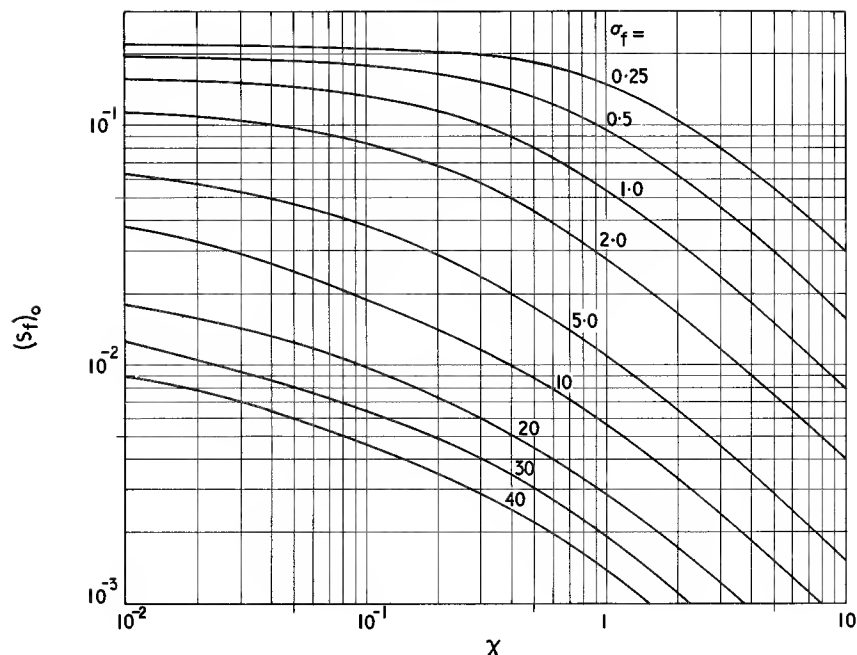


Fig. 8.16. Time factor for amplitude to fall to zero, $(S_f)_0$, as a function of χ with σ_f as a parameter

Referring to the various responses shown in Figs. 8.11 to 8.15 it is interesting to consider the net area under the trailing edge and backswing curves. If either of Eqns 8.13 or 8.14 is integrated over the time period from the closure of the switch (Fig. 8.10) to infinity the result is

$$\int_0^{\infty} \frac{u'_b}{U'_b} dt = -t_d$$

$$\text{thus } \int_0^{\infty} \frac{u'_b}{R'_b} dt = -\frac{U'_b t_d}{R'_b}$$

$$\text{or } \int_0^{\infty} i dt = -It_d$$

where I is the current in the load resistor at the end of the pulse, i.e. immediately before the trailing edge starts, and i is the instantaneous load current thereafter. In words; the net amp.seconds in the load during the backswing exactly balances the amp.seconds in the load during the pulse. The analysis assumes zero droop but the result is generally true; the positive and negative areas of the pulse balance, i.e. the transformer does not transmit a d.c. level. If the shunt inductance is made very large so that the amplitude of the backswing is very small, the time constant becomes very large and the balance is maintained.

If a subsequent pulse follows the first before its trailing edge transient has completely decayed, the second pulse

will cut off a part of the backswing area and disturb the balance. But the second pulse will be displaced (e.g. downwards) by the residual current of the first pulse. Succeeding pulses will be similarly displaced until the area balance is restored. Thus as the mark/space ratio is increased towards unity the zero-current line moves upwards relative to the pulse wave-form and approaches a level approximately midway between the maximum positive and negative excursions, always maintaining equal areas.

8.3. DETERMINATION OF THE ELEMENT VALUES

In the preceding sections the relations between the element values and the pulse distortion have been expressed in graphical form. However, since these relations usually involve more than one circuit element and as each circuit element is the subject of several, often conflicting, requirements, the treatment so far does not lend itself to transformer design other than by the trial and error method of calculation.

If the pulse transformer is fully specified, complete design can be a long process. Wilds¹ has proposed a design procedure which leads without ambiguity to the permitted range of values for each circuit element. This is of great value to the designer who is regularly concerned with the design of pulse transformers having stringent requirements. However, most low power pulse

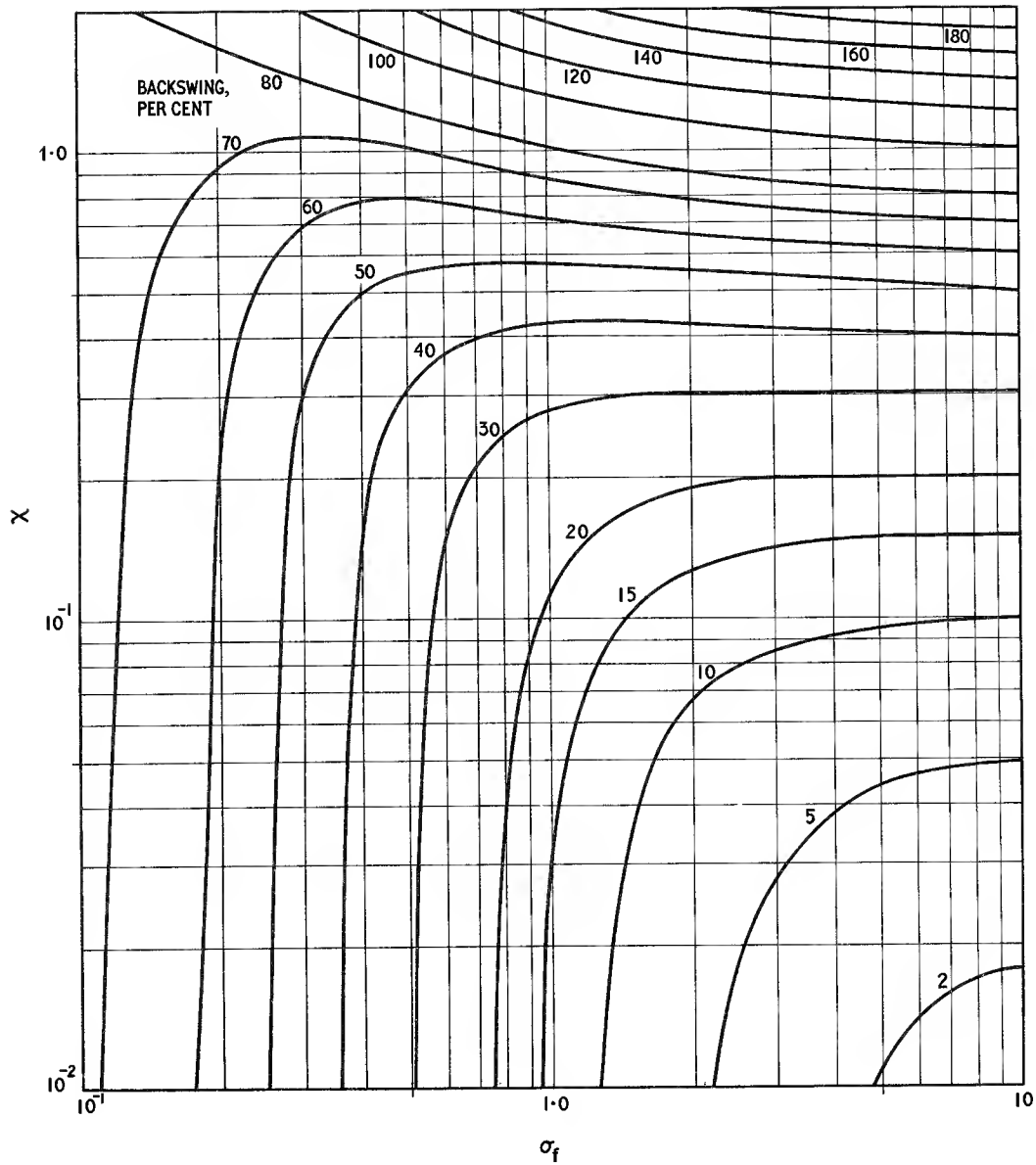


Fig. 8.17. χ as a function of σ_f with backswing (percent of U'_b) as a parameter

transformers are not fully specified and it is useful to have a procedure that may be readily adapted to design requirements. Such a procedure is set out in the following section. It is based on that described by Wilds but is somewhat less comprehensive and more direct. If, as is often the case, the trailing edge is not specified in detail, some or all of the latter part of the procedure may be omitted. After the steps in the procedure have been given in general terms they are illustrated by means of a worked example in Section 8.3.2.

It often happens that a simple pulse transformer is required quickly for a low power circuit. If the specification is confined to the bare necessities, a formal design procedure is not justified. To meet this situation a rapid, rather empirical, method may be adopted. Such a method is described in Section 8.3.3.

8.3.1. A complete design procedure

A pulse transformer specification will list some or all of the following requirements: (the figures in brackets refer to the example to be worked in the next section)

Primary pulse amplitude	(6V)
Pulse duration, t_d	(4 μ s)
Source resistance, R_a	(50 Ω)
Load resistance, R_b	(600 Ω)
Shunt capacitance of the load	(150 pF)
Turns ratio, r	(2)
Maximum rise time, t_r from 10 to 90% amplitude	(0.1 μ s)
Maximum overshoot	(5%)
Maximum droop, D	(5%)
Maximum fall time to zero amplitude, t_f	(1 μ s)
Maximum backswing	(10%)
Whether trailing edge oscillations are permissible	(No)
Type of winding, e.g. isolation, phase reversing, autotransformer, etc.	

First the load-source mismatch factor η must be calculated. For a step-up transformer

$$\eta = \frac{R'_b}{R_a} = \frac{R_b}{R_a r^2}$$

From the overshoot limitation and Fig. 8.5, $(\sigma_r)_{\min}$ is obtained. This is the minimum value of σ_r assuming overshoot is the only restriction (see Section 8.2.1). A horizontal line may now be drawn on Fig. 8.6 at $\sigma_r = (\sigma_r)_{\min}$. If it intersects the curve for the given value of η in two places then x must lie outside the range enclosed by these two intersections. It is usually preferable to choose the lower region because, if the load capacitance is appreciable, it is easier to make L_l/C small than large.

This procedure will be assumed. Therefore $L_l/CR_aR'_b$ may, so far, have any value below that at the lower intersection of $(\sigma_r)_{\min}$ and the appropriate η curve. As previously explained, if the $(\sigma_r)_{\min}$ line does not intersect the appropriate η curve then the value of σ_r at the minimum of that curve must be taken as $(\sigma_r)_{\min}$ and there is no restriction on $L_l/CR_aR'_b$.

The rise time must now be considered. Fig. 8.4 will show, for any value of σ_r the corresponding value of S_r for typical fractions of the leading edge used to specify the rise time. This value may be designated $(S_r)_{\min}$. If for any value of σ_r the factor S_r is greater than $(S_r)_{\min}$, it merely means that more of the leading edge will be traversed in a given time so that the rise time will be shorter than specified. For any value of $(S_r)_{\min}$ Eqn 8.7 will give a maximum value of L_lC .

A simple table may now be constructed e.g. Table 8.1

- | | |
|---------|--|
| Col. 1: | σ_r in progressive steps starting at $(\sigma_r)_{\min}$. Since in the final design σ_r will not differ greatly from $(\sigma_r)_{\min}$, three or four values will usually be sufficient. |
| Col. 2: | Corresponding to the values of σ_r in col. 1, values of $L_l/CR_aR'_b$ from Fig. 8.6. |
| Col. 3: | $(L_l/C)^{\frac{1}{2}}$ from col. 2. |
| Col. 4: | $(S_r)_{\min}$ from σ_r and Fig. 8.4. |
| Col. 5: | $(L_lC)^{\frac{1}{2}}_{\max}$ from $(S_r)_{\min}$ in col. 4 and Eqn 8.7, i.e. $(L_lC)^{\frac{1}{2}}_{\max} = (t_r/2\pi(S_r)_{\min})(1 + 1/\eta)^{\frac{1}{2}}$ |
| Col. 6: | $(C)_{\max} = (L_lC)^{\frac{1}{2}}_{\max} \times (L_l/C)^{-\frac{1}{2}}$ |
| Col. 7: | $(L_l)_{\max} = (L_lC)^{\frac{1}{2}}_{\max} \times (L_l/C)^{\frac{1}{2}}$ |

If there is no trailing edge specification, cols. 6 and 7 give the range of values within which C and L_l may be chosen. For each value of σ_r , C and L_l may not be larger than the corresponding maximum values because this would violate $(L_lC)_{\max}$ and the permitted rise time would be exceeded. They may have smaller values provided L_l/C does not pass outside the range permitted by the $(\sigma_r)_{\min}$ line in Fig. 8.6. If $(\sigma_r)_{\min}$ is greater than the value at $x = 1$ then this means that $(L_l/C)^{\frac{1}{2}}$ must not be greater than the first value in col. 3; if $(\sigma_r)_{\min}$ equals the value at $x = 1$ then there is no restriction on L_l/C provided $(C)_{\max}$ and $(L_l)_{\max}$ are not exceeded.

Again in the absence of a trailing edge specification, the minimum value of the shunt inductance $(L_p)_{\min}$ may easily be obtained from the permitted droop, D , and Fig. 8.9. The transformer design then involves choosing a core and winding configuration to satisfy the limits of shunt inductance, leakage inductance and shunt capacitance (part of which may be external to the transformer). In practice the design should allow margins for manufacturing tolerances.

The additional restrictions on L_p , C and L_p which arise from the specification of the trailing edge response will now be considered. First the least value of the damping factor, i.e. $(\sigma_r)_{\min}$ must be decided. If oscillations are not

permitted then $(\sigma_f)_{\min} = 1$; if a certain amplitude of oscillation is acceptable $(\sigma_f)_{\min}$ may be less than unity and its value may be estimated from Figs. 8.11 and 8.12 by assuming a provisional value of χ . Following a procedure similar to that for the leading edge, a table may now be constructed for a range of values of σ_f e.g. Table 8.2.

- Col. 1: σ_f in progressive steps starting at $(\sigma_f)_{\min}$.
 Col. 2: Corresponding to the values of σ_f in col. 1, values of $(\chi)_{\max}$ from Fig. 8.17 and the specified backswing. It may happen that for the lower values of σ_f there are no corresponding values of $(\chi)_{\max}$; it follows that these values of σ_f are inadmissible.
 Col. 3: $(L_p)_{\min}$ from $(\chi)_{\max} = t_d R / (L_p)_{\min}$. It will be found that $(L_p)_{\min}$ becomes substantially constant as σ_f increases, and a value of $(L_p)_{\min}$ may be taken that is valid over a reasonable range of σ_f values. This value may be compared with the $(L_p)_{\min}$ calculated earlier from the droop specification. A value of L_p may be provisionally chosen such that it is larger, by a reasonable margin, than the value of $(L_p)_{\min}$ obtained from either criterion. The corresponding value of χ may be calculated from $\chi = t_d R / L_p$. This value of χ is provisionally fixed, i.e. it is independent of σ_f and may be used in the next column of the table.
 Col. 4: $(S_f)_o$, i.e. the value of S_f corresponding to the fall time, from Fig. 8.16, σ_f and χ .
 Col. 5: $(L_p C)_{\max} = \{t_f / 2\pi(S_f)_o\}^2$; see Eqn 8.16,
 Col. 6: $(C)_{\max} = (L_p C)_{\max} / L_p$,
 Col. 7: $C = L_p / (2\sigma_f R)^2$; see Eqn 8.18.

The values of $(C)_{\max}$ in col. 6 are the maximum values of C for the specified maximum fall time. They increase in value from the top to the bottom of the column. But because L_p has been fixed there is a value of C corresponding to each value of σ_f ; see Eqn 8.18. These values of C are calculated in col. 7; they decrease in value as σ_f increases. Fig. 8.18 indicates the variation of $(C)_{\max}$ and C with σ_f . If any value of C is chosen from col. 7 then σ_f is fixed and col. 6 gives the maximum permissible value of C to meet the fall time requirement; if both criteria are to be observed then clearly the permissible values of σ_f are those for which $C \leq (C)_{\max}$ and the maximum value of C equals $(C)_{\max}$ at the cross-over point.

The value of $(C)_{\max}$ obtained from the trailing edge requirements may now be compared with the range of values obtained in the table of leading edge parameters and a suitable limit value may be chosen, e.g. if the largest value of $(C)_{\max}$ in the leading edge table is less than $(C)_{\max}$ obtained from the trailing edge table then the former value would be selected as the limit. In practice the actual value chosen would be lower than this by a

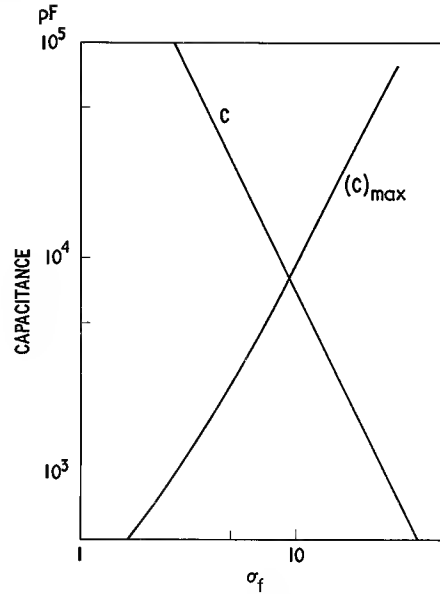


Fig. 8.18. Variation of C and $(C)_{\max}$ with σ_f for worked example

suitable margin to allow for manufacturing tolerances. A check should be made that it is a reasonable value when the shunt capacitance associated with the load is taken into account. The corresponding maximum value of leakage inductance may now be calculated; in most cases $(L_l/C)^{\frac{1}{2}}$ must not exceed the value corresponding to $(\sigma_f)_{\min}$ at the top of col. 3 of the first table (see the discussion following the description of this table).

The element values having been determined, all the response parameters should be checked to ensure that they do not lie outside the limits given in the specification.

8.3.2. An example of design

The foregoing procedure will now be illustrated by a worked example of a step-up pulse transformer, the specification values being the figures in brackets in the list at the beginning of the previous section.

The load-source mismatch factor is

$$\eta = R_b / R_a r^2 = 600 / 50 \times 4 = 3$$

Other useful values are

$$R'_b = 600 / 4 = 150 \Omega$$

$$R = R_a R'_b / (R_a + R'_b) = 37.5 \Omega$$

$$R_a R'_b = 7500$$

Referring to Fig. 8.5, a 5% overshoot will not be exceeded if $(\sigma_f)_{\min} = 0.7$. A line drawn at this value on Fig. 8.6 intersects the $\eta = 3$ curve at $x = 0.177$ and 5.7 . Assuming that it is preferable to use the lower region then x must be less than 0.177 .

Table 8.1. CALCULATION OF LEADING EDGE PARAMETERS

1	2	3	4	5	6	7
σ_r	$x =$ L_l/CR_aR_b (from Fig. 8.6)	$(L_l/C)^{\frac{1}{2}}$ (col. 2)	$(S_r)_{\min}$ (from Fig. 8.4)	$(L_lC)^{\frac{1}{2}}_{\max}$ $=$ $\left(\frac{t_r}{2\pi(S_r)_{\min}}\right)(1+1/\eta)^{\frac{1}{2}}$	$(C)_{\max}$ $=$ $(L_lC)^{\frac{1}{2}} \times (L_l/C)^{-\frac{1}{2}}$	$(L_l)_{\max}$ $=$ $(L_lC)^{\frac{1}{2}} \times (L_l/C)^{\frac{1}{2}}$
0.7	0.177	36.4	0.34	5.4×10^{-8}	1480pF	1.97μH
1	0.072	23.2	0.54	3.4×10^{-8}	1470	0.79
1.5	0.0296	14.9	0.94	1.96×10^{-8}	1320	0.29
2.0	0.0161	11.0	1.32	1.39×10^{-8}	1260	0.15

The first table may now be constructed as described in the previous section.

For each value of σ_r , the values of C and L_l may not be larger than those given in columns 6 and 7 respectively because this would violate $(L_lC)^{\frac{1}{2}}_{\max}$ and lead to an excessive rise time. They may have smaller values provided $(L_l/C)^{\frac{1}{2}}$ is not greater than 36.4; if this value is exceeded then σ_r will be less than 0.7 and the overshoot limitation will be exceeded. Thus 740 pF and 1.97 μH are not permissible but 740 pF and 0.98 μH would be acceptable.

If, on the other hand, L_l is made disproportionately small so that $(L_l/C)^{\frac{1}{2}}$ is much smaller than the value corresponding to the minimum value of σ_r , the damping factor will be larger than necessary. Provided the value of C does not exceed the limit, the resulting rise time will not be greater than the specified value. However, because the damping factor σ_r is greater than the minimum value, the rise time will be greater than it need be (see the effect of σ_r in Fig. 8.3). If C can be reduced so that $(L_l/C)^{\frac{1}{2}}$ approaches the value corresponding to $(\sigma_r)_{\min}$ the rise time will be decreased, and the leading edge response

will be optimized well within the specification. However, in practice it is often quite difficult to meet the $(L_l)_{\min}$ limit and the question of the disproportionately low value of L_l does not arise.

Returning to the example, the top of the pulse must now be considered. The permitted droop is 5%. From Fig. 8.9, $L_p/t_dR = 19.5$.

$$(L_p)_{\min} = 19.5 \times 4 \times 10^{-6} \times 37.5 = 2.93 \text{ mH}$$

The backswing limitation may modify this value.

The second table may now be constructed. The requirement that the trailing edge must not be oscillatory limits σ_t to values equal to or greater than one. The maximum fall time is 1 μs and the maximum backswing is 10%.

An inspection of the tables shows that the maximum value of the shunt capacitance is determined by leading edge requirements; the crossover capacitance in the second table is outside the range permitted by the first table. A value of 1480 pF would be possible but it would be better to choose a lower value, e.g. 1000 pF to allow some margin for manufacturing tolerances. It must not be made too low because (1) when referred to the second-

Table 8.2. CALCULATION OF THE TRAILING EDGE PARAMETERS

1	2	3	4	5	6	7
σ_t	$(\chi)_{\max}$ (from Fig. 8.17 and backswing)	$(L_p)_{\min}$ $=$ $t_dR/(\chi)_{\max}$	$(S_t)_o$ (from σ_t and χ in Fig. 8.16)	$(L_pC)_{\max}$ $=$ $\left(\frac{t_f}{2\pi(S_t)_o}\right)^2$	C_{\max} $=$ $\frac{(L_pC)_{\max}}{L_p}$	C $=$ $\frac{L_p}{(2\sigma_tR)^2}$
1	—	mH Provisionally choose	0.15	1.13×10^{-12}	280pF	710 000pF
2	0.067	2.14 $L_p = 4 \text{ mH}$	0.1	2.53×10^{-12}	630	180 000
5	0.095	1.5 $\therefore \chi =$	0.05	10×10^{-12}	2 500	29 000
10	0.1	1.5 $\frac{4 \times 10^{-6} \times 37.5}{4 \times 10^{-3}}$	0.027	35×10^{-12}	8 800	7 100
20	0.1	1.5	0.013	150×10^{-12}	38 000	1 800
30	0.1	1.5 $= 0.0375$	0.009	310×10^{-12}	78 000	790

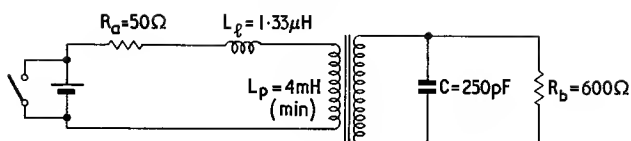


Fig. 8.19. Element values for worked examples

ary it must not approach too closely the load capacitance and (2) the maximum leakage inductance must be reduced in proportion to satisfy the $(\sigma_r)_{\min}$ requirements (i.e. the overshoot) and even with $L_l = 1.97 \mu\text{H}$ the ratio L_p/L_l is rather large. In practice it will normally be necessary to add external capacitance to achieve the design value and so avoid excessive overshoot. In the present example the total secondary shunt capacitance must be $1000/4 = 250 \text{ pF}$ of which 150 pF exists across the specified load. Taking $C = 1000 \text{ pF}$, the maximum value of the leakage inductance is $L_l = 1.97 \times 1000/1480 = 1.33 \mu\text{H}$. It may be less than this without invalidating the design.

Fig. 8.19 shows the element values in the equivalent circuit and Table 8.3 shows the calculated values of all the main parameters based on these element values.

Table 8.3.

Parameter	Remarks	Calculated value	Spec. value
x	$= L_l/CR_aR_b$	0.177	
σ_r	from Fig. 8.6	0.7	
Overshoot	corresponding to σ_r	5%	5% max
$S_r(10-90\%)$	from Fig. 8.4	0.34	
Rise time (10-90%)	from Eq. 8.6	0.067 μs	<0.1 μs
L_p/t_dR		26.7	
Droop	from Fig. 8.9	3.7%	<5%
σ_r	from Eq. 8.17	26.7	>1 for no oscillation
χ	$= t_dR/L_p$	0.0375	
$(S_t)_0$	from Fig. 8.16	0.01	
Fall time to zero	from Eq. 8.15	0.13 μs	<1 μs
Backswing	from Fig. 8.17	3.7%	<10%

The practical realization of a low power pulse transformer having the required transformation ratio and the calculated element values is almost identical to the realization of a wide band transformer. This has been discussed in detail in Section 7.3. Basically it consists of choosing a core and a winding configuration that will give the required shunt and leakage inductance with an acceptable value of self capacitance. For most purposes the number of turns may be calculated from the initial

effective permeability, from α or from A_L . If the flux density in the core is not negligible the pulse magnetization may lower the permeability so that the initial permeability is no longer the appropriate parameter. This aspect is considered in Section 8.5.

8.3.3. A rapid design procedure

It often happens that a small pulse transformer having a simple specification is required quickly for experimental purposes. The following method, which is partly experimental, will often provide a satisfactory transformer.

- From the required pulse duration, permissible droop and circuit impedance, R , obtain $(L_p)_{\min}$ from Fig. 8.9.
- Select a suitable core, and using the published value of α or A_L (see Table 7.1) determine the number of primary turns.
- Calculate the number of turns on the other winding(s) from the required turns ratio(s) and wind the transformer using a reasonably low leakage inductance configuration, e.g. single layer windings (see Fig. 11.18).
- Measure the pulse distortion of the transformer in the circuit. If the leading edge transient is oscillatory this is due to the load not being matched to the source. It may or may not be possible to improve the matching. If the overshoot is excessive, shunt capacitance may be added; this will reduce the overshoot but increase the rise time. If it is not possible to meet the leading edge and pulse top requirements by this simple approach then some or all of the full design of Section 8.3.1 procedure must be followed.

8.4. PULSE DISTORTION IN RELATION TO BANDWIDTH

Any transformer connected between a source and load may be represented by the elements of the equivalent circuit. From these elements it is possible to calculate the bandwidth for the transmission of sinusoidal currents and, separately, the distortion which occurs when a given pulse is transmitted. Clearly these two aspects of the performance of the transformer are related, indeed some designers attempt to translate a pulse distortion speci-

fication into an approximately equivalent bandwidth in order to visualize the requirement more easily.

Wilds⁴ has analysed the relation between the two aspects of performance to discover how feasible it is to predict the pulse distortion from the transmission bandwidth. He shows that it is possible if only the leading edge and the pulse top are of interest. To predict the leading edge response it is necessary to know not only the attenuation/frequency relation at the upper end of the transmission band but also the corresponding phase-shift/frequency response. Since for a given transformer the latter is usually not known, he points out that there is little to be gained from the analogy; it would be better to measure the principal elements of the equivalent circuit of a given transformer and then use these values directly to predict the pulse distortion using functions such as those given earlier in this chapter.

However, the droop of the pulse top is very simply related to the attenuation at the lower end of the transmission band and, as it may be useful in certain circumstances, this relation is now derived.

From Eqn 7.14 or Fig. 7.6, the attenuation due to the shunt inductance, L_p , is 3 dB at $\omega = \omega_1$ when

$$\frac{\omega_1 L_p}{R} = 1$$

Let $L_p = \mu_i L_o$ where L_o is defined in Eqn 2.14 and μ_i is the initial permeability, assuming low amplitude signals.

$$\therefore \mu_i L_o = \frac{R}{\omega_1} \quad \text{H} \quad (8.19)$$

From Eqn 8.12 the pulse top droop is related to L_p by the following expression

$$\left. \begin{aligned} L_p &= -\frac{t_d R}{\log_e(1 - D/100)} \quad \text{H} \\ &= \mu_p L_o \end{aligned} \right\} \quad (8.20)$$

where μ_p is the pulse permeability, i.e. that value of permeability which characterizes the behaviour of the material under pulse conditions, (see Section 8.5). Combining these equations, the pulse droop of a given transformer may be expressed in terms of the frequency at which the insertion loss due to the shunt inductance reaches 3 dB:

$$\begin{aligned} \frac{\mu_p}{\mu_i} &= -\frac{\omega t_d}{\log_e(1 - D/100)} \\ \text{or } f_1 t_d &= -\frac{\mu_p}{\mu_i} \cdot \frac{\log_e(1 - D/100)}{2\pi} \end{aligned} \quad (8.21)$$

Similar expressions may be written for other values of insertion loss due to L_p , e.g. 0.1, 0.5 and 1 dB at f_1 . The results may be shown graphically as in Fig. 8.20. It is interesting to note that a 5% droop on a 4 μ s pulse corresponds to a 3 dB insertion loss at 2 kHz, assuming that $\mu_p/\mu_i = 1$. This example shows that the energy spectrum of a typical pulse extends down to a surprisingly low frequency. It also shows that even this

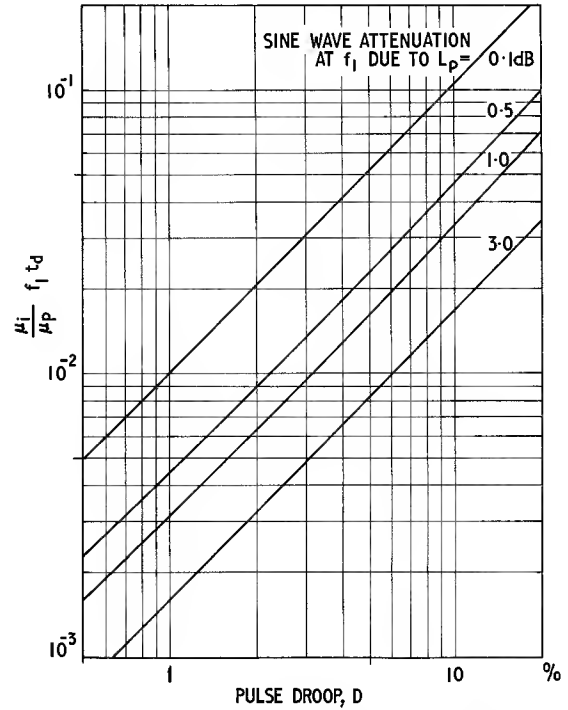


Fig. 8.20. Pulse droop in time t_d related to the frequency f_1 at which the low frequency sine wave attenuation of the transformer, due to L_p , has a given value

limited correspondence between pulse and wide band performance is only possible if the ratio μ_p/μ_i is known. The pulse permeability is considered in the next section.

8.5. PULSE PERMEABILITY

As for wide band transformers, the core of a pulse transformer must provide sufficient shunt inductance with a reasonable number of turns on the winding. Ignoring the effect of any residual air gap, the inductance at low amplitude alternating currents is given by

$$L_p = \frac{\mu_o \mu_i N^2 A_c}{l_e} \quad \text{H} \quad (8.22)$$

$$(8.22) \quad L_p = 4\pi \mu_i N^2 A_c 10^{-9} / l_e \quad \text{H}$$

The problem is to find a substitute for the initial permeability, μ_i , which will give the appropriate value of L_p under pulse conditions. If the flux density, B , were directly proportional to the field strength, H , over the excursions considered then the permeability and inductance would be constant. If a constant direct voltage U were applied to such an inductance then by definition

$$U = L_p \frac{di}{dt} \quad \text{V} \quad (8.23)$$

From Eqn 2.11,

$$U = -e = NA \frac{dB}{dt} \quad \text{V} \quad (8.24)$$

The current and flux density would rise linearly with time. When the current reaches a value I the energy stored in the core is

$$\frac{1}{2} L_p I^2 = V \int_0^{AB} H dB \quad \text{J} \quad (8.25)$$

where ΔB is the change in flux density corresponding to I , and V is the core volume. This assumes a uniform distribution of flux density; if this is not so the R.H.S. must also be integrated with respect to volume.

In a practical transformer there is in general a non-linear relation between B and H , and the inductance L_p is a function of the instantaneous amplitude. From Eqns 8.23 and 8.24, by integration,

$$\int_0^{t_d} U dt = \int_0^I L_p di = NA \int_0^{AB} dB \quad (8.26)$$

It may usually be assumed that during the interval t_d (the pulse duration) the variation of U is negligible (i.e. the droop is small) so this integration may be written

$$U t_d = L_p \Delta I = NA \Delta B \quad \text{V.s (Wb)} \quad (8.27)$$

where L_p is now an effective value, defined by this Eqn.

$$\text{Now } \Delta I = \frac{\Delta H l}{N} \quad \text{A} \quad (8.28)$$

Therefore the effective value of L_p is given by

$$L_p = \frac{N^2 A}{l} \cdot \frac{\Delta B}{\Delta H} = \frac{N^2 A}{l} \cdot \mu_o \mu_p \quad \text{H} \quad (8.29)$$

This value of inductance may be used in the equivalent circuit of the pulse transformer; it will give the same value of magnetizing current and magnetic energy at the end of the pulse as the actual, varying, inductance. In the above equation the pulse permeability is introduced and it is defined by

$$\mu_p = \frac{\Delta B}{\mu_o \Delta H} \quad (8.30)$$

which is formally the same as the definition of amplitude permeability in the a.c. case. Therefore in calculations of inductance and number of turns for pulse transformers the normal expressions may be used, e.g. Eqn 8.22, but μ_p is substituted for μ_i .

Before discussing the nature of $\Delta B/\Delta H$ for pulsed magnetic cores it is necessary to be able to evaluate the magnitude of the change of flux density. From Eqn 8.27

$$\Delta B = \frac{U t_d}{NA} \quad \text{T} \quad (8.31)$$

where, for small droops, U may be taken as the average voltage across the winding during the pulse. If the cross-sectional area A is not uniform then ΔB will depend on the cross-section taken. In practice, provided the non-uniformity is not large, a mean value of A may be used or, if known, the effective value A_e .

In the majority of small pulse transformers used in electronic equipment, e.g. data handling transformers, the value of ΔB is less than 10 mT (100 Gs). At these low flux densities the core material is operated substantially at the origin of the B - H loop and, for a ferrite, the pulse permeability as defined by Eqn 8.30 may be taken as equal to the initial permeability without significant error. In illustration, the example transformer design considered earlier in this chapter may be used. The relevant parameters are: pulse duration, $t_d = 4 \mu\text{s}$, the primary inductance, $L_p = 4 \text{ mH}$ and the primary pulse amplitude

$$(8.24) \quad U = NA \frac{dB}{dt} \times 10^{-8} \quad \text{V}$$

$$(8.25) \quad \frac{1}{2} L_p I^2 = \frac{V}{4\pi} \int_0^{AB} H dB \times 10^{-7} \quad \text{J}$$

$$(8.26) \quad \int_0^{t_d} U dt = \int_0^I L_p di = NA \int_0^{AB} dB \times 10^{-8} \quad \text{V.s}$$

$$(8.27) \quad U t_d = L_p \Delta I = NA \Delta B \times 10^{-8} \quad \text{V.s}$$

$$(8.29) \quad L_p = \frac{4\pi N^2 A}{l} \frac{\Delta B}{\Delta H} \times 10^{-9} = 4\pi N^2 \frac{A}{l} \times \mu_p \times 10^{-9} \quad \text{H}$$

$$(8.30) \quad \mu_p = \frac{\Delta B}{\Delta H}$$

$$(8.31) \quad \Delta B = \frac{U t_d}{NA} \times 10^8 \quad \text{Gs}$$

= 6V. A suitable core for such a transformer might be the 14 mm pot core listed in Table 7.1. Referring to that table:

$$N = \alpha \sqrt{L_{mH}} = 24.3 \times 2 = 48.6 \\ \approx 50 \text{ turns}$$

$$A_e = 25.9 \text{ mm}^2$$

\therefore from Eqn 8.31

$$\Delta B = \frac{6 \times 4 \times 10^{-6}}{50 \times 25.9 \times 10^{-6}} \approx 1.9 \text{ mT} \quad (19 \text{ Gs})$$

This flux density is attained after $4 \mu\text{s}$, i.e. $dB/dt = 0.48 \text{ mT}/\mu\text{s}$. This is equivalent to the maximum rate of change of flux density in a sine wave of frequency 200 kHz and $\hat{B} = 0.36 \text{ mT}$ (3.6 Gs). So it is seen that in such a transformer the pulse magnetization is not very great or rapid; eddy current and permeability dispersion effects may usually be ignored and initial permeability may be used in the design.

It is appropriate now to consider pulses of larger energies. If the flux density excursion becomes appreciable then the core material magnetization will no longer be confined to a region near the origin of the B - H loop. It becomes very difficult to predict, in general terms, over which minor B - H loop the core will operate. Until this loop has been established the pulse permeability ($= \Delta B/\Delta H$) cannot be determined. The pulse permeability may determine the number of turns on the primary winding and this in turn affects the flux density excursion (see Eqn 8.31). Thus there is a closed loop of relations which can only be made to yield the best design conditions by a process of preparing a table of parameters such as N_1 , ΔB , μ_p and L_p and interpolating for the most suitable design.

Melville⁵ has described in detail various modes of magnetization in ferromagnetic cores; only a brief and simplified account of his description will be given here. In the present context it is first assumed that effects depending on the rate of change of flux and on the velocity of propagation within the ferrite may be ignored, i.e. the magnetization is similar to that occurring during the determination of B - H loops with direct current. This assumption is probably valid for most ferrite pulse transformers; the limitations will be discussed later.

Fig. 8.21 shows the B - H curve traced in a ferrite core, initially demagnetized, when a succession of unidirectional pulses are applied. The interval between pulses is sufficient to ensure that the flux changes due to one pulse have finished before the next pulse arrives. Each pulse is of such an amplitude and duration that the change of flux is ΔB (see Eqn 8.31). During each pulse the flux density increases by ΔB and when the pulse has ceased it returns to a residual value on the B -axis. A series of unclosed minor loops will be described until the curvature of the

B - H loop permits a fall of flux density equal to ΔB and a closed minor loop is achieved.

If for a given ferrite there is available a series of B - H loops of successively increasing size such as shown diagrammatically in Fig. 8.22, the minor loop corresponding to a given ΔB may readily be determined. A loop is found in which the flux density change from the tip to the remanent value is ΔB ; this section of the curve coincides with the upper arm of the minor loop, and the slope of the line joining the tip to the remanent value gives the pulse permeability.

For a given material, the maximum available flux density excursion is limited by the shape and size of the B - H loop and this limits the energy that may be transmitted by a given size of transformer core made from this material. However there are two ways in which the flux density excursion may be increased beyond the value obtainable in the simple case just considered. The first is to introduce an air gap so that the loop is sheared as described in Section 4.2.2. This reduces the residual flux density for a given peak flux density and so increases ΔB as shown in Fig. 8.23. The pulse permeability will generally be reduced to the corresponding effective value, so this method is only applicable where a design is limited by ΔB rather than pulse permeability (or droop, or back-swing).

The other method is to introduce some reverse magnetic field so that between pulses the material is returned to a point on the curve to the left of the B -axis. This may be done by applying a negative reset pulse between the main pulses or by providing a d.c. or permanent magnet bias to the core.⁶ A reset pulse will set the core to a point on the B -axis below the normal residual flux density, indeed a negative value is quite feasible. A steady field or current bias will result in the flux density returning to the value where the minor loop cuts the bias line (b - b' in Fig. 8.22). A substantial increase in ΔB may be achieved in this way.

Sets of B - H loops for ferrites suitable for pulse transformers are shown in Fig. 3.2. Using these loops and the above method, the operating minor loop may be determined and the pulse permeability may be scaled off see Fig. 3.2.6. This procedure will give sufficiently accurate results for most ferrite pulse transformers.

Eddy currents, which have such a pronounced effect in laminated alloy cores, cause relatively little disturbance of the magnetization loop in ferrites. Instead the velocity of propagation within the ferrite must be considered. It was shown in Section 2.2.4 that the velocity of propagation of the magnetization in a manganese zinc ferrite is about $3 \times 10^4 \text{ m.s.}^{-1}$. If it is assumed that the surface change of flux density must reach the centre of the core by the shortest route in a time that is less than a tenth of the pulse duration, t_d , then it may readily be shown that the least cross-sectional dimension of the core, b , must be less than about $6t_d$ where b is in mm and t_d is in μs .

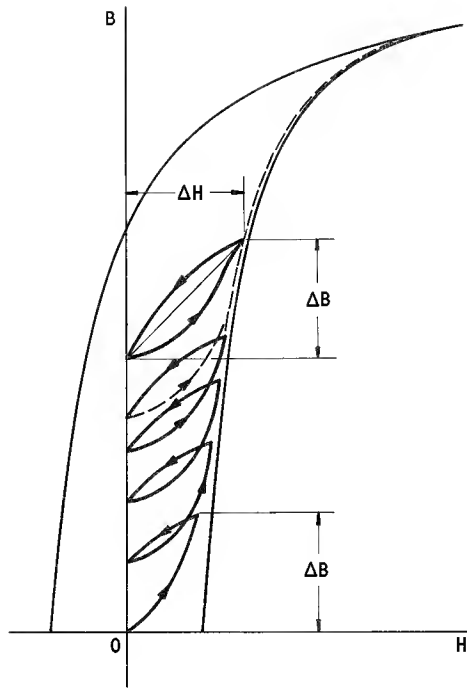


Fig. 8.21. The B-H curves of an initially demagnetized ferrite core, when a succession of unidirectional voltage pulses are applied to a magnetizing winding. (Courtesy Melville⁵)

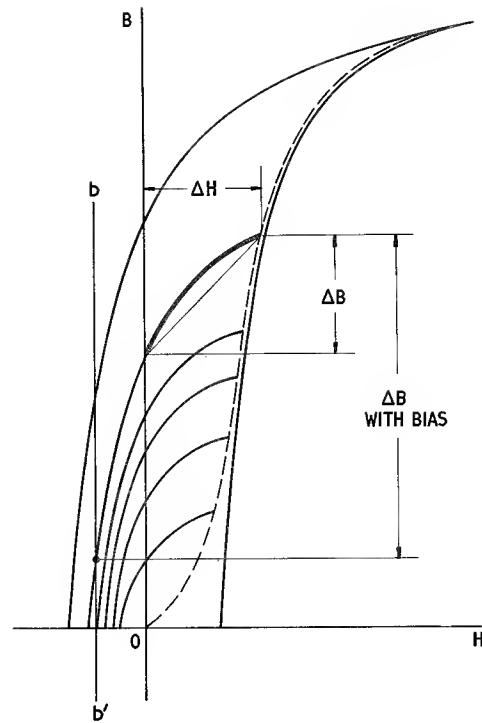


Fig. 8.22. A diagrammatic representation of an increasing series of B-H loops showing how the minor loop corresponding to a series of flux density excursions ΔB , may be determined

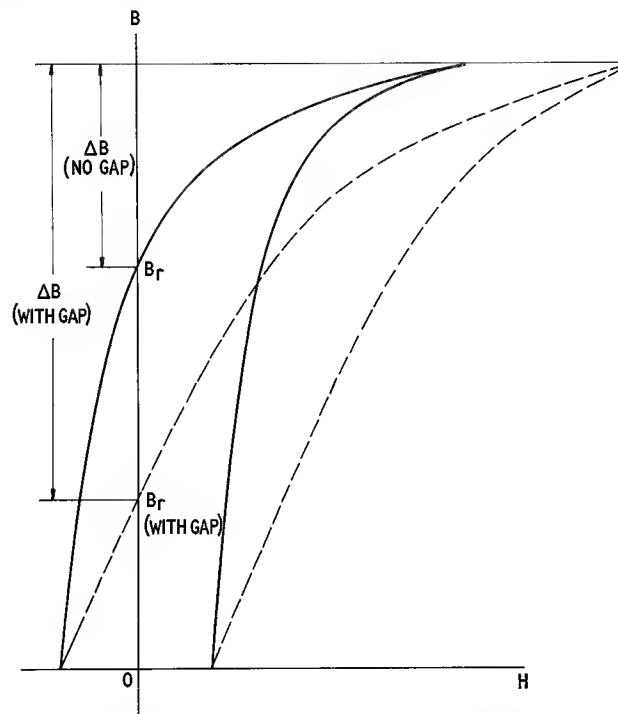


Fig. 8.23. The increase of available flux density excursion due to shearing the B-H loop by the introduction of an air gap

Before leaving this discussion of cores for higher power ferrite pulse transformers some mention must be made of core losses. During the pulse the flux density rises steadily from its residual or bias value to its maximum value, a total change of ΔB . At the end of the pulse the flux will decay back to the starting value at a rate which depends on χ and σ_f (see Figs. 8.11 to 8.15; dB/dt is proportional to the voltage amplitude). Thus a minor B - H loop will be traversed and the rates of change of flux density will not normally be high even if the voltage pulse is very square. The hysteresis core loss depends to some extent on dB/dt but a reasonable estimate may be made from the area of the minor loop. Since there is an infinite variety of possible minor loops it is not usually possible to give data on this subject; perhaps the best approach is to estimate the fraction of the full B - H loop that is enclosed and take this fraction of the energy loss per cycle of the full loop. This energy is dissipated at the pulse repetition rate and therefore the power loss may be calculated. At pulse repetition rates below 5 kHz this loss will not be appreciable in manganese zinc ferrite unless the magnetization approaches the full B - H loop.

Eddy current core loss could be significant at higher pulse energies. It is easily shown that for a core having a resistivity ρ and a circular cross-sectional area A the eddy current loss density when the flux density changes linearly by ΔB in time t is given by

$$P_F = \frac{(\Delta B)^2 A}{8\pi\rho t^2} \quad \text{W.m}^{-3} \text{ during time } t \quad (8.32)$$

Taking a rather extreme example, suppose $\Delta B = 0.1$ T (1000 Gs), $A = 10^{-4}$ m² (1 cm²), $\rho = 1$ Ω m (100 Ω cm) and $t = t_d = 1$ μ s, then P_F is 4×10^4 W.m⁻³ or 40 mW.cm⁻³. The mean dissipation would be much less than this because normally the duty cycle (mark/space ratio) is small. Thus even taking into account both rising and decaying flux density, the eddy current core loss is not likely to be serious.

Winding losses under pulse conditions present, in a general case, a somewhat complex problem and the reader is referred to Glasoe⁷ for a detailed treatment. However a useful upper limit to the effective resistance may be obtained by using the results for the high frequency resistance of windings given in Section 11.4.4 and putting

$$f = \frac{1}{2t_d} \quad (8.33)$$

The loss in the winding resistance occurs only during the pulse and therefore the winding loss so obtained must be reduced by the duty cycle ratio.

Summarizing the characteristics of ferrite cores at higher pulse powers, the achievement of a sufficient flux density excursion is the main limitation. Polarization or gapping can improve the performance in this respect but it cannot approach that of the alloy cores. On the other hand core losses are unlikely to be a limitation in the use of ferrite cores.

8.6. PRACTICAL CONSIDERATIONS

8.6.1. General

As previously observed, the realization of a low power pulse transformer is similar to the realization of a wide band transformer and much of Section 7.3 applies. In low power pulse transformer design there is less emphasis on winding resistance because this has little effect on the shape of the transmitted pulse. However, winding resistance will reduce the pulse amplitude and if this is an important aspect of performance it may easily be taken into account by using the following equation:

$$U'_b = \left(\frac{E_a R'_b}{R_a + R'_b + R_1 + R'_2} \right) \quad (8.34)$$

where R_1 is the resistance of the primary winding and R'_2 is the resistance of the secondary winding referred to the primary.

If there is a pulse attenuation limit the corresponding limit of winding resistance may thus be readily found. This could lead to the evaluation of $(R_{dc}/L)_\frac{1}{2}$, i.e. the resistance/inductance ratio for one of the windings, e.g. the primary. Table 7.1 could then be used for the selection of a suitable ferrite core.

Another important design parameter is the ratio of shunt inductance to leakage inductance, L_p/L_l . It has been seen that the energy spectrum of a pulse transformer can be very wide and this tends to lead to large values for L_p/L_l . This ratio has been discussed in Section 7.3.1. It is often the case that a large value of L_p/L_l is more important than a low value of $(R_{dc}/L)_\frac{1}{2}$. This tends to lead to a winding that occupies only a small fraction of the available winding height, a shallow winding giving low leakage inductance at the expense of a higher resistance.

Whichever criterion is used in selecting a core, a high value of effective permeability is always desirable. Any of the core shapes listed in Table 7.1 p. 256 may be used for low power pulse transformers but clearly the H cores with their very high values of μ_e are particularly suitable.

$$(8.32) \quad P_F = \frac{(\Delta B)^2 A}{8\pi\rho t^2} \times 10^{-16} \quad \text{W.cm}^{-3}$$

8.6.2. A practical example of a low power pulse transformer

To illustrate the realization of a low power pulse transformer, the theoretical design considered in Section 8.3.2 will be used. Fig. 8.19 shows the equivalent circuit and Table 8.3 compares the predicted performance with the specification.

Due to the severe specification, the ratio L_p/L_l is required to be rather high (> 3000) so the transformer is not easy to realize. It was proposed to use a ferrite pot core and to select a size of core that would allow the low impedance winding to be accommodated in one layer using a reasonable conductor diameter, thus minimizing the leakage inductance.

The core chosen was the 18 mm pot core from Table 7.1; $\alpha = 19.5$ turns for 1 mH, winding breadth, $b_w = 6.3$ mm and the mean turn length, $l_w = 37.1$ mm.

Required primary inductance > 4 mH

\therefore Number of turns on the primary winding = 39

\therefore Maximum overall conductor diameter = $6.3/39 = 0.161$ mm

The conductor selected was 0.0044 in (0.112 mm) fine enamelled covered wire, $d_o = 0.132$ mm (see Appendix Table A1.2.1). The secondary winding would consist of

Primary inductance = 4.3 mH

Leakage inductance = 1.32 μ H

Self capacitance referred to the secondary side = 58 pF

The design shunt capacitance referred to the secondary side is $1000/4 = 250$ pF, therefore an external shunt capacitance of about 190 pF must be added.

Plate 8.1 shows oscillograms obtained during pulse tests with the transformer connected between a 50 Ω source and a 150 Ω load. It is seen that with the proper external capacitor the measured pulse distortions are close to the design values, allowing for the difficulty of measuring small deviations on oscillograms. In particular the use of the initial permeability in calculating the shunt inductance is shown to be justified.

The interwinding screen was included in case the interwinding capacitance (otherwise present) should give rise to a spike on the leading edge of the output pulse. The likelihood of such a spike in the absence of a screen depends on the time constants involved; when the screen was disconnected in the above example the leading edge waveform was unchanged. The presence of the screen makes the attainment of a low leakage inductance more difficult. An alternative design of transformer,

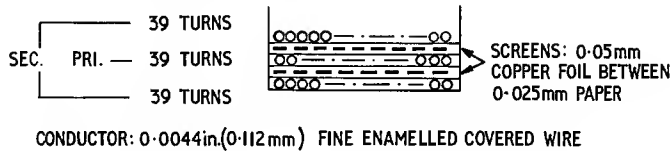


Fig. 8.24. Winding arrangement of the example pulse transformer

two layers, each identical to the primary, placed one above and one below the primary as shown in Fig. 8.24.

From Fig. 11.18 the leakage inductance referred to the primary is given by

$$L_l = 4\pi 10^{-4} \frac{N_1^2 l_w}{4b_w} \left(\frac{\Sigma x}{3} + \Sigma x_d \right) \quad \mu\text{H}$$

$$l_w = 37.1 \text{ mm}$$

$$b_w = 6.3 \text{ mm}$$

$$\Sigma x = 3 \times 0.112 \text{ mm}$$

$$\Sigma x_d = 2 \times 0.1 \text{ mm} + 0.02 \text{ due to the enamel covering}$$

$$\therefore L_l = 4\pi 10^{-4} \frac{39^2 \cdot 37.1}{4 \times 6.3} (0.112 + 0.22) \approx 1 \mu\text{H}$$

A model of this transformer was constructed and had the following measured properties.

without a screen, was also realized. This consisted of three equal windings wound trifilar on a 14 mm pot core. There was no sign of a leading edge spike. The leakage inductance was much less (0.36 μ H) but this reduction of leakage inductance by itself led to a somewhat longer rise time (0.075 μ s) because it increased the damping factor, σ_r (see Table 8.1, Fig. 8.6 and Fig. 8.3) and this was only partly offset by a decrease in $(L_l C)^{\frac{1}{2}}$ (see Eqn 8.7). The new value of σ_r was 1.2 and the observed overshoot was zero as would be expected. A reduction of C to restore the ratio L_l/C would have decreased the rise time significantly below the value obtained with the first version.

REFERENCES AND BIBLIOGRAPHY

Section 8.1.

1. WILDS, C. F., 'Determination of core size in pulse transformer design', *Electronic Engng*, 33, 566, (1961).

Section 8.2.1.

2. POSTMA, W., unpublished report.

3. FENOGLIO, P., PECK, C. W., RICHARDSON, F. R., LORD, H. W. and BOYAJIAN, A., 'High power, high voltage pulse transformer design criteria and data', *General Electric Contract report, Req. No. NWK 60F200*, (1953).

Section 8.3.

1. WILDS, C. F., see ref. 1.

Section 8.4.

4. WILDS, C. F., 'Pulse transformers, frequency response, and wide band transformers', *Electronic Engng*, **34**, 608, (1962).

Section 8.5.

5. MELVILLE, W. S., 'The measurement and calculation of pulse magnetization characteristics of nickel irons from 0.1 to 5 microseconds', *Proc. Instn elect. Engrs*, **97 Part 2**, 165, (1950).
6. 'The Application of Ferroxdure for premagnetizing cores in power carrying coils', *Matronics*, no. 9, 153, (1955).
7. GLASOE, G. N., *et al.*, see General.
BROWN, D. R., BUCK, D. A. and MENYUK, N., 'A comparison of metals and ferrites for high speed pulse

operation', *Trans. Am. Inst. elect. Engrs*, **73 Part 1**, 631, (1955).

SHARPLES, T. K., 'Saturation and gain characteristics of pulse transformers using various core materials', *Trans. I.E.E.E.*, **CP11**, 317, (1964).

Section 8.6.

WILDS, C. F., 'Graded windings for pulse transformers', *Proc. Instn elect. Engrs*, **109 Part C**, 589, (1962).

General

GLASOE, G. N. and LEBACQZ, J. V., (Editors), 'Pulse generators', *M.I.T. Radiation Lab. Series*, McGraw-Hill Book Company, Inc., (1948).

BRUIJNING, H. G., 'Pulse transformers', *Commun. News*, **10**, 126, (1950).

TSCHIEGG, C., 'NBS pulse transformers', *Radio Electron. Engrg*, **13**, (1952).

BADY, I., 'Measurements of parameters that determine the front edge response of step-up transformers', *Conv. Rec. Inst. Radio Engrs*, **3, Part 10**, 26, (1955).

GROSSNER, N. R., 'Pulse transformer circuits and analysis', *Electro-Technology*, **69**, no. 2, 71, (Part 1), and no. 3, 80, (Part 2), (1962).

GROSSNER, N. R., *Transformers for electronic circuits*, McGraw-Hill Book Company, (1967).

Power Transformers

9.1. INTRODUCTION

The transformers considered in this chapter are those which transmit relatively large powers such that the design is mainly limited by saturation or the heating of the core or windings. Although the treatment is related to the use of ferrite cores much of it is quite general in its application. Current transformers and high energy inductors are not specifically included but a large proportion of the treatment is relevant to the design of these devices also.

Power transformers may be required to transmit at a single frequency, e.g. in a power distribution network, or over a narrow band of frequencies, e.g. in the output of an ultrasonic generator, or over a wide band of frequencies, e.g. in an aerial matching unit.

Single frequency and narrow band transformers sometimes have a regulation specification which may override the limitations arising from saturation or heating. The regulation depends not only on the winding losses but also on the leakage inductance; indeed the design of such transformers may be determined mainly by the winding resistance and leakage inductance.

Wide band power transformers will normally have to meet a return loss requirement over a given frequency band as well as having acceptable losses. Therefore the design of such transformers is a combination of the

principles discussed in Chapter 7 and the procedure for single frequency power transformers. Normally such a transformer would be initially designed as a single frequency power transformer at the lower frequency of the transmission band and then the design would be checked, again as a single frequency transformer, at the upper frequency of the band. Having achieved a satisfactory design as a power transformer, the wide band transmission requirements, e.g. return loss (see Section 7.2), would then be considered and the design would be developed accordingly.

It will be seen later that as the frequency to be transmitted becomes lower then, for a given temperature rise, the flux density at which the core may operate becomes higher, until a frequency is reached below which the design is limited by the saturation of the core. For a silicon iron core the maximum working flux density is typically 1.5T (1.5×10^4 Gs) and the saturation value is typically 2T (2×10^4 Gs). It has been seen that for ferrites the corresponding figures would be typically 0.35 and 0.5T (3500 and 5000 Gs) respectively. Therefore at the lower power frequencies, e.g. 50 Hz and 400 Hz, the transformer steels have a distinct advantage over ferrites. However, at higher frequencies, where loss considerations dominate the design, the ferrite cores find a wide variety of applications. Typical examples are a 2 kW, 30 kHz output transformer to supply an ultrasonic power trans-

ducer and a 5 kW antenna matching transformer operating over a frequency band from 2 to 30 MHz. As suggested above, the design procedure will depend on which factors predominate in the particular problem and this information must be deduced at the commencement of the design.

Common to most power transformer designs is the heat transfer problem and this is considered first. Then there is a general discussion of the electrical design of transformers operating at frequencies that are not so high that the eddy current losses in the windings are significant. This is followed by a more detailed study of three types of design, namely the regulation limited, the saturation limited and the core loss limited design. Finally the problems of the higher frequency power transformer are considered.

9.2. HEAT TRANSFER AND TEMPERATURE RISE

9.2.1. General

This subject is treated extensively in text books on heat and elsewhere and the reader is referred to the literature for a more detailed study than is possible here. This section will be confined to interpreting some of the more straightforward results in terms that are applicable to transformer design.

A part of the power applied to the primary of a transformer is dissipated in the form of heat due to losses in the windings, in the core and in the dielectric materials that insulate the winding. The latter loss is usually negligible but may become significant in high voltage transformers. These losses cause a rise in temperature, the equilibrium temperature being reached when the heat lost balances the heat produced in the transformer. Since the production of heat per unit volume will in general vary from one part of the transformer to another and because the thermal conductivities involved are finite, the temperature, and therefore the rate of heat transfer, will in general vary from place to place on the surface of the transformer.

From the engineering point of view the temperature is important mainly because of its effects, usually deleterious, on the properties of the materials composing the transformer, e.g. increase of copper resistance, increase of core losses, reduction of the saturation flux density of the core material and degradation of the insulating materials. Since these effects concern the interior of the transformer it is the interior temperature that is important and this will be higher than the surface temperature by an amount depending on the thermal conductivities of the transformer materials and the distribution of the heat sources.

Sometimes the designer is more concerned with the heat dissipation than the temperature rise, e.g. the

efficiency of the transformer may be important or its contribution to the ambient temperature inside an equipment may be a design criterion. At equilibrium, the calculation of the rate of heat dissipation usually presents no problems of heat transfer because it equals the total power loss. The present discussion is therefore concerned mainly with the temperatures attained by the transformer.

As indicated above, the surface temperature is a function of the rate of production of heat, i.e. power loss, and the heat dissipating properties of the transformer assembly. The heat will in general be transferred to the surroundings by means of conduction, convection and by radiation, and each of these processes may be natural or may be artificially aided. The way in which the total heat transfer is proportioned between these means of dissipation will vary widely from one design to another.

Enough has been said to illustrate the complexity presented by a proper analysis of the heat transfer problem. However since great accuracy is not normally required, simplifying assumptions may be made. In the extreme case these lead to the rule of thumb that a heat loss of about $300 \mu\text{W}$ per square millimeter of surface (0.2 W.in^{-2}) is a reasonable design figure. The design of a highly rated power transformer usually requires a more reliable guide. Accordingly data will now be given that will enable most transformer temperature problems to be solved with reasonable accuracy. Since the transformers under discussion are not large by power engineering standards they attain equilibrium temperature in a relatively short time and it is this equilibrium temperature that is of main concern. The transient heating and cooling problem arises when the operation is intermittent or when the transformer is so large that the thermal time constant is too long for convenient measurement of the equilibrium temperature. The transient problem is dealt with in most text books on power transformers.

A transformer is usually cooled mainly by convection (forced or natural) assisted by radiation. The amount of cooling by conduction is significant only if special means are adopted to make it so, e.g. some transformers are equipped with special heat conductors and heat sinks so that conduction is the principal means of cooling. However the majority of transformers are not designed in this way so attention will be devoted mainly to the other two types of cooling.

A transformer may be operated in contact with surrounding air or it may be contained in an oil filled vessel. In either design the transfer of heat depends ultimately on the radiation and convection from the surface in contact with the air (incidental conduction and the possibility of water cooling being ignored). The convection may be natural, or forced air cooling may be provided. The treatment below starts with the cooling of a body in air.

If the transformer is contained in an oil filled vessel

then the heat must be transferred from the transformer surface to the volume of oil before being dissipated to the surrounding air. This process is next considered. Finally attention is given to the passage of heat from the interior of the transformer to its surface. Applying these calculations in the above order enables the complete heat transfer problem to be solved in principle. In practice the procedure is reasonably reliable unless some factor is present which either invalidates the assumptions, e.g. significant conduction, or complicates the calculation, e.g. an unusual winding arrangement.

9.2.2. Radiation

This is taken first not because it is necessarily the most important means of cooling but because it does not depend on the ambient air conditions.

The rate of dissipation of heat from a surface follows from the Stefan-Boltzmann law and is given by:

$$P_{\text{rad}} = 5.67 \cdot 10^{-8} E (T_s^4 - T_o^4) \quad \mu\text{W} \cdot \text{mm}^{-2} \quad (9.1)$$

where E is the emissivity of the surface
 T_s is the surface temperature of the transformer in $^{\circ}\text{K}$

and T_o is the temperature of the surrounding objects in $^{\circ}\text{K}$

The values of emissivity for a number of surfaces are given in Table 9.1.

In subsequent calculations involving radiation, T_o will be assumed to be 300°K (27°C) and E will be taken as 0.95. These data have been used to calculate the broken curve in Fig. 9.1; this expresses the relation given in Eqn 9.1 and may be used to find the heat lost by radiation

Table 9.1. THE EMISSIVITIES OF VARIOUS SURFACES (AFTER KING¹)

Surface	Emissivity E
Polished aluminium and brass	0.05
Clean, smooth iron and steel	0.2
Polished silver	0.025
Oxidized aluminium	0.1–0.2
Oxidized brass	0.25–0.6
Oxidized iron and steel	0.6–0.9
Metallic paint	0.5
Non-metallic solids such as porcelain glass, paper and non-metallic paints of any colour	0.9–0.95

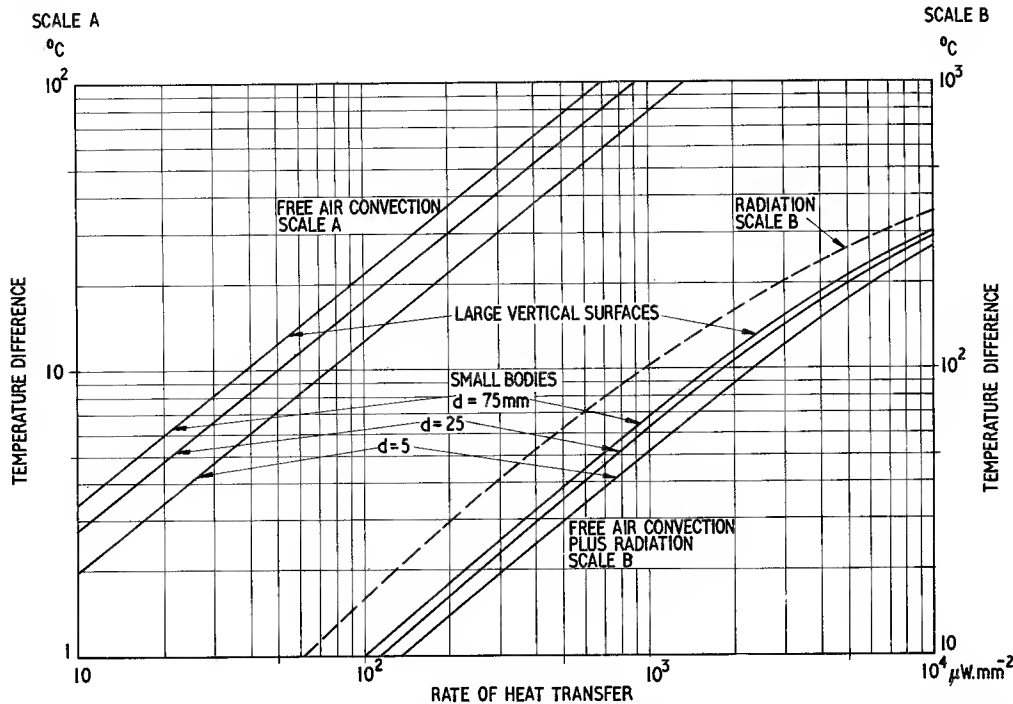


Fig. 9.1. Heat transfer by free air convection and radiation. The temperature difference between the surface and the surrounding air as a function of the rate of heat transfer for: large vertical surfaces (heights $> 0.6\text{ m}$ or 24 in.), and small bodies having various values of d in mm where $d = \text{dia.}$ for long horizontal cylinders or $d = \frac{d_{\text{hor}} d_{\text{vert}}}{d_{\text{hor}} + d_{\text{vert}}}$ for more compact bodies in which the horizontal length d_{hor} becomes comparable with the vertical height, d_{vert} . For small spheres $d = \text{radius}$. The L.H. group of curves is for free air convection, the broken curve is for radiation assuming a surface emissivity of 0.95 and an ambient temperature of 27°C , and the R.H. group is for the sum of the convection and radiation. Based on data given by King² and Montsinger³

in most practical situations. Radiation loss under other conditions may be readily obtained from the above equation.

9.2.3. Convection

Convection is the removal of heat by the passage of a fluid over a surface.

The fluid in close proximity to the surface may be regarded as a stagnant film transmitting heat by conduction to the main body of the fluid which due to its movement may be regarded as a constant temperature heat sink. There is, of course, a gradual transition between the stagnant film and the main body of the fluid. The rate of heat dissipation depends on the properties of the fluid and the difference in temperature between the surface and the fluid; it does not depend on the fine texture or the colour of the surface.

In free convection the movement of the fluid arises from its reduced density when heated. It gathers heat as it rises over the heated surface and subsequently loses it to the surrounding fluid or containing vessel, becomes more dense as it cools and descends, perhaps to recycle past the heated surface indefinitely. Clearly the rate of heat transfer per unit area of surface will be influenced by the geometry of the surface, e.g. a vertical surface will lose heat by free convection at a rate different to that from a horizontal surface.

In forced convection the fluid is passed over the surface at a velocity determined only by the performance of the pump or blower. Thus the rate of cooling is less dependent on the geometry of the surface but obviously depends on the fluid velocity.

Free convection in air

Two formulae are quoted from the literature. For a long horizontal cylinder in air at atmospheric pressure the following formula is derived from one quoted by King²

$$P_{\text{conv}} = 6.3 \frac{\theta^{1.25}}{d^{0.25}} \quad \mu\text{W} \cdot \text{mm}^{-2} \quad (9.2)$$

where P_{conv} is the rate of heat transfer by convection,

θ is the difference in temperature in °C between the surface and the air,

d is the diameter of the cylinder in mm

When the diameter exceeds 150 to 200 mm (6 to 8 in) the rate of heat transfer per unit area tends to become independent of the diameter, and the body may be treated as a number of large plane surfaces. A formula is given below for the heat transfer from a large vertical

surface. Before considering this however it should be mentioned that Eqn 9.2 may be extended to apply to all bodies having dimensions which are small enough to affect the convection per unit area, i.e. linear dimensions of less than about 300 mm (12 in). This is done by giving d an effective value depending on the horizontal dimension and the vertical dimension of the given body, d_{hor} and d_{vert} respectively.³

$$\text{Then } \frac{1}{d} = \frac{1}{d_{\text{hor}}} + \frac{1}{d_{\text{vert}}} \quad (9.3)$$

Thus for a sphere $1/d = 2/\text{diameter}$, therefore d equals the radius of the sphere. This method is applicable to most power transformers used with electronic apparatus.

For vertical surfaces having heights greater than 600 mm (24 in) Montsinger⁴ gives a formula which may be stated as follows

$$P_{\text{conv}} = 2.17 \theta^{1.25} \quad \mu\text{W} \cdot \text{mm}^{-2} \quad (9.4)$$

(θ is defined in Eqn 9.2)

From the upper side of a plane horizontal surface the rate of heat loss will be 15 to 25% more than for a vertical surface, and for a similar downward facing surface the rate of heat loss will be less and will decrease as the surface becomes larger; a reduction of 33% relative to the vertical surface is quoted by King.

If the air pressure is n atmospheres then both of the heat transfer expressions, i.e. the R.H.S. of Eqn 9.2 and 9.4, must be multiplied by \sqrt{n} , thus natural convection at high altitudes is much less effective.

Fig. 9.1 shows the surface temperature rise above ambient as a function of the rate of heat transfer at normal atmospheric pressure. The left hand group of curves are for free convection cooling of horizontal cylinders or small bodies in accordance with Eqn 9.2 and for large vertical surfaces in accordance with Eqn 9.4. The broken curve is for radiation cooling under the conditions mentioned in connection with Eqn 9.1. The right hand group of curves are for free convection plus radiation and, neglecting conduction losses, represent the equilibrium temperatures of typical bodies cooling under normal atmospheric conditions.

For free convection at normal atmospheric pressures the thickness of the stagnant film referred to above is about 2–3 mm. This must be remembered when considering clearances. If the space between the surface of the winding and the outside leg of a shell type core is less than 10 mm then the convection cooling from these surfaces will be less than the calculated value. If the spacing approaches 3 mm it may be assumed that no cooling by free convection will occur in that space and the areas concerned must be disregarded in calculating the total cooling surface of the transformer. Similarly any surface which clears an adjacent obstruction by less

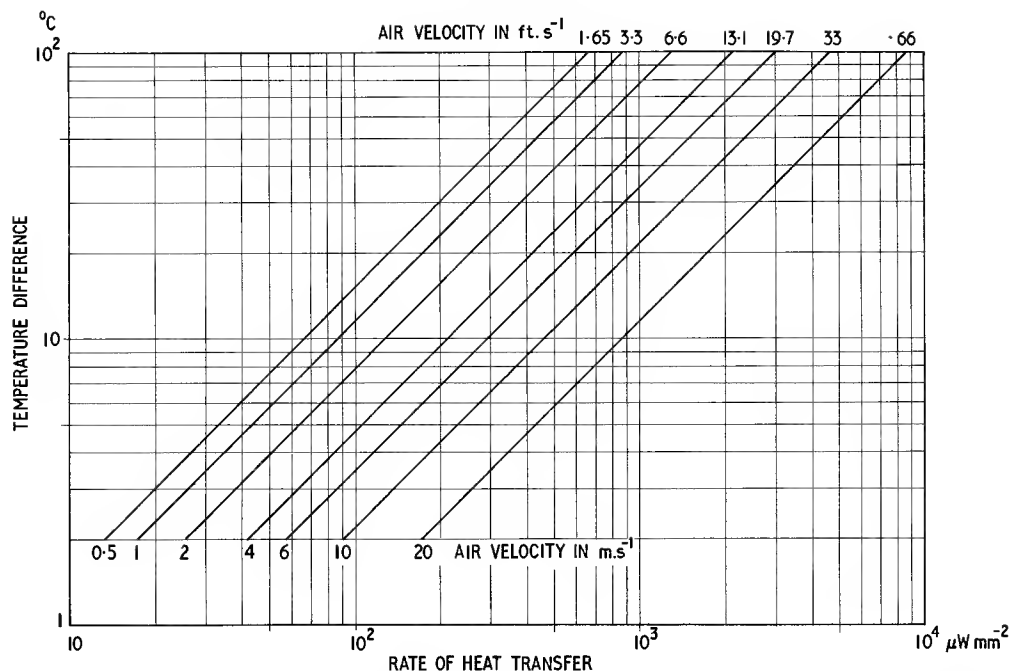


Fig. 9.2. Heat transfer by forced air convection. The temperature difference between the surface and the surrounding air as a function of the rate of heat transfer for various air velocities. These data apply to air flow parallel to a smooth surface. If the surface is rough the transfer may be 10 to 40% greater; if the air meets the surface at an oblique angle the transfer is somewhat less. Based on data quoted by King⁵

than about 5 mm will lose relatively little heat by free convection. If the transformer or its case is fitted with cooling fins these should be at least 12 mm (1/2 in) apart if they are to contribute to cooling by free convection. In fact the effective area of such fins may be estimated by assuming that their surfaces (but not their exposed edges) and the surfaces from which they project are covered by a 6 mm thickness of conductive material. The derived surface, including the (now thickened) exposed edges of the fins may be used to calculate the effective area.

Forced convection in air

For air flowing over a plane surface King⁵ gives a formula from which the following expressions may be obtained

$$P_{\text{conv}} = (4.54 + 4.1v)\theta \quad \mu\text{W}.\text{mm}^{-2} \quad (9.5)$$

where v is the velocity of the air stream at a distance of about 25 mm from the surface, in m.s^{-1} , and θ is the temperature difference between the surface and the air in $^{\circ}\text{C}$

$$\text{or } P_{\text{conv}} = (4.54 + 1.25v)\theta \quad \mu\text{W}.\text{mm}^{-2}$$

where the symbols are as before except that v is in ft.s^{-1}

Fig. 9.2 shows the relative surface temperature as a function of the rate of heat transfer due to forced air cooling. The amount of radiation cooling is usually relatively small but if it is significant it may be added from the data given in Fig. 9.1.

Free convection in oil

In an oil immersed transformer the heat is normally transferred from the transformer surface to the walls of the containing vessel by free convection. The rate of heat transfer per unit area depends on the viscosity and other properties of the oil and also on the temperature difference, θ , between the transformer surface and the main body of the oil. In practice the main body of the oil may be assumed to be at a temperature that is not much higher than the walls of the containing vessel when these are cooled by air convection. King⁶ quotes results obtained by Montsinger and Metrovick, and suggests that these results may be approximately represented by

$$P_{\text{conv}} = \frac{112 \theta^{1.25}}{v^{0.4}} \quad \mu\text{W}.\text{mm}^{-2} \quad (9.6)$$

where v is the oil viscosity in centipoises measured at a temperature that is a mean between that of the dissipating surface and the bulk of the oil.

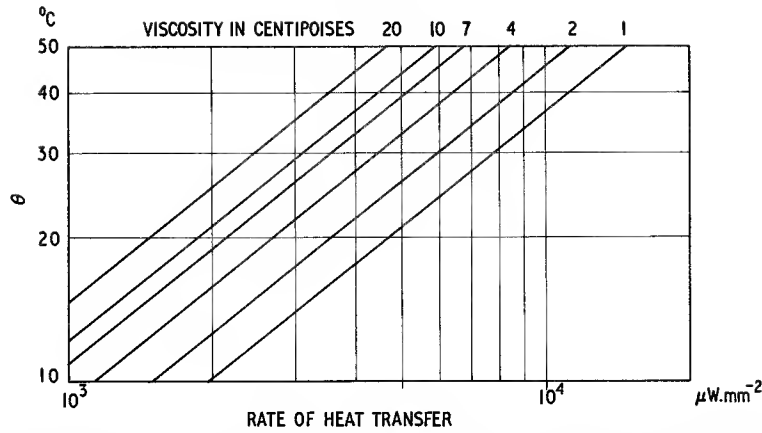


Fig. 9.3. Heat transfer by free convection in oil. The approximate temperature difference between a large dissipating surface and the average temperature of the surrounding oil, shown as a function of the rate of heat transfer with the oil viscosity as a parameter. The viscosity is the value corresponding to a temperature that is a mean between that of the dissipating surface and the bulk of the oil. Based on data quoted by King⁶

This expression is shown graphically in Fig. 9.3.

The remarks made concerning the effect of the stagnant layer between the surface and the convection currents apply here also except that the effective skin thickness is about 1 to 1.5 mm. Thus if convection cooling is to be assisted by providing vertical ducts in the core or winding these should have least dimensions of not less than 3 mm. If this limitation is observed then the surface area of the duct may be added to the total cooling area.

9.2.4. Conduction

The rate of heat flow perpendicular to a lamina of area A , thickness δx and thermal conductivity λ when the temperature difference is $\delta\theta$ is given by $\lambda A \delta\theta / \delta x$

$$\text{or } P_{\text{cond}} = \frac{\lambda \delta\theta}{\delta x} \quad \mu\text{W.mm}^{-2} \quad (9.7)$$

where P_{cond} is the rate of heat transfer by conduction per unit area

δx is in mm

$\delta\theta$ is in °C

λ is in $\mu\text{W.mm}^{-1} \cdot ^\circ\text{C}^{-1}$.

This may conveniently be regarded as the 'ohms law' of heat flow by conduction:

$$P_{\text{cond}} = \frac{\delta\theta}{R_T} \quad \mu\text{W.mm}^{-2} \quad (9.8)$$

where R_T is the thermal resistance = $\frac{\delta x}{\lambda}$

and has the units: $^\circ\text{C.mm}^2 \cdot \mu\text{W}^{-1}$.

Given the thermal resistance of a layer through which a uniform perpendicular heat transfer is occurring, the

temperature difference across the layer may be readily calculated. Where the heat flow is divergent, P_{cond} is not constant across the thickness and the temperature drop must be obtained by integration.

The thermal conductivities of some commonly used transformer materials are given in Table 9.2.

Pursuing the electrical analogy, a complex arrangement of heat sources and heat transfer paths may be represented by an equivalent electrical circuit of current sources and resistances (e.g. see Fig. 9.5). In the transient case capacitors would be included to represent thermal capacitances.

Before considering an example to illustrate the equivalent electrical circuit it will be convenient to consider the heat transfer in a homogeneous ferrite core. Fig. 9.4 shows the cross-section of a cylindrical core of radius r and axial length l . The power converted to heat in

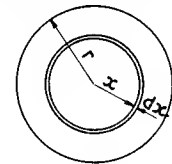


Fig. 9.4. Cross section of a homogeneous cylindrical ferrite core

unit volume of the ferrite, P_m , is assumed to be uniform and therefore at thermal equilibrium the heat passing through an elementary surface of radius x is

$$P_m \pi x^2 l \quad \text{W}$$

The heat flow per unit area is

$$\frac{P_m \pi x^2 l}{2\pi x l} = \frac{P_m x}{2} = P_{\text{cond}}$$

Therefore from Eqn 9.7

$$d\theta = \frac{P_m x}{2} \frac{dx}{\lambda}$$

Integrating from $x = 0$ to $x = r$, the temperature difference between the centre and the surface is

$$\theta_{cs} = \frac{P_m r^2}{4\lambda} = \frac{P_m d^2}{16\lambda} \quad ^\circ\text{C} \quad (9.9)$$

If λ is in $\mu\text{W}.\text{mm}^{-1}.\text{}^\circ\text{C}^{-1}$, and the diameter d is in mm then P_m is in $\mu\text{W}.\text{mm}^{-3}$ or $\text{mW}.\text{cm}^{-3}$.

Table 9.2. THERMAL CONDUCTIVITIES OF SOME MATERIALS COMMONLY USED IN POWER TRANSFORMERS

Material	Thermal Conductivity, λ in $\mu\text{W}.\text{mm}^{-1}.\text{}^\circ\text{C}^{-1}$ at 20°C
Metals	
Aluminium, 90% pure	220×10^3
Brass	111×10^3
Copper	385×10^3
Lead	38×10^3
Silver	410×10^3
Steel	43×10^3
Insulating materials	
Alumina ceramics	$(10-30) \times 10^3$
Cotton cloth, varnished	160-220
Bitumen	420-700
Epoxy resin, cast without filler	170-210
Epoxy resin, cast with silica filler	400-850
Ferrite	3500-4300
Glass	720-1200
Glass bonded mica	380-600
Mica	400-600
Paper, dry	50-140
Paper board, varnished	250
Phenol formaldehyde (Bakelite etc)	
moulded without filler	125-250
moulded with wood flour filler	170-350
paper laminate	240-260
fabric laminate	320
Polyamide resin (Nylon etc)	
moulded without filler	220-280
moulded with glass fibre filler	210-280
Polycarbonate, moulded without filler	190
Polyester resins, cast without filler	170-260
moulded with glass fibre filler	420-670
glass cloth laminate	210
Polyethylene, moulded without filler	330-520
Polystyrene, moulded without filler	40-140
Polytetrafluoroethylene (P.T.F.E.)	
moulded without filler	250
Polyvinylchloride (P.V.C.) moulded	
without filler	125-300
Rubber	130-280
Silicone rubber	210-400
Silk, varnished	160
Wax, paraffin	230
microcrystalline	200-250

Note. In the literature thermal conductivities are often quoted in the units:

$\text{Btu}.\text{h}^{-1}.\text{ft}^{-2}.\text{}^\circ\text{F}^{-1}.\text{in.}$ Multiply the figures so quoted by 144 to convert to $\mu\text{W}.\text{mm}^{-1}.\text{}^\circ\text{C}^{-1}$.

For normal sizes of ferrite cores operating at typical frequencies and flux densities this conductive temperature drop is not large. Where it is large then Eqn 9.9 becomes invalid since both P_m and λ are functions of temperature and this should be allowed for in the integration.

For cores with cross-sections approximating to a square, Eqn 9.9 may be used with reasonable accuracy if the effective diameter d is taken as the diameter of the circle having the same area, A , as the rectangular core, i.e. $d = (4A/\pi)^{1/2}$.

A similar treatment of ferrite cores having cross-sections with rectangular dimensions $b \times d$ where $b \gg d$, i.e. relatively thin slabs of ferrite, yields a temperature difference between the central plane and the parallel surfaces given by:

$$\theta_{cs} = \frac{P_m d^2}{8\lambda} \quad ^\circ\text{C} \quad (9.10)$$

In the derivation of this expression it is assumed that the heat flow is normal to the plane of the slab; for a slab of finite thickness and limited superficial dimensions some heat will flow towards the edges and this will reduce the central temperature.

A comparison of the last two equations shows that for an infinite slab the temperature at the centre is twice that for a cylinder having a diameter equal to the slab thickness. In practice a general rectangular core will have an intermediate value.

9.2.5. An example of a heat transfer calculation

An example illustrating the calculation of the temperatures within a transformer will now be considered. Fig. 9.5 shows a cross-section of a cylindrical ferrite core carrying two windings. Details of the dimensions, currents and core loss are also given in the figure. Alongside the cross-section of the transformer is the equivalent electrical circuit of the heat transfer path. The current sources are analogous to heat sources and the resistances are analogous to parts of the heat transfer path having relatively low conductivity. The core loss is represented by a distributed current source and the thermal resistance of the windings is neglected. It is assumed that the heat flow is radial and parallel to the plane of the diagram. This is a reasonable assumption in the case of these windings since they are wide and shallow so that the heat loss through the ends may be neglected. Considering the core, the part with which this example is concerned may be regarded as one limb of a closed core, the closing limbs carrying no windings. The temperature of these limbs may be separately calculated and will clearly be less than that of the limb carrying the windings. Thus there will in practice be some flow of heat axially along the core. Three-dimensional flow of heat presents a complex

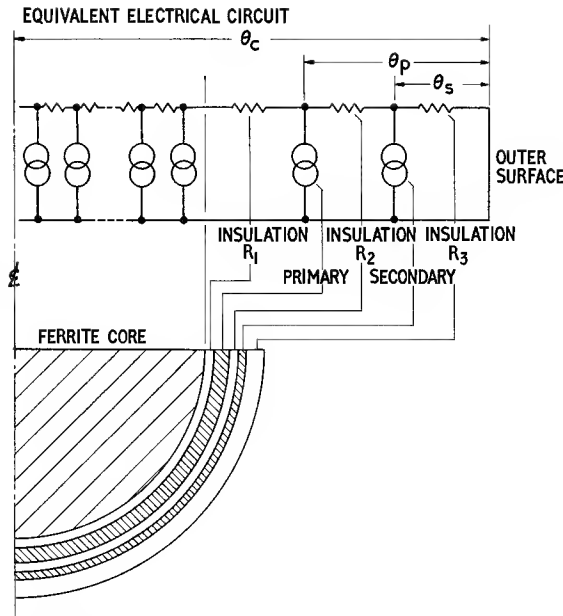


Fig. 9.5. Diagram for the example calculation of temperature distribution in a ferrite cored transformer, showing the cross-section of the core and windings and the equivalent electrical circuit of the heat transfer path.

The following data are used in the example:

Ferrite core: Axial length: 50 mm

Diameter: 20 mm

Power loss in core: $150 \mu\text{W} \cdot \text{mm}^{-3}$

Thermal conductivity: $4000 \mu\text{W} \cdot \text{mm}^{-1} \cdot ^\circ\text{C}^{-1}$

Windings: Primary winding consists of 50 turns of 0.032 in (0.813 mm) dia. enamelled copper wire and carries an r.m.s. current of 2A.

Secondary winding consists of 100 turns of 0.0164 in (0.417 mm) dia. enamelled copper wire and carries an r.m.s. current of 1A.

Axial length of windings = 50 mm

Insulation: Varnished cotton, $\lambda = 160 \mu\text{W} \cdot \text{mm}^{-1} \cdot ^\circ\text{C}^{-1}$

Insulation thicknesses

R_1 , 0.5 mm

R_2 , 0.5 mm

R_3 , 1.0 mm

problem so the axial flow is neglected here; this will make the answer somewhat pessimistic.

Proceeding with the calculation in simple stages, the heat generated at each of the main sources is first deduced.

Heat generated in the core =

$$150 \times 10^{-6} \times (\pi/4) \times 20^2 \times 50 = 2.36\text{W}$$

Heat generated in the primary windings:

$$\text{Mean turn length} \approx (20 + 1.8)\pi = 68.5 \text{ mm}$$

\therefore Total length of the conductor =

$$50 \times 68.5 = 3430 \text{ mm}$$

For 0.032 in. dia. copper wire

$$\text{the specific resistance, } R_c = 0.0327 \Omega \cdot \text{m}^{-1}$$

$$\therefore \text{Resistance} = 3.43 \times 0.0327 = 0.112 \Omega$$

\therefore Heat generated in the primary =

$$I^2 R = 4 \times 0.112 = 0.45\text{W}$$

Heat generated in the secondary winding:

$$\text{Mean turn length} \approx 75.4 \text{ mm}$$

$$\therefore \text{Total length of the conductor} = 7540 \text{ mm}$$

$$R_c = 0.124 \Omega \cdot \text{m}^{-1}$$

$$\therefore \text{Resistance} = 7.54 \times 0.124 = 0.935 \Omega$$

$$\therefore \text{Heat generated in the secondary} =$$

$$1 \times 0.935 \approx 0.94\text{W}$$

The total rate of heat flow through R_3 is

$$\frac{2.36 + 0.45 + 0.94}{80.0 \times 50} = 0.00094 \text{ W} \cdot \text{mm}^{-2}$$

$$= 940 \mu\text{W} \cdot \text{mm}^{-2}$$

where 80.0 = mean circumference of R_3 in mm.

$$\text{The thermal resistance of } R_3 = \frac{1.0}{160} = 0.00625^\circ\text{C} \cdot \text{mm}^2 \cdot \mu\text{W}^{-1}$$

Therefore the temperature drop across R_3 , given by Eqn 9.8, is

$$\theta_3 = 0.00625 \times 940 = 5.9^\circ\text{C}$$

The rate of heat flow through R_2 is less than that through R_3 by the heat generated in the secondary winding. Its value is

$$\frac{2.36 + 0.45}{72.6 \times 50} = 0.00077 \text{ W} \cdot \text{mm}^{-2}$$

$$= 770 \mu\text{W} \cdot \text{mm}^{-2}$$

where 72.6 = mean circumference of R_2 in mm.

$$\text{The thermal resistance of } R_2 = \frac{0.5}{160} = 0.00312^\circ\text{C} \cdot \text{mm}^2 \cdot \mu\text{W}^{-1}$$

Therefore the temperature drop across R_2 is

$$\theta_2 = 0.00312 \times 770 = 2.4^\circ\text{C}$$

Similarly the temperature drop across R_1

$$\theta_1 = 0.00312 \times \frac{2.36 \times 10^6}{64.4 \times 50} = 2.3^\circ\text{C}$$

The temperature drop between the centre and the surface of the core is given by Eqn 9.9

$$\frac{P_m d^2}{16\lambda} = \frac{150 \times 400}{16 \times 4000} \approx 0.9^\circ\text{C}$$

Therefore the temperatures relative to the coil surface are

$$\theta_s = \text{relative temperature of secondary} = + 5.9^\circ\text{C}$$

$$\theta_p = \text{relative temperature of primary} = + 8.3^\circ\text{C}$$

$$\theta_c = \text{relative temperature at centre of}$$

$$\text{core} = + 11.5^\circ\text{C}$$

*See Appendix Table A.1.1.

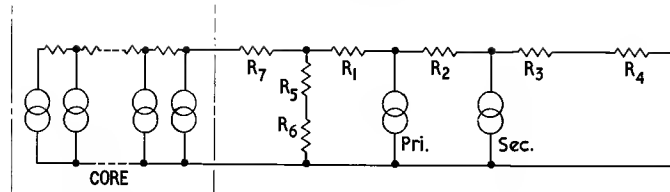


Fig. 9.6. Modification of equivalent circuit shown in previous figure so that it includes a thermal shunt

Assuming the surface of the winding is being cooled by free air convection and radiation, reference to Fig. 9.1 shows that the temperature of the surface when the dissipation is $940 \mu\text{W}.\text{mm}^{-2}$ (= the rate of heat flow through R_3) is about 60°C . The curve for $d = 25 \text{ mm}$ has been used because the present case may be regarded as a long cylinder, it being assumed that there is no heat loss at the ends. The actual internal temperatures are

Actual temperature of secondary $\approx 65.9^\circ\text{C}$

Actual temperature of primary $\approx 68.3^\circ\text{C}$

Actual temperature at centre of core $\approx 71.5^\circ\text{C}$

It is seen that, in this example, the heat transfer at the surface accounts for the major temperature rise. The temperature gradient within the ferrite core is negligible. Had the insulation been thicker or if the windings had consisted of many layers interleaved with paper the internal temperature drop would have been greater. However the example serves to show the temperature distribution in a typical ferrite power transformer.

9.2.6. Thermal shunts and thermal isolation

A thermal shunt is a means of making the cooling due to conduction a significant if not a major factor. One means of doing this is to use a coil former made of a metal such as aluminium, provided, of course, with a slit to prevent the occurrence of a shorted turn. The flange of the coil former might be fastened to a heat sink such as a chassis, a panel or a large cooling fin, again taking care to avoid an electrical short circuit. The temperature of the heat sink would depend on the heat flowing into it from the thermal shunt and on its rate of cooling due to convection, etc. This may be readily obtained from the heat transfer graphs shown earlier in this section. Usually the heat sink temperature will be near that of the equipment ambient so a very effective heat transfer path is provided.

The equivalent circuit of Fig. 9.5 may be modified to illustrate the resulting analytical problem. The reference temperature in this case must be the ambient temperature and not that of the coil surface, so the closing short circuit must be replaced by a resistance, R_4 , which represents the thermal resistance of the surface of the transformer, i.e. $R_4 = \theta/P_{\text{tot}}^\circ\text{C}.\text{mm}^2.\mu\text{W}^{-1}$ where θ is the

temperature difference between the surface and the ambient, and P_{tot} is the total rate of heat transfer from the surface in $\mu\text{W}.\text{mm}^{-2}$. This resistance may be estimated from the appropriate heat transfer graph. Then a shunt resistance, R_5 , is connected from a point a little to the left of the primary winding. This resistance represents the thermal resistance of the shunt and would normally have quite a low value. In series with it would be connected the thermal resistance, R_6 , representing the heat transfer of the heat sink. If this is being cooled by air having the same temperature as that cooling the transformer surface this resistance, R_6 , would be connected to the common potential at the bottom of the circuit. Fig. 9.6 shows the resulting circuit; R_1 now represents the thermal resistance between the primary winding and the coil former, and R_7 the thermal resistance between the coil former and the core. Ordinary network analysis will yield the temperatures of the various points.

An alternative or additional means of reducing winding temperatures is to isolate the heat coming from the core and prevent it from entering the windings. This may be done, for example, by making a sufficiently large gap between core and coil former so that all the core heat is carried away by direct convection. This situation could be represented in Fig. 9.6 by making R_7 open circuit and connecting a thermal shunt from the core surface. The numerical value of this shunt would depend on the rate of heat transfer from the core surface.

Further ways of dealing with the heat transfer problem are to be found in the literature. Sufficient has been included here to enable the designer to obtain a reasonably accurate estimate of the equilibrium temperatures within a proposed transformer.

9.3. GENERAL ELECTRICAL DESIGN CONSIDERATIONS

The basic relation is the e.m.f. equation (see Eqn 4.16)

$$E = \frac{\omega \hat{B}_c A_c N}{\sqrt{2}} \quad \text{V} \quad (9.11)$$

$$(9.11) \quad E = \frac{\omega \hat{B}_c A_c N 10^{-8}}{\sqrt{2}} \quad \text{V}$$

where \hat{B}_e is the peak value of the effective* flux density in teslas

A_e is the effective* core cross-sectional area in m^2
and N is the number of turns

The freedom of design implicit in this equation is usually restricted by other considerations; the more important of these will be considered later. For the moment it is useful to discuss qualitatively the e.m.f. equation in relation to a given source voltage U_1 ($\approx E$ in practice) and a given core.

Since the core losses rise with frequency and flux density, the flux density at high frequencies is usually limited to relatively low values by the permissible core loss. At high frequencies the necessary low flux densities may be obtained with relatively few turns. If the number of turns required to obtain the permissible flux density is too small to provide sufficient shunt impedance then N must be suitably increased; this will reduce the flux density and both the reactive and core loss components of the magnetizing current will be reduced.

For a given voltage and core, $\hat{B}_e N \propto 1/f$. The core loss expressed in watts is approximately proportional to $f \hat{B}_e^n$ where n lies between 1.9 and 2.9 (see Fig. 3.19). Thus for a given core loss $\hat{B}_e \propto 1/f^{1/n}$. It follows that as the frequency is decreased, both the flux density and the number of turns will increase if the core loss is maintained at a specified value. Under these conditions the design is core loss limited. In such a design it may be advantageous to obtain a certain ratio between core loss and copper loss in order to achieve optimum performance with respect to efficiency or volume, etc.

At lower frequencies the flux density will approach the saturation value and will become limited. Below this frequency the design is saturation limited. At progressively lower frequencies the core loss decreases and the winding loss rises because N must now rise in inverse proportion to f in order to keep \hat{B}_e constant. The total power loss, or temperature rise is still the factor limiting the throughput.

At even lower frequencies the winding resistance or leakage inductance will become large enough to result in an unacceptable regulation. Below this frequency the design is regulation limited and the temperature rise ceases to be a restriction.

The shunt inductance has been mentioned above. This is often a major parameter in transformer design. If it is too low, the magnetizing current will be too great; in a wide band transformer this will cause excessive attenuation or insufficient return loss at the lower end of the transmission band (see Section 7.2.4). Except for tuned

transformers, the shunt inductance is usually required to be greater than a specified value. However, excessive values may be accompanied by a leakage inductance or a winding resistance that is too high to meet other specification requirements.

The e.m.f. equation is often combined with the expression for inductance to give a relation that is independent of the number of turns. From Eqns 4.16 and 4.18

$$N^2 = \frac{2E^2}{\omega^2 \hat{B}_e^2 A_e^2} = \frac{L l_e}{\mu_0 \mu_e A_e}$$

$$\therefore A_e l_e = V_e = \frac{2\mu_0 \mu_e E^2}{\omega^2 L \hat{B}_e^2} \quad m^3 \quad (9.12)$$

This equation gives the core volume required to satisfy simultaneously the flux density and inductance requirements. However, an inspection of this relation shows that caution is required in its use. It states that the higher the effective permeability or the lower the required inductance the larger is the required core volume. This surprising result is obtained because the inductance has been given a specific value rather than a minimum value. Thus if for a given frequency, voltage and flux density the inductance is fixed at a very low value the required core volume may be very large. The cross-sectional area of the core must be large enough to satisfy the flux density requirements but at the same time the core reluctance must be high so that the shunt inductance is not exceeded; for a given value of μ_e this may mean that the magnetic path length must be long to obtain the required high reluctance. Hence the large volume. Alternatively the core volume may be kept within reasonable limits by reducing μ_e , e.g. by introducing an air gap. This would be the right course in the design of a tuned transformer requiring a specified shunt inductance value. However, for a normal power or wide band transformer it offers no advantage; an excessive shunt inductance in these cases is detrimental only inasmuch as it may cause the leakage inductance or winding resistance to be too high and these parameters are unaffected by a reduction of μ_e .

Eqn 9.12 is often quoted. The above discussion has shown that it can lead to unexpected results. If the flux density and inductance are the main consideration in a design then it is probably better to consider them separately. If the flux density is the limiting parameter, due to core loss or saturation, then for a given core the minimum number of turns is determined by Eqn 9.11. The shunt inductance may then be calculated, e.g. from Eqn 4.18. Since it was postulated that the design was flux density limited, the inductance will be greater than the minimum required to meet the magnetizing current or

*In this chapter the effective flux density and effective area as defined in Section 4.2.1 will generally be used although for high flux densities the assumption used in their derivation, i.e. core loss $\propto \hat{B}^3$, is not usually very accurate.

$$(9.12) \quad A_e l_e = V_e = \frac{8\pi \mu_e E^2 10^7}{\omega^2 L \hat{B}_e^2} \quad cm^3$$

transmission band specification. The leakage inductance and resistance may then be estimated (see Chapter 11); if they are excessive it may be necessary to use a larger core. If, on the other hand, the design is inductance limited the required shunt inductance will determine the number of turns and the resultant flux density will be acceptable. At the start of a design it may not be known which is the limiting parameter so the number of turns is calculated by both criteria and the larger number is used.

In connection with these basic calculations it should be noted that the core permeability is a function of flux density and in power transformers the amplitude permeability at the maximum working flux density may be

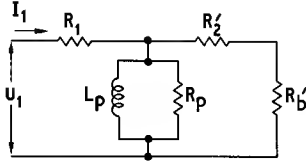


Fig. 9.7. Simplified equivalent circuit of a power transformer, the elements referred to the primary side.

- U_1 = Primary voltage
- R_1 = Primary winding resistance
- I_1 = Primary current
- R_2' = Secondary winding resistance
- R_b' = Load resistance
- L_p = Shunt inductance of primary
- R_p = Shunt core loss resistance

appreciably larger than the initial permeability (see Fig. 3.4). Which value of permeability is used depends on whether the transformer is to be operated only at the rated voltage or whether it must give a satisfactory performance at voltages down to zero. If the latter requirement applies the initial permeability must be used.

Continuing the discussion of general design considerations some basic relations concerning power will now be considered.

It is often stated that for maximum efficiency in a transformer the core loss should equal the winding losses. This arises from the following argument based on the equivalent circuit shown in Fig. 9.7. Assuming that

$$R_1 + R_2' \ll R_b' \ll |L_p \text{ and } R_p \text{ in parallel}|,$$

the winding and core losses are given by:

$$\left. \begin{aligned} \text{winding loss} &= P_w = I_1^2(R_1 + R_2') \\ \text{core loss} &= P_m V_e = U_1^2/R_p \end{aligned} \right\} \quad \text{W} \quad (9.13)$$

where P_m is the core loss density and

V_e is the effective core volume (see Section 4.2.1)

and the power in the load is

$$P_b = I_1^2 R_b' = U_1^2/R_b'$$

$$\therefore \frac{P_w + P_m V_e}{P_b} = \frac{R_1 + R_2'}{R_b'} + \frac{R_b'}{R_p} \quad (9.14)$$

This expression for the ratio of the total power loss to the output power may be differentiated with respect to R_b' to obtain the condition for minimum power loss. This condition is that $(R_1 + R_2')/R_b' = R_b'/R_p$, i.e. the value of load resistance is such that the core loss equals the winding loss. This result is not valid generally because if the output power is constant the applied voltage will depend on R_b' and so, consequently, will the flux density. Under these conditions R_p , the core loss resistance, will not, in general, be constant.

The more practical situation is the design of a transformer on a given core to give minimum total power loss when delivering a given power into a given load. The number of primary turns, N_1 , is the variable. If N_1 is large the winding loss will be high and the flux density and core loss will be low; if N_1 is small the reverse applies. The problem is to find the correct ratio of core and winding loss for minimum total loss. It is assumed that the winding fills the winding space, the copper factor is constant and eddy current effects in the winding are negligible. If R_s represents the total winding resistance referred to the primary winding then, making the same assumptions as in the previous analysis:

$$P_w = I_1^2 R_s = \frac{U_1^2 R_s}{(R_b')^2} \quad (\text{see Fig. 9.7})$$

$$\text{and} \quad P_m V_e \propto \bar{B}_e^n \quad (\text{see Fig. 3.19})$$

$$= \frac{K_1 U_1^n}{N_1^n} \quad \begin{array}{l} \text{From Eqn 9.11,} \\ K_1 \text{ being a constant of} \\ \text{proportionality} \end{array}$$

$$\therefore P_w + P_m V_e = K_1 \left(\frac{U_1}{N_1} \right)^n + \left(\frac{U_1}{R_b'} \right)^2 R_s$$

From Eqn 11.11 $R_s = K_2 N_1^2$ where K_2 is another constant of proportionality

$$\therefore P_w + P_m V_e = K_1 \left(\frac{U_1}{N_1} \right)^n + K_2 \left(\frac{U_1 N_1}{R_b'} \right)^2$$

Differentiating with respect to N and equating to zero, the following condition for minimum total power loss is obtained

$$K_1 \left(\frac{U_1}{N_1} \right)^n = \frac{2K_2}{n} \left(\frac{U_1 N_1}{R_b'} \right)^2$$

$$\text{i.e. } P_m = \frac{2}{n} P_w \quad (9.15)$$

It has been seen (Fig. 3.19) that the value of n lies between about 2 and 3; only when it is 2 does the equating

of the core and winding losses give minimum total loss.

It is not always possible or desirable to apply this result. As described at the beginning of this section, low frequency power transformer designs are often regulation or saturation limited; under these conditions the winding loss predominates. At higher frequencies where the design is limited by core loss (temperature rise) it is possible to choose the most suitable ratio of core and winding loss. When small size is more important than efficiency it is usual for transformers with laminated iron cores to be designed to have high core loss relative to the winding loss. The resulting heat may be removed from the core by conduction to a heat sink, so the core temperature is prevented from being excessive.

The calculation of winding resistance and the optimum ratio of primary and secondary winding areas are discussed in Section 11.3. Data on the losses in ferrite cores at high flux densities are given in Fig. 3.19. In using these graphs it must be remembered that the loss so obtained does not include eddy current loss in the core. This is a function of the core shape and in some cores it may be appreciable. Section 2.2.4 describes eddy current phenomena in ferrite cores and gives an expression for the eddy current power loss. There is a further discussion in Section 4.2.3.

9.4. LOW FREQUENCY POWER TRANSFORMERS

9.4.1. General

The transformers to be considered under this heading are those for which the winding resistance may be taken as substantially equal to the d.c. value. The frequency at which this ceases to be true depends on the output power, e.g. a 1 kW transformer may have an appreciable increase of winding resistance due to eddy currents at frequencies above about 3 kHz. The problems peculiar to the design of these higher frequency transformers are considered in Section 9.5.

It was shown in the previous section that the design of a power transformer is dominated by the permissible flux density. At very low frequencies it is usually the saturation flux density that limits the design while at higher frequencies it is usually the flux density corresponding to the permissible core loss. Given a limit value for the flux density, the design of a transformer on a given core may be very straightforward. The number of primary turns may be calculated from Eqn 9.11 in which E is put equal to the primary voltage. The number of turns on the other windings may be provisionally calculated from the specified voltage ratios. The conductor diameters and resistances may readily be calculated from the equations given in Sections 11.2 and 11.3. The internal

voltage drops due to winding resistances and, if significant, the leakage inductance may then be calculated, and the number of secondary turns may be increased if necessary to obtain the specified full load secondary voltages.

At this stage of the design it may be found that the winding resistance is too high, leading either to excessive regulation or to excessive power loss in the windings. If so, a larger core must be selected and the design repeated.

When the design satisfies the flux density and winding loss requirements, the shunt inductance should be calculated to ensure that it is adequate to meet the specification for magnetizing current or possibly return loss.

This trial and error approach can, with experience, lead quite quickly to a satisfactory design. However it is helpful to have some advance information of the power-handling capacity of available cores. In the following sections the three main classes of design are analysed with the object of providing core parameters that will enable the most suitable core to be rapidly selected.

9.4.2. Regulation limited transformers

Because regulation becomes a limitation only at very low frequencies it is rarely a factor in the design of ferrite-cored transformers. However, the following analysis may be useful in certain circumstances.

The voltage regulation may be defined as the difference between the output voltage on open circuit and that on full load, expressed as a fraction or percentage of the open circuit voltage. From Fig. 9.7 the voltage regulation due to the winding resistance, referred to the primary side, is given by

$$\text{Voltage regulation} \approx \frac{I_1(R_1 + R'_2)}{U_1} = \frac{I_1^2(R_1 + R'_2)}{\text{input power}}$$

If the winding loss, $I_1^2(R_1 + R'_2)$, is denoted by P_w and P_i and P_o denote the input and output power respectively, then for a voltage regulation of x per cent:

$$\begin{aligned} \frac{x}{100} &= \frac{P_w}{P_i} \\ \therefore P_i &= P_w \cdot \frac{100}{x} \\ \therefore P_o &= P_i - P_w = P_w \left(\frac{100}{x} - 1 \right) \quad \text{W} \end{aligned} \quad (9.16)$$

Assuming that the transformer has two windings and that each has the same cross-sectional area (see Section 11.3), then from Eqn 11.11

$$R_1 = \frac{2m\rho_c N_1^2 l_w}{A_a F_a} \quad \Omega$$

where ρ_c is the conductor resistivity at 20°C,

A_a is the total window area,
 F_a is the corresponding copper factor and
 m is the fractional increase of conductor resistivity above the value at 20°C. For values of m see caption of Table 9.3.

$$\therefore R_1 + R_2' = \frac{4m\rho_c N_1^2 l_w}{A_a F_a} \quad \Omega \quad (9.17)$$

$$\therefore P_w = \frac{4I_1^2 m\rho_c N_1^2 l_w}{A_a F_a} \quad \text{W} \quad (9.18)$$

The number of turns may be eliminated by substitution from Eqn 9.11 putting $U_1 = E$. Thus

$$\left. \begin{aligned} P_w &= \frac{8I_1^2 U_1^2 m\rho_c l_w}{A_c^2 A_a F_a \omega^2 \hat{B}_e^2} \quad \text{W} \\ &= \frac{P_i^2 m k_1}{f^2 \hat{B}_e^2} \quad \text{W} \end{aligned} \right\} \quad (9.19)$$

where $k_1 = \frac{2\rho_c l_w}{\pi^2 A_c^2 A_a F_a} \quad \Omega \cdot \text{m}^{-4}$

But $P_w = P_i \cdot \frac{x}{100}$

$$\therefore P_i = \frac{f^2 \hat{B}_e^2}{m k_1} \cdot \frac{x}{100}$$

It is easily shown from the definition of x or by Eqn 9.16 that

$$\begin{aligned} P_i &= \frac{P_o}{1 - \frac{x}{100}} \\ \therefore P_o &= \frac{f^2 \hat{B}_e^2}{m k_1} \cdot \frac{x}{100} \left(1 - \frac{x}{100}\right) \\ \therefore P_o &= \frac{f^2 \hat{B}_e^2}{m k_1} \cdot \frac{(x - 0.01x^2)}{100} \quad \text{W} \end{aligned} \quad (9.20)$$

$$\text{or } k_1 = \frac{f^2 \hat{B}_e^2}{m P_o} \cdot \frac{(x - 0.01x^2)}{100} \quad \Omega \cdot \text{m}^{-4} \quad (9.21)$$

If the regulation is 10%

$$k_1 = 0.09 \frac{f^2 \hat{B}_e^2}{m P_o}$$

For a given core material, \hat{B}_e is limited to a value determined by the saturation flux density; the frequency, the required output power and the permissible regulation

$$(9.19) \quad P_w = \frac{P_i^2 m k_1}{f^2 \hat{B}_e^2} \quad \text{W}$$

$$\text{where } k_1 = \frac{2\rho_c l_w 10^{16}}{\pi^2 A_c^2 A_a F_a} \quad \Omega \cdot \text{cm}^{-4}$$

are given parameters in the design. Therefore the design value of k_1 may be obtained from Eqn 9.21. It is then necessary to find a core having a value of k_1 (from Eqn 9.19) that is equal to or smaller than the design value. The core selection is facilitated if the available cores are tabulated with their k_1 values. Table 9.3, which is introduced in Section 9.4.5, gives data for a range of ferrite cores suitable for power transformers. It includes values of k_1 calculated on the assumption that the overall copper factor, F_a , is 0.30.

Finally the possibility of poor regulation due to excessive leakage inductance must again be mentioned. At the low frequencies used in power distribution the regulation is almost invariably due to winding resistance. However, at higher frequencies it is advisable to check the contribution of the leakage inductance, the voltage drop across it being $jI\omega L_r$. If it is too large the winding must be sectionalized as described in Section 11.7 or a larger core must be used.

9.4.3. Saturation limited transformers

If the transformer is not regulation limited, and this will be true for most ferrite-cored power transformers, then the next limitation encountered is that imposed by the saturation of the core. The core is operated at a flux density, \hat{B}_e , which is suitably less than the saturation value and the core loss, $P_{m\phi}$, is less than the value dictated by temperature rise.

The following method of core selection has been proposed.⁷ To any given core plus winding, a nominal value of the total power dissipation, P_{tot} , may be assigned. This assumes a certain standard of cooling, e.g. free air convection and radiation from all exposed surfaces of the core and winding, and it assumes a certain permissible temperature rise. In the present treatment, P_{tot} is taken as corresponding to a uniform rate of heat transfer of $300 \mu\text{W} \cdot \text{mm}^{-2}$ (approx. $0.2 \text{ W} \cdot \text{in}^{-2}$) from all the exposed surfaces. Expressed in terms of the core and winding losses

$$\begin{aligned} P_{\text{tot}} &= P_m V_c + P_w \\ &= P_m V_c + \frac{P_i^2 m k_1}{f^2 \hat{B}_e^2} \end{aligned}$$

from Eqn 9.19

$$\therefore P_{\text{tot}} \approx P_m V_c + \frac{P_o^2 m k_1}{f^2 \hat{B}_e^2} \quad \text{W} \quad (9.22)$$

since, for a reasonably efficient transformer,

$$P_i \approx P_o$$

For a given core made of a specified material, the core loss, $P_{m\phi}$, is determined when f and \hat{B}_e are determined. Thus

corresponding to the value of P_{tot} there is a value of P_o which is the output rating of the core at a specified frequency. It depends on the geometry and material of the core and winding but is substantially independent of the number of turns. This nominal output power may be calculated for a suitable range of cores and the tabulated results would be a useful guide to the selection of a core for a saturation limited transformer. In practice allowance would have to be made if (1) the rate of cooling or the permissible temperature rise were different from the values assumed, and (2) if the copper factor were other than the average value used in calculating k_1 , (e.g. a high voltage transformer or a transformer having many windings would have a copper factor that was smaller than average).

Since both terms of Eqn 9.22 depend on frequency, a tabulation of P_o is only practical for cores that are used at a standard frequency, e.g. silicon iron laminated cores for 50 or 60 Hz, or strip wound cut cores (C cores) for 400 Hz. As ferrite cores may be used over a wide frequency range, P_o cannot be given as a core parameter for ferrite cores. However if P_m can be expressed as a function of frequency then a graph of P_o against frequency may be constructed for a given core. E.g. if the energy lost in a unit volume of the core is w_m joules per cycle:

$$P_{\text{tot}} = w_m V_e f + P_o^2 \frac{mk_1}{f^2 \hat{B}_e^2}$$

$$\therefore P_o^2 = (P_{\text{tot}} - w_m V_e f) \frac{f^2 \hat{B}_e^2}{mk_1} \quad \text{W} \quad (9.23)$$

This method of expressing core performance is illustrated in Section 9.4.5 where a representative range of cores is considered.

9.4.4. Core loss limited transformers

At frequencies above about 1 kHz the design of a ferrite-cored power transformer ceases to be governed by the saturation flux density; the core loss limits the flux density to a value lower than that corresponding to the onset of saturation.

It was shown in Section 9.3 that for maximum efficiency the core loss should equal $(2/n) \times$ the winding loss, where n is the Steinmetz exponent (see Eqn 9.15) and lies between approximately 2 and 3. It was also observed that practical considerations may lead to a loss ratio other than this optimum. For the purpose of calculating design parameters it is reasonable to assume that the core and winding losses will be equal. The results will not be appreciably affected by a moderate departure from equality; the exact loss ratio will emerge during the final design calculations.

Given a suitable core the design procedure is, as before,

quite straightforward. The total permissible loss is decided on heating considerations. If half is allocated to the core, the permissible core loss density is determined. Since this depends on f and \hat{B}_e the latter is readily obtained from graphs such as those in Fig. 3.19. The core parameters and the e.m.f. equation 9.11 will enable the number of turns to be calculated. From this the conductor diameter and copper loss may be obtained. The main difficulty again is that at the start of a design it is not known which core size is the most suitable.

The following procedure is based on a method suggested by MacFadyan⁸ and it enables the designer to select from a range of cores one which will have approximately the required performance. It is necessary to know only the output power, P_o , and to estimate the overall copper factor and a core loss parameter.

From Eqn 9.18 the total winding loss referred to the primary side is

$$P_w = \frac{4I_1^2 m \rho_c N_1^2 l_w}{A_a F_a} \quad \text{W}$$

For equal core and winding loss:

$$P_w = P_m V_e = \frac{P_{\text{tot}}}{2}$$

$$\therefore \frac{4I_1^2 m \rho_c N_1^2 l_w}{A_a F_a} = \frac{P_{\text{tot}}}{2}$$

The output power is very nearly equal to $I_1^2 R'_b$, therefore by substituting P_o/R'_b for I_1^2 , the following expression is obtained:

$$P_o = \frac{P_{\text{tot}}}{8} \cdot \frac{R'_b A_a F_a}{m \rho_c N_1^2 l_w} \quad \text{W} \quad (9.24)$$

The number of turns must be eliminated. This may be done by introducing the core loss in terms of some convenient parameter. Such a parameter is a normalized value of the shunt core loss resistance, R_p , and this may be obtained as follows.

The total core loss = $P_m V_e = U_1^2/R_p$. Using the e.m.f. Eqn 9.11 to eliminate U_1^2 , (assuming that $U_1 = E$):

$$P_m V_e R_p = 2\pi^2 \hat{B}_e^2 A_e^2 N_1^2 f^2 \quad \text{for sinusoidal voltages.}$$

For a given frequency, flux density and core loss density

$$R_p = \frac{2\pi^2 \hat{B}_e^2 f^2}{P_m} \cdot \frac{N_1^2 A_e}{l_e} \quad \Omega \quad (9.25)$$

since $V_e = A_e \cdot l_e$

This shunt resistance may be normalized to a value

$$(9.25) \quad R_p = \frac{2\pi^2 \hat{B}_e^2 f^2}{P_m} \cdot \frac{N_1^2 A_e}{l_e} \cdot 10^{-16} \quad \Omega$$

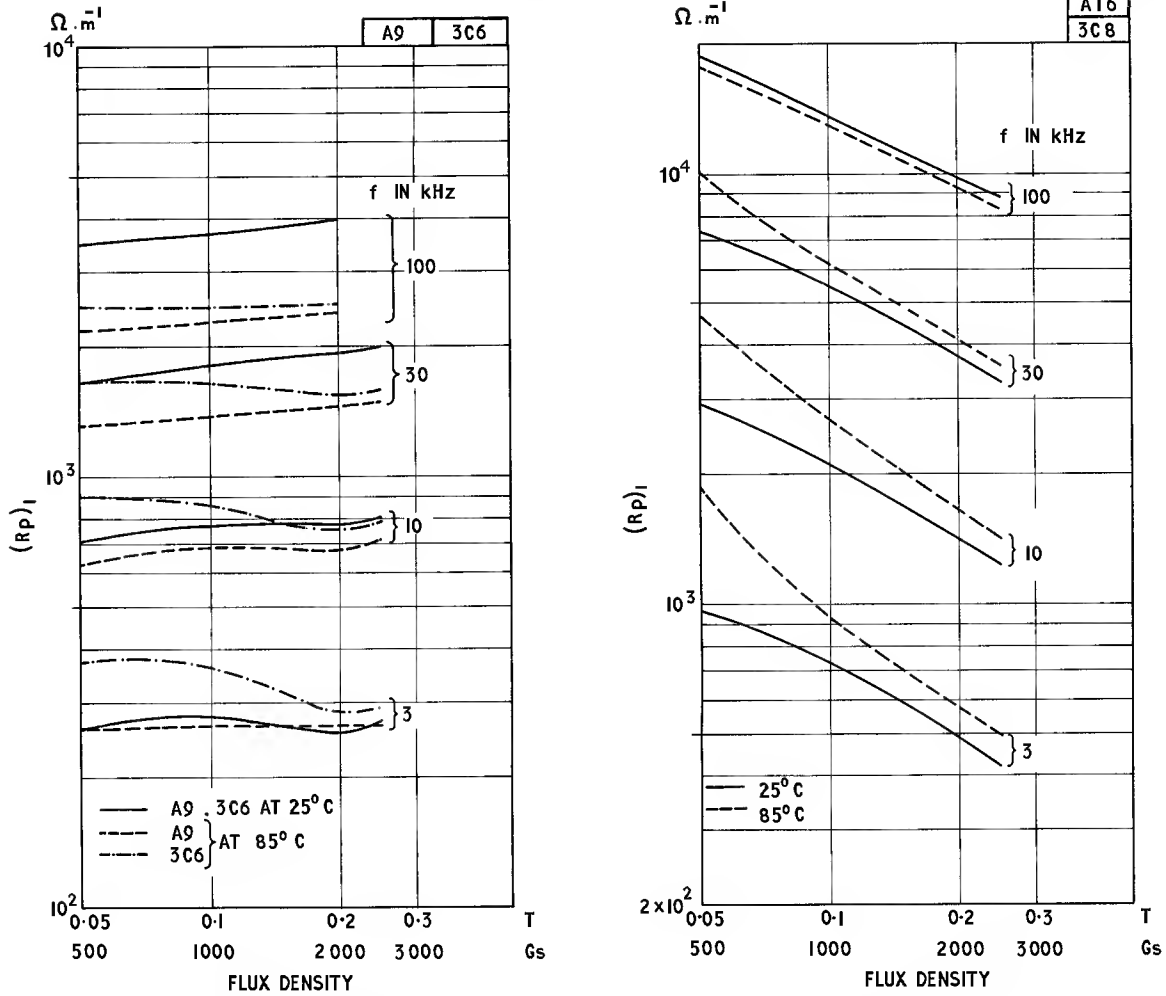


Fig. 9.8. Normalized shunt core loss resistance $(R_p)_1$, (i.e. R_p when $N = 1$ and $C_1 = 1 \text{ m}^{-1}$) as a function of flux density at various frequencies for three transformer grades of manganese zinc ferrite.

corresponding to one turn on a core having $C_1 (= l_e/A_e)$ equal to 1 m^{-1} . If this value is denoted by $(R_p)_1$ then

$$\left. \begin{aligned} (R_p)_1 &= \frac{2\pi^2 \hat{B}_e^2 f^2}{P_m} \quad \Omega \cdot \text{m}^{-1} \\ \text{and } R_p &= (R_p)_1 \frac{N_1^2}{C_1} \quad \Omega \end{aligned} \right\} \quad (9.26)$$

It has been seen that the power loss in a core is approximately proportional to B_e^n .

Therefore

$$\frac{U_1^2}{R_p} \propto B_e^n \propto U_1^n \text{ at a given frequency.}$$

Fig. 3.19 shows that n may have any value between 2 and 3 but it may also be seen that for the particular manganese zinc ferrite grades suitable for power transformers $n \approx 2$ (e.g. see the graphs for A9, N27, 3C6 and A16 (3C8)). Therefore for these materials R_p and $(R_p)_1$ are approximately independent of flux density up to values approaching saturation. If there is eddy current loss in the core this is proportional to \hat{B}_e^2 , see Eqn 2.48, and thus enhances the constancy of R_p .

Fig. 9.8 shows $(R_p)_1$ as a function of flux density calculated at various frequencies from the data given for ferrites A9, 3C6 and A16 (3C8), appropriate allowance having been made for the eddy current loss in a core having an assumed $15 \times 15 \text{ mm}$ cross section. The higher

$$(9.26) \quad (R_p)_1 = \frac{2\pi^2 \hat{B}_e^2 f^2 10^{-16}}{P_m} \quad \Omega \cdot \text{cm}^{-1} \quad \text{and } R_p = (R_p)_1 \frac{N_1^2}{C_1} \quad \Omega$$

($N = 1, C_1 = 1 \text{ cm}^{-1}$)

the value of $(R_p)_1$ the more suitable is the material. To the extent that the curves are approximately horizontal it is relatively easy to estimate $(R_p)_1$ at a given frequency with reasonable accuracy in spite of the fact that the flux density to be used is unknown. The curves for A16 (3C8) have an appreciable negative slope due to n being greater than 2 (see Fig. 3.19.11), however a reasonable estimate of $(R_p)_1$ may still be made.

It is now possible to eliminate N_1 from Eqn 9.24. From Eqn 9.26.

$$P_m V_e = \frac{U_1^2}{R_p} = \frac{U_1^2 l_e}{(R_p)_1 N_1^2 A_e}$$

$$= \frac{P_{\text{tot}}}{2} \text{ for equal core and winding losses.}$$

$$\therefore N_1^2 = \frac{2U_1^2 l_e}{P_{\text{tot}} (R_p)_1 A_e}$$

This may be substituted in Eqn 9.24 so that

$$P_o = \frac{P_{\text{tot}}^2 R_b'}{16 U_1^2} \cdot \frac{F_a (R_p)_1 A_e A_a}{m \rho_c l_e l_w}$$

Since $U_1^2/R_b' = P_o$:

$$P_o \sqrt{\left[\frac{m}{F_a (R_p)_1} \right]} = \frac{P_{\text{tot}}}{4} \sqrt{\left[\frac{A_e A_a}{\rho_c l_e l_w} \right]} = k_2$$

$$\text{W} \cdot \Omega^{-\frac{1}{2}} \cdot \text{m}^{\frac{1}{2}} \quad (9.27)$$

The constant k_2 is a property of the core geometry, and values may be listed for suitable cores. It is then only necessary to calculate $P_o [m/F_a (R_p)_1]^{\frac{1}{2}}$; the output power is specified in the design requirements, the overall copper factor may be estimated by the designer by reference to Section 11.2, m depends on the working temperature (see caption of Table 9.3) and $(R_p)_1$ may be estimated from a graph such as that in Fig. 9.8. A core may then be selected such that it has k_2 equal to or larger than this calculated value. In the next section this and the foregoing procedures are applied to a range of cores and their performance is discussed.

9.4.5. Core performance

In the preceding sections parameters have been derived which, if they were made available for various ferrite cores, would facilitate the selection of the core most suitable to meet a given requirement. A difficulty is that, whereas there are standard ranges of silicon iron cores, there is at present no recognised range of ferrite cores designed specifically for power transformers. It is desirable to have such a range of cores to illustrate the design approach used in this chapter and to relate it to reality. For this purpose the author has postulated a

range of cores based on assemblies of U cores. There are two unit U cores: the only difference is that one has longer legs than the other. They are illustrated in Fig. 9.9 together with a range of assemblies. The unit U cores have been dimensioned and proportioned in such a way that the assemblies are not too far from the shape that is optimum for least R_{dc}/L and total loss. Although this range is, to some extent, arbitrary it may be regarded as realistic; is not expensive to manufacture and it does cover a useful range of sizes. The performance of any other given core that is within the general range of sizes may be inferred approximately by comparison with members of the range or, if such a core is in frequent use, its parameters may be calculated so that it may be included in the list.

Data for this range of cores are given in Table 9.3. In addition to the usual dimensional parameters of the core and winding space, a number of performance parameters are given. The first of these is the exposed surface area, A_e , of the core plus a full winding, i.e. the total available cooling area. From this the value of the nominal power dissipation, P_{tot} , has been calculated assuming a uniform heat transfer of $300 \mu\text{W} \cdot \text{mm}^{-2}$ (approx. $0.2 \text{ W} \cdot \text{in}^{-2}$). The next column lists the values of k_1 (see Eqn 9.19) using $\rho_c = 1.694 \times 10^{-8} \Omega \cdot \text{m}$ and $F_a = 0.3$. Values of k_2 from Eqn 9.27 are then given. The next two columns give parameters relevant to the resistance/inductance ratio. The first is $k_3 = 2 \rho_c l_e l_w / \mu_c A_a A_e$; this equals $(R_{dc}/L)^{\frac{1}{2}}$ normalized with respect to μ_c and F_a ; i.e. it depends only on the geometry of the core. The second is $(R_{dc}/L)^{\frac{1}{3}}$, i.e. the d.c. resistance/inductance ratio for a winding that occupies half the winding space, assuming that the overall copper factor, F_a , of the half winding space is 0.3 and $\mu_c = 1000$. The next column lists a figure of merit, ψ . This is proportional to R_{dc}/L when this ratio is made independent of the volume of the smallest rectangular box that will enclose the core plus winding; a low ψ indicates a good core shape. Finally approximate weights of core and core plus winding are given.

For regulation limited transformers k_1 is the relevant parameter. From Eqn 9.21, k_1 is calculated using the specified frequency, flux density, output power and regulation, and a core is selected which has a value of k_1 equal to or less than the calculated value. The flux density is determined by the saturation and is often taken as that flux density at which the amplitude permeability has fallen to a value equal to the initial permeability at a typical working temperature, see Fig. 3.4. For ferrites suitable for L.F. power transformer applications, i.e. the higher saturation manganese zinc ferrites such as A9, 3C6, N27, A16 and 3C8, this criterion leads to a working flux density of about 0.3T (3000 Gs). If it is wished to work nearer the limit this value might be raised to 0.35T for certain ferrites.

The parameter k_1 is also used in saturation limited

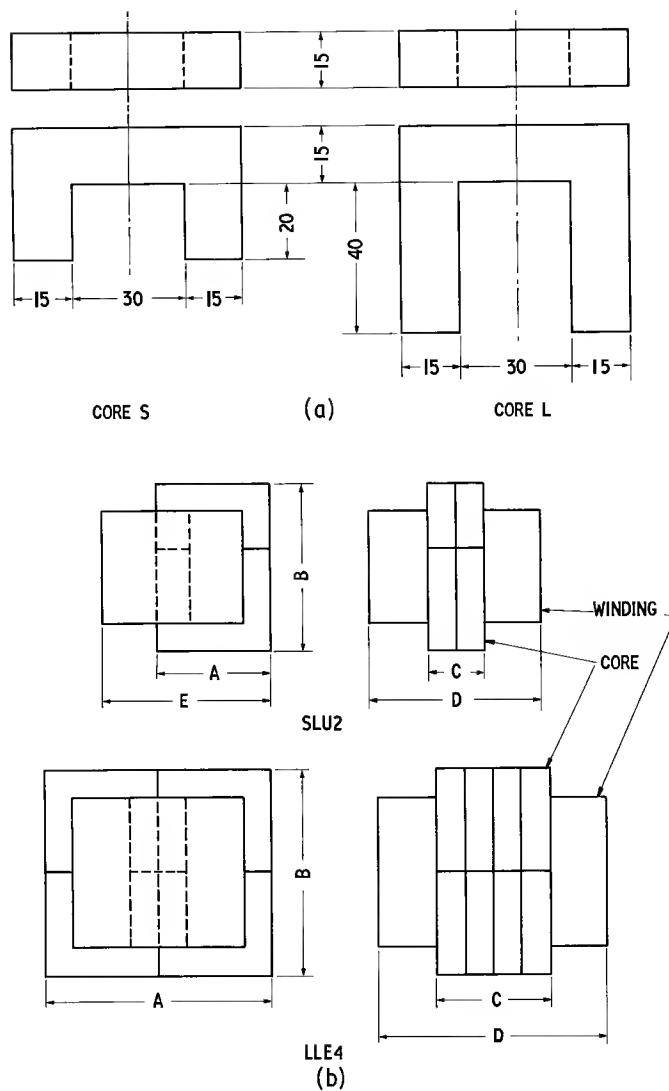


Fig. 9.9. Unit U cores. (a) Dimensions of the two unit cores, in mm. (b) Definition of overall dimension symbols used in Table 9.3, and illustration of assembly code.

Assembly code:

S—short U core

L—long U core

First two letters indicate which of the three possible combinations of S and L is used.

The third letter is U for the single aperture core and E for the double aperture core.

The final cypher is the number of U cores stacked side by side in the assembly.

Table 9.3. PROPERTIES OF TRANSFORMER CORES

In compiling this table the following constants were used:

Nominal rate of heat dissipation $= 300 \mu\text{W}.\text{mm}^{-2}$

$\approx 0.2 \text{ W.in}^{-2}$

Overall copper factor,

$F_a = 0.3$

Resistivity of copper,

$\rho_c = 1.694 \times 10^{-8} \Omega.\text{m}$

Effective permeability,

$\mu_e = 1000$

If other values apply then appropriate allowance must be made.

Core ref.	Physical dimensions (see Fig. 9.9)					Dimensional parameters of the core					Dimensions of winding aperture (see Fig. 11.1)			
	A	B	C	D	E	l_e	A_e	V_e	C_1 $= \frac{l_e}{A_e}$	d_{cs} effective cooling dia. of largest cross-section	b_a	h_a	A_a	l_w
	mm					mm	mm ²	mm ³	mm ⁻¹	mm	mm	mm	mm ²	mm
SSU1	60	70	15	75	90	187	225	42.1×10^3	0.832	17	40	30	1220	154
SLU1	60	90	15	75	90	227	225	51.1×10^3	1.01	17	60	30	1800	154
LLU1	60	110	15	75	90	267	225	60.1×10^3	1.19	17	80	30	2400	154
SSU2	60	70	30	90	90	187	450	84.2×10^3	0.416	19	40	30	1200	184
SSE1	120	70	15	75	—	187	450	84.2×10^3	0.416	19	40	30	1200	184
SLU2	60	90	30	60	90	227	450	102.2×10^3	0.505	19	60	30	1800	184
SLE1	120	90	15	75	—	227	450	102.2×10^3	0.505	19	60	30	1800	184
LLU2	60	110	30	90	90	267	450	120.2×10^3	0.594	19	80	30	2400	184
LLE1	120	110	15	75	—	267	450	120.2×10^3	0.594	19	80	30	2400	184
SSU3	60	70	45	105	90	187	675	126.3×10^3	0.277	20	40	30	1200	214
SLU3	60	90	45	105	90	227	675	153.3×10^3	0.337	20	60	30	1800	214
SSU4	60	70	60	120	90	187	900	168.4×10^3	0.208	20.5	40	30	1200	244
SSE2	120	70	30	90	—	187	900	168.4×10^3	0.208	34	40	30	1200	214
LLU3	60	110	45	105	90	267	675	180.3×10^3	0.396	20	80	30	2400	214
SLU4	60	90	60	120	90	227	900	204.4×10^3	0.252	20.5	60	30	1800	244
SLE2	120	90	30	90	—	227	900	204.4×10^3	0.252	34	60	30	1800	214
LLU4	60	110	60	120	90	267	900	240.4×10^3	0.297	20.5	80	30	2400	244
LLE2	120	110	30	90	—	267	900	240.4×10^3	0.297	34	80	30	2400	214
SSE3	120	70	45	105	—	187	1350	252.6×10^3	0.139	36	40	30	1200	244
SLE3	120	90	45	105	—	227	1350	306.6×10^3	0.168	36	60	30	1800	244
SSE4	120	70	60	120	—	187	1800	336.8×10^3	0.104	38	40	30	1200	274
LLE3	120	110	45	105	—	267	1350	360.6×10^3	0.198	36	80	30	2400	244
SLE4	120	90	60	120	—	227	1800	408.6×10^3	0.126	38	60	30	1800	274
LLE4	120	110	60	120	—	267	1800	480.6×10^3	0.148	38	80	30	2400	274

ASSEMBLED FROM UNIT U CORES AS ILLUSTRATED IN FIG. 9.9.

In particular if the winding is to be operated at temperatures other than 20°C the change of copper resistivity should be taken into account. As far as k_1 and k_2 are concerned this has been done by including a factor m in design Eqns 9.19, 9.23 and 9.27. This factor is the fractional change of copper resistivity with temperature:

Copper temperature	20	40	60	80	100°C
m	1	1.079	1.157	1.236	1.314

Performance parameters (see Section 9.4.5)								
A_c , exposed (cooling) area of core and winding	P_{tot} permissible dissipation at $300 \mu\text{W} \cdot \text{mm}^{-2}$	k_1 $= \frac{2\rho_c l_w}{\pi^2 A_c^2 A_a F_a}$	k_2 $= \frac{P_{\text{tot}}}{4} \sqrt{\frac{A_c A_a}{\rho_c l_w}}$	k_3 $= \frac{2\rho_c l_w}{\mu_o A_c A_a}$	$\left[\frac{R_{dc}}{L} \right]^{\frac{1}{2}}$ $= \frac{k_3}{\mu_o F_a}$	ψ , figure of merit	Approx. weight of core	Approx. weight of core and winding
mm^2	W	$\Omega \cdot \text{m}^{-4}$	$\text{W} \cdot \Omega^{-\frac{1}{2}} \cdot \text{m}^{\frac{1}{2}}$	$\Omega \cdot \text{H}^{-1}$	$\Omega \cdot \text{H}^{-1}$	—	kg	kg
25.8×10^3	7.7	29.1	45.3	2882	9.61	495	0.22	0.72
31.4×10^3	9.4	19.4	61.4	2332	7.77	474	0.26	1.0
36.9×10^3	11.1	14.5	76.8	2058	6.86	477	0.30	1.3
30.6×10^3	9.2	8.68	69.8	1722	5.74	334	0.43	1.0
34.5×10^3	10.3	8.68	78.3	1722	5.74	469	0.43	1.0
36.8×10^3	11.0	5.78	92.9	1392	4.64	319	0.52	1.4
41.3×10^3	12.4	5.78	104	1392	4.64	449	0.52	1.4
42.9×10^3	12.9	4.34	116	1228	4.10	322	0.60	1.8
48.0×10^3	14.4	4.34	130	1228	4.10	453	0.60	1.8
35.4×10^3	10.6	4.48	91.3	1334	4.45	287	0.65	1.3
42.2×10^3	12.6	2.99	121	1080	3.60	274	0.78	1.8
40.2×10^3	12.1	2.88	112	1140	3.80	268	0.86	1.7
40.2×10^3	12.1	2.52	120	1000	3.33	308	0.86	1.6
48.9×10^3	14.7	2.24	150	952	3.17	277	0.91	2.3
47.6×10^3	14.3	1.92	148	924	3.08	256	1.0	2.2
47.6×10^3	14.3	1.68	158	910	2.70	295	1.0	2.1
54.9×10^3	16.5	1.44	182	914	2.71	259	1.2	2.8
54.9×10^3	16.5	1.26	194	714	2.38	297	1.2	2.6
45.9×10^3	13.8	1.28	157	760	2.54	259	1.3	2.1
53.9×10^3	16.2	0.852	205	616	2.05	248	1.6	2.7
51.6×10^3	15.5	0.807	193	640	2.14	239	1.7	2.6
61.8×10^3	18.6	0.639	251	542	1.81	250	1.8	3.4
60.2×10^3	18.0	0.538	250	518	1.73	229	2.1	3.4
68.7×10^3	20.6	0.404	304	458	1.52	230	2.4	4.2

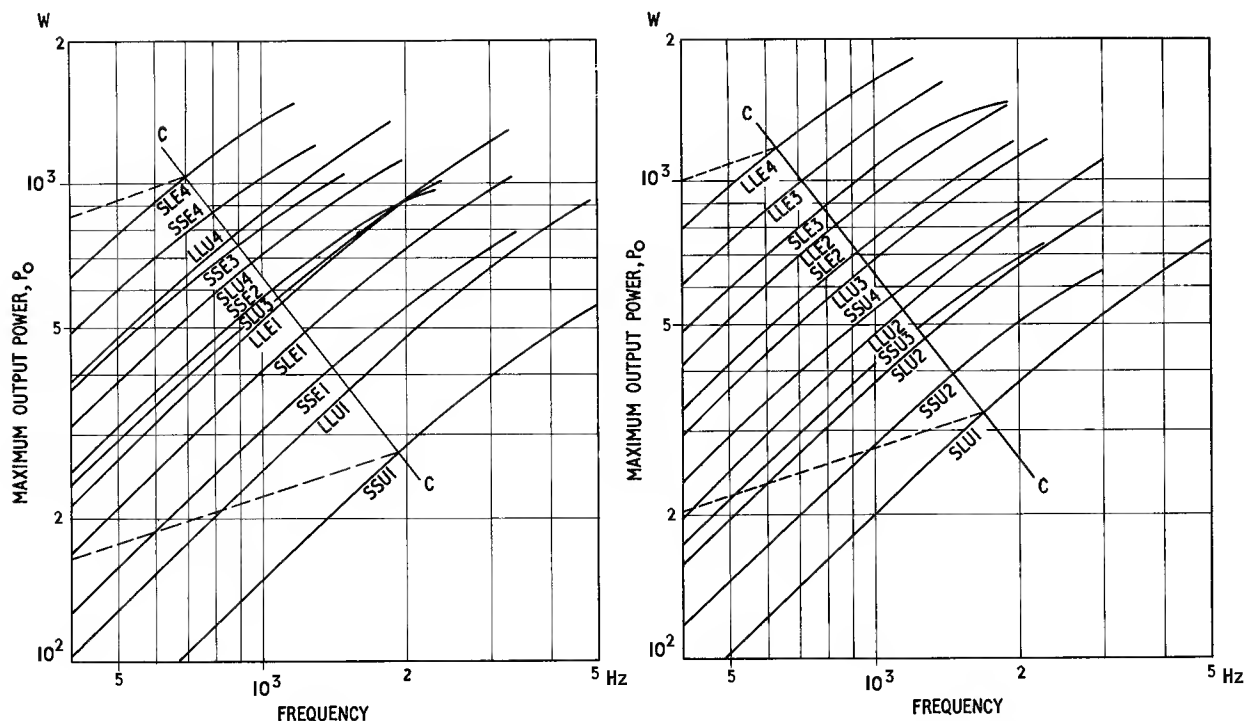


Fig. 9.10. The performance of saturation limited ferrite transformers.

The nominal value of P_o , the maximum output power, as a function of frequency for the 24 core assemblies listed in Table 9.3. The computation uses Eqn 9.23 and assumes $w_m = 18.10^{-9} \text{ J.mm}^{-3} \cdot \text{cycle}^{-1}$ at $\hat{B}_e = 0.3 \text{ T}$, that the nominal cooling rate of $300 \mu\text{W.mm}^{-3}$ applies, that the overall copper factor, F_a is 0.3 and that the temperature is 20°C .

The curves are terminated at the upper end at the frequency at which the core loss equals the winding loss; at higher frequencies the design would be loss limited. The line CC indicates the approximate region below which 0.004 in grain oriented silicon steel cores of equivalent size have superior performance. The broken lines indicate the course of the P_o curves for such cores.

transformers, see Eqn 9.23. Again \hat{B}_e is determined by the core saturation and may be taken as 0.3T (3000 Gs) for suitable ferrites at a typical working temperature. To calculate P_o , the value of w_m must be estimated. For ferrites suitable for L.F. power transformer applications w_m at $\hat{B}_e = 0.30 \text{ T}$ (3000 Gs) and a temperature of 85°C is typically $18.10^{-9} \text{ J.mm}^{-3} \cdot \text{cycle}^{-1}$. Using these figures P_o has been calculated as a function of frequency for each of the listed transformer cores and the results are shown in Fig. 9.10. These curves provide a means of selecting a core to transmit a given power at a given frequency. Over the range of frequencies occupied by these curves the winding loss predominates and the core loss is limited by the saturation of the core. Each curve is terminated at the upper end at the frequency at which the core loss has risen to equal the winding loss. Beyond this frequency the design is core loss limited.

If the heat transfer from the transformer differs from the value used in calculating P_{tot} , i.e. $300 \mu\text{W.mm}^{-2}$ (0.2 W.in^{-2}) allowance must be made for this. It is not easy to make an allowance in such a way that the curves of Fig. 9.10 can still be used. However, when the core loss is negligible Eqn 9.23 shows that $P_o^2 \propto P_{\text{tot}} f^2$, i.e. the

curves of Fig. 9.10 have unity slope; the falling off at the upper end is due to the increasing core loss. If the heat dissipation is a factor k greater than the assumed value then P_{tot} is increased by the same factor and, where the core loss is negligible, P_o is increased by the factor \sqrt{k} . Therefore Fig. 9.10 may still be useful in estimating the core size provided (1) the specified value of P_o is divided by \sqrt{k} before being used to select a core and (2) the droop due to core loss is disregarded, i.e. the curves are extrapolated with unity slope. With the increased dissipation the core loss will remain negligible up to higher frequencies and therefore the droops and the terminating points (at which the core loss has risen to $P_{\text{tot}}/2$) will be removed to higher frequencies.

As observed earlier in this Chapter, silicon iron cores are used for power frequency transformers due to their higher values of saturation flux density, thus over much of the lower frequency range of Fig. 9.10 the curves for the ferrite cores would indicate a lower output power than corresponding curves for silicon iron. To give an indication of the extent of this region, the nominal output power, P_o , has been recalculated for each of the cores in Table 9.3 on the assumption that the core material was

0.004 in (0.1 mm) grain oriented silicon steel having a loss that is typical of strip-wound cut cores (C cores), the geometric factors remaining unchanged. It was found that over most of the region covered by the graph the silicon iron transformers were not saturation limited but core loss limited, so the value of P_o was calculated as shown in the previous section. The results are indicated by the broken lines in Fig. 9.10, one for the largest core and one for the smallest. The line CC shows the approximate region of intersection. Above this line the ferrite core, due to its lower loss, is superior.

Most transformer designs involving ferrite cores will be in the core loss limited region. In this case core selection is quite simple. As shown in the previous section (see Eqn 9.27) it is only necessary to calculate $P_o[m/F_a(R_p)_1]^{\frac{1}{2}}$ and find a core that has k_2 equal to or larger than this value. If the heat transfer is other than the $300 \mu\text{W}.\text{mm}^{-2}$ ($0.2 \text{ W}.\text{in}^{-2}$) assumed in calculating the nominal dissipation, P_{tot} , then a correction must be made. If the actual dissipation is a factor k times greater than the above nominal value, the figure obtained from $P_o[m/F_a(R_p)_1]^{\frac{1}{2}}$ must be divided by k before the core is selected.

Finally it must be remembered that transformers which are designed to transmit powers of the order of 1 kW tend to be wound with rather heavy conductors. At frequencies of more than a few kHz eddy current effects in the winding can raise the winding resistance by a large factor and the foregoing analyses and procedures are invalidated. When eddy currents are likely to be present it is far more difficult to select a core. Section 9.5 discusses these problems.

9.4.6. Example design of a low frequency power transformer

To illustrate the application of ferrite cores to a practical transformer the following specification will be used as an example:

Output power	1 kW at 1 kHz
Primary voltage	1 kV
Secondary voltage	200V at full load
Regulation	< 5%

Nominal cooling conditions will be assumed. Reference to Fig. 9.10 shows the design falls in the saturation limited class and that cores SLE3 and SSE4 should both be suitable. As the former has a slightly smaller volume it will be used for this design. The properties of core SLE3, taken from Table 9.3 are:

Core cross-sectional area	$A_e = 1350 \text{ mm}^2$
Effective volume	$V_e = 307 \times 10^3 \text{ mm}^3$
Core factor	$C_1 = 0.168 \text{ mm}^{-1}$
Window width	$b_a = 60 \text{ mm}$
Window height	$h_a = 30 \text{ mm}$

Window area	$A_a = 1800 \text{ mm}^2$
Mean turn length	$l_w = 244 \text{ mm}$
Nominal total loss	$P_{\text{tot}} = 16.2$ (corresponding to $300 \mu\text{W}.\text{mm}^{-2}$)

The maximum flux density is taken as 0.3T (3000 Gs) as this was the value assumed in deriving the curves in Fig. 9.10. From Eqn 9.11 the number of primary turns,

$$N_1 = \frac{\sqrt{2 \times 1000}}{2\pi \times 10^3 \times 0.3 \times 1350 \times 10^{-6}} = 556 \text{ turns}$$

$$\therefore N_2 = 111 \text{ turns (uncorrected for regulation)}$$

The net winding breadth will be taken as 50 mm and the net winding height, after allowing for a coil former, bowing of the winding, etc., will be taken as 22 mm. The net winding area, $A_w = 22 \times 50 = 1100 \text{ mm}^2$. Thus the approximate cross-sectional area available for each winding is 550 mm^2 .

An approximate value of the primary overall conductor diameter may be obtained from Eqn 11.1. This ignores the presence of interleaving insulation so a somewhat smaller conductor diameter must be used in practice.

$$d_o \approx \sqrt{\frac{550}{556}} = 0.994 \text{ mm}$$

If medium covered enamelled copper wire is used, Tables A.1.1 and A.1.2.2 in Appendix A show that a suitable conductor diameter is $d = 0.813 \text{ mm}$ (0.032 in). This has a maximum overall diameter of 0.8966 mm. Allowing a factor of 0.95 for the residual spacing between turns in a closely wound layer, the number of turns per layer is given by

$$\frac{50 \times 0.95}{0.8966} = 53$$

$$\therefore \text{number of layers} = \frac{556}{53} \approx 10.5 \quad \text{or 11 rounded to the next higher integer.}$$

The actual height occupied by this winding may be estimated as $11(0.8966 + t) \text{ mm}$ where t is the thickness of the layer interleaving material. Assuming $t = 0.1 \text{ mm}$ the primary winding height will be 11 mm.

The corresponding calculation for the secondary is as follows. Approximate overall conductor diameter, $d_o \approx (550/111)^{\frac{1}{2}} = 2.23 \text{ mm}$. The wire Tables A.1.1 and A.1.2.2 in Appendix A show that a suitable conductor diameter would be $d = 1.83 \text{ mm}$ (0.072 in). This has a maximum overall diameter of 1.943 mm. The maximum number of turns per layer is $50 \times 0.95/1.943 = 24.4$ and the number of layers is $111/24.4 = 4.55$. The actual winding height of the secondary, allowing for 0.2 mm interleaving, is $5(1.943 + 0.2) = 10.7 \text{ mm}$.

Allowing an extra 0.3 mm for the insulation and, if required, a screen between the windings, the total winding height is 22 mm. This is exactly equal to the maximum winding height assumed at the outset so it must be expected that the winding will be rather full. If a more generous margin is considered desirable the conductors of each winding may be reduced by one gauge. However, with heavy conductors the difference between adjacent standard diameters is rather large and it is often difficult to achieve well-balanced winding resistances within the height and winding resistance limitations.

If the mean turn length, 244 mm, is taken to apply to both windings, the winding resistances are

$$\begin{aligned}\text{Primary: } & 556 \times 0.03265 \times 0.244 = 4.43 \, \Omega \\ \text{Secondary: } & 111 \times 0.006449 \times 0.244 = 0.175 \, \Omega\end{aligned}$$

The second figure in each multiplication is the resistance of the conductor in ohms per metre obtained from Table A.1.1 in Appendix A. These figures are the room temperature values and are used for convenience. In a practical design the resistances at the working temperature would be calculated using the temperature coefficient of the resistivity, see Section 11.3, or more conveniently multiplying the 20°C values by the factor m (see the caption of Table 9.3). The errors introduced by taking the mean turn length to apply to each winding individually tend to cancel when the total winding resistance or loss is considered.

The total power loss:

$$\begin{aligned}\text{Primary winding loss: } I^2 R &= 1 \times 4.43 = 4.43 \text{ W} \\ \text{Secondary winding loss} &= 25 \times 0.175 = 4.38 \text{ W}\end{aligned}$$

$$\begin{aligned}\text{Core loss: } w_m V_c f &= 18 \times 10^{-9} \times 307 \times 10^3 \times 10^3 \\ &= 5.53 \text{ W}\end{aligned}$$

where w_m is the core loss density per cycle and has been assumed to be

$$18 \times 10^{-9} \text{ J} \cdot \text{mm}^{-3} \cdot \text{cycle}^{-1}, \text{ as in Fig. 9.10}$$

Total	14.34 W
-------	---------

This compares with a nominal total loss, P_{tot} , of 16.2 W, thus the transformer will be operating inside its nominal rating. It is interesting to note that the nominal total copper area of the primary is 288 mm² and, of the secondary, 292 mm². The sum of these copper areas divided by the total window area, A_w , 1800 mm², gives an overall copper factor, F_a , of 0.321. This compares with 0.30 assumed in compiling Table 9.3 and Fig. 9.10. The rather high value is due to the very full winding that has been fortuitously obtained and it accounts for the total loss being less than the nominal value.

The full load voltage drop in the winding resistance referred to the secondary side is

$$I_2(R_2 + R_1/r^2) = 5(0.175 + 4.43/25) = 1.76 \text{ V}$$

This is less than 1% of the open circuit secondary voltage and there is no need for turns adjustment on this account.

It remains to check the voltage drop due to leakage inductance. Using the formula in Fig. 11.18 and assuming the primary and secondary are simply wound one on top of the other then, referring the leakage inductance to the secondary side

$$\begin{aligned}N &= 111 & l_w &= 244 \text{ mm} \\ M &= 1 & Y &= 50 \text{ mm} \\ \Sigma x &= 11 + 10.7 = 21.7 \text{ mm} & \Sigma x_A &= 0.3 \text{ mm} \\ L_l &= 4\pi 10^{-4} \frac{12300 \times 244}{50} \left(\frac{21.7}{3} + 0.3 \right) \mu\text{H} \\ &= 570 \mu\text{H}\end{aligned}$$

The voltage drop across this reactance is $I_2 \omega L_l = 5 \times 2\pi \times 10^3 \times 570 \times 10^{-6} = 18 \text{ V}$. The output voltage at full load, ignoring winding resistance and assuming an induced e.m.f. of 200 V, is $\sqrt{(200^2 - 18^2)} \approx 199.2 \text{ V}$. Thus the voltage drop at full load due to the leakage inductance is 0.8 V which is also negligible. Had it been outside the limit so that a correction would have been required, it would be normal practice to increase the number of secondary turns to give the nominal output voltage at full load. If such adjustment is likely to be required it is an advantage for the secondary winding to have an incomplete last layer so that the extra turns may be easily accommodated. On the other hand if the leakage inductance were excessive it could be reduced by sandwiching the secondary between two sections of the primary, one above and one beneath, see Section 11.7.

Finally the magnetizing current may be checked. Assuming that the effective permeability of the core is 1000, the primary shunt inductance is

$$\begin{aligned}L_p &= \frac{\mu_0 \mu_e N^2}{C_1} = \frac{4\pi \times 10^{-7} \times 10^3 \times 556^2}{0.168 \times 10^3} \\ &= 2.31 \text{ H}\end{aligned}$$

\therefore the magnetizing current is

$$\begin{aligned}U_1/\omega L_p &= 10^3/6.28 \times 10^3 \times 2.31 \\ &= 0.069 \text{ A}\end{aligned}$$

which is quite satisfactory in relation to the primary full load current of 1 A.

This example illustrates the design procedure for a low frequency, saturation limited, power transformer. Had the design been loss limited the main difference would have been in the core selection. This would have been made in accordance with the procedure given in Section 9.4.4 and then the design would have proceeded as in this example, the core loss being calculated from $(R_p)_1$ obtained from Fig. 9.8.

9.5. HIGHER FREQUENCY POWER TRANSFORMERS

9.5.1. General

The power transformers discussed in this section are those in which eddy current considerations influence the design or performance of the windings. The actual frequency at which this occurs depends on the circumstances, e.g. a transformer designed to deliver 1 kW into 10Ω will have such thick conductors that the a.c. resistance may be as much as five times the d.c. resistance at frequencies as low as a few kilohertz, while on the other hand a transformer delivering relatively little power into a high impedance load might have negligible winding loss at several hundred kilohertz. In low power wide band transformers the attenuation limits the winding resistance but in power transformers it is more often the heat dissipation that is the limiting factor. Thus the higher the transmitted power the more important is the effect of eddy currents; high power implies high currents, and heavy conductors imply relatively high a.c. resistance due to eddy currents.

The design procedures for higher frequency power transformers are complicated by these eddy current losses in the windings. The methods of core selection described in the foregoing sections no longer apply and to some extent it is necessary to resort to trial and error methods. However a number of guiding principles are available to the designer. These will be discussed in the following sections.

Given proper data, the core performance is readily predictable but the winding gives rise to losses, leakage inductance and self capacitance all of which must be within limits if the transformer performance is to be satisfactory. Thus the optimum winding geometry usually presents the major problem in the design of a high frequency transformer.

Another general problem is cooling. If the transmitted power is large there will be an appreciable amount of power converted to heat. It is often impracticable to make the transformer large enough to dissipate this heat at a safe temperature by natural air convection; to meet leakage inductance and self capacitance specifications it is usually necessary to restrict the size. It follows, therefore, that more effective cooling methods, e.g. oil cooling, are usually used for H.F. high power transformers; the rate of heat transfer is a major design parameter.

9.5.2. Core selection

The majority of transformers operating in the higher frequency range will be core loss limited in the design. Possible exceptions are wide band transformers that have

to meet a severe attenuation or return loss specification at the lower end of the transmission band; in such cases the shunt inductance may determine the number of turns.

The higher frequency range has been defined as that in which eddy currents influence the winding design or performance. At the lower end of this range the transformers will not be very different in application or appearance to the low frequency transformers considered earlier in this chapter. They will probably be single frequency or narrow band devices, they will have windings that occupy a large proportion of the available winding space and the total cooling area will be approximately as expressed by A_e in Table 9.3. Under these circumstances the discussion of low frequency transformers in Section 9.4.4 is relevant.

Previous designs or other considerations may suggest that a particular core should be used. Where such guidance is not available it is inevitable that some guesses will have to be made. A guess may be made in choosing a probable core for a trial design, the first in a series of successive approximations. The alternative is to make a guess concerning the effect of eddy currents on the winding resistance. Basic data for estimating the a.c. winding resistance is given in Section 11.4.4. For a given winding it is possible to calculate the factor, F_R , by which the a.c. resistance exceeds the d.c. value. It depends on the conductor diameter, the geometry of the winding and the frequency; it may vary widely from one design to another. Some guiding considerations are discussed in the next section and from these it may be possible to guess a value for F_R . This may be included in Eqn 9.27:

$$\frac{P_o}{\sqrt{[F_a(R_p)_1]}} = \frac{P_{tot}}{4} \sqrt{\frac{A_a A_e}{\rho_c l_w l_e F_R}} = \frac{k_2}{\sqrt{F_R}}$$

As this method provides only a rough guide the factor m has for convenience been put equal to unity.

$$P_o \sqrt{\frac{F_R}{F_a(R_p)_1}} = k_2 \quad W.\Omega^{-\frac{1}{2}} m^{\frac{1}{2}} \quad (9.28)$$

If it is possible to make a reasonable guess for the ratio F_R/F_a the method of core selection becomes the same as that described in Section 9.4.4, i.e. a core is chosen that has a value of k_2 that is equal to or greater than the value calculated by Eqn 9.28, using Fig. 9.8 to estimate the value of $(R_p)_1$. The a.c. resistance factor has been coupled with the copper factor, F_a , because they both depend on the winding geometry. If the winding fills the available space so that $F_a \approx 0.3$ as assumed for low frequency transformers, the conductor diameter may be large enough to make F_R very high, e.g. 50. F_R may be reduced by using a smaller diameter; indeed it is shown in the next section that for least a.c. resistance F_R should be in the region of

1.5. A straightforward reduction of conductor diameter will also reduce F_a , hence the need to consider the two factors together. The use of bunched conductors to make eddy currents negligible would return the design to the low frequency category, i.e. $F_R \approx 1$, but the copper factor would be somewhat less than 0.3.

In Eqn 9.28, k_2 is a core constant that depends on the rate of heat transfer. The values quoted in Table 9.3 assume an average rate of heat dissipation of $300 \mu\text{W.mm}^{-2}$ (0.2 W.in^{-2}). If a different rate is proposed a correction must be made as described in Section 9.4.5.

A core having been selected, by one means or another, the trial design may proceed. Assuming the core is listed in a table such as 9.3 the permissible dissipation may be obtained from the appropriate column or, if the average rate of heat transfer differs from $300 \mu\text{W.mm}^{-2}$ (0.2 W.in^{-2}), the actual rate of heat transfer must be multiplied by the total cooling area to obtain the total dissipation. Some fraction of this, e.g. a half, may be allocated to the core and, from the core volume, the core loss density may be calculated. Using core loss data such as given in Fig. 3.19 a value of flux density may be obtained corresponding to the permissible core loss density at the operating frequency. If the transformer is to operate over a band of frequencies, this and the following steps should be made using frequencies corresponding to each end of the band so that the design may accommodate the worst case. From the frequency, flux density and terminal voltages the number of turns may be evaluated using the e.m.f. equation, e.g. Eqn 9.11.

A trial winding design may now be made, using the recommendations of the next section as a guide to the best conductor diameter. The d.c. winding resistance follows from Eqn 11.9. The factor F_R may be calculated for each portion of the winding according to the procedure described in Section 11.4.4 and the a.c. resistance of each winding may be obtained. For a wide band transformer with a maximum load current that is independent of frequency, the upper frequency limit must be used in calculating the a.c. resistances. The maximum power loss in the windings may now be calculated from the full-load currents and the a.c. winding resistances. If this is excessive, or in the wrong proportion to the core loss, a different core or winding arrangement must be used and the design process repeated until a satisfactory solution is found. If there is a minimum inductance limit, each design should be checked to ensure that this limit is not infringed. In some cases, e.g. wide band transformers operating at relatively low power, the inductance consideration overrides that of core loss in determining the number of turns and the design procedure approaches that described for wide band transformers in Section 7.3.2.

As explained at the beginning of this section, the foregoing remarks apply to transformers designed for the lower end of the higher frequency region. Attention may

now be turned to the situation at much higher frequencies. Transformers designed to operate at these higher frequencies differ appreciably in application and appearance to the previously considered low frequency transformers. They are usually required to transmit a band of frequencies, a typical bandwidth ratio being 10. They will consequently need to have low leakage inductance and low self capacitance, and so the windings will usually be designed as single layers, well spaced from the core and from each other. The cooling area will not therefore correspond to that used for low frequency transformers. To ease the problem of designing the winding to meet the high frequency specification it is necessary to restrict the size of the transformer. This usually entails a more effective means of heat transfer than free air convection; oil cooling is often used.

It follows from these considerations that H.F. power transformers tend to have an open construction in which the entire core surface can transfer heat directly to the convection medium. If this type of construction is assumed, the thermal balance of the core is almost entirely isolated from that of the winding and so the design of the core may be largely independent of the winding design.

It is assumed that the frequency and core size are such that, to avoid eddy current losses in the core, the choice of ferrite must be confined to the nickel zinc grades. To avoid an excessive core loss density at high frequencies it is usually necessary to restrict the flux density to quite low values, e.g. less than 10 mT (100 Gs). Under these conditions the residual loss is the main component of the magnetic loss in the core (see Section 2.2.5). Therefore the magnetic core loss density may be related to the residual loss factor by transposing Eqn 2.56:

$$P_m = \left(\frac{\tan \delta_r}{\mu} \right) \cdot \frac{\pi f \hat{B}_e^2}{\mu_0} \quad \text{W.m}^{-3} \quad (9.29)$$

The residual loss factor $(\tan \delta_r)/\mu$ is a function of frequency and temperature, see Figs. 3.12 and 3.13. The ferrite with the lowest residual loss factor under the appropriate conditions will be the most suitable. Given a grade of ferrite, Eqn 9.29 relates the core loss density to the flux density.

In the problem of core selection the starting parameters depend to some extent on the circumstances. One approach is to start with the core temperatures and base the selection on thermal equilibrium. To establish the relevant relations, a hypothetical core having a uniform circular cross-section of diameter d and a volume V may be considered. The temperature difference between the

$$(9.29) \quad P_m = \left(\frac{\tan \delta_r}{\mu} \right) \frac{f \hat{B}_e^2 10^{-7}}{4} \quad \text{W.cm}^{-3}$$

centre and the surface of the core is designated θ_{cs} and is related to the core loss density by Eqn 9.9:

$$\theta_{cs} = \frac{P_m d^2}{16\lambda} \quad ^\circ\text{C} \quad (9.30)$$

Assuming the flux density is uniform the total power dissipated in the core is $P_m V$ and at equilibrium this equals the total rate of heat transfer, i.e.

$$P_m V = P_{\text{conv}} A_c \quad \text{W} \quad (9.31)$$

where A_c is the surface area of the core

and P_{conv} is the heat transfer per unit area

Combining this in Eqn 9.30:

$$\begin{aligned} P_{\text{conv}} &= \frac{16V\lambda\theta_{cs}}{A_c d^2} \\ &= \frac{4\lambda\theta_{cs}}{d} \quad \text{W.m}^{-2} \end{aligned} \quad (9.32)$$

If d is in mm and λ for ferrite is $4000 \mu\text{W.mm}^{-1}.\text{C}^{-1}$:

$$P_{\text{conv}} = \frac{16 \times 10^3 \times \theta_{cs}}{d} \quad \mu\text{W.mm}^{-2} \quad (9.33)$$

If thermal considerations enable the designer to decide the temperature of the core surface and the temperature of the core centre these equations enable the corresponding diameter and core loss density to be determined. The method of heat transfer and the permissible surface temperature together determine the rate of heat transfer P_{conv} (e.g. see Fig. 9.3). The difference between the surface and centre temperatures equals θ_{cs} . Thus Eqn 9.33 yields d and Eqn 9.30 yields P_m and hence the flux density.

These parameters are not dependent on the total power to be transmitted because the only design criterion was temperature distribution. If the transformer is required to transmit a band of frequencies, the flux density calculation must be made at several frequencies within the band so that when the corresponding numbers of turns are subsequently calculated the limiting case, i.e. that yielding the largest number of turns, may be determined.

It is interesting to note that if, for the purpose of facilitating the H.F. aspects of the design, it is desired to minimize the length of the winding conductor then it is necessary to minimize πdN

or $d/\bar{B}A$ from Eqn 9.11

i.e. maximize $\bar{B}d$ since $A = \pi d^2/4$

or $\sqrt{P_m}d$ since $P_m \propto \bar{B}^2$ approx

Applying this to Eqn 9.30 it is clear that θ_{cs} should be made as high as thermal considerations will allow.

From the e.m.f. equation, the number of turns may be calculated and the subsequent winding design will

determine the winding breadth required. The cross-sectional area and the winding breadth having been determined, a suitable core may be selected. In practice a uniform cylindrical core will not normally be available and the selection will probably be made from a standard range having rectangular cross-sections, e.g. a range such as that shown in Table 9.3. Under these circumstances the core diameter, d , must be replaced by an effective cross-sectional dimension. Such values have been listed in Table 9.3 under the designation d_c . When the core has a double E shape the centre leg is the limb that will reach the highest temperature and therefore where appropriate d_c refers to this limb.

The above approach will lead to the selection of a suitable core provided the design is core loss limited. This is not always true; if the bandwidth is wide the minimum shunt inductance will determine the number of turns. Therefore when the core has been selected on magnetic loss considerations and the corresponding number of turns has been calculated, the shunt inductance must be checked using Eqn 4.18 and the value of C_1 for the selected core. If it is found that the inductance is insufficient to meet the attenuation or return loss specification a number of courses are open. It would, for example, be possible simply to increase the number of turns but this would probably make it more difficult to meet the leakage inductance and self capacitance requirements, and since it would lower the flux density it would result in the core being operated at temperatures lower than the permitted values. A better course is to repeat the design on a ferrite having a higher permeability. This will probably have a higher value of loss factor ($\tan \delta_r/\mu$) so the design approach starting from core temperatures will, in fact, result in a higher number of turns.

However, the number of turns required to obtain the specified inductance will be less than for the previous design because the permeability is higher. In principle it would be possible to balance the design so that the specified inductance and the specified core temperatures were simultaneously achieved, giving the most economical use of the core material.

If it is difficult to obtain sufficient heat transfer from the core, cooling ducts may be provided. When the core is made from units such as the U cores in Table 9.3 cooling ducts may easily be provided by spacing the units. For oil cooling the spacing should not be less than 3 mm (see Section 9.2.3).

So far all the core loss has been assumed as magnetic in origin. Where there are high frequency, high voltage terminals adjacent to the ferrite the intense electric fields can give rise to high dielectric losses in the core. The resultant local heating may fracture the ferrite. The remedy is to screen those parts of the core that are exposed to intense H.F. electric fields. The screens should

be applied in such a way as to avoid excessive interception of the magnetic fields, e.g. a cylindrical core might be covered by an earthed screen which is divided into narrow strips parallel to the axis. In the application of such screens the cooling of the core must not be impeded and the clearance to the winding must be adequate to prevent excessive capacitance or the chance of voltage breakdown.

Summarizing the problem of core selection for the higher frequency transformer, the temperature limitations will narrow the choice to cores of particular cross sectional dimensions (d_c in Table 9.3) and the inductance considerations may in addition determine the core factor C_1 . The final selection will depend on the winding; in particular the core must provide sufficient winding breadth. Some of the aspects of winding design will be considered in the next section.

9.5.3. Windings

In the context of this chapter the higher frequency range is defined as that in which copper eddy currents influence the winding design. As in the previous section the problem may be considered in two parts, starting with transformers for the lower frequency end of this range. In such transformers the windings will normally occupy an appreciable proportion of the winding space and usually an attempt will be made to relate the core and winding losses. The presence of eddy currents makes it difficult to estimate the latter in advance. The way in which this difficulty influences the choice of a core was considered at the beginning of the previous section. Assuming that a core has been selected for an initial design, the problem is to design the winding for minimum loss. Before considering this problem analytically it is instructive to apply the method of Section 11.4.4 to a given winding. For the purpose of illustration the example transformer design in Section 9.4.6 will be used and the a.c. resistance of the windings at an arbitrary frequency of 5 kHz will be calculated.

The simple winding arrangement shown in Fig. 11.9(a) will be assumed, so that each complete winding constitutes one winding portion. For each portion it is necessary to obtain the number of turns per layer, N_l , the effective conductor height, h , the layer copper factor, F_l , and the number of layers, p .

Considering the primary winding first, this consists of 556 turns of 0.813 mm (0.032 in) diameter copper wire. From the calculation in Section 9.4.6, $N_l = 53$, $p = 11$, and the d.c. resistance is 4.43 Ω . From Fig. 11.10, $h = 0.886 \times 0.813 = 0.72$ mm and from Eqn 11.27 $F_l = 53 \times 0.72/50 = 0.76$.

From Table 11.2, the penetration depth, Δ , for copper at 5 kHz and 20°C is 0.925 mm (in a practical design the

value of Δ would correspond to the working temperature). Thus the value of the variable in Fig. 11.11 is

$$\frac{h\sqrt{F_l}}{\Delta} = \frac{0.72\sqrt{0.76}}{0.925} = 0.68$$

From Fig. 11.11, putting $p = 11$, the value of F_R is about 3.9 so the a.c. resistance of the primary is $3.9 \times 4.43 = 17\Omega$.

Similarly for the secondary,

$$N_l = 24.4 \quad p = 5 \quad R_{dc} = 0.175 \Omega$$

$$h = 1.62 \quad F_l = 0.79$$

$$\therefore \frac{h\sqrt{F_l}}{\Delta} = 1.56$$

$$\therefore F_R = 13$$

and the a.c. resistance of the secondary is $13 \times 0.175 = 2.3\Omega$. It should be noted that in the earlier d.c. resistance calculation the mean turn length was assumed to be the same for both windings. For the simple arrangement where one winding is wound over the other this assumption leads to one winding resistance being lower than calculated and the other being higher. In the summation the error is cancelled. But when calculating the a.c. resistance, each d.c. winding resistance is in general increased by a different factor F_R and this can lead to error if the mean turn lengths for the two windings are significantly different. In such a case the mean turn length should be calculated for each winding; in the foregoing example this has been ignored for the sake of simplicity.

This example demonstrates that the eddy current loss in heavy gauge windings can be appreciable even at quite low frequencies. In this particular case considerable improvement could be obtained by changing the winding configuration to that shown in Fig. 11.9(b).

The problem of choosing the optimum conductor cross-section will now be considered analytically, extending Dowell's results⁹ described in Section 11.4.4 and elsewhere. First it is necessary to emphasize the significance of the parameter p . This is the number of layers in a winding portion as defined in Section 11.4.4. A winding portion is that part between the surface of a winding and the surface of zero m.m.f. (see Fig. 11.9). This may include the whole winding as in Fig. 11.9(a) or it may be half a winding as in the primary winding of Fig. 11.9(b). Thus a winding portion for which $p = 2.5$ will be half a 5-layer winding, i.e. it will occupy a winding height equal to 2.5 times the layer thickness. In all cases the layers are assumed to be complete: indeed incomplete layers invalidate the theory and should be avoided as they will give rise to excessive eddy current losses when only a few layers are used. Although the derivation involves a layer copper factor, F_l (see Eqn 11.27), if this

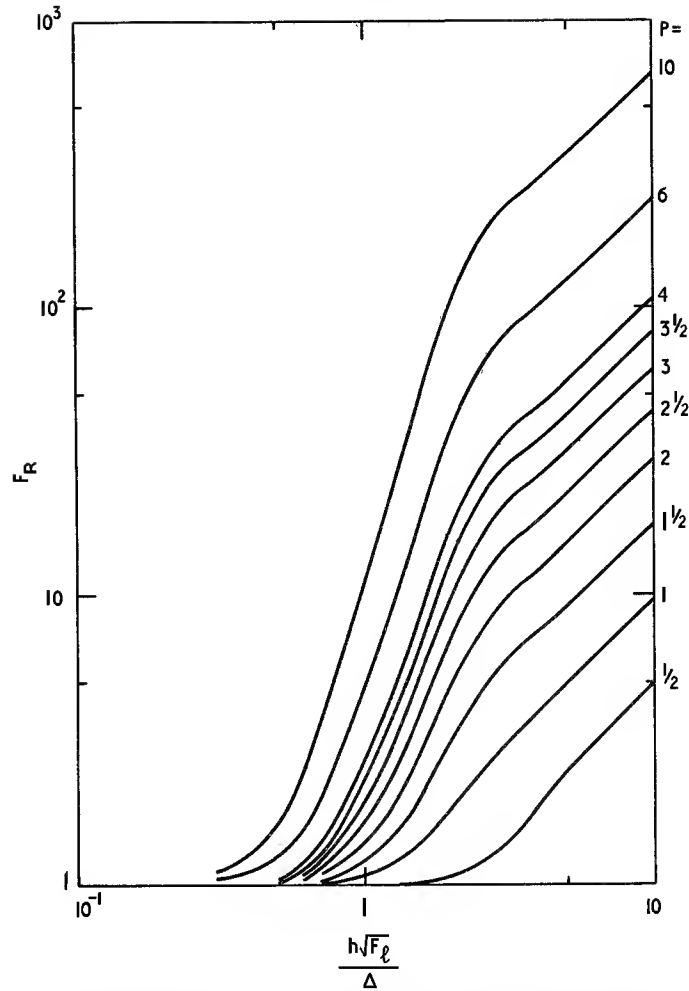


Fig. 9.11. Simplified version of Fig. 11.11; fractional rise in winding resistance due to eddy currents as a function of $h\sqrt{F_l}/\Delta$ with number of layers, p , per winding portion as a parameter

becomes too small, i.e. turns too widely spaced, the theory becomes unreliable.

The most interesting case is the close-packed multi-layer winding of N turns occupying a winding breadth b_w . Assuming solid round wire is to be used the problem is to determine the wire diameter that will give minimum a.c. resistance. Fig. 9.11 is a simplified version of Fig. 11.11 produced here for convenience. It is seen that each curve starts at the lower end by an upward curvature, then there is a steep straight portion and this is followed by a straight portion in which $F_R \propto h\sqrt{F_l}/\Delta$ (in the present context $h = 0.886 \times \text{copper dia.}$).

The a.c. resistance of the winding is $F_R R_{dc}$. For the close packed winding under consideration it may be seen from Section 11.3 that

$$R_{dc} \propto \frac{1}{h^2} \quad (9.34)$$

It follows that in the upper straight region of the curves

$$R_{AC} = F_R R_{dc} \propto \frac{1}{h} \quad (9.35)$$

so the largest possible conductor should be used. However when $h\sqrt{F_l}/\Delta$ is less than about 2 a different situation occurs. It is clear that the steepness of the curve will cause $F_R R_{dc}$ to be a minimum towards the lower curved region. In this region Dowell's expression for the curve may be approximated to

$$F_R = 1 + \frac{1}{45} (5p^2 - 1) \left[\frac{h\sqrt{F_l}}{\Delta} \right]^4 \quad (9.36)$$

$$\therefore R_{AC} \propto \frac{1}{h^2} \left\{ 1 + \frac{1}{45} (5p^2 - 1) \left[\frac{h\sqrt{F_l}}{\Delta} \right]^4 \right\} \quad (9.37)$$

Now $F_l = \frac{N_h}{b_w}$ (see Eqn 11.27)

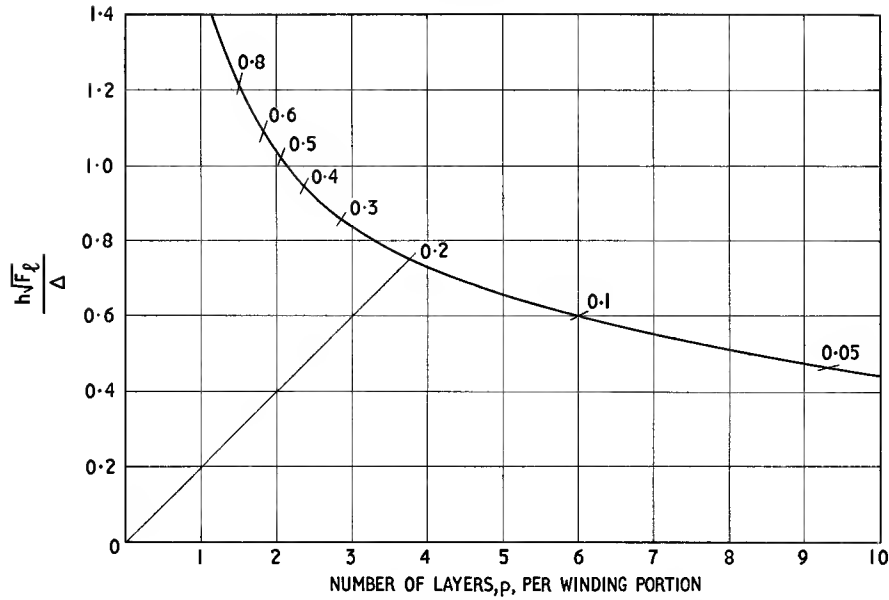


Fig. 9.12. $h\sqrt{F_l}/\Delta$ as a function of p for minimum high frequency resistance of a close packed winding of round wire. The marks are the intersects of the curve with straight lines from the origin having the indicated slope; the slope $= b_w F_l^{3/2}/N\Delta$. The latter function is calculable from given data; its intersection with the curve gives the optimum values of $h\sqrt{F_l}/\Delta$ and p

$$\therefore p = \frac{N}{N_l} = \frac{Nh}{b_w F_l} \quad (9.38)$$

$$\therefore R_{AC} \propto \frac{1}{h^2} + \frac{N^2 h^4}{9b_w^2 \Delta^4} - \frac{h^2 F_l^2}{45\Delta^4} \quad (9.39)$$

Differentiating this expression with respect to h and equating to zero, R_{AC} is minimum when

$$\left[\frac{h\sqrt{F_l}}{\Delta} \right]^4 = \frac{45}{10p^2 - 1} \quad (9.40)$$

If this is substituted in Eqn 9.36

$$\left. \begin{aligned} F_R &= 1 + \frac{5p^2 - 1}{10p^2 - 1} \\ &\rightarrow 1.5 \text{ when } p > 1 \end{aligned} \right\} \quad (9.41)$$

Thus as a general rule, when the conductor diameter cannot be so large that $d/\Delta \gg 2$, the diameter should be such that $F_R \approx 1.5$. To find the optimum diameter, the values of h and p must be found that simultaneously satisfy Eqns 9.38 and 9.40. The latter equation is plotted in Fig. 9.12 and the points are marked where the curve intersects with straight lines from the origin having various values of slope.

The slope of these lines is

$$\frac{h\sqrt{F_l}}{\Delta p} = \frac{h\sqrt{F_l}}{\Delta} \cdot \frac{b_w F_l}{Nh} = \frac{b_w F_l^{3/2}}{N\Delta} \quad (9.42)$$

from Eqn 9.38

N , b_w and Δ are known for the given winding at a given frequency, and $F_l \approx 0.78$ ($F_l^{3/2} \approx 0.69$) for a close-packed winding. Thus the required slope is readily calculated and hence p may be obtained. This should be rounded to the nearest integer for a simple winding, e.g. Fig. 11.9(a), or to the nearest (integer plus a half) for a winding having a zero m.m.f. surface at the centre. The optimum is not usually critical.

Having found the optimum number of layers, the conductor diameter may be calculated in the normal way assuming closely wound layers. As an example the windings considered earlier in this section will be optimized.

The starting data are

$$f = 5 \text{ KHz} \quad \therefore \quad \Delta = 0.925$$

$$b_w = 50 \text{ mm} \quad F_l^{3/2} = 0.69 \text{ (assumed)}$$

$$l_w = 244 \text{ mm (assumed the same for both primary and secondary)}$$

For the primary, $N = 556$ turns therefore

$$\frac{b_w F_l^{3/2}}{N\Delta} = \frac{50 \times 0.69}{556 \times 0.925} = 0.067$$

Constructing a line having a slope of 0.067 on Fig. 9.12, it intersects the curve at $p = 7.6$. Using $p = 8$ the data yields the following provisional values: $h\sqrt{F_l}/\Delta = 0.52$ and $F_R = 1.5$.

Making a conventional winding design using $p = 8$:

$$N_l = \frac{556}{8} \approx 69.5$$

\therefore the theoretical overall conductor diameter allowing a layer packing factor of 0.95 is given by

$$d_o = \frac{50 \times 0.95}{69.5} = 0.684 \text{ mm}$$

Referring to the Tables in Appendix A, the nearest suitable wire has a copper diameter, $d = 0.61 \text{ mm}$; the resistance, R_c , is $0.05804 \Omega \cdot \text{m}^{-1}$ and the diameter of medium enamelled covering is 0.686 mm . The resistance of this practical winding at 5 kHz may now be calculated as before:

$$h = 0.886 \times 0.61 = 0.540 \text{ mm}$$

$$F_l = 69.5 \times 0.540/50 = 0.751$$

$$\frac{h\sqrt{F_l}}{\Delta} = \frac{0.540 \times 0.867}{0.925} \approx 0.51$$

From Fig. 11.11, $F_R \approx 1.5$

The d.c. resistance $= N \cdot R_c \cdot l_w = 556 \times 0.05804 \times 0.244 = 7.87 \Omega$

$$\therefore R_{AC} = 1.5 \times 7.87 = 11.8 \Omega$$

This compares with 15.9 for the previous design, which used the largest possible wire diameter.

The corresponding calculation for the secondary is as follows:

$$N = 111 \text{ turns}$$

$$\frac{b_w F_l^{3/2}}{N \Delta} = \frac{50 \times 0.69}{111 \times 0.925} = 0.336$$

From Fig. 9.12 $p \approx 2.7$

Using $p = 3$, provisional data are

$$h\sqrt{F_l}/\Delta = 0.84$$

$$F_R \approx 1.5$$

Proceeding with a conventional winding design

$$N_l = \frac{111}{3} = 37$$

Theoretical value of $d_o \approx 1.28 \text{ mm}$

From the wire tables the most suitable wire has

$$d = 1.02 \text{ mm}, R_c = 0.0209 \Omega \cdot \text{m}^{-1} \text{ and } d_o = 1.11 \text{ mm}$$

Therefore the resistance of this secondary winding at 5 kHz is calculated as above

$$h = 0.886 \times 1.02 = 0.904 \text{ mm}$$

$$F_l = \frac{37 \times 0.904}{50} = 0.669$$

$$\frac{h\sqrt{F_l}}{\Delta} = \frac{0.904 \times 0.818}{0.925} = 0.80$$

From Fig. 11.11 $F_R \approx 1.45$

The d.c. resistance is $111 \times 0.0209 \times 0.244 = 0.566 \Omega$

$$\therefore R_{AC} = 1.45 \times 0.566 = 0.821 \Omega$$

This compares with 2.1Ω for the previous design.

Returning to the general case, if the indicated number of layers approaches unity a different situation exists. Because a partly filled layer is inadmissible the design must be based on one full layer, i.e. $p = 1$ or, if the zero m.m.f. surface divides the winding, $p = \frac{1}{2}$. Considering the curves for $p = 1$ and $p = \frac{1}{2}$ in Fig. 11.11 it is seen that almost the whole region above the lower curvature has a slope of approximately unity. Under these conditions it has been deduced (see Eqn 9.35) that $R_{AC} \propto 1/h$ so if round conductor is used it should have the largest possible diameter, i.e. allowing a layer packing factor of 0.95

$$d_o = \frac{0.95 b_w}{N} \quad (9.43)$$

If the single layer is to consist of conductor having rectangular cross-section, $b \times h$ (see Fig. 11.10), then $R_{dc} \propto 1/bh$. If the unity slope part of the F_R curve applies, $R_{AC} = F_R R_{dc} \propto 1/b$. So if $h\sqrt{F_l}/\Delta$ is less than about 2 the conductor thickness h should be increased until the part of the curve having unity slope is reached; further increase has no advantage because the current flows on or near only one of the conductor surfaces.

When the current flow is confined to a surface layer of effective thickness Δ the a.c. resistance is clearly given by $\rho_c N l_w / b \Delta$. Substituting from Eqn 11.15 and putting the relative permeability of the conductor equal to unity,

$$R_{AC} = \frac{N l_w}{b} \sqrt{(\pi \mu_o \rho_c f)} \quad \Omega \quad (9.44)$$

Thus $R_{AC} \propto \sqrt{\rho_c}$; a reduction of ρ_c reduces the d.c. resistance in proportion but this is partly offset by a decrease in penetration depth. Changing from copper to silver or silver plated conductor will reduce R_{AC} by a factor of approximately $\sqrt{0.96} \approx 0.98$.

So far windings of solid round or rectangular conductors have been considered. It might be deduced from the above considerations that a winding might have least a.c. resistance if it were wound in spiral form using foil of width equal to the net winding breadth. It has been found experimentally that such windings are unsatisfactory because (a) they are difficult to wind without accidentally producing shorted turns, and (b) if thin foil is used the copper factor is poor (the interleaving insulation may exceed the foil in thickness). The rise of resistance due to eddy currents can be quite small but is much greater than the value predicted by the above procedure. This is

$$(9.44) \quad R_{AC} = \frac{2\pi N l_w}{b} \sqrt{(\rho_c f 10^{-9})} \quad \Omega$$

probably due to eddy currents circulating in the surface of the foil, induced by convergent components of the field.

If the a.c. resistance of solid conductors cannot be made small enough then bunched conductors of the type used for inductors and described in Section 11.4.3 may offer advantage. A design procedure would be to calculate the maximum overall conductor diameter from the required number of turns and the net space available for the winding portion. From this the number of layers per portion may be deduced; this will be the minimum value of p . Since p and h (the effective strand diameter) are no longer related, the strand diameter may be chosen so that $h\sqrt{F_l}/\Delta$ gives $F_R \approx 1.5$ at the appropriate value of p in Fig. 11.11; a value of F_l must be assumed, e.g. 0.6. A bunched conductor may then be selected such that it has the required strand diameter and overall diameter.

Other winding properties, e.g. leakage inductance and self capacitance may be calculated from the relations given in Chapter 11. Concerning leakage inductance at high frequencies it should be remembered that the current flows on the conductor surface nearest the winding interface, i.e. nearest the maximum m.m.f. surface (see Fig. 11.9). When there is only one or a few layers this effect reduces the leakage inductance. It may easily be taken into account by making the dimensions Σx and Σx_A in Fig. 11.18 apply to the current configuration rather than that of the conductors.

The foregoing discussion of the design of windings for high frequency high power transformers has concentrated on the problems arising from eddy currents. The more usual design problems will probably be present also. Leakage inductance and self capacitance limits will normally have to be observed; Sections 11.6 and 11.7 provide data on these subjects. If a wide band return loss requirement is imposed, it is probable that a filter design technique such as that described in Section 7.2.5. will have to be used.

Finally the winding construction and insulation will need to be carefully chosen so that the windings will

adequately withstand the high frequency high voltage conditions to which they will be subjected.

REFERENCES AND BIBLIOGRAPHY

Section 9.2.

KING, W. J., 'The basic laws and data of heat transmission', *Mech. Engrg.*, **54**, 190, (Part 1), 275, (Part 2), 347, (Part 3), 410, (Part 4) and 492, (Part 5), (1932).

GROSSNER, N. R., 'Analysis of transient loading and heating of the electronic transformer', *Trans. I.E.E.E.*, **PMP3**, 30, (1967).

Section 9.2.2.

1. KING, W. J., (see above), table 1, p. 494.

Section 9.2.3.

2. KING, W. J., *ibid.*, p. 351.

3. KING, W. J., *ibid.*, p. 350.

4. BLUME, L. F., *et al.*, see General.

5. KING, W. J., (see above), p. 426.

6. KING, W. J., *ibid.*, p. 353.

Section 9.4.3.

7. MACFADYAN, K. A., see General.

Section 9.4.4.

8. MACFADYAN, K. A., see General.

Section 9.5.

WOOD, J., 'The design of H.F. baluns for high powers', *Electron. Engrg.*, **37**, 164, (1965).

Section 9.5.3.

9. DOWELL, P. L., 'Effects of eddy currents in transformer windings', *Proc. Instn. elect. Engrs*, **113**, 1387, (1966).

General

BLUME, L. F., BOYAJIAN, A., CAMILLI, G., LENNOX, T. C., MINNECI, S. and MONTSINGER, V. M., *Transformer engineering*, John Wiley and Sons, Inc., New York, (1951).

MACFADYAN, K. A., *Small transformers and inductors*, Chapman and Hall Ltd, London, (1953).

STAFF OF DEPT. ELECT. ENGG, M.I.T., *Magnetic circuits and transformers*, John Wiley & Sons, Inc., New York, (1943).

GROSSNER, N. R., *Transformers for electronic circuits*, McGraw-Hill Book Company, (1967).

Ferrite Antennas

10.1. INTRODUCTION

As domestic radio receivers became more portable and self-contained there was a trend towards the use of built-in antennas. At first these were frame windings consisting of a number of turns enclosing the largest available area within the dimensions of the receiver. The received signal was the e.m.f. induced in the winding by the magnetic component of the electromagnetic field. As receivers became smaller it became increasingly difficult to achieve sufficient sensitivity with frame windings. The difficulty was relieved by the introduction of ferrite cores. The dimensions of the winding could then be reduced to those of a small R.F. tuning coil and it could be provided with a high permeability core which could magnify by at least a hundred times the actual area enclosed by the winding. In this way sufficient sensitivity could be obtained within the dimensions of a very small receiver. Almost all A.M. broadcast receivers now manufactured are provided with ferrite antennas; indeed this is true not only of personal receivers but also of large radiograms where the ferrite antenna is a convenient means of avoiding external antenna connections.

The theory of cylindrical ferrite cores is considered in detail in Section 4.3. The basic relations are established and data concerning the magnetization of cylinders are

given. These results will now be applied to the use of ferrite cores specifically for antennas.

In practice the majority of antenna cores are cylindrical, but the dimensions of the receiver may be such that other shapes, notably a slab or plate, may be preferable. Although the following treatment is based on the use of cylindrical cores it applies in principle to cores of any cross section. This is also true of the definitions of μ_{rod} and μ_{coil} , but the data concerning these properties given in Section 4.3 will not in general apply to cores having cross sections departing appreciably from circular.

10.2. ANTENNA CIRCUIT THEORY

The approach used in this section is based on that used by Maanders and van der Vleuten.¹

10.2.1. Induced e.m.f., effective height

If a short circular winding of N turns enclosing an effective area A_N is placed in a uniform alternating magnetic field with the axis of the winding parallel to the field strength vector H , then the e.m.f., E_s , induced in it will, by the e.m.f. equation, be:

$$E_s = \mu_0 \omega H A_N N \quad \text{V} \quad (10.1)$$

If the aperture of the winding is now filled with a long ferrite cylinder coaxial with the winding and having its centre coinciding with the centre of the winding, then the flux density at the centre of the winding will, by the definition given in Section 4.3.1, be increased by the factor μ_{rod} . If the cross-sectional area of the rod is A then the total flux linking the winding will be $\mu_0 \mu_{\text{rod}} H A$ (neglecting the air flux that passes through any area difference between A_N and A). Therefore

$$E_s = \mu_0 \mu_{\text{rod}} \omega H A N \quad \text{V} \quad (10.2)$$

The strength of an electromagnetic field is usually expressed in terms of the electric field strength E . Using the fundamental relation:

$$H = \sqrt{\left(\frac{\epsilon_0}{\mu_0}\right)} E \quad \text{A.m}^{-1}$$

where E is in V.m^{-1}

$$\mu_0 H = \sqrt{(\mu_0 \epsilon_0)} \cdot E = \frac{E}{c_0}$$

where $c_0 = 1/\sqrt{(\mu_0 \epsilon_0)} = \text{velocity of electromagnetic waves in vacuo} \approx 3 \times 10^8 \text{ m.s.}^{-1}$

This may be substituted into the previous equation:

$$E_s = \mu_{\text{rod}} \omega E A N / c_0 \quad \text{V} \quad (10.3)$$

The effective height, h_e , of an antenna is defined as the ratio of the induced e.m.f. to the electric field strength:

$$h_e = \frac{E_s}{E} \quad \text{m} \quad (10.4)$$

Therefore for a ferrite rod antenna

$$\begin{aligned} h_e &= \mu_{\text{rod}} \omega A N / c_0 \\ &= \mu_{\text{rod}} 2\pi A N / \lambda \quad \text{m} \end{aligned}$$

where λ is the wavelength in m

If the winding is not short compared with the rod or if it is not central on the rod, the induced e.m.f. will be less than the value given by Eqn 10.3. The reduction is proportional to the e.m.f. averaging factor F_A ; this factor is defined in Section 4.3.2 and data are given which enable it to be estimated in certain cases. The foregoing equations may now be re-written in a more general form:

$$E_s = \mu_{\text{rod}} \omega E A N F_A / c_0 \quad \text{V} \quad (10.5)$$

$$\left. \begin{aligned} \text{and } h_e &= \mu_{\text{rod}} \omega A N F_A / c_0 \\ &= \mu_{\text{rod}} 2\pi A N F_A / \lambda \end{aligned} \right\} \quad \text{m} \quad (10.6)$$

$$(10.1) \quad E_s = \omega H A N 10^{-8} \quad \text{V}$$

$$(10.2) \quad E_s = \mu_{\text{rod}} \omega H A N 10^{-8} \quad \text{V}$$

10.2.2. Signal strength

The magnetic antenna described above behaves as a signal source having an e.m.f., E_s , and a reactance ωL . Associated with this reactance there will be a loss tangent, $\tan \delta$, which will arise from the radiation resistance and the losses in the winding and the core. The radiation resistance of a ferrite antenna is usually negligible compared with the losses. The estimation of losses will be considered in Section 10.3.3 but for the purpose of the present discussion it is sufficient to represent the losses, whatever their origin, by a shunt resistance, R_p , so that the unloaded Q -factor of the antenna is given by

$$Q = R_p / \omega L$$

The inductance of the antenna is usually resonated, at the frequency of the signal to be detected, by a capacitance, C . This resonant circuit is in general loaded by the first

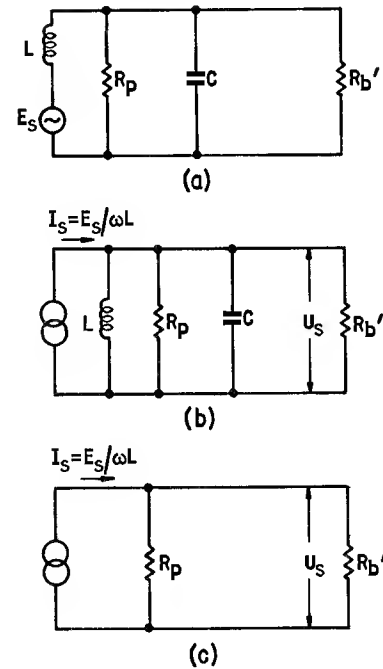


Fig. 10.1. Equivalent circuits of a rod antenna connected to a signal source

amplification stage of the receiver. Fig. 10.1(a) shows the equivalent circuit; for convenience the loss element R_p is shown in parallel with C . There may be, in practice, an impedance transformation between the capacitance and the load and this is usually achieved by connecting the load to a tap on the winding. However, in the following discussion this transformation will be ignored and R_b' will be defined as the load resistance referred to the primary circuit. If the amplification stage is voltage operated the value of R_b' is high so the antenna operates substantially

on open circuit. In a conventional circuit using semi-conductors, R'_b is usually comparable to R_p and the circuit design is governed by power transfer, noise or bandwidth considerations.

The presence of the load lowers the Q -factor to a loaded value denoted by

$$Q_L = \frac{R_p R'_b}{\omega L (R_p + R'_b)} \quad (10.7)$$

$$\text{Thus } \frac{Q_L}{Q} = \frac{R'_b}{R_p + R'_b} \quad (10.8)$$

The above circuit may be converted to the constant current equivalent (see Fig. 10.1(b), by applying Thevenin's theorem. Since at resonance $\omega L = -(1/\omega C)$ the circuit reduces to that shown in Fig. 10.1(c).

The signal voltage, U_s , developed across the load, R'_b , is given by

$$\begin{aligned} U_s &= I_s \frac{R_p R'_b}{R_p + R'_b} \\ &= \frac{E_s}{\omega L} \cdot \frac{R_p R'_b}{R_p + R'_b} = E_s Q_L \quad \text{V} \end{aligned} \quad (10.9)$$

This result is rather obvious; the e.m.f. induced in the antenna is magnified by the value of the loaded Q -factor. Thus the voltage appearing across the load referred to the primary will be Q_L times the e.m.f. given by Eqn 10.5:

$$U_s = \mu_{\text{rod}} \omega E Q_L A N F_A / c_o = E h_e Q_L \quad \text{V} \quad (10.10)$$

The voltage appearing at the terminals of the first amplifier stage will of course differ from U_s if there is an impedance transformation.

If the first stage of amplification is voltage operated then the maximum sensitivity will be obtained when the R.H.S. of Eqn 10.10 is a maximum i.e. when $h_e Q_L$ is maximum. For a given antenna loss, Q_L will be maximum when the circuit has negligible load ($R'_b \gg R_p$). If on the other hand the first stage is current operated, as in the case of a transistor, it is the power in the load that is of interest.

From Eqn 10.9

$$P_s = \frac{U_s^2}{R'_b} = \frac{E_s^2}{\omega^2 L^2} \frac{R_p^2 R'_b}{(R_p + R'_b)^2} = \frac{E_s^2 Q R_p R'_b}{\omega L (R_p + R'_b)^2} \quad \text{W} \quad (10.11)$$

where P_s is the signal power delivered to the load.

This will be a maximum when $R'_b = R_p$ i.e. when $Q_L = Q/2$. The maximum signal power that may be delivered to the load is:

$$(P_s)_{\text{max}} = \frac{E_s^2 Q}{4\omega L} = \frac{E^2 h_e^2 Q}{4\omega L}$$

In practice, bandwidth and signal/noise ratio considerations usually lead to $R'_b > R_p$. In either case the signal power is proportional to $h_e^2 Q$.

10.2.3. Noise power

Fig. 10.2 shows a source, having resistance R_p , connected to an active 4-pole having input resistance R'_b referred to the primary side of any transformer that may be in the circuit. A noise generator having an e.m.f. of r.m.s. value

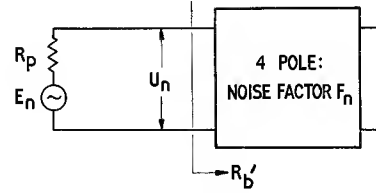


Fig. 10.2. An active 4-pole connected to a noise source

E_n is shown connected in series with R_p to represent the thermal noise due to the source resistance. The noise voltage is given by

$$E_n = \sqrt{(4kT\Delta f R_p)} \quad \text{V} \quad (10.12)$$

where k = Boltzmann's constant = $1.380 \times 10^{-23} \text{ J}^\circ\text{K}^{-1}$

T = temperature in $^\circ\text{K}$

Δf = bandwidth at the 3 dB points

If the 4-pole consisted of only a shunt resistor R'_b then the noise voltage U_n at the input terminals would simply correspond to that due to the thermal noise of a resistance equal to the parallel combination of R_p and R'_b :

$$U_n = \sqrt{\left(\frac{4kT\Delta f R_p R'_b}{R_p + R'_b} \right)} = E_n \sqrt{\left(\frac{R'_b}{R_p + R'_b} \right)} \quad \text{V} \quad (10.13)$$

However as the 4-pole in practice is an active device, e.g. an amplifier, the input resistance R'_b itself is not regarded as a noise source. Instead the 4-pole is said to have a noise factor F_n which may be defined by:

$$F_n = \left[\frac{\text{Output noise power due to source and 4-pole}}{\text{Output noise power if source was only noise contribution}} \right] \quad (10.14)$$

This ratio may also be expressed in decibels. Because R'_b is not regarded as a source of noise, the input noise voltage, U_n , due to the source E_n is given by

$$U_n = \frac{E_n R'_b}{R_p + R'_b} \quad \text{V} \quad (10.15)$$

and the input noise power is

$$P_n = \frac{U_n^2}{R'_b} = \frac{E_n^2 R'_b}{(R_p + R'_b)^2} \quad \text{W} \quad (10.16)$$

If the 4-pole contributes no noise and has a gain G , the output noise power is

$$\frac{GE_n^2 R'_b}{(R_p + R'_b)^2} \quad \text{W} \quad (10.17)$$

The noise factor, F_n , is the factor by which the output noise power of an actual 4-pole exceeds this value.

It is interesting to note that if the only source of noise in the 4-pole were a resistance corresponding to R'_b then from Eqn 10.13 the output noise power would be

$$\frac{GE_n^2}{R_p + R'_b} \quad \text{and then} \quad F_n = \frac{GE_n^2}{R_p + R'_b} \cdot \frac{(R_p + R'_b)^2}{GE_n^2 R'_b} = \frac{R_p + R'_b}{R'_b} \quad (10.18)$$

If, under these conditions, the source is matched to the 4-pole, i.e. $R_p = R'_b$, then $F_n = 2$ or alternatively this may be expressed as 3 dB.

In practice F_n may be greater or smaller than this value even if the input is matched since in an active 4-pole R'_b does not normally exist as a physical resistance and there will in general be gain and noise generation distributed in a complex manner throughout the network. For any active 4-pole, F_n is an approximately quadratic function of the source resistance R_p and has a minimum at a particular value of this resistance.

It follows from Eqns 10.14 and 10.17 that the noise power at the output of the 4-pole is

$$P_{no} = \frac{GE_n^2 R'_b}{(R_p + R'_b)^2} \times F_n = GF_n \frac{4kT\Delta f R_p R'_b}{(R_p + R'_b)^2} \quad \text{W} \quad (10.19)$$

It has been assumed that the only noise arising from the antenna is due to the loss resistance R_p . There will of course be noise induced in the aerial from the noise components of the electromagnetic field (atmospherics, etc.). However, this noise is transmitted through the antenna circuit in the same way as the signal, so its amplitude in relation to that of the signal is unaffected by the circuit design. Its only significance in the present context is that it can provide a measure of the relative importance of the thermal noise generated in the circuit.

10.2.4. Signal-to-noise ratio

It is readily seen from Eqn 10.11 that the signal power in the output of the 4-pole is

$$P_{so} = \frac{GE^2 h_c^2 Q R_p R'_b}{\omega L (R_p + R'_b)^2} \quad \text{W} \quad (10.20)$$

Therefore the signal-to-noise ratio is

$$\frac{P_{so}}{P_{no}} = \frac{E^2 h_c^2 Q}{4kT\Delta f F_n \omega L} \quad (10.21)$$

This expression applies to those stages of the receiver up to but not including the detector. The bandwidth Δf is the total bandwidth of the part of the receiver being considered.

After detection the signal-to-noise ratio may be shown to be²:

$$\left(\frac{P_{so}}{P_{no}} \right)_{AF} = \frac{m^2 E^2 h_c^2 Q}{4kT\Delta f F_n \omega L} \quad (10.22)$$

where m is the modulation factor of the signal, and Δf is the effective noise bandwidth of the receiver. For an input signal/noise ratio greater than 4, this bandwidth may be taken as twice the audio frequency bandwidth.

For the maximum signal-to-noise ratio the antenna circuit should have the highest possible value of $h_c^2 Q/F_n$. The effective height is limited by the permissible size of the antenna, the noise factor may be minimized by proper choice of source resistance referred to the input of the 4-pole, and the unloaded Q -factor is limited by the bandwidth requirements or the impedance requirements or the losses in the antenna.

10.2.5. Bandwidth and impedance requirements

The bandwidth at the 3 dB points is given by the well-known relation:

$$\Delta f = \frac{f}{Q_L} \quad (10.23)$$

so from Eqn 10.8

$$\Delta f = \frac{f(R_p + R'_b)}{Q R'_b} \quad (10.24)$$

To obtain the best compromise between the various requirements, an impedance transformation is required

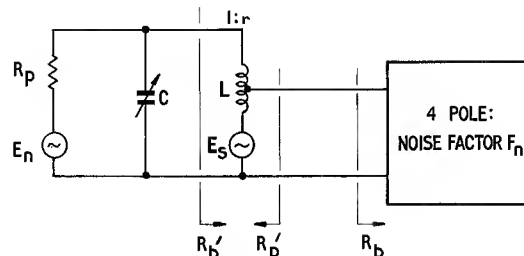


Fig. 10.3. The equivalent circuit of a rod antenna having both signal and noise sources, and connected to an active 4-pole

between the antenna and the input of the 4-pole. This is shown in Fig. 10.3, where the transformation, of voltage ratio r , is obtained by tapping into the antenna winding L , (tight coupling is assumed). C is the resonating capacitor; the choice of a convenient value for C will usually

determine the value of L and hence the number of primary turns. R_b is determined by the design of the 4-pole (the 4-pole being a thermionic or semiconductor amplifier or frequency changer), R'_p is the value of source impedance that will make the noise factor minimum and R_p is determined by the losses in antenna and the number of turns on the antenna winding.

Re-writing Eqn 10.8 for the secondary side of the transformer:

$$Q_L = \frac{QR_b}{r^2 R_p + R_b}$$

$$\text{since } R_b = r^2 R'_p$$

$$\therefore Q_L = \frac{QR_b}{R'_p + R_b}$$

$$\therefore Q = \frac{Q_L(R'_p + R_b)}{R_b} \quad (10.25)$$

All the quantities on the R.H.S. of this equation are determined by bandwidth or impedance requirements, so the unloaded Q -factor may be calculated. From this value, R_p may be obtained:

$$R_p = \omega L Q \quad \Omega \quad (10.26)$$

where L is determined by the tuning requirements. Finally the transformation ratio is calculated:

$$r = \left(\frac{R'_p}{R_p} \right)^{\frac{1}{2}} \quad \text{assuming tight coupling.} \quad (10.27)$$

These conditions may be met, in general, only at one frequency since r cannot be varied with frequency within a given band. It is usual to obtain the best design at the middle of a broadcast band and accept some departure from optimum as the frequency departs from mid-band. For another broadcast band a separate antenna circuit is designed, the additional winding usually being placed on the same antenna rod.

10.2.6. A design example

To illustrate the antenna circuit theory, a basic design will be derived using the data provided in the paper by Maanders and van der Vleuten.¹

The 4-pole is assumed to have an OC170 or AF125 transistor as a mixer at the input. At 1 MHz the input resistance is 2,500 Ω , and the noise factor has a minimum of 2.75 when the source resistance is 400 Ω , i.e.

$$R_b = 2500 \Omega$$

$$F_n = 2.75 \text{ (4.4 dB)}$$

$$R'_p = 400 \Omega$$

It is assumed that the broadcast band extends from 0.5 to 1.5 MHz and that at 1 MHz, the value of Δf is 10 kHz. From Eqn 10.23 $Q_L = 100$. From Eqn 10.25

$$Q = 100 \frac{(400 + 2500)}{2500} = 116$$

From Eqn 10.26, assuming $L = 200 \mu\text{H}$

$$R_p = 6.28 \times 10^6 \times 200 \times 10^{-6} \times 116 = 1.46 \times 10^5 \Omega$$

\therefore from Eqn 10.27

$$r = \left(\frac{400}{1.46 \times 10^5} \right)^{\frac{1}{2}} = 1/19$$

Fig. 10.4 shows a typical graph of F_n against source resistance (R'_p) for an OC170 or AF125 transistor at 1 MHz. R'_p and Q are related by Eqn 10.25; putting $Q_L = 100$ (10 kHz bandwidth) and $R_b = 2500 \Omega$, the values of Q corresponding to R'_p may be calculated and these have been marked off along the abscissa. (From Eqn 10.27 the turns ratio is also a function of R'_p .) From Eqn 10.21 the signal-to-noise ratio is proportional to Q/F_n . For each value of Q the ratio Q/F_n has been calculated and plotted.

For maximum signal-to-noise ratio the unloaded Q -factor (i.e. 120 from Fig. 10.4) is somewhat higher than the above Q -factor calculated for minimum F_n , but it is much less than for the condition of maximum signal (which is $Q = 2Q_L$). Often a compromise is made; Fig. 10.4 shows that Q may be raised towards 200 without too great a loss of signal-to-noise ratio, e.g. $Q = 140$ would be a reasonable compromise. This would make $R'_p = 1000$, $R_p = 1.76 \times 10^5$ and $r = 1/13.3$.

As stated above, when the frequency differs from the value used in the circuit design the performance will differ from that calculated. Considering only the bandwidth, adjacent channel selectivity requirements usually limit the bandwidth of the I.F. amplifier in small receivers to about 8 kHz, and the bandwidth of the antenna circuit need not appreciably exceed this value. Thus for best overall performance the antenna circuit bandwidth should be constant over the broadcast band, i.e. f/Q_L should be constant. Therefore from Eqns 10.8 and 10.26

$$Q = Q_L \left(\frac{\omega L Q}{R_b} + 1 \right) = \frac{Q_L}{1 - \frac{Q_L \omega L}{R_b}}$$

For $L = 200 \mu\text{H}$, $R_b = 2500 \Omega$ (assumed const.), $Q_L = f/10^4$ and $r = 1/19$

$f(\text{MHz})$	Q_L	Q
0.5	50	52
1.0	100	116
1.5	150	218

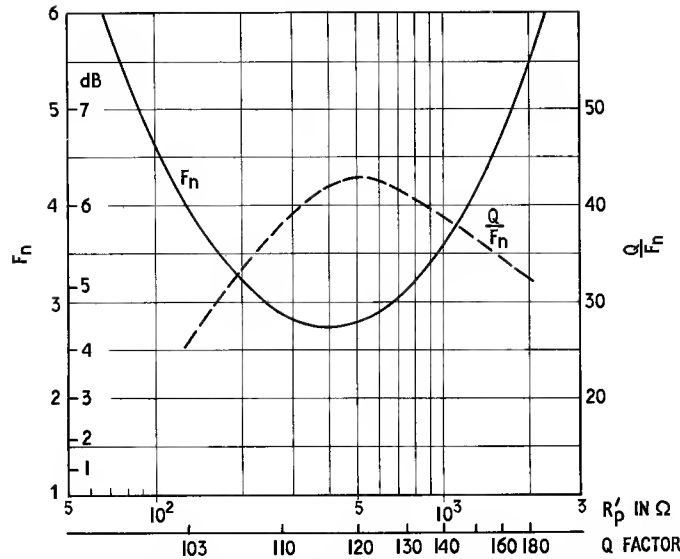


Fig. 10.4. Noise factor, F_n , as a function of source resistance, R'_p , for a transistor type OC170 or AF125 operating as a frequency changer at 1 MHz. The abscissa has been scaled in terms of Q using Eqn 10.25 putting $Q_i = 100$ (10 kHz bandwidth at 1 MHz) and $R_p = 2,500 \Omega$. A curve of Q/F_n (proportional to signal-to-noise ratio) has been added

Within the limitations of present-day ferrites and the permissible rod dimensions it is not possible to obtain a Q -factor that rises with frequency in this way, so the ferrite antenna usually has excessive bandwidth at the upper end of the medium wave broadcast band.

In the long wave band, e.g. at 200 kHz, a bandwidth of 10 kHz requires a Q -factor of not more than 20. In practice a value nearer 30 is used and usually the antenna circuit has to be artificially degraded to restrict the Q -factor to this value.

If the amplifier or frequency changer is voltage operated, as in the case of a thermionic circuit, the situation is a little different. Since such a circuit imposes negligible load on the antenna, $Q \approx Q_L$. Thus for the same bandwidth the value of Q will need to be a little lower than for the loaded case.

10.3. PRACTICAL ASPECTS OF DESIGN

10.3.1. General

It has been seen (Eqn 10.21) that for the greatest signal-to-noise ratio, $h_e^2 Q/L$ should be as large as possible. It was subsequently shown that Q and L are often determined by requirements of bandwidth and tuning respectively. Thus the primary considerations in ferrite antenna design are:

- (i) The effective height should be as large as possible within the permissible dimensions.
- (ii) The unloaded Q -factor should be reasonably near the design value.

- (iii) The inductance of the winding should be as close as possible to the design value.

In addition there may be a secondary consideration, e.g. the temperature coefficient of inductance will, in general, have to be within specified limits.

These factors will now be studied from the design point of view.

10.3.2. Maximum effective height

From Eqn 10.6, the effective height:

$$\left. \begin{aligned} h_e &= \mu_{\text{rod}} \omega A N F_A / c_0 \\ \text{or } \mu_{\text{rod}} 2\pi A N F_A / \lambda \end{aligned} \right\} \quad \text{m}$$

The number of turns N and the e.m.f. averaging factor F_A are usually determined by the inductance and temperature coefficient requirements and are not variables in the attainment of maximum effective height.

Therefore:

$$h_e \propto \mu_{\text{rod}} A \quad (10.28)$$

It is shown in Section 4.3.1 that μ_{rod} depends on the permeability of the rod material and the length/diameter ratio, m , of the rod. Fig. 4.9 shows the relations. For maximum μ_{rod} the ferrite permeability should be high and the rod should be long compared with its diameter, d . However, considering only μ_{rod} , the graph shows that for a given ferrite permeability there is a limit to the useful increase in m while for a given value of m there is a limit to the useful increase in ferrite permeability.

Table 10.1. PROPERTIES OF SOME TYPICAL FERRITE ANTENNA RODS

This table illustrates the influence of factors that affect the effective height. The effective height is based on a frequency of 1 MHz and a short central winding of 40 turns ($F_A = 1$). Such a winding would have an inductance between 200 μ H and 400 μ H depending on which of the rods is used.

μ	l	d	m	N	μ_{rod}	A	h_e	Vol	h_e/Vol
	mm in	mm in	l/d			m^2	m	m^3	m^{-2}
175	200 8	9.5 0.375	21	0.0043	100	71×10^{-6}	5.9×10^{-3}	14.2×10^{-6}	420
175	200 8	12.7 0.50	15.8	0.0070	79	127×10^{-6}	8.4×10^{-3}	25.4×10^{-6}	330
175	150 6	9.5 0.375	15.8	0.0070	79	71×10^{-6}	4.7×10^{-3}	10.7×10^{-6}	440
175	150 6	12.7 0.50	11.8	0.0112	59	127×10^{-6}	6.3×10^{-3}	19.1×10^{-6}	330
500	200 8	9.5 0.375	21	0.0045	159	71×10^{-6}	9.5×10^{-3}	14.2×10^{-6}	670
500	200 8	12.7 0.50	15.8	0.0073	111	127×10^{-6}	11.8×10^{-3}	25.4×10^{-6}	460
500	150 6	9.5 0.375	15.8	0.0073	111	71×10^{-6}	6.6×10^{-3}	10.7×10^{-6}	620
500	150 6	12.7 0.50	11.8	0.0115	76	127×10^{-6}	8.1×10^{-3}	19.1×10^{-6}	420

From Eqn 10.28, it is the product $\mu_{\text{rod}} A$ that should be maximized. Referring again to Fig. 4.9 it is seen that none of the curves has a slope as steep as 2, therefore the quotient μ_{rod}/m^2 ($= \mu_{\text{rod}} d^2/l^2$) increase monotonically as m decreases. It follows that, for a given length, l , the products $\mu_{\text{rod}} d^2$ and $\mu_{\text{rod}} A$ increase as the diameter is increased.

The maximum effective height is therefore obtained when the ferrite material has the highest permeability consistent with loss limitations, the length of the rod is the maximum permitted by the space limitations and the diameter is as large as weight and cost considerations will allow.

If the maximum effective height per unit core volume is required it is necessary to maximize $\mu_{\text{rod}} A/l d^2$, i.e. maximize μ_{rod}/l . From Eqn 4.65:

$$\frac{\mu_{\text{rod}}}{l} \approx \frac{1}{l \left(\frac{1}{\mu} + N \right)}$$

Fig. 4.8 shows N as a function of m for various magnetic bodies. For rods and similar bodies N decreases as m increases, therefore μ_{rod}/l will increase as m becomes larger. It follows that for a given rod length the maximum effective height per unit core volume will be obtained when the rod is as thin as possible. Alternatively if the value of m is fixed the effective height per unit core volume will increase as the rod becomes shorter.

Some of these relations are illustrated numerically in Table 10.1 in which the calculated properties of some typical antenna rods are shown.

Brief mention may be made at this point about the possible use of tubular cores. If a given ferrite rod is made into a tube of the same overall dimensions, the value of μ_{rod} does not change nor does the flux density in the central portion of the ferrite tube. Therefore the total flux due to a given field is diminished in the ratio of the ferrite cross-sectional areas. It follows that in the expression for the effective height the value of A must be that of the cross-sectional area of the tube. Thus for the same overall dimensions the tube will give a smaller effective height. The volume of material would be better utilized in a rod of the same length and cross-sectional area as this would have a larger value of m and therefore a higher μ_{rod} . If the rod becomes too slender then mechanical considerations would invalidate this conclusion.

10.3.3. Unloaded Q-factor

The Q -factor of a resonant circuit is the reciprocal of the sum of all the contributory loss tangents. If the inductive element is a rod antenna the principal loss tangents to be considered are:

- (a) $(\tan \delta_m)_{\text{rod}}$ = loss tangent due to magnetic losses in the rod.
- (b) $\tan \delta_{\text{AC}}$ = loss tangent due to total (a.c.) copper losses
- (c) $\tan \delta_{\text{rad}}$ = loss tangent due to radiation
- (d) $\tan \delta_{\text{mc}}$ = loss tangent due to the magnetic coupling of the rod to adjacent conductive parts e.g. metal supports or chassis.

Table 10.2. UNLOADED Q-FACTORS OF TYPICAL ANTENNA RODS

Q is the value measured with the rod in isolation

Q' is the value measured with the rod *in situ* in a receiver.

Winding details:

L = 200 μ H, N = 44 turns for B2 ferrite
= 37 turns for A10 ferrite

Winding was short and central

Rod details:

Length = 200mm (8 in)

Diameter = 9.5mm (0.375 in)

Ferrite grade	Frequency MHz	Bunched Conductors									
		45		28		20		12		8	
		strands of 0.0016 in (0.04 mm) dia. copper									
		Q	Q'	Q	Q'	Q	Q'	Q	Q'	Q	Q'
B2 or 4B	0.5	282	125	234	122	221	117	180	108	142	92
	0.75	272	133	238	131	231	128	199	120	165	107
	1.0	246	130	222	128	215	128	191	120	164	111
	1.2	206	120	193	118	191	118	172	112	150	107
	1.5	170	105	175	105	166	105	154	98	140	96
A10 or 3D3	0.5	376	136	316	128	274	125	228	112	166	98
	0.75	332	145	300	140	260	137	238	127	188	114
	1.0	256	145	246	142	232	140	212	131	179	121
	1.2	195	140	191	135	182	135	172	127	153	119
	1.5	135	128	135	125	128	125	125	119	120	113
		Solid copper wire (approx. dia.)									
		0.0164 in 0.4 mm		0.0116 in 0.3 mm		0.0076 in 0.2 mm		0.0060 in 0.16 mm		0.0048 in 0.12 mm	
B2 or 4B	0.5	163	87	180	106	204	112	190	109	153	97
	0.75	149	89	172	109	200	115	197	118	172	110
	1.0	140	88	159	107	185	112	186	118	172	112
	1.2	126	82	143	100	164	104	168	110	158	108
	1.5	112	73	126	89	140	93	145	99	140	97
A10 or 3D3	0.5	195	94	240	109	260	115	238	113	187	101
	0.75	183	100	216	112	252	121	241	124	205	115
	1.0	163	100	186	112	212	121	210	126	192	122
	1.2	141	97	155	107	181	117	179	122	165	118
	1.5	114	92	124	101	137	110	137	113	133	112

All of these losses depend on the distribution of the flux density along the rod due to current in the winding. This distribution is in general different from and independent of the distribution of flux density due to the magnetic component of the incident electromagnetic field. This is because the e.m.f. induced in the winding by the incident field has a phase that is 90° in advance of that of the incident field. If the winding is at resonance the current is in phase with this e.m.f. so the resultant secondary or self-induced field is in quadrature with the incident field. Thus the e.m.f. that energizes the circuit arises wholly from the incident field, while the secondary or self-induced field determines the inductance and magnetic loss associated with the winding.

The calculation of $(\tan \delta_m)_{\text{rod}}$ has been discussed in some detail in Section 4.3.5; its value may readily be obtained

from a knowledge of the loss tangent of the material and the geometry of the rod. The loss tangent of the material of a given rod may be obtained by measurement in the following way. The rod is closely wound along its entire length with a bunched conductor composed of many strands of fine wire, so chosen that the copper loss may be neglected. This may be checked by subsequently replacing the winding with another using a conductor having a somewhat higher H.F. resistance and ensuring that the measured loss tangent is unaffected. Provided $\tan \delta_{\text{rad}}$ and $\tan \delta_{\text{mc}}$ are negligible the measured loss tangent will equal $(\tan \delta_m)_{\text{rod}}$. The material loss tangent may then be calculated from Eqn 4.73. This value may then be used in evaluating $(\tan \delta_m)_{\text{rod}}$ for more practical winding configurations.

The prediction of $\tan \delta_{\text{AC}}$ is difficult. This loss tangent

depends on the H.F. resistance of the winding which in turn depends on the type of conductor, the shape of the winding and the configuration of the secondary magnetic field. An adequate method of evaluating this loss would require a large amount of empirical data and the results would probably be too unwieldy for convenient use. As a guide, the discussion of copper losses in the chapter on inductors (Section 5.7.3) may be consulted in conjunction with Section 11.4. The principles established in these sections will indicate in a general way how a given copper loss will be influenced by a given change in conductor composition or configuration. A practical difficulty is the isolation of the copper loss for the purpose of measurement. This may be overcome by using a rod of known material loss angle and calculating the value of $(\tan \delta_m)_{\text{rod}}$. If $\tan \delta_{\text{rad}}$ and $\tan \delta_{\text{mc}}$ are made negligible, the value of $\tan \delta_{\text{AC}}$ may be obtained by subtracting $(\tan \delta_m)_{\text{rod}}$ from the measured loss tangent. In practice it is not difficult to make the winding loss small compared with the core loss, although economy may dictate a design or type of conductor for which the winding loss is by no means negligible.

The value of $\tan \delta_{\text{rad}}$ is always negligibly small. This follows from the fact that the effective height (see Section 10.2.1 and Table 10.1) is always very much smaller than that of the equivalent dipole antenna.

In practice the loss due to the proximity of conductive parts is usually quite large. In the lay-out of a portable radio receiver it is always essential to make a compact assembly, indeed the main advantage of a ferrite antenna is that it may be contained physically in quite a small volume. It is therefore inevitably placed near other components and metal parts. The resultant degradation of performance compared with that obtained when the rod antenna is isolated may amount to a doubling of the total loss tangent, i.e. a halving of Q -factor.

Because of this last consideration there seems to be little point in elaborating on methods of calculating Q -factor. The usual procedure is to make a trial winding giving the required inductance. For A.M. broadcast bands the conductor usually consists of a number of strands, e.g. 24, of 0.0016 in (0.04 mm) dia. wire. The Q -factor may then be measured in isolation and *in situ*; if a higher Q -factor is required the number of strands may be increased or the length of the winding reduced. The magnetic loss in the rod eventually limits the Q -factor that may be obtained.

The effect on the Q -factor of varying the length of the winding may be deduced from Eqns 4.73, 4.74 and 4.76. The longer winding gives the higher value of $(\tan \delta_m)_{\text{rod}}$ because the flux density distribution is more uniform or, putting it in a different way, μ_{coil} is higher.

As examples of unloaded Q -factors, Table 10.2, shows results quoted by Maanders and van der Vleuten¹ for various rod antennas in both isolated and *in situ* positions.

10.3.4. Inductance

The inductance of a winding centrally placed on a ferrite cylinder has been considered in Section 4.3.4. From Fig. 4.12 the inductance of any central winding on any rod may be estimated with reasonable accuracy. An experimental winding based on such an estimate may be made and its inductance measured; the number of turns may then be altered if necessary. Final adjustment is often made by moving the winding along the rod until the correct inductance is obtained.

It is quite common for one rod to be used for two frequency bands. In such cases it is usual to place one winding towards one end of the rod and the other winding towards the other end of the rod. A winding that is midway between the centre and the end of the rod will have about 10% less inductance than the same winding placed centrally.

10.3.5. Temperature coefficient

From Eqn 4.77 the temperature coefficient of inductance of a winding on a ferrite rod is given approximately by:

$$(T.F.) \times \mu_{\text{coil}}$$

where T.F. is the temperature factor, $\Delta\mu/\mu^2\Delta\theta$, of the ferrite and is a material parameter. If μ_{coil} is 20 and T.F. is $10 \times 10^{-6} \text{ } ^\circ\text{C}^{-1}$ then the temperature coefficient

$$\frac{\Delta L}{L\Delta\theta} = 200 \text{ ppm}/^\circ\text{C}$$

The temperature coefficient of frequency, assuming that the temperature coefficient of the resonating capacitance is negligible,

$$\frac{\Delta f}{f\Delta\theta} \approx -\frac{1}{2} \frac{\Delta L}{L\Delta\theta} \quad \text{since } f \propto L^{-\frac{1}{2}}$$

$$= -100 \text{ ppm}/^\circ\text{C} \text{ for the above example. If } \Delta\theta \text{ is } 20^\circ\text{C} \text{ and } f \text{ is } 1 \text{ MHz, } \Delta f \text{ is } -2 \text{ kHz.}$$

The temperature coefficient may be somewhat reduced by reducing the length of the winding in relation to the length of the rod; this reduces μ_{coil} .

REFERENCES AND BIBLIOGRAPHY

Section 10.2.

1. MAANDERS, E. J., *et al.*, see General.

Section 10.2.4.

2. BLOCK, H. and RIETVELD, J. J., 'Inductive aerials in modern broadcast receivers', *Philips tech. Rev.*, **16**, 181, (1955).
- BAELDE, A., 'Theory and experiments on the noise of transistors', *Philips Res. Rep. Supplement No. 4*, (1965).

- MEYER, R. G., 'Noise in transistor mixers at low frequencies', *Proc. Instn elect. Engrs*, **114**, 611, (1967).

Section 10.2.6.

1. MAANDERS, E. J., *et al.*, see General.

General

- VAN SUCHTELEN, H., 'Ferroxcube aerial rods', *Electron Applic. Bull.* **13**, 88, (1952).
- CRAWTHORNE, M. J., 'Ferroxcube aerial rods for medium and long wave reception', *Mullard tech. Commun.*, **1**, 181, (1954).
- GRIMMETT, C. A., 'Ferrite cored antennae', *Conv. Rec. Inst. Radio Engrs*, **2**, Part 7, 3, (1954), also *Proc. Instn Radio Engrs Aust.* **16**, 31, (1955).
- 'Ferroxcube aerial rods for medium wave reception', *Matronics*, no. 3, 41, (1953).
- DUPUIS, J., 'Cadres utilisant des ferrites', *Onde élect.*, **35**, 379, (1955).
- POLYDOROFF, W. J., 'Magnetic field antenna', *Electron. Inds*, **17**, no. 3, 66, (1958).
- WRIGHT, C. M., 'Ferrite rods for broadcast receiver antenna coils', *Proc. Instn Radio Engrs Aust.*, **21**, 410, (1960).
- MAANDERS, E. J. and VAN DER VLEUTEN, H., 'Ferrite aerials for transistor receivers', *Matronics*, no. 18, 354, (1961).
- NILSEN, O. K., 'A nondirectional ferrite rod antenna arrangement suitable for A.M. radios', *Proc. Inst. Radio Engrs*, **49**, 1222, (1961).
- POLYDOROFF, W. J., 'Recent advances in ferromagnetics', *Electronic Inds*, **20**, no. 9, 102, (1961).
- LAURENT, H. J. and CARVALHO, C. A. B., 'Ferrite antennas for A.M. broadcast receivers', *Trans. Inst. Radio Engrs*, **BTR-8**, no. 2, 50, (1962).
- 'Ferrite und Ferritantennen', *Radio Fernsehen*, 660, (1962).
- SHIEFER, G., 'A small ferroxcube aerial for VHF reception', *Philips tech. Rev.*, **24**, 332, (1962-63).
- HUMPHREY, L. C., 'Design of ferrite-cored antennas', *Solid St. Des.*, **5**, no. 1, 24, (1964).
- BITTERLICH, W., 'Magnetische Dipolantennen für Feldstärkemessungen im LF- und VLF-Bereich', *Elektron. Rdsch.* **21**, 225, (1967).

Properties of Windings

11.1. INTRODUCTION

The ferrite manufacturer usually supplies his product as a set of ferrite parts and possibly ancillary parts from which the user may construct a wound component to meet specific requirements. The winding, with all its possible variety in design and execution, is usually the concern of the user. In this the magnetic component differs from other electrical components. Whereas a resistor or a capacitor leaves the manufacturer as a finished and tested component, the quality of a wound magnetic component depends on both the core manufacturer and the user.

The core manufacturer normally provides data on the magnetic properties of the core; these are the properties that he can test and control. Where the application of the core involves a well-established design technique, e.g. cores for inductors or transformers, the manufacturer will usually give some additional design information to enable the properties of the core to be fully exploited. This information, e.g. winding data, Q -curves, etc., may usually be taken as a guide only, since so much depends on the techniques of winding design and construction that will be used. Also, it usually applies only to specific cores. Often such data are not available and the winding must be designed from first principles.

In most of the preceding chapters on the applications of ferrites, the relations between the winding properties

and the overall design have been established for each type of application. The purpose of the present chapter is to consider these winding properties and the way in which they may be related to or calculated from the winding design.

In any calculations involving windings the first essential is adequate data on the wires or conductors which make up the winding. Because such information is often scattered and is sometimes in inconvenient form, tables have been specially prepared for the more common conductor ranges and these are given in Appendix A. Where the range of sizes was originally in inches, the metric dimensions have been given additionally. The tables cover the properties of bare round conductors, enamel insulated solid conductors and enamelled bunched conductors; the quoted properties range from the dimensional limits of the conductor to special functions used later in this chapter.

11.2. NUMBER OF TURNS IN A GIVEN WINDING AREA

The number of turns of a given conductor that may be wound into a given winding area depends not only on the overall diameter of the conductor and the dimensions of the winding area but also on the following factors:

- (i) whether the winding is in regular layers,
- (ii) how much insulation is used to interleave or cover the windings,
- (iii) the winding tension,
- (iv) how many separate windings and connections there are, and the technique used for bringing out the connections.

The possible number of turns predicted from calculation will depend on a proper allowance for these factors; the result will also depend on whether dimensions of the conductor and winding area are the nominal values or whether they are respectively maximum and minimum limit values. Fig. 11.1 defines some of the symbols used in calculations relating to the winding.

Two ideal arrangements of conductors are shown in cross-section in Fig. 11.2; these will be referred to as the square and hexagonal arrangement respectively. If the overall conductor diameter, d_o , is much smaller than the dimensions of the available winding space, then the number of turns, N , in a winding area, A_w , is given for the square arrangement by:

$$N = \frac{A_w}{d_o^2} \quad (11.1)$$

If the winding copper (space) factor is defined as

$$F_w = \frac{\text{total cross-sectional area of copper in winding}}{\text{actual cross-sectional area of the winding space}}$$

then for the perfect square arrangement:

$$F_w = \frac{\pi}{4} \left(\frac{d}{d_o} \right)^2 \quad (11.2)$$

where d is the bare diameter of the conductor.

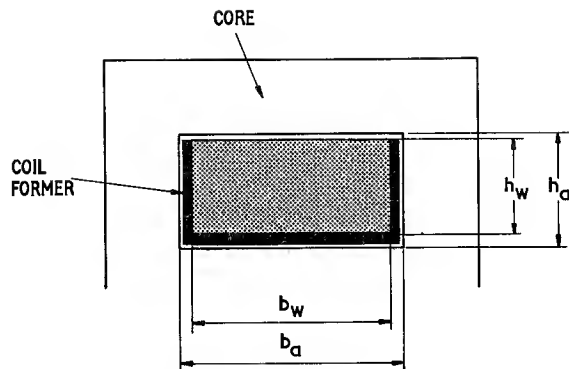
This factor is given in the wire Tables A.1.2.1, etc., in Appendix A for all the commonly used insulated conductors. It is calculated from Eqn 11.2 using the nominal value of d and the maximum overall value of d_o . When $d/d_o \rightarrow 1$, $F_w \rightarrow 0.785$.

The square arrangement is one extreme of close packed ordering; the other is the hexagonal arrangement. In this case the winding copper factor is given, for a large number of turns, by

$$F_w = \frac{\pi}{2\sqrt{3}} \left(\frac{d}{d_o} \right)^2 \quad (11.3)$$

When $d/d_o \rightarrow 1$, $F_w \rightarrow 0.907$

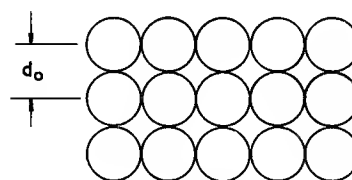
In a practical winding the conductor pattern will correspond to neither ideal. However, in a carefully wound coil, without interlayer insulation, the hexagonal arrangement will occur over large regions of the winding. Although successive layers approximate to helices of opposite lay, in practice the conductor will tend to lay in the groove formed by the previous layer for the



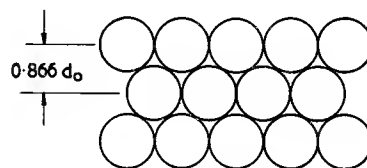
$$A_a = \text{WINDOW AREA} = b_a h_a$$

$$A_w = \text{NET WINDING CROSS-SECTIONAL AREA} = b_w h_w$$

Fig. 11.1. Some symbols used in winding calculations



(a) SQUARE



(b) HEXAGONAL

Fig. 11.2. Cross-sections of ideal arrangements of conductors in a winding

majority of the turn before being forced to cross over into the next groove. In the region of the crossover the square configuration will occur.

From the above definition of winding copper factor, its value for a practical winding is given by

$$F_w = \frac{N\pi d^2}{4} \cdot \frac{1}{A_w} \quad (11.4)$$

and will usually be somewhat less than the value of F_w given in the Appendix wire tables against the appropriate value of d .

Another useful factor is the overall copper factor F_a defined by

$$F_a = \frac{\text{total cross-sectional area of copper in winding}}{\text{actual window area in the core}}$$

$$F_a = \frac{N\pi d^2}{4} \cdot \frac{1}{A_a} \quad (11.5)$$

where A_a is defined in Fig. 11.1.

Plate 11.1 shows sections of some cylindrical windings, obtained by encapsulating, cutting and photographing. The most common type of winding is the scramble or random winding. The wire is guided by hand or by mechanical traverse but because the diameter is small and there is no interleaving between layers a fully-ordered arrangement is not often possible. In the first

Table 11.1.

Overall conductor diameter		F_p
mm	in	
0.03-0.07	$(1.2-2.8) \times 10^{-3}$	0.77-0.86
0.10-0.15	$(4-6) \times 10^{-3}$	0.81-0.90
0.20-0.4	$(8-16) \times 10^{-3}$	0.86-0.95
0.50-2.0	$(20-80) \times 10^{-3}$	0.81-0.90

cross-section the winding has been hand controlled by a skilled winder; almost perfect ordering has been achieved. In the second, the traverse was mechanical and some disordering has occurred. The third photograph, (c) shows the cross-section of a random winding, hand-controlled without much care. The first few layers are well-ordered but then disordering sets in and spreads from the flanges of the coil former. If the wire is fed onto the coil former with the same traverse or pitch that would be used for close-wound layers, the winding area will be well filled, varying from the theoretical maximum filling of the hexagonal arrangement in some places to a somewhat spaced version of the square arrangement in others. In practice the number of turns that may be randomly wound into a given area may be calculated from Eqn 11.1 provided a suitable packing factor, F_p , is used:

$$N = \frac{A_w}{d_o^2} \times F_p \quad (11.6)$$

The packing factor depends on the overall diameter of the conductor, the winding technique (wire tension, traverse, skill of the operator, etc.) and to some extent on the dimensions of the winding area. Table 11.1 gives some experimentally-determined values applying to cylindrical windings on all but the smallest coil formers.

The higher figure in the F_p range, combined with nominal values of A_w and d_o , will give a typical number of turns; the lower figure combined with a minimum value of A_w and a maximum value of d_o will give a fairly safe limit value for N , i.e. the number of turns that may be specified with reasonable certainty that they can be wound in the given winding area. The value of F_p has been calculated for each of the cross-sections in Plate

11.1 and the results are quoted in the caption. If the winding area dimensions are very small the above values of F_p must be reduced, e.g. by 10%.

If the overall conductor diameter is not very small compared to the dimensions of the winding area, then it becomes relatively easy to wind the whole coil in regular layers. Such a coil is shown in Plate 11.1(d). The conductor arrangement is close-packed and varies from the square to the hexagonal pattern. For most purposes the number of turns may be calculated from Eqn 11.6. However, when the conductor diameter is so large that only a few turns are possible then it is necessary to calculate the number of turns per layer and the possible number of layers to arrive at the number of turns. The possible number of layers, assuming a square pattern of conductors, is given by h_w/d_o rounded to the next lower integer.

Another type of winding is that in which the layers are insulated with paper or plastic foil. Plate 11.1(e) shows an actual cross-section. Normally this type of winding uses a coil former without flanges. The winding breadth, b_w , must be less than the width of the interleaving to prevent the end turns from collapsing onto the layer below; the size of the margin depends on the conductor diameter and the stiffness of the interleaving. If h_w is the permissible winding height and the layers are in tight contact (see also last paragraph of this section), the number of turns is given by

$$N = p \times \frac{b_w}{d_o} \times F_p \quad (11.7)$$

where p is the number of layers = $h_w/(d_o + t)$ rounded to the next lower integer

t is the thickness of the interleaving

and F_p is a packing factor

A good winder will attain this number of turns with unity packing factor if d_o used in the calculation is the maximum value. If a safety margin is required F_p may be put equal to 0.95.

Where a self-supporting, low-capacitance winding is required, wave-winding is often used. In this the conductor is made to traverse across the whole winding breadth and back one or more times during each revolution. Its main use is for H.F. coils in radio receivers, antenna rod coils and E.H.T. coils in television line scanning transformers. Since wave windings rarely have to fill the available winding space the design is not usually critical. A successful winding depends on the proper choice of gear ratios on the winding machine so that the correct traverse is obtained. Instructions for gear wheel selection are usually available with the winding machine.

Returning to layer or random winding it has been assumed in calculations involving winding height that successive layers are in close contact. This is justified

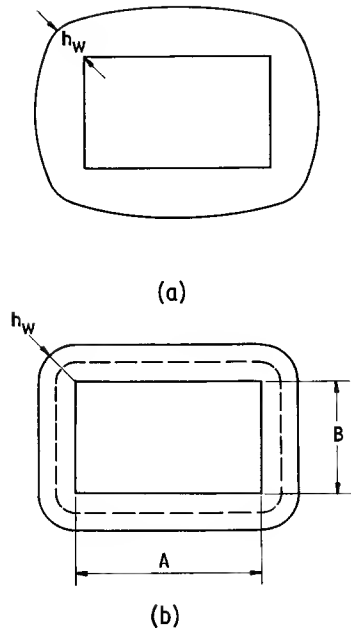


Fig. 11.3. Geometry of a winding on a rectangular coil former

in the case of round coils but when the coil former is rectangular as in Fig. 11.3(a) the actual winding height in the region covered by the core will be greater than the calculated winding height, h_w , due to the bowing of the windings. The amount of the bowing depends on the proportions of the coil former and the height of the winding. Usually the nett available winding height should be reduced by 15 to 20% to obtain the value of h_w to be used in the above calculations.

11.3. THE D.C. WINDING RESISTANCE

The d.c. resistance of a winding consisting of a total length, l , of conductor of cross-sectional area A is

$$R_{dc} = \frac{\rho_c l}{A} \quad \Omega \quad (11.8)$$

where ρ_c is the resistivity of the conductor material. For copper at a temperature of 20°C the nominal value of ρ_c is $1.694 \times 10^{-8} \Omega \cdot m$. The temperature coefficient of this resistivity is 0.00393 per °C.

If d is the bare conductor diameter, l_w is the mean turn length and N is the number of turns on the winding, then Eqn 11.8 becomes

$$R_{dc} = \frac{4\rho_c N l_w}{\pi d^2} = N l_w R_c \quad \Omega \quad (11.9)$$

where R_c is the resistance per unit length of conductor $= 4\rho_c/\pi d^2$

Values of R_c are given in the wire tables in Appendix A. For a circular winding the mean turn length is readily calculated from the mean diameter. When the winding is wound on a rectangular coil former as shown in Fig. 11.3, the bowing of the winding may usually be ignored in its effect on the mean turn length and this may be calculated, by reference to Fig. 11.3(b), from

$$l_w = 2(A+B) + \pi h_w \quad (11.10)$$

Combining Eqns 11.9 and 11.4 or 11.5

$$R_{dc} = \frac{\rho_c N^2 l_w}{A_w F_w} = \frac{\rho_c N^2 l_w}{A_a F_a} \quad \Omega \quad (11.11)$$

Thus for a winding fully occupying a given winding space, $R_{dc} \propto N^2$. If the winding embraces a magnetic core, the inductance, L , is also proportional to N^2 (see Eqn 4.23 for example). It follows that a given core may be characterized by a particular value of R_{dc}/L , i.e. the ratio of the resistance to the inductance for a winding which occupies the full winding space. From the expressions for R_{dc} and L it follows that

$$\left. \begin{aligned} R_{dc}/L &= \frac{\rho_c}{\mu_o \mu_e} \times \frac{l_w C_1}{F_w A_w} \quad \Omega \cdot H^{-1} \\ &= \frac{\rho_c l_w x^2}{F_w A_w} \quad \Omega \cdot mH^{-1} \\ \text{or} \quad &\frac{\rho_c l_w 10^9}{F_w A_w A_L} \quad \Omega \cdot H^{-1} \end{aligned} \right\} \quad (11.12)$$

from Eqns 5.6 and 5.8.

Inasmuch as F_w is not greatly affected by the conductor diameter, R_{dc}/L is approximately independent of the number of turns and depends mainly on the core geometry. This ratio is often used to compare the merits of alternative core designs.

If the winding is made with bunched conductors consisting of n strands, each of diameter d , then provided the twist of the bunch is neglected, the resistance of the conductor or winding may be calculated from Eqns 11.8 or 11.9 by using d or R_c for a single strand and dividing the result by n .

So far the discussion has been confined to a single winding occupying substantially all the available winding space. Another important case is the transformer which, in its simplest form, consists of two windings having in general unequal numbers of turns, e.g. N_1 and N_2 , and carry currents I_1 and I_2 respectively such that

$$I_1 N_1 = I_2 N_2$$

Continuing to use the subscripts to distinguish the properties of the windings, the power dissipated in the windings is, using Eqn 11.11

$$P = I_1^2 \cdot \frac{\rho_c N_1^2 l_{w1}}{A_{w1} F_{w1}} + I_2^2 \cdot \frac{\rho_c N_2^2 l_{w2}}{A_{w2} F_{w2}}$$

if $l_{w1} \approx l_{w2} = l_w$, $F_{w1} = F_{w2} = F_w$ and $A_{w1} + A_{w2} =$ the total winding area, A_w , then

$$P = \frac{\rho_c I_1^2 N_1^2 l_w}{F_w} \left(\frac{1}{A_{w1}} + \frac{1}{A_w - A_{w1}} \right)$$

Differentiating w.r.t. A_{w1} and equating to zero:

$$\frac{1}{A_{w1}^2} = \frac{1}{(A_w - A_{w1})^2}$$

$$\text{or } A_{w1} = \frac{A_w}{2} \quad (11.13)$$

Therefore for minimum power loss in the windings the winding areas should be approximately equal. If l_{w1} is significantly less than l_{w2} then A_{w2} should be somewhat greater than A_{w1} . An exact result may be obtained in specific cases by expressing l_{w1} and l_{w2} in terms of A_{w1} before differentiating. In practice the minimum is fairly flat, so equal or nearly equal winding areas may be used for the first trial calculation. If, as a result, the winding resistance R_1 differs significantly from $R_2(N_1/N_2)^2$ (this may be due to unequal copper factors as well as a poor division of the winding space) then the ratio of winding areas must be suitably adjusted until the resistances referred to one side of the transformer are approximately equal.

11.4. POWER LOSS DUE TO EDDY CURRENTS IN THE WINDING

11.4.1. General

A conductor immersed in an alternating magnetic field will have e.m.f.'s induced in it and these will give rise to eddy currents and associated power losses.¹ The magnetic fields may be due to currents flowing in other conductors or due to current flowing in the conductor in question. The losses may be represented as an increase in resistance of the current-carrying conductors above the value measured with direct current; this increase of resistance becomes larger as the frequency increases.

A conductor which forms a part of a current-carrying winding will in general experience the magnetic field due to its own alternating current and also the field due to all the other current carrying conductors in the vicinity. Usually these two contributions are considered separately and the resultant losses or resistance increments are added together. This approach is considered in the two sections immediately following. However, it is only valid if the field due to the winding as a whole is approximately uniform across the diameter of the individual conductors. If the winding consisted, for example, of a single layer of large diameter wire, the transverse field would vary greatly across the thickness of the layer and the simple

approach might lead to appreciable error in the estimation of eddy current losses. Instead it is preferable to analyse the eddy current losses as a whole. The results of such analysis, applicable particularly to transformer design, are given in Section 11.4.4.

11.4.2. Skin effect

A single straight isolated conductor carrying an alternating current, see Fig. 11.4(a), will be surrounded by, and at low frequencies permeated by, a concentric magnetic field. This field will induce opposing eddy currents within the conductor itself as shown in the centre diagram. These currents tend to oppose the main current in the vicinity of the axis of the conductor and to

Table 11.2. PENETRATION DEPTH, $\Delta = k f^{-\frac{1}{2}}$

Conductor Material	Temperature	k	
	°C	m.Hz ^½	mm.Hz ^½
Copper	20	0.0655	65.5
	70	0.072	72
Aluminium	20	0.082	82
	70	0.090	90
Silver	20	0.064	64
	70	0.070	70

enhance it at the surface. Thus the current distribution tends to become non-uniform across the section, the current being least at the centre and greatest at the surface of the conductor. As the frequency increases, the induced e.m.f.'s increase and the non-uniformity becomes more pronounced until the current is virtually confined to a thin skin at the surface, and the inner region plays no part in the conduction.

The a.c. resistance of a straight conductor of circular cross-section is given by

$$R_{ac} = R_{dc} + R_{se} = R_{dc}(1 + F) \quad \Omega \quad (11.14)$$

where R_{se} is the increase in resistance due to skin effect and F is the skin effect factor.

The skin effect factor is a function of d/Δ where Δ is the penetration depth. This is a property of a conducting material and is strictly the depth beneath an infinite plane surface at which an incident plane e.m. wave is attenuated to $1/e$ or 37% of its surface value due to the effect of eddy currents.²

$$\Delta = \sqrt{(\rho_c / \pi \mu_0 \mu_r f)} \quad \text{m} \quad (11.15)$$

where ρ_c is the conductor resistivity

μ_r is the relative permeability of the conductor

$$(11.15) \Delta = \frac{1}{2\pi} \left(\frac{\rho_c 10^9}{\mu_r f} \right)^{\frac{1}{2}} \quad \text{cm}$$

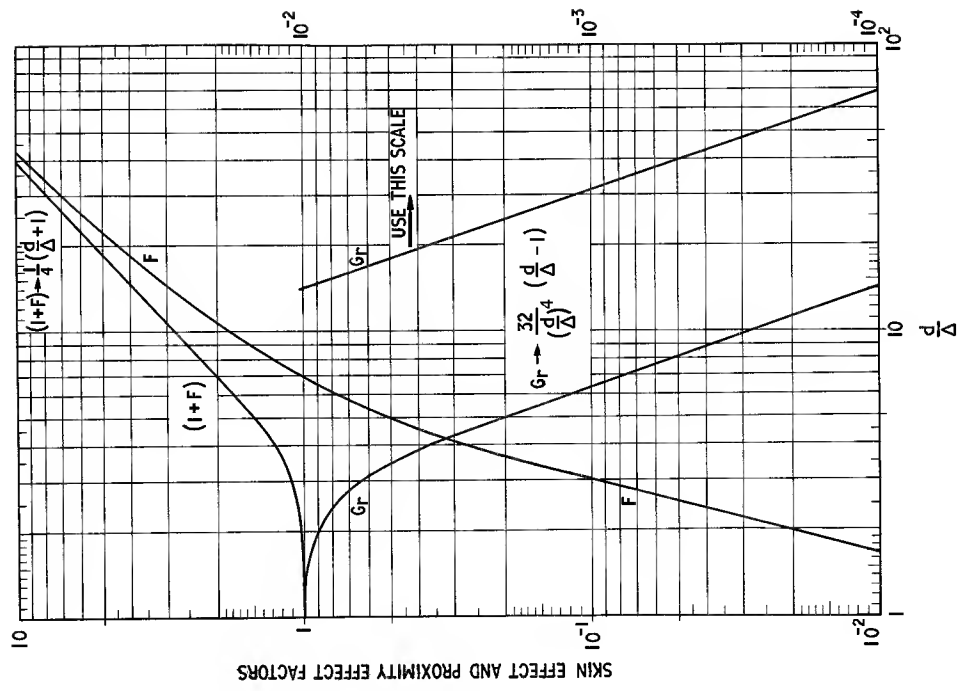


Fig. 11.5. Skin effect factor, F , and proximity effect factor, G_r , as functions of d/Δ for round conductors based on figures given by Butterworth³

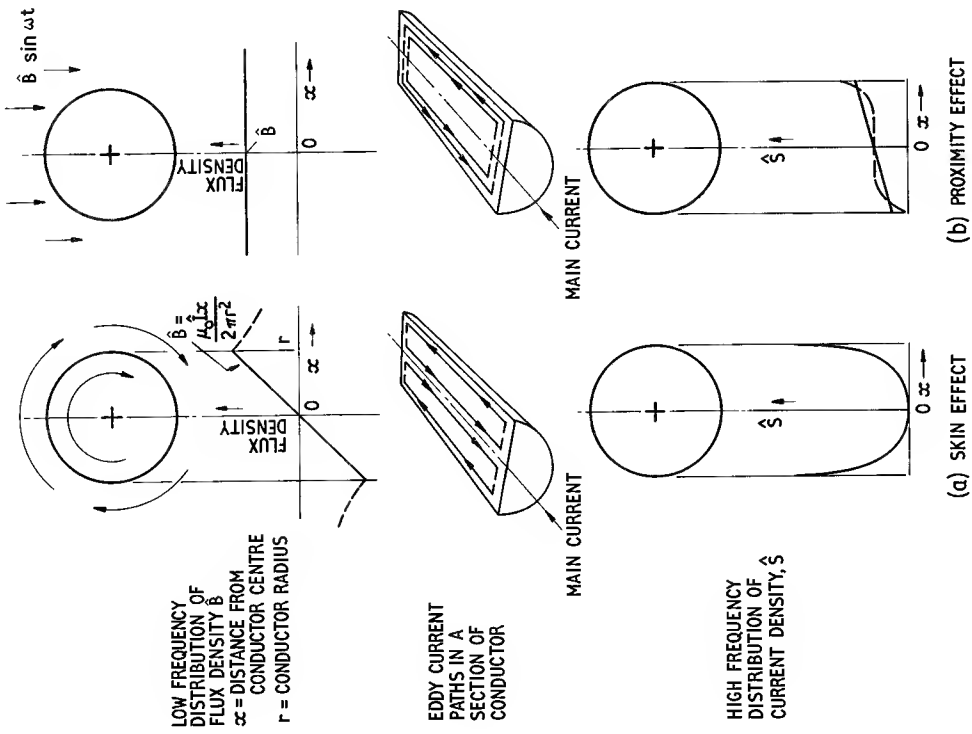


Fig. 11.4. Skin and proximity effect in round conductors

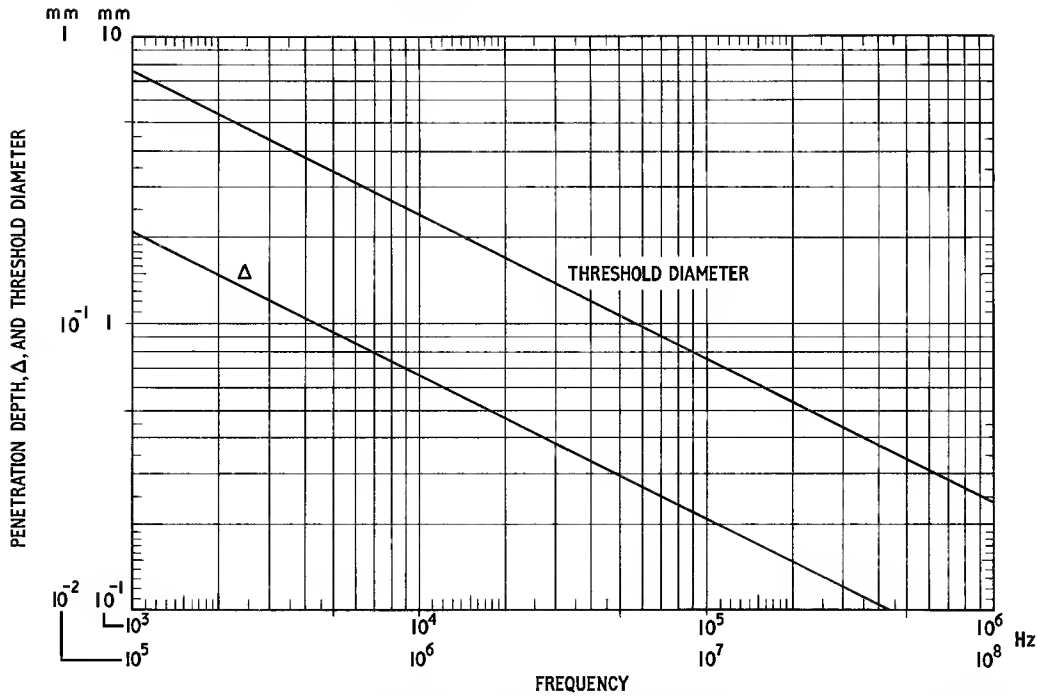


Fig. 11.6. Skin effect in round copper conductors at 20°C. Penetration depth, Δ , and the threshold diameter (diameter at which $1+F = 1.2$) as functions of frequency

When the current in a round conductor is confined by skin effect to a depth beneath the surface that is much less than the diameter, this depth, measured as the distance over which the current falls to $1/e$ of its surface value, tends to the value Δ . Some values of Δ in terms of frequency are given in Table 11.2 for three common conducting materials at two temperatures.

Fig. 11.5 gives F and $1+F$ as functions of d/Δ . For convenience in calculations involving copper conductors Fig. 11.6 gives Δ for copper as a function of frequency, and also the threshold diameter, i.e. the diameter at which the skin effect has increased the resistance of the conductor to 1.2 times the d.c. value.

Referring to Fig. 11.5 it is seen that when d/Δ for a round conductor is less than 2 the skin effect is negligible. It increases rapidly as d/Δ increases and when d/Δ is greater than 5:

$$1+F \approx \frac{1}{4} \left(\frac{d}{\Delta} \right)^2 \quad (11.16)$$

When d/Δ is very large, $1+F$ approximates to $d/4\Delta$ and the a.c. resistance,

$$R_{ac} = R_{dc} + R_{se} \approx R_{dc} d/4\Delta = \frac{l}{d} \sqrt{\left(\frac{\mu_0 \mu_c \rho_c f}{\pi} \right)} \Omega \quad (11.17)$$

from Eqn 11.15 and $R_{dc} = \frac{4\rho_c l}{\pi d^2}$

This equation shows that, although an increase in diameter will increase the ratio of a.c. resistance to d.c. resistance, it will always reduce the actual value of a.c. resistance due to skin effect at any frequency. At the higher frequencies at which Eqn 11.17 holds the current effectively flows in a surface layer of depth Δ . This follows from Eqn 11.17 since

$$R_{dc} + R_{se} \approx R_{dc} d/4\Delta = \frac{4\rho_c l}{\pi d^2} \times \frac{d}{4\Delta} = \frac{\rho_c l}{\pi d \Delta} \quad (11.18)$$

and $\pi d \Delta$ is the cross-sectional area of a surface layer of depth Δ .

Skin effect may be virtually eliminated by using conductors consisting of thin insulated strands so composed that individual strands weave cyclically from the centre of the conductor to the outside and back as they run along the length of the conductor. Such a stranding and transposition makes the current density uniform. However, since skin effect is not usually the most important form of eddy current loss in winding conductors, it is not usual to use this special stranding. To combat the proximity effect loss described in the next section bunched conductor is often used. This consists of a number of thin insulated strands simply twisted into the form of a rope. If the strands formed perfect

$$(11.17) \quad R_{ac} = R_{dc} + R_{se} \approx R_{dc} d/4\Delta = \frac{2l\sqrt{(\mu_c f \rho_c 10^{-9})}}{d} \Omega$$

helical paths, keeping at a constant distance from the axis, the skin effect would be the same as for a solid conductor having the same copper cross section, assuming that all the strands were connected together at each end of the conductor. In practice, however, such bunched conductors are usually made up of groups of strands and appreciable transposition of the strands occurs. Careful measurements have shown that most bunched conductors behave as though the strands are transposed almost perfectly and the skin effect can be ignored.

In isolation, a perfectly transposed bunched conductor will be subject to a further eddy current loss due to its own field traversing the strands, each of which carries the same current. This may be called internal proximity effect. It may be comparable to, and at high frequencies may be larger than, the skin effect in an equivalent conductor consisting of perfectly untransposed strands. However when a perfectly transposed bunched conductor is in a winding, the field due to the bunch, as such, largely disappears due to the proximity of the other turns; the winding behaves as though it consists only of strands, all carrying equal current. Under these conditions only the normal proximity effect described in the next section is important.

Returning to the consideration of skin effect loss in general, the loss tangent due to skin effect in an inductor of L henries follows from Eqn 11.14

$$\tan \delta_{se} = \frac{R_{dc}F}{\omega L} \quad (11.19)$$

At low values of d/Δ , F is proportional to $(d/\Delta)^4$ and is therefore proportional to f^2 . Thus at low frequencies $\tan \delta_{se}$ is proportional to f . It may easily be shown that it reaches a peak when $d/\Delta \approx 6$. Thereafter it falls; as F becomes approximately proportional to $f^{-\frac{1}{2}}$, $\tan \delta_{se}$ approaches proportionality to $f^{-\frac{1}{2}}$.

11.4.3. Proximity effect

This is the eddy current effect in a conductor due to the alternating magnetic field of other conductors in the vicinity. In practice this may usually be interpreted as the eddy current effect in the conductors of a winding due to the field of the winding as a whole. The field will, in general, depend on the geometry of the core, if any. It must be remembered that any additional windings or conductors in the same field will have eddy currents induced in them whether or not they are carrying a main current; the resultant energy loss will simply add to the corresponding loss in the current-carrying winding and will be apparent as an additional resistance in that winding.

The field of a current-carrying winding will normally cut the conductors of that winding, or associated windings,

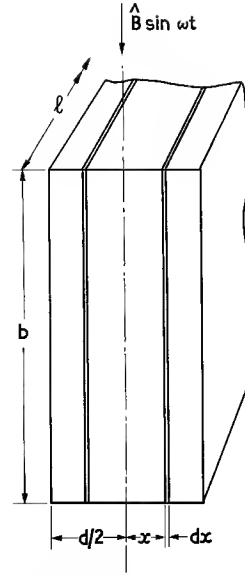


Fig. 11.7. Calculation of eddy currents in a thin tape

perpendicular to the conductor axis. The resultant eddy current paths and current distribution are shown in Fig. 11.4(b) for a round wire for which d/Δ is not large.

When d/Δ is less than unity the effect of the magnetic fields of the eddy currents themselves may be ignored and the calculations of the eddy current loss are quite simple; the following derivation of proximity effect in a thin tape illustrates the principles.

Fig. 11.7 shows the cross-section of a tape having width b and thickness d . An alternating magnetic flux density, $\hat{B} \sin \omega t$, is everywhere parallel to the plane of the tape. The e.m.f. induced in a loop consisting of the two elementary laminae is given by

$$E = \omega \hat{B} 2xl / \sqrt{2} \quad \text{V} \quad (11.20)$$

where l is the length of tape being considered.

An eddy current will flow along the laminae parallel to the length of the tape, in one direction on one side of the axis and in the opposite direction on the other side. Neglecting the short paths connecting the laminae at the ends of the tape, the resistance of the elementary eddy current circuit is given by

$$R = \frac{2\rho_e l}{bdx} \quad \Omega$$

Therefore the power loss due to proximity effect is

$$dP_{pe} = E^2/R = \omega^2 \hat{B}^2 x^2 l b dx / \rho_e$$

$$(11.20) \quad E = \frac{\omega \hat{B} 2xl}{\sqrt{2}} \cdot 10^{-8} \quad \text{V}$$

$$P_{pe} = \frac{\omega^2 \bar{B}^2 lb}{\rho_c} \int_0^{d/2} x^2 dx$$

$$= \frac{\omega^2 \bar{B}^2 l b d^3}{24 \rho_c} \quad \text{W} \quad (11.21)$$

It must be remembered that this result applies only when the flux density is parallel to the plane of the tape; a small inclination may result in much greater losses. An analogous expression may be obtained for a round conductor of diameter d , namely

$$P_{pe} = \frac{\pi \omega^2 \bar{B}^2 l d^4}{128 \rho_c} \quad \text{W} \quad (11.22)$$

Since the latter case is the more common, the following discussion will be in terms of round conductors. If the transverse magnetic field is associated with a main current in the conductor, the eddy currents cause a distortion of the current density, enhancing it on one side of the axis and diminishing it on the other, as shown by the full line in the lower diagram of Fig. 11.4(b).

At higher frequencies or with larger conductor diameters such that ratio d/Δ becomes larger than unity the field due to these eddy currents significantly reduces the flux density inside the conductor and the associated current distribution becomes non-linear as shown by the broken line.

When this happens there will also be some skin effect tending to cause the current to flow near the surface as shown on the lower diagram of Fig. 11.4(a). Provided the transverse flux density is uniform in the vicinity of the conductor the two effects are additive and the current tends to be concentrated towards one side of the conductor.

Returning to the current distribution due to the transverse field only, the effect of the eddy current field and the associated non-linear current distribution is to reduce the proximity effect loss that would otherwise be present. Butterworth calculated the eddy current loss in round conductors taking this eddy current screening into account. His results are most conveniently expressed by introducing a proximity effect factor, G_r , into Eqn 11.22:

$$P_{pe} = \frac{\pi \omega^2 \bar{B}^2 l d^4 G_r}{128 \rho_c} \quad \text{W} \quad (11.23)$$

This factor, which is a dimensionless function of d/Δ is plotted in Fig. 11.5; it is valid only for round conductors. When d/Δ decreases to unity, $G_r \rightarrow 1$; when d/Δ is increasing beyond 4,

$$G_r \rightarrow \frac{32}{(d/\Delta)^4} \left(\frac{d}{\Delta} - 1 \right) \quad (11.24)$$

It is often necessary to express this loss as the tangent of the proximity effect loss angle, δ_{pe} , referred to the current-carrying winding. For simplicity it will be assumed that there is only one winding concerned and that it is embraced by a magnetic core, e.g. a ferrite pot core. The flux density in the winding space, although non-uniform, is everywhere assumed proportional to the ampere-turns in the winding. Eqn 11.23 may be combined with the following relations:

$$P_{pe} = I^2 R_{pe} \quad \text{where } R_{pe} \text{ is the series increase in resistance of the winding due to proximity effect,}$$

$$\bar{B}^2 = k N^2 I^2 \quad \text{where } \bar{B}^2 \text{ is } B^2 \text{ averaged over the winding space and } k \text{ is a constant,}$$

$$\tan \delta_{pe} = R_{pe} / \omega L \text{ and}$$

$$L = \mu_0 \mu_c N^2 / C_1$$

It follows that

$$\tan \delta_{pe} = \frac{P_{pe}}{\omega L I^2} = \frac{P_{pe} C_1}{I^2 \omega \mu_0 \mu_c N^2}$$

$$= \frac{\pi \omega^2 k N^2 I^2 d^4 G_r}{64 \rho_c} \times \frac{C_1}{I^2 \omega \mu_0 \mu_c N^2}$$

$$= \frac{\pi^2 k C_1}{32 \rho_c \mu_0} \times \frac{f l d^4 G_r}{\mu_c} \quad (11.25)$$

When d/Δ is less than unity, e.g. at low frequencies, $G_r \approx 1$ and $\tan \delta_{pe}$ is proportional to the frequency. At higher frequencies the proximity effect usually makes an appreciable contribution to the total loss of a wound component. When $d/\Delta \approx 3.5$ the value of $\tan \delta_{pe}$ reaches a maximum. At higher frequencies G_r approaches proportionality to $(d/\Delta)^{-3}$ or $f^{-3/2}$, so $\tan \delta_{pe}$ approaches proportionality to $f^{-1/2}$.

A reduction of conductor diameter, d , will be very effective in reducing proximity effect but, by itself, this reduction will rapidly increase the value of R_{dc} and may result in a greater over-all loss. The usual method of combating proximity effect is to use bunched conductors consisting of n insulated strands of diameter d . At each end of the winding the strands are soldered together; at low frequencies the winding has an effective area of $n\pi d^2/4$. The conductor is twisted so that, in its simplest form, each strand follows a helical path. Fig.

$$(11.21) \quad P_{pe} = \frac{\omega^2 \bar{B}^2 l b d^3}{24 \rho_c} 10^{-16} \quad \text{W}$$

$$(11.22) \quad P_{pe} = \frac{\pi \omega^2 \bar{B}^2 l d^4}{128 \rho_c} 10^{-16} \quad \text{W}$$

$$(11.23) \quad P_{pe} = \frac{\pi \omega^2 \bar{B}^2 l d^4 G_r}{128 \rho_c} 10^{-16} \quad \text{W}$$

$$(11.25) \quad \tan \delta_{pe} = \frac{\pi k C_1}{128 \rho_c} \times \frac{f l d^4 G_r}{\mu_c} \times 10^{-7}$$

11.8 shows a side view of two strands in such a bunched conductor; the e.m.f.'s induced in each half-twist are cancelled by those in the next. If the bunched conductor has a more complicated composition, e.g. seven twisted bunches each of seven twisted strands, cancellation will still occur. Provided the number of twists in a winding is greater than about ten the eddy currents circulating between the strands may be ignored and only those circulating within the strands need to be considered.

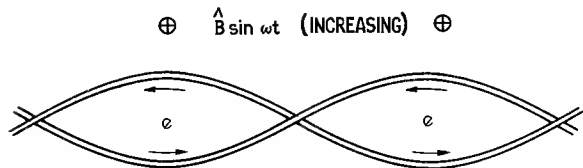


Fig. 11.8. The cancellation of eddy-current e.m.f.'s induced in twisted strands of bunched conductors by a transverse flux

Thus Eqn 11.25 may be applied to the strands of the conductor; d then refers to the bare diameter of the strand and l refers to the total length of strands, i.e. Nnl_w , where l_w is the mean turn length. The above equation may now be written in more general form

$$\begin{aligned} \tan \delta_{pe} &= \frac{\pi^2 k_l C_1}{32 \rho_d \mu_o} \times \frac{f N n d^4 G_r}{\mu_e} \\ &= \left. \begin{aligned} &\frac{k_e f N n d^4 G_r}{\mu_e} \\ \text{or } &\frac{k_E f N n d^4 G_r}{A_L} \end{aligned} \right\} \quad (11.26) \end{aligned}$$

where k_e and k_E are alternative forms of proximity effect constant; $k_e = 10^{-9} k_E C_1 / \mu_o$. The constant k_e has the basic units $[\text{s.m}^{-4}]$ but may be more conveniently expressed in $[\text{s.mm}^{-4}]$ in which case d is in mm. The constant k_E has the basic units $[\text{s.m}^{-4}.\text{H}]$ but may similarly be expressed in terms of mm and nanohenries.

If solid conductors are being considered the same equations may be used but then $n = 1$.

Since the flux density in the winding space is not uniform and is not easily calculated, the value of k_e or k_E must usually be determined experimentally for a given core. It will depend on the geometry of the core, air gap and the winding. The experimental method is basically as follows. Two coils are wound, each having the overall cross-section for which the constant is to be determined, e.g. a full coil former. One is wound with solid conductor of such a diameter that, at the measuring frequency, d/Δ is about 3.5 so that $\tan \delta_{pe}$ is near maximum. The diameter should be preferably on the high side so that the number of turns is not excessive, bearing in mind the need to make self-capacitance loss negligible. Further, the frequency should not be so high

that the core loss is large compared with the proximity effect loss. The other coil is wound with the same number of turns of a bunched conductor of the same over-all diameter. The strand diameter is chosen so that the proximity effect loss is negligible and if the strands are well transposed the skin effect loss may also be ignored. After the d.c. resistance has been measured, each coil is placed in turn in the given core and the overall loss tangent is determined. The inductances are also measured.

From the overall loss tangent for the stranded winding, the loss tangent due to the d.c. resistance $R_{dc}/\omega L$, is subtracted. For the solid winding, both the d.c. resistance and skin effect loss tangents are calculated and subtracted from the overall loss tangent. The resulting loss tangents, containing no d.c. or skin effect components, are subtracted. This eliminates the core loss and the difference equals the proximity effect loss tangent of the solid winding; that due to the stranded winding having been made negligible.

Thus k_e may be obtained from Eqn 11.26 since all the other quantities are known (G_r may be obtained by reference to Fig. 11.5). The proximity effect constant, having been determined for a given core (with a given air gap), may be used to calculate the proximity effect loss tangent of any winding on that core type (with the same air gap) provided the overall geometry of the winding is similar to that used for the experimental determination. Typical values of k_e and k_E are given in Table 5.4.

The graphs of Fig. 5.11 show the relative magnitudes of the winding resistance and eddy current loss tangents calculated for comparable windings of solid and bunched conductors placed in a typical ferrite pot core.

11.4.4. Total eddy current loss in transformer windings

The two previous sections have considered eddy currents in conductors using an approach which enables the total eddy current loss in inductors to be estimated reasonably well provided an experimental constant of the core is known. It assumes that the transverse flux density is uniform in the vicinity of the conductor. This approach cannot easily be used for transformers because in this case the winding geometry depends greatly on the design requirements and if there are few layers the uniform flux density assumption is invalid.

Dowell⁴ has adapted the analysis of eddy current losses in armature slots⁵ to the case of transformers and his results are used in this section. In a transformer the transverse field in the winding space may be taken as being parallel to the interfaces between windings and its magnitude may be easily evaluated. This enables a general analysis to be made. Qualitatively the combination of the transverse and the conductor fields in a

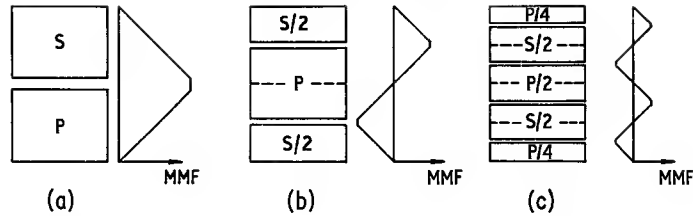
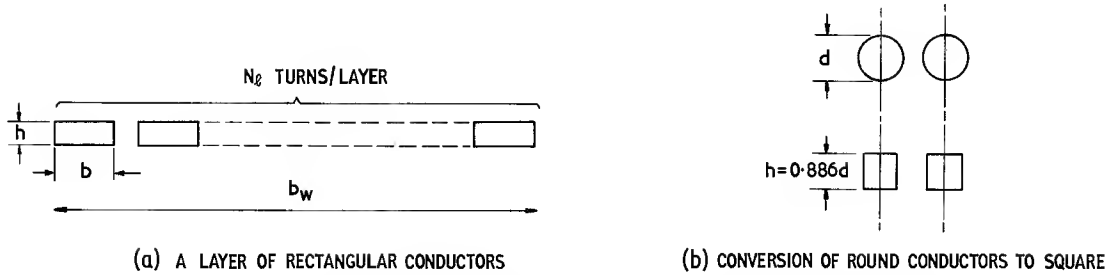


Fig. 11.9. Some transformer winding arrangements and the corresponding m.m.f. diagrams


 Fig. 11.10. Winding layer parameters (note: h , b and d refer to bare conductors)

normal transformer causes the current density to increase towards the surface of the conductor that faces the nearest winding interface. This will result in an increase of winding resistance and also in a fall in the leakage inductance (see Section 11.7) as the frequency rises. This section is only concerned with the rise in resistance. The analysis leads to a factor, F_R , by which the d.c. resistance may be multiplied. This factor is a function of the winding geometry and to a ratio analogous to d/Δ ; the method of determining it will now be described.

In a transformer, the ampere turns due to the primary are very nearly balanced by those due to the secondary. In Section 11.7 the m.m.f. diagram is introduced (see Fig. 11.17); moving from the innermost or outermost surface of the windings the m.m.f. increases linearly from zero until it reaches a maximum at a primary/secondary interface after which it begins to fall linearly. Fig. 11.9 shows some typical winding arrangements and the corresponding m.m.f. diagrams. For the purpose of the present calculation it is necessary to divide the windings into portions in which the low frequency m.m.f. varies linearly from zero. Thus in Fig. 11.9(b) the half secondaries are portions and the primary must be divided into two equal portions. In general each portion must be considered separately, but if, for example, two are identical the value of F_R calculated for one of them would apply to both.

For each portion the following parameters are required:

- The number of turns per layer, N_t
- The effective conductor height, h
- The layer copper factor, F_t

Fig. 11.10(a) shows a typical layer of rectangular conductors. The layer copper factor is defined by

$$F_t = \frac{N_t b}{b_w} \quad (11.27)$$

where b_w is the overall winding breadth and b is the conductor breadth. If the conductors are round, the equivalent square conductors must first be derived as in Fig. 11.10(b) and then the above parameters may be calculated, putting $h = b = 0.886d$.

The only other information about the portion of winding that is required is the number of layers, p . In most transformers the m.m.f. diagram will be such that the number of layers will either be an integral number or, if the dividing line cuts through the middle of a layer, an integral number plus a half.

From the above parameters the variable $h\sqrt{F_t}/\Delta$ must be calculated; for the given frequency, Δ may be obtained from Eqn 11.15, Table 11.2 or Fig. 11.6. The variable $h\sqrt{F_t}/\Delta$ corresponds to the ratio d/Δ used in the previous sections. Fig. 11.11 gives F_R as a function of $h\sqrt{F_t}/\Delta$ with the number of layers per portion as a parameter. If R_{dc} , see Section 11.3, is the resistance of the portion of the winding, or of the whole winding if it has been divided into identical portions, then the corresponding resistance at the given frequency is $R_{dc}F_R$. For further details of the method and its derivation see ref. 4.

This rapid method of estimating the a.c. resistance of transformer windings has been verified experimentally and has given reliable results over a wide range of winding configurations. However it was found to be inaccurate for windings consisting of foil extending across the whole winding width; the actual value of R_{AC} is larger than that predicted, presumably due to the presence of a small component of the leakage flux perpendicular to the foil.

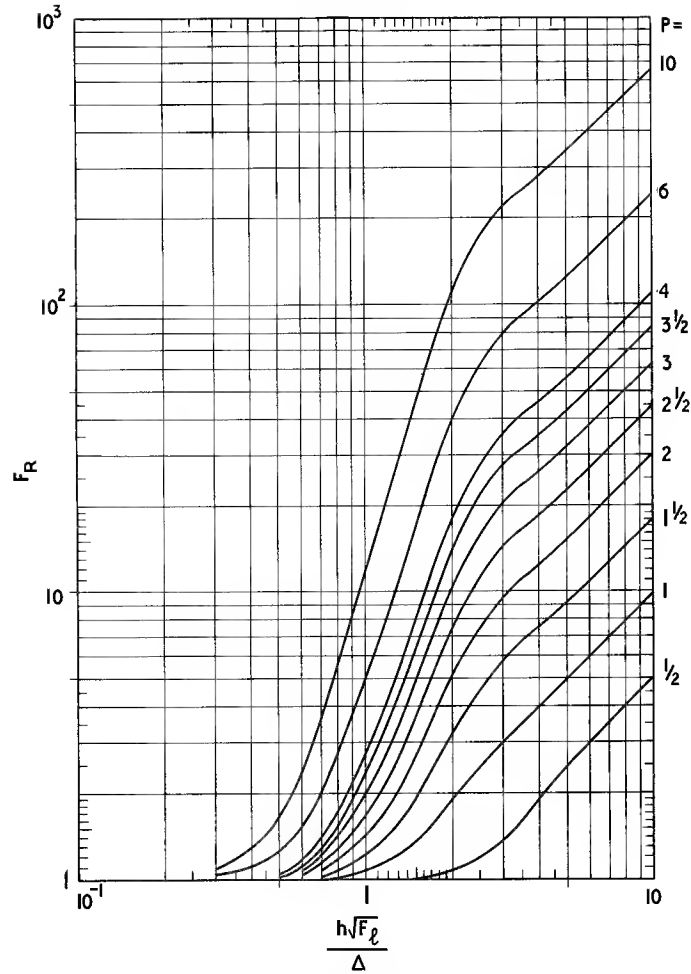


Fig. 11.11. F_R as a function of $h\sqrt{F_l}/\Delta$ with number of layers, p , per winding portion as a parameter. (After Dowell⁴)

$$R_{AC} = R_{dc}F_R \quad \text{When } \frac{h\sqrt{F_l}}{\Delta} > 5 \quad F_R \rightarrow \frac{2p^2 + 1}{3} \cdot \frac{h\sqrt{F_l}}{\Delta}$$

If it is found that the increase in resistance due to eddy currents is excessive, one remedy is to use bunched conductors as described in the previous section. The permissible strand diameter may be estimated by applying the above method to the winding as if it consisted only of strands i.e. $N \times n$ turns each consisting of one strand. Then $h = 0.886 \times$ the strand diameter and F_l is approximately equal to the copper factor F_w .

The practical application of the method described in this section is considered in more detail in Section 9.5.3.

11.5. THE INDUCTANCE OF AN AIR-CORED COIL

The inductance of a cylindrical air-cored solenoid having N turns is given by Nagaoka's formula:⁶

$$L = \frac{\mu_0 \pi D^2 N^2 K}{4l_c} \times 10^6 \quad \mu\text{H} \quad (11.28)$$

where D is the mean diameter of the coil in m

l_c is the axial length of the coil in m

and K is a constant depending on l_c/D ; as l_c/D becomes larger $K \rightarrow 1$.

If K is modified to take account of the radial thickness of the coil, the above equation may be used to calculate the inductance of any cylindrical coil having a rectangular winding section. Since the constant will depend among other things on l_c/D the equation may be simplified to:

$$(11.28) \quad L = \frac{\pi^2 D^2 N^2 K 10^{-3}}{l_c} \quad \mu\text{H}$$

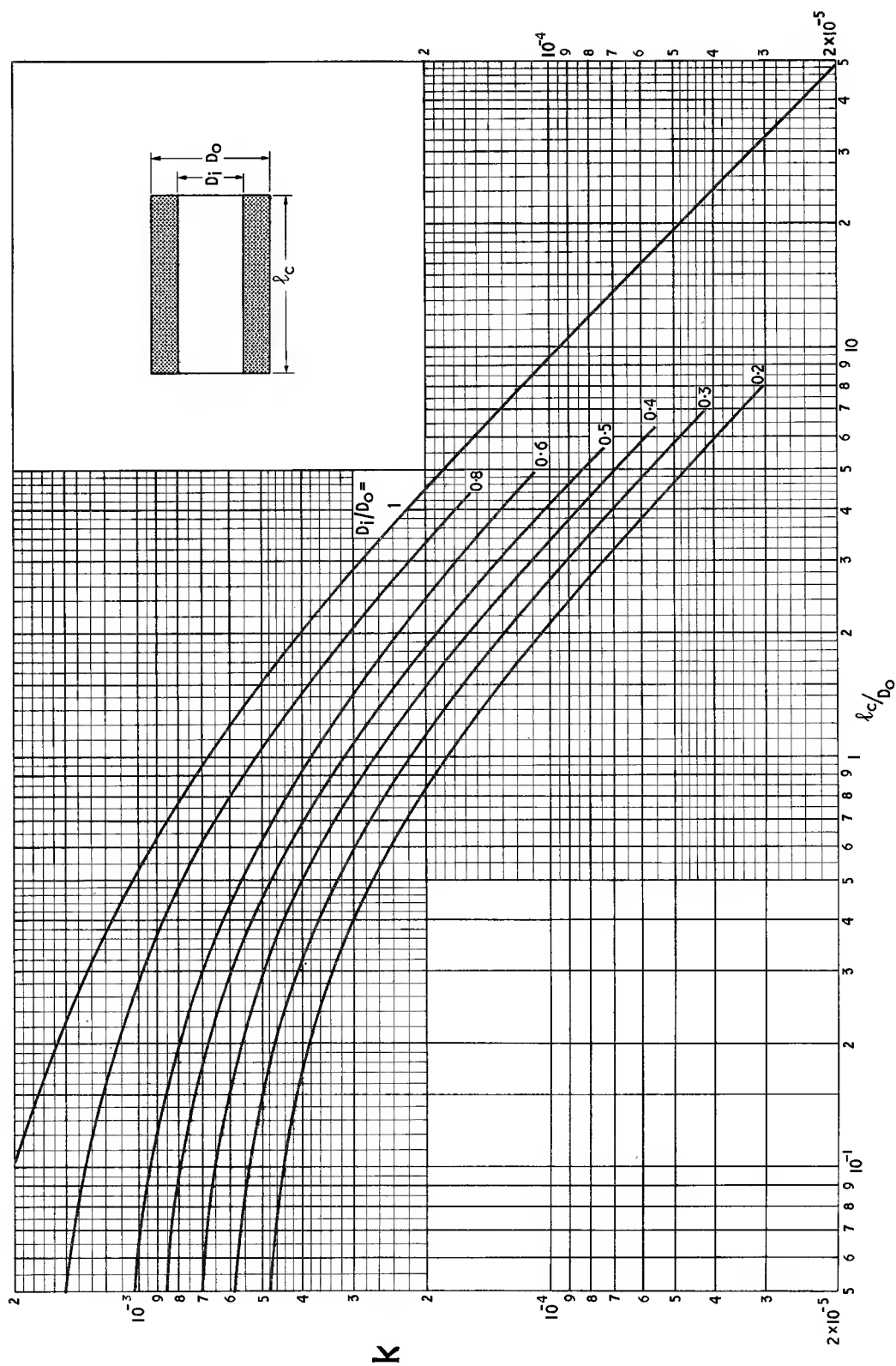


Fig. 11.12. Inductance of air-cored coils; k in Eqn 11.29 as a function of l_c/D_o and D_i/D_o .

$$L = D_o N^2 k \quad \mu\text{H} \quad (11.29)$$

where D_o is the outside diameter of the coil in mm, and k is a function of l_c/D_o and D_i/D_o , where D_i is the internal diameter of the coil in mm, and l_c is in mm.

The function k has been calculated from data given by Grover⁷ and it is plotted in Fig. 11.12. Using this graph and Eqn 11.29 the inductance of any cylindrical air-cored coil may easily be obtained with reasonable accuracy. For greater precision reference should be made to the data by Grover, mentioned above.

11.6. THE SELF CAPACITANCE OF A WINDING

11.6.1. Introduction

This subject has been extensively discussed in the literature,^{8,9,10} in the present context it is only necessary to describe briefly the basic approach and to summarize the more important results.

It is usually assumed in the analysis of self capacitance that the current distribution in the winding is not significantly different from that which exists at low frequency. More specifically, it is assumed that the voltage between any two points on a winding is proportional to the number of turns separating them. This assumption is adopted in the analytical results quoted here.

The distributed capacitance between turns of a winding, and between the winding and the surroundings, may for most purposes be represented by a self capacitance C_s connected across the winding. The end capacitances shown in Fig. 5.10(a) may or may not be included in C_s depending on the circumstances (see also Eqn 5.16). The general method of calculating C_s is to equate the energy stored in it, i.e. $\frac{1}{2}C_s U^2$, to the sum of all the energy in the distributed capacitance. Assuming that the winding consists of one or more regular layers wound over a screen or a conductive core, three main categories of distributed capacitance may be distinguished, namely, that between adjacent layers, that between layers and screen (or core) and that between adjacent turns. The self capacitance reflected across the terminals of a winding having N turns, due to the capacitance between a pair of adjacent turns, is $(1/N)^2 \times$ the adjacent-turn capacitance so the total contribution of the adjacent-turn capacitance is only significant when there are few turns. Thus it is in single layer windings that it becomes important. In such windings the capacitance between non-adjacent turns may also contribute significantly. The problem of the isolated single layer winding is considered at the end of this section.

11.6.2. A general method of analysis

It follows from the above discussion that the problem is to find an expression for C_s in terms of the inter-layer and/or the layer-to-screen capacitance. In the following treatment, which is based on a paper by Duerdoth,⁹ the term 'screen' is taken to include any conductive surface, such as a core, adjacent to the first layer.

Fig. 11.13 shows two adjacent surfaces representing winding layers or a layer and a screen. In general the

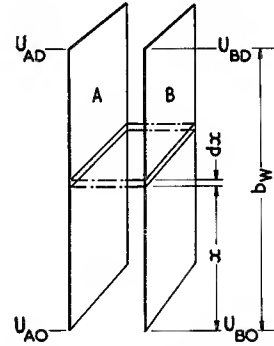


Fig. 11.13. Calculation of self capacitance due to winding layers. Representation of two adjacent conductive layers each having a linear potential distribution. (After Duerdoth⁸)

potential of surface A may be taken as varying linearly from U_{AO} at the lower end to U_{AD} at the upper end. Similarly the potential of the surface B varies linearly from U_{BO} to U_{BD} . If surface A is a screen, the surface is at uniform potential and $U_{AO} = U_{AD}$. The potential difference between the two surfaces will in general vary linearly along the length from $U_o = U_{BO} - U_{AO}$ at the bottom to $U_d = U_{BD} - U_{AD}$ at the top, possibly becoming zero at some point depending on the polarity and distribution of the surface potentials.

The potential difference at the element dx is

$$U_o + (U_d - U_o) \frac{x}{b_w} \quad V$$

where b_w is the width of the layer. The associated electrical energy is

$$dW = \frac{1}{2} C_l \frac{dx}{b_w} \left\{ U_o + (U_d - U_o) \frac{x}{b_w} \right\}^2 \quad J$$

where C_l is the capacitance between the two surfaces considered as a parallel plate capacitor, i.e. when there is a uniform voltage distribution over each surface. Integrating over the surface, the total energy is

$$W = \frac{C_l}{6} (U_o^2 + U_o U_d + U_d^2) \quad J$$

U_o and U_d must be of consistent sign convention. If one of the surfaces represents a layer of a winding having

a total voltage U_p across it then the self capacitance, C_s , appearing across the terminals of that winding due to the distributed capacitance may be obtained by equating energies:

$$\frac{1}{2}C_s U_p^2 = \frac{C_l}{6}(U_o^2 + U_o U_D + U_D^2)$$

$$\therefore C_s = \frac{C_l}{3U_p^2}(U_o^2 + U_o U_D + U_D^2) \quad \text{F} \quad (11.30)$$

If there are several layers of distributed capacitance contributing to the total self capacitance of a winding, the contributions of these layers must be added to the

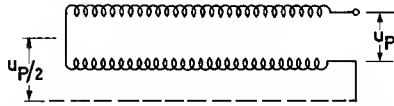


Fig. 11.14. Representation of two layers wound over a screen
(After Duerdohth⁸)

R.H.S. of this equation to obtain the total self capacitance, observing that C_l may not necessarily be the same for each layer.

As an example, an expression will be derived for the self capacitance of the two-layer winding over a screen illustrated in Fig. 11.14. Let the total applied voltage be U_p and let C_m and C_l represent the parallel-plate capacitance between layer and screen, and between layers, respectively. Applying Eqn 11.30 to each part.

$$C_s = \frac{C_m}{3U_p^2} \left(0 + 0 + \frac{U_p^2}{4} \right) + \frac{C_l}{3U_p^2} (U_p^2 + 0 + 0)$$

$$C_s = \frac{C_m}{12} + \frac{C_l}{3} \quad (11.31)$$

Table 11.3 gives expressions for the self capacitance of a number of commonly used winding arrangements. The first part of this table is concerned with single windings varying in configuration from one layer to a multi-layer winding having several sections. In most cases the screen is also shown and this is connected to some point on the winding. In practice, even if no physical connection is made, the screen or core may often be considered to be at a potential equal to that at some point on the winding. It has been convenient in the table to consider the windings as wound *over* the screen but the results are of course true for the inverted arrangement.

The second part of Table 11.3 is concerned with the winding arrangements commonly used in wide band transformers. These are all simple single-layer arrangements and there is usually a screen which is connected to, or considered to be equal in potential to, a point on one of the windings. The windings are connected together at points which are assumed to be of equal potential.

For transformers having many layers it may be possible to neglect the winding-winding or the winding-screen capacitances and calculate the self capacitance of each winding considered separately as in the first part of the table. For the intermediate cases of transformers having a few layers the self capacitance must be calculated from first principles by the method described above.

It should be noted that in the second section of the table a number of additional variations are implied. E.g. for item 8 the variations may be set out as follows:

	Self capacitance referred to primary, C_s	Self capacitance referred to secondary, $C'_s = C_s/r^2$
r very large	$\frac{C_m}{3} + \frac{C_l r^2}{3}$	$\frac{C_m}{3r^2} + \frac{C_l}{3}$
r very small	$\frac{C_m}{3} + \frac{C_l}{3}$	$\frac{C_m}{3r^2} + \frac{C_l}{3r^2}$
$r = 1$	$\frac{C_m}{3}$	$\frac{C_m}{3r^2}$

To use the expressions for self capacitance it is necessary to determine C_l and C_m . This may be done experimentally by measuring the direct capacitance between two single layers or between a layer and a screen; the winding conductor and interleaving insulation must correspond with the proposed winding but any difference in superficial area may be corrected by proportion.

Alternatively the values may be calculated by treating the adjacent surfaces as a parallel plate capacitor in which

$$C = \frac{\epsilon_o \epsilon A}{S_e} \cdot 10^{12} \quad \text{pF} \quad (11.32)$$

where $\epsilon_o = 8.854 \times 10^{-12}$

ϵ is the effective permittivity of the dielectric

A is the area of the surface ($= b_w l_w$) in m^2

and S_e is the effective thickness of the dielectric in m.

If the dimensions are in mm

$$C = 0.008854 \frac{\epsilon A}{S_e} \quad \text{pF} \quad (11.32(a))$$

Since one or both of the surfaces consist of a layer of round conductors the effective thickness of the dielectric is not defined.

Empirical formulae for calculating S_e were proposed by Zuhr¹¹ and are quoted in Fig. 11.15. These are claimed to be accurate to 2% provided d is between 0.5c and 0.9c and S is between 1.2c and 1.8c

$$(11.32) \quad C = 0.08854 \frac{\epsilon A}{S_e} \quad \text{pF}$$

Table 11.3a. SELF CAPACITANCE OF VARIOUS ARRANGEMENTS OF A SINGLE WINDING AND SCREEN.

C_m is the low-frequency capacitance that would be measured between layer and screen when disconnected, (see Eqn 11.32).

C_l is the low-frequency capacitance that would be measured between adjacent layers when disconnected, (see Eqn 11.32).

C_m and C_l refer to layers extending across the full winding width except in case 6 where they refer to the layers in each section.

p is the number of layers wound one above another.

q is the number of sections.

N is the number of turns.

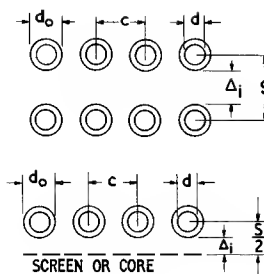
	Winding arrangement	Description	Self capacitance
1		Unbalanced single layer winding and screen	$\frac{C_m}{3}$
2		Balanced single layer winding and screen	$\frac{C_m}{12}$
3		Balanced double layer winding and screen	$\frac{1}{12} \left(\frac{C_m}{4} + C_l \right)$
4		Double layer winding, both layers starting at R.H.S. Start connected to screen	$\frac{C_m}{12} + \frac{C_l}{4}$
5		Normal winding of p layers, start connected to screen	$\frac{C_m}{3p^2} + \frac{4C_l(p-1)}{3p^2}$
		Normal winding with q sections, each with p layers: without screen—	$\frac{4C_l(p-1)}{3p^2q}$
6		Additional self capacitance due to screen:	
		$q = 2$	$\frac{C_m}{3} \cdot \frac{3p^2 + 3p + 2}{4p^2}$
		$q = 3$	$\frac{C_m}{3} \cdot \frac{5p^2 + 3p + 1}{3p^2}$
		$q = 4$	$\frac{C_m}{3} \cdot \frac{42p + 18p + 4}{16p^2}$
7		Single spiral of flat strip	$C_l \cdot \frac{N-1}{N^2}$

In the absence of more specific data the value of the effective permittivity of the dielectric may be taken as 4 if the winding is impregnated with wax and 3.5 if it is unimpregnated.

A useful guide to the self capacitance of a simple multilayer winding may be obtained from expression 5 of Table 11.3a and Eqn 11.32. Considering only the interlayer capacitance and assuming that there are a large number of layers

$$C_s \propto \frac{C_l}{p} \propto \frac{A}{pS_e} \propto \frac{b_w l_w}{pS_e}$$

where b_w = width of the winding
 l_w = mean turn length



$$S_e = S - 1.15d + 0.26c$$

$$= \Delta_i + d_o - 1.15d + 0.26c$$

FOR UNSPACED WINDING $c = d_o$
 THEN $S_e = \Delta_i + 1.26d_o - 1.15d$

$$S_e = \frac{1}{2} (S - 1.15d + 0.26c)$$

$$= \Delta_i + \frac{1}{2} (d_o - 1.15d + 0.26c)$$

FOR UNSPACED WINDING $c = d_o$
 THEN $S_e = \Delta_i + \frac{1}{2} (1.26d_o - 1.15d)$

Fig. 11.15. Effective thickness of dielectric between adjacent winding layers or between a winding layer and a screen. (After Zuhr¹¹) See wire tables in Appendix A for d and d_o . Also, under "Functions of copper wire diameter" in the Appendix tables the values of $d_o - 1.15d$ and $1.26d_o - 1.15d$ are listed for enamelled wires and bunched conductors

Table 11.3b. SELF CAPACITANCES OF VARIOUS ARRANGEMENTS OF TRANSFORMER WINDINGS AND SCREEN

The self capacitances are referred to the primary winding, i.e. the lower winding in each diagram.

r = Secondary e.m.f./primary e.m.f. = turns ratio. The expressions given apply when both primary and secondary are wound in the same direction. If the winding directions

are opposite, r must be treated as a negative number.

The connection shown between primary and secondary need not be a physical one; it is intended to indicate points of common potential.

Other symbols as in Table 11.3a.

	Winding arrangement	Description	Self capacitance referred to primary
8		Unbalanced single layer windings, both connected to the screen at one end	$\frac{C_m}{3} + \frac{C_l}{3}(1-r)^2$
9		Unbalanced single layer windings, opposite ends connected to the screen	$\frac{C_m}{3} + \frac{C_l}{3}(1+r+r^2)$
10		Unbalanced single layer windings connected to interposed screen. Winding to screen capacitances equal	$\frac{C_m}{3}(1+r^2)$
11		Balanced to unbalanced single layer windings without screen	$\frac{C_l}{3} \left(1 - \frac{r}{2} + \frac{r^2}{4} \right)$
12		Balanced to unbalanced single layer windings with interposed screen. Winding to screen capacitances equal	$\frac{C_m}{3} \left(1 + \frac{r^2}{4} \right)$
13		Balanced to balanced single layer windings without screen	$\frac{C_l}{12}(1-r)^2$

For a given winding cross-sectional area $A_w (= b_w h_w)$ and a given number of turns it follows from Eqn 11.1 that

$$p = \frac{h_w}{d_o} = h_w \sqrt{(N/A_w)} \propto h_w$$

S_e will be constant because if the winding cross-sectional area and the number of turns are both constant the wire diameter is constant,

$$\therefore C_s \propto \frac{b_w l_w}{h_w} \quad (11.33)$$

This expression shows the relation between self capacitance and the geometry of the winding. Clearly it is an advantage to use a winding area which is tall in comparison with its breadth. Sectionalizing is an artificial method of achieving this if the given winding area is unfavourable.

For random or scramble wound coils the calculation of self capacitance will obviously be less reliable than the corresponding calculation for multilayer coils. However provided the winding is laid evenly using a traversing pitch appropriate to a layer winding then a reasonable

guide to the self capacitance of a cylindrical winding may be obtained by assuming that it is built up as shown in Fig. 11.2(a) and using expression 5 of Table 11.3a. The number of layers may be taken as the winding height divided by the overall wire diameter, and C_l may be calculated from equation 11.32 and Fig. 11.15 by putting $\Delta_i = 0$.

As an example, consider a 25 mm dia. ferrite pot core. The winding height h_w is 4.0 mm, the winding breadth is 9.0 mm and the mean turn length is 52.7 mm. Therefore the area of the mean layer is 470 mm². Assuming the winding consists of 0.0092 in ($d_o = 0.264$ mm) fine enamel covered wire unimpregnated

$$\varepsilon = 3.5$$

$$\text{and } S_e = 1.26d_o - 1.15d$$

$$= 0.0545 \text{ mm for } 0.0092 \text{ in wire (from Table A.1.2.3 in Appendix A)}$$

Therefore from Eqn 11.32

$$C_1 = \frac{8.854 \times 10^{-12} \times 3.5 \times 470 \times 10^{-3} \times 10^{12}}{0.0545}$$

$$= 278 \text{ pF}$$

$$\text{The number of layers, } p = 4.0/0.264 = 15$$

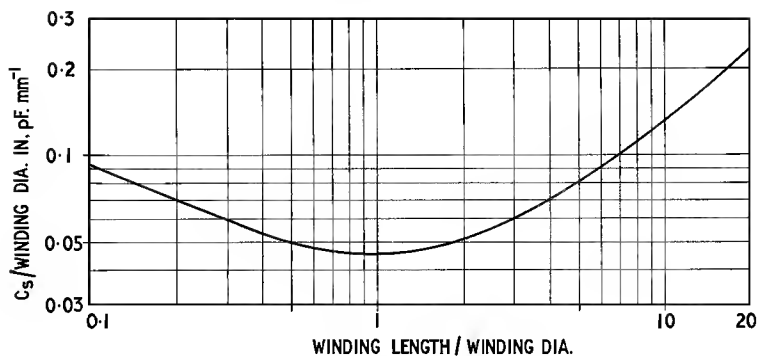


Fig. 11.16. Self capacitance of a physically isolated single layer winding according to Medhurst¹². One end of the winding is earthed and the capacitance due to the connection leads has not been included.

Therefore from expression 5 of Table 11.3(a)

$$C_1 = \frac{4}{3} \cdot \frac{14}{225} \cdot 278 = 23 \text{ pF}$$

This corresponds to the element designated C_a in Fig. 5.10 and is in close agreement with the results quoted in Table 5.3. The value of C_a obtained on a given coil former wound to a given winding height depends very little on the number of turns because as the wire diameter gets smaller, the number of layers increases (tending to reduce C_a) while S_e decreases (tending to increase C_a).

To calculate the capacitance between the start of a multilayer winding and the core, assuming that the core is isolated from the winding and that the number of layers is large, Eqn 11.32 may again be used, S_e being obtained from the lower part of Fig. 11.15 by putting Δ_i equal to the separation of the first layer from the core and choosing an appropriate value of ϵ . If Δ_i is large compared with the wire diameter then S_e may be taken as equal to Δ_i .

The discussion so far has not applied to physically isolated single layer windings. The single layer windings considered have been in the proximity of a conductive layer so that the capacitance between the turns and that layer have made the major contribution to the self capacitance. For an isolated single layer winding the capacitance between turns and the capacitance between the winding as a whole and its (distant) surroundings are both important.

Medhurst¹² studied this subject and came to the conclusion that the self capacitance is independent of the conductor diameter and the spacing of the turns; it depends only on the diameter and length of the winding. His experimental results, based on measurements of a wide variety of single layer windings, are summarized in Fig. 11.16. These results may also be used to estimate the self capacitance of a single layer winding located approximately half way up the winding area of a ferrite core,

e.g. a pot core, particularly if the ferrite is of a high resistivity grade.

11.7. LEAKAGE INDUCTANCE IN TRANSFORMERS

11.7.1. General

The flux linkage between two windings or parts of the same winding is never complete. In addition to the mutual flux, which does link both of the windings, there are various leakage fluxes. Some are those which fail to link all the turns of the winding which generates them, while others, having completely linked the generating winding, fail to link all the turns of an adjacent winding. This situation is obvious in the case of an air-cored mutual inductance, but, to a lesser degree, it also applies to windings surrounded by a high permeability core as shown in Fig. 11.17.

If the primary winding, P , is energized by a current flowing in the direction shown then, if the secondary winding is loaded, the secondary current will flow in the reverse direction. The instantaneous difference between the primary and secondary ampere turns will equal the

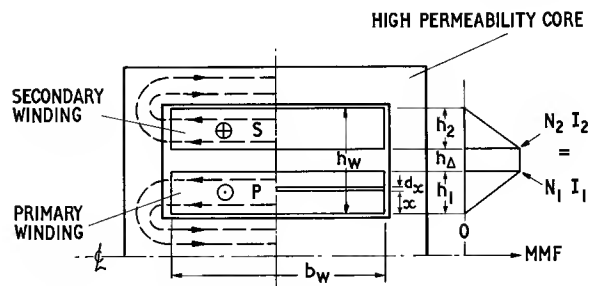


Fig. 11.17. Leakage inductance in a simple transformer. The L.H.S. of the diagram represents the leakage flux paths; the R.H.S. shows how the magneto motive force varies with the distance, x , from the inner surface of the winding

instantaneous magnetizing ampere turns and determine the instantaneous mutual flux. In addition there will be leakage fluxes shown diagrammatically by broken lines in the L.H.S. of Fig. 11.17. In practice these fluxes combine, within the core, with the main flux and so lose their individual identities. The resultant flux pattern not only depends on the geometry of the winding and core but also varies with time over the cycle.

If the secondary is short-circuited, the main flux which links both windings will be negligible because the primary and secondary ampere turns almost cancel. The flux pattern will then be as shown in the L.H.S. of Fig. 11.17. The fluxes contributed by each winding are in the same direction in the winding space and mutually repel. The residual e.m.f. due to this flux will appear as inductance in series with the primary terminals and is termed the leakage inductance referred to the primary. The symbol L_l will be used to denote leakage inductance. Its magnitude may be calculated by equating its energy, $\frac{1}{2}L_l I_1^2$, to the magnetic energy of the leakage flux.

The R.H.S. of Fig. 11.17 shows an elementary layer of winding, of thickness dx , situated at a distance x from the inner surface of the winding. The field strength along the flux path which includes this layer depends on the number of ampere turns linked by the path i.e.

$$\oint H ds = N_1 I_1 \frac{x}{h_1} \quad A$$

where s is the distance along the flux path
 N_1 is the number of primary turns
 and I_1 is the primary current

Since the reluctance of the path within the magnetic core is negligible compared with that of the path in the winding, H may be taken as the field strength in the winding layer dx . It is assumed to be constant along the layer and this is supported by the experimental results. The uniformity arises mainly from the mutual repulsion of the winding fluxes which ensures that the flux direction is substantially parallel to the interface between the windings (if the primary and secondary were wound side-by-side, the leakage flux would be perpendicular to the direction shown in Fig. 11.17).

Thus

$$H = \frac{N_1 I_1}{b_w} \frac{x}{h_1} \quad A.m^{-1} \quad (11.34)$$

It is usual to use the winding breadth, b_w , rather than the window breadth, b_a , because the flux disperses rapidly on leaving the winding and the associated energy is much reduced. This is particularly so at winding edges

that may be outside the confines of the core, e.g. an E or U core.

The magnetomotive force will vary linearly from zero when $x = 0$ to $N_1 I_1$ when $x = h_1$, as shown in the diagram on the R.H.S. of Fig. 11.17. It will be constant across the interwinding space because the ampere turns embraced by the line integral in this region are constant. As the secondary winding space is traversed the magnitude of the magnetomotive force will fall linearly to zero since $N_1 I_1 = -N_2 I_2$.

The volume of the elementary layer is $l_w \cdot b_w \cdot dx$, therefore the energy stored in the field is

$$\frac{\mu_0}{2} \int_0^{h_1} H^2 dx l_w b_w$$

The mean length, l_w , is usually taken as a constant for the windings as a whole, i.e. it is based on $h_w/2$. The energy in the total winding space is then

$$\begin{aligned} \frac{\mu_0 l_w b_w}{2} \left\{ \int_0^{h_1} \left(\frac{N_1 I_1 x}{b_w h_1} \right)^2 dx + \left(\frac{N_1 I_1}{b_w} \right)^2 h_d \right. \\ \left. + \int_0^{h_2} \left(\frac{N_2 I_2 x}{b_w h_2} \right)^2 dx \right\} \\ = \frac{1}{2} L_l I_1^2 \text{ by definition} \end{aligned}$$

Since $|N_1 I_1| = |N_2 I_2|$ this equation reduces to

$$\begin{aligned} \frac{1}{2} L_l I_1^2 &= \frac{\mu_0 l_w}{2 b_w} \left(\frac{h_1 + h_2}{3} + h_d \right) N_1^2 I_1^2 \\ \therefore L_l &= \mu_0 N_1^2 \frac{l_w}{b_w} \left(\frac{h_1 + h_2}{3} + h_d \right) \quad H \quad (11.35) \end{aligned}$$

This equation gives the value of the leakage inductance referred to the primary. The value referred to the secondary may be obtained by simply substituting N_2 for N_1 .

If the physical dimensions are in millimetres:

$$L_l = 4\pi 10^{-4} N_1^2 \frac{l_w}{b_w} \left(\frac{h_1 + h_2}{3} + h_d \right) \quad \mu H \quad (11.36)$$

This method of derivation may be extended to a variety of winding arrangements. Fig. 11.18 gives results for windings sectionalized various ways. Other arrangements are considered in the literature.

It often happens that Σx_d is negligible compared with Σx so that $(\Sigma x/3 + \Sigma x_d) \propto X$, the total winding dimen-

$$(11.34) \quad H = \frac{4\pi N_1 I_1}{10 b_w} \frac{x}{h_1} \quad \text{Oe}$$

$$(11.35) \quad L_l = 4\pi 10^{-9} N_1^2 \frac{l_w}{b_w} \left(\frac{h_1 + h_2}{3} + h_d \right) \quad H$$

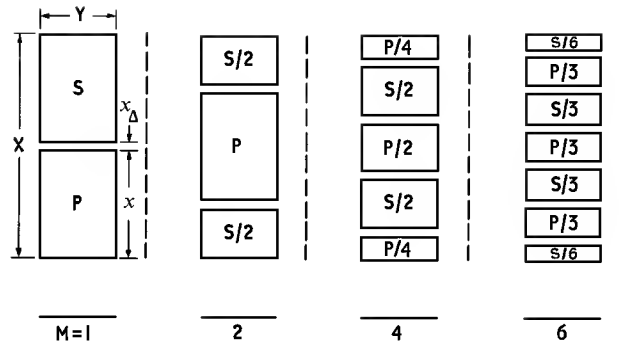


Fig. 11.18. The leakage inductance of commonly used winding arrangements. The diagram and the equation below may be used for transformers in which the primary and secondary sections are wound one above the other, i.e. where $X = h_w$, $Y = b_w$ and the solid line represents the winding axis, or for transformers in which the sections are wound side-by-side, i.e. where $X = b_w$, $Y = h_w$ and the broken line represents the coil axis.

$$L_l = 4\pi \cdot 10^{-4} \frac{N^2 l_w}{M^2 Y} \left(\frac{\sum x}{3} + \sum x_A \right) \quad \mu H$$

where N is the number of turns on the winding to which the leakage inductance is to be referred.

M is the number of section interfaces.

l_w is the mean turn length in mm.

Y is the winding dimension parallel to the section interfaces, in mm.

X is the overall winding dimension perpendicular to the section interfaces.

$\sum x$ is the sum of all section dimensions perpendicular to the section interfaces, in mm, i.e. $X - \sum x_A$

$\sum x_A$ is the sum of all inter-section layer thicknesses, in mm

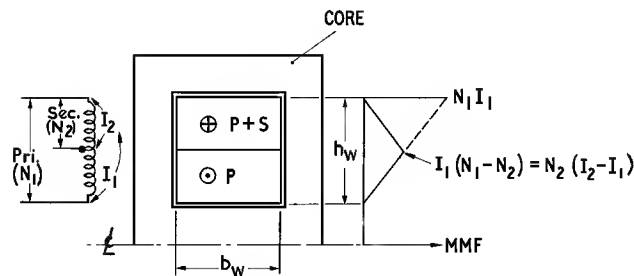


Fig. 11.19. Leakage inductance in an auto-transformer. The R.H.S. of the diagram shows how the magnetomotive force varies with the distance from the inner surface of the winding

sion perpendicular to the inter-section layers (see Fig. 11.18). Therefore, for a given winding arrangement $L_l \propto N^2 l_w X/Y$. For a transformer having winding sections wound one above another $X = h_w$, the winding height, and $Y = b_w$, the winding breadth, so

$$L_l \propto N_1^2 \frac{l_w h_w}{b_w} \quad (11.37a)$$

while for a transformer having sections wound side-by-side $X = b_w$ and $Y = h_w$ so

$$L_l \propto N_1^2 \frac{l_w b_w}{h_w} \quad (11.37b)$$

The latter arrangement requires a winding area which is tall and narrow if the leakage inductance is to be made as small as possible. Some of the advantage would be lost because such a winding shape would lead to a larger value of l_w . For these reasons the side-by-side arrangements is not often used. The more conventional method of winding the sections one above another leads to a leakage inductance which is related to the winding area geometry as shown in Eqn 11.37a i.e. for minimum leakage inductance the winding area is wide and shallow. This is the reverse of the requirement for least self-capacitance (see Eqn 11.33).

The presence of an air gap in the core usually has little effect on the leakage inductance provided it is not so large as to cause appreciable distortion of the field in the winding space. Since the air gap reduces the primary open-circuit inductance, L_p , the ratio L_p/L_l is reduced and this, as discussed in Chapter 7, reduces the possible bandwidth of the transformer.

At high frequencies the current distribution in the conductors will be disturbed due to eddy currents. The effect is to cause the current to concentrate at the surface of the conductor that faces the nearest winding interface. This results in a lower leakage inductance, although the reduction is only significant when the windings consist of few layers of fairly thick conductors. Dowell⁴ has analysed this effect and has given data for the calculation of high frequency leakage inductance. It is related to the high frequency resistance of transformer windings discussed in Section 11.4.4 and is only significant when there is an appreciable high frequency contribution to the winding resistance.

11.7.2. Auto-transformer windings and bifilar windings

A diagram of a typical auto-transformer is shown in Fig. 11.19. Between the start of the primary and the secondary tap the magnetomotive force rises linearly as before, reaching $I_1(N_1 - N_2)$. The secondary ampere-

turns are then superimposed on those of the primary so that viewed from the other end of the winding the magnetomotive force at the tap is

$$N_2(I_2 - I_1) = N_2(I_1 N_1/N_2 - I_1) = I_1(N_1 - N_2)$$

Integrating as before, the leakage inductance referred to the primary winding is found to be

$$L_l = \frac{\mu_0 l_w}{b_w} (N_1 - N_2)^2 \cdot \frac{h_w}{3} \quad \text{H} \quad (11.38)$$

If the physical dimensions are in mm

$$L_l = 4\pi 10^{-4} \frac{l_w}{b_w} (N_1 - N_2)^2 \frac{h_w}{3} \quad \mu\text{H} \quad (11.39)$$

Thus an auto-transformer has lower leakage inductance than the corresponding two-winding transformer.

A bifilar wound transformer is one in which the primary and secondary windings are wound together by feeding on the two winding conductors side-by-side so that each layer consists of alternate primary and secondary conductors. This represents the ultimate intermingling of the windings and if the primary and secondary have equal numbers of turns then the leakage inductance will be extremely small; the self-capacitance may however be prohibitively large. If the numbers of turns are not equal then there will be a part of the larger winding in which there is no bifilar cancellation of the field. The situation is then similar to the auto-transformer and the result derived above may be used.

REFERENCES AND BIBLIOGRAPHY

Section 11.4.1.

1. WELSBY, V. G., *The theory and design of inductance coils*, Macdonald and Co. (Publishers) Ltd., London, 2nd Edition, (1960).

Sections 11.4.2. and 11.4.3.

2. HOWE, G. W. O., 'The application of telephone transmission formulae to skin effect problems', *J. Instn elect. Engrs*, **54**, 473, (1916).
3. BUTTERWORTH, S., 'Effective resistance of inductance coils at radio frequency', *Expl. Wireless*, **3**, 203, (1926).
- HOWE, G. W. O., 'The high frequency resistance of wires and coils', *J. Instn elect. Engrs*, **58**, 152, (1920).
- BUTTERWORTH, S., 'Eddy current losses in cylindrical conductors with special applications to the alternating current resistance of short coils', *Phil. Trans. R. Soc.*, **A222**, 57, (1922).
- CASIMIR, H. B. G. and UBBINK, J., 'The skin effect', *Philips tech. Rev.*, **28**, 271, (Part 1) and 300, (Part 2), (1967).

$$(11.38) \quad L_l = 4\pi 10^{-9} \frac{l_w}{b_w} (N_1 - N_2)^2 \frac{h_w}{3} \quad \text{H}$$

Section 11.4.4.

4. DOWELL, P. L., 'Effects of eddy currents in transformer windings', *Proc. Instn elect. Engrs*, **113**, 1387, (1966).
5. FIELD, A. B., 'Eddy currents in large slot-wound conductors', *Proc. Am. Inst. elect. Engrs*, **25**, 659, (1905).

Section 11.5.

6. NAGAOKA, H., 'The inductance coefficients of solenoids', *J. Coll. Sci. imp Univ. Tokyo*, **27**, art 6, (1909).
7. GROVER, F. W., *Inductance calculations*, van Nostrand Company Inc. (1946).

Section 11.6.

8. DUERDOTH, W. T., 'Equivalent capacitances of transformer windings', *Wireless Engr*, **23**, 161, (1946).
9. MAURICE, D. and MINNS, R. H., 'Very-wide band radio frequency transformers', *Wireless Engr*, **24**, 168, (Part 1) and 209, (Part 2), (1947).
10. MACFADYAN, K. A., *Small transformers and inductors*, Chapman and Hall, Ltd., (1953).

Section 11.6.2.

DUERDOTH, see section 11.6.

11. ZUHRT, H., 'Einfache Näherungsformeln für die Eigenkapazität Mehrlagiger-Spulen', *Elektrotech. Z.*, **55**, 662, (1934).
12. MEDHURST, R. G., 'H.F. resistance and self-capacitance of single-layer solenoids', *Wireless Engr*, **24**, 35, (1947).

Section 11.7.

STAFF OF DEPT. OF ELECT. ENGG, M.I.T., *Magnetic circuits and transformers*, John Wiley and Sons Inc., New York, (1943).

MAURICE, D., *et al.*, see section 11.6.

MATSCH, W. M., *Capacitors, magnetic circuits, and transformers*, Prentice-Hall, Inc., Englewood Cliffs N.J., (1964).

GROSSNER, N. R., *Transformers for electronic circuits*, McGraw-Hill Book Company, (1967).

Appendix A

Wire Tables

A.1. SWG

A.2. METRIC

A.3. AWG

A.4. BUNCHED CONDUCTORS

Table A.1.1. PROPERTIES OF BARE COPPER WIRES—SWG
(BASED ON BS 156: 1951)

Gauge No.	Copper diameter (d)						Nominal Copper Area		Nominal resistance per unit length, (R_c)	
SWG	Nominal		Maximum		Minimum		in ²	mm ²	Ω/100 in	Ω/m
	in	mm	in	mm	in	mm				
50	0.001 0	0.025 4	0.001 08	0.027 43	0.000 92	0.023 37	$0.785 4 \times 10^{-6}$	$0.506 7 \times 10^{-3}$	84.91	33.43
49	0.001 2	0.030 5	0.001 28	0.032 51	0.001 12	0.028 45	1.131×10^{-6}	$0.729 7 \times 10^{-3}$	58.97	23.22
48	0.001 6	0.040 6	0.001 68	0.042 67	0.001 52	0.038 61	2.011×10^{-6}	1.297×10^{-3}	33.17	13.06
47	0.002 0	0.050 8	0.002 08	0.052 83	0.001 92	0.048 77	3.142×10^{-6}	2.027×10^{-3}	21.23	8.357
46	0.002 4	0.061 0	0.002 48	0.062 99	0.002 32	0.058 93	4.524×10^{-6}	2.919×10^{-3}	14.74	5.804
45	0.002 8	0.071 1	0.002 89	0.073 41	0.002 71	0.068 83	6.158×10^{-6}	3.973×10^{-3}	10.83	4.264
44	0.003 2	0.081 3	0.003 29	0.083 57	0.003 11	0.078 99	8.042×10^{-6}	5.189×10^{-3}	8.292	3.265
43	0.003 6	0.091 4	0.003 7	0.093 98	0.003 5	0.088 9	10.18×10^{-6}	6.567×10^{-3}	6.553	2.580
42	0.004 0	0.102	0.004 1	0.104 1	0.003 9	0.099 06	12.57×10^{-6}	8.107×10^{-3}	5.307	2.089
41	0.004 4	0.112	0.004 5	0.114 3	0.004 3	0.109 2	15.21×10^{-6}	9.810×10^{-3}	4.386	1.727
40	0.004 8	0.122	0.004 9	0.124 5	0.004 7	0.119 4	18.10×10^{-6}	11.68×10^{-3}	3.685	1.451
39	0.005 2	0.132	0.005 3	0.134 6	0.005 1	0.129 5	21.24×10^{-6}	13.70×10^{-3}	3.140	1.236
38	0.006 0	0.152	0.006 1	0.154 9	0.005 9	0.149 9	28.27×10^{-6}	18.24×10^{-3}	2.359	0.928 6
37	0.006 8	0.173	0.006 9	0.175 3	0.006 7	0.170 2	36.32×10^{-6}	23.43×10^{-3}	1.836	0.723 0
36	0.007 6	0.193	0.007 7	0.195 6	0.007 5	0.190 5	45.36×10^{-6}	29.27×10^{-3}	1.470	0.578 7
35	0.008 4	0.213	0.008 5	0.215 9	0.008 3	0.210 8	55.42×10^{-6}	35.75×10^{-3}	1.203	0.473 8
34	0.009 2	0.234	0.009 3	0.236 2	0.009 1	0.231 1	66.48×10^{-6}	42.89×10^{-3}	1.003	0.395 0
33	0.010 0	0.254	0.010 1	0.256 5	0.009 9	0.251 5	78.54×10^{-6}	50.67×10^{-3}	0.849 2	0.334 3
32	0.010 8	0.274	0.010 9	0.276 9	0.010 7	0.271 8	91.61×10^{-6}	59.10×10^{-3}	0.728 1	0.286 6
31	0.011 6	0.295	0.011 7	0.297 2	0.011 5	0.292 1	105.7×10^{-6}	68.18×10^{-3}	0.631 1	0.248 5
30	0.012 4	0.315	0.012 5	0.317 5	0.012 3	0.312 4	$0.120 8 \times 10^{-3}$	0.077 91	0.552 2	0.217 4
29	0.013 6	0.345	0.013 7	0.348 0	0.013 5	0.342 9	$0.145 3 \times 10^{-3}$	0.093 72	0.459 1	0.180 7
28	0.014 8	0.376	0.014 9	0.378 5	0.014 7	0.373 4	$0.172 0 \times 10^{-3}$	0.111 0	0.387 6	0.152 6
27	0.016 4	0.417	0.016 6	0.421 6	0.016 2	0.411 5	$0.211 2 \times 10^{-3}$	0.136 3	0.315 7	0.124 3
26	0.018 0	0.457	0.018 2	0.462 3	0.017 8	0.452 1	$0.254 5 \times 10^{-3}$	0.164 2	0.262 1	0.103 2
25	0.020	0.508	0.020 2	0.513 1	0.019 8	0.502 9	$0.314 2 \times 10^{-3}$	0.202 7	0.212 3	0.083 58
24	0.022	0.559	0.022 2	0.563 9	0.021 8	0.553 7	$0.380 1 \times 10^{-3}$	0.245 3	0.175 4	0.069 07
23	0.024	0.610	0.024 2	0.614 7	0.023 8	0.604 5	$0.452 4 \times 10^{-3}$	0.291 9	0.147 4	0.058 04
22	0.028	0.711	0.028 3	0.718 8	0.027 7	0.703 6	$0.615 8 \times 10^{-3}$	0.397 3	0.108 3	0.042 64
21	0.032	0.813	0.032 3	0.820 4	0.031 7	0.805 2	$0.804 2 \times 10^{-3}$	0.518 9	0.082 92	0.032 65
20	0.036	0.914	0.036 4	0.924 6	0.035 6	0.904 2	1.018×10^{-3}	0.656 7	0.065 53	0.025 80
19	0.040	1.02	0.040 4	1.026	0.039 6	1.005 8	1.257×10^{-3}	0.810 7	0.053 07	0.020 89
18	0.048	1.22	0.048 5	1.232	0.047 5	1.206 5	1.810×10^{-3}	1.168	0.036 85	0.014 51
17	0.056	1.42	0.056 6	1.438	0.055 4	1.407	2.463×10^{-3}	1.589	0.027 08	0.010 66
16	0.064	1.63	0.064 6	1.641	0.063 4	1.610	3.217×10^{-3}	2.076	0.020 73	0.008 162
15	0.072	1.83	0.072 7	1.847	0.071 3	1.811	4.072×10^{-3}	2.627	0.016 38	0.006 449
14	0.080	2.03	0.080 8	2.052	0.079 2	2.012	5.027×10^{-3}	3.243	0.013 27	0.005 223
13	0.092	2.34	0.092 9	2.360	0.091 1	2.314	6.648×10^{-3}	4.289	0.010 03	0.003 950
12	0.104	2.64	0.105 0	2.667	0.103 0	2.616	8.495×10^{-3}	5.481	0.007 850	0.003 091
11	0.116	2.95	0.117 2	2.977	0.114 8	2.916	10.57×10^{-3}	6.818	0.006 311	0.002 485
10	0.128	3.25	0.129 3	3.284	0.126 7	3.218	12.87×10^{-3}	8.302	0.005 183	0.002 040

Table A.1.2.1. PROPERTIES OF FINE ENAMELLED COPPER WIRES—SWG (BASED ON BS 1844: 1952—FINE COVERING)

SWG	Copper dia. (d)	Overall dia. (max.) (d _o)		Increase in dia. due to insulation (min)		Approximate weight		Turns per unit winding breadth (1/d _o)		Turns per unit winding area (1/d _o ²)		Winding space factor $F_w = \frac{\pi}{4} \left(\frac{d}{d_o} \right)^2$
		in	mm	in	mm	lb/100 in	g/m	in ⁻¹	mm ⁻¹	in ⁻²	mm ⁻²	
50*	0.001 0	0.001 4*	0.035 56	0.000 12	0.003 05	0.027 22 × 10 ⁻³	0.004 861	714	28.1	510 000	791	0.400 7
49*	0.001 2	0.001 6*	0.040 64	0.000 14	0.003 56	0.038 89 × 10 ⁻³	0.006 945	625	24.6	391 000	605	0.441 8
48*	0.001 6	0.002 0*	0.050 80	0.000 17	0.004 32	0.068 06 × 10 ⁻³	0.012 15	500	19.7	250 000	387	0.502 7
47	0.002 0	0.002 4	0.060 96	0.000 20	0.005 08	0.104 2 × 10 ⁻³	0.018 60	417	16.4	174 000	269	0.545 4
46	0.002 4	0.002 9	0.073 66	0.000 25	0.006 35	0.150 6 × 10 ⁻³	0.026 89	345	13.6	119 000	184	0.537 9
45	0.002 8	0.003 3	0.083 82	0.000 3	0.007 62	0.204 4 × 10 ⁻³	0.036 51	303	11.9	91 800	142	0.565 4
44	0.003 2	0.003 8	0.096 52	0.000 3	0.007 62	0.266 9 × 10 ⁻³	0.047 67	263	10.4	69 300	107	0.557 0
43	0.003 6	0.004 2	0.106 7	0.000 3	0.007 62	0.336 4 × 10 ⁻³	0.060 07	238	9.37	56 700	87.9	0.577 0
42	0.004 0	0.004 7	0.119 4	0.000 4	0.010 2	0.416 9 × 10 ⁻³	0.074 46	213	8.38	45 300	70.2	0.568 9
41	0.004 4	0.005 2	0.132 1	0.000 4	0.010 2	0.504 7 × 10 ⁻³	0.090 13	192	7.57	37 000	57.3	0.562 3
40	0.004 8	0.005 6	0.142 2	0.000 4	0.010 2	0.598 9 × 10 ⁻³	0.106 9	179	7.03	31 900	49.4	0.577 0
39	0.005 2	0.006 1	0.154 9	0.000 5	0.012 7	0.704 7 × 10 ⁻³	0.125 9	164	6.45	26 900	41.7	0.570 7
38	0.006 0	0.006 9	0.175 3	0.000 5	0.012 7	0.934 7 × 10 ⁻³	0.166 9	145	5.71	21 000	32.6	0.593 9
37	0.006 8	0.007 9	0.200 7	0.000 7	0.017 8	1.205 × 10 ⁻³	0.215 2	127	4.98	16 000	24.8	0.581 9
36	0.007 6	0.008 7	0.221 0	0.000 7	0.017 8	1.499 × 10 ⁻³	0.267 8	115	4.53	13 200	20.5	0.599 3
35	0.008 4	0.009 6	0.243 8	0.000 7	0.017 8	1.830 × 10 ⁻³	0.326 8	104	4.10	10 900	16.8	0.601 3
34	0.009 2	0.010 4	0.264 2	0.000 7	0.017 8	2.191 × 10 ⁻³	0.391 3	96.2	3.79	9 250	14.3	0.614 6
33	0.010 0	0.011 3	0.287 0	0.000 8	0.020 3	2.589 × 10 ⁻³	0.462 3	88.5	3.48	7 830	12.1	0.615 1
32	0.010 8	0.012 2	0.309 9	0.000 8	0.020 3	3.017 × 10 ⁻³	0.538 7	82.0	3.23	6 720	10.4	0.615 5
31	0.011 6	0.013 0	0.330 2	0.000 8	0.020 3	3.469 × 10 ⁻³	0.619 6	76.9	3.03	5 920	9.17	0.625 3
30	0.012 4	0.013 9	0.353 1	0.000 9	0.022 9	3.972 × 10 ⁻³	0.709 4	71.9	2.83	5 180	8.02	0.625 0
29	0.013 6	0.015 2	0.386 1	0.001 0	0.025 4	4.778 × 10 ⁻³	0.853 2	65.8	2.59	4 330	6.71	0.628 8
28	0.014 8	0.016 6	0.416 6	0.001 0	0.025 4	5.647 × 10 ⁻³	1.009	61.0	2.40	3 720	5.76	0.639 6
27	0.016 4	0.018 2	0.462 3	0.001 1	0.027 9	6.928 × 10 ⁻³	1.237	54.9	2.16	3 020	4.68	0.637 7
26	0.018 0	0.019 9	0.505 5	0.001 1	0.027 9	8.339 × 10 ⁻³	1.489	50.3	1.9	2 530	3.91	0.642 6
25	0.020	0.022 0	0.558 8	0.001 2	0.030 5	10.28 × 10 ⁻³	1.836	45.5	1.79	2 070	3.20	0.649 1
24	0.022	0.024 0	0.609 6	0.001 2	0.030 5	12.43 × 10 ⁻³	2.220	41.7	1.64	1 740	2.69	0.660 0
23	0.024	0.026 1	0.662 9	0.001 2	0.030 5	14.78 × 10 ⁻³	2.640	38.3	1.51	1 470	2.28	0.664 1
22	0.028	0.030 3	0.769 6	0.001 3	0.033 0	20.08 × 10 ⁻³	3.585	33.0	1.30	1 090	1.69	0.670 7
21	0.032	0.034 4	0.873 8	0.001 4	0.035 6	26.20 × 10 ⁻³	4.678	29.1	1.14	845	1.31	0.679 6
20	0.036	0.038 6	0.980 4	0.001 4	0.035 6	33.13 × 10 ⁻³	5.916	25.9	1.02	671	1.04	0.683 2
19	0.040	0.042 7	1.085	0.001 5	0.038 1	40.85 × 10 ⁻³	7.296	23.4	0.922	548	0.850	0.689 2
18	0.048	0.050 9	1.293	0.001 6	0.040 6	58.78 × 10 ⁻³	10.50	19.7	0.773	386	0.598 5	0.698 5
17	0.056	0.059 1	1.501	0.001 7	0.043 2	79.89 × 10 ⁻³	14.27	16.9	0.666	286	0.444	0.705 2
16	0.064	0.067 2	1.707	0.001 7	0.043 2	104.3 × 10 ⁻³	18.62	14.9	0.586	221	0.343	0.712 4
15	0.072	0.075 4	1.915	0.001 7	0.043 2	131.9 × 10 ⁻³	23.55	13.3	0.522	176	0.273	0.716 2
14	0.080	0.083 6	2.123	0.001 8	0.045 7	163.9 × 10 ⁻³	29.27	12.0	0.471	143	0.222	0.719 2
13	0.092	0.095 8	2.433	0.001 9	0.048 3	216.7 × 10 ⁻³	38.69	10.4	0.411	109	0.169	0.724 3
12	0.104	0.108 0	2.743	0.002 0	0.050 8	275.0 × 10 ⁻³	49.11	9.26	0.365	85.7	0.133	0.728 3
11	0.116	0.120 3	3.056	0.002 1	0.053 3	341.7 × 10 ⁻³	61.01	8.31	0.327	69.1	0.107	0.730 3
10	0.128	0.132 5	3.366	0.002 2	0.055 9	416.7 × 10 ⁻³	74.41	7.55	0.297	57.0	0.088 3	0.733 0

*First three rows refer to oleo enamel wire to BS 156:1951—normal covering as these gauges are not included in BS 1844:1952

Table A.1.2.2. PROPERTIES OF MEDIUM ENAMELLED COPPER WIRES—SWG (BASED ON BS 1844: 1952—MEDIUM COVERING)

SWG	Copper dia. (d)	Overall dia. (max.) (d _o)		Increase in dia. due to insulation (min)		Approximate weight		Turns per unit winding breadth (1/d _o)		Turns per unit winding area (1/d _o ²)		Winding copper space factor $F_w = \frac{\pi}{4} \left[\frac{d}{d_o} \right]^2$
		in	mm	in	mm	lb/100 in	g/m	in ⁻¹	mm ⁻¹	in ⁻²	mm ⁻²	
47	0.002 0	0.002 6	0.066 04	0.000 3	0.007 62	0.106 4 × 10 ⁻³	0.019 00	385	15.1	148 000	229	0.464 7
46	0.002 4	0.003 1	0.078 74	0.000 4	0.010 2	0.153 6 × 10 ⁻³	0.027 43	323	12.7	104 000	161	0.470 7
45	0.002 8	0.003 6	0.091 44	0.000 5	0.012 7	0.209 4 × 10 ⁻³	0.037 40	278	10.9	77 200	120	0.475 1
44	0.003 2	0.004 2	0.106 7	0.000 6	0.015 2	0.275 3 × 10 ⁻³	0.049 16	238	9.37	56 700	87.9	0.455 9
43	0.003 6	0.004 6	0.116 8	0.000 6	0.015 2	0.345 8 × 10 ⁻³	0.061 76	217	8.56	47 300	73.3	0.481 0
42	0.004 0	0.005 1	0.129 5	0.000 7	0.017 8	0.427 5 × 10 ⁻³	0.076 34	196	7.72	38 400	59.6	0.483 1
41	0.004 4	0.005 6	0.142 2	0.000 8	0.020 3	0.517 8 × 10 ⁻³	0.092 47	179	7.03	31 900	49.4	0.484 9
40	0.004 8	0.006 1	0.154 9	0.000 8	0.020 3	0.614 4 × 10 ⁻³	0.109 7	164	6.45	26 900	41.7	0.486 3
39	0.005 2	0.006 6	0.167 6	0.000 9	0.022 9	0.721 7 × 10 ⁻³	0.128 9	152	5.97	23 000	35.6	0.487 5
38	0.006 0	0.007 4	0.188 0	0.000 9	0.022 9	0.953 9 × 10 ⁻³	0.170 3	135	5.32	18 300	28.3	0.516 3
37	0.006 8	0.008 4	0.213 4	0.001 1	0.027 9	1.227 × 10 ⁻³	0.219 2	119	4.69	14 200	22.0	0.514 7
36	0.007 6	0.009 3	0.236 2	0.001 1	0.027 9	1.527 × 10 ⁻³	0.272 7	108	4.23	11 600	17.9	0.524 5
35	0.008 4	0.010 2	0.259 1	0.001 2	0.030 5	1.864 × 10 ⁻³	0.332 9	98.0	3.86	9 610	14.9	0.532 7
34	0.009 2	0.011 1	0.281 9	0.001 2	0.030 5	2.229 × 10 ⁻³	0.398 1	90.1	3.55	8 120	12.6	0.539 5
33	0.010 0	0.012 0	0.304 8	0.001 3	0.033 0	2.632 × 10 ⁻³	0.470 0	83.3	3.28	6 940	10.8	0.545 4
32	0.010 8	0.012 9	0.327 7	0.001 3	0.033 0	3.064 × 10 ⁻³	0.547 2	77.5	3.05	6 010	9.31	0.550 5
31	0.011 6	0.013 7	0.348 0	0.001 3	0.033 0	3.525 × 10 ⁻³	0.629 5	73.0	2.87	5 330	8.26	0.563 1
30	0.012 4	0.014 6	0.370 8	0.001 5	0.038 1	4.031 × 10 ⁻³	0.719 8	68.5	2.70	4 690	7.27	0.566 5
29	0.013 6	0.015 9	0.403 9	0.001 6	0.040 6	4.839 × 10 ⁻³	0.864 1	62.9	2.48	3 960	6.13	0.574 6
28	0.014 8	0.017 1	0.434 3	0.001 6	0.040 6	5.714 × 10 ⁻³	1.020	58.5	2.30	3 420	5.30	0.588 3
27	0.016 4	0.019 0	0.482 6	0.001 7	0.043 2	7.011 × 10 ⁻³	1.252	52.6	2.07	2 770	4.29	0.585 2
26	0.018 0	0.020 7	0.525 8	0.001 8	0.045 7	8.436 × 10 ⁻³	1.507	48.3	1.90	2 330	3.62	0.593 9
25	0.020	0.022 8	0.579 1	0.001 9	0.048 3	10.39 × 10 ⁻³	1.856	43.9	1.73	1 920	2.98	0.604 3
24	0.022	0.024 9	0.632 5	0.001 9	0.048 3	12.54 × 10 ⁻³	2.240	40.2	1.58	1 610	2.50	0.613 1
23	0.024	0.027 0	0.685 8	0.002 0	0.050 8	14.91 × 10 ⁻³	2.663	37.0	1.46	1 370	2.13	0.620 6
22	0.028	0.031 2	0.792 5	0.002 1	0.053 3	20.24 × 10 ⁻³	3.614	32.1	1.26	1 030	1.59	0.632 6
21	0.032	0.035 3	0.896 6	0.002 2	0.055 9	26.38 × 10 ⁻³	4.711	28.3	1.12	803	1.24	0.645 4
20	0.036	0.039 6	1.006	0.002 3	0.058 4	33.35 × 10 ⁻³	5.956	25.3	0.994	638	0.988	0.649 1
19	0.040	0.043 7	1.110	0.002 4	0.061 0	41.10 × 10 ⁻³	7.339	22.9	0.901	524	0.812	0.658 0
18	0.048	0.051 9	1.318	0.002 5	0.063 5	59.06 × 10 ⁻³	10.55	19.3	0.759	371	0.575	0.671 8
17	0.056	0.060 2	1.529	0.002 6	0.066 0	80.22 × 10 ⁻³	14.33	16.6	0.654	276	0.428	0.679 6
16	0.064	0.068 3	1.735	0.002 7	0.068 6	104.7 × 10 ⁻³	18.69	14.6	0.576	214	0.332	0.689 6
15	0.072	0.076 5	1.943	0.002 8	0.071 1	132.4 × 10 ⁻³	23.64	13.1	0.515	171	0.265	0.695 7
14	0.080	0.084 7	2.151	0.002 9	0.073 7	163.9 × 10 ⁻³	29.27	11.8	0.465	139	0.216	0.700 7
13	0.092	0.097 0	2.464	0.003 0	0.076 2	216.7 × 10 ⁻³	38.69	10.3	0.406	106	0.165	0.706 5
12	0.104	0.109 2	2.774	0.003 1	0.078 7	275.0 × 10 ⁻³	49.11	9.16	0.361	83.9	0.130	0.712 4
11	0.116	0.121 5	3.086	0.003 2	0.081 3	341.7 × 10 ⁻³	61.01	8.23	0.324	67.7	0.105	0.715 9
10	0.128	0.133 7	3.396	0.003 3	0.083 8	416.7 × 10 ⁻³	74.41	7.48	0.294	55.9	0.086 7	0.719 9

Table A.1.2.3. FUNCTIONS OF COPPER WIRE DIAMETERS—SWG (BASED ON BS 1844: 1952)

SWG	Nominal copper dia. (d)		d^4	Fine covering			Medium covering		
				Nominal overall dia. (d_o)	$S_1 = 1.26d_o - 1.15d$	$S_2 = d_o - 1.15d$	Nominal overall dia. (d_o)	$S_1 = 1.26d_o - 1.15d$	$S_2 = d_o - 1.15d$
	in	mm	mm ⁴	mm	mm	mm	mm	mm	mm
50*	0.001 0	0.025 4	4.16×10^{-7}	0.030 99*	0.009 83	0.001 78			
49*	0.001 2	0.030 5	8.63×10^{-7}	0.036 32*	0.010 7	0.001 27			
48*	0.001 6	0.040 6	2.73×10^{-6}	0.046 86*	0.012 3	0.000 127			
47	0.002 0	0.050 8	6.66×10^{-6}	0.057 40	0.013 9	-0.001 02	0.061 21	0.018 7	0.002 80
46	0.002 4	0.061 0	1.38×10^{-5}	0.069 47	0.017 4	-0.000 635	0.073 91	0.023 0	0.003 81
45	0.002 8	0.071 1	2.56×10^{-5}	0.080 14	0.019 2	-0.001 65	0.086 49	0.027 2	0.004 70
44	0.003 2	0.081 3	4.36×10^{-5}	0.091 57	0.021 9	-0.001 91	0.100 5	0.033 1	0.006 99
43	0.003 6	0.091 4	6.99×10^{-5}	0.101 6	0.022 9	-0.003 56	0.110 5	0.034 0	0.005 33
42	0.004 0	0.102	1.07×10^{-4}	0.114 3	0.027 2	-0.002 54	0.123 2	0.038 4	0.006 35
41	0.004 4	0.112	1.56×10^{-4}	0.125 7	0.029 9	-0.002 79	0.135 9	0.042 7	0.007 37
40	0.004 8	0.122	2.21×10^{-4}	0.135 9	0.031 0	-0.004 32	0.147 3	0.045 4	0.007 11
39	0.005 2	0.132	3.04×10^{-4}	0.148 6	0.035 3	-0.003 30	0.160 0	0.049 7	0.008 13
38	0.006 0	0.152	5.39×10^{-4}	0.168 9	0.037 6	-0.006 35	0.180 3	0.052 0	0.005 08
37	0.006 8	0.173	8.90×10^{-4}	0.194 3	0.046 2	-0.004 31	0.205 7	0.060 6	0.007 11
36	0.007 6	0.193	1.39×10^{-3}	0.214 6	0.048 4	-0.007 37	0.227 3	0.064 4	0.005 33
35	0.008 4	0.213	2.07×10^{-3}	0.236 2	0.052 3	-0.009 14	0.250 2	0.069 9	0.004 83
34	0.009 2	0.234	2.98×10^{-3}	0.256 5	0.054 5	-0.012 2	0.271 8	0.073 7	0.003 05
33	0.010 0	0.254	4.16×10^{-3}	0.279 4	0.060 0	-0.012 7	0.294 6	0.079 2	0.002 54
32	0.010 8	0.274	5.66×10^{-3}	0.301 0	0.063 8	-0.014 5	0.316 2	0.083 0	0.000 76
31	0.011 6	0.295	7.54×10^{-3}	0.321 3	0.066 0	-0.017 5	0.336 6	0.085 2	-0.002 29
30	0.012 4	0.315	9.84×10^{-3}	0.344 2	0.071 5	-0.018 0	0.360 7	0.092 3	-0.001 52
29	0.013 6	0.345	1.42×10^{-2}	0.377 2	0.078 0	-0.020 1	0.393 7	0.098 8	-0.003 56
28	0.014 8	0.376	2.00×10^{-2}	0.407 7	0.081 4	-0.024 6	0.424 2	0.102	-0.008 13
27	0.016 4	0.417	3.01×10^{-2}	0.450 9	0.089 0	-0.028 2	0.468 6	0.111	-0.010 4
26	0.018 0	0.457	4.37×10^{-2}	0.492 8	0.095 1	-0.033 0	0.511 8	0.119	-0.014 0
25	0.020	0.508	6.66×10^{-2}	0.546 1	0.104	-0.038 1	0.565 2	0.128	-0.019 1
24	0.022	0.559	9.75×10^{-2}	0.596 9	0.109	-0.045 7	0.617 2	0.135	-0.025 4
23	0.024	0.610	1.38×10^{-1}	0.649 0	0.117	-0.052 1	0.670 6	0.144	-0.030 5
22	0.028	0.711	2.56×10^{-1}	0.753 1	0.131	-0.064 8	0.774 7	0.158	-0.043 2
21	0.032	0.813	4.36×10^{-1}	0.857 3	0.145	-0.077 5	0.878 8	0.173	-0.055 9
20	0.036	0.914	6.99×10^{-1}	0.960 1	0.158	-0.091 4	0.984	0.189	-0.067 3
19	0.040	1.02	1.07	1.064	0.173	-0.104	1.088	0.203	-0.080 0
18	0.048	1.22	2.21	1.270	0.198	-0.132	1.294	0.229	-0.108
17	0.056	1.42	4.09	1.476	0.224	-0.160	1.501	0.256	-0.135
16	0.064	1.63	6.98	1.680	0.248	-0.189	1.707	0.281	-0.163
15	0.072	1.83	11.2	1.885	0.272	-0.218	1.913	0.307	-0.191
14	0.080	2.03	17.0	2.090	0.297	-0.246	2.118	0.333	-0.218
13	0.092	2.34	29.8	2.398	0.334	-0.290	2.427	0.371	-0.260
12	0.104	2.64	48.7	2.705	0.371	-0.333	2.734	0.407	-0.304
11	0.116	2.95	75.4	3.012	0.407	-0.376	3.042	0.444	-0.347
10	0.128	3.25	112	3.320	0.444	-0.419	3.349	0.481	-0.390

*First three rows refer to oleo enamel wire to BS 156:1951—normal covering, as these gauges are not included in BS 1844: 1952

Table A.2.1. PROPERTIES OF BARE COPPER WIRES—METRIC (BASED ON BS 2039: 1953)

It is proposed that in due course BS 2039:1953 should be superseded by one based on I.E.C. Publication 182. This lists a series of conductor diameters based on the logarithmic progressions of the R series (see I.S.O. Publication R3). How-

ever, as the data on this list does not at present go beyond the nominal conductor diameters and the maximum overall diameters, it is not possible to include comprehensive wire tables based on this proposal.

Copper diameter (d)			Nominal copper area	Nominal resistance per unit length, (R _c)	Copper diameter (d)			Nominal copper area	Nominal resistance per unit length, (R _c)
Nom. mm	Max. mm	Min. mm	mm ²	Ω/m	Nom. mm	Max. mm	Min. mm	mm ²	Ω/m
0-050	0-052 00	0-048 00	1.964×10^{-3}	8-781	0-650	0-656 5	0-643 5	331.8×10^{-3}	0-051 96
0-055	0-057 00	0-053 00	2.376×10^{-3}	7-257	0-680	0-686 8	0-673 2	363.2×10^{-3}	0-047 27
0-060	0-062 00	0-058 00	2.827×10^{-3}	6-098	0-700	0-707 0	0-693 0	384.8×10^{-3}	0-044 80
0-065	0-067 25	0-062 75	3.318×10^{-3}	5-196	0-720	0-727 2	0-712 8	407.2×10^{-3}	0-042 32
0-070	0-072 25	0-067 75	3.849×10^{-3}	4-480	0-750	0-757 5	0-742 5	441.8×10^{-3}	0-038 97
0-075	0-077 25	0-072 75	4.418×10^{-3}	3-903	0-780	0-787 8	0-772 2	477.8×10^{-3}	0-036 05
0-080	0-082 25	0-077 75	5.027×10^{-3}	3-430	0-800	0-808 0	0-792 0	502.7×10^{-3}	0-034 25
0-085	0-087 5	0-082 5	5.675×10^{-3}	3-038	0-850	0-858 5	0-841 5	567.5×10^{-3}	0-030 34
0-090	0-092 5	0-087 5	6.362×10^{-3}	2-710	0-900	0-909 0	0-891 0	636.2×10^{-3}	0-027 05
0-095	0-097 5	0-092 5	7.088×10^{-3}	2-432	0-950	0-959 5	0-940 5	708.8×10^{-3}	0-024 30
0-100	0-102 5	0-097 5	7.854×10^{-3}	2-195	1-00	1-010 0	0-9900	785.4×10^{-3}	0-021 91
0-110	0-112 5	0-107 5	9.503×10^{-3}	1-814	1-05	1-060 5	1-039 5	865.9×10^{-3}	0-019 90
0-120	0-122 5	0-117 5	11.31×10^{-3}	1-525	1-10	1-111 0	1-089 0	950.3×10^{-3}	0-018 08
0-130	0-132 5	0-127 5	13.27×10^{-3}	1-299	1-15	1-161 5	1-138 5	$1\ 039 \times 10^{-3}$	0-016 56
0-140	0-142 5	0-137 5	15.39×10^{-3}	1-120	1-20	1-212 0	1-188 0	$1\ 131 \times 10^{-3}$	0-015 22
0-150	0-152 5	0-147 5	17.67×10^{-3}	0-975 7	1-25	1-262 5	1-237 5	$1\ 227 \times 10^{-3}$	0-014 03
0-160	0-162 5	0-157 5	20.11×10^{-3}	0-857 5	1-30	1-313 0	1-287 0	$1\ 327 \times 10^{-3}$	0-013 03
0-170	0-172 5	0-167 5	22.70×10^{-3}	0-759 5	1-35	1-363 5	1-336 5	$1\ 431 \times 10^{-3}$	0-012 08
0-180	0-182 5	0-177 5	25.45×10^{-3}	0-677 5	1-40	1-414 0	1-386 0	$1\ 539 \times 10^{-3}$	0-011 18
0-190	0-192 5	0-187 5	28.35×10^{-3}	0-608 1	1-45	1-464 5	1-435 5	$1\ 651 \times 10^{-3}$	0-010 45
0-200	0-202 5	0-197 5	31.42×10^{-3}	0-548 8	1-50	1-515 0	1-485 0	$1\ 767 \times 10^{-3}$	0-009 742
0-210	0-212 5	0-207 5	34.64×10^{-3}	0-497 8	1-55	1-565 5	1-534 5	$1\ 887 \times 10^{-3}$	0-009 200
0-220	0-222 5	0-217 5	38.01×10^{-3}	0-453 6	1-60	1-616 0	1-584 0	$2\ 011 \times 10^{-3}$	0-008 536
0-230	0-232 5	0-227 5	41.55×10^{-3}	0-415 0	1-65	1-666 5	1-633 5	$2\ 138 \times 10^{-3}$	0-008 163
0-240	0-242 5	0-237 5	45.24×10^{-3}	0-381 1	1-70	1-717 0	1-683 0	$2\ 270 \times 10^{-3}$	0-007 572
0-250	0-252 5	0-247 5	49.09×10^{-3}	0-351 2	1-75	1-767 5	1-732 5	$2\ 405 \times 10^{-3}$	0-007 233
0-260	0-262 6	0-257 4	53.09×10^{-3}	0-324 7	1-80	1-818 0	1-782 0	$2\ 545 \times 10^{-3}$	0-006 731
0-270	0-272 7	0-267 3	57.26×10^{-3}	0-301 0	1-90	1-919 0	1-881 0	$2\ 835 \times 10^{-3}$	0-006 060
0-280	0-282 8	0-277 2	61.58×10^{-3}	0-280 0	2-0	2-020 0	1-980 0	$3\ 142 \times 10^{-3}$	0-005 499
0-290	0-292 9	0-287 1	66.05×10^{-3}	0-261 0	2-1	2-121 0	2-079 0	$3\ 464 \times 10^{-3}$	0-004 956
0-300	0-303 0	0-297 0	70.69×10^{-3}	0-243 9	2-2	2-222	2-178	$3\ 801 \times 10^{-3}$	0-004 557
0-310	0-313 1	0-306 9	75.48×10^{-3}	0-228 4	2-3	2-323	2-277	$4\ 155 \times 10^{-3}$	0-004 113
0-320	0-323 2	0-316 8	80.42×10^{-3}	0-214 4	2-4	2-424	2-376	$4\ 524 \times 10^{-3}$	0-003 821
0-330	0-333 3	0-326 7	85.53×10^{-3}	0-201 6	2-5	2-525	2-475	$4\ 909 \times 10^{-3}$	0-003 511
0-340	0-343 4	0-336 6	90.79×10^{-3}	0-189 9	2-6	2-626	2-574	$5\ 309 \times 10^{-3}$	0-003 334
0-350	0-353 5	0-346 5	96.21×10^{-3}	0-179 1	2-7	2-727	2-673	$5\ 726 \times 10^{-3}$	0-002 995
0-360	0-363 6	0-356 4	101.8×10^{-3}	0-169 4	2-8	2-828	2-772	$6\ 158 \times 10^{-3}$	0-002 773
0-370	0-373 7	0-366 3	107.5×10^{-3}	0-160 3	2-9	2-929	2-871	$6\ 605 \times 10^{-3}$	0-002 645
0-380	0-383 8	0-376 2	113.4×10^{-3}	0-152 0	3-0	3-030	2-970	$7\ 069 \times 10^{-3}$	0-002 439
0-390	0-393 9	0-386 1	119.5×10^{-3}	0-144 3	3-1	3-131	3-069	$7\ 548 \times 10^{-3}$	0-002 290
0-400	0-404 0	0-396 0	125.7×10^{-3}	0-137 3	3-2	3-232	3-168	$8\ 042 \times 10^{-3}$	0-002 124
0-420	0-424 2	0-415 8	138.5×10^{-3}	0-124 5	3-3	3-333	3-267	$8\ 553 \times 10^{-3}$	0-001 994
0-450	0-454 5	0-445 5	159.0×10^{-3}	0-097 44	3-4	3-434	3-366	$9\ 079 \times 10^{-3}$	0-001 881
0-480	0-484 8	0-475 2	181.0×10^{-3}	0-095 26	3-5	3-535	3-465	$9\ 621 \times 10^{-3}$	0-001 792
0-500	0-505 0	0-495 0	196.3×10^{-3}	0-087 82	3-6	3-636	3-564	$10\ 180 \times 10^{-3}$	0-001 695
0-520	0-525 2	0-514 8	212.4×10^{-3}	0-081 15	3-7	3-737	3-663	$10\ 750 \times 10^{-3}$	0-001 603
0-550	0-555 5	0-544 5	237.6×10^{-3}	0-072 51	3-8	3-838	3-762	$11\ 340 \times 10^{-3}$	0-001 520
0-580	0-585 8	0-574 2	264.2×10^{-3}	0-065 29	3-9	3-939	3-861	$11\ 950 \times 10^{-3}$	0-001 438
0-600	0-606 0	0-594 0	282.7×10^{-3}	0-061 03	4-0	4-040	3-960	$12\ 570 \times 10^{-3}$	0-001 370
0-620	0-626 2	0-613 8	301.9×10^{-3}	0-057 09					

Table A.2.2.1. PROPERTIES OF FINE ENAMELLED COPPER WIRES—METRIC (BASED ON BS 2039: 1953—FINE COVERING)

Nom. copper dia. (d)	Overall dia., (d _o) (max)	Increase in dia. due to insula- tion (min.)	Approx. weight	Turns per unit winding breadth (1/d _o)	Turns per unit winding area (1/d _o ²)	Winding copper space factor $F_w = \frac{\pi}{4} \left[\frac{d}{d_o} \right]^2$	Nom. copper dia., (d)	Overall dia., (d _o) (max)	Increase in dia. due to insula- tion (min.)	Approx. weight	Turns per unit winding breadth (1/d _o)	Turns per unit winding area (1/d _o ²)	Winding copper space factor $F_w = \frac{\pi}{4} \left[\frac{d}{d_o} \right]^2$
mm	mm	mm	g/m	mm ⁻¹	mm ⁻²		mm	mm	mm	g/m	mm ⁻¹	mm ⁻²	
0.050	0.060	0.005 0	0.018 3	16.7	278	0.545 4	0.650	0.705	0.030	3.006	1.42	2.01	0.667 6
0.055	0.068	0.005 0	0.022 2	14.7	216	0.513 8	0.680	0.738	0.033	3.292	1.36	1.84	0.666 8
0.060	0.073	0.006 0	0.026 3	13.7	188	0.530 6	0.700	0.758	0.033	3.485	1.32	1.74	0.669 8
0.065	0.078	0.006 0	0.030 8	12.8	164	0.545 4	0.720	0.778	0.033	3.686	1.29	1.65	0.672 7
0.070	0.083	0.007 5	0.035 7	12.0	145	0.558 6	0.750	0.808	0.033	3.997	1.24	1.53	0.676 7
0.075	0.090	0.007 5	0.041 1	11.1	123	0.545 4	0.780	0.841	0.036	4.324	1.19	1.41	0.675 6
0.080	0.095	0.007 5	0.046 6	10.5	111	0.557 0	0.800	0.861	0.036	4.547	1.16	1.35	0.678 1
0.085	0.100	0.007 5	0.052 5	10.0	100	0.567 5	0.850	0.912	0.036	5.129	1.10	1.20	0.682 2
0.090	0.105	0.007 5	0.058 7	9.52	90.7	0.577 0	0.900	0.965	0.036	5.749	1.04	1.07	0.683 2
0.095	0.113	0.010 0	0.065 8	8.85	78.3	0.555 1	0.950	1.015	0.036	6.397	0.985	0.971	0.688 0
0.100	0.118	0.010 0	0.072 8	8.48	71.8	0.564 1	1.00	1.070	0.038	7.091	0.935	0.873	0.686 0
0.110	0.130	0.010 0	0.087 9	7.69	59.2	0.562 3	1.05	1.120	0.038	7.811	0.893	0.797	0.690 3
0.120	0.140	0.010 0	0.104 3	7.14	51.0	0.577 0	1.10	1.170	0.038	8.569	0.855	0.731	0.694 2
0.130	0.153	0.012 5	0.122 8	6.54	42.7	0.567 0	1.15	1.220	0.038	9.362	0.820	0.672	0.697 9
0.140	0.163	0.012 5	0.142 0	6.14	37.6	0.579 4	1.20	1.275	0.041	10.19	0.784	0.615	0.695 7
0.150	0.173	0.012 5	0.162 6	5.78	33.4	0.590 4	1.25	1.325	0.041	11.05	0.755	0.570	0.699 0
0.160	0.185	0.015 0	0.185 5	5.41	29.2	0.587 5	1.30	1.375	0.041	11.95	0.727	0.529	0.702 1
0.170	0.198	0.018 0	0.210 0	5.05	25.5	0.579 0	1.35	1.425	0.041	12.88	0.702	0.493	0.704 9
0.180	0.208	0.018 0	0.234 9	4.81	23.1	0.588 2	1.40	1.480	0.043	13.85	0.676	0.457	0.702 8
0.190	0.218	0.018 0	0.261 1	4.59	21.0	0.596 6	1.45	1.530	0.043	14.86	0.654	0.427	0.705 4
0.200	0.230	0.018 0	0.289 3	4.35	18.9	0.593 9	1.50	1.580	0.043	15.89	0.633	0.401	0.707 9
0.210	0.240	0.018 0	0.318 4	4.17	17.4	0.601 3	1.55	1.630	0.043	16.97	0.613	0.376	0.710 2
0.220	0.250	0.018 0	0.348 8	4.00	16.0	0.608 2	1.60	1.680	0.043	18.07	0.595	0.354	0.712 4
0.230	0.260	0.018 0	0.380 8	3.85	14.8	0.614 6	1.65	1.735	0.043	19.22	0.576	0.332	0.710 3
0.240	0.270	0.018 0	0.414 1	3.70	13.7	0.620 6	1.70	1.785	0.043	20.40	0.560	0.314	0.712 4
0.250	0.283	0.020	0.450 1	3.53	12.5	0.612 9	1.75	1.835	0.043	21.65	0.545	0.297	0.714 3
0.260	0.293	0.020	0.486 2	3.41	11.6	0.618 4	1.80	1.885	0.043	22.86	0.531	0.281	0.716 2
0.270	0.306	0.020	0.524 7	3.27	10.7	0.611 5	1.90	1.990	0.043	25.4	0.503	0.253	0.716 0
0.280	0.316	0.020	0.563 6	3.17	10.0	0.616 6	2.0	2.090	0.046	28.0	0.478	0.229	0.719 2
0.290	0.326	0.020	0.603 9	3.07	9.41	0.621 5	2.1	2.190	0.046	30.9	0.457	0.209	0.722 2
0.300	0.336	0.023	0.647 0	2.98	8.86	0.626 1	2.2	2.295	0.048	34	0.436	0.190	0.721 7
0.310	0.349	0.023	0.690 8	2.87	8.21	0.619 7	2.3	2.395	0.048	37	0.418	0.174	0.724 3
0.320	0.359	0.023	0.735 4	2.79	7.76	0.624 0	2.4	2.500	0.048	41	0.400	0.160	0.723 8
0.330	0.369	0.023	0.781 3	2.71	7.34	0.628 2	2.5	2.600	0.051	44	0.385	0.148	0.726 1
0.340	0.382	0.025	0.830 5	2.62	6.85	0.622 2	2.6	2.700	0.051	48	0.370	0.137	0.728 3
0.350	0.392	0.025	0.879 4	2.55	6.51	0.626 1	2.7	2.805	0.051	51	0.357	0.127	0.727 7
0.360	0.402	0.025	0.929 9	2.49	6.19	0.629 9	2.8	2.905	0.053	55	0.344	0.119	0.729 6
0.370	0.412	0.025	0.981 0	2.43	5.89	0.633 4	2.9	3.010	0.053	59	0.332	0.110	0.729 0
0.380	0.424	0.025	1.035	2.36	5.56	0.630 8	3.0	3.110	0.056	63	0.322	0.103	0.730 8
0.390	0.435	0.025	1.090	2.30	5.28	0.631 3	3.1	3.210	0.056	68	0.312	0.097 0	0.732 5
0.400	0.445	0.028	1.147	2.25	5.05	0.634 6	3.2	3.315	0.056	72	0.302	0.091 0	0.731 9
0.420	0.467	0.028	1.264	2.14	4.59	0.635 3	3.3	3.415	0.056	77	0.293	0.085 7	0.733 4
0.450	0.498	0.028	1.448	2.01	4.03	0.641 3	3.4	3.515	0.056	81	0.284	0.080 9	0.734 8
0.480	0.531	0.030	1.649	1.88	3.55	0.641 8	3.5	3.620	0.058	86	0.276	0.076 3	0.734 2
0.500	0.551	0.030	1.787	1.82	3.29	0.646 7	3.6	3.720	0.058	91	0.269	0.072 3	0.735 5
0.520	0.571	0.030	1.931	1.75	3.07	0.651 4	3.7	3.820	0.058	96	0.262	0.068 5	0.736 8
0.550	0.601	0.030	2.158	1.66	2.77	0.657 8	3.8	3.925	0.061	102	0.255	0.064 9	0.736 2
0.580	0.634	0.030	2.398	1.58	2.49	0.657 3	3.9	4.025	0.061	107	0.248	0.061 7	0.737 4
0.600	0.654	0.030	2.564	1.53	2.34	0.661 1	4.0	4.125	0.061	112	0.242	0.058 8	0.738 5
0.620	0.674	0.030	2.737	1.48	2.20	0.664 6							

Table A.2.2.2. PROPERTIES OF MEDIUM ENAMELLED COPPER WIRES—METRIC (BASED ON BS 2039: 1953—MEDIUM COVERING)

Nom. copper dia., (d)	Overall dia. (d _o) (max)	Increase in dia. due to insula- tion (min.)	Approx. weight	Turns per unit winding breadth (1/d _o)	Turns per unit winding area (1/d _o ²)	Winding copper space factor $F_w = \frac{\pi}{4} \left[\frac{d}{d_o} \right]^2$	Nom. copper dia., (d)	Overall dia. (d _o) (max)	Increase in dia. due to insula- tion (min.)	Approx. weight	Turns per unit winding breadth (1/d _o)	Turns per unit winding area (1/d _o ²)	Winding copper space factor $F_w = \frac{\pi}{4} \left[\frac{d}{d_o} \right]^2$
mm	mm	mm	g/m	mm ⁻¹	mm ⁻²		mm	mm	mm	g/m	mm ⁻¹	mm ⁻²	
0.050	0.065	0.007 5	0.018 7	15.4	237	0.464 7	0.650	0.728	0.051	3.037	1.37	1.89	0.626 1
0.055	0.070	0.007 5	0.022 5	14.3	204	0.484 9	0.680	0.761	0.053	3.323	1.31	1.73	0.627 1
0.060	0.078	0.010 0	0.027 0	12.8	164	0.464 7	0.700	0.781	0.053	3.517	1.28	1.64	0.630 9
0.065	0.083	0.010 0	0.031 5	12.0	145	0.481 7	0.720	0.801	0.053	3.719	1.25	1.56	0.634 6
0.070	0.090	0.012 5	0.036 7	11.1	123	0.475 1	0.750	0.831	0.053	4.031	1.20	1.45	0.639 7
0.075	0.100	0.015 0	0.042 6	10.0	100	0.441 8	0.780	0.864	0.056	4.360	1.16	1.34	0.640 1
0.080	0.105	0.015 0	0.048 2	9.52	90.7	0.455 9	0.800	0.884	0.056	4.584	1.13	1.28	0.643 2
0.085	0.110	0.015 0	0.054 2	9.09	82.6	0.469 0	0.850	0.935	0.056	5.168	1.07	1.14	0.649 1
0.090	0.115	0.015 0	0.060 5	8.70	75.6	0.481 0	0.900	0.990	0.058	5.792	1.01	1.02	0.649 1
0.095	0.123	0.018 0	0.067 7	8.13	66.1	0.468 5	0.950	1.041	0.058	6.446	0.961	0.923	0.654 1
0.100	0.128	0.018 0	0.074 9	7.81	61.0	0.479 4	1.00	1.095	0.061	7.141	0.913	0.834	0.655 0
0.110	0.140	0.020 0	0.090 5	7.14	51.0	0.484 9	1.05	1.145	0.061	7.865	0.873	0.763	0.660 5
0.120	0.153	0.020 0	0.107 5	6.54	42.7	0.483 1	1.10	1.195	0.061	8.623	0.837	0.700	0.665 5
0.130	0.166	0.023 0	0.126 4	6.02	36.3	0.481 7	1.15	1.245	0.061	9.419	0.803	0.645	0.670 1
0.140	0.176	0.023 0	0.145 8	5.68	32.3	0.497 0	1.20	1.300	0.064	10.26	0.769	0.592	0.669 2
0.150	0.186	0.023	0.166 6	5.38	28.9	0.510 8	1.25	1.350	0.064	11.12	0.741	0.549	0.673 4
0.160	0.198	0.025	0.189 7	5.05	25.5	0.512 9	1.30	1.400	0.064	12.02	0.714	0.510	0.677 2
0.170	0.211	0.028	0.214 5	4.74	22.5	0.509 8	1.35	1.450	0.064	12.95	0.690	0.476	0.680 8
0.180	0.223	0.028	0.240 0	4.48	20.1	0.511 7	1.40	1.505	0.066	13.92	0.664	0.442	0.679 6
0.190	0.233	0.028	0.266 5	4.29	18.4	0.522 3	1.45	1.555	0.066	14.93	0.643	0.414	0.682 9
0.200	0.246	0.030	0.295 7	4.07	16.5	0.519 1	1.50	1.605	0.066	15.97	0.623	0.388	0.686 0
0.210	0.256	0.030	0.325 0	3.91	15.3	0.528 5	1.55	1.660	0.069	17.06	0.602	0.363	0.684 8
0.220	0.268	0.030	0.356 3	3.73	13.9	0.529 3	1.60	1.710	0.069	18.17	0.585	0.342	0.687 6
0.230	0.278	0.030	0.388 5	3.60	12.9	0.537 6	1.65	1.760	0.069	19.32	0.568	0.323	0.690 3
0.240	0.288	0.030	0.422 1	3.47	12.1	0.545 4	1.70	1.810	0.069	20.50	0.552	0.305	0.692 8
0.250	0.301	0.033	0.458 8	3.32	11.0	0.541 8	1.75	1.865	0.071	21.75	0.536	0.288	0.691 5
0.260	0.311	0.033	0.495 1	3.22	10.3	0.548 9	1.80	1.915	0.071	22.96	0.522	0.273	0.693 9
0.270	0.324	0.033	0.534 0	3.09	9.53	0.545 4	1.90	2.015	0.071	25.5	0.496	0.246	0.698 3
0.280	0.334	0.033	0.573 2	2.99	8.96	0.552 0	2.0	2.120	0.074	28.1	0.472	0.223	0.699 0
0.290	0.344	0.033	0.613 8	2.91	8.45	0.558 2	2.1	2.220	0.074	31.0	0.450	0.203	0.702 8
0.300	0.354	0.036	0.656 9	2.83	7.98	0.564 1	2.2	2.325	0.076	34	0.430	0.185	0.703 2
0.310	0.366	0.038	0.701 8	2.73	7.47	0.563 4	2.3	2.425	0.076	37	0.412	0.170	0.706 5
0.320	0.377	0.038	0.747 0	2.65	7.04	0.565 9	2.4	2.530	0.076	41	0.395	0.156	0.706 8
0.330	0.387	0.038	0.793 4	2.58	6.68	0.571 1	2.5	2.630	0.079	44	0.380	0.145	0.709 7
0.340	0.399	0.041	0.843 0	2.51	6.28	0.570 3	2.6	2.735	0.079	48	0.366	0.134	0.709 8
0.350	0.409	0.041	0.892 1	2.45	5.98	0.575 1	2.7	2.835	0.079	51	0.353	0.124	0.712 4
0.360	0.420	0.041	0.943 2	2.38	5.67	0.577 0	2.8	2.935	0.081	55	0.341	0.116	0.714 8
0.370	0.430	0.041	0.994 9	2.33	5.41	0.581 5	2.9	3.040	0.081	59	0.329	0.108	0.714 7
0.380	0.445	0.043	1.051	2.25	5.05	0.572 7	3.0	3.140	0.084	64	0.318	0.101	0.716 9
0.390	0.455	0.043	1.107	2.20	4.83	0.577 0	3.1	3.245	0.084	68	0.308	0.095 0	0.716 8
0.400	0.465	0.043	1.163	2.15	4.62	0.581 2	3.2	3.345	0.084	72	0.299	0.089 4	0.718 8
0.420	0.488	0.046	1.282	2.05	4.20	0.581 8	3.3	3.445	0.084	77	0.290	0.084 3	0.720 7
0.450	0.518	0.046	1.467	1.93	3.73	0.592 7	3.4	3.550	0.084	82	0.282	0.079 3	0.720 4
0.480	0.551	0.048	1.669	1.82	3.29	0.596 0	3.5	3.650	0.086	86	0.274	0.075 1	0.722 2
0.500	0.571	0.048	1.808	1.75	3.07	0.602 2	3.6	3.750	0.086	91	0.267	0.071 1	0.723 8
0.520	0.591	0.048	1.953	1.69	2.86	0.608 0	3.7	3.850	0.086	96	0.260	0.067 5	0.725 4
0.550	0.624	0.048	2.184	1.60	2.57	0.610 2	3.8	3.955	0.089	102	0.253	0.063 9	0.725 0
0.580	0.657	0.051	2.426	1.52	2.32	0.612 1	3.9	4.055	0.089	107	0.247	0.060 8	0.726 5
0.600	0.677	0.051	2.593	1.48	2.18	0.616 9	4.0	4.155	0.089	113	0.241	0.057 9	0.727 9
0.620	0.697	0.051	2.766	1.44	2.06	0.621 5							

Table A.2.2.3. FUNCTIONS OF COPPER WIRE DIAMETERS—METRIC (BASED ON BS 2039: 1953)

Nominal copper dia. (<i>d</i>)	<i>d</i> ⁴	Fine covering			Medium covering		
		Nominal overall dia. (<i>d</i> _o)	<i>S</i> ₁ = 1.26 <i>d</i> _o - 1.15 <i>d</i>	<i>S</i> ₂ = <i>d</i> _o - 1.15 <i>d</i>	Nominal overall dia. (<i>d</i> _o)	<i>S</i> ₁ = 1.26 <i>d</i> _o - 1.15 <i>d</i>	<i>S</i> ₂ = <i>d</i> _o - 1.15 <i>d</i>
mm	mm ⁴	mm	mm	mm	mm	mm	mm
0.050	6.25 × 10 ⁻⁶	0.056 50	0.013 7	-0.001 00	0.060 25	0.018 4	0.002 75
0.055	9.15 × 10 ⁻⁶	0.063 00	0.016 1	-0.000 25	0.065 25	0.019 0	0.002 00
0.060	1.30 × 10 ⁻⁵	0.068 50	0.017 3	-0.000 50	0.073 00	0.023 0	0.004 00
0.065	1.79 × 10 ⁻⁵	0.073 38	0.017 7	-0.001 38	0.077 87	0.023 4	0.003 12
0.070	2.40 × 10 ⁻⁵	0.079 13	0.019 2	-0.001 38	0.085 13	0.026 8	0.004 63
0.075	3.16 × 10 ⁻⁵	0.085 13	0.021 0	-0.001 13	0.093 88	0.032 0	0.007 63
0.080	4.10 × 10 ⁻⁵	0.090 13	0.021 6	-0.001 88	0.098 87	0.032 6	0.006 88
0.085	5.22 × 10 ⁻⁵	0.095 00	0.022 0	-0.002 75	0.103 8	0.033 0	0.006 00
0.090	6.56 × 10 ⁻⁵	0.100 0	0.022 5	-0.003 50	0.108 8	0.033 5	0.005 25
0.095	8.15 × 10 ⁻⁵	0.107 8	0.026 5	-0.001 50	0.116 8	0.037 9	0.007 50
0.100	1.00 × 10 ⁻⁴	0.112 8	0.027 1	-0.002 25	0.121 8	0.038 4	0.006 75
0.110	1.46 × 10 ⁻⁴	0.123 8	0.029 4	-0.002 75	0.133 8	0.042 0	0.007 25
0.120	2.07 × 10 ⁻⁴	0.133 8	0.030 5	-0.004 25	0.145 3	0.045 0	0.007 25
0.130	2.86 × 10 ⁻⁴	0.146 5	0.035 0	-0.003 00	0.158 3	0.049 9	0.008 75
0.140	3.84 × 10 ⁻⁴	0.156 5	0.036 2	-0.004 50	0.168 3	0.051 0	0.007 25
0.150	5.06 × 10 ⁻⁴	0.166 5	0.037 3	-0.006 00	0.178 3	0.052 1	0.005 75
0.160	6.55 × 10 ⁻⁴	0.178 8	0.041 2	-0.005 25	0.190 3	0.055 7	0.006 25
0.170	8.35 × 10 ⁻⁴	0.191 8	0.046 1	-0.003 75	0.203 3	0.060 6	0.007 75
0.180	1.05 × 10 ⁻³	0.201 8	0.047 2	-0.005 25	0.214 3	0.063 0	0.007 25
0.190	1.30 × 10 ⁻³	0.211 8	0.048 3	-0.006 75	0.224 3	0.064 1	0.005 75
0.200	1.60 × 10 ⁻³	0.222 8	0.050 7	-0.007 25	0.236 8	0.068 3	0.006 75
0.210	1.94 × 10 ⁻³	0.232 8	0.051 8	-0.008 75	0.246 8	0.069 4	0.005 25
0.220	2.34 × 10 ⁻³	0.242 8	0.052 9	-0.010 3	0.257 8	0.071 8	0.004 75
0.230	2.80 × 10 ⁻³	0.252 8	0.054 0	-0.011 8	0.267 8	0.072 9	0.003 25
0.240	3.32 × 10 ⁻³	0.262 8	0.055 1	-0.013 3	0.277 8	0.074 0	0.001 75
0.250	3.91 × 10 ⁻³	0.275 3	0.059 3	-0.012 3	0.290 8	0.078 8	0.003 25
0.260	4.57 × 10 ⁻³	0.285 2	0.060 4	-0.013 8	0.300 7	0.079 9	0.001 70
0.270	5.31 × 10 ⁻³	0.296 7	0.063 3	-0.013 9	0.312 2	0.082 8	0.001 65
0.280	6.15 × 10 ⁻³	0.306 6	0.064 3	-0.015 4	0.322 1	0.083 9	0.000 10
0.290	7.07 × 10 ⁻³	0.316 6	0.065 4	-0.017 0	0.332 1	0.084 9	-0.001 45
0.300	8.10 × 10 ⁻³	0.328 0	0.068 3	-0.017 0	0.343 5	0.087 8	-0.001 50
0.310	9.24 × 10 ⁻³	0.339 5	0.071 2	-0.017 1	0.355 5	0.091 4	-0.001 05
0.320	1.05 × 10 ⁻²	0.349 4	0.072 2	-0.018 6	0.365 9	0.093 0	-0.002 10
0.330	1.19 × 10 ⁻²	0.359 4	0.073 3	-0.020 2	0.375 9	0.094 1	-0.003 65
0.340	1.34 × 10 ⁻²	0.371 8	0.077 5	-0.019 2	0.388 3	0.098 3	-0.002 70
0.350	1.50 × 10 ⁻²	0.381 8	0.078 5	-0.020 8	0.398 3	0.099 3	-0.004 25
0.360	1.68 × 10 ⁻²	0.391 7	0.079 5	-0.022 3	0.408 7	0.101	-0.005 30
0.370	1.87 × 10 ⁻²	0.401 7	0.080 6	-0.023 9	0.418 7	0.102	-0.006 85
0.380	2.09 × 10 ⁻²	0.412 6	0.082 9	-0.024 4	0.432 1	0.107	-0.004 90
0.390	2.31 × 10 ⁻²	0.423 1	0.084 5	-0.025 5	0.442 1	0.108	-0.006 45
0.400	2.56 × 10 ⁻²	0.434 5	0.087 5	-0.025 5	0.452 0	0.110	-0.008 00
0.420	3.11 × 10 ⁻²	0.455 4	0.090 8	-0.027 6	0.474 9	0.115	-0.008 10
0.450	4.10 × 10 ⁻²	0.485 8	0.094 5	-0.031 8	0.504 8	0.118	-0.012 7
0.480	5.31 × 10 ⁻²	0.518 1	0.101	-0.033 9	0.537 1	0.125	-0.014 9
0.500	6.25 × 10 ⁻²	0.538 0	0.103	-0.037 0	0.557 0	0.127	-0.018 0
0.520	7.31 × 10 ⁻²	0.557 9	0.105	-0.040 1	0.576 9	0.129	-0.021 1
0.550	9.15 × 10 ⁻²	0.587 8	0.108	-0.044 8	0.608 3	0.134	-0.024 2
0.580	1.13 × 10 ⁻¹	0.619 1	0.113	-0.047 9	0.641 1	0.141	-0.025 9
0.600	1.30 × 10 ⁻¹	0.639 0	0.115	-0.051 0	0.661 0	0.143	-0.029 0
0.620	1.48 × 10 ⁻¹	0.658 9	0.117	-0.054 1	0.680 9	0.145	-0.032 1

cont.

Table A.2.2.3. (continued)

Nominal copper dia. (<i>d</i>)	d^4	Fine covering			Medium covering		
		Nominal overall dia. (d_o)	S_1 $= 1.26 d_o - 1.15 d$	S_2 $= d_o - 1.15 d$	Nominal overall dia. (d_o)	S_1 $= 1.26 d_o - 1.15 d$	S_2 $= d_o - 1.15 d$
mm	mm ⁴	mm	mm	mm	mm	mm	mm
0.650	1.79×10^{-1}	0.689 3	0.121	-0.058 3	0.711 3	0.149	-0.036 3
0.680	2.14×10^{-1}	0.722 1	0.128	-0.059 9	0.743 6	0.155	-0.038 4
0.700	2.40×10^{-1}	0.742 0	0.130	-0.063 0	0.763 5	0.157	-0.041 5
0.720	2.69×10^{-1}	0.761 9	0.132	-0.066 1	0.783 4	0.159	-0.044 6
0.750	3.16×10^{-1}	0.791 8	0.135	-0.070 8	0.813 3	0.162	-0.049 3
0.780	3.70×10^{-1}	0.824 6	0.142	-0.072 4	0.846 1	0.169	-0.050 9
0.800	4.10×10^{-1}	0.844 5	0.144	-0.075 5	0.866 0	0.171	-0.054 0
0.850	5.22×10^{-1}	0.894 8	0.150	-0.082 8	0.916 3	0.177	-0.061 3
0.900	6.56×10^{-1}	0.946 0	0.157	-0.089 0	0.969 5	0.187	-0.065 5
0.950	8.15×10^{-1}	0.995 8	0.162	-0.096 8	1.020	0.192	-0.072 8
1.00	1.00	1.049	0.172	-0.101	1.073	0.202	-0.077 0
1.05	1.22	1.099	0.177	-0.109	1.123	0.207	-0.084 8
1.10	1.46	1.148	0.182	-0.117	1.173	0.212	-0.092 5
1.15	1.75	1.198	0.187	-0.124	1.222	0.218	-0.100
1.20	2.07	1.252	0.198	-0.128	1.276	0.228	-0.104
1.25	2.44	1.302	0.203	-0.136	1.326	0.233	-0.112
1.30	2.86	1.352	0.208	-0.144	1.376	0.238	-0.120
1.35	3.32	1.401	0.213	-0.151	1.425	0.243	-0.127
1.40	3.84	1.455	0.223	-0.156	1.479	0.253	-0.132
1.45	4.42	1.504	0.228	-0.163	1.528	0.258	-0.139
1.50	5.06	1.554	0.233	-0.171	1.578	0.263	-0.147
1.55	5.77	1.604	0.238	-0.179	1.632	0.274	-0.151
1.60	6.55	1.654	0.243	-0.187	1.682	0.279	-0.159
1.65	7.41	1.706	0.252	-0.192	1.731	0.284	-0.166
1.70	8.35	1.756	0.257	-0.200	1.781	0.289	-0.174
1.75	9.38	1.805	0.262	-0.207	1.834	0.299	-0.178
1.80	1.05×10	1.855	0.267	-0.215	1.884	0.304	-0.186
1.90	1.30×10	1.957	0.281	-0.228	1.984	0.314	-0.202
2.00	1.60×10	2.058	0.293	-0.242	2.087	0.330	-0.213
2.10	1.94×10	2.158	0.303	-0.258	2.187	0.340	-0.229
2.20	2.34×10	2.261	0.318	-0.270	2.290	0.355	-0.241
2.30	2.80×10	2.360	0.329	-0.285	2.389	0.365	-0.256
2.40	3.32×10	2.462	0.342	-0.298	2.491	0.379	-0.269
2.50	3.91×10	2.563	0.354	-0.312	2.592	0.391	-0.283
2.60	4.57×10	2.663	0.365	-0.328	2.694	0.404	-0.296
2.70	5.31×10	2.765	0.378	-0.341	2.794	0.415	-0.312
2.80	6.15×10	2.865	0.390	-0.355	2.894	0.426	-0.326
2.90	7.07×10	2.967	0.403	-0.368	2.996	0.440	-0.339
3.00	8.10×10	3.068	0.416	-0.382	3.097	0.452	-0.353
3.10	9.24×10	3.168	0.426	-0.398	3.199	0.466	-0.366
3.20	1.05×10^2	3.270	0.440	-0.411	3.299	0.476	-0.382
3.30	1.19×10^2	3.369	0.450	-0.426	3.398	0.486	-0.397
3.40	1.34×10^2	3.469	0.460	-0.442	3.500	0.500	-0.410
3.50	1.50×10^2	3.572	0.475	-0.454	3.601	0.512	-0.425
3.60	1.68×10^2	3.671	0.485	-0.469	3.700	0.522	-0.440
3.70	1.87×10^2	3.771	0.496	-0.485	3.800	0.532	-0.456
3.80	2.09×10^2	3.874	0.511	-0.496	3.903	0.548	-0.467
3.90	2.31×10^2	3.974	0.522	-0.512	4.003	0.558	-0.483
4.00	2.56×10^2	4.073	0.532	-0.527	4.102	0.569	-0.498

Table A.3.1. PROPERTIES OF BARE COPPER WIRES—AWG (B. & S.) (BASED ON BS 156: 1951)

AWG (B. & S.)	Copper diameter (d)						Nominal copper area		Nominal resistance per unit length (R_c)	
	Nominal in mm		Maximum in mm		Minimum in mm		in ²	mm ²	$\Omega/100$ in	Ω/m
50	0.000 99	0.025 2	0.001 07	0.027 18	0.000 91	0.023 11	$0.769 8 \times 10^{-6}$	0.497×10^{-3}	88.18	34.72
49	0.001 11	0.028 2	0.001 19	0.030 23	0.001 03	0.026 16	$0.967 7 \times 10^{-6}$	0.624×10^{-3}	70.15	27.62
48	0.001 24	0.031 5	0.001 32	0.033 53	0.001 16	0.029 46	1.208×10^{-6}	0.779×10^{-3}	56.21	22.13
47	0.001 40	0.035 6	0.001 48	0.037 59	0.001 32	0.033 53	1.539×10^{-6}	0.993×10^{-3}	44.09	17.36
46	0.001 57	0.039 9	0.001 65	0.041 91	0.001 49	0.037 85	1.936×10^{-6}	1.249×10^{-3}	35.06	13.80
45	0.001 76	0.044 7	0.001 84	0.046 74	0.001 68	0.042 67	2.433×10^{-6}	1.570×10^{-3}	27.90	10.98
44	0.001 98	0.050 3	0.002 06	0.052 32	0.001 90	0.048 26	3.079×10^{-6}	1.987×10^{-3}	22.04	8.679
43	0.002 22	0.056 4	0.002 30	0.058 42	0.002 14	0.054 36	3.871×10^{-6}	2.497×10^{-3}	17.54	6.904
42	0.002 49	0.063 3	0.002 58	0.065 53	0.002 40	0.060 96	4.870×10^{-6}	3.142×10^{-3}	13.94	5.488
41	0.002 80	0.071 1	0.002 89	0.073 41	0.002 71	0.068 83	6.158×10^{-6}	3.973×10^{-3}	11.03	4.341
40	0.003 14	0.079 8	0.003 23	0.082 04	0.003 05	0.077 47	7.744×10^{-6}	4.996×10^{-3}	8.767	3.451
39	0.003 53	0.089 7	0.003 63	0.092 20	0.003 43	0.087 12	9.787×10^{-6}	6.314×10^{-3}	6.936	2.731
38	0.003 97	0.100 8	0.004 07	0.103 4	0.003 87	0.098 30	12.38×10^{-6}	7.986×10^{-3}	5.484	2.159
37	0.004 45	0.113 0	0.004 55	0.115 6	0.004 35	0.110 5	15.55×10^{-6}	10.03×10^{-3}	4.364	1.718
36	0.005 00	0.127 0	0.005 10	0.129 5	0.004 90	0.124 5	19.63×10^{-6}	12.67×10^{-3}	3.457	1.361
35	0.005 60	0.142 2	0.005 7	0.144 8	0.005 5	0.139 7	24.63×10^{-6}	15.89×10^{-3}	2.756	1.085
34	0.006 30	0.160 0	0.006 4	0.162 6	0.006 2	0.157 5	31.17×10^{-6}	20.11×10^{-3}	2.178	0.857 3
33	0.007 10	0.180 3	0.007 2	0.182 9	0.007 0	0.177 8	39.59×10^{-6}	25.54×10^{-3}	1.714	0.675 0
32	0.008 00	0.203 2	0.008 1	0.205 7	0.007 9	0.200 7	50.27×10^{-6}	32.43×10^{-3}	1.350	0.531 6
31	0.008 90	0.226 1	0.009 0	0.228 6	0.008 8	0.223 5	62.21×10^{-6}	40.14×10^{-3}	1.091	0.429 6
30	0.010 00	0.254 0	0.010 1	0.256 5	0.009 9	0.251 5	78.54×10^{-6}	50.67×10^{-3}	0.864 2	0.340 2
29	0.011 30	0.287 0	0.011 4	0.289 6	0.011 2	0.284 5	100.3×10^{-6}	64.70×10^{-3}	0.677 0	0.266 5
28	0.012 60	0.320 0	0.012 7	0.322 6	0.012 5	0.317 5	124.7×10^{-6}	80.44×10^{-3}	0.543 9	0.214 2
27	0.014 20	0.360 7	0.014 3	0.363 2	0.014 1	0.358 1	158.4×10^{-6}	$0.102 2$	0.428 6	0.168 7
26	0.015 90	0.403 9	0.016 1	0.408 9	0.015 7	0.398 8	198.6×10^{-6}	$0.128 1$	0.341 9	0.134 6
25	0.017 90	0.454 7	0.018 1	0.459 7	0.017 7	0.449 6	251.6×10^{-6}	$0.162 4$	0.269 7	0.106 2
24	0.020 10	0.510 5	0.020 3	0.515 6	0.019 9	0.505 5	317.3×10^{-6}	$0.204 7$	0.213 9	0.084 22
23	0.022 60	0.574 0	0.022 8	0.579 1	0.022 4	0.569 0	401.1×10^{-6}	$0.258 8$	0.169 2	0.066 62
22	0.025 30	0.642 6	0.025 6	0.650 2	0.025 0	0.635 0	502.7×10^{-6}	$0.324 3$	0.135 0	0.053 16
21	0.028 50	0.723 9	0.028 8	0.731 5	0.028 2	0.716 3	637.9×10^{-6}	$0.411 6$	0.106 4	0.041 89
20	0.032 00	0.812 8	0.032 3	0.820 4	0.031 7	0.805 2	804.2×10^{-6}	$0.518 9$	0.084 39	0.033 22
19	0.035 90	0.911 9	0.036 3	0.922 0	0.035 5	0.901 7	$1 012 \times 10^{-6}$	$0.653 0$	0.067 06	0.026 40
18	0.040 30	1.024	0.040 7	1.033	0.039 9	1.013	$1 276 \times 10^{-6}$	$0.822 9$	0.053 21	0.020 95
17	0.045 30	1.151	0.045 8	1.163	0.044 8	1.138	$1 612 \times 10^{-6}$	1.040	0.042 12	0.016 58
16	0.050 80	1.290	0.051 3	1.303	0.050 3	1.278	$2 027 \times 10^{-6}$	1.308	0.033 49	0.013 19
15	0.057 10	1.450	0.057 7	1.466	0.056 5	1.435	$2 561 \times 10^{-6}$	1.652	0.026 51	0.010 44
14	0.064 10	1.628	0.064 7	1.643	0.063 5	1.613	$3 227 \times 10^{-6}$	2.082	0.021 03	0.008 281
13	0.072 00	1.829	0.072 7	1.847	0.071 3	1.811	$4 072 \times 10^{-6}$	2.627	0.016 67	0.006 564
12	0.080 80	2.052	0.081 6	2.073	0.080 0	2.032	$5 128 \times 10^{-6}$	3.308	0.013 24	0.005 212
11	0.090 70	2.304	0.091 6	2.327	0.089 8	2.281	$6 461 \times 10^{-6}$	4.168	0.010 51	0.004 136
10	0.101 90	2.588	0.102 9	2.614	0.100 9	2.563	$8 155 \times 10^{-6}$	5.261	0.008 322	0.003 277
9	0.114 40	2.906	0.115 5	2.934	0.113 3	2.878	$10 280 \times 10^{-6}$	6.631	0.006 603	0.002 600
8	0.128 50	3.264	0.129 8	3.297	0.127 2	3.231	$12 970 \times 10^{-6}$	8.367	0.005 234	0.002 061
7	0.144 30	3.665	0.145 7	3.701	0.142 9	3.630	$16 350 \times 10^{-6}$	10.55	0.004 151	0.001 634
6	0.162 00	4.115	0.163 6	4.155	0.160 4	4.074	$20 610 \times 10^{-6}$	13.30	0.003 293	0.001 296

Table A.3.2.1. PROPERTIES OF FINE ENAMELLED COPPER WIRES—AWG (B. & S.) (BASED ON BS 1844: 1952—FINE COVERING)

AWG (B. & S.)	Copper dia. (d)		Overall dia. (max.) (d _a)		Increase in dia. due to insulation (min)		Approximate weight		Turns per unit winding breadth (1/d _w)		Turns per unit winding area (1/d _w ²)		Winding copper space factor $F_w = \frac{\pi}{4} \left[\frac{d}{d_a} \right]^2$
	in	mm	in	mm	in	mm	lb/100 in	g/m	in ⁻¹	mm ⁻¹	in ⁻²	mm ⁻²	
50*	0.000 99	0.035 56	0.001 4	0.035 56	0.000 12	0.003 05	0.026 95 × 10 ⁻³	0.004 81	714	28.1	510 000	791	0.392 7
49*	0.001 11	0.038 10	0.001 5	0.038 10	0.000 13	0.003 30	0.033 33 × 10 ⁻³	0.005 95	667	26.2	444 000	689	0.430 1
48*	0.001 24	0.040 64	0.001 6	0.040 64	0.000 14	0.003 56	0.041 11 × 10 ⁻³	0.007 34	625	24.6	391 000	605	0.471 7
47*	0.001 40	0.045 72	0.001 8	0.045 72	0.000 15	0.003 81	0.052 50 × 10 ⁻³	0.009 38	556	21.9	309 000	478	0.475 1
46*	0.001 57	0.050 80	0.002 0	0.050 80	0.000 17	0.004 32	0.065 83 × 10 ⁻³	0.011 8	500	19.7	250 000	387	0.484 0
45*	0.001 76	0.055 88	0.002 2	0.055 88	0.000 18	0.004 57	0.082 50 × 10 ⁻³	0.014 7	454	17.9	207 000	320	0.502 7
44	0.001 98	0.060 96	0.002 4	0.060 96	0.000 2	0.005 08	0.104 2 × 10 ⁻³	0.018 6	417	16.4	174 000	269	0.534 6
43	0.002 22	0.068 58	0.002 7	0.068 58	0.000 2	0.005 08	0.126 7 × 10 ⁻³	0.022 6	370	14.6	137 000	213	0.531 0
42	0.002 49	0.076 20	0.003 0	0.076 20	0.000 25	0.006 35	0.163 3 × 10 ⁻³	0.029 1	333	13.1	111 000	172	0.541 1
41	0.002 80	0.083 82	0.003 3	0.083 82	0.000 25	0.006 35	0.204 4 × 10 ⁻³	0.036 5	303	11.9	91 800	142	0.565 4
40	0.003 14	0.093 98	0.003 7	0.093 98	0.000 3	0.007 62	0.261 1 × 10 ⁻³	0.046 6	270	10.6	73 000	113	0.565 6
39	0.003 53	0.104 1	0.004 1	0.104 1	0.000 3	0.007 62	0.327 8 × 10 ⁻³	0.058 5	244	9.60	59 500	92.2	0.582 2
38	0.003 97	0.119 4	0.004 7	0.119 4	0.000 4	0.010 2	0.416 7 × 10 ⁻³	0.074 3	213	8.38	45 300	70.2	0.560 4
37	0.004 45	0.134 6	0.005 3	0.134 6	0.000 4	0.010 2	0.509 7 × 10 ⁻³	0.091 0	189	7.43	35 600	55.2	0.553 7
36	0.005 00	0.149 9	0.005 9	0.149 9	0.000 5	0.012 7	0.652 8 × 10 ⁻³	0.116 5	169	6.67	28 700	44.5	0.564 1
35	0.005 6	0.165 1	0.006 5	0.165 1	0.000 5	0.012 7	0.815 6 × 10 ⁻³	0.145 1	154	6.06	23 700	36.7	0.583 0
34	0.006 3	0.185 4	0.007 3	0.185 4	0.000 6	0.015 2	1.033 × 10 ⁻³	0.184 5	137	5.39	18 800	29.1	0.585 0
33	0.007 1	0.208 3	0.008 2	0.208 3	0.000 7	0.017 8	1.313 × 10 ⁻³	0.234 3	122	4.80	14 900	23.1	0.588 8
32	0.008 0	0.233 7	0.009 2	0.233 7	0.000 7	0.017 8	1.663 × 10 ⁻³	0.296 3	109	4.28	11 800	18.3	0.593 9
31	0.008 9	0.256 5	0.010 1	0.256 5	0.000 7	0.017 8	2.053 × 10 ⁻³	0.366 5	99.0	3.90	9 800	15.2	0.609 9
30	0.010 0	0.287 0	0.011 3	0.287 0	0.000 8	0.020 3	2.589 × 10 ⁻³	0.462 2	88.5	3.48	7 830	12.1	0.615 1
29	0.011 3	0.322 6	0.012 7	0.322 6	0.000 8	0.020 3	3.300 × 10 ⁻³	0.589 0	78.7	3.10	6 200	9.61	0.621 8
28	0.012 6	0.358 1	0.014 1	0.358 1	0.000 9	0.022 9	4.103 × 10 ⁻³	0.732 0	70.9	2.79	5 030	7.80	0.627 2
27	0.014 2	0.401 3	0.015 8	0.401 3	0.001 0	0.025 4	5.206 × 10 ⁻³	0.929 0	63.3	2.49	4 010	6.21	0.634 4
26	0.015 9	0.449 6	0.017 7	0.449 6	0.001 0	0.025 4	6.519 × 10 ⁻³	1.164	56.5	2.22	3 190	4.95	0.633 8
25	0.017 9	0.502 9	0.019 8	0.502 9	0.001 1	0.027 9	8.247 × 10 ⁻³	1.472	50.5	1.99	2 550	3.95	0.641 9
24	0.020 1	0.561 3	0.022 1	0.561 3	0.001 2	0.030 5	10.44 × 10 ⁻³	1.854	45.2	1.78	2 050	3.17	0.649 7
23	0.022 6	0.627 4	0.024 7	0.627 4	0.001 2	0.030 5	13.11 × 10 ⁻³	2.340	40.5	1.59	1 640	2.54	0.657 5
22	0.025 3	0.698 5	0.027 5	0.698 5	0.001 2	0.030 5	16.41 × 10 ⁻³	2.925	36.4	1.43	1 320	2.05	0.664 8
21	0.028 5	0.782 3	0.030 8	0.782 3	0.001 3	0.033 0	20.80 × 10 ⁻³	3.714	32.5	1.28	1 050	1.63	0.672 5
20	0.032 0	0.873 8	0.034 4	0.873 8	0.001 4	0.035 6	26.20 × 10 ⁻³	4.677	29.1	1.14	845	1.31	0.679 6
19	0.035 9	0.977 9	0.038 5	0.977 9	0.001 4	0.035 6	32.93 × 10 ⁻³	5.880	26.0	1.02	675	1.05	0.682 9
18	0.040 3	1.092	0.043 0	1.092	0.001 5	0.038 1	41.47 × 10 ⁻³	7.404	23.3	0.916	541	0.838	0.689 9
17	0.045 3	1.222	0.048 1	1.222	0.001 5	0.045 7	52.34 × 10 ⁻³	9.348	20.8	0.819	432	0.670	0.696 6
16	0.050 8	1.364	0.053 7	1.364	0.001 6	0.040 6	65.75 × 10 ⁻³	11.74	18.6	0.733	347	0.538	0.702 9
15	0.057 1	1.529	0.060 2	1.529	0.001 7	0.043 2	83.00 × 10 ⁻³	14.78	16.6	0.654	276	0.428	0.706 6
14	0.064 1	1.709	0.067 3	1.709	0.001 7	0.043 2	104.6 × 10 ⁻³	18.68	14.9	0.585	221	0.342	0.712 5
13	0.072 0	1.915	0.075 4	1.915	0.001 7	0.043 2	131.9 × 10 ⁻³	23.54	13.3	0.522	176	0.273	0.716 2
12	0.080 8	2.144	0.084 4	2.144	0.001 8	0.045 7	166.7 × 10 ⁻³	29	11.8	0.466	140	0.218	0.719 8
11	0.090 7	2.400	0.094 5	2.400	0.001 9	0.048 3	208.3 × 10 ⁻³	37	10.6	0.417	112	0.174	0.723 5
10	0.101 9	2.690	0.105 9	2.690	0.002 0	0.050 8	263.9 × 10 ⁻³	47	9.44	0.372	89.2	0.138	0.727 2
9	0.114 4	3.015	0.118 7	3.015	0.002 1	0.053 3	333.3 × 10 ⁻³	59	8.43	0.332	71.0	0.110	0.729 5
8	0.128 5	3.378	0.133 0	3.378	0.002 2	0.055 9	419.4 × 10 ⁻³	71	7.52	0.296	56.5	0.087 6	0.733 1
7	0.144 3	3.785	0.149 0	3.785	0.002 3	0.058 4	527.8 × 10 ⁻³	94	6.71	0.264	45.0	0.069 8	0.736 6
6	0.162 0	4.242	0.167 0	4.242	0.002 4	0.061 0	669.4 × 10 ⁻³	119	5.99	0.236	35.9	0.055 6	0.739 1

*First six rows refer to oilo enamel wire to BS 156:1951—normal covering, as these gauges are not included in BS 1844:1952

Table A.3.2.2. PROPERTIES OF MEDIUM ENAMELLED COPPER WIRES—AWG (B. & S.) (BASED ON BS 1844: 1952—MEDIUM COVERING)

AWG (B. & S.)	Copper dia. (d)	Overall dia. (max.) (d _o)		Increase in dia. due to insulation (min)		Approximate weight		Turns per unit winding breadth (1/d _o)		Turns per unit winding area (1/d _o ²)		Winding copper space factor $F_w = \frac{\pi}{4} \left[\frac{d}{d_o} \right]^2$
		in	mm	in	mm	lb/100 in	g/m	in ⁻¹	mm ⁻¹	in ⁻²	mm ⁻²	
44	0.001 98	0.002 6	0.066 04	0.000 3	0.007 62	0.106 1 × 10 ⁻³	0.018 9	385	15.1	148 000	229	0.455 5
43	0.002 22	0.002 9	0.073 66	0.000 4	0.010 2	0.128 9 × 10 ⁻³	0.023 1	345	13.6	119 000	184	0.460 3
42	0.002 49	0.003 2	0.081 28	0.000 4	0.010 2	0.166 4 × 10 ⁻³	0.010 2	313	12.3	97 700	151	0.475 5
41	0.002 80	0.003 6	0.091 44	0.000 5	0.012 7	0.209 4 × 10 ⁻³	0.037 3	278	10.9	77 200	120	0.475 1
40	0.003 14	0.004 1	0.104 1	0.000 6	0.015 2	0.270 0 × 10 ⁻³	0.048 2	244	9.60	59 500	92.2	0.460 7
39	0.003 53	0.004 5	0.114 3	0.000 6	0.015 2	0.336 1 × 10 ⁻³	0.060 0	222	8.75	49 400	76.5	0.483 3
38	0.003 97	0.005 1	0.129 5	0.000 7	0.017 8	0.426 9 × 10 ⁻³	0.076 2	196	7.72	38 400	59.6	0.475 9
37	0.004 45	0.005 7	0.144 8	0.000 8	0.020 3	0.523 3 × 10 ⁻³	0.093 4	175	6.91	30 800	47.7	0.478 7
36	0.005 00	0.006 4	0.162 6	0.000 9	0.022 9	0.669 2 × 10 ⁻³	0.119 5	156	6.15	24 400	37.8	0.479 4
35	0.005 6	0.007 0	0.177 8	0.000 9	0.022 9	0.833 9 × 10 ⁻³	0.148 9	143	5.62	20 400	31.6	0.502 7
34	0.006 3	0.007 8	0.198 1	0.001 0	0.025 4	1.053 × 10 ⁻³	0.188 1	128	5.05	16 400	25.5	0.512 4
33	0.007 1	0.008 8	0.223 5	0.001 1	0.027 9	1.339 × 10 ⁻³	0.239 1	114	4.47	12 900	20.0	0.511 3
32	0.008 0	0.009 8	0.248 9	0.001 2	0.030 5	1.694 × 10 ⁻³	0.302 1	102	4.02	10 400	16.1	0.523 4
31	0.008 9	0.010 8	0.274 3	0.001 2	0.030 5	2.091 × 10 ⁻³	0.373 3	92.6	3.65	8 570	13.3	0.533 4
30	0.010 0	0.012 0	0.304 8	0.001 3	0.033 0	2.632 × 10 ⁻³	0.466 0	83.3	3.28	6 940	10.8	0.545 4
29	0.011 3	0.013 4	0.340 4	0.001 3	0.033 0	3.347 × 10 ⁻³	0.597 1	74.6	2.94	5 570	8.63	0.558 5
28	0.012 6	0.014 8	0.375 9	0.001 5	0.038 1	4.158 × 10 ⁻³	0.742 2	67.6	2.66	4 570	7.08	0.569 3
27	0.014 2	0.016 5	0.419 1	0.001 6	0.040 6	5.269 × 10 ⁻³	0.941 0	60.6	2.39	3 670	5.69	0.581 7
26	0.015 9	0.018 5	0.469 9	0.001 7	0.043 2	6.594 × 10 ⁻³	1.177	54.1	2.13	2 920	4.53	0.580 2
25	0.017 9	0.020 6	0.523 2	0.001 8	0.045 7	8.342 × 10 ⁻³	1.489	48.5	1.91	2 360	3.65	0.593 0
24	0.020 1	0.022 9	0.581 7	0.001 9	0.048 3	10.50 × 10 ⁻³	1.874	43.7	1.72	1 910	2.96	0.605 1
23	0.022 6	0.025 6	0.650 2	0.002 0	0.050 8	13.25 × 10 ⁻³	2.365	39.1	1.54	1 530	2.37	0.612 1
22	0.025 3	0.028 4	0.721 4	0.002 0	0.050 8	16.55 × 10 ⁻³	2.955	35.2	1.39	1 240	1.92	0.623 3
21	0.028 5	0.031 7	0.805 2	0.002 1	0.053 3	20.96 × 10 ⁻³	3.743	31.5	1.24	995	1.54	0.634 8
20	0.032 0	0.035 3	0.896 6	0.002 2	0.055 9	26.38 × 10 ⁻³	4.710	28.3	1.12	802	1.24	0.645 4
19	0.035 9	0.039 5	1.003	0.002 3	0.058 4	33.16 × 10 ⁻³	5.922	25.3	0.997	641	0.993	0.648 8
18	0.040 3	0.044 0	1.118	0.002 4	0.061 0	41.72 × 10 ⁻³	7.450	22.7	0.895	517	0.801	0.658 9
17	0.045 3	0.049 1	1.247	0.002 4	0.061 0	52.60 × 10 ⁻³	9.392	20.4	0.802	415	0.643	0.668 5
16	0.050 8	0.054 7	1.389	0.002 5	0.063 5	66.08 × 10 ⁻³	11.80	18.3	0.720	334	0.518	0.677 4
15	0.057 1	0.061 3	1.557	0.002 6	0.066 0	83.42 × 10 ⁻³	14.92	16.3	0.642	266	0.412	0.681 5
14	0.064 1	0.068 4	1.737	0.002 7	0.068 6	105.0 × 10 ⁻³	18.75	14.6	0.576	214	0.331	0.689 8
13	0.072 0	0.076 5	1.943	0.002 8	0.071 1	132.4 × 10 ⁻³	23.64	13.1	0.515	171	0.265	0.695 7
12	0.080 8	0.085 5	2.172	0.002 9	0.073 7	166.7 × 10 ⁻³	29	11.7	0.460	137	0.212	0.701 4
11	0.090 7	0.095 7	2.431	0.003 0	0.076 2	211.1 × 10 ⁻³	37	10.4	0.411	109	0.169	0.705 5
10	0.101 9	0.107 1	2.720	0.003 1	0.078 7	263.9 × 10 ⁻³	47	9.34	0.368	87.2	0.135	0.711 0
9	0.114 4	0.119 9	3.045	0.003 2	0.081 3	333.3 × 10 ⁻³	59	8.34	0.328	69.6	0.108	0.715 0
8	0.128 5	0.1342	3.409	0.003 3	0.083 8	422.2 × 10 ⁻³	75	7.45	0.293	55.5	0.086 1	0.720 1
7	0.144 3	0.1502	3.815	0.003 4	0.086 4	530.6 × 10 ⁻³	94	6.66	0.262	44.3	0.068 7	0.724 9
6	0.162 0	0.1682	4.272	0.003 5	0.088 9	669.4 × 10 ⁻³	119	5.95	0.234	35.3	0.054 8	0.728 6

Table A.3.2.3. FUNCTIONS OF COPPER WIRE DIAMETERS—AWG (B. & S.)

AWG (B. and S.)	Nominal copper dia. (d)		d^4	Fine covering			Medium covering		
				Nominal overall dia. (d_o)	S_1 $= 1.26 d_o - 1.15 d$	S_2 $= d_o - 1.15 d$	Nominal overall dia. (d_o)	S_1 $= 1.26 d_o - 1.15 d$	S_2 $= d_o - 1.15 d$
	in	mm	mm ⁴	mm	mm	mm	mm	mm	mm
50*	0.000 99	0.025 2	4.00×10^{-7}	0.030 86	0.009 97	0.001 94			
49*	0.001 11	0.028 2	6.32×10^{-7}	0.033 78	0.010 1	0.001 36			
48*	0.001 24	0.031 5	9.84×10^{-7}	0.036 83	0.010 2	0.000 610			
47*	0.001 40	0.035 6	1.60×10^{-6}	0.041 53	0.011 4	0.000 635			
46*	0.001 57	0.039 9	2.53×10^{-6}	0.046 48	0.012 7	0.000 622			
45*	0.001 76	0.044 7	3.99×10^{-6}	0.051 56	0.013 6	0.000 152			
44	0.001 98	0.050 3	6.40×10^{-6}	0.057 15	0.014 2	-0.000 686	0.060 96	0.019 0	0.003 12
43	0.002 22	0.056 4	1.01×10^{-5}	0.064 01	0.015 8	-0.000 838	0.069 09	0.022 2	0.004 24
42	0.002 49	0.063 3	1.60×10^{-5}	0.071 76	0.017 7	-0.000 978	0.076 20	0.023 3	0.003 47
41	0.002 80	0.071 1	2.56×10^{-5}	0.079 50	0.018 4	-0.002 29	0.086 49	0.027 2	0.004 70
40	0.003 14	0.079 8	4.05×10^{-5}	0.089 54	0.021 1	-0.002 18	0.098 43	0.032 3	0.006 71
39	0.003 53	0.089 7	6.46×10^{-5}	0.099 44	0.022 2	-0.003 67	0.108 3	0.033 4	0.005 22
38	0.003 97	0.100 8	1.03×10^{-4}	0.113 9	0.027 6	-0.002 05	0.122 8	0.038 8	0.006 85
37	0.004 45	0.113 0	1.63×10^{-4}	0.127 6	0.030 8	-0.002 35	0.137 8	0.043 6	0.007 81
36	0.005 00	0.127 0	2.60×10^{-4}	0.143 5	0.034 8	-0.002 54	0.154 9	0.049 2	0.008 89
35	0.005 6	0.142 2	4.09×10^{-4}	0.158 8	0.036 5	-0.004 83	0.170 2	0.050 9	0.006 60
34	0.006 3	0.160 0	6.56×10^{-4}	0.179 1	0.041 6	-0.004 95	0.190 5	0.056 0	0.006 48
33	0.007 1	0.180 3	1.06×10^{-3}	0.201 9	0.047 0	-0.005 46	0.214 6	0.063 0	0.007 24
32	0.008 0	0.203 2	1.70×10^{-3}	0.226 1	0.051 2	-0.007 62	0.240 0	0.068 8	0.006 35
31	0.008 9	0.226 1	2.61×10^{-3}	0.248 9	0.053 7	-0.011 0	0.264 2	0.072 9	0.004 19
30	0.010 0	0.254 0	4.16×10^{-3}	0.279 4	0.059 9	-0.012 7	0.294 6	0.079 2	0.002 54
29	0.011 3	0.287 0	6.79×10^{-3}	0.313 7	0.065 2	-0.016 4	0.328 9	0.084 4	-0.001 14
28	0.012 6	0.320 0	1.05×10^{-2}	0.349 3	0.072 0	-0.018 8	0.365 8	0.092 8	-0.002 29
27	0.014 2	0.360 7	1.69×10^{-2}	0.392 4	0.079 7	-0.022 4	0.408 9	0.100	-0.005 84
26	0.015 9	0.403 9	2.66×10^{-2}	0.436 9	0.086 0	-0.027 6	0.455 9	0.110	-0.008 51
25	0.017 9	0.454 7	4.27×10^{-2}	0.490 2	0.094 8	-0.032 6	0.509 3	0.119	-0.013 6
24	0.020 1	0.510 5	6.79×10^{-2}	0.548 6	0.104	-0.038 5	0.567 7	0.128	-0.019 4
23	0.022 6	0.574 0	1.09×10^{-1}	0.613 4	0.113	-0.046 7	0.635 0	0.140	-0.025 1
22	0.025 3	0.642 6	1.71×10^{-1}	0.682 0	0.120	-0.057 0	0.703 6	0.148	-0.035 4
21	0.028 5	0.723 9	2.75×10^{-1}	0.765 8	0.132	-0.066 7	0.787 4	0.160	-0.045 1
20	0.032 0	0.812 8	4.36×10^{-1}	0.857 3	0.145	-0.077 5	0.878 8	0.173	-0.055 9
19	0.035 9	0.911 9	6.91×10^{-1}	0.957 6	0.158	-0.091 1	0.981 7	0.188	-0.066 9
18	0.040 3	1.024	1.10	1.072	0.173	-0.105	1.096	0.204	-0.081 2
17	0.045 3	1.151	1.75	1.199	0.187	-0.124	1.223	0.218	-0.100
16	0.050 8	1.290	2.77	1.341	0.206	-0.143	1.365	0.236	-0.119
15	0.057 1	1.450	4.42	1.504	0.227	-0.164	1.529	0.259	-0.139
14	0.064 1	1.628	7.03	1.683	0.248	-0.190	1.709	0.282	-0.163
13	0.072 0	1.829	11.2	1.885	0.272	-0.218	1.912	0.307	-0.191
12	0.080 8	2.052	17.7	2.111	0.299	-0.249	2.139	0.335	-0.221
11	0.090 7	2.304	28.2	2.365	0.330	-0.285	2.394	0.367	-0.255
10	0.101 9	2.588	44.9	2.652	0.365	-0.325	2.681	0.402	-0.296
9	0.114 4	2.906	71.3	2.973	0.404	-0.369	3.002	0.441	-0.339
8	0.128 5	3.264	113	3.332	0.445	-0.421	3.362	0.482	-0.392
7	0.144 3	3.665	180	3.736	0.493	-0.479	3.766	0.530	-0.449
6	0.162 0	4.115	287	4.188	0.545	-0.544	4.218	0.582	-0.514

*First six rows refer to oleo enamel wire to BS 156:1951—normal covering, as these gauges are not included in BS 1844:1952.

Table A.4.1. PROPERTIES OF BUNCHED CONDUCTORS—0.0016 in (≈ 0.04 mm) DIA. (48 SWG) STRANDS

Number of strands (n)	Single (S) or Double (D) silk covering	Maximum overall diameter of bunch		Approximate weight		Turns per unit winding breadth		Turns per unit winding area		Nominal resistance per unit length (R_d/n)	Winding copper space factor (F_w)	nd^4	Nominal overall diameter of bunch	S_1	S_2
		in	mm	lb/100 in	g/m	in ⁻¹	mm ⁻¹	in ⁻²	mm ⁻²						
3	S	0.0067	0.169	3.22×10^{-4}	0.0575	150	5.90	22 500	348	11.1	0.135	8.19×10^{-6}	0.144	0.060	0.0221
4	S	0.0073	0.186	4.01×10^{-4}	0.0717	136	5.37	18 600	289	8.29	0.150	1.09×10^{-5}	0.159	0.061	0.0198
5	S	0.0078	0.197	4.77×10^{-4}	0.0852	129	5.07	16 600	257	6.63	0.166	1.36×10^{-5}	0.169	0.062	0.0184
7	S	0.0084	0.212	6.24×10^{-4}	0.111	120	4.71	14 300	22.1	4.74	0.200	1.91×10^{-5}	0.182	0.064	0.0163
9	S	0.0097	0.246	7.83×10^{-4}	0.140	103	4.07	10 700	16.6	3.69	0.193	2.46×10^{-5}	0.212	0.067	0.0119
10	S	0.0105	0.266	8.65×10^{-4}	0.155	95.5	3.76	9 120	14.1	3.32	0.183	2.73×10^{-5}	0.231	0.069	0.0091
12	S	0.0115	0.292	1.02×10^{-3}	0.182	87.0	3.43	7 570	11.7	2.76	0.182	3.28×10^{-5}	0.244	0.071	0.0071
15	S	0.0117	0.296	1.23×10^{-3}	0.219	85.7	3.37	7 350	11.4	2.21	0.221	4.09×10^{-5}	0.257	0.072	0.0052
16	S	0.0122	0.310	1.30×10^{-3}	0.233	81.9	3.22	6 710	10.4	2.07	0.215	4.37×10^{-5}	0.270	0.073	0.0031
19	S	0.0127	0.322	1.52×10^{-3}	0.271	79.0	3.11	6 230	9.66	1.75	0.238	5.19×10^{-5}	0.281	0.075	0.0015
21	S	0.0136	0.344	1.67×10^{-3}	0.298	73.8	2.90	5 440	8.44	1.58	0.229	5.73×10^{-5}	0.302	0.077	0.0016
24	S	0.0142	0.360	1.88×10^{-3}	0.336	70.6	2.78	4 980	7.72	1.38	0.240	6.55×10^{-5}	0.317	0.079	0.0038
27	S	0.0148	0.375	2.10×10^{-3}	0.375	67.8	2.67	4 600	7.12	1.23	0.249	7.37×10^{-5}	0.330	0.080	0.0058
30	S	0.0155	0.393	2.31×10^{-3}	0.413	64.7	2.55	4 180	6.48	1.11	0.252	8.19×10^{-5}	0.347	0.082	0.0084
36	S	0.0170	0.431	2.75×10^{-3}	0.491	58.9	2.32	3 470	5.38	0.921	0.251	9.83×10^{-5}	0.384	0.086	0.0139
45	S	0.0189	0.479	3.40×10^{-3}	0.606	53.0	2.09	2 810	4.35	0.737	0.290	1.23×10^{-4}	0.428	0.091	0.0205
54	D	0.0216	0.549	4.44×10^{-3}	0.792	46.3	1.82	2 140	3.32	0.614	0.232	1.47×10^{-4}	0.494	0.127	0.0011
63	D	0.0231	0.587	5.10×10^{-3}	0.911	43.3	1.70	1 870	2.90	0.527	0.237	1.72×10^{-4}	0.528	0.131	0.0062
72	D	0.0245	0.622	5.77×10^{-3}	1.03	40.8	1.61	1 670	2.58	0.461	0.240	1.97×10^{-4}	0.561	0.135	0.0111
81	D	0.0258	0.656	6.42×10^{-3}	1.15	38.7	1.53	1 500	2.33	0.410	0.244	2.21×10^{-4}	0.591	0.138	0.0156
90	D	0.0272	0.692	7.09×10^{-3}	1.27	36.7	1.45	1 350	2.09	0.369	0.243	2.46×10^{-4}	0.624	0.142	0.0205
100	D	0.0286	0.725	7.81×10^{-3}	1.40	35.0	1.38	1 230	1.90	0.332	0.246	2.73×10^{-4}	0.654	0.145	0.0251
108	D	0.0296	0.751	8.39×10^{-3}	1.50	33.8	1.33	1 140	1.77	0.307	0.247	2.95×10^{-4}	0.677	0.148	0.0285
135	D	0.0327	0.831	1.03×10^{-2}	1.85	30.6	1.20	935	1.45	0.246	0.253	3.69×10^{-4}	0.750	0.155	0.0394
162	D	0.0355	0.903	1.23×10^{-2}	2.19	28.1	1.11	792	1.23	0.205	0.258	4.42×10^{-4}	0.815	0.163	0.0492
189	D	0.0381	0.969	1.42×10^{-2}	2.54	26.2	1.03	687	1.07	0.176	0.262	5.16×10^{-4}	0.875	0.169	0.0583
216	D	0.0409	1.038	1.61×10^{-2}	2.88	24.5	0.963	599	0.928	0.154	0.259	5.90×10^{-4}	0.938	0.176	0.0677
243	D	0.0432	1.097	1.81×10^{-2}	3.23	23.2	0.912	537	0.832	0.137	0.262	6.63×10^{-4}	0.991	0.182	0.0757
270	D	0.0453	1.152	2.00×10^{-2}	3.57	22.1	0.868	486	0.754	0.123	0.264	7.37×10^{-4}	1.04	0.188	0.0832
297	D	0.0474	1.204	2.19×10^{-2}	3.91	21.1	0.830	445	0.689	0.112	0.265	8.11×10^{-4}	1.09	0.193	0.0903
324	D	0.0494	1.255	2.38×10^{-2}	4.25	20.2	0.797	410	0.635	0.102	0.266	8.85×10^{-4}	1.13	0.198	0.0972

Note 1.

$$F_w = \frac{\pi n}{4} \left(\frac{d}{\text{nom. dia. of bunch over covering}} \right)^2$$

where d = bare strand dia.

Note 2.

$$S_1 = 1/26 \text{ (nom. dia. of bunch over covering)}$$

$$= 1/15 \text{ (eff. copper dia. of bunch)}$$

$$S_2 = \text{(nom. dia. of bunch over covering)}$$

$$= 1/15 \text{ (eff. copper dia. of bunch)}$$

Table A.4.2. PROPERTIES OF BUNCHED CONDUCTORS—0.002 0 in (\approx 0.051 mm) DIA. (47 SWG) STRANDS

Number of strands (n)	Single (S) or Double (D) silk covering	Maximum overall diameter of bunch		Approximate weight		Turns per unit winding breadth		Turns per unit winding area		Nominal resistance per unit length (R_p/n)		Winding copper space factor (F_w)	nd^4	Nominal overall diameter of bunch	S_1	S_2
		in	mm	lb/100 in	g/m	in ⁻¹	mm ⁻¹	in ⁻²	mm ⁻²	$\Omega/100\text{in}$	Ω/m					
—	—	—	—	—	—	—	—	—	—	—	—	—	—	—	—	—
3	S	0.007 6	0.193	4.47×10^{-4}	0.079 8	131	5.17	17 300	26.8	7.08	2.79	0.163	2.00×10^{-6}	0.168	0.062	0.018 5
4	S	0.008 4	0.213	5.65×10^{-4}	0.101	119	4.69	14 200	22.0	5.31	2.09	0.178	2.66×10^{-5}	0.187	0.064	0.015 7
5	S	0.008 9	0.227	6.78×10^{-4}	0.121	112	4.41	12 500	19.4	4.25	1.67	0.197	3.33×10^{-5}	0.198	0.066	0.013 9
7	S	0.009 6	0.245	8.99×10^{-4}	0.161	104	4.08	10 700	16.7	3.03	1.19	0.237	4.66×10^{-5}	0.215	0.067	0.011 5
9	S	0.011 2	0.285	1.14×10^{-3}	0.203	89.2	3.51	7 960	12.3	2.36	0.929	0.224	5.99×10^{-5}	0.252	0.071	0.006 0
10	S	0.012 2	0.309	1.26×10^{-3}	0.224	82.2	3.24	6 750	10.5	2.12	0.836	0.213	6.66×10^{-5}	0.274	0.074	0.002 6
12	S	0.013 4	0.340	1.49×10^{-3}	0.265	74.6	2.94	5 570	8.63	1.77	0.696	0.210	7.99×10^{-5}	0.291	0.076	0.000 1
15	S	0.013 6	0.346	1.80×10^{-3}	0.322	73.5	2.89	5 400	8.37	1.42	0.557	0.254	9.99×10^{-5}	0.306	0.077	0.002 2
16	S	0.014 3	0.362	1.92×10^{-3}	0.343	70.1	2.76	4 920	7.63	1.33	0.522	0.274	1.07×10^{-4}	0.323	0.079	0.004 7
19	S	0.014 8	0.376	2.24×10^{-3}	0.400	67.5	2.66	4 560	7.07	1.12	0.440	0.272	1.27×10^{-4}	0.336	0.081	0.006 7
21	S	0.015 9	0.403	2.47×10^{-3}	0.441	63.0	2.48	3 970	6.15	1.01	0.398	0.262	1.40×10^{-4}	0.362	0.083	0.010 5
24	S	0.016 6	0.422	2.79×10^{-3}	0.499	60.2	2.37	3 630	5.62	0.884	0.348	0.273	1.60×10^{-4}	0.380	0.085	0.013 2
27	S	0.017 3	0.440	3.12×10^{-3}	0.557	57.8	2.27	3 340	5.17	0.786	0.310	0.283	1.80×10^{-4}	0.396	0.087	0.015 7
30	S	0.018 2	0.461	3.45×10^{-3}	0.615	55.1	2.17	3 030	4.70	0.708	0.279	0.286	2.00×10^{-4}	0.417	0.090	0.018 8
36	S	0.020 0	0.507	4.10×10^{-3}	0.733	50.1	1.97	2 510	3.89	0.590	0.232	0.284	2.40×10^{-4}	0.462	0.094	0.025 5
45	S	0.022 3	0.565	5.08×10^{-3}	0.907	44.9	1.77	2 020	3.13	0.472	0.186	0.285	3.00×10^{-4}	0.515	0.100	0.033 6
54	D	0.025 4	0.644	6.52×10^{-3}	1.16	39.4	1.55	1 560	2.41	0.393	0.155	0.264	3.60×10^{-4}	0.591	0.138	0.015 6
63	D	0.027 1	0.689	7.52×10^{-3}	1.34	36.8	1.45	1 360	2.10	0.337	0.133	0.268	4.20×10^{-4}	0.633	0.143	0.021 9
72	D	0.028 8	0.732	8.52×10^{-3}	1.52	34.7	1.37	1 200	1.87	0.295	0.116	0.273	4.80×10^{-4}	0.672	0.147	0.027 8
81	D	0.030 4	0.772	9.51×10^{-3}	1.70	32.9	1.30	1 080	1.68	0.262	0.103	0.276	5.39×10^{-4}	0.709	0.151	0.033 4
90	D	0.032 1	0.815	1.05×10^{-2}	1.88	31.2	1.23	971	1.50	0.236	0.092 9	0.274	5.99×10^{-4}	0.750	0.155	0.039 4
100	D	0.033 7	0.855	1.16×10^{-2}	2.07	29.7	1.17	882	1.37	0.212	0.083 6	0.278	6.66×10^{-4}	0.787	0.160	0.045 0
108	D	0.034 9	0.886	1.25×10^{-2}	2.23	28.7	1.13	822	1.27	0.197	0.077 4	0.278	7.19×10^{-4}	0.815	0.163	0.049 2
135	D	0.038 6	0.982	1.54×10^{-2}	2.75	25.9	1.02	670	1.04	0.157	0.061 9	0.285	8.99×10^{-4}	0.904	0.172	0.062 5
162	D	0.042 1	1.068	1.84×10^{-2}	3.28	23.8	0.936	565	0.876	0.131	0.051 6	0.288	1.08×10^{-3}	0.984	0.181	0.074 6
189	D	0.045 2	1.148	2.13×10^{-2}	3.80	22.1	0.871	490	0.759	0.112	0.044 2	0.291	1.26×10^{-3}	1.06	0.189	0.085 6
216	D	0.048 5	1.231	2.42×10^{-2}	4.32	20.6	0.813	426	0.660	0.098 3	0.038 7	0.289	1.44×10^{-3}	1.13	0.198	0.097 2
243	D	0.051 2	1.301	2.71×10^{-2}	4.84	19.5	0.769	381	0.591	0.087 4	0.034 4	0.291	1.62×10^{-3}	1.20	0.205	0.107
270	D	0.053 8	1.367	3.00×10^{-2}	5.36	18.6	0.731	345	0.535	0.078 6	0.031 0	0.293	1.80×10^{-3}	1.26	0.212	0.116
297	D	0.056 3	1.430	3.29×10^{-2}	5.88	17.8	0.699	315	0.489	0.071 5	0.028 1	0.294	1.98×10^{-3}	1.32	0.218	0.125
324	D	0.058 7	1.490	3.58×10^{-2}	6.40	17.0	0.671	290	0.450	0.065 5	0.025 8	0.296	2.16×10^{-3}	1.38	0.224	0.133

See notes to Table A.4.1.

Table A.4.3. PROPERTIES OF BUNCHED CONDUCTORS—0.002 4 in (= 0.061 mm) DIA. (46 SWG) STRANDS

Number of strands (n)	Single (S) or Double (D) silk covering	Maximum overall diameter of bunch		Approximate weight		Turns per unit winding breadth		Turns per unit winding area		Nominal resistance per unit length (R_c/n)		Winding copper space factor (F_w)	nd ⁴	Nominal overall diameter of bunch	S ₁	S ₂
		in	mm	lb/100 in	g/m	in ⁻¹	mm ⁻¹	in ⁻²	mm ⁻²	Ω/100in	Ω/m					
—	—	—	—	—	—	—	—	—	—	—	—	—	—	—	—	—
3	S	0.008 8	0.223	6.07×10^{-4}	0.108	114	4.48	13 000	20.1	4.91	1.93	0.176	4.14×10^{-5}	0.195	0.065	0.0144
4	S	0.009 7	0.247	7.74×10^{-4}	0.138	103	4.04	10 500	16.3	3.69	1.45	0.191	5.52×10^{-5}	0.218	0.068	0.011 0
5	S	0.010 4	0.264	9.36×10^{-4}	0.167	96.3	3.79	9 280	14.4	2.95	1.16	0.210	6.90×10^{-5}	0.232	0.069	0.008 9
7	S	0.011 2	0.286	1.25×10^{-3}	0.224	88.9	3.50	7 910	12.3	2.11	0.829	0.252	9.66×10^{-5}	0.252	0.071	0.005 9
9	S	0.013 1	0.334	1.59×10^{-3}	0.283	76.2	3.00	5 800	8.99	1.64	0.645	0.237	1.24×10^{-4}	0.296	0.076	0.000 8
10	S	0.014 3	0.363	1.76×10^{-3}	0.314	70.0	2.75	4 890	7.59	1.47	0.580	0.222	1.38×10^{-4}	0.324	0.079	0.004 8
12	S	0.015 8	0.401	2.09×10^{-3}	0.372	63.4	2.49	4 020	6.22	1.23	0.484	0.218	1.66×10^{-4}	0.344	0.081	0.007 8
15	S	0.016 0	0.407	2.54×10^{-3}	0.454	62.4	2.46	3 890	6.03	0.983	0.387	0.264	2.07×10^{-4}	0.362	0.084	0.010 6
16	S	0.016 8	0.427	2.71×10^{-3}	0.483	59.5	2.34	3 540	5.48	0.921	0.363	0.256	2.21×10^{-4}	0.383	0.086	0.013 7
19	S	0.017 5	0.444	3.17×10^{-3}	0.566	57.2	2.25	3 270	5.07	0.776	0.305	0.282	2.62×10^{-4}	0.398	0.088	0.016 1
21	S	0.018 8	0.477	3.49×10^{-3}	0.624	53.3	2.10	2 840	4.40	0.702	0.276	0.270	2.90×10^{-4}	0.430	0.091	0.020 7
24	S	0.019 7	0.499	3.96×10^{-3}	0.701	50.9	2.00	2 590	4.01	0.614	0.242	0.281	3.31×10^{-4}	0.452	0.093	0.024 0
27	S	0.020 5	0.521	4.43×10^{-3}	0.791	48.8	1.92	2 380	3.69	0.546	0.215	0.291	3.73×10^{-4}	0.471	0.096	0.027 0
30	S	0.021 5	0.547	4.90×10^{-3}	0.874	46.4	1.83	2 160	3.34	0.491	0.193	0.293	4.14×10^{-4}	0.497	0.098	0.030 8
36	S	0.023 7	0.602	5.84×10^{-3}	1.04	42.2	1.66	1 780	2.76	0.409	0.161	0.290	4.97×10^{-4}	0.551	0.104	0.038 9
45	S	0.026 5	0.673	7.24×10^{-3}	1.29	37.8	1.49	1 430	2.21	0.328	0.129	0.291	6.21×10^{-4}	0.616	0.111	0.048 7
54	D	0.030 0	0.762	9.19×10^{-3}	1.64	33.3	1.31	1 110	1.72	0.273	0.107	0.271	7.45×10^{-4}	0.702	0.150	0.032 2
63	D	0.032 2	0.818	1.06×10^{-2}	1.90	31.1	1.22	965	1.50	0.234	0.092 1	0.276	8.69×10^{-4}	0.753	0.156	0.039 9
72	D	0.034 2	0.869	1.20×10^{-2}	2.15	29.2	1.15	855	1.32	0.205	0.080 6	0.278	9.94×10^{-4}	0.800	0.161	0.047 0
81	D	0.036 1	0.917	1.35×10^{-2}	2.41	27.7	1.09	767	1.19	0.182	0.071 7	0.282	1.12×10^{-3}	0.845	0.166	0.053 7
90	D	0.038 2	0.969	1.49×10^{-2}	2.66	26.2	1.03	686	1.06	0.164	0.064 5	0.279	1.24×10^{-3}	0.894	0.171	0.061 1
100	D	0.040 1	1.018	1.65×10^{-2}	2.94	25.0	0.982	623	0.965	0.147	0.058 0	0.282	1.38×10^{-3}	0.939	0.176	0.067 8
108	D	0.041 5	1.055	1.77×10^{-2}	3.17	24.1	0.948	580	0.899	0.137	0.053 7	0.284	1.49×10^{-3}	0.973	0.180	0.072 9
135	D	0.046 1	1.170	2.20×10^{-2}	3.92	21.7	0.854	471	0.730	0.109	0.043 0	0.288	1.86×10^{-3}	1.08	0.192	0.089 1
162	D	0.050 2	1.275	2.62×10^{-2}	4.67	19.9	0.784	397	0.615	0.091 0	0.035 8	0.291	2.24×10^{-3}	1.18	0.203	0.104
189	D	0.054 0	1.371	3.04×10^{-2}	5.42	18.5	0.729	343	0.532	0.078 0	0.030 7	0.294	2.61×10^{-3}	1.27	0.212	0.117
216	D	0.057 9	1.472	3.46×10^{-2}	6.17	17.3	0.680	298	0.462	0.068 3	0.026 9	0.292	2.98×10^{-3}	1.36	0.223	0.131
243	D	0.061 3	1.556	3.87×10^{-2}	6.92	16.3	0.643	266	0.413	0.060 7	0.023 9	0.293	3.35×10^{-3}	1.44	0.231	0.143
270	D	0.064 4	1.636	4.29×10^{-2}	7.67	15.5	0.611	241	0.373	0.054 6	0.021 5	0.294	3.73×10^{-3}	1.51	0.239	0.154
297	D	0.067 4	1.713	4.71×10^{-2}	8.41	14.8	0.584	220	0.341	0.049 6	0.019 5	0.296	4.10×10^{-3}	1.58	0.247	0.165
324	D	0.070 3	1.785	5.13×10^{-2}	9.15	14.2	0.560	202	0.314	0.045 5	0.017 9	0.297	4.47×10^{-3}	1.65	0.255	0.175

See notes to Table A.4.1.

Table A.4.4. PROPERTIES OF BUNCHED CONDUCTORS—0.0028 in (≈ 0.071 mm) DIA. (45 SWG) STRANDS

Number of strands (n)	Single (S) or Double (D) silk covering	Maximum overall diameter of bunch		Approximate weight		Turns per unit winding breadth		Turns per unit winding area		Nominal resistance per unit length (R_c/n)		Winding copper space factor (F_w)	nd^4	Nominal overall diameter of bunch	S_1	S_2
		in	mm	lb/100 in	g/m	in ⁻¹	mm ⁻¹	in ⁻²	mm ⁻²	$\Omega/100$ in	Ω/m					
—	—	—	—	—	—	—	—	—	—	—	—	—	—	—	—	—
3	S	0.0097	0.247	7.85×10^{-4}	0.140	103	4.05	10 600	16.4	3.61	1.42	0.195	7.68×10^{-5}	0.219	0.068	0.010 8
4	S	0.010 8	0.275	1.01×10^{-3}	0.180	92.5	3.64	8 550	13.3	2.71	1.07	0.211	1.02×10^{-4}	0.246	0.071	0.006 9
5	S	0.011 5	0.293	1.23×10^{-3}	0.219	86.7	3.41	7 510	11.6	2.17	0.853	0.230	1.28×10^{-4}	0.262	0.073	0.004 4
7	S	0.012 5	0.318	1.65×10^{-3}	0.295	79.8	3.14	6 380	9.88	1.55	0.609	0.275	1.79×10^{-4}	0.285	0.075	0.000 9
9	S	0.014 7	0.373	2.10×10^{-3}	0.375	68.2	2.68	4 650	7.20	1.20	0.474	0.257	2.30×10^{-4}	0.336	0.081	0.000 7
10	S	0.016 0	0.406	2.33×10^{-3}	0.415	62.5	2.46	3 910	6.06	1.08	0.426	0.241	2.56×10^{-4}	0.367	0.084	0.001 4
12	S	0.017 7	0.449	2.77×10^{-3}	0.494	56.5	2.23	3 200	4.95	0.903	0.355	0.236	3.07×10^{-4}	0.391	0.087	0.001 4
15	S	0.018 0	0.456	3.38×10^{-3}	0.604	55.6	2.19	3 100	4.80	0.722	0.284	0.286	3.84×10^{-4}	0.412	0.089	0.001 8
16	S	0.018 9	0.479	3.60×10^{-3}	0.644	53.0	2.09	2 810	4.36	0.677	0.267	0.277	4.10×10^{-4}	0.435	0.092	0.002 1
19	S	0.019 6	0.498	4.23×10^{-3}	0.755	51.0	2.01	2 600	4.03	0.570	0.224	0.304	4.86×10^{-4}	0.454	0.094	0.002 4
21	S	0.021 1	0.536	4.67×10^{-3}	0.833	47.4	1.87	2 250	3.49	0.516	0.203	0.291	5.38×10^{-4}	0.490	0.098	0.002 8
24	S	0.022 1	0.561	5.30×10^{-3}	0.946	45.3	1.78	2 050	3.17	0.451	0.178	0.302	6.14×10^{-4}	0.515	0.100	0.003 6
27	S	0.023 1	0.586	5.93×10^{-3}	1.06	43.4	1.71	1 880	2.91	0.401	0.158	0.312	6.91×10^{-4}	0.538	0.103	0.003 7
30	S	0.024 2	0.616	6.56×10^{-3}	1.17	41.3	1.62	1 700	2.64	0.361	0.142	0.315	7.68×10^{-4}	0.567	0.106	0.004 3
36	S	0.026 7	0.679	7.83×10^{-3}	1.40	37.4	1.47	1 400	2.17	0.301	0.118	0.310	9.22×10^{-4}	0.629	0.113	0.005 0
45	S	0.029 9	0.758	9.73×10^{-3}	1.74	33.5	1.32	1 120	1.74	0.241	0.094 8	0.311	1.15×10^{-3}	0.705	0.121	0.006 2
54	D	0.033 8	0.857	1.22×10^{-2}	2.18	29.6	1.17	878	1.36	0.201	0.079 0	0.292	1.38×10^{-3}	0.800	0.161	0.006 9
63	D	0.036 2	0.920	1.42×10^{-2}	2.53	27.6	1.09	762	1.18	0.172	0.067 7	0.295	1.61×10^{-3}	0.859	0.167	0.005 8
72	D	0.038 5	0.978	1.61×10^{-2}	2.87	26.0	1.02	674	1.04	0.150	0.059 2	0.297	1.84×10^{-3}	0.914	0.174	0.006 4
81	D	0.040 7	1.033	1.80×10^{-2}	3.21	24.6	0.968	605	0.937	0.134	0.052 6	0.301	2.07×10^{-3}	0.965	0.179	0.007 1
90	D	0.043 0	1.093	1.99×10^{-2}	3.56	23.2	0.915	540	0.837	0.120	0.047 4	0.299	2.30×10^{-3}	1.02	0.185	0.008 0
100	D	0.045 2	1.148	2.20×10^{-2}	3.94	22.1	0.871	490	0.759	0.108	0.042 6	0.301	2.56×10^{-3}	1.07	0.191	0.008 8
108	D	0.046 8	1.190	2.37×10^{-2}	4.24	21.3	0.840	456	0.706	0.100	0.039 5	0.303	2.76×10^{-3}	1.11	0.195	0.009 3
135	D	0.052 0	1.322	2.94×10^{-2}	5.26	19.2	0.757	369	0.573	0.080 2	0.031 6	0.307	3.46×10^{-3}	1.24	0.209	0.011 3
162	D	0.056 7	1.441	3.51×10^{-2}	6.27	17.6	0.694	311	0.482	0.066 9	0.026 3	0.310	4.15×10^{-3}	1.35	0.221	0.012 9
189	D	0.061 0	1.550	4.08×10^{-2}	7.28	16.4	0.645	269	0.416	0.057 3	0.022 6	0.312	4.84×10^{-3}	1.45	0.233	0.014 5
216	D	0.065 5	1.664	4.65×10^{-2}	8.30	15.3	0.601	233	0.361	0.050 1	0.019 7	0.310	5.53×10^{-3}	1.56	0.245	0.016 1
243	D	0.069 3	1.761	5.21×10^{-2}	9.31	14.4	0.568	208	0.323	0.044 6	0.017 6	0.312	6.22×10^{-3}	1.65	0.255	0.017 5
270	D	0.072 9	1.852	5.78×10^{-2}	10.3	13.7	0.540	188	0.292	0.040 1	0.015 8	0.313	6.91×10^{-3}	1.74	0.264	0.018 7
297	D	0.076 3	1.938	6.34×10^{-2}	11.3	13.1	0.516	172	0.266	0.036 5	0.014 4	0.314	7.60×10^{-3}	1.82	0.273	0.020 0
324	D	0.079 6	2.021	6.90×10^{-2}	12.3	12.6	0.495	158	0.245	0.033 4	0.013 2	0.315	8.29×10^{-3}	1.90	0.282	0.021 1

See notes to Table A.4.1.

Appendix B

Calculation of the Core Factors of a Pot Core

Two core factors are used in the calculation of the effective magnetic dimensions of a magnetic circuit. They are introduced and defined in Section 4.2.1:

$$C_1 = \Sigma l/A, \quad C_2 = \Sigma l/A^2$$

where A is the cross-sectional area of an element, of length l , in the magnetic path.

The procedures for calculating these core factors have

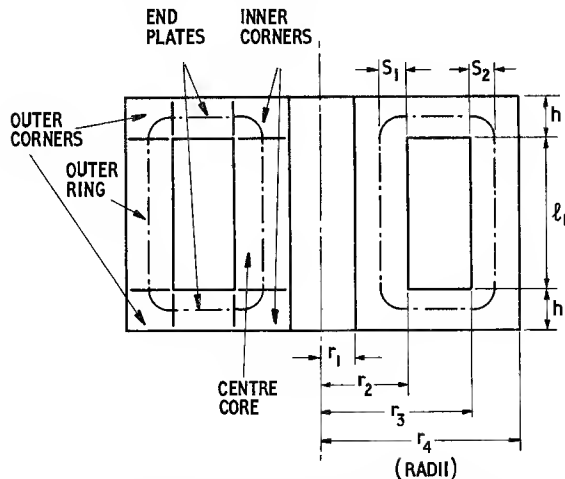


Fig. B.1. Cross-section of a simple pot core, defining symbols and indicating sections of the magnetic path

been laid down in IEC Publication 205 (1966). Thus the following procedure is in accordance with that recommendation.

Fig. B.1 represents the essential geometry of a pot core and defines the symbols used. The object is to derive expressions for $\Sigma l/A$ and $\Sigma l/A^2$ for each section of the magnetic path; the core factors C_1 and C_2 are then the sum of the respective expressions. The mean magnetic path is assumed to divide the main cross-sections into equal areas, thus the dimensions S_1 and S_2 are not identically equal to half the radial thickness of the inner and outer rings respectively.

The outer ring

Cross-sectional area of the ring = $\pi(r_4^2 - r_3^2)$

$$\therefore \Sigma l/A = \frac{l_1}{\pi(r_4^2 - r_3^2)}$$

$$\Sigma l/A^2 = \frac{l_1}{\pi^2(r_4^2 - r_3^2)^2}$$

The end plates

For an elementary ring at a radius x in the end plate

$$\frac{l}{A} = \frac{dx}{2\pi xh}$$

$$\therefore \Sigma l/A = \frac{1}{2\pi h} \int_{r_2}^{r_3} \frac{dx}{x} = \frac{1}{2\pi h} \log_e \frac{r_3}{r_2}$$

$$\text{and } \Sigma l/A^2 = \frac{1}{4\pi^2 h^2} \int_{r_2}^{r_3} \frac{dx}{x^2} = \frac{1}{4\pi^2 h^2} \left(\frac{1}{r_2} - \frac{1}{r_3} \right)$$

$$\therefore \text{ For both plates } \Sigma l/A = \frac{1}{\pi h} \log_e \frac{r_3}{r_2}$$

$$\Sigma l/A^2 = \frac{1}{2\pi^2 h^2} \left(\frac{r_3 - r_2}{r_2 r_3} \right)$$

The centre core

Cross-sectional area of the centre core = $\pi(r_2^2 - r_1^2)$

$$\therefore \Sigma l/A = \frac{l_1}{\pi(r_2^2 - r_1^2)}$$

$$\Sigma l/A^2 = \frac{l_1}{\pi^2(r_2^2 - r_1^2)^2}$$

The outer corners

The magnetic path divides the cross-sectional areas of the end plate and outer ring into equal parts. The magnetic path is taken as a quadrant having a mean radius and the cross-sectional area is taken as the mean of the two terminating areas.

First it is necessary to evaluate an expression for S_2 . By the equal-area definition

$$\pi(r_3 + S_2)^2 - \pi r_3^2 = \frac{\pi}{2}(r_4^2 - r_3^2)$$

$$\therefore S_2^2 + 2r_3 S_2 - \frac{1}{2}(r_4^2 - r_3^2) = 0$$

$$\therefore S_2 = -r_3 + \sqrt{\left[\frac{r_3^2 + r_4^2}{2} \right]}$$

$$\text{The length of one magnetic path} = \frac{\pi}{4}(S_2 + h/2)$$

The mean cross-sectional area

$$= \frac{1}{2}(2\pi r_3 h + \pi(r_4^2 - r_3^2))$$

$$= \frac{\pi}{2}(2r_3 h + r_4^2 - r_3^2)$$

Therefore, for the combination of both outer corners:

$$\Sigma l/A = \frac{(S_2 + h/2)}{2r_3 h + r_4^2 - r_3^2}$$

$$\Sigma l/A^2 = \frac{2(S_2 + h/2)}{\pi(2r_3 h + r_4^2 - r_3^2)^2}$$

The inner corners

The same procedure is followed. To find an expression for S_1 :

$$\pi r_2^2 - \pi(r_2 - S_1)^2 = \frac{\pi}{2}(r_2^2 - r_1^2)$$

$$\therefore S_1^2 - 2r_2 S_1 + \frac{1}{2}(r_2^2 - r_1^2) = 0$$

$$\therefore S_1 = r_2 - \sqrt{\left[\frac{r_1^2 + r_2^2}{2} \right]}$$

$$\text{The length of one magnetic path} = \frac{\pi}{4}(S_1 + h/2)$$

The mean cross-sectional area

$$= \frac{1}{2}(2\pi r_2 h + \pi(r_2^2 - r_1^2))$$

$$= \frac{\pi}{2}(2r_2 h + r_2^2 - r_1^2)$$

Therefore, for the combination of both inner corners

$$\Sigma l/A = \frac{(S_1 + h/2)}{(2r_2 h + r_2^2 - r_1^2)}$$

$$\Sigma l/A^2 = \frac{2(S_1 + h/2)}{\pi(2r_2 h + r_2^2 - r_1^2)^2}$$

These expressions ignore any slots that might be provided for winding connections, e.g. see Fig. 5.1*b*. IEC Publication 205 includes correction expressions to take such slots into account; in effect the cross-sectional areas of the outer ring, the outer corners and the end plates are reduced in proportion to the total angle of the slots subtended at the centre.

It must be appreciated that these calculations are standardized approximations for the purposes of comparing similar cores; the need for relatively simple expressions limits the accuracy.

Appendix C

Symbols

Following each symbol and definition there is, in general a reference to the equation (in brackets), the figure or section in which the symbol is introduced or first used.

a	a dimension	Fig. 4.2	$A_1 A_2$	particular cross-sectional areas of a core	(6.1)
a	a parameter used in the leading edge analysis of a pulse transformer	(8.3) (8.5)			
a	a parameter used in the trailing edge analysis of a pulse transformer	(8.13)	b	a dimension	Fig. 4.2
a	hysteresis loss coefficient due to Legg	(2.67)	b	conductor breadth	Fig. 11.10
a_{10}, a_{11} a_{02} }	Peterson coefficients	{ (2.37) (2.38)	b	a parameter used in the leading edge analysis of a pulse transformer	(8.3) (8.5)
A	area	(2.11)	b	a parameter used in the trailing edge analysis of a pulse transformer	(8.13)
A	a dimension	Fig. 11.3	b_a	breadth of core window	Fig. 11.1
A_a	window area of a core	Fig. 11.1	b_w	actual winding breadth	Fig. 11.1
A_c	exposed (cooling) area of core plus winding	Table 9.3	B	magnetic flux density	(2.2)
A_e	effective cross-sectional area of a core	(4.3)	B	a dimension	Fig. 11.3
A_e	effective loss of a network	Fig. 7.2	B_a, B_{3a}	flux densities at frequencies $f_a, 3f_a$ and $2f_a \pm f_b$ respectively	(2.76) (2.77)
A_g	cross-sectional area of air gap	(4.19)	$B_{2a \pm b}$		Table 2.2
A_i	insertion loss of a network	Fig. 7.2	B_{av}	flux density averaged over a length of core	Fig. 4.10
A_L	inductance factor	(5.8)	B_c	flux density at the centre of a cylindrical core	(4.62)
A_m	cross-sectional area of a magnetic core	(4.19)	B_e	effective flux density	(4.15)
A_N	effective area enclosed by an air cored coil	(4.75)	B_r	remanence	Fig. 2.1
A_r	return loss of a network	Fig. 7.2	B_{sat}	saturation flux density	Table 3.4
A_w	cross-sectional area of a winding	Fig. 11.1	$(B)_0$	flux density in core with zero air gap	(4.33)
			B_1, B_2	flux density at particular cross sections of a core	(6.1)

c	a dimension	Fig. 4.2	D_o	outer diameter of air cored coil	Fig. 11.12
c	residual loss coefficient due to Legg	(2.67)	e	instantaneous value of e.m.f.	(2.10)
c_o	the velocity of electro-magnetic waves in vacuo	(2.51)	e	eddy current loss coefficient due to Legg	(2.67)
c	pitch of turns in a winding layer	Fig. 11.15	E	e.m.f.	
c_h, c_e, c_r	magnetic loss coefficients due to Snoek	(2.69)	E	emissivity of a surface	(9.1)
C	capacitance	Fig. 5.12	E	electric field strength	(10.3)
C	$= C_1 + C_2$	(7.18)	E_a	source e.m.f.	Fig. 7.2
C_a, C_b, C_c	components of the self capacitance of a single section winding	Fig. 5.10	$E_{a, E_{3a}}$	e.m.f.'s at frequencies $f_a, 3f_a$ and $2f_a \pm f_b$ respectively	(2.78) Table 2.2
C'_a, C'_b, C'_c	components of the self capacitance of a multi-section winding	Fig. 5.10	$E_{2a \pm b}$	e.m.f. induced in a short coil placed centrally on a cylindrical core	Section 4.3.2 (10.12)
C_x	capacitance between two adjacent winding layers considered as a parallel plate capacitor	Table 11.3	E_n	noise e.m.f.	
C_i	capacitance between a winding layer and a screen (or other conducting surface) considered as a parallel plate capacitor	Table 11.3	E_{na}	distortion e.m.f. at frequency ηf_a	Fig. 4.6 (10.1)
C_m	shunt capacitance	(2.43)	E_s	signal e.m.f.	(3.5), Fig. 3.20
C_p	total capacitance required to resonate an inductance at a given frequency	(5.23)	E_ρ	activation energy	
C_{res}	total self capacitance of a winding or windings	(5.16)	f	frequency	(2.48)
C_s	core factor $= l_e/A_e$	(4.8)	f_a, f_b	frequencies	(2.79)
C_1	core factor, C_1 , for a pot core of unit radius	(5.4)	f_{res}	resonant frequency	(3.2), Fig. 3.11
$(C_1)_1$	core factor $= l_e/A_e^2$	(4.10)	Δf	bandwidth at 3 dB points	(10.12)
C_2	total capacitance appearing across the primary winding	Fig. 7.3	f_1, f_2	frequency of the lower and upper ends respectively of a transformer pass band	Fig. 7.1
C_1	total capacitance appearing across the secondary winding	Fig. 7.3	F	eddy current loss coefficient due to Jordan	(2.62)
d	dimension	(2.48)	F	a_{11}/a_{02}	Table 2.2
d	diameter	Fig. 4.2	F	skin effect factor	(11.14)
d	diameter of bare conductor	Fig. 1.7	F	a function	(7.46) (7.50)
d_{hor}	horizontal dimension of a body subject to convection	(9.3)	F_a	overall copper factor	(11.5)
d_i	inner diameter	(7.54)	F_A	averaging factor	Fig. 4.11(b)
d_o	outer diameter	Fig. 7.15	F_b	core hysteresis factor	(4.41)
d_o	diameter of conductor over the insulation	(11.1)	F_K	eddy current loss coefficient due to Jordan	Section 2.2.6. (11.27)
d_{vert}	vertical dimension of a body subject to convection	(9.3)	F_l	layer copper factor	(10.14)
D	droop of the top of a pulse, percent	(8.12)	F_n	noise factor	(11.6)
D	disaccommodation	(2.27)	F_p	packing factor	
D_i	inner diameter of air cored coil	Fig. 11.13	F_R	factor by which the a.c. resistance of a transformer winding exceeds the d.c. value	Fig. 11.11
			F_w	winding copper factor	(11.2)
			F_1	particular value of function F	(7.47) (7.51)
			G	conductance	(2.55)
			G	gain	(10.17)
			G_h	conductance due to hysteresis loss	(4.52)
			G_r	factor expressing the screening effect of eddy currents in a round conductor	(11.23)
			G_s	conductance expressing the loss in the self capacitance of a winding	(5.22)

h	thickness of a toroidal core	Fig. 4.1	K	constant	(11.28)
h	dimension	Fig. 4.2	K_1, K_2	constants	(9.15)
h	effective conductor height	Fig. 11.10			
h	hysteresis loss coefficient due to Jordan	(2.62)	l	length	(2.1)
h	hysteresis loss coefficient due to Jordan	(2.65)	l	length of magnetic shunt in pot core adjuster	Fig. 5.3
h_a	height of core window	Fig. 11.1	l_c	length of a coil	Fig. 4.11(a)
h_e	effective height of an antenna	(10.4)	l_e	effective path length of a magnetic circuit	(4.3)
h_K	hysteresis loss coefficient due to Jordan	(2.66)	l_g	path length of an air gap	(4.19)
h_w	actual height of a winding perpendicular to layers	Fig. 11.1	L_l	total leakage inductance	{ Fig. 7.3 Fig. 11.18
$h\Delta$	distance separating primary and secondary windings	Fig. 11.17	l_m	path length in a magnetic core	(4.19)
h_1, h_2	height of primary and secondary windings respectively	Fig. 11.17	l_w	mean turn length of a winding	(5.2)
			l_1, l_2	path lengths of parts of a magnetic core	(6.2)
H	magnetic field strength	(2.1)	L	inductance	(2.14)
H_a	field strength at the fundamental frequency	(2.76)	L_a	the air inductance of a coil	(4.66)
H_c	coercivity	(4.34)	L_{l1}	leakage inductance associated with the primary winding	Fig. 7.3
H_c	field strength at centre of rod	Section 4.3.1.	L_{l2}	leakage inductance associated with the secondary winding	Fig. 7.3
H_D	demagnetizing field strength	(4.61)		inductance/ μ	(2.14)
H_i	internal field strength	(2.3)	L_o	parallel inductance	(2.17)
H_2	field strength in a particular part of a core	(6.4)	L_p	series inductance	(2.15)
			L_s		
i	instantaneous current	(8.23)	m	dimensional ratio of a cylindrical or ellipsoidal core	Fig. 4.8
I	current				
I_{na}	distortion current at frequency nf_a	(4.58)	m	fractional increase of conductor resistivity above the value at 20°C	(9.17)
I_s	signal current	(10.9)			
I_1	current in winding having N_1 turns	(7.4)	m	modulation factor	(10.22)
I_2	current in winding having N_2 turns	(7.4)	M	magnetization	(2.3)
j	$\sqrt{-1}$		M	number of section interfaces in a transformer	Fig. 11.19
J	magnetic polarization (intrinsic flux density)	(2.5)	M_c	magnetization at centre of cylindrical core	(4.61)
J_c	magnetic polarization at the centre of a cylindrical core	(4.61)	M_{sat}	saturation magnetization	(3.2), Fig. 3.11
k	constant	Table 2.2	n	Steinmetz exponent	(3.4), Fig. 3.12
k	constant	(11.29)	n	number of insulated strands in a bunched conductor	(5.21)
k	Boltzmann's constant	(3.5), Fig. 3.20, (10.12)			
k	coupling factor	(7.27)			
k_e, k_E	proximity effect constants	(11.26)	N	number of turns	(2.14)
k_1, k_2, k_3	magnetic loss coefficients	(2.61)	N	demagnetizing factor	(4.61)
k_1, k_2, k_3	proportions of a pot core	Fig. 5.1.	N_a	normalized number of turns	(7.48)
k_1	parameter used in power transformer design	(9.19)	N_i	number of turns in a winding layer	(11.27)
k_2	parameter used in power transformer design	(9.27)	N_1	number of turns on a primary winding	(2.1)
k_3	parameter used in power transformer design	Table 9.3	N_2	number of turns on a secondary winding	(2.11)

p	$2\pi f$	(2.75)	$(R_{dc}/L)_{\frac{1}{2}}$	ratio of d.c. resistance to inductance for a winding half filling the available winding height	(7.36)
p	porosity	(3.1)			
p	number of layers in a winding	(11.7)			
P	power		R_F	eddy current series loss resistance	(2.49)
P_a	applied power	Fig. 7.2			
P_{av}	average power	(8.1)	R_h	series resistance representing hysteresis loss	(2.34)
P_b	power in load	Fig. 7.2			
P_{cond}	rate of heat transfer due to conduction	(9.7)	R_p	parallel resistance representing magnetic and/or circuit losses	(2.17), Fig. 2.2
P_{conv}	rate of heat transfer due to convection	(9.2)	$(R_p)_1$	shunt resistance representing normalized core loss	(9.26)
P_F	eddy current power loss (volume) density	(2.48)	R_{pe}	shunt resistance representing proximity effect in a winding	Section 11.4.3
P_h	hysteresis power loss (volume) density	(2.33)			
P_i	input power	(9.16)	R_s	series resistance representing magnetic and/or circuit losses	(2.15), Fig. 2.2
P_m	power loss (volume) density in a magnetic material due to any cause	(2.56)	R_s	total winding resistance of a transformer referred to the primary winding	(7.11)
P_n	noise power	(10.16)			
P_{no}	noise output power	(10.19)			
P_o	output power	(9.16)	R_{sc}	increase in conductor resistance due to skin effect	(11.14)
P_p	power during pulse	(8.1)			
P_{pe}	power loss due to proximity effect in a winding	(11.21)	R_T	thermal resistance	(9.8)
P_r	reflected power	Fig. 7.2	R_o	nominal resistance of a half section filter	(7.23)
P_{rad}	rate of heat transfer due to radiation	(9.1)	R_1	resistance of primary winding	Fig. 7.3
P_s	signal power	(10.11)	R_2	resistance of secondary winding	Fig. 7.3
P_{so}	signal output power	(10.20)			
P_{tot}	power loss in core plus winding	(9.22)	s	length along a path	(4.1)
P_w	power loss in windings	(9.13)	S	pitch of adjacent winding layers	Fig. 11.15
q	number of side-by-side sections in a winding	Table 11.3	S_e	effective thickness of dielectric	(11.32)
q_2	C.C.I.F. hysteresis factor	(2.70)	S_t	time factor associated with trailing edge of a pulse	(8.13)
$q_{2-24 \times 100}$	hysteresis coefficient based on q_2	(2.72)	$(S_t)_0$	value of S_t corresponding to the fall time to zero (t_f)	Fig. 8.16
Q	quality (Q) factor	(5.17)	S_r	time factor associated with leading edge of a pulse	(8.3)
Q_L	Q-factor of a loaded circuit	(10.7)	S_1, S_2	functions of wire diameter dimensions relating to the magnetic path in pot core	Fig. B.1
r, r_1, r_2	radius and particular radii	Fig. 4.1			
r	transformation ratio	(7.3)	S_1, S_2		
R	resistance		t	time	
R	$= R_a R'_b / (R_a + R'_b)$	(7.12)	t	residual loss coefficient due to Jordan	(2.62)
R_a	source resistance	Fig. 7.2	t	thickness of layer insulation	(11.7)
R_{ac}	d.c. resistance of a conductor plus the resistance due to skin effect	(11.14)	t_d	pulse duration	Fig. 8.1
R_{AC}	d.c. resistance of a winding plus the resistance due to general eddy current phenomena	(9.35)	t_f	pulse fall time	Fig. 8.1
R_b	load resistance	Fig. 7.2	t_K	residual loss coefficient due to Jordan	(2.66)
R_c	resistance per unit length of conductor	(11.9)	t_P	time between leading edges of consecutive pulses	Fig. 8.1
R_{dc}	d.c. resistance of a winding	(11.9)	t_r	pulse rise time	Fig. 8.1

t_1	pulse rise time of source	(8.2)	Z	impedance	(2.15)
t_2	pulse rise time of oscilloscope	(8.2)	Z_a	source impedance	Fig. 7.2,
			Z_A	source impedance	Fig. 4.6
T	absolute temperature	(3.5), Fig. 3.20	Z_b	load impedance	Fig. 7.2
T_s	absolute temperature of a surface	(9.1)	Z_B	load impedance	Fig. 4.6
T_o	absolute temperature of objects surrounding a radiating surface	(9.1)	Z_i	input impedance	Fig. 7.7
			Z_m	impedance due to the magnetic properties of a core	Fig. 4.6
U	voltage		α	coefficient of linear expansion	Section 1.4.2
U_a	voltage at fundamental frequency f_a	Fig. 4.6	α	ratio of boundary thickness to crystallite thickness	Fig. 2.5
U_b	voltage across load	Fig. 7.2	α	angle	(4.39)
U_{AO}, U_{AD} U_{BO}, U_{BD}	voltage potentials at each end of winding layers A and B respectively	Fig. 11.13	α	turns factor	(5.6)
U_D	voltage difference $U_{BD}-U_{AD}$	(11.30)	β	eddy current shape factor	(2.48)
U_n	noise voltage	(10.13)	γ	gyromagnetic ratio	(3.2), Fig. 3.11
U_{na}	distortion voltage at frequency nf_a	Fig. 4.6	δ_{ac}	loss angle due to the d.c. resistance plus skin effect in a conductor	Fig. 5.11(a)
U_p	voltage applied across a winding	(11.30)	δ_{AC}	loss angle due to the total (a.c.) resistance in a conductor	Section 10.3.3
U_s	signal voltage	(10.9)	δ_{cp}	loss angle of an inductor due to dielectric loss in its self capacitance	(5.23)
U_o	voltage difference $U_{BO}-U_{AO}$	(11.30)	δ_{cs}	loss angle due to the self capacitance of a series resonated inductance	(5.26)
v	velocity of propagation of e.m. waves in material	(2.50)	δ_d	dielectric loss angle = ϵ_p''/ϵ_p'	(2.45)
v	air velocity	(9.5)	δ_{dc}	loss angle due to d.c. winding resistance	(5.18)
V	volume		δ_F	loss angle due to eddy currents in core	(2.49)
V_e	effective (or hysteresis) volume of a core	(4.6)	δ_h	hysteresis loss angle	(2.35)
V_T	overall volume of a pot core	(5.5)	δ_L	loss angle of an inductor in the absence of self capacitance	(5.26)
w_h	hysteresis energy loss (volume) density	(2.33)	δ_m	loss angle due to any magnetic loss	(2.16)
W_h	hysteresis energy loss	(4.14)	δ_{mc}	loss angle of a rod antenna due to magnetic coupling to adjacent conductive parts	Section 10.3.3
x	a length or distance variable		δ_{pe}	loss angle due to proximity effect	(11.26)
x	a parameter used in the leading edge analysis of a pulse transformer	(8.8)	δ_r	residual loss angle	(2.53)
x	voltage regulation	(9.16)	δ_{rad}	loss angle due to antenna radiation	Section 10.3.3
Σx	transformer winding dimension	Fig. 11.18	S_{r+F}	loss angle due to residual plus eddy current loss in core	Table 5.5
Σx_A	transformer winding dimension	Fig. 11.18	δ_{se}	loss angle due to skin effect	(11.19)
X	transformer winding dimension	Fig. 11.18	δ_{tot}	total loss angle of an inductor	(5.17)
Y	admittance	(2.17)			
Y	transformer winding dimension	Fig. 11.18			
z	variable	Fig. 7.5			

Δ	penetration depth	(2.52), (11.15)	ν	Rayleigh hysteresis coefficient	(2.30)
ε	permittivity	(2.43)	ν	viscosity	(9.6)
$\varepsilon'_p, \varepsilon''_p$	real and imaginary components respectively of the complex permittivity expressed in parallel terms	(2.44)	ρ	resistivity	(2.43)
ε_0	electric constant = $8.854 \times 10^{-12} \text{ F.m}^{-1}$	(2.43)	ρ	nominal mismatch factor	(7.24)
$\varepsilon_1, \varepsilon_2$	real components of the permittivity of crystallite and boundary respectively	Fig. 2.5	ρ_c	resistivity of winding conductor	(11.8)
η	load-source mismatch factor	Fig. 8.2	ρ_s	sintered (mass) density	(3.1)
η_B	I.E.C. hysteresis loss coefficient of a material	(2.74)	ρ_x	X-ray (mass) density	(3.1)
η_i	I.E.C. hysteresis loss factor of a core	(4.43)	ρ_1, ρ_2	resistivity of crystallite and boundary respectively	Fig. 2.5
θ	temperature in $^{\circ}\text{C}$		ρ_{∞}	resistivity of polycrystalline ferrite extrapolated to $T = \infty$	(3.5), Fig. 3.20
θ_{cs}	temperature difference between the centre and the surface of a magnetic core	(9.9)	σ_r	damping factor associated with leading edge of a pulse	(8.3)
θ_1, θ_2	particular temperatures	(2.21)	σ_f	damping factor associated with trailing edge of a pulse	(8.13)
κ	susceptibility	(2.7)	τ	relaxation time = $1/\omega_r$	(2.47)
λ	wavelength	(2.50)	ϕ	phase shift	(7.16)
λ	thermal conductivity	(9.7)	ϕ	magnetic flux	(2.10)
μ	permeability	(2.8)	χ	a parameter used in the trailing edge analysis of a pulse transformer	(8.13)
μ_a	amplitude permeability	(2.30)			
μ_c	conductor permeability	(11.15)	ψ	figure of merit for a transformer core, $\propto R_{dc}/L$ when this ratio is made independent of the volume of the smallest rectangular box that will just enclose the core plus winding	Table 9.3
μ_{coil}	ratio of inductance of a coil with and without a core	(4.66)			
μ_e	effective permeability	(4.23)	ω	$2\pi \times$ frequency	
μ_i	initial permeability	(2.30)	ω_c	$2\pi \times$ cut off frequency	(7.24)
μ'_p, μ''_p	real and imaginary components respectively of the complex permeability expressed in parallel terms	(2.17)	ω_r	$2\pi \times$ relaxation frequency	(2.47)
μ_p	pulse permeability	(8.30)	ω_1	$2\pi \times$ frequency at lower end of transformer pass band	(8.19)
μ_r	reversible permeability	Section 2.1			
μ_{rod}	rod permeability	(4.64)	\hat{x}	maximum value of x	
μ'_s, μ''_s	real and imaginary components respectively of the complex permeability expressed in series terms	(2.15)	\check{x}	minimum value of x	
μ_{Δ}	incremental permeability	{ Section 2.1 Fig. 3.6	\bar{x}	average value of x	
μ_0	magnetic constant = $4\pi 10^{-7}$	(2.2)	Δx	change of x	
μ_1, μ_2	permeability at particular places, temperatures or times	(2.21)	δx	small change of x	
			x'	real part of x	
			x''	imaginary part of x	
			x'	value of x referred to the other side of a transformer	

Index

- Absolute permeability 19
- a.c. winding resistance. *See* Winding resistance
- Adhesives, choice of 14–15
- Admittance, in terms of complex permeability 21–22, 109
- Air-cored coil 348–50
- Air gap, effect of 174–82, 196, 205, 253, 258, 357
 - residual reluctance 258
- Amplitude permeability 20, 36, 65
- Anisotropy 4, 5
- Antennas 327–36
 - bandwidth and impedance requirements 330–31
 - circuit theory 327–32
 - design aspects 332–35
 - design example 331–32
 - effective height 328, 332–33
 - equivalent circuits 328, 330
 - inductance 335
 - noise power 329–30
 - properties of ferrite rods 333
 - Q*-factor 328–35
 - signal strength 328–29
 - signal-to-noise ratio 330, 331
 - temperature coefficient 335
 - tubular cores 333
 - tuning, high frequency transductor 230
- Apparent permeability 189
- Applied power 238, 240
- Atmosphere control in kilns 12
- Attenuation in transformers 238–40, 249, 290
- Autotransformer windings, leakage inductance 357
- Backswing 278
- Bandwidth, antennas 330–31
 - pulse distortion in relation to 289–90
- B-H* curve 19, 228, 292
- B-H* loop 20, 24, 25, 47–53, 291, 292, 294
 - minor 54–60
 - non-linearity 36
 - obtained by special heat treatment 47
 - shearing of 176–77
 - transition from parabolic to elliptical 36
- B-H* relation 24, 25
- Binders, use of in ferrite manufacture 8
- Bloch walls 4
- Boltzmann's constant 157, 329
- Bonding. *See* Cementing of ferrite cores
- Bunched conductors. *See* Windings
- Capacitance, distributed, in windings 350, 351
 - see also* Self capacitance; Stray capacitance
- Capacitor, polystyrene 202
- silvered mica 202
- Cementing of ferrite cores 14–15
- Chemical co-precipitation 6
- Cobalt, effect of addition to NiZn ferrite 53
- Code numbers, ferrite, index to 40–41
- Coercivity 20
 - typical values of 44, 45
- Coil, air-cored, inductance of 348–50
- Colour television, raster correction in 230–32
- Combined loss tangent 214–15
- Complex permeability. *See* Permeability
- Conduction, heat transfer by 302–03, 305
- Conductor, arrangements in winding 338–39
 - bunched. *See* Windings and Wire
 - resistivity 340
 - see also* Wire
- Convection, heat transfer by 300–02
- Cooling in power transformers 298–305, 319, 321
- Copper factor 195, 308–09, 319, 320, 338
 - layer 322–26, 347, 348
- Copper loss conductance 179
- Copper wires, bare, properties of (table) 360, 364, 369
 - diameters, functions of (table) 363, 367, 372
 - fine enamelled, properties of (table) 361, 365, 370
 - medium enamelled, properties of (table) 362, 366, 371

- Core dimensions, effective 172-74, 377-78
- Core factor 173, 195, 196, 265, 266, 377-78
- Core losses 178, 253, 260, 294, 306-12, 316, 318
high frequency transductor 228
inductors 213-14
- Coupling factor 250
- Cracking of T.V. deflection yokes 13
- Crystal anisotropy 4
- Crystal structure 2, 3
- Curie point, and initial permeability 91
and magnetic saturation 61
typical values of 44, 45
- Cylindrical cores 183-91
effective loss tangent of 191
energized by winding, flux density distribution along 189
immersed in uniform magnetic field, flux density distribution along 186-88
inductance of windings on 189
magnetic losses in 189
permeability relations 185-86
temperature coefficient of inductance 191
- Damping factor 271, 274, 278
- d.c. winding resistance. *See* under Windings
- Demagnetizing factor 183, 184, 186
- Demagnetizing field 183
- Diamond machining 14
- Dielectric loss in a ferrite core 26, 28-29, 321
in self capacitance 212-13, 217, 220
see also Eddy current core loss
- Dielectric loss factor 26
- Dielectric properties of ferrites 26-29, 157-65
- Differential permeability 20
- Dilution ratio 176, 203-04
- Dimensional resonance 28-29, 180-81, 251, 253, 256, 264
- Disaccommodation 11, 23, 105-07, 203
- Disaccommodation factor 23, 105-06
typical values of 44
- Distortion, magnetic 33-36, 143-47, 181-82, 221
pulse. *See* Pulse distortions
- Domain boundaries (walls) 4-5
- Drilling, ultrasonic 14
- Droop, in transmission characteristic of a wide band transformer 237, 240, 242, 244, 247, 262, 264
in a pulse waveform 270, 275-77, 286, 288, 290
- Dry pressing 8-9
- Eddy current core loss 27-29, 32, 180-01, 253, 294
- Eddy current loss coefficients 30-3
- Eddy current loss in conductors and windings 209-12, 322-26, 341-48
- Eddy current loss tangent 27, 30-2
- Effective dimensions, (area, length and volume) of a core 172-74
- Effective loss of a transformer 238, 240, 244
- Effective loss tangent of cylinder 190-01
- Effective permeability 30, 175-76, 196-98, 250-01
- Electric constant 26
- Electric field strength 328
- Electric fields, intense, effect on transformer cores 321
- Electrolytic co-precipitation 6
- Electromagnetic wave propagation in ferrites 28
- e.m.f., averaging factor 187-89
equation 19, 174, 190, 305, 327-28
induced 19, 327-28
- Emissivities of various surfaces 299
- Encapsulation 15-16, 235
- Extrusion 9-10
- Ferrimagnetic oxides. *See* Ferrites
- Ferrimagnetic resonance 108, 122, 141, 148
- Ferrimagnetism, Ferromagnetism 4
- Ferrite antennas. *See* Antennas
- Ferrites, magnetically hard 2
magnetically soft 1
magnetic and electrical properties of 44-168
mechanical properties of 42-3
thermal properties of 43
magnetism in 2-5
manufacture of. *See* Manufacture
microwave 2
naturally occurring 1
nature of 1
permanent magnet 2
rectangular loop 2
spinel 2-3
see also Manganese zinc ferrites; Nickel zinc ferrites
- Filter techniques, wind band transformers, higher frequency region 242-47
lower frequency region 248
- Finishing, processes in core manufacture 12-13
processes available to user 13-16
- Flux density, amplitude of third harmonic and intermodulation products 33-34
B-H loops 47-53
minor 54-60
distribution along cylinder energized by winding 188-89
immersed in uniform magnetic field 186-87
effective 174
expressions for 18, 19, 24, 25, 174, 305
high, power loss as function of frequency at 148-56
hysteresis loss factor as function of 138-40
- Flux density *continued*
in antennas 328, 334
in cylindrical cores 182-89
in power transformer design 306, 308-12
intrinsic 19
minor *B-H* loops 54
permeability, as function of high amplitude 65-71
as function of low amplitude 72-73
Peterson's expression for 25
Rayleigh's expression for 24
shunt core loss resistance as function of 311
see also Saturation flux density
- Flux distribution. *See* Flux density, distribution
- Flux linkage per unit current 21
- Forming 8-10
miscellaneous methods 10
see also Extrusion; Pressing
- Frequency, complex permeability as function of 108-21
hysteresis loss factor as function of 141
magnetic distortion as function of 143-47
permittivity as function of 160-63
power loss as function of, at high flux densities 148-56
range of ferrites 108
residual loss tangent as function of 122-31
with superimposed steady field as parameter 135-37
resistivity as function of 160-63
resonant, dependence on temperature, in antennas 335
in inductors 201-03
- Fringing flux, at air gap 175-76
at around cylindrical core 183
- Grain growth 10
- Granulation 8
- Green state 9
- Grinding 12, 14
- Hanna curves 84-90, 253
- Hardness of ferrites 46
- Heat sink 305
- Heat transfer, by conduction 302-03
by convection 300-02
by radiation 299-300
in power transformers 298-305, 309, 312, 320, 321
- High-amplitude properties, expression of 36
- High frequency transducers 225-36
antenna tuning 230
applications 225, 230-33
closed loop control circuit 234-35
core loss 228
design 233-35
general mode of operation 226-30
operating techniques 233-35

Index

- High frequency transducers *continued*
 proton synchrotron field control 230
 raster correction in colour television 230–32
 temperature dependence 228
 Hot pressing 10
 Hysteresis 5, 23–25
 Hysteresis effects, in transducers 228
 in inductors 194
 Hysteresis energy loss (volume) density 24, 25
 Hysteresis loop 5, 20, 24
see also B-H loop
 Hysteresis loss 23–25, 30–33
 in inductors 213–14
 in pulse transformers 294
 in wide band transformers 254
 Hysteresis (loss) coefficient 23–25, 30–33, 214–15
 IEC 32–33
 Jordan 30–32
 Legg 31–32
 Peterson 25, 32
 Rayleigh 23–24, 32
 Snoek 31–33
 summary of expressions 32
 typical values of 44, 45
 Hysteresis (loss) factor 178, 213–14
 as function of flux density 138–40
 as function of frequency 141
 as function of temperature 142
 Hysteresis loss resistance 24–25, 31, 33, 178
 Hysteresis loss tangent 24–25, 178–79, 214
 summary of expressions for 32
 Hysteresis properties of gapped cores 178
- Impact strength 42
 Impedance, in terms of complex permeability 21–22
 conversion of series to parallel 21–22
 Incremental permeability. *See* Permeability
 Inductance 21, 174–75
 low 201
 of a winding having a cylindrical core 189–90
 of air-cored coil 348–50
 of antennas 35
 of inductors 193–94, 196–98
 adjustment of 198–201
 constancy of 201–06
 of pulse transformers 290–91
 of wide band transformers 265–66
 ratio of d.c. winding resistance to 195–96, 253–54
 temperature coefficient of 202, 234, 335
 variability. *See* Inductors
 Inductance factor 198, 251
 Inductance ratio 189
 Induction law 19
 Inductors 193–224
 adjustment of 198–201
- Inductors *continued*
 applications 193
 basic requirements 193
 combined loss tangents 214–15
 core form 195–96
 core losses 213–14
 future developments 224
 hysteresis effects in 194
 intermodulation 221, 224
 loss due to d.c. winding resistance 208–09
 loss due to eddy currents in winding conductors 209–12
 loss due to stray capacitance 212–13
 magnetic coupling between 194
 performance requirements 193
 Q-factor 194, 195, 208–21
 self capacitance 206–08
 summary of loss expressions 214
 temperature coefficient of 194, 202
 variability 201–06
 due to ferrite 202–04
 due to non-ferrite parts 204–05
 overall 205–06
 waveform distortion 221, 224
 Initial permeability. *See* Permeability
 Insertion loss 238–48, 261–64
 Inspection 13
 Instability factor 23, 176
 Intermodulation 33–36, 181–82, 221, 224
 as function of frequency 143–47
 Internal magnetic field 19
 Intrinsic flux density 19
 Iso-static pressing 10
- Jordan loss expression 30–32
- Kilns 11–12
- LC product 194, 200–03
 Leakage flux 175, 183, 354–55
 Leakage inductance, calculation of 354–57
 in power transformers 308–09, 318, 320
 in pulse transformers 271, 274–75, 286, 287, 289, 294, 295
 in wide band transformers 240, 242–44, 247, 250, 255, 260, 264, 267
 Legg hysteresis coefficient 31, 33, 138, 178–80, 182, 214
 Legg loss expression 31–33
 Loss angle 21–22
 Loss coefficients 30, 33
 Loss expressions 29–33
 discussion on 33
 Loss factor 29–33, 179
see also Residual loss
 Loss resistance, series 21, 178
 Loss tangent 21–22, 24–33, 179
 due to eddy currents in winding 344–45
 in antennas 333–35
- Loss tangent *continued*
 in inductors 208–15
 in wide band transformers 261
 Low-amplitude properties 21–36
- Machining 13–14
 Magnetic area moment 19
 Magnetic circuit theory 171–92
 Magnetic constant 18
 Magnetic core loss density 148–57
 Magnetic cores, closed 172–82
 open 182–91
 Magnetic coupling, inductors 194
 Magnetic distortion 33–36, 181–82, 221, 224
 as a function of frequency 143–47
 Magnetic field, internal 19
 Magnetic field strength 18, 183
 incremental permeability as function of 74–83
 Magnetic hysteresis 5, 23–25
 Magnetic loss 21, 148–56, 177–81, 189–91
 at low field strength, summary of expressions 33
see also Eddy current loss, Hysteresis loss and Residual loss
 Magnetic moment 18
 Magnetic oxides 1
 Magnetic polarization 19
 Magnetic properties
 expression of 18–36
 graphical data 46–168
 typical values of, for ferrites 44–45
 Magnetic shunt adjustment 199–201
 Magnetism in ferrites 2–5
 Magnetite 1
 Magnetization 18–21
 of ferrites 4–5
 saturation 108
 Magnetization curves 5, 20, 54, 176–77
 Magnetizing current 306, 318
 Magnetomotive force 347, 354–56
 Magnetostriction in transducers 235
 static, as function of field strength 166
 Manganese zinc ferrites 1
 applications 2
 classification by application 39
 dimensional resonance 28–29, 180
 graphical data 46–168
 typical values of specification parameters 46
 Manufacture 5–13
 flow diagram 6
 processes 5–6
 Manufacturer reference and code numbers 40–41
 Mating surfaces 13
 Mechanical properties 42–43
 Mechanical resonance 235
 Microwave devices, ferrites 2
 Mid-series impedance 244
 Mid-shunt impedance 244
 Minor B-H loops 54–60
 Mismatch 238–39, 274

- Mismatch factor 244, 247, 274, 286
 Mixing of raw materials 7
- Nickel zinc ferrites 1
 applications 2
 classification by application 39
 cobalt additions 53
 dimensional resonance 180
 graphical data 46–186
 typical values of specification parameters 46
- Noise factor 329–32
 Noise power 329–30
 Noise voltage 329
- Overshoot in pulse transformers 270–75
 Oxygen, in sintering kiln 10–11
- Packing factor 339
 Penetration depth, in ferrite 29
 in conductors 322–26, 341–48
 Permanent magnetic ferrites 2
 Permeability, absolute 19
 amplitude 20
 apparent 189
 as function of high amplitude flux density 65–71
 as function of low amplitude flux density 72–73
 complex 21–22
 complex initial, as function of frequency 108–21
see also Permeability, initial
 corresponding to slope of minor loop 54
 differential 20
 effective 30, 175–76, 196–200, 250–51
 incremental 20, 54, 225–26, 228
 as function of steady field strength 74–83
 as function of temperature with steady field strength as parameter 101–04
 initial, as function of stress 167–68
 as function of temperature 91–100
 Curie point and 91
 typical values of 44, 45
see also Permeability, complex
 initial
 of free space 18
 pulse 290–94
 relative 19
 reversible 20
 rod 186, 328
 temperature dependence of 22–23, 91–100, 202–03
 time-change of. *See* Disaccommodation
- Permittivity 25–27
 as function of frequency 160–63
 as function of temperature at high frequency 164–65
 of free space 26
- Permittivity *continued*
 parallel complex 26
 Peterson coefficient 25, 32, 72, 138
 Peterson loss expression, relations 25, 172
 Phase angle 21
 Phase shift 240, 242, 244, 247–48
 Polystyrene capacitor, temperature coefficient of 202
 Porosity 43
 typical values 43
 Pot cores 195–201, 254–55, 258
 core factor calculation 377–78
 geometry of 377
 proportions for 195–96
 standard ranges 195–97
 Power dissipation in transformer windings 340
 Power loss, due to eddy currents in windings 341–48
 due to proximity effect 344–46
 due to skin effect 341–44
 per unit volume 33
 Power loss (volume) density 29, 30, 181
 as function of frequency at high flux densities 148–56
 typical values of 44
 Power transformers 297–326
 applications 297
 cooling 298–305, 319, 321
 core data 314–15
 electrical design considerations 305–08
 heat transfer and temperature rise 298–305, 316, 320, 321
 calculation example 303–05
 conduction 302–03
 convection 300–02
 radiation 299–300
 higher frequency 319–26
 core selection 319–22
 winding design 320, 322–26
 low frequency 308–18
 core loss limited 310–12
 core performance 312–17
 design example 317–18
 regulation limited 308–09
 saturation limited 309
 minimum total power loss 307
 Pre-sintering 7
 Pressing, dry 8–9
 hot 10
 iso-static 10
 slurry 10
 Proton synchrotron field control 230
 Proximity effect 209–12, 344–46
 Proximity effect constant 210, 346
 Proximity effect factor 342, 345
 Proximity effect loss tangent 210–12, 345–46
 Pulse permeability 290–93
 Pulse transformers 269–96
 applications 269
 core materials 269
 core requirements 290–94
 design procedure 284–89
 droop 275
- Pulse transformers *continued*
 leading edge of pulse 271–75
 practical considerations 294–95
 pulse distortions 270
 in relation to bandwidth 289–90
 in terms of equivalent circuit elements 271–84
 pulse droop. *See* Droop
 pulse permeability 290–93
 rectangular pulses, ideal and distorted 270
 specification 270, 285
 step-down 271
 step-up 271
 terms and definitions 270
 top of pulse 275
 trailing edge of pulse 278–84
- Q-chart 216, 217, 220
 Q-contours 216
 Q-curves 215–16
 Q-factors
 antennas 333–35
 in H.F. transformer design 262
 inductors 194, 208–21
 transducers 228–31
- Radiation, heat transfer by 299–300
 Radiation resistance 328
 Raster correction in colour television 230, 232
 Raw materials 6–7
 Rayleigh coefficient 23–24, 32, 72, 138
 Rayleigh loop 24
 Rayleigh region 24–25
 Rayleigh relations 23–25
 Rectangular loop ferrites 2
 Reflection coefficient 239
 Regulation limited transformers. *See* Power transformers, low frequency
 Relative permeability 19
 Relaxation frequency of composite dielectric 27
 Reluctance 173–74
 Remanence, typical values of 44, 45
 Residual loss 29, 30–32, 181, 190
 summary of expressions 32
 Residual loss coefficient 30–32
 Residual loss factor 181, 213
 as function of frequency 122–31
 as function of temperature 132–34
 typical values of 44, 45
 Residual loss tangent 29
 as function of frequency with superimposed steady field as parameter 135–37
 of gapped core 181
 Resistivity 25–27
 as function of frequency 160–63
 as function of temperature 157–59
 at high frequency 164–65
 typical values of 44, 45
 Resonance, dimensional 28–29, 180–81, 251, 253
 ferrimagnetic 108, 122, 141, 148, 181
 mechanical 235

Index

- Resonant dimension 29
 Return loss 239, 241–46, 262–63
 Reversible permeability 20
 Rise time 271, 274–75, 286
 Rod permeability 186, 328
 Rods. *See* Cylindrical cores

 Saturation flux density
 as function of temperature 61–64
 typical values of 44, 45
 Saturation limited transformers. *See*
 Power transformers, low frequency
 Saturation magnetization 108
 Screen 234, 267, 295, 321–22, 351–53
 Self capacitance
 dielectric loss in 212–13, 217, 220
 of windings 206–08, 257, 260, 350–54
 analysis method 350–51
 expressions for 352–53
 relation between geometry and 352–53
 Series hysteresis resistance 24–25, 31, 33, 178
 Series loss resistance 178
 Shearing of B – H loop 176–77
 Shrinkage 10
 Shunt capacitance 242–47, 271, 275, 278, 286, 287–89
 Shunt core loss resistance 22, 241–42, 261–62, 310
 as function of flux density 311
 Shunt impedance in H.F. transformer design 262
 Shunt inductance 250–03, 259, 261, 275, 278, 286, 287, 290–91, 294, 306–08, 318
 Signal power 329
 Signal-to-noise ratio 329–31
 Signal voltage 329
 Silvered mica capacitor, temperature coefficient of 202
 Silvering of ferrite core 267
 Sintered density 42
 typical values 43
 Sintering 10–12
 typical cycle 11
 Skin effect, in ferrites 180, 181
 in conductors 209, 212, 220, 341–44
 Skin effect factor 209, 341
 Skin effect loss tangent 209
 Slurry pressing 10
 Snoek loss expressions 31–33
 Solenoid 183
 cylindrical air-cored 348
 ideal 18–21
 Specification parameters, typical values of 44–46
 Spin direction, transition of 4
 Spin orientation 4
 Spin precession resonance 108
 Spinel ferrite 1, 3
 Spinel lattice 2–3
 unit cell of 2–3
 Spray drying 8
 incremental permeability as function of 74–83

 Stefan-Boltzmann law 299
 Steinmetz exponent 148
 Stray capacitance. *See* Self capacitance
 Stress, initial permeability as function of 167–68
 Stress effects; variability in inductors 204
 Sub-lattices 3, 4
 Surface preparation for cementing 15
 Susceptibility 19
 Symbols, list of 379–84

 Television, colour, raster correction 232
 Temperature, a factor in variability 22–23, 202–06
 hysteresis loss factor as function of 142
 incremental permeability as function of, with steady field strength as parameter 101–04
 initial permeability as function of 91–100
 permittivity as function of, at high frequency 164–65
 residual loss factor as function of 132–34
 resistivity, as function of 157–59
 at high frequency 164–65
 saturation flux density as function of 61–64
 Temperature coefficient, antennas 335
 of cylindrical core 191
 of effective permeability 176
 of inductance 191, 201–05, 234, 335
 of inductors 194, 201–05
 of initial permeability 22
 of transductor 228, 234
 Temperature control of kilns 12
 Temperature dependence, of disaccommodation 106
 of high frequency transductor 228
 of LC product 202–03
 Temperature factor 23, 176, 191, 202, 335
 typical values of 44, 45
 Tensile strength 42–43
 Thermal conductivities, transformer materials 303
 Thermal isolation 305
 Thermal properties of ferrites, typical values of 43
 Thermal shunt 305
 Third harmonic distortion 34–36, 143–47, 181–82
 Third order summation products 34–36, 143–46
 Time-change of permeability. *See* Disaccommodation
 Time factor in pulse analysis 271, 278
 Tolerances of dimensions 12
 Toroid, effective dimensions of 172–73
 ideal 21
 reluctance of 173
 Trace elements 7
 Transducers, high frequency. *See* High frequency transducers

 Transformers, leakage inductance in 354–57
 power. *See* Power transformers
 pulse. *See* Pulse transformers
 wide band. *See* Wide band transformers
 winding areas in 340–41
 Turns factor 197–98

 U cores 312–13
 Ultimate compressive strength 42
 Ultimate tensile strength 42
 Ultrasonic drilling 14
 Unit cell of spinel lattice 2–3
 Unit U cores 312–13

 Vacancies 11
 Variability 22–23
 of inductors. *See* Inductors, variability

 Waveform distortion. *See* Distortion, magnetic
 Wide band transformers 237–68
 applications 237
 basic network concepts 238–40
 equivalent circuit 240–41
 filter techniques, higher frequency region 242–47
 lower frequency region 248
 high frequency 261–68
 core contribution 261–64
 core form 265–66
 core geometry 264–65
 windings 264–67
 low and medium frequency 250–61
 bandwidth 256–57
 core contribution 250–56
 core form 258–59
 core geometry 256–58
 core properties 258
 core selection 259
 design procedure 259–61
 number of turns 251, 254, 259
 practical design in terms of element values 250–59
 relations arising from core and winding geometry 256–58
 passive networks 238–40
 reflexion characteristics in terms of equivalent circuit elements 238–48
 specification 240, 248
 transmission characteristic 237, 240, 249, 267
 higher frequency region, filter techniques 242–47
 in terms of equivalent circuit elements 238–49
 lower frequency region 242
 lower frequency region, filter techniques 248
 mid-band region 241–42
 Winding areas in transformers 340–41
 Winding calculations, symbols used 338

Winding conductors, loss due to eddy currents in 209–12, 322–26, 341–48

Winding resistance, a.c. 322–26, 341–48
d.c. 340–41
inductors 208–12
power transformers 307–08, 317–18, 319–20, 322–26
pulse transformers 294
wide band transformers 241–42, 247, 259

Winding resistance/inductance ratio 196, 256, 340

Winding resistance loss tangent 208–12

Windings, properties of 337–58
arrangements, and m.m.f. diagrams 347
in wide band transformers 353
bowing of 340
bunched conductors 340, 344–46, 348
properties of (table) 373–76
conductor arrangements 338–39
copper (space) factor 338
cross-sections of 339
distributed capacitance in 350, 351
eddy current loss in 341–48

Index

Windings *continued*

inductance of air-cored coil 348–50
isolated single layer, self capacitance of 354
layer parameters 347
leakage inductance 354–57
mean turn length 340
number of layers 339
number of turns in given winding area 337–40
on rectangular coil former 340
packing factor 339
penetration depth 341
power loss due to eddy current loss 341–48
proximity effect 344–46
resistance of. *See* Winding resistance
self capacitance of 206–08, 257, 260, 350–54
analysis method 350–54
expressions for 351–53
relation between geometry and 352–53
skin effect 341–44
see also under specific applications

Wire, properties of, (tables) 359–76

AWG, bare 369
diameter functions 372
fine enamelled 370
medium enamelled 371
bunch conductors 373–76

Metric, bare 364
diameter functions 367
fine enamelled 365
medium enamelled 366

S.W.G., bare 360
diameter functions 363
fine enamelled 361
medium enamelled 362

X-core 195, 254–57, 258

Young's modulus of elasticity 42

Zinc content, effect on permeability/
temperature relation 91
effect on saturation flux density/
temperature relation 61

Soft Ferrites – Properties and Applications – E. C. Snelling

Table 3.1. SURVEY OF SOME FERRITE GRADES

APPLICATION CLASSIFICATION											
Class	I	II	III	IV	V	VI	VII	VIII	IX	X	XI
Initial permeability	800-2500	500-1000	1500-10 000	1000-3000	> 1000	500-1000	160-490	70-150	36-65	12-30	< 10
Main applications	Inductors	Inductors Antenna rods	Wide band & pulse transformers	High B_{sat} applns., T.V. & power transformers	Wide band & pulse transformers	H.F. Wide band & power transformers, Antenna rods	Antenna rods, H.F. power transformers	Inductors, Antenna rods, H.F. power transformers	Inductors	Inductors	Inductors
Approx. frequency range	< 200 kHz	100 kHz-2 MHz	LF-200 MHz	< 100 kHz	1-300 MHz	100 kHz 300 MHz	500 kHz-5 MHz	2-30 MHz	10-40 MHz	20-60 MHz	> 30 MHz
Manufacturer and trade name											
UNITED KINGDOM											
1 Aladdin Components Ltd. Feradin							R1	R4 R5	R6 R8	R9 R10	
2 Mullard Ltd. Ferroxcube	A1 A5 A13	A10	A5T A8 A7 A15	A2 A3 A9 A16		B1	B2	B10	B4	B5	
3 Neosid Ltd.	F7 F8 F8A	F11	F7 F8A				F14A	F16 F17	F25		F29
4 The Plessey Company Ltd.	M2 T5 T11	T21 T31	T5 T5T	NW27 NW29 NW26			NW25	NW6 NW10 H32			
5 S.E.I. Ltd. Feralex	P R	S	P	R		K2	K4	K6	K8		
6 S.T.C. Ltd. Stanferite	SA503 SA502 SA500L	SA401	SA500T SA601			SB700	SB600	SB500	SB400	SB300	
HOLLAND											
7 N.V. Philips Ferroxcube	3B 3B3 3B5 3H1 3B7	3D3	3E1 3E2 3E3	3C2 3C6 3C7 3C8		4A1 4A4	4B1	4C1 4C6 4C7	4D1 4D2	4E1	1Z3
FRANCE											
8 Cofelec Ferrinox	T4 T6 T10 T14 T22	B10* T31*	B50 T6	B30 B42 B50			H20	H30 H32	H50	H60 H52	
9 Coprim Ferroxcube	3B 3B3 3B5 3H1 3B7	3D3	3E1 3E2 3E3	3C6 3C7 3C8		4A1 4A3	4B1	4C1 4C7	4D1	4E1	
10 L.T.T. Fermalite Femilite	2002 1004 1002 2005	1005	2002 2003	3002 3001	2101	1101	1102	1112 1103	1104	1105	
GERMANY											
11 Krupp Widia-Fabrie Hyperox	D1S4 D1S2 D1S3		C3 D1 D1S1	C2 C22 C21	E1	E2 E3	E4	E5	E6	E7	
12 Neosid Pemetzrieder GmbH						F1	F2	F106	F20	F40	F100
13 Siemens A.G. Siferrit	N22 N28 N29	M33	T26 N30 T35 T38	N20 N27			M11	K1		K12	U17 U60
14 Steatite Magnesia Kerapern	417	615	417	407 417		503	606 612	602		704 814	
15 Valvo GmbH Ferroxcube	3B 3B3 3B5 3H1 3B7	3D3	3E1 3E2 3E3	3C6 3C7 3C8		4A1 4A3 4A4	4B1	4C1 4C6 4C7	4D1	4E1	
U.S.A.											
16 Allen-Bradley Co.	W-O3 W-5			W-O3 W-O4 W-5		W-O1	R-O2				
17 Ceramic Magnetics Inc.	MN-30 MN-60	MN-30 MN-31	MN-30	MN-31	CM-2002	CN-20 C-2025	C-2050 C-2075	C-2075 N-51	N-50	N-40	
18 Fair-rite Products Corp.	71 72 73	31 32 33					64 62	61 65 51	63		
19 Ferroxcube Corp. Ferroxcube	3B9 3B7	3D3	3E 3E2A 3E3	3E 3C5	4A6	4A	4B	4C 4C4	4D	4E	1Z2
20 Indiana General Corp. Ferramic	TC-6 TC-7	TC-3	O-5 O-6	O-5		H		TC-4 Q-1	Q-2	Q-3	
21 Magnetics Inc.	C D G	A	A C D G	C D				N			
22 National Moldite Co. Inc.	D*	71*						M	M2*		
23 Stackpole Carbon Co. Ceramag	C24 C26	C27A	C24	C24A		C7A C5N	C9	C11 C11A	C12	C2285	C2285A
24 D. M. Steward Manufacturing Co.	F-112					F4S-1		F-220		F6-21	
JAPAN											
25 Nippon Electric Co. Ltd. Neferrite	C*		D1* D2 D3								
26 Nippon Ferrite Industrial Co. Ltd.	VL-71 VL-74 FQ-2 GP-5 GP-3 GQ-2 SB-5 FB-5	AL-3 CL-81	VL-71 VL-74 FB-3 GP-5	VL-71 VL-74 SB-5 FB-5 FB-3		L-84 L-85 T-314 TH-100 CL-81	LK-100 QL-400 L-81 QM-051 KQ-1 L-82	QM-101 QM-201 LM-81	MH-81 VH-40 KM-45 1T-1 MH-90	VH-50 VH-100 VH-150 VH-200	VH-300
27 Sony Corp.	407*FBM FB1 FB4 FB4A	503* 403 FB1	204 FBL FC1 FC2 FC4	304 307	4B1*	5A5 KT23	KT21 KT41	6A6 KM21	6A7	KH51 KH72	KH75
28 Tohoku Metal Industries Ltd.	1801F	801F	4000H 7000H 12000H	1300B 1500B 3000B	2000L		250L 400L	80L 100L	40L	20L	10L

- (i) See text for the description of this table.
(ii) The application classifications are summarized at the heads of the columns; they are defined more completely in the text.
(iii) As far as is known classifications I to IV are basically manganese zinc ferrites and V to XI are basically nickel zinc ferrites. Exceptions are 1Z2 and 1Z3, which are hexagonal structures, and AL-3 and CL-81 which, although appearing in column II are nickel zinc ferrites.

*(iv) Often associated companies use the same code number for equivalent material grades. However, sometimes quite different ferrites manufactured by unrelated companies have by chance identical code numbers; to avoid ambiguity in the graphical data only those material grades printed in bold type are quoted in Figs. 3.1 to 3.24.